

Sheffield Hallam University

Assessing the daylight transmittance of atria roofs in real buildings.

LASH, Daniel.

Available from the Sheffield Hallam University Research Archive (SHURA) at:

<http://shura.shu.ac.uk/19942/>

A Sheffield Hallam University thesis

This thesis is protected by copyright which belongs to the author.

The content must not be changed in any way or sold commercially in any format or medium without the formal permission of the author.

When referring to this work, full bibliographic details including the author, title, awarding institution and date of the thesis must be given.

Please visit <http://shura.shu.ac.uk/19942/> and <http://shura.shu.ac.uk/information.html> for further details about copyright and re-use permissions.

SHEFFIELD HALLAM UNIVERSITY
LEARNING CENTRE
CITY CAMPUS, FOND STREET,
SHEFFIELD S1 1WB.



Fines are charged at 50p per hour

- 1 APR 2008

APM

REFERENCE

ProQuest Number: 10697248

All rights reserved

INFORMATION TO ALL USERS

The quality of this reproduction is dependent upon the quality of the copy submitted.

In the unlikely event that the author did not send a complete manuscript and there are missing pages, these will be noted. Also, if material had to be removed, a note will indicate the deletion.



ProQuest 10697248

Published by ProQuest LLC (2017). Copyright of the Dissertation is held by the Author.

All rights reserved.

This work is protected against unauthorized copying under Title 17, United States Code
Microform Edition © ProQuest LLC.

ProQuest LLC.
789 East Eisenhower Parkway
P.O. Box 1346
Ann Arbor, MI 48106 – 1346

Assessing the Daylight Transmittance of Atria Roofs in Real Buildings

Daniel Lash

A thesis submitted in partial fulfilment of the requirements of Sheffield
Hallam University for the degree of Doctor of Philosophy



August 2004

Abstract

The displacement of artificial lighting with daylighting in buildings has been shown to reduce energy consumption and provide preferable spaces for building occupants. The atrium is one means of achieving daylighting objectives in medium to large scale buildings. The transmittance of daylight through atria roofs is the least understood area of atrium design, with a particular dearth of information concerning roof transmittance in real buildings.

This study aims to further the current knowledge base with regard to roof transmittance through the measurement of transmittance in real buildings, and comparison to a newly proposed photoanalysis technique. This has the potential advantage of being able to assess the transmittance of existing roofs far more efficiently than physical illuminance measurement approaches.

The daylight factor at points immediately beneath the roof was measured in two case study buildings, one of which was a simple a-frame, the other a space frame monopitched roof with significant over-shading from the urban context. Hemispherical photographs were taken in these buildings, and the proportion of visible sky seen at the corresponding viewpoints found using the program HemiView. The effects of changing the photograph viewpoint, quality, and using the classifying tool within HemiView were investigated. The buildings were then modelled on a computer and a comparison made with hemispherical images of the roofs derived through a rendering process. Illuminance simulations were then run using the program Radiance. The effects of the well and external obstructions were isolated, and the relationship between illuminance at the photocell point and average roof plane illuminance found. The consequence of parametrically adjusting the structure reflectance and glazing transmittance was explored, and simple relationships relating these two factors to average roof plane transmittance derived.

Further roof types were modelled on a computer and analysed in the same manner. A means of relating the photographic technique to transmittance is presented, and a methodology described for application of the procedure to existing roofs. The process was demonstrated on 15 roofs in Sheffield. The thesis concludes with a summary and suggestions for future work.

Acknowledgements

Undertaking a PhD is ultimately a great personal and rather self-indulgent test of mettle. Upon this voyage, there are those who are of assistance at various points, and those who sail beside you all the way. The greatest debt of thanks must go to my supervisor, Professor Steve Sharples, who put faith in me in the first instance, and was an invaluable source of wisdom and experience throughout.

The success of the field measurements were in no small part down to the practical ingenuity of Les Goodwin. A thank you also to the various health and safety parties, along with the relevant maintenance personnel and porters. To Tamer Gado for his incessant plugging of Ecotect, and to Dr. Andrew Marsh for the live demonstration. To Dr. John Mardalijevic and the members of the Radiance online discussion boards for help with this initially bewildering program. To the owners of all the buildings in which field measurements were performed. To the support staff, and my fellow researchers within the department, thank you.

A special thank you to the EPSRC and Sheffield Hallam University for providing the financial backing for this research.

Finally, and without whom none of this would have been possible, is the fantastic network of family and friends I am fortunate to find myself a part of. To all flatmates, catmates, coursemates, oldmates and soulmates, to the city of Sheffield, and its dark little holes and wide open spaces, to my family across the globe, and most especially, to my mother and father, and sister, love and the biggest of thank you's.

I declare that as far as I am aware any work referred to has been correctly attributed and that all other content of the submission represents solely my own work. No portion of this thesis has been submitted in support of an application for another degree at this or any other institution of learning.

Table of Contents

0. Preface

<i>Title Sheet</i>	<i>i</i>
<i>Abstract</i>	<i>ii</i>
<i>Acknowledgements</i>	<i>iii</i>
<i>Table of Contents</i>	<i>iv</i>
<i>List of Figures</i>	<i>ix</i>
<i>List of Tables</i>	<i>xvi</i>

1. Introduction	1
1.1 Background	2
1.2 Overview	3

2. Daylighting in Atrium Buildings: A Literature Review	6
2.1 Daylighting: A Background	7
2.1.1 <i>A Very Brief History of Daylighting & Buildings</i>	7
2.1.2 <i>Daylighting and Energy</i>	7
2.1.3 <i>Daylight and Human Beings</i>	8
2.1.4 <i>As Things Stand Now</i>	9
2.2 Human Perception of Illuminated spaces	11
2.3 The Atrium	14
2.3.1 <i>Historical Context</i>	14
2.3.2 <i>The Advantages of Atria</i>	15
2.3.3 <i>Atrium Nomenclature</i>	17
2.3.4 <i>Lighting Objectives of Atria</i>	20
2.3.5 <i>The Passage of Light Flux</i>	21
2.4 External Conditions	22
2.4.1 <i>Sky Luminance Distribution and Models</i>	22
2.4.2 <i>Application to Daylight Analysis</i>	28
2.4.3 <i>External Obstructions</i>	29
2.5 The Fenestration	30
2.5.1 <i>Form and Structure</i>	30
2.5.2 <i>Surface</i>	36
2.5.3 <i>Control of Direct Sunlight</i>	38
2.5.4 <i>Light Transport</i>	39
2.5.5 <i>Maintenance</i>	40
2.6 The Well	40
2.6.1 <i>Geometry</i>	40
2.6.2 <i>Surface Reflectance</i>	46
2.6.3 <i>Internal Well Obstructions</i>	48
2.6.4 <i>Adjacent Spaces</i>	48
2.7 Artificial Lighting Control: A Brief Discussion	51
2.8 From Knowledge to Practice: Application in the Field	53
2.8.1 <i>The Process of Design and the Role of the Design Tool</i>	53
2.8.2 <i>Types of Design Tool</i>	54
2.8.2.1 <i>Simple Design Ideas and Tools</i>	54

2.8.2.2 <i>Study of Precedents</i>	56
2.8.2.3 <i>Modelling</i>	58
2.8.2.3.1 <i>Scale Models</i>	58
2.8.2.3.2 <i>Computer Models</i>	59
2.8.3 <i>Which Tool is Appropriate?</i>	60
2.9 Conclusions	61

3. Project Outline and Methodology	63
3.1 Outline: Aims and Objectives	64
3.1.1 <i>Chapter Outline</i>	64
3.1.2 <i>Current Gaps in Knowledge: A Very Brief Recap</i>	64
3.1.3 <i>Aims and Objectives</i>	65
3.2 Methodology: An Overview	65
3.3 Physical Illuminance Measurements	69
3.3.1 <i>Measuring the Roof Transmittance</i>	69
3.3.2 <i>The Hardware</i>	72
3.3.3 <i>The Case Study Atria</i>	74
3.3.3.1 <i>Selecting the Case Study Atria</i>	74
3.3.3.2 <i>The Sheaf Building; A Simple Scenario</i>	75
3.3.3.2.1 <i>A Description</i>	75
3.3.3.2.2 <i>Set-up and Rationale</i>	77
3.3.3.3 <i>The Owen Building; A More Complex Scenario</i>	80
3.3.3.3.1 <i>A Description</i>	80
3.3.3.3.2 <i>Set-up and Rationale</i>	82
3.3.4 <i>Running the Experiment</i>	86
3.3.4.1 <i>Logging the Weather Conditions</i>	86
3.3.4.2 <i>Length of Logging Period</i>	86
3.4 Photoanalysis with HemiView	87
3.4.1 <i>The HemiView Software</i>	87
3.4.1.1 <i>Background</i>	87
3.4.1.2 <i>HemiView; The Process</i>	87
3.4.2 <i>Methodology for Photo Derivation</i>	92
3.4.2.1 <i>The Base Position</i>	92
3.4.2.2 <i>Varying Location of Photograph</i>	93
3.4.2.3 <i>Varying Quality of Photograph</i>	98
3.4.2.4 <i>Processing the Image in HemiView</i>	98
3.4.2.5 <i>The Plan Area of Obstruction</i>	101
3.4.3 <i>Deriving the Image using Radiance</i>	102
3.4.3.1 <i>The Benefits of Image Generation from Radiance</i>	102
3.4.3.2 <i>Generating the Images</i>	103
3.5 Computer Simulation of Daylight in Buildings: Selecting the Right Tool	107
3.5.1 <i>Computer Simulation of Daylighting</i>	107
3.5.2 <i>The Objectives of a Global Illumination Model</i>	107
3.5.3 <i>Early Programs and Simple Models</i>	108
3.5.4 <i>Radiosity</i>	110
3.5.4.1 <i>The Workings</i>	110
3.5.4.2 <i>In Practice and Validation</i>	112
3.5.5 <i>Ray-tracing and Radiance</i>	114

3.5.5.1	<i>The Workings</i>	114
3.5.5.2	<i>In Practice and Validation</i>	119
3.6	Summary	123
4.	Deriving Transmittance Values for Atria Roofs in Real Buildings	124
4.1	Introduction	125
4.2	The Sheaf Building: Results and Analysis	125
4.2.1	<i>Example Sky Types</i>	125
4.2.2	<i>Classifying Sky Conditions</i>	129
4.2.3	<i>An Analysis of the Overcast Results</i>	131
4.3	The Owen Building: Results and Analysis	133
4.3.1	<i>Sorting the Data</i>	133
4.3.2	<i>The External Obstructions</i>	134
4.3.3	<i>The Influence of Artificial Lighting</i>	135
4.3.4	<i>Example Sky Types</i>	136
4.3.5	<i>Overcast Sky Analysis</i>	140
4.4	Conclusions	143
5.	An Investigation of Skylight Gap Fraction through the Analysis of Hemispherical Imagery	145
5.1	Introduction	146
5.2	Results from a Simple Scenario: The Sheaf Building	146
5.2.1	<i>The Base Position</i>	146
5.2.2	<i>Varying Location of Photograph Position</i>	147
5.2.3	<i>Assessing the Legitimacy of the Classified Results</i>	150
5.2.4	<i>Varying the Quality of the Image</i>	154
5.3	Results from a Complex Scenario: The Owen Building	158
5.3.1	<i>The Base Position</i>	158
5.3.2	<i>Varying Location of Photograph Position</i>	159
5.3.3	<i>Assessing the Legitimacy of the Classified Results</i>	164
5.4	Results from Computer Generated Images: Sheaf	167
5.5	Results from Computer Generated Images: Owen	176
5.5.1	<i>Replicating the Physically Acquired Photograph Positions</i>	176
5.5.2	<i>Changing Depth of Photo Viewpoint: Owen</i>	182
5.6	Synthesised Imagery: The Simple and Complex Findings Discussed	193
5.7	Conclusions	195
6.	Expanding Scenario Possibilities: Computer Simulation	196
6.1	Introduction	197
6.2	A methodology for Lighting Simulation	197
6.2.1	<i>A Step Back from Radiance</i>	197
6.2.2	<i>Creating the Geometry</i>	201
6.2.3	<i>The Ecotect Platform</i>	204

6.2.4	<i>Procuring and Application of Material Photometric Information</i>	209
6.2.4.1	<i>Obtaining the Correct Data from the Field</i>	209
6.2.4.2	<i>Editing the *.rad File to Change Photometric Settings</i>	214
6.3	Setting Radiance Ambient Parameters	218
6.3.1	<i>The Simulation Parameters</i>	218
6.3.2	<i>The Ambient Parameters</i>	219
6.3.2.1	<i>Ambient Value and Weight</i>	219
6.3.2.2	<i>Ambient Divisions and Supersample</i>	220
6.3.2.3	<i>Ambient Bounces</i>	223
6.3.2.4	<i>Ambient Accuracy and Resolution</i>	226
6.4	Base Case Simulations: Results	227
6.4.1	<i>The Simple Scenario (Sheaf Building)</i>	227
6.4.1.1	<i>Roof Plane Results</i>	227
6.4.1.2	<i>The Well Contribution</i>	230
6.4.2	<i>The Complex Scenario (Owen Building)</i>	231
6.4.2.1	<i>Roof Plane Results</i>	231
6.4.2.2	<i>External Obstruction Contribution</i>	233
6.4.2.3	<i>The Well Contribution</i>	235
6.5	Examining the Impact of Structural Reflectance and Glazing Transmittance	237
6.5.1	<i>The Need for Parametric Experimentation</i>	237
6.5.2	<i>Methodology</i>	237
6.5.3	<i>Findings: The Simple Atrium Scenario</i>	238
6.5.3.1	<i>Magnitudes</i>	238
6.5.3.2	<i>Distribution</i>	242
6.5.4	<i>Findings: The Complex Atrium Scenario</i>	246
6.5.4.1	<i>Magnitudes</i>	246
6.5.4.2	<i>Distribution</i>	250
6.6	Physical Illuminance Measurements and Computer Simulations Compared	251
6.6.1	<i>The Sheaf Building</i>	251
6.6.2	<i>The Owen Building</i>	252
6.6.2.1	<i>Including External Obstructions</i>	252
6.6.2.2	<i>Excluding External Obstructions</i>	252
6.6.3	<i>Discussion</i>	252
6.7	Conclusions	253

7. Expansion of Roof Typology and Application of Findings **255**

7.1	Introduction	256
7.2	Computer Models: Approach	256
7.3	Results and Analysis	259
7.3.1	<i>A Description of Result Presentation</i>	259
7.3.2	<i>Magnitudes of Transmittance</i>	277
7.3.3	<i>Distribution of Transmittance</i>	278
7.3.4	<i>A Comparison of Results with SkyVision</i>	282
7.3.5	<i>Effect of Viewpoint within the Various Roof Types</i>	283
7.3.6	<i>Relating the Photograph to Transmittance of the Roofs</i>	286
7.3.7	<i>A Discussion of the Relevance of Application</i>	290

7.4 Application to the Field	292
7.4.1 <i>Divergence between Real and Simulated Conditions:</i>	292
<i>Application of the Photographic Method to Real Buildings</i>	
7.4.2 <i>The Buildings Selected and Methodology</i>	294
7.4.3 <i>Discussion</i>	312
7.5 Conclusions	317
8. Conclusions	319
8.1 Summary	320
8.2 Suggestions for Future Work	323
9. Bibliography	327
Appendix A : Configuring the Dataloggers	342
Appendix B : Weather Log	345
Appendix C : Full Illuminance Results from Sheaf & Owen Buildings	360
Appendix D : Statistical Equations	378

List of Figures

Chapter 1: Introduction

Chapter 2: Daylighting in Atrium Buildings: A Literature Review

Figure 2-1	Bland artificial lighting conditions typically found in office buildings in the mid to late part of the century (Baker et. al. 1993)	7
Figure 2-2	Illuminance mapping from the Perolles area (Compagnon 2004)	10
Figure 2-3	An example of a well daylit space, Westgate School, Winchester, UK (Bell & Burt 1995)	11
Figure 2-4	The Palm House, Kew, London, 1848 (Baker et. al. 1993)	14
Figure 2-5	The Hyatt Regency Hotel, USA	15
Figure 2-6	Atria have the potential to address and solve complex and often conflicting issues simultaneously (Bednar 1986)	15
Figure 2-7	Atrium spaces are often dynamic, and well liked by building users (Bryn 1995)	16
Figure 2-8	a. Centre for New Business, Reze, France (Baker et. al. 1993). b. Harlequin Centre, Watford, UK; c. Bentalls, Kingston-Upon-Thames, UK; d. Burrell Collection, Glasgow, UK. (all Burt & Bell 1995)	17
Figure 2-9	Four types of atria typology (Hung & Chow 2001)	18
Figure 2-10	Possible paths of light from the sky to point P in a room	20
Figure 2-11	Probabilities of three sky conditions (overcast, intermediate, clear) relative to sunshine duration (Rahim et. al. 2004)	24
Figure 2-12	Illuminance results from IDMP, Lyon (Dumortier 1994)	25
Figure 2-13	The distribution of the 15 sky types in Sheffield, November 1993-February 1994 (Markou et. al. 2004.)	27
Figure 2-14	The novel rotating sky simulator used to measure PDF (Michel & Scartezzini 2002)	29
Figure 2-15	There are a multitude of structural roof configurations open to the designer	31
Figure 2-16	A model study under an artificial sky investigating the effects of 14 atrium roof types (Navvab & Selkowitz 1984)	32
Figure 2-17	A model study under an artificial sky investigating the effects of 3 atrium roof types (Boubekri 1995)	33
Figure 2-18	Transmittance profiles of clear and diffusing circular domes and flat skylights (Laouadi 2004)	34
Figure 2-19	Daylight factor at floor level under different roof types (Dewey & Littlefair 1998).	35
Figure 2-20	The redirection of light towards the ceiling using an LCP (left) and mirrored reflective blind (right) (Kischkoweit-Lopin 2002)	38
Figure 2-21	The efficiency of circular lightwells as a function of aspect ratio (H/r) for various angles of solar altitude (Tsangrassoulis & Santamouris 2000)	41
Figure 2-22	Effect on DF of varying PAR (Liu et. al. 1991)	42
Figure 2-23	The relationship between well index and daylight factor is one of exponential decay (Calcagni & Paroncini 2004)	43
Figure 2-24	The various attempts made by authors to relate well index to daylight factor (Wright & Letherman 1998)	44

Figure 2-25	The findings of Atif et. al. (1995) relating well index, surface reflectance and roof transmittance to average daylight factor on the atrium floor	44
Figure 2-26	The relationship between theoretically derived, physically measured and computer simulated results for sky component within an open well (Aizlewood et. al. 1997)	45
Figure 2-27	Splaying is a strategy which can be adopted to improve the efficiency of deeper wells up to angles of approximately 60° (Laouadi 2004)	46
Figure 2-28	Daylight factor in spaces adjacent to the well on top (5 th) and ground floors (Cole 1990)	49
Figure 2-29	A monograph addresses multiple parameters in a user friendly manner (Szerman 1992)	50
Figure 2-30	The varying nature of transmittance with angle from horizontal in the Jewellery School (left) and Centre Court (right) for application to a simple equation (Littlefair 1998)	56
Figure 2-31	Dragvoll University Centre, Trondheim, Norway (Fontoynt 1999)	57
Figure 2-32	Illuminance measurements taken under overcast sky conditions were consistently lower in a scale model than from the full scale building (Cannon-Brookes 1997)	59

Chapter 3: Project Outline and Methodology

Figure 3-1	Schematic of methodology for this thesis	69
Figure 3-2	Skye DataHog and internal photocell used to measure and log illuminance	72
Figure 3-3	Response curve of SKL 310 photocell used relative to the CIE standard curve. The agreement is good.	72
Figure 3-4	The Sheaf building	76
Figure 3-5	Location of Sheaf photocells	79
Figure 3-6	The Owen Building	81
Figure 3-7	Potential depths within the roof from which 'transmittance' could be measured	82
Figure 3-8	Location of Owen photocells	85
Figure 3-9	Nikon 950 Coolpix camera with fisheye adaptor	87
Figure 3-10	a. The horizon circle is resized to fit the are of captured image; b. Splitting the window ensures accuracy of fit	89
Figure 3-11	Terminology of sky dome	89
Figure 3-12	Correction factor applied by HemiView to actual camera lenses	90
Figure 3-13	The classifier menu box. The threshold can be set, and the 'ignore red' option checked.	90
Figure 3-14	Toggling from the original image (left) to the classified image (right) facilitates the classification process	91
Figure 3-15	The trolley used to capture the image from the position of the photocell, suspended over the well	93
Figure 3-16	Photograph positions in the Sheaf building	95
Figure 3-17	Photograph positions in the Owen building	97
Figure 3-18	Processing the derived photographs	100
Figure 3-19	Detail of Sheaf roof as viewed from the ground at resolutions of a. 512, b. 1024, c. 2048, d. 4096 and e. 8192	104

Figure 3-20	Schematic indicating incremental deepening of viewpoint within the well of the Sheaf building, at the end position	105
Figure 3-21	Location of Radiance derived fisheye images in the Owen building	106
Figure 3-22	Three views of the same boardroom (Ward Larson & Shakespeare 1998)	108
Figure 3-23	A comparison of a theoretical model and two computer programs (Tsangrassoulis & Bourdakis 2003)	109
Figure 3-24	The simple BRE split-flux method is used to calculate daylight in the built in lighting analysis tool within Ecotect	110
Figure 3-25	A Lambertian (perfectly diffuse) surface assumes no bias in any direction of reflection (Summerfield 2004)	111
Figure 3-26	A comparison of 2 measured field datasets with 4 computer programs, including the most widely known radiosity program, Lightscape (Ashmore & Richens 2001 (figure from Roy 2000))	114
Figure 3-27	Image generation using a. purely deterministic approach, b. purely stochastic approach and c. the hybrid approach taken by Radiance (Ward Larson & Shakespeare 1998)	115
Figure 3-28	The completed view of the yellow sphere (top left) is the resultant combination of a direct light calculation (top right), indirect specular component calculation (bottom left) and diffuse calculation (bottom right) (Ward Larson & Shakespeare 1998)	116
Figure 3-29	Incoming incident light to a surface is considered direct (deterministic tracing back to a source), indirect (hemispherical stochastic sampling) and specular terms (Summerfield 2004)	117
Figure 3-30	Possible combinations of reflection with ambient bounce parameter set at a. 0 and b. 1	119
Figure 3-31	Results of sky luminance scan and illuminance values physically measured and predicted by Radiance for a. an overcast sky, and b. an intermediate sunny sky	120
Figure 3-32	Illuminance values physically measured and predicted using Radiance (Galasiu 2002)	121
Figure 3-33	The close match between physically measured and simulated daylight factors in a museum space (Ng et. al. 1999)	122

Chapter 4: Deriving Transmittance Values for Atria Roof in Real Buildings

Figure 4-1	7 th September 2002. A demonstration of the dynamic nature of sky luminance distribution	126
Figure 4-2	October 15 th 2002. A completely overcast day	127
Figure 4-3	September 1 st 2002. A day with clear skies	128
Figure 4-4	The variation of daylight factor over the course of a day under clear sky conditions	128
Figure 4-5	Illuminance values over the course of a day under clear skies	129
Figure 4-6	Internal illuminance against external illuminance for all sky conditions between 6 am and 9 pm	130
Figure 4-7	The distribution of sky into three bins, between 8 am and 6 pm, July to October 2002	131
Figure 4-8	Internal illuminance against external illuminance under overcast skies between 8 am and 6 pm	132

Figure 4-9	The distribution of sky into three bins, between 8 am and 6 pm, February to April 2004	134
Figure 4-10	Obstructed external illuminance against unobstructed external illuminance under overcast skies	134
Figure 4-11	Illuminance levels for sample days one week apart from 14 th February to 17 th April 2004, with their corresponding sunrise and sunset times (the dashed vertical lines)	136
Figure 4-12	12 th March 2004. An almost entirely overcast day	137
Figure 4-13	2 nd March 2004. A day with clear skies	138
Figure 4-14	The variation of illuminance over the course of a day under clear skies	138
Figure 4-15	The obstructed measuring points are potentially under direct illumination between 11.15 am and 1 pm on February 14 th	139
Figure 4-16	The variation of daylight factor over the course of a day under clear skies	140
Figure 4-17	Internal illuminance against obstructed external illuminance under overcast skies	141
Figure 4-18	Internal illuminance against unobstructed external illuminance under overcast skies	141
Figure 4-19	The distribution of DF (or more correctly, I_I/I_E in the case of the obstructed results) values derived from the obstructed and unobstructed external photocells	142
Figure 4-20	The variation of DF (or more correctly, I_I/I_E) over the course of a day under overcast skies	143

Chapter 5: An Investigation of Skylight Gap Fraction through the Analysis of Hemispherical Imagery

Figure 5-1	View from the S1 (left) and S2 (right)	148
Figure 5-2	As the viewpoint moves deeper into the well (i.e. further from the roof), the area of interest diminishes, and the lines of perspective approach plan conditions (i.e. parallel)	149
Figure 5-3	For practical reasons, the photograph at S1 could not be taken under even skies. The resultant partially cloudy sky made classification more problematic	152
Figure 5-4	Moving the classifier from 100-180 at increments of 10.	153
Figure 5-5	Detail from position S5 at hi, fine and normal quality (l-r)	156
Figure 5-6	Overall results from the Sheaf building	157
Figure 5-7	Visible sky, structure blockage and external blockage proportions as seen from the 12 viewpoints	160
Figure 5-8	The view from O4	161
Figure 5-9	The view from O6	162
Figure 5-10	The view from O7	162
Figure 5-11	Overall results from the photographs analysed at the Owen building	167
Figure 5-12	The effect on gap fraction of increasing depth from the roof plane at end and central positions	168
Figure 5-13	Views at end (left) and central (right) positions at depths of 0m and 4m	169
Figure 5-14	Narrow omissions of structure running along the length due to saturation of the side of the structural member by the intense light source (the 'sun')	171

Figure 5-15	The gap fraction results from the physically captured photographs overlaid onto the curves from the generated images.	171
Figure 5-16	Side-by-side comparisons of the physically acquired photos to the computer generated images	172
Figure 5-17	Comparison of photo S4 before and after modifying the right hand edge from black to red	175
Figure 5-18	A comparison between physically captured photographs and generated images for visible sky, structure blockage and external blockage values	177
Figure 5-19	A side-by-side comparison of physically captured photographs with computer generated images	178
Figure 5-20	Gap fraction results from obstructed and unobstructed computer generated images with increasing depths within the well along west, central and east axis	183
Figure 5-21	Visible sky and derived structure and external blockage values with increasing depths within the well along west, central and east axis	185
Figure 5-22	The changing view with lateral and vertical displacement of viewpoint	186
Figure 5-23	Illustration of geometric parameters defined in equations 5.4 and 5.5	188
Figure 5-24	The rise of gap to external obstruction ratio with increasing well depth	188
Figure 5-25	Computer generated views along east, centre and west axis	191
Figure 5-26	The Canon EOS-1D Mark II	194

Chapter 6: Expanding Scenario Possibilities: Computer Simulation

Figure 6-1	The workings of Radiance (adapted from Radiance manual pages)	198
Figure 6-2	A rendering of an atrium space (Ward Larson & Shakespeare 1998)	199
Figure 6-3	An overview of the simulation process used in this study	200
Figure 6-4	The right hand rule	201
Figure 6-5	The Sheaf building modelled to a high and low level of detail	203
Figure 6-6	The materials dialogue box	205
Figure 6-7	Position of analysis grid in the Sheaf building	205
Figure 6-8	Position of analysis grid in the Owen building	206
Figure 6-9	The Radiance file conversion window	207
Figure 6-10	The Radiance grid point results are imported to the Ecotect grid	208
Figure 6-11	Output display option in Ecotect	208
Figure 6-12	The Minolta LS-100 Luminance	211
Figure 6-13	The reference material of known reflectance 0.87	212
Figure 6-14	Optics5 allows the building of layered glazing systems from an extensive database of glass types and coated films	213
Figure 6-15	Effect of changing ambient divisions across one row of a grid in the Sheaf building	221
Figure 6-16	Three settings of ambient division	222
Figure 6-17	The cost in time of running a more accurate simulation by increasing the -ad parameter	223

Figure 6-18	The effect of changing the τ_{ab} parameter across an analysis row in the Sheaf building	224
Figure 6-19	Error associated with varying τ_{ab} parameter against computational cost Sheaf	225
Figure 6-20	Error associated with varying τ_{ab} parameter against computational cost for the Owen scenario	225
Figure 6-21	Analysis plane daylight factor results for the Sheaf building, with roof plan overlaid and without.	229
Figure 6-22	Analysis plane daylight factor results with the well reflectance set at 0% and with a well of 70.3% reflectance	230
Figure 6-23	Daylight factor at analysis plane in the Owen building with the roof overlaid and without	232
Figure 6-24	Average daylight factor per grid row in the N-S direction	233
Figure 6-25	Average difference at analysis row between simulations with and without external obstructions	234
Figure 6-26	Analysis plane daylight factor results with the well reflectance set at 0% and with a reflective well	236
Figure 6-27	The contribution of the well to DF calculated at the analysis plane	236
Figure 6-28	The effects of changing structural reflectance and glazing transmittance on overall roof transmittance	238
Figure 6-29	The effect of changing structural reflectance on overall roof transmittance for various levels of glazing transmittance	239
Figure 6-30	The effect of changing glazing transmittance on overall roof transmittance for various levels of structural reflectance	241
Figure 6-31	Structural reflectance against Transmittance Ratio	242
Figure 6-32	The distribution of values of Coefficient of Variation obtained for 56 simulations of the Sheaf building	242
Figure 6-33	The effect of structural reflectance and glazing transmittance on coefficient of variation	243
Figure 6-34	The effect of increasing the structural reflectance at 10% increments on transmittance of the roof for a fixed glazing transmittance of 80%	244
Figure 6-35	Histogram showing distribution of transmittance values measured at the analysis points at low and high value scenarios	245
Figure 6-36	Transmittance contours for low and high scenarios	245
Figure 6-37	The effects of changing structural reflectance and glazing transmittance on overall roof transmittance	246
Figure 6-38	The effect of changing structural reflectance on overall roof transmittance for various levels of glazing transmittance	247
Figure 6-39	The effect of changing glazing transmittance on overall roof transmittance for various levels of structural reflectance	248
Figure 6-40	Structural reflectance against Transmittance Ratio for the Owen and Sheaf buildings	249
Figure 6-41	Schematic of A-frame and monopitched roofs	249
Figure 6-42	The distribution of values of Coefficient of Variation obtained for 56 simulations of the Owen building	250
Figure 6-43	The effect of structural reflectance and glazing transmittance on coefficient of variation	251

Chapter 7: Expansion of Roof Typology and Application of Findings

Figure 7-1	The 20x20 analysis grid assigned to the 10m3 black box, upon which various roofs were placed	258
Figure 7-2	The depths at which hemispherical views of the roofs were generated for HemiView analysis	259
Figure 7-3	Computer Simulation Analysis: Pyramid	261
Figure 7-4	Computer Simulation Analysis: Dome 1	263
Figure 7-5	Computer Simulation Analysis: Dome 2	265
Figure 7-6	Computer Simulation Analysis: Flat	267
Figure 7-7	Computer Simulation Analysis: Waffle	269
Figure 7-8	Computer Simulation Analysis: Sawtooth	271
Figure 7-9	Computer Simulation Analysis: Monopitch Space Frame (Owen)	273
Figure 7-10	Computer Simulation Analysis: (A-Frame (Sheaf)	275
Figure 7-11	TR against structure reflectance for the eight roof types simulated	279
Figure 7-12	Coefficient of variation against structure reflectance for the eight roofs simulated	280
Figure 7-13	Gap fraction against relative depth for the eight roof types investigated	285
Figure 7-14	The % difference between coefficient c and calculated gap fraction. The dashed line represents the % difference of c from the PAG i.e. depth = infinity	289
Figure 7-15	Correction factor to be applied to physically captured photographs using the specific set-up of this experiment, for linear atria	294
Figure 7-16	The Meadowhall Shopping Centre, Sheffield, completed in 1990 incorporates a multitude of skylight types	295
Figure 7-17	Application to Real Skylights: Meadowhall A	297
Figure 7-18	Application to Real Skylights: Meadowhall B	298
Figure 7-19	Application to Real Skylights: Meadowhall C	299
Figure 7-20	Application to Real Skylights: Meadowhall D	300
Figure 7-21	Application to Real Skylights: Meadowhall E	301
Figure 7-22	Application to Real Skylights: Meadowhall F	302
Figure 7-23	Application to Real Skylights: Showroom Cinema	303
Figure 7-24	Application to Real Skylights: Natwest Offices	304
Figure 7-25	Application to Real Skylights: Orchard Square Shopping Centre	305
Figure 7-26	Application to Real Skylights: Blue Moon Cafe	306
Figure 7-27	Application to Real Skylights: Millennium Galleries A	307
Figure 7-28	Application to Real Skylights: Millennium Galleries B	308
Figure 7-29	Application to Real Skylights: Winter Gardens	309
Figure 7-30	Application to Real Skylights: Sheffield Hallam University	310
Figure 7-31	Application to Real Skylights: TK Maxx	311
Figure 7-32	Schematic of possible automated program to assess roof transmittance using a photograph and simple input information	316

Chapter 8: Conclusions

Chapter 9: Bibliography

List of Tables

Chapter 1: Introduction

Chapter 2: Daylighting in Atrium Buildings: A Literature Review

Table 2-1	A description of the 15 sky types proposed by Kittler	26
Table 2-2	The findings of selected studies into potential energy savings due to various lighting control mechanisms	52

Chapter 3: Project Outline and Methodology

Chapter 4: Deriving Transmittance Values for Atria Roof in Real Buildings

Chapter 5: An Investigation of Skylight Gap Fraction through the Analysis of Hemispherical Imagery

Table 5-1	Gap fraction results from the five photo positions, and their deviation from the photocell value (S1)	147
Table 5-2	Reference and Classified gap fraction results from the five viewpoints, together with the relative differences between the classified results and S1 and the relative difference between the classified and reference results from that viewpoint	151
Table 5-3	The lower and upper values of gap fraction reasonably possible for these scenarios and the relative differences to the adjusted value	152
Table 5-4	Classified gap fraction results from taking the photographs at the three quality settings of the camera for positions S2-5, along with the relative difference to the reference value	154
Table 5-5	Gap fraction results for the lower and upper boundaries at the three camera quality settings for positions S2-5	155
Table 5-6	Mean errors for the three camera quality settings	155
Table 5-7	Adjusted and unobstructed gap fractions for the 12 Owen viewpoints, together with the differences from the O1 position, and derived structure blockage and external blockage values	160
Table 5-8	A comparison between adjusted and classified gap fraction results	165
Table 5-9	Classification upper and lower bounds of the obstructed images	166
Table 5-10	Classification upper and lower bounds of the unobstructed images	166
Table 5-11	Gap fraction values at end and central axis positions with increasing depth of the Sheaf building	168
Table 5-12	Comparison of physically captured photograph with computer generated images for obstructed and unobstructed images	176
Table 5-13	Visible sky and derived external and structure blockage values with increasing depths within the well along west, central and east axis.	184

Chapter 6: Expanding Scenario Possibilities: Computer Simulation

Table 6-1	The files created by Ecotect in the export to Radiance	207
Table 6-2	Reflectance values for principle surfaces in the Sheaf and Owen buildings	212
Table 6-3	Transmissivity values for increments of transmittance	215
Table 6-4	Effect of changing the $-ad$ (with $-as$) parameter	220
Table 6-5	Effect of increasing the $-ab$ parameter	224
Table 6-6	Minimum distances from after which stochastic hemispherical sampling takes place for various values of $-ar$.	226
Table 6-7	Equations of lines derived from figure 6-29	239
Table 6-8	Equations of lines derived from figure 6-38	247

Chapter 7: Expansion of Roof Typology and Application of Findings

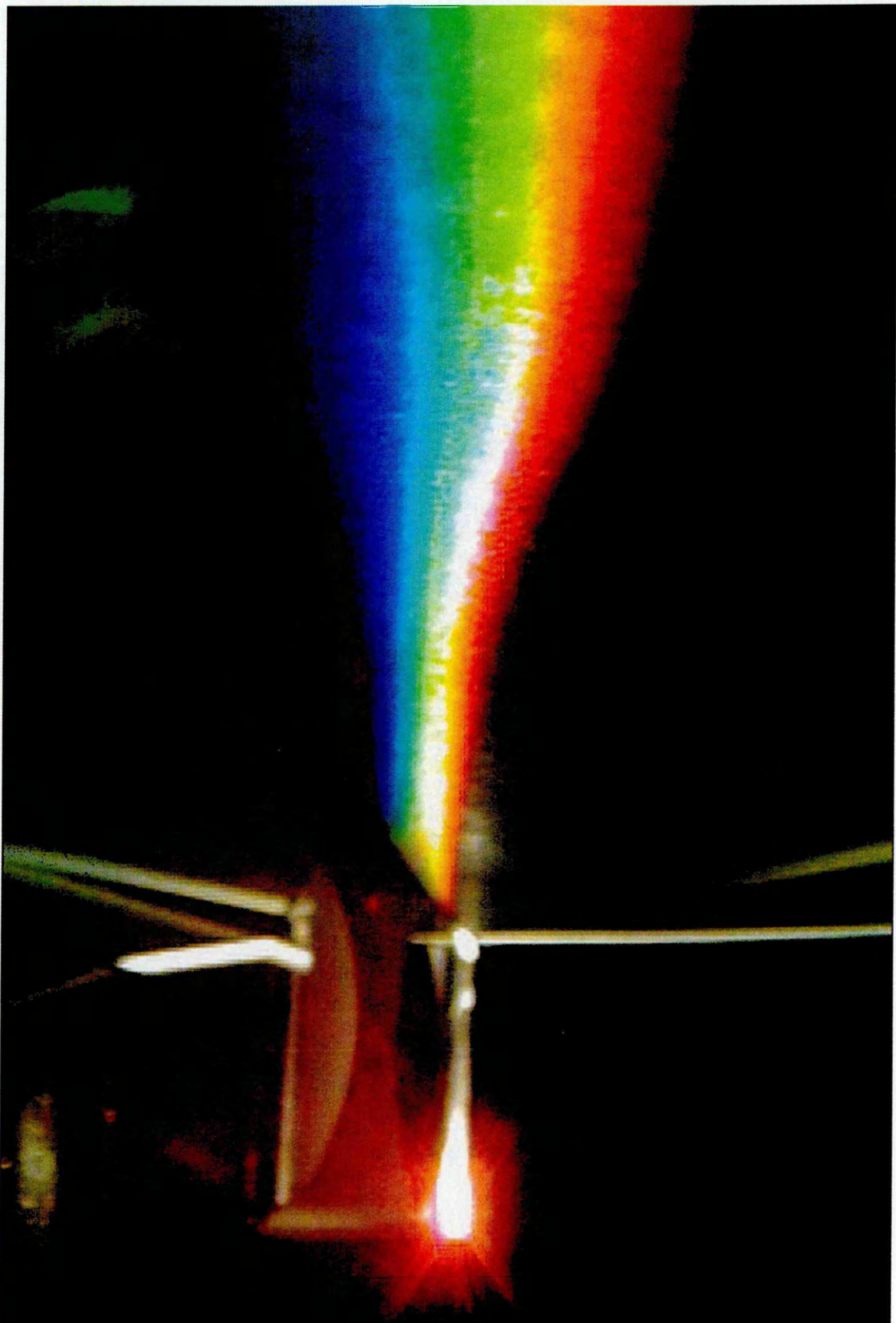
Table 7-1	The coefficients from the derived polynomials describing the TR relative to the structure reflectance of the 8 roof types simulated, as well as the PAG.	277
Table 7-2	SkyVision results for transmittance at roof plane level, together with the difference from the Radiance output	282
Table 7-3	Transmittance results for the 15 roofs examined	310
Table 7-4	Transmittance results for the 15 roofs examined with $\rho = 70\%$ and $T_g = 78\%$	311
Table 7-5	SkyVision output, together with difference from the photoanalysis method	311

Chapter 8: Conclusions

Chapter 9: Bibliography

Chapters A-B: Appendices

Table A-1	Scale Values Used for the Configuration of the Photocells	343
Table B-1	The Weather Log	347



And God said, "Let there be light"; and there was light. And God saw that the light was good; and God separated the light from the darkness. GENESIS, CHAPTER I

1

Introduction

1.1 Background

1.2 Overview

'Who are YOU?' said the Caterpillar. This was not an encouraging opening for a conversation. Alice replied, rather shyly, 'I--I hardly know, sir, just at present-- at least I know who I WAS when I got up this morning, but I think I must have been changed several times since then.' ALICE IN WONDERLAND, LEWIS CARROLL

1.1 Background

The use of daylight as a principle means of lighting our buildings is becoming a more pertinent issue in today's environmentally conscious climate. Within the myriad of published and ongoing daylighting research, which include topics such as the performance of daylighting systems, daylight responsive lighting control systems, design tools, case studies, user interaction and more, the work described in this thesis focuses on a very small 'window', that is, the daylight transmittance of atria roofs in real buildings. As such, the findings will be of potential use to any party involved in the design and operation of atrium roof systems. This includes the architectural profession, lighting engineers and glazing manufacturers. It will also be of interest to any researchers in the field of daylighting in buildings, as part of the ongoing drive towards the reestablishment of natural lighting as the chief internal source of illuminance.

The ultimate aim of this thesis is to greatly further the currently available information on the transmittance of daylight through atria fenestration systems. This will increase the potential for real daylighting benefits to be achieved in newly built (and through retrofitting, existing) atrium spaces. The fulfilment of this aim is achieved through meeting the following four objectives:

1. to assess the transmittance of daylight through skylights by conducting measurements in real working buildings under dynamic sky conditions
2. to propose and test a new photoanalysis technique whose aim is to rapidly assess the transmittance of daylight through skylights
3. to investigate further the multiple parameters of roof configuration, and their effect on transmittance, by comparing physically measured with computer simulated results
4. to propose useable advice for building designers, or at least suggest avenues for continuation of this research

1.2 Overview

The thesis opens with a thorough review of the literature concerning daylighting in atria buildings (Chapter 2). The arguments for daylighting in terms of energy and human factors are outlined. The atrium as a concept is introduced as a means of meeting daylighting objectives, and the passage of light flux broken down at its various stages of travel through the atrium. The impact of the external sky conditions, the fenestration and the well are described in depth, together with the shortcomings of current research based knowledge, and areas in which further work is needed. The pragmatics of artificial lighting and its role in conjunction with daylighting are briefly discussed, before the role of the designer and the tools at his/her disposal are considered.

Chapter 3 outlines the aims and objectives of the project, before detailing the methodology for the field element of the experimental work. This comprises the physical measurement of illuminance levels, and a novel photoanalysis technique. For the illuminance measurements, this involves the exact set-up configuration and rationale, together with notes on the running of the experiment, including logging the weather conditions. With regard to the photoanalysis technique, the experimental procedure for image capture, processing and analysis is described, as well as the methodology for investigating the location and quality of the photograph and the generation of images for analysis through computer modelling. Amongst this, the two detailed case study buildings of this thesis are introduced. The chapter concludes with a discussion of global illumination models, with descriptions of two leading approaches - radiosity and (backwards) ray-tracing. The program of choice for use in this thesis is stated.

Chapter 4 presents the results from the illuminance measurements within the two case study buildings. Analysis for each of these roofs is undertaken separately. Illuminance results under different sky conditions are displayed, before the data is binned into three discrete categories. From the results under overcast skies, the daylight factor at the point of the internal measurement point was derived. In the case of the more complex case study (which is subject to site obstructions), a ratio of internal illuminance to external 'obstructed' illuminance is also obtained.

Chapter 5 discusses the results of the photoanalysis experiments. This is split into four parts, these being the two case study buildings for images captured in the field, and through generation from computer models of the real buildings. For the field captured photographs this involves a discussion of changing the photograph viewpoint, assessing the legitimacy of the classification process, and in the case of the simple case study, the effect of varying the quality of the image. With regard to the synthesised imagery this involves a discussion of methodically increasing the distance of image viewpoint from the atrium roof. The two methods of image derivation are compared, and guidelines for successful image capture stated.

Chapter 6 is concerned with the computer simulation of the case study buildings. The first part of the chapter deals with the methodology, firstly through the interaction of Radiance and Ecotect, and secondly through the tuning of the Radiance ambient parameters. The results from simulations at high quality settings for both buildings are presented, and the differences from the physically measured results derived. The relationship between the illuminance level at the photocell position and the average roof plane levels are found. Through further simulation, the effects of the well and external obstructions (in the case of the complex case study) are isolated. Parametric changes to the reflectance of the structural elements and the transmittance of the glazed elements are made, and the results in terms of magnitude and distribution for both case studies discussed. The relationship between these two dependant variables and the overall roof transmittance is expressed using simple equations. The differences between the calculated transmittance results from these equations, and from average roof transmittances as estimated from the measured data (which was modified using the information concerning the effects discussed and isolated at the start of the chapter) were found and stated.

Chapter 7 expands on the methods and findings of Chapters 3-6 through the computer modelling of six further roof types, and a repetition of the computer simulation and photoanalysis processes. A brief comparison of trends found between these roof types follows, in terms of illuminance magnitudes, distribution and of image gap fraction. The results are also compared with output from the specialist skylight program SkyVision. A means of relating the results from the photoanalysis technique to the transmittance of the roof is proposed, and where possible, pragmatic correction

factors suggested accounting for divergences between artificial and real world conditions. The new methodology is demonstrated in fifteen case study roofs in Sheffield, and the results compared to SkyVision output.

Chapter 8 summarises the findings of the thesis, and suggests potential paths for future work.

2

Daylighting in Atrium Buildings: A Literature Review

- 2.1 Daylighting: A Background
- 2.2 Human Perceptions of Illuminated Spaces
- 2.3 The Atrium
- 2.4 External Conditions
- 2.5 The Fenestration
- 2.6 The Well
- 2.7 Artificial Lighting Control: A Brief Discussion
- 2.8 From Knowledge to Practice: Application in the Field
- 2.9 Conclusions

'The man who doesn't read good books has no advantage over the man who can't read them'. MARK TWAIN

2.1 Daylighting: A Background

2.1.1 A Very Brief History of Daylighting & Buildings

Daylighting has been the chief form of internal illumination in man made buildings up till the widespread use of artificial lighting. The advancement in building techniques over the past two millennia has seen the window form evolve from small open apertures to large planes of glazing capable of spanning considerable distances. The advent of cheap and efficient artificial lighting, first through incandescent sources (invented by Thomas Edison in 1879), and then particularly fluorescent tube luminaires in the 1940's permitted architects to design buildings of deep plan without concern for natural daylighting (Scartezzini 2003). This freedom, coupled with great advances in HVAC systems, enabled a building typology to develop that was totally autonomous of the external environment, the building skin defining where artificial conditioning began, the windows serving only to provide views. This is evident in many of the characterless buildings of the 1950's, 60's and 70's (Baker et. al. 1993) (Figure 2-1). A shift back towards daylighting has arisen in the last quarter of the twentieth century, due predominantly to two factors; energy and human perception.

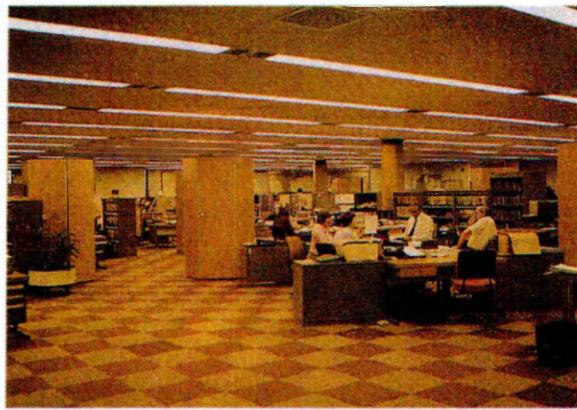


Figure 2-1: Bland artificial lighting conditions typically found in office buildings in the mid to late part of the century (Baker et. al. 1993)

2.1.2 Daylighting and Energy

The oil crisis of 1973 has highlighted the need to conserve energy (Wotton 1998, DTI 2001). Artificial lighting (and the associated cooling loads, which have been quantified at 90% of the lighting power (Love 1998 b)) account for as much as 50% of

non-domestic energy use depending on the figures used (Windheim & Daly 1983, Vischer 1986, Baker et. al. 1993). This equates to \$50 billion annually in the USA alone (Love 1998 b). In the UK electric lighting consumes about 58000 GWh per annum, or about 20% of all generated electricity (Loe 2003). Targets set at the Kyoto Protocol of 1997 mean that by the year 2010, new buildings will need to achieve a 60% reduction in carbon emissions (Battle 2001). Whilst walls with windows are more costly to construct and maintain, they also have a higher market value and command greater rental revenue (Boyce et. al. 2003). Accreditation schemes rewarding daylight spaces may potentially magnify this factor into the future. Increased self-sufficiency of buildings with regard to energy consumption will mean less reliance on the energy infrastructure; a potential target for an act of terror in the politically uncertain waters since September 11th 2001 (Gordes et. al. 2003).

2.1.3 Daylight and Human Beings

Alongside energy concerns, research had simultaneously been undertaken championing daylighting on psychological grounds, due to its quality, changeability and variability (Wotton & Borkow 1983, Heerwagen 1986, Terman et. al. 1986, Vischer 1986, Baker 2000). One hour of worker salary is equivalent to the cost of one year of lighting energy for that worker. The strongest economic argument would therefore appear to be in terms of improved worker productivity, job satisfaction and reduced absenteeism (Leslie 2003). A study analysing the presence of daylight on the test score performance of schoolchildren found a statistically significant correlation between the two factors (Heschong & Wright 2002). The positive results for both vertical and roof openings suggests the relationship was due to daylight and not necessarily the view out. Boyce et. al. (2003) applaud the effort but state some limitations of the study, chiefly that sample sizes were not large enough to be accepted by epidemiologists, and that it was not necessarily daylight *per se* that improved performance, rather the way in which it was delivered.

Physically daylight is just another source of electromagnetic radiation in the visible range, whose properties can be closely matched by artificial lighting. Natural and artificial lighting can be described by the same parameters, however natural light varies in intensity and colour, suggesting measuring approaches with average,

maximum and minimum values as well as probabilities to exceed given thresholds (Fontoynt 2002). There are no proven physical or physiological reasons for daylight to be more desirable than the equivalent artificial lighting; the reason must be psychological.

Daylight fulfils two very basic requirements; to be able to see both the task and the space well, and to receive some environmental stimulation (Boyce 1998). Daylight is characterised by high illuminances and excellent colour rendering, and is often accompanied by a view (Fontoynt 2002). Those of higher status in organisations are often given spaces closer to/with more windows (Boyce 1998). Whilst surrogate daylight can already be provided by artificial light, the surrogate view is missing. Heerwagen (1986) observes occupants of windowless offices attempt to replicate view through posters. Millet (1998) writes that *'daylight keeps us connected to our physical environment'*. The thorough review of Boyce et. al. (2003) concludes by saying that *'the biophilia hypothesis [that humans have an innate need to be in contact with nature] is the main reason why windows are inherently better than electric lighting. All the other psychological effects of windows can, in principle, be fulfilled by electric lighting, given enough care and expenditure [though this author has not to date found lighting a system that simulates the variable sky luminance distribution as effectively as nature itself]. But if contact with nature is really an essential part of life for people, then windows should be a legally required component of many buildings, as they are in some European countries'*.

It has also been shown that UV-B light (found in daylight) helps the body produce vitamin D, although glazing blocks this part of the spectrum, perhaps indicating that architects should provide more outdoor habitable space (Mead 2003). This clearly brings up practicality issues. Strong light levels (naturally found in daylight) may stimulate our circadian cycles by activating serotonin (an antidepressant) and suppressing melatonin (a sleep inducer).

2.1.4 As Things Stand Now

The potential is there; there is sufficient daylight to meet the requirements of 50-70% of the occupancy period in the temperate zones of the earth (Fontoynt 2002) yet,

for too many designers, lighting is seen as a piece of hardware fitted to resolved architectural solutions (Julian 1998). The irradiance mapping studies of Compagnon (2004) potentially enable the daylight availability in any context to be revealed (Figure 2-2). Architects, having turned their collective back on daylighting for a generation have had to relearn old skills and fuse them with current building needs (e.g. Figure 2-3). Collaborative international research is one strong means of achieving this. IEA Task 21; Daylight in Buildings is divided into four subtasks (Johnsen 1998);

- A. Performance and evaluation of daylighting systems
- B. Daylight responsive lighting and control systems
- C. Daylighting design tools
- D. Case studies

This chapter will explain in further detail some of the findings of this research.

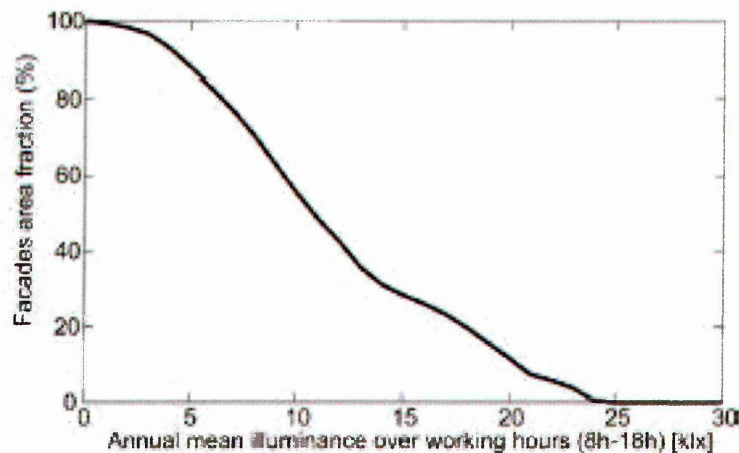


Figure 2-2: Through simulation of urban contexts, the luminance or illuminance patterns on the facades of buildings can be mapped, enabling the potential for daylighting systems to be assessed. For example, 10kLux (the threshold for deploying daylighting systems) is reached on approximately 60% of facades (vertical and roofs) in the Perolles area (Compagnon 2004). This seemingly high value was due to the specifics of the buildings on site, which have relatively large building footprints to their height.



Figure 2-3: An example of a well daylighted space, Westgate School, Winchester, UK (Bell & Burt 1995).

2.2 Human Perception of Illuminated spaces

Light is a fundamental entity for life. The interaction of light with man made space enables us to experience architecture. Millet (1998) cites Richard Kelly's poetic interpretation of the three types of light;

'Focal glow is 'the campfire of all time,...the sunburst through the clouds, and the shaft of sunshine that warms the far end of the valley. Focal glow commands attention and attracts interest. It fixes the gaze, concentrates the mind, and tells people what to look at. [It] separates the important from the unimportant.'...Ambient luminescence is 'a snowy morning in the open country. It is underwater in the sunshine, or inside a tent at high noon. Ambient luminescence minimises the importance of all things and of all people. It fills people with a sense of freedom, of space and can suggest infinity'...Play of brilliants is 'the aurora borealis,...the Versailles Hall of Mirrors with its thousands of candle flames. Play of brilliants is Times Square at night,...the magic of the Christmas tree, Fourth of July skyrockets. It quickens the appetite and heightens all sensation. It can be distracting or it can be entertaining'

Through our perception of light, we determine the extents to which a space is, at the least, acceptable whilst at best, actively enhancing our existence. In essence, our response to lit scenes is a subjective one. Difficulties are therefore an inevitability when quantifying lighting environments. In her review, Veitch (2001a) breaks down our psychobiological process into *visibility*, *photobiology* and *arousal and stress*. *Photobiology* relates to circadian rhythms and mental conditions such as Seasonal Affective Disorder (SAD). The concept is a relatively new one and further research is recommended. *Arousal* is the general state of mental and physical activation whilst *stress* is the name for a set of physiological and hormonal changes that arise in response to threatening or unpleasant events e.g. glare. Support for these factors is relatively weak. One study examined the effect of increasing illuminance (from low (70 Lux) to medium (486 Lux) to high (1962 Lux)) on task performance. The only correlation was found in moving directly from low to high illuminances, though when a 15 minute adaptation time was allowed, performance was similar. This indicates that people can adapt to a wide range of luminous conditions, and can perform well over a broad range of illuminances. These findings illustrate the shortcomings of guidelines and regulations stipulating minimum design values.

Much of the literature in *visibility* concerns the quantifying of the subjective measure into the quantifiable measure of luminance. This quantity is based upon the theoretically approximated v - λ relationship of human visual response to varying wavelengths of the electromagnetic spectrum. Such relationships must be viewed with caution. Most studies concentrate on the distribution of luminance in a field of view. Franta et. al. (2003) state that our eyes adjust to the brightest spot within the field of view, and thus our perception of brightness will vary with the same light levels. The area surrounding a bright patch will appear dark, and so if the lighting conditions are more uniform, the overall perception of a space may be brighter. In most spaces therefore, the goal is to minimise luminance ratios.

In their comprehensive study, Loe et. al. (1994) investigated the effects of various interior lighting conditions (measured using an automated luminance scanning device) on human perception through the use of traditional semantic differential scale techniques (which were then analysed in terms of visual interest and visual brightness). The scale which best described visual brightness was found to be 'dim-bright', and when

the subjective results were compared to the average luminance over a horizontal band of width 40° (the approximate area covered by a normal human field of view when looking horizontally), a value of 30 cd/m^2 was found to correspond to the point where assessment changes from generally dim to generally bright. Likewise, visual interest (most appropriate scale 'interesting-uninteresting') was compared to the ratio of maximum to minimum luminance in the 40° horizontal field of view, and a value of 13 was found to be the point where the lit environment changed from uninteresting to interesting (with little gains over 80, though one would presume glare would at some point become a contradictory issue). A ratio of between 10 and 50 was suggested as a working guide. The authors state that *'what the lighting designer should understand from this, is that lighting needs to be a composition of light and shade put together in such a way that it complements the architecture in a holistic manner...'*

Ozturk (2003) found that 2.3 is the maximum ratio of luminance across a surface of constant reflectance (as opposed to across the whole scene) that is permissible for human comfort, though this recommendation is by no means a panacea for lighting success. Light stains may be caused in a scene through specular surfaces or light sources. Practical recommendations include using matt surfaces, and diffusing light sources/distributors.

Lighting quality has been presented in two ways; guidelines based on past experience and visual comfort criteria based on measurable quantities. The former are often too abstract to be applicable, whilst the latter are often unsuccessful or too complicated to implement (Parpairi et. al. 2002). The Daylight Glare Index, for example, was found to either over or under-predict the glare sensation. *'Imprecise use of theories about psychological processes has likely contributed more heat than light in our literature'* (Veitch 2001 b). Some consistent trends have however arisen. Whilst a generally uniform luminance distribution is necessary in terms of overall brightness perception, an element of variability is required for interest. Of particular importance are bright and interesting vertical surfaces (Veitch 2001 b). This can be created through uniform surface reflectances with variable illuminances, or variable reflectances and uniform illuminances. The latter is preferable as it is normally as a result of visual interest (e.g. moving from a wall, to a bookshelf, to a window) (Parpairi et. al. 2002).

There is no consensus on the quantitative luminance values that are preferred (Veitch 2001 b).

When designing with daylight it is therefore as important to achieve a harmonious distribution as it is to draw in sufficient magnitudes of light flux. It has been shown that occupants in poorly distributed daylit spaces raise artificial lighting levels to even the distribution (Boyce 1998). This negates any benefits sought through the daylit solution.

2.3 The Atrium

2.3.1 Historical Context

The atrium has emerged as a possible solution to bringing natural light into deep-plan buildings, with 60% of building floor surface in the USA directly beneath a roof (Laouadi 2004). An atrium can be described as a covered courtyard, a courtyard being an internal void within or between buildings that is open to the sky (Lam 1986, Gordon & Andersson 1989, Aizlewood 1995). Courtyard buildings extend back to ancient civilisations based in warmer climates such as the Greeks or Romans, and Arabian culture whereby the central court performed important social and space conditioning functions. The roofed court first appeared in London, 1837 at the Reform club by Sir Charles Barry, and was as a result of advances made in iron and glazing manufacturing technology (Figure 2-4).

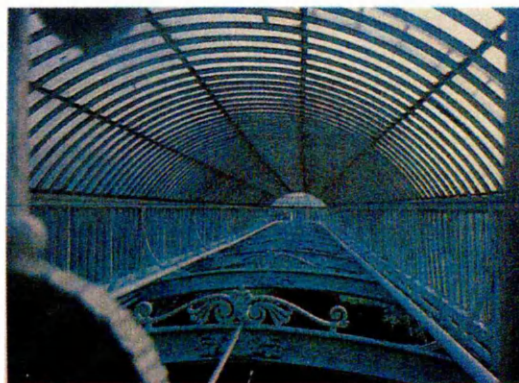


Figure 2-4: Material advances, for example the proliferation in use of glass and iron enabled the construction of buildings such as the Palm House, Kew, London, 1848 (Baker et. al. 1993).

Poor fire performance however meant that it was not to become a major building component until the 1970's, catalysed by Portman's Hyatt Regency hotel in Atlanta, 1967 (Bednar 1986) (Figure 2-5).

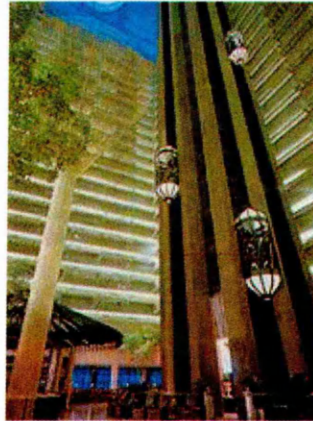


Figure 2-5: The Hyatt Regency Hotel, USA (<http://atlanta.morehotels.com/hyatt-regency-atlanta-photo.html>)

2.3.2 The Advantages of Atria

Atria are generally found in commercial establishments, though there are examples of extended usage. Kotani et. al. (2003) note an increased trend for this building typology in high rise residential apartments in Japan over the past 10 years, due to a resolution of environmental issues and efficient earthquake resistance. The popularity of atria can be attributed to their performance under the three broad headings of *social, financial and environmental* (Figure 2-6).

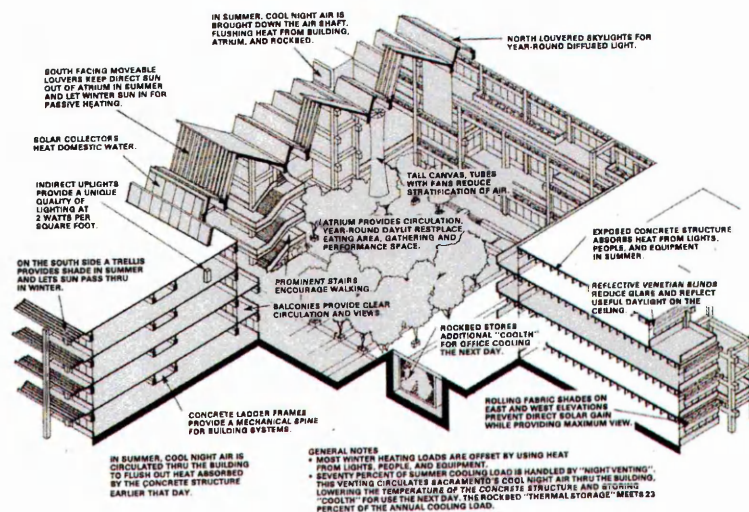


Figure 2-6: Atria have the potential to address and solve complex and often conflicting issues simultaneously (Bednar 1986)

-
- *Socially*, they unify disparate elements of a building(s), acting as highly visual communication tools. This is why they are often the circulation and/or social heart of a building. Building users like atrium spaces and the openness of the roof, and often use them as meeting places (Bryn 1995) (Figure 2-7). From an architectural design standpoint an irregularly shaped atrium surrounded by standard building mass may help resolve awkwardly shaped site issues (Hung & Chow 2001).

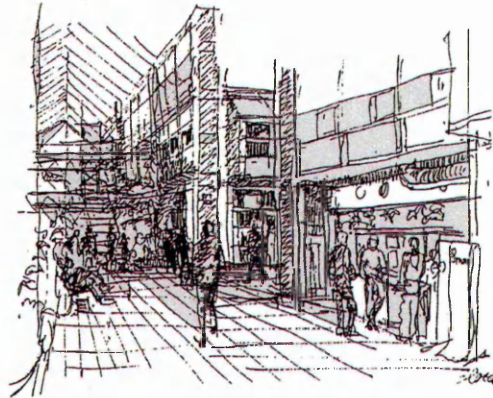


Figure 2-7: Atrium spaces are often dynamic and well liked by building users (Bryn 1995).

- *Financially*, the pleasantness of the space created may result in increased lettable values for rooms overlooking the space, and increased productivity of workers within those rooms. There is also increased potential for retail activity at the ground floor (Hung & Chow 2001).
- *Environmentally* (and financially), atria have the potential to reduce energy loads of buildings through various processes. Treating them as a buffer zone, they can alleviate heating loads of buildings, whilst manipulating the stack effect, natural ventilation can be encouraged. Such phenomena can only occur through effective design. It should be noted that conditioning the atrium to the same state as the remainder of the internal spaces may result in increased energy loads, as it is the intermediate nature of the atrium between inside and out that makes such savings possible. Indeed fully climatized atria often have poor energy economy and high energy consumption (Bryn 1995). Care must also be taken with the shape of the well to prevent air stratification (Kainlauri 1991). Perhaps the most important benefit of an atrium is in allowing natural daylight to penetrate deep into the plan of a building, and it is on this aspect that this study will concentrate (Treado & Gillette 1986, Gillette & Treado 1988). Indeed some of the most successful daylighting

solutions have been in toplighted spaces (Selkowitz 1998). Some of these environmental objectives can be contradictory. Hopkirk details a preliminary design tool to best determine the configuration necessary for maximised energy savings in rooms adjacent to atria, concerning lighting and cooling loads (Hopkirk 1998).

Working examples of daylit atrium spaces can be seen in Figure 2-8.

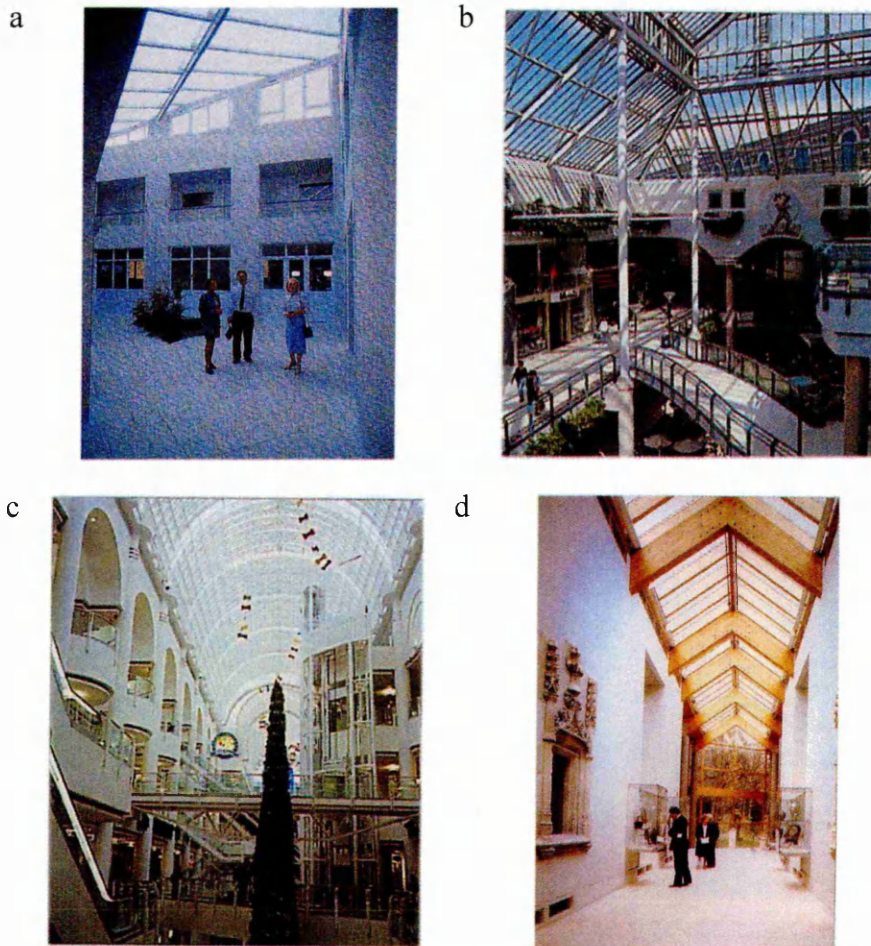


Figure 2-8: a. Centre for New Business, Reze, France (Baker et. al. 1993). b. Harlequin Centre, Watford, UK; c. Bentalls, Kingston-Upon-Thames, UK; d. Burrell Collection, Glasgow, UK. (all Burt & Bell 1995)

2.3.3 Atrium Nomenclature

Atria are classified according to how many sides are surrounded by the building mass so for example a 4-sided atrium is one that is totally internal and a 3-sided atrium has one open end. Hung and Chow (2001) refer to these as centralised and semi-enclosed respectively, along with descriptions for attached and linear atria (Figure 2-9). This study will examine 4-sided atria, whereby the internal spaces are entirely top-lit.

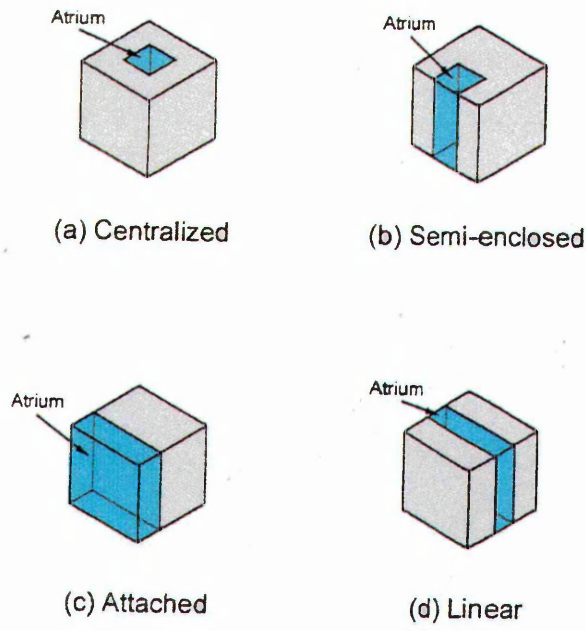


Figure 2-9: Four types of atria typology (Hung & Chow 2001)

A top-lit atrium has glazing on the roof plane such that it is lit from above, whereas a side-lit atrium receives its light from vertical glazing at one or more end(s) (Saxon 1983). The geometry of the well can be expressed in a number of manners. The plan aspect ratio (PAR) and section aspect ratio (SAR) relate the width to the length and the height to the width respectively. The well index (WI) relates the vertical surface area to the horizontal surface area, and thus combines the three parameters involved in the PAR and SAR, as can be seen below (Liu et. al. 1991);

$$PAR = \frac{w}{l} \quad [2-1]$$

$$SAR = \frac{h}{w} \quad [2-2]$$

$$WI = \frac{h \times (l + w)}{2 \times l \times w} \quad [2-3]$$

therefore,

$$WI = \frac{SAR \times (PAR + 1)}{2} \quad [2-4]$$

where,

l = well length

w = well width

h = well height

A high well index or SAR indicates a deep well. It should be noted that different combinations of PAR and SAR can be used to give the same WI for example a well with a PAR of 1 and an SAR of 2 of gives a WI of 2. This is the same as for a well with PAR of 1/3 and SAR 3. The PAR can be used to classify rectilinear atria, such that PAR's between 0.9 and 1 constitute square atria, 0.4 - 0.9 are rectangular and under 0.4 are linear.

Reflectances are expressed as the percentage of light reflected back off a surface, and are denoted by the symbol ρ . For walls with more than one material (hence different reflectances), the area weighted reflectance is used which is found by multiplying the area of each material by its individual reflectance, summing them and dividing by the total area. This value should be used with caution, as though it gives an impression of a space, it says little about the distribution of light, which is more dependent on the arrangement and contrast of reflective surfaces (Sharples & Lash 2004).

The natural lighting conditions of a space (in terms of magnitude) are often quoted as the daylight factor (DF) which is the ratio expressed as a percentage of the internal illumination to the unobstructed external illumination (excluding sunlight). The daylight factor can be divided into three components, the sky component (SC), that which comes directly from the sky, the externally reflected component (ERC), that which has been reflected by the external environment (e.g. buildings, trees, the ground) and the internally reflected component (IRC), that which has been reflected off the internal room surfaces. This is demonstrated in Figure 2-10.

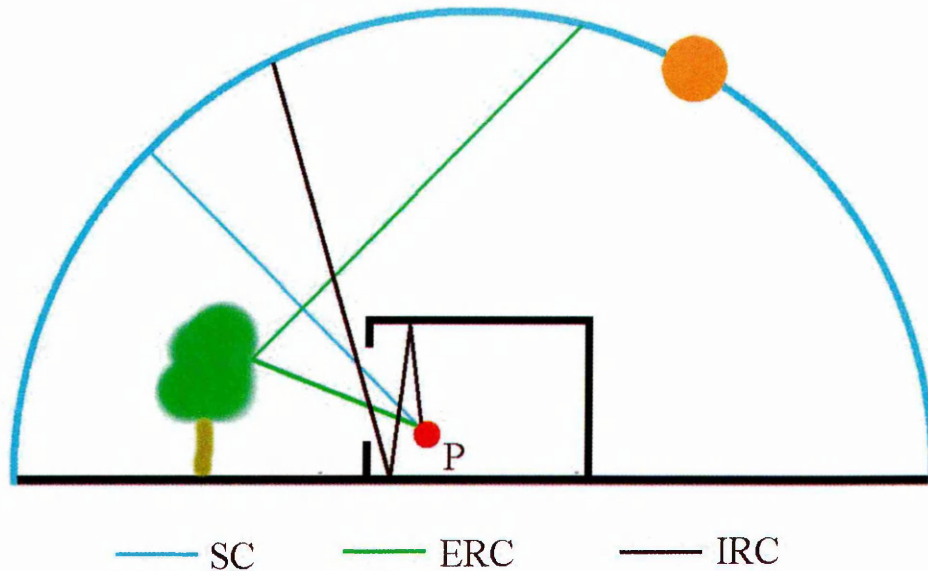


Figure 2-10: Possible paths of light from the sky to point P in a room arriving direct from the sky (SC), reflected from the external environment (ERC) and reflected from the internal room surfaces (IRC).

2.3.4 Lighting Objectives of Atria

The atrium can be used to achieve four various lighting objectives at increasing levels of difficulty (Aizlewood 1995). Perhaps the easiest of these is providing sufficient levels of illumination for occupancy within the atrium itself. A designer will normally be able to achieve this without difficulty, though an over-obsession with target illuminance values (which become relatively unimportant after a few hundred Lux) is a dangerous strategy (Julian 1998). Secondly, the designer will aim to control direct sunbeam so as to prevent glare and overheating. From a psychological standpoint occupants should have lighting arriving from as many directions as possible, and if this is unattainable through natural sources, an element of balancing by use of artificial lighting may be necessary (Boyer 1998). Rea (1998) cites the absence of occupant complaints as the first commandment of lighting design. Emphasis on this will be different depending on the local climatic conditions, for example Texas (where much of the research in this field is concentrated) has more clear days and higher sun altitudes than in the UK, and thus solar control may be a more pertinent issue. Solutions to these first two objectives need to be developed in tandem, as they have the potential to contradict each other (Saridar & Elkadi 2002). The third objective is providing sufficient illumination to maintain plant growth within the atrium.

This can be a problematic issue, and should be addressed towards the start of the design process, as changes towards the end are harder and costlier. Plants require plentiful amounts of illumination, to provide them with energy, to give them seasonal guidance and to regulate their shape. Daylighting remains the element of plant maintenance most difficult to predict and control in the interior environment (Weiner & Milne 2003). Typical needs lie in the range of 700 to 1000 Lux for twelve hours a day, rising to more for more exotic species (Saxon 1983). These demands may well prove challenging in certain climates, and could result in the need for supplementary artificial lighting. It should also be noted that plants have low reflectances, and will reduce the overall light flux in the well. The fourth and hardest objective is providing sufficient illumination to displace artificial lighting in spaces adjacent to the well. It is here where current buildings have been least successful, and also where there is most potential for saving energy.

2.3.5 The Passage of Light Flux

All daylight originates from the sun, and it is this passage of flux from the sun to the working plane that determines which parameters must be considered and which are at the disposal of the designer. The route can be broken down into four broad headings, which are;

- passage of flux externally
- transmission through the fenestration
- distribution within the well
- arrival at adjoining spaces

This study concentrates on the effects of the fenestration, although it is necessary to have prior knowledge of the other factors in order to gain a better understanding of the processes concerned, due to the overlapping nature of the parameters involved.

2.4 External Conditions

2.4.1 Sky Luminance Distribution and Models

The prevalent sky conditions will be intrinsically linked to the target objectives of the fenestration system and the organisation of the well and adjoining spaces. Sky luminance distributions are a result of several factors interacting with incoming solar radiation from the sun. Visible light is the component of the electromagnetic spectrum to which the human eye is sensitive towards and lies within the wavelength range of 380-770nm. As this flux enters the atmosphere of the earth, it is absorbed, reflected and dispersed according to latitude, season, time of day, altitude, cloud type and cover and atmospheric turbidity (Kittler & Ruck 1984, Baker et. al. 1993). Attempts have been made to define global daylight zones, although a review of illuminance measurements has highlighted significant differences between countries with similar climates (Ruck 1986). The dynamic nature of the sky luminance can be attributed to the constant state of flux under which the earth's weather systems are in operation. The cloud type, the way in which they form (orthographic, frontal, convection (Baker et. al. 1993)) and the effect of the wind on their duration and distribution (McCluney & Bornemann 1986) are strongly affected by local as well as global factors. These discrepancies are further highlighted through localised variation in turbidity (the content of water and particles in the atmosphere), such that individual regions may have their own fairly specific daylight patterns. Whilst turbidity can be theoretically calculated for a region (Navvab et. al. 1984), comparing measurements taken under real skies from different daylight zones is a difficult proposition, demonstrating the challenge posed to designers when trying to produce relatively stable environments through the harness of a dynamic source.

Several sky luminance models are available, in order that some element of standardisation can be applied to data from different sources. The uniform sky is the simplest, and assumes a constant luminance across the entire sky hemisphere. It is characterised by a sky of thick milky white clouds in an atmosphere full of dust (Baker et. al. 1993). Homogenous skies include the CIE overcast and clear skies, and are defined where any turbidity, pollution, nebulosity or cloudiness within the atmosphere

is evenly dispersed and uniformly distributed over the entire sky hemisphere (Kittler 1986).

The CIE overcast sky (sometimes known as the Moon and Spencer overcast sky) (Seshadri 1960) describes a sky with clear atmosphere that is wholly covered by dark cloud, and is defined through the luminance relative to the zenith luminance according to the formula;

$$L_{\theta} = \frac{L_z (1 + 2 \sin \theta)}{3} \quad [2-5]$$

where,

L_{θ} = luminance at angle θ to zenith

L_z = zenith luminance

It should be noted that application of this equation has been found to underestimate illuminance levels, due to different luminance distributions found in ‘dark overcast’ and ‘bright overcast’ days (Muneer 1998).

The overcast sky model is often used as a worst case scenario in terms of illuminance availability, and is easily replicated in simulation facilities (notably the sky chamber, mirror sky and artificial sky) which have been evolving since the early part of the 20th century (Navvab 1996). Whilst it is extremely difficult if not impossible to exactly mimic the CIE overcast luminance distribution in the most common simulator – the mirror box - they do represent a decent pragmatic approach for analysis of scale models (Cooksy et. al. 1991).

The CIE clear sky model has an uneven distribution of luminance, and is dependent on solar altitude and azimuth. It is representative of a cloudless sky with clear atmosphere, and disregards sunbeam in the calculations (Baker et. al. 1993). The overcast and clear sky models represent opposite extremes of cloud cover, who in their pure forms seldom occur, and thus other means are necessary to define those skies that fall in between the two. The mean sky is a model which takes into account models for overcast, intermediate and clear skies along with their probability of occurrence

(Nakamura et. al. 1986) whilst the All Sky Model which is expressed as a function of solar altitude and normalised global illuminance is capable of representing luminance distribution from clear to overcast skies (Igawa & Nakamura 2001).

The nebulosity index classes skies into five categories ranging from overcast through to clear. Several methodologies exist for converting the continuous nature of real skies into discrete types. Li et. al. (2004) identify six means of describing the overcast condition;

1. Cloud cover – carried out by trained observers, with 8 Oktas (an Okta being one eighth of the sky) being overcast
2. Sunshine hour (zero = overcast). This is available from meteorological stations, and coupled with sky type probability distributions, have been found to agree with methodologies involved with derivation of irradiance data. (Nakamura 1986, Rahim et. al. 2004) (Figure 2-11). Kittler & Darula (1999) observed an inversely linear relationship between relative sunshine duration and probability of overcast skies – which are ‘*very important for window design*’.

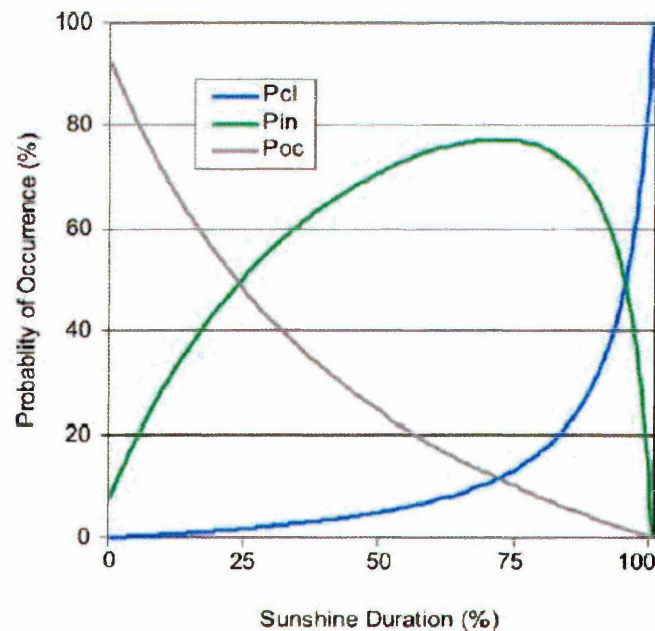


Figure 2-11: Probabilities of three sky conditions (overcast, intermediate, clear) relative to sunshine duration (Rahim et. al. 2004).

3. Clearness index i.e. global solar irradiance to extraterrestrial solar irradiance ratio. A value of under 0.15 indicates an overcast sky. This method is often used as it is dependant on only one measured parameter (global solar irradiance)
4. Diffuse ratio, (sometimes called cloud ratio) i.e. diffuse solar irradiance to global solar irradiance ratio. Such data for horizontal and vertical planes is available from International Daylight Measuring Program (IDMP) stations, of which there are 33 in Europe. Yearly data for Lyon, France can be seen in Figure 2-12 (Dumortier 1994). A high value indicates most light flux is diffuse, which is an indicator of overcast conditions. A value over 0.98 is considered overcast.

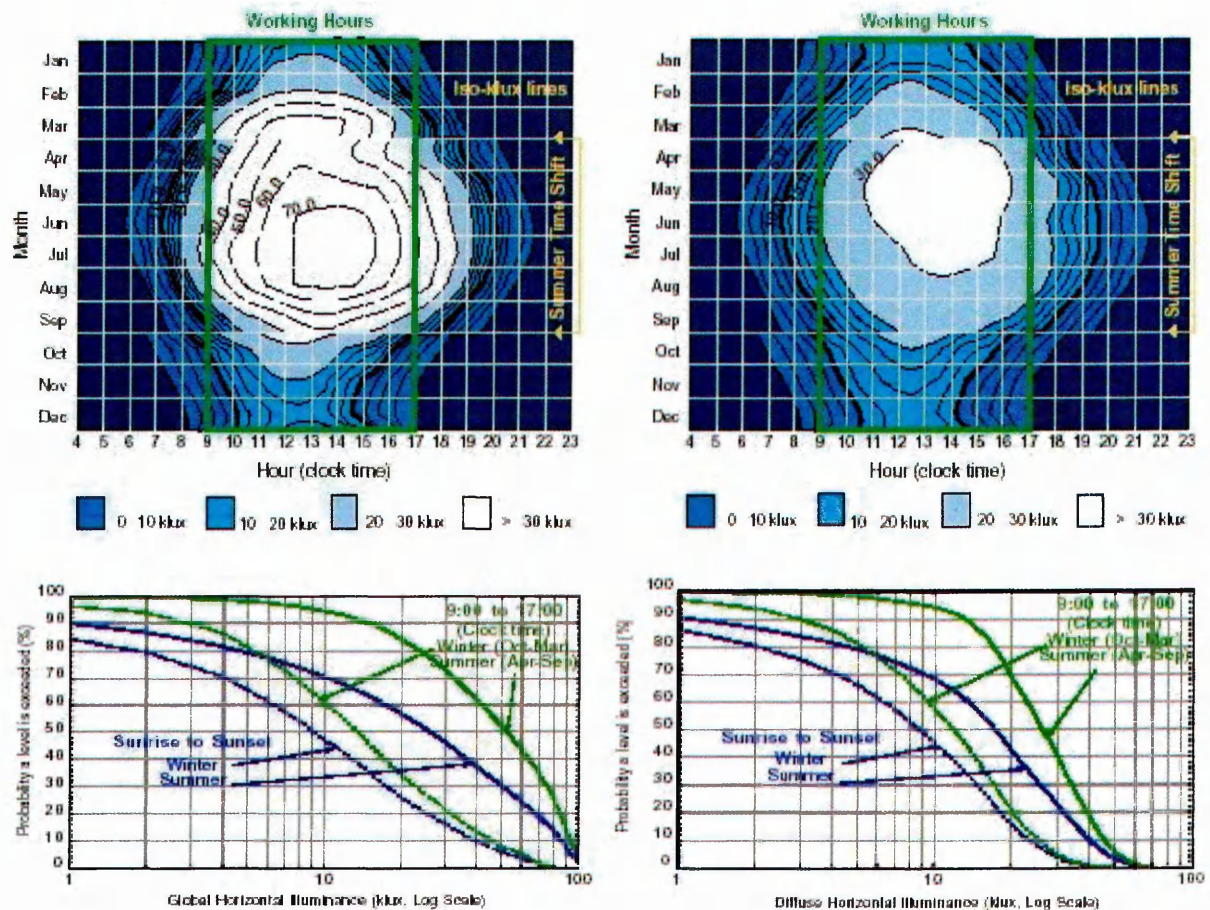


Figure 2-12: Illuminance results from IDMP, Lyon, France (Latitude 45.78N, longitude 4.93E). Left images show global illuminance values, right images show diffuse illuminance values. Top images show temporal patterns, bottom images indicate % of time target illuminances are exceeded (Dumortier 1994).

5. Zenith luminance to diffuse illuminance ratio (L_z/D_v). Kittler & Darula (2002) have proposed the standardised classification of sky conditions into 15 types based upon this approach (Table 2-1). With access to long term L_z/D_v data, the daylight climate for specific regions can be derived thus enabling universal application of localised research. Such an analysis has recently been undertaken for Sheffield, the site for this research. Data was analysed over the period between November 1993 and February 1994 (Markou et. al. 2004). The most frequent sky was types were 2 (19.5% of cases), 1 (10.5%) and 3 (9.7%). Overall, overcast sky types (1-5) constituted 49% of all sky conditions. The exact distribution can be seen in Figure 2-13.

Table 2-1: A description of the 15 sky types proposed by Kittler

<i>Sky</i>	<i>Code</i>	<i>Sky description</i>
1	I.1	Overcast, with steep gradation and with azimuthal uniformity
2	I.2	Overcast, with steep gradation and slight brightening towards the sun
3	II.1	Overcast, moderately graded, with azimuthal uniformity
4	II.2	Overcast, moderately graded, with slight brightening towards the sun
5	III.1	Overcast, foggy or cloudy, with overall uniformity
6	III.2	Partly cloudy, with uniform gradation & slight brightening towards the sun
7	III.3	Partly cloudy, with a bright circumsolar effect and uniform gradation
8	III.4	Partly cloudy, rather uniform, with a clear solar corona
9	IV.2	Partly cloudy, with shaded sun position
10	IV.3	Partly cloudy, with a bright circumsolar effect
11	IV.4	White–blue sky with a clear solar corona
12	V.4	Very clear/non-turbid, with a clear solar corona
13	V.5	Cloudless, polluted, with a broad solar corona
14	VI.5	Cloudless, turbid, with a broad solar corona
15	VI.6	White–blue turbid sky with a wide solar corona effect

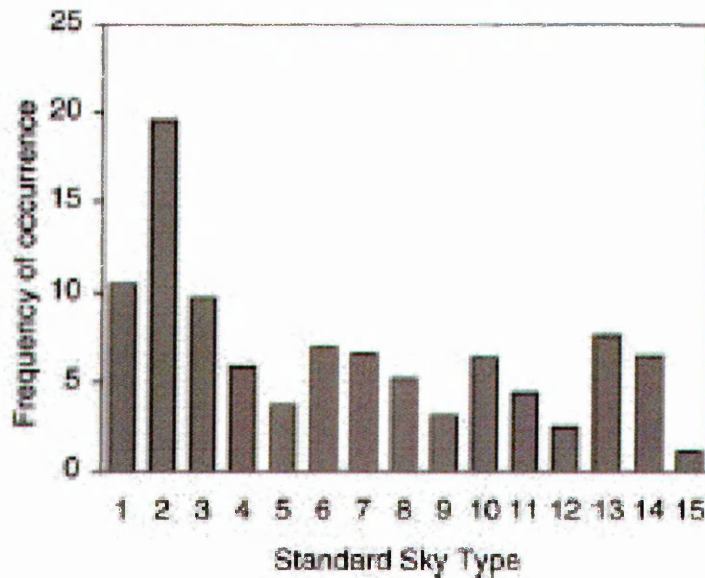


Figure 2-13: The distribution of the 15 sky types in Sheffield, November 1993-February 1994 (Markou et. al. 2004).

6. Sky patch to zenith luminance ratio.

It was found that no single index was capable of comprehensively describing the fully overcast sky patterns, with root mean square errors from the Moon and Spencer sky ranging from approximately 10-20%. Skies in the United Kingdom are generally cloudy, with a proportion of the sky covered by low cloud. They are clearest in late spring and early summer whereas cloud amounts tend to reach a maximum in November and December (Ruck 1986, Baker 1993).

An accessible means of obtaining sky luminance distributions in the field without the need for the kind of specialist equipment that is typically found at monitoring stations involves sky mapping using digital cameras. The zenith luminance is calculated based on the shutter speed, and as such luminance values for the sky vault can be derived, with results for many skies archived (Roy et. al. 1998). Using High Dynamic Range (HDR) imagery a calibrated camera can be used to derive real luminance values directly from the field, and analysed in programs such as Radiance for glare etc.

2.4.2 Application to Daylight Analysis

In an ideal world, there would be the resources for every study into the behaviour of daylighting and building to be undertaken for all sky conditions. Limited time and finances have generally led to research focusing on one particular sky distribution, most commonly the overcast sky which is seen as a worst case scenario (Littlefair 1993). In designing to meet worst case conditions, one can assume that, provided other factors such as control of glare etc. have been considered, lighting requirements will have been met at all times. Clearly, as sky conditions change the luminance distributions alter and so architects will often have to adapt their designs to satisfy the most appropriate sky condition. The most important variables at their disposal are envelope shape, aperture geometry, orientation and location, and surface characteristics (Baker et. al. 1993). The fenestration and artificial lighting systems will also form a key part of the strategy.

Sometimes designing to satisfy worst case conditions may prove to be less beneficial than designing for the overall annual pattern of conditions the building will experience. For example, oversizing openings may lead to adequate daylight levels for heavily overcast days, but if such days are few and far between, the most economical design will likely lie elsewhere. It is here where new techniques such as annual luminance mapping (Compagnon 2004) may prove ultimately beneficial over existing simple techniques. Such approaches however are still in their infancy, and whilst they may take on more relevance in the future, it is not within the scope of this study to attempt to invalidate current research standards.

As has been mentioned in Section 2.3.3 natural lighting conditions are often quoted as daylight factors, a quantity that is specific to overcast sky conditions. The main advantage of the daylight factor is that it provides a standardised, measurable quantity, which can be compared against criterion values or used to predict likely internal illuminances and electric light use (Littlefair 1993). The daylight factor remains constant under changing magnitudes of illuminance (provided the luminance distribution remains fixed, as its use in solely overcast skies implies) (Tregenza 1984). A method using partial daylight factors (PDF) has been suggested, which involves the use of a novel rotating sky simulator (Michel & Scartezzini 2002) (Figure 2-14). This

has the advantage of implementing a daylight factor type approach which is valid over a range of sky luminance distributions. The universal lack of these sky simulators however, means that like luminance or irradiation mapping, the implementation and whole scale adoption of such methods may only become evident in future work. This study will focus on overcast sky conditions, and the measurable quantities associated with them.

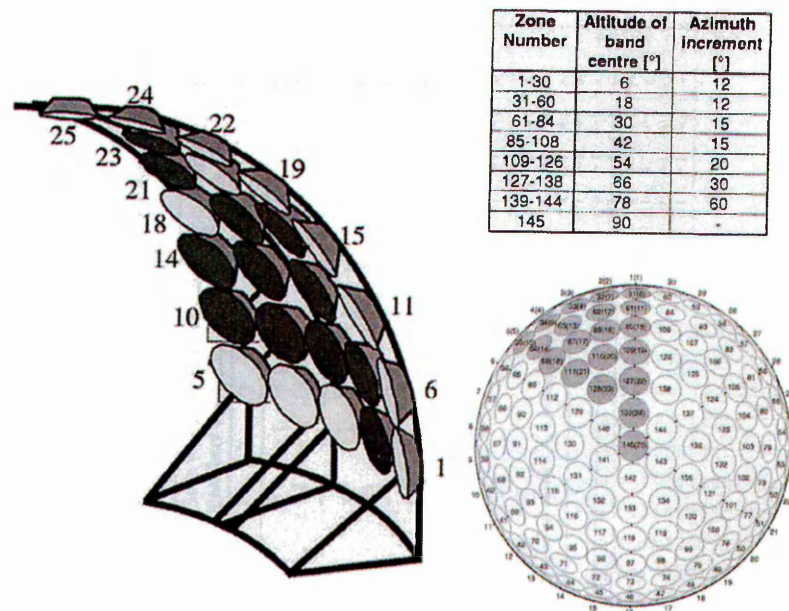


Figure 2-14: The novel rotating sky simulator used to measure PDF. The model is rotated six times relative to the sky to simulate the entire sky vault (Michel & Scartezzini 2002).

2.4.3 External Obstructions

External obstructions will reduce incident flux where adjacent buildings are taller than the atria in question (Wright & Letherman 1998). This is due to a reduction in the visible part of the sky vault, though this is slightly offset by the externally reflected component (ERC) of light coming from the obstruction, which acts as a secondary weaker luminance source. The mean luminance of the obstruction has been approximated at 10% of the average sky luminance it obstructs (BRE digest 309), which equates to 20% of the luminance of a standard CIE overcast sky (which are characterised by lower levels of luminance at horizon altitudes relative to zenith altitudes). This is found to overestimate the luminance and is therefore unsuitable for use in built up urban sites. New algorithms are given relating the ratio between

reflected component and sky component to the angle of visible sky from the working plane (Lee 1992). The relationship follows the law of diminishing returns approaching a maximum daylight factor which represents an unobstructed site condition.

The effects of an irregular skyline (as opposed to the unrealistic continuous strips used in traditional calculations) are investigated by Capeluto (2003). The Sustarc program is used to assess the Sky Solid Angle (SSA) as seen from vertical windows. A strong relationship was found between SSA and daylight factor in a room. An SSA of at least 1 steradian was needed to obtain a DF of 2% in the test case room used (dimensions 5m(W)x8m(D)x2.7m(H), glazing ratio 15%).

2.5 The Fenestration

2.5.1 Form and Structure

The objectives of the fenestration system are twofold. Primarily it should admit as much diffuse light as possible, whilst simultaneously regulating incoming sunbeams. Direct sunlight is potentially problematic in that the visible component is an obvious source of glare, the ultra violet component damages sensitive surfaces whilst the infra red component is a source of thermal heat gain, which may or may not be desirable (Baker et. al. 1993). Care should be taken to prevent totally masking the sun pattern so as to provide sparkle, liveliness and dynamic qualities (Boyer 1990). Clearly attempting to block out direct sunbeam will reduce a portion of the visible sky, and hence diffuse light, thus a designer will have to resolve the balance of direct and indirect flux, dependant on climate and use of the space. Reduction of light due to glazing will be at least 20% (10% for the structure, 10% for the glazing) (Baker et. al. 1993), rising as high as 80% (Song & Boyer 1994) or 40% if an element of sunbeam is permitted (Boyer & Song 1995). The atrium roof is perhaps the least understood area of atrium design, as is demonstrated by the scarcity of papers available to designers (Aizlewood 1995).

Roofs come in a variety of shapes and sizes, whose exact configuration is limited only by the designer's imagination. The roof chosen will depend upon the size

(span), usage, materials, objectives and many more factors. Roof types can be broken down into approximate structural forms, some of which can be seen in Figure 2-15 (Stroud Foster & Harington 1990).

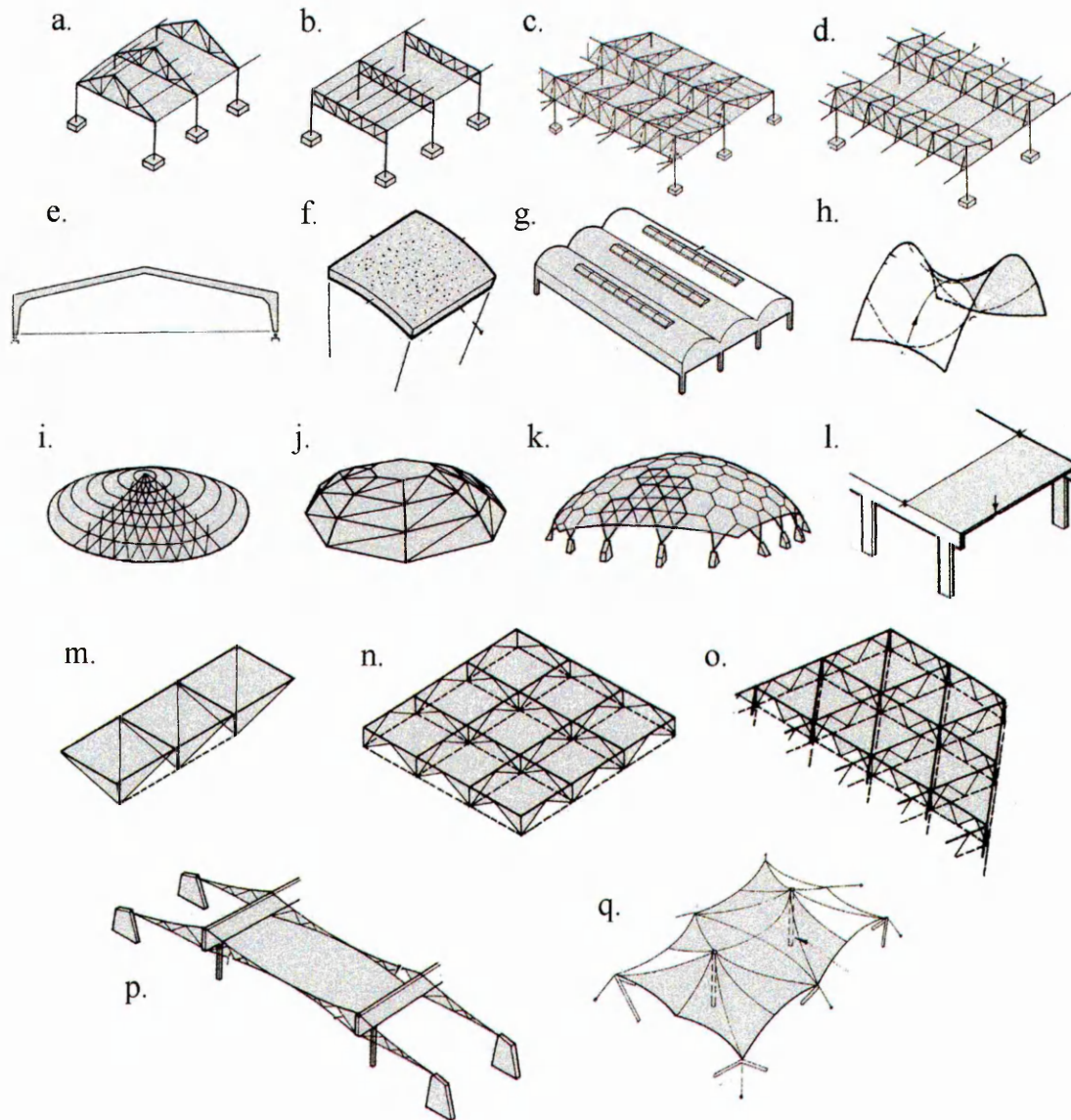


Figure 2-15: There are a multitude of structural roof configurations open to the designer; a. trussed; b. girder; c. northlight; d. monitor; e. portal frame; f. shell; g. barrel; h. saddle; i. grid dome; j. polygonal dome; k. geodesic dome; l. slab; m. space frame; n. flat grid; o. lattice; p. suspended; q. membrane (Stroud Foster & Harington 1990).

The most comprehensive paper examines fourteen roof structures with different glazing options under different sky conditions (Navvab & Selkowitz 1984). The roof types and results are presented in Figure 2-16. Sawtooth and monitor configurations are found to have the highest sensitivity to solar altitude when compared to pyramids,

vaults and A-frames. Results are based on the daylight factor taken with an azimuth of 0° at the centre of a well of unrealistically high reflectance (86% where typical values are 30% (Boyer & Kim 1988)). It would be interesting to note the effects of roof configuration on illumination around the vertical walls, at different times of the day (varying azimuth). Lowering the transmittance of the glazing through using diffuse and tinted glazing lowered illumination levels as expected.

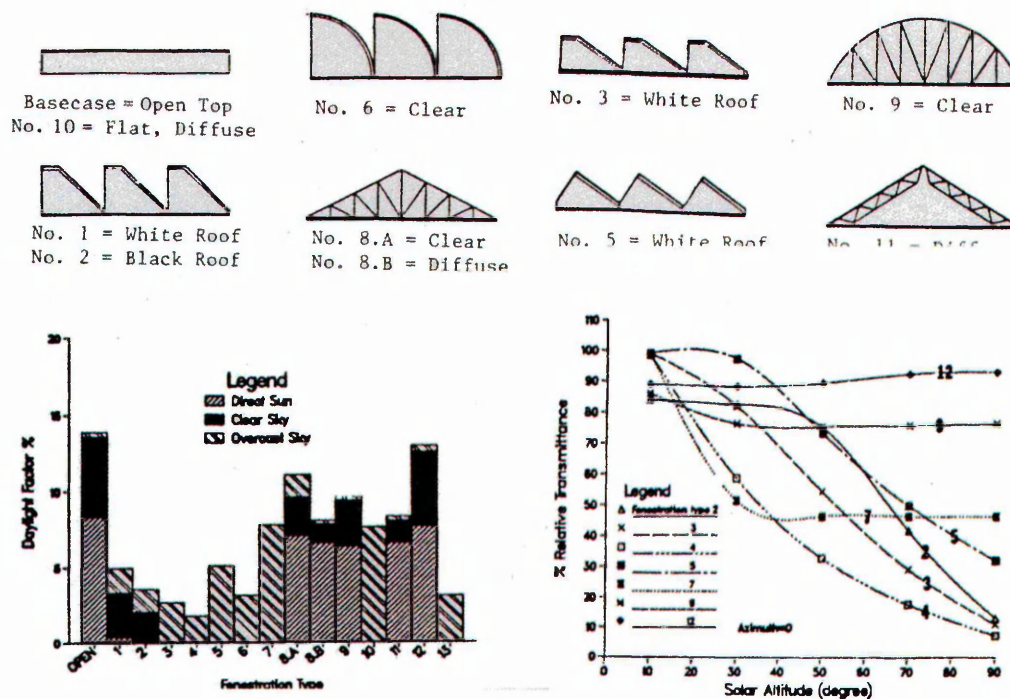


Figure 2-16: A model study under an artificial sky investigating the effects of 14 atrium roof types: Top images; roof types investigated. Bottom left; daylight factor at the centre of the well floor for various roof configurations. Bottom right; relative transmittances of the roof configurations as a function of solar altitude (Navvab & Selkowitz 1984).

Further study into roof configuration on daylighting has shown it to be the factor that has the greatest effect on intensity and direction (Boubekri 1995). Three types were tested in an artificial sky and vertical daylight factors on each wall at every storey were taken for a seven storey high well (reflectance unspecified). The flat top roof was found to admit the most daylight whilst the sawtooth roof had the strongest directional properties, receiving most light on the walls facing the openings (Figure 2-17). These directional properties were less noticeable at increased depths within the well. This is backed up in previous work where the impact of roof structure was found to be markedly lower with increasing distance from the well (Sharples & Neal 1993). The

monitor roof admitted least light, though the balance of light between top and bottom of the well was most even. Further work is necessary to determine the effects of the various configurations on vertical daylight distribution with the addition of sunbeam, and the effect of other roof types. The methodology should be extended to real buildings as well as simplified scale model conditions.

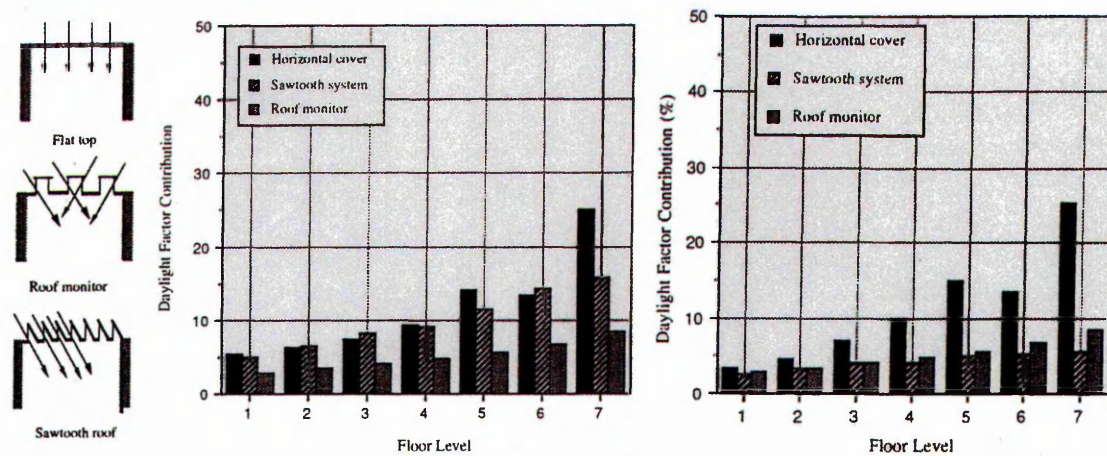


Figure 2-17: A model study under an artificial sky investigating the effects of 3 atrium roof types: Left, roof types examined; centre, maximum daylight factors; right, minimum daylight factors (Boubekri 1995).

One study that attempts to incorporate direct sunlight looks at the effect of waffle and sawtooth roof systems in three daylight climates (Boyer & Song 1995). Illumination results are found on seven points of the well floor, and results presented as maximum, minima and average for solstice and equinox conditions in an atrium of well index 1.2. The study looks at 36 canopy configurations, though results for only four are presented which are two sawtooth and two waffle types with reflectances of 85%. Though only limited results are printed, it is clear that choosing the most appropriate canopy system is largely dependent on daylight climate (defined in this case through latitude). Waffle systems were found to have similar daylight performance under clear and overcast skies, and performed well in limiting sunlight entry in all but the highest solar altitudes, where sunlight penetration was very high. Sawtooth roofs only admitted half the diffuse skylight of the waffle roofs under overcast conditions, but were more effective at blocking out the summer sun, whilst allowing entry of lower altitude sun may be a factor in promoting thermal heat gain in the winter. Comparing the luminance ratios of bright patches has highlighted the need to properly consider the effects of

admitting direct sunlight in terms of glare, which may be problematic, particularly on specular surfaces.

Laouadi (2004) found that domes were the best shape for admitting low solar altitude winter sun (Figure 2-18). Further studies of low altitude sun angles were conducted by Matusiak & Aschehoug (1998). Horizontal glazing was found to perform the poorest; blocking low altitude sun when it was needed the most, and allowing in high altitude summer sun. The optimum angle of slope was found to be 18° - 30° . A monopitched roof orientated north (assuming the vertical element of the roof was glazed, and not part of the internal wall) outperformed a south facing slope by allowing in low altitude sun (even magnifying it through reflection off the internal sloped surface of the roof) whilst controlling rays from higher angles.

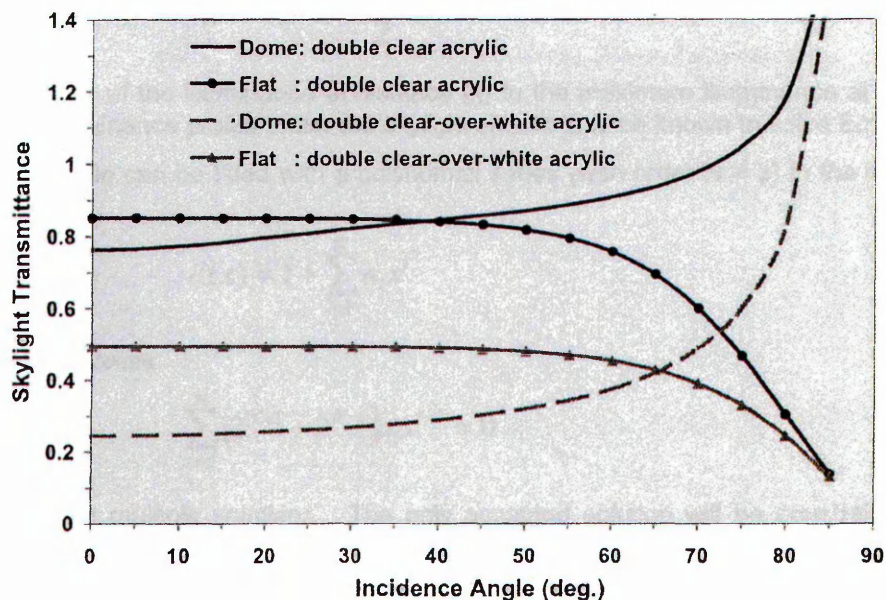


Figure 2-18: Transmittance profiles of clear and diffusing circular domes and flat skylights (Laouadi 2004).

Where more than one roof opening is required, the careful spacing of the openings is essential. One study investigated the spacing for six roof shapes; flat, shed, vertical sawtooth, northlight (sloping sawtooth), vertical monitor and domes (Dewey & Littlefair 1998). Monitor roofs were found to have the best distribution, domes the worst, whilst also providing low illuminances to the vertical walls, making the space feel gloomy. Figure 2-19 shows the results, though it is not valid to compare the magnitudes, as different roof opening areas were used for each type (e.g. the sawtooth had ten times more opening than the domes). Another study confirms the potential for use of multiple rooflights in European sites, in this case for use in underground spaces

(Bouchet & Fontoynt 1996). Asdrubali (2003) derives a calculation method for deriving illuminance values at the working plane under sawtooth roofs based on external solar radiation and surface and geometric properties. The method can be used to estimate performance at the design phase or for optimising performance by varying the roof shape or materiality.

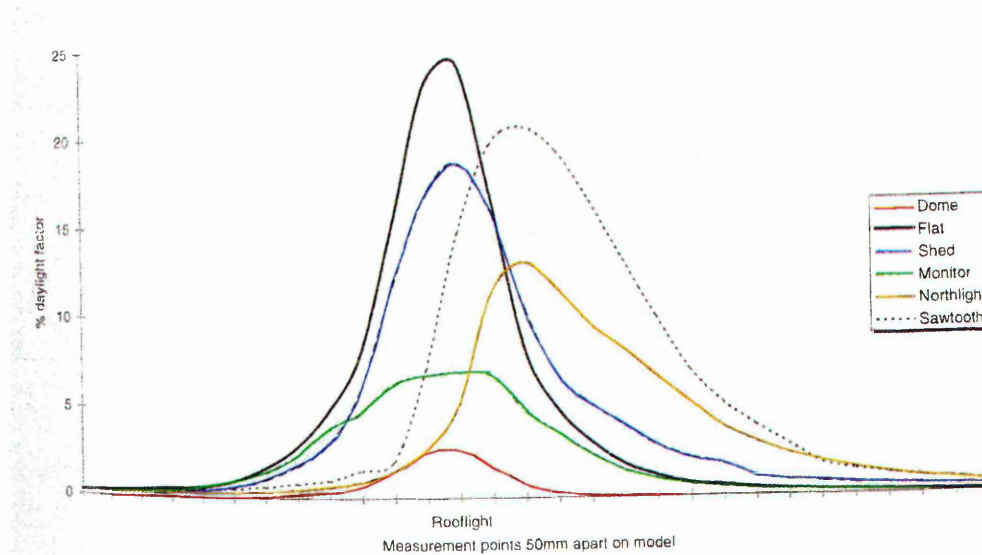


Figure 2-19: Daylight factor at floor level under different roof types (Dewey & Littlefair 1998). For comparison purposes, the form is more significant than the magnitude of the curves as different sized openings were used for the various roof types.

The effects of roof structure on daylight within the well under real overcast sky conditions have been assessed (Sharples & Shea 1999). Illuminance levels at varying height on the four walls and centre of the floor of a well of scale model, well index 2, and reflectance 2% were found for three glazed roof structures relative to an unstructured flat glazed roof. The south-sloping monopitch roof appeared to have the highest transmittance with the flat and A-frame performing similarly. It was observed that taking the plan area obstruction (PAO) as a correction factor will underestimate the losses due to attenuation in section. This underestimation lies within the region of 10-15%, with specific values given in Shea's (2000) thesis. Extending the study to include partly cloudy skies has revealed that inter-reflections within the structure may actually increase illumination levels on the north and east walls relative to having no roof structure (Sharples & Shea 2000). Once again, further study is needed to further investigate this activity in the sections of roof systems, as well as more roof types, and in real buildings.

The underestimation of the PAO is confirmed in further studies (Harrison 1998, Calcagni et. al. 2000, Calcagni & Paroncini 2004). A model study under an artificial sky investigated with and without an A-frame roof found reductions due to the roof to be 65-70% (read from graphs). The stated PAO and glazing transmittance of 11% and 65% respectively would imply an overall transmittance of approximately 59%. Further idiosyncrasies are observed by Harrison (1998). The transmittance of light through an essentially glazed roof is poorest when the truss porosity is a mid (or low, dependant upon roof shape) range value. A solid plane truss provides greater illuminance in the atrium than a moderately braced example of the same truss. This unexpected result could be due to the very low reflective surfaces used in the well. This meant that light passing through the more porous trusses would arrive at the well, and most likely be absorbed, whilst light which hit the more solid truss was more likely to inter-reflect deep towards the centre of the well, where the photocell was positioned. Nonetheless, this observation could provide a useful strategy for redirecting light deep into atria wells whilst reducing glare issues towards the top. Definite further study is required to assess the behaviour of more complex real structures on daylight distribution.

A large potential source for investigating the performance of roof type can be found within the existing built environment. However, little information on performance of real buildings was found within the literature. A systematic and comprehensive examination of this area could highlight issues that have been missed by simplified scale or computer modelling, and as such there is a definite need for further study in this field.

2.5.2 Surface

The presence of glazing will reduce transmission through flux reflected and absorbed by the glass, when compared to a non-glazed (i.e. totally open) scenario. The exact transmission is dependent on the angle at which the flux is incident, with rays at high angles of incidence beginning to reflect specularly thus reducing transmittance. For 6mm clear glass the value is around 0.85, although this decreases to 0.61 at high angles (Littlefair 1982). Using frosted or tinted glazing can be used as a strategy to control direct sunlight, although these will also reduce the amount of 'useful' light entering, and could result in bland uniform lighting conditions.

Spectrally selective glazing can be used to reject non-visible parts of the electromagnetic spectrum (Smith 2004). More intelligent materials such as photochromic (Jain 2003) and electrochromic (Selkowitz 1998, Jain 2003) films alter their transmittance properties dependant on external stimuli (i.e. light levels or voltage signal). In an investigation of such a material, Inoue (2003) found that '*despite being a relatively simple system, large energy savings by shading solar radiation and making efficient use of natural light [are possible]. Through practical application to a research institute building, the system is demonstrated to work well and to be considered by most occupants to improve the comfort in the office*'.

Alternatives to the more traditional approach of glass include ETFE (Pearson 2000, Robinson-Gayle et. al. 2001, Spring 2001 and 2004), transparent refractive index matched polymers (TRIMM) (Smith 2004), polycarbonate (Lane 2001, Smith 2004) and aerogel (Rouanet & Bobkowicz 2003). Each of these offer added benefits to glass, be it thermal, reduced weights or improved fire performance. Despite theoretical analyses of this new generation of materials (e.g. Pfrommer et. al. 1995), the relatively recent implementation of such transmissive surfaces means there is little reported evidence as to their performance in practice. One study looks at the subjective response to five materials used to roof an atrium well, those being; clear glazing, tinted glazing, prismatic glazing, louvers and diffusing material (Weiss 2004). Four factors of subjective impression were assessed; clarity, complexity, enclosedness and degree of pleasantness. The louvers and diffusing material performed least well, whilst the clear, tinted and prismatic glazings were well liked. The former two transformed the exterior light into that more akin to a luminaire, increasing the feeling of enclosedness and decreasing the impression of scale within the well. The asymmetric light distribution and sharp shadows caused by the latter three seemed to be the most welcoming in a circulation and relaxation zone. A major shortcoming of the study was that the subjective responses were to a observations of a scale model, and recommendations were made to repeat the study in full scale spaces.

2.5.3 Control of Direct Sunlight

Although this study will focus on overcast skies, transmissive surfaces may incorporate an element of shading to control incoming sunbeam, with the associated overheating and glare issues (especially where there is an abundance of VDU's, which have the effect of shifting the working plane from the horizontal to the vertical (Veitch 2001 b)). *'For maximum efficiency, shading should be sufficiently flexible to use the overall solar gain and daylight on dull days to reduce the loads on heating and artificial lighting systems. This will involve adjustable shading devices'* (Littlefair 2000). It has been stated that occupants value window blinds as much as the windows themselves (Rea 1998).

Specific strategies include the use of light diffusing glass, capillary glass, frosted glass, lightshelves, laser cut panels (LCP), prismatic panels, holographic optical elements (HOE) and light guiding glass (Matusiak & Aschehoug 1998, Littlefair 2000, Kischkoweit-Lopin 2002) (Figure 2-20). Shading systems that block sunlight but admit skylight include prismatic panels, prisms and Venetian blinds, sun protecting mirror elements, directional selective shading systems with concentrating HOE, transparent shading systems with HOE based on total internal reflection and anidolic zenithal openings. Systems with mechanical elements (known as 'active' systems) are inappropriate in climates such as the UK, where overcast days predominate (Littlefair 1989).

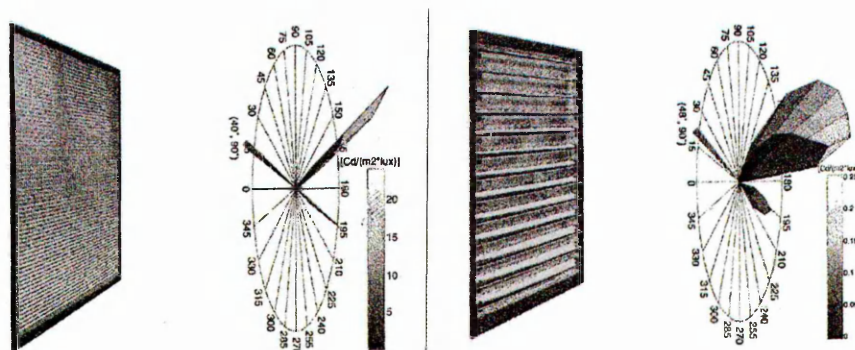


Figure 2-20: The redirection of light towards the ceiling using an LCP (left) and mirrored reflective blind (right) (Kischkoweit-Lopin 2002).

Where blinds are used manual control is best in shared offices. Automatic blinds are more effective in 'unowned' spaces such as circulation zones. Care must be

taken to prevent the frequent automated movement of the blinds for psychological reasons. Human dissatisfaction with automated blinds is discussed by Iwata & Tokura (2003). They find that once blinds are drawn down (through manual over-ride) they were never drawn up. Reflection from VDU's was also a problem amongst building users.

When dealing with atria the conditions are somewhat different to those for side-lit spaces (where much of the literature is concentrated). The scale and lighting levels found within atria often give them the feel of somewhere between an indoor and outdoor space, and as such higher levels of sunbeam may be permitted. Indeed, some sunbeam may be desirable to add 'sparkle'. As the activity occurring within the atrium well may not require the levels of concentration as those in the adjacent spaces, the lighting conditions too may not need to be as strictly regulated. Finally, in side lit spaces the opening is generally within the resting eye line of a building user, whereas in a top lit space the bright opening is more likely to be outside the field of view. Nevertheless consideration of incoming direct solar energy from the standpoint of overheating and glare should be considered, and any shading device installed should aim to maximise the amount of incoming skylight whilst controlling direct sunlight. The designer will have to decide whether to provide shading for the principal opening in the well, or internal shading systems for the spaces adjoining the well, or a combination thereof (Douvoulou & Pitts 2000). A means of assessing the performance of existing systems, particularly in terms of diffuse light admittance would be welcomed, as there is little reported quantified information, especially on horizontal openings.

2.5.4 Light Transport

Recent material advances have resulted in the ability to efficiently transport light. The principal systems available are hollow highly reflective piping (e.g. light pipes, solar tubes) and glass fibres which work by total internal reflection (e.g. multi core glass or the cheaper ultra-clear flexible polymer) (Smith 2004). These transport systems could be used to transport artificial light, for example at night or under heavily overcast days (Kischkoweit-Lopin 2002) and could potentially take their collection point from atria wells, enabling buildings of deeper plan. Whilst this addresses the energy issue, the lighting conditions in light piped spaces are often akin to a blanket

layer of artificial lighting, and as such may not have the psychologically beneficial variability and view which can be found in spaces immediately adjacent to the well.

2.5.5 Maintenance

Dirt accumulation will also reduce transmitted flux. A crude system currently exists for applying correction factors based on location, type of work and glazing slope (BRE Estimating daylight in buildings: Part 1 1986, BS 8206-2 1992). These values are based on pre-1940's studies, when environmental conditions were markedly different. A recent comprehensive study of the effect of dirt on transmittance has put forward new correction values based upon location, room function, glazing slope and exposure to rain (Tregenza et. al. 1999, Sharples et. al. 2001). They are based on the monitoring of approximately 500 windows in Sheffield, and range from 0.98 (residential, vertical, rural, and exposed) to 0.20 (industrial, horizontal, urban, and sheltered). The typical atrium scenario of horizontal glazing in an urban area for commercial use applies 0.70 to daylight calculations. Interestingly, there was no significant relationship between frequency of window cleaning and light transmittance. Cannon-Brookes (1997) offers a word of caution in applying these arbitrary factors stating that they may be applicable for deriving worst case scenarios, but potentially unreliable if quantitative accuracy is required.

Extra thought may have to be given as to how the transparent surfaces of the fenestration system are to be maintained. Large areas of shading for example could pose a practical challenge with regard to easy access. New technologies such as Pilkington's self cleaning glazing¹ could become more prominent in the future.

2.6 The Well

2.6.1 Geometry

Light attenuation and distribution within the atrium well is dependent on two main parameters, the well geometry and the nature of the surfaces. Previous research

¹ <http://www.pilkington.com/>

has concentrated on how controlled changes to these variables influence illumination levels using mainly the daylight factor as the indicator.

For atria of equal plan area and depth, the generic shape will influence illumination levels. Circular atria are found to have the highest illumination levels, followed by square, equilateral triangle, rectangular then linear (Oretskin 1982, Willbold-Lohr 1989). The specific efficiency of circular wells are discussed by Tsangrassoulis & Santamouris (2000) (Figure 2-21). Although each shape will see approximately the same proportions of the sky and hence receive a similar sky component, the higher volume to surface area ratio of the circular form means that there are fewer reflections, and hence less flux absorbed by the surfaces and so a higher IRC value.

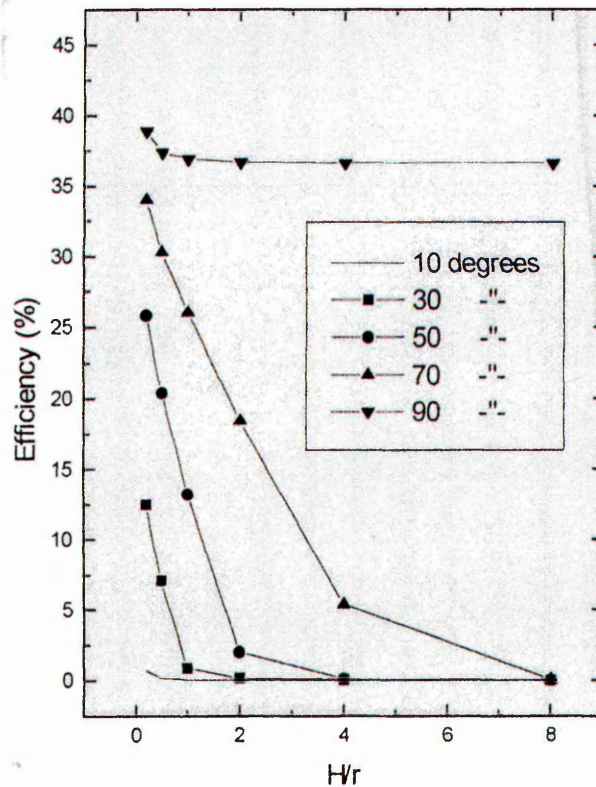


Figure 2-21: The efficiency of circular lightwells as a function of aspect ratio (H/r) for various angles of solar altitude (Tsangrassoulis & Santamouris 2000)

It is noted that whilst the square and circular forms are more efficient, there is more potential in rectangular and linear atria for vertical fenestration. For any fixed section, increasing the length, and hence reducing the PAR will increase daylight levels,

with the spread of distribution slightly more uneven across the width of the atrium as it becomes more linear (Liu et. al. 1991) (Figure 2-22). This stands to reason as the light admitting area has increased. Daylight levels will be highest in the centre of the well, dropping off towards the corners, with the longer side wall receiving greater levels of illumination than the shorter one (Kim & Boyer 1986). This difference becomes greater as the well becomes more linear, which raises the issue of orientation. Clearly under theoretically perfect overcast conditions this is not crucial, but for clear skies, linear atria oriented east-west will receive direct sunlight at the top of the south facing wall, whilst sunlight will penetrate deep into those oriented north-south yet less into adjacent spaces.

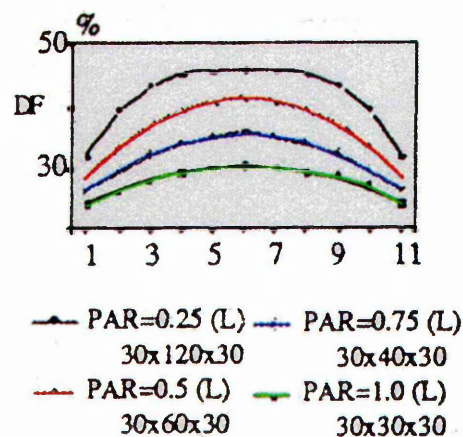


Figure 2-22: For a fixed section, increasing the length (and hence reducing PAR) increases the light admitting opening and hence daylight levels increase. The distribution flattens out towards the centre of the well (considering lengthways direction), with sharp drop-offs towards the edges (Liu et. al. 1991).

For shallow atria, daylight levels are highest in the centre, diminishing towards the edges. As the atrium becomes deeper (increasing SAR), daylight levels fall and the spread across the width evens out (Liu et. al. 1991). This can be explained by the dominance of the SC in shallow atria, whilst for deeper atria the IRC becomes more prevalent. There are several papers available relating daylight factor (as a whole and separated into SC and IRC) to geometry, chiefly well index. These range from general observations to developing design algorithms. Where quantitative proposals have been suggested, the general form is of an exponential decay as the well index increases (becomes deeper) (Kim & Boyer 1986, Degelman et. al. 1988, Neal & Sharples 1992, Atif et. al. 1995, Calcagni & Paroncini 2004 (Figure 2-23)), though Liu et. al. (1991) provide a polynomial equation. These are mainly based on empirically derived

approaches, though some theoretical approaches have been attempted (Tregenza 1997, Laouadi & Atif 2000).

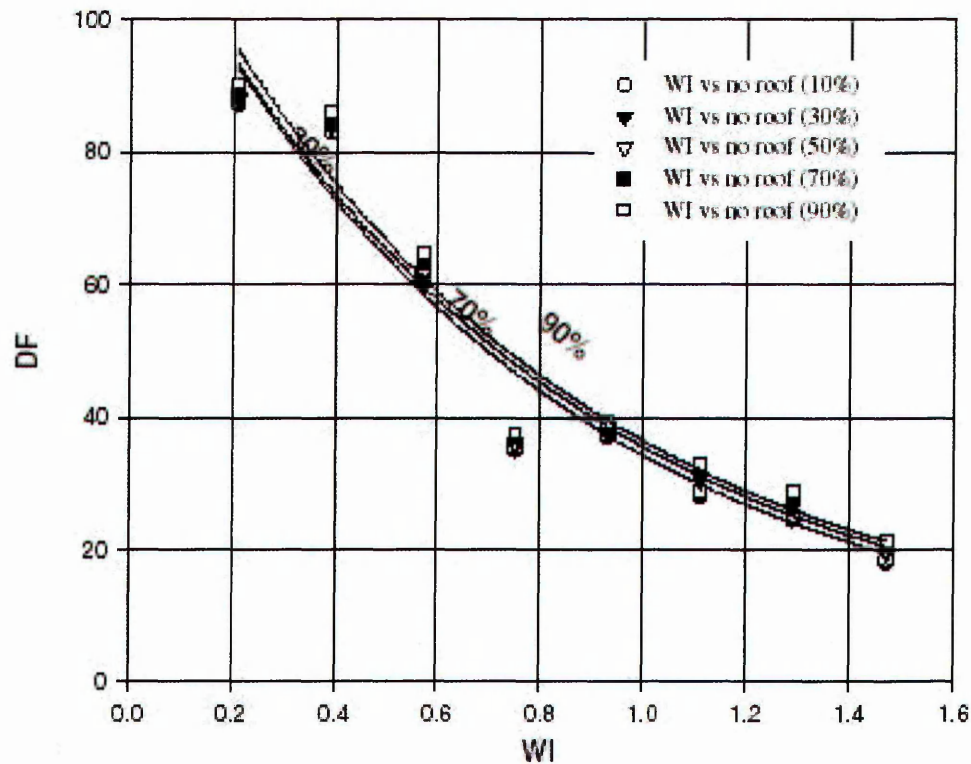


Figure 2-23: The relationship between well index and daylight factor is one of exponential decay (Calcagni & Paroncini 2004).

Comparison of these various prediction algorithms have shown that they agree with each other in their general form, but do not correlate well in terms of absolute numbers (Wright & Letherman 1998) (Figure 2-24). A first reason for this divergence is that some papers quote DF in the centre of the well (which is likely to be higher) (Kim & Boyer 1986, Neal & Sharples 1992) whilst others take average DF (Atif et. al. 1995) (Figure 2-25). Differences between SC measurements are due to the fact that similar values of WI can be derived from atria of significantly different proportions and indicates that caution must be taken when using WI. Moeck & Selkowitz (1996) offer a word of caution in applying too much faith in such numeric output when they say that *'...numbers are performance criteria derived from specific formulae. They are established, changed or discarded by experts' associations for a particular design domain. The formulae are subject to change over time. In addition, numbers may be ambiguous since different designs can produce identical numerical performance values'*.

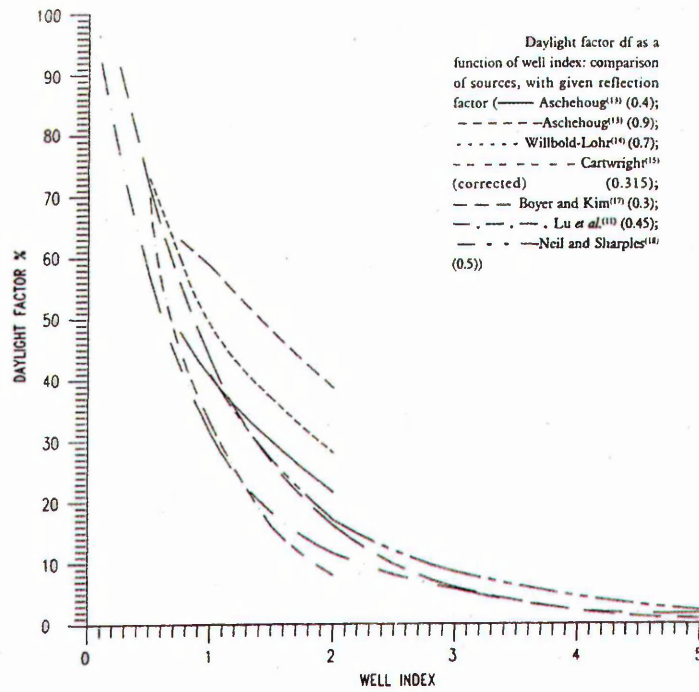


Figure 2-24: The various attempts made by authors to relate well index to daylight factor agree in general form though differ numerically (Wright & Letherman 1998).

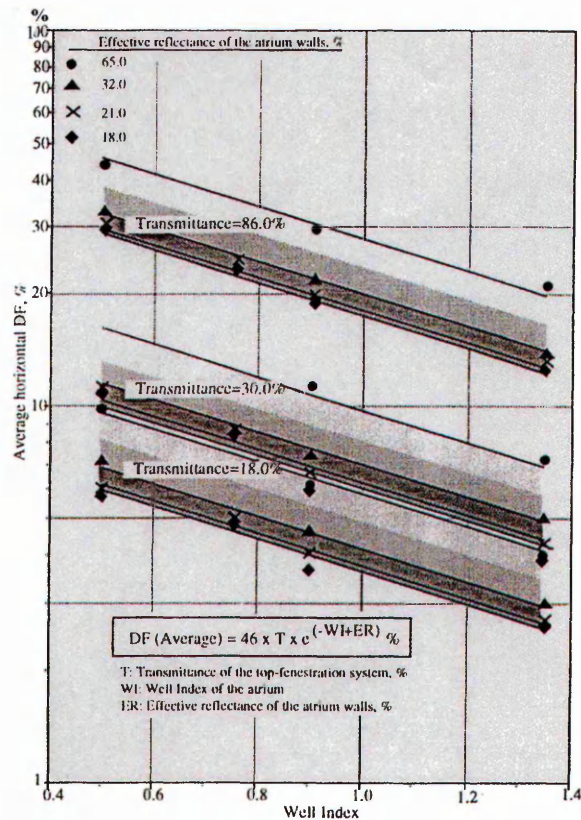


Figure 2-25: The findings of Atif *et. al.* (1995) relating well index, surface reflectance and roof transmittance to average daylight factor on the atrium floor.

Aizlewood et. al. (1997) have successfully managed to accurately predict the SC as a function of WI by approximating the square plan of his atrium as a circle, and comparing derived values with measured values (from a scale model) and those from the computer programme Radiance (Figure 2-26). This technique would probably become less accurate as the atrium becomes more linear.

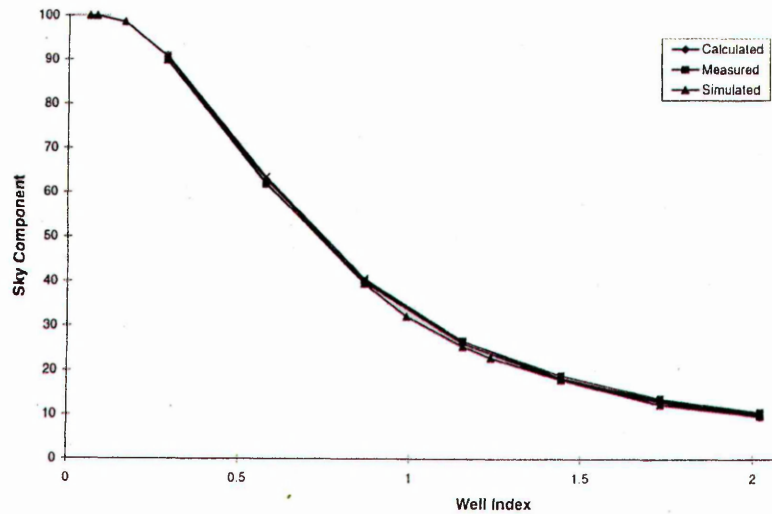


Figure 2-26: The agreement between theoretically derived, physically measured and computer simulated results for sky component within an open well was found to be good (Aizlewood et. al. 1997).

Differences between IRC values between authors are due to the aforementioned geometric paradox and differences in values of reflectance used in the models. The general graphical form for IRC at floor level is that of a curve rising and peaking at a WI of about 1, before gradually tailing off. The complexity of reflected flux makes it seem improbable that a simple algorithm can accurately predict the IRC, particularly when real atria are normally far more complicated than unobstructed rectilinear boxes of uniform reflectance. The most effective current means of accurately deriving reflected flux values is through computer simulation.

The addition of side glazing to atria will increase illumination levels within the well. Algorithms are developed for 3-sided atria with open and opaque tops for a well of 30% reflectance (Degelman 1988, Kim & Boyer 1988). Boubekri & Anninos (1996) derive tables of daylight efficiency factors under top and side-lit conditions for atria as functions of PAR (0.2 to 1.0) and SAR (0.5 to 4.0) for reflectances of 0.3, 0.5 and 0.7. The effect of the top aperture diminishes with increasing depth of the well and it is here

that the addition of side glazing will become more beneficial. It is observed that the benefits of adding glazing a second side are not as great as the first addition of glazing. Extra thought is required in the use of side glazing with respect to the control of glare. By comparing glazing to envelope ratio, 4-sided atria were found to be more efficient than 3-sided then 2-sided ones, as for the same ratio they produced far higher daylight efficiency factors, albeit without managing to attain as high absolute values.

Splaying the well has been identified as a means of improving daylight levels at the base of atria (Neal & Sharples 1992). Splay angles shallower than 60° do not significantly improve the efficiency of the well (Figure 2-27) (Laouadi 2004). It should be noted however that splaying will result in less rentable floor area compared to an unsplayed atria of equal base area. They are also structurally more challenging to design, and the deeper nature of the lower floors may make them harder to light, though this may be offset by the daylighting gains.

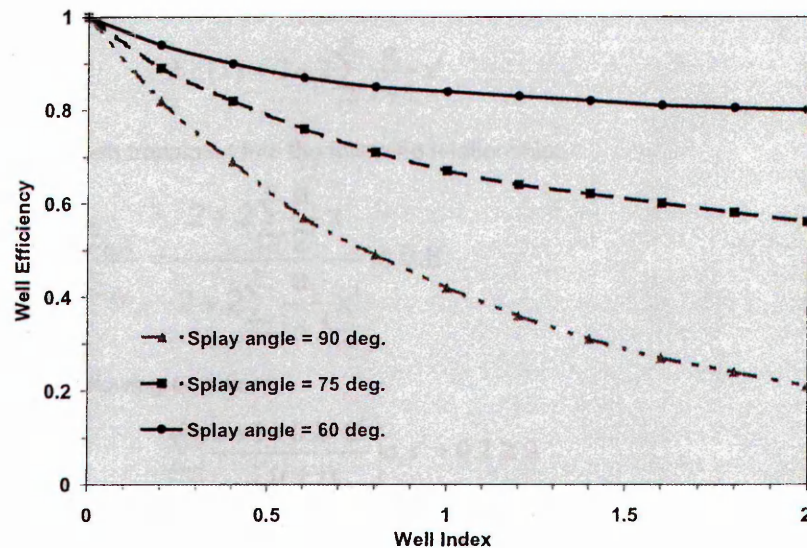


Figure 2-27: Splaying is a strategy which can be adopted to improve the efficiency of deeper wells up to angles of approximately 60° (Laouadi 2004).

2.6.2 Surface Reflectance

The effect of changing reflectance has been investigated by a number of authors, with the simplest examinations assuming surfaces of uniform reflectance across the whole well. Increasing reflectance is found to be more effective deeper down the well. Reading from a graph, the relative difference in DF at the top of two 5-storey wells of

respective reflectances 1.5% and 86% is 15%, increasing to 100% at the base (Navvab & Selkowitz 1984). Despite the simplicity of these models, Aizlewood failed to correlate measured IRC values with calculated values, demonstrating the complex and as yet poorly understood behaviour of reflected flux, particularly when highly reflective surfaces are used (Aizlewood et. al. 1997). More realistic studies include openings in the well that calculate average weighted reflectances (Willbold-Lohr 1989, Atif & Boyer 1991, Iyer-Raniga 1994, Atif et. al. 1995, Boubekri 1995). It is clear that increasing the reflectance of the well increases illumination levels due to the higher values of IRC, though the exact magnitude would seem to be specific to the form of the atrium examined. Boubekri (1995) found a quadrupling in reflectance resulted in a doubling of daylight factor on the vertical walls. This can be misleading in that different configurations of reflective surface can produce the same weighted-value, yet dissimilar magnitudes of daylight factor at various positions. The differences become less noticeable as the density of contrasting reflective surfaces increase (Sharples & Mahambrey 1999, Sharples & Lash 2004). The addition of specular surfaces reflects flux deeper into atria providing higher illuminance, though this must be balanced with the increased potential for glare (Willbold-Lohr 1989, Matusiak 1999 et. al., Sharples & Mahambrey 1999).

A solution to the disparity between light flux at the top and bottom of the well is to increase the openings to the well progressively at each level. This is practical in that the bottom floor has access to the well and so requires larger openings, whilst the differences in opening can help speak an architectural language of hierarchy. Throughout history builders have done this intuitively in narrow streets. Cole (1990) studied a 5-storey well and found the percentage opening configuration of ground - 100%, 2nd - 80%, 3rd - 60%, 4th - 40% and 5th - 20% most effective (Figure 2-31). Aschehoug (1992) looked at a 4-storey glazed street and found the glazing distribution of 100% (ground), 70%, 60%, 50% (fourth) to be optimal. The most detailed study investigates the changing of glazing transmittance as well as opening size between levels (Matusiak et. al. 1999). Both strategies performed similarly well compared to a base case, though it was noted that changing the glazing type is a less flexible option due to the limited availability of glass which has different transmittance properties yet similar colour.

Increasing the reflectance of the floor will increase daylight levels due to an increased IRC (Cole 1990, Boubekri 1995, Matusiak 1999). This improvement is most noticeable at the base of the well, and becomes imperceptible towards the top. Thought should be given as to the nature of the floor, for example covering in plants will greatly reduce its reflectance, and therefore daylight levels at the base of the well. Increasing floor reflectance at the edges of the well will enhance illumination levels in adjacent spaces, the area required dependent on the size and location of the openings to the space (Iyer-Raniga 1994).

2.6.3 Internal Well Obstructions

Many atria have circulation routes between the well and adjoining spaces consisting of walkways with balconies. For deep wells or wide balconies, difficulties may occur in achieving adequate light levels and even distribution, particularly directly under the balconies (Kim et. al. 1994). This may result in the need for supplementary artificial lighting. The configuration of the balcony edge (solid or rail) was found to have a comparatively low impact on daylight levels. The presence of other major architectural objects such as staircases should be carefully considered, as they will affect lighting levels and distribution, and potentially create large areas of shadow.

2.6.4 Adjacent Spaces

The main area for potential savings lies in the ability of atria to displace artificial lighting in their adjacent spaces. Several studies have specifically examined the effects of parametric changes to the well on daylight levels in the adjoining spaces. These generally take the form of illumination readings at defined distances from the atrium (Cole 1990, Iyer-Raniga 1994, Al-Turki & Schiler 1997, Matusiak et. al. 1999). The various papers agree on the general trend, that there is some form of decay of illumination with increasing distance from the atrium (e.g. Figure 2-28). This effect is most pronounced on higher floors and closer to the well, as it is here where the sky component is most pronounced. Positions located further away become more reliant on weaker reflected flux. The aforementioned parametric changes to the well strongly affect the daylighting properties of their adjacent spaces, as well as the conditions of the spaces themselves. Most studies detail modular like boxes with high reflectance

ceilings, mid-reflectance walls and low reflectance floors. The vast difference in illumination levels across the plan of the room can be partially rectified through either adding openings to the outside on the external side, or through controlling incoming light from the well using devices such as lightshelves. This can be a useful strategy as for most of the results, illumination levels only reached 500 Lux (an adequate level for standard office tasks (Baker et. al. 1993)) at locations very close to the well, with particularly low levels in the lower portions of the building. It should be noted however that they reduce the absolute quantity of flux due to absorption and maintenance losses from the shelf.

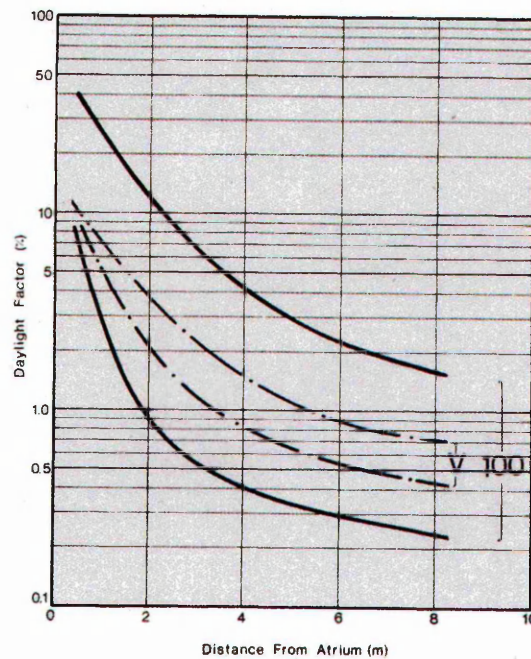


Figure 2-28: Daylight factor in spaces adjacent to the well on top (5th) and ground floors. The bold lines are for spaces which are 100% glazed to the well, the dashed lines have variable glazing (small openings at the top, increasing in size towards the bottom). It can be seen that such an opening strategy can help even light distribution throughout the building (Cole 1990).

A second way to determine daylighting properties of a space adjacent to an atrium is to treat that space as a side-lit room, and applying the lumen method in a conventional manner (Degelman 1988). This uses the illuminance incident to the atrium wall as the departure point, and so has the advantage of being able to interchange results between different authors. Distribution is represented as maximum (5 feet (approximately 1.5m) from opening), middle and minimum (5 feet from rear wall). Al-Turki & Schiler (1997) display graphs for readings derived from the lumen method and

from physical measurement. Whilst no absolute values are given, the agreement appears to be good. The advantages of having many points of measurement with the model approach can be seen over just the three from the calculated method as interestingly, the minimum value of illuminance does not occur immediately adjacent to the rear wall, but 5 feet before it. This is due to the presence of reflected light in the vicinity of the back wall.

Szerman (1992) presents a monograph for deriving mean daylight factor in rooms adjacent to atria as a function of room position, atrium width, SAR, atrium wall and floor reflectances and glazing types, based on typical office specifications (Figure 2-29). The low range of SAR possibilities (0.4-1.6) excludes deeper atria, though the ability of such atria to provide light for adjacent spaces is questionable. The relative simplicity at which so many interdependent variables have been correlated when so many authors have failed to produce concrete methods casts aspersions over the accuracy, though in terms of ease of use it seems a good early design tool. Some form of modelling will be required at a later stage to validate the findings and assess distribution; something the mean daylight factor on its own fails to demonstrate.

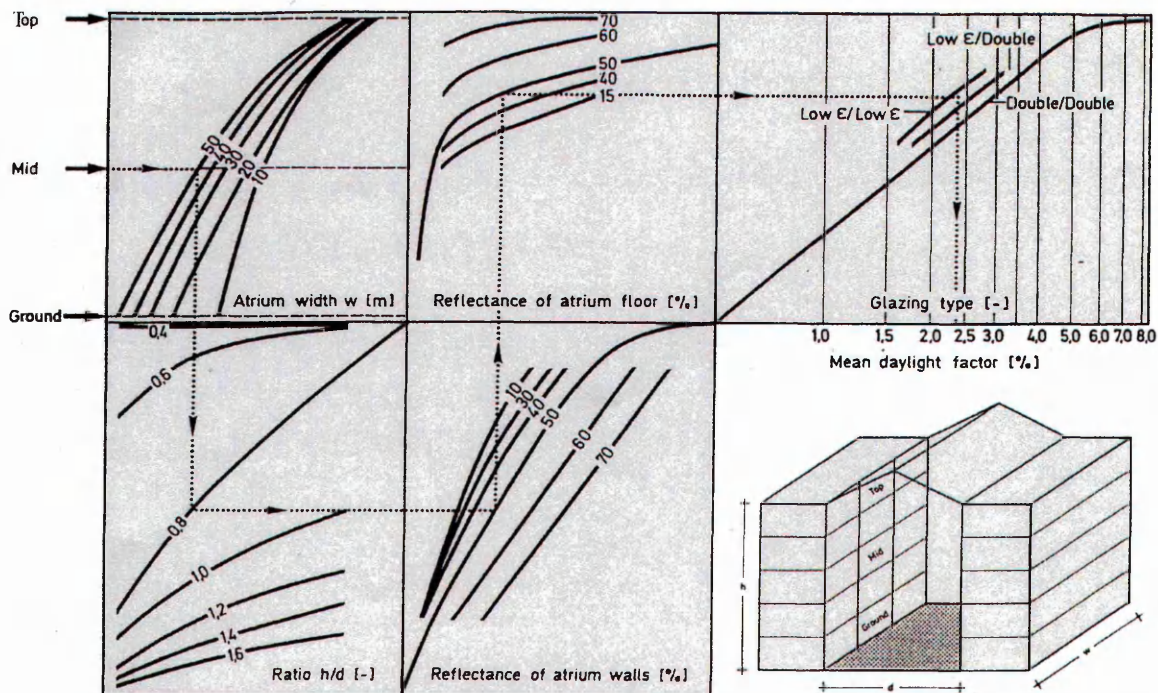


Figure 2-29: A monograph addresses multiple parameters in a user friendly manner (Szerman 1992)

2.7 Artificial Lighting Control: A Brief Discussion

In all but the most exceptional of circumstances, an artificial lighting system will need to be installed such that target illuminance levels can be reached, to extend activity into the night and to reduce contrasts between the bright atrium and dimmer adjoining spaces. *'Energy is not saved by daylighting; energy is saved by dimming down or switching off electric lights that are not needed because of daylight'* (Leslie 2003). Coyne et. al (1998) suggest that whilst daylighting is often appropriate for ambient lighting levels, it is important to provide localised task lighting such that individual users can be flexible towards their specific task. Costs associated with artificial lighting consist of initial fixtures and control systems, as well as running and maintenance costs, whilst natural lighting costs nothing to run. Initially however, daylighting may result in higher ceilings, more expensive artificial lighting controls and higher design fees (Cole 1986).

The ability to save energy is reliant upon an efficient system that activates the artificial lighting as and when necessary (Gillette 1989). Broadly speaking, control falls into two categories, switching and dimming. The switching may be manually controlled, or automated. It may be timer controlled, though as Rae et. al. (1998) state, *'an occupant will not tolerate being plunged into darkness forty feet from the light switch'*. Many studies have attempted to quantify the potential energy savings due to the perfect integration of daylighting and artificial lighting through control systems. These experiments have taken the form of computer simulations and actual field measurements (see Table 2-2).

In reality, these potential savings are almost never realised. Several factors explain this phenomenon, the first concerning practicalities. Atif & Galasiu (2002) observed a reduction in efficiency of 30-65% of a dimming system due to incorrectly adjusted phases of dimming control, improper maintenance of the skylight (i.e. snow cover), an oversizing of the artificial lighting system and inadequate positioning of the photosensor. The poor performance of photosensors as a representative of actual work plane illuminance levels is also quoted by Ehrlich et. al. (2002). Configuration issues aside, the photosensor coupled with a dimming system will aim to maintain a constant illuminance level. 1 Lux of daylight however, is not necessarily equal to 1 Lux of

artificial lighting (Fontoynt 2002). Daylight generally enters from the side and is of mixed spectra whereas artificial light comes from lamps located above the occupant and are of fixed spectra.

Table 2-2: The findings of selected studies into potential energy savings due to various lighting control mechanisms.

<i>Author(s)</i>	<i>Year</i>	<i>Location</i>	<i>Potential Savings</i>	<i>Notes</i>
Bodart & De Herde	2002	Belgium	50-80%	Office building
Hestnes & Aschehoug	1995	Norway & USA	50-55% & 60-70%	Top floor office building
Onaygil	2003	Turkey	30%	More savings in summer (45%) and clear days (35%) than winter (21%) and overcast (16%)
Li & Lam	2001	Hong Kong	50%	Perimeter office space
Li & Lam	2002	Hong Kong	65%	Automated dimming in daylight corridor
Laouadi	2004	-	-	Dimming 28% more effective than switching
Atif & Galasiu	2002	Canada	68% dimming, 31.5% switching	
Reinhart	2004	-	0-60%	Using program 'Lightswitch-2002' which takes probability of user over-ride into account.

Zonneveldt & Mallory-Hill (1998) write that '*although a system may function very efficiently, the user acceptance of the system may be disappointing*'. Theoretically automatic dimming systems may potentially save the most energy. Countless anecdotal studies have found simple manual systems perform better (Love 1998 b, Rea & Rutledge 1998). Leslie (2003) observes that the most effective strategy could involve switch sticker reminders coupled with encouragement from management.

Clearly the integration of daylighting and the artificial lighting system needs to be such that artificial lighting is disabled when not needed. Given the failure of many automated system, it would suggest that building users either are not sufficiently educated, have not the incentive, or can not make such decisions if the artificial lighting is shared with other occupants. Further work is needed in this area, in particular expressing explicitly the interaction between artificial lighting systems and existing atria buildings.

2.8 From Knowledge to Practice: Application in the Field

2.8.1 The Process of Design and the Role of the Design Tool

It is recognised that successful daylight designs are often characterised by high levels of design team skill and experience (Selkowitz 1998). The participation of a knowledgeable professional from conception through commissioning appears to be important in successful attainment of objectives (provision of good quality daylighting, comprehensive scope of design and consideration of user preferences and control) with respect to daylighting (Love 1998 a).

At the genesis of a project, the designer/design team is armed with a set of predefined objectives and a blank canvas. These objectives in combination with specific site, budget, personnel, material availability and a host of other influencing factors will begin to shape the project. The more of these influences exerted onto the 'canvas', the less freewill the designer has, and the more the design follows a path of predestined inevitability (to use the logic of Tolstoy). The designer will use the tools at his disposal to coalesce these influencing factors into the most appropriate solutions.

But what is a design tool? Milne and Zurich (1998) state that *'the object of a Design Tool is to help architects create a better building...when using a Design Tool, two different models of the building exist: one is a three-dimensional picture in the architect's mind, and the other is a mathematical abstraction of its energy performance in the computer. These two models are almost totally separate'*. A design tool differs from a simulation tool in that it is used at the start of the design process, where ideas are most malleable and easily adjustable. Changes further down the path are both harder and more costly to implement. Navvab (1996) reinforces this, stating that no single tool has the capability to solve all lighting design problems, and so design tools should vary during the design process. Degelman (1998) asserts that the exact numerical values are not necessarily desirable at the early stages of the design process; there is always the artificial lighting system to back us up when daylighting levels are inadequate. Indeed *'it is much more interesting to have rough but early information than precise information which comes too late'* (Paule et. al. 1998). There are four criteria necessary for design tools (Milne & Zurich 1998). Most important is user confidence. Secondly

accuracy, though not in terms of absolute numerical quantities, rather trends in sequences of answers derived from successive design revisions. The remaining two criterion are response time and amount of detail.

2.8.2 Types of Design Tool

The competent designer will be equipped with a whole kit of design tools at his disposal. For the purposes of this discussion they are broken down into three headings;

1. Simple design ideas and tools
2. Study of precedents
3. Modelling
 - a. Physical
 - b. Simulated

2.8.2.1 Simple Design Ideas and Tools

The most basic design tools consist of simple measurements and rules of thumb. Such guidelines are easy to understand and implement, and are aimed directly at designers. A good example of this is the BRE (Building Research Establishment) published *Designing buildings for daylight* (Bell & Burt 1995), which contains simple design guidelines, rules of thumb, simple formula, example buildings and self assessment exercises. Another example is *Daylight performance of buildings* by Marc Fontoynt (1999) where statements such as ‘*simple designs often perform better*’ and ‘*in atria, secondary windows need to be at least 50% of wall surfaces*’ may be vague, but provide useful departure points. Further such advice is given by Leslie (2003) such as configuring buildings properly, elongating buildings along east-west axis, locating critical tasks near the building perimeter, bringing light in high, admitting daylight from more than one side of a space, controlling direct light, using light coloured surfaces and locating computer screens perpendicular to windows. The Heschong Mahone Group² provides useful generalised information for building designers. Specific information on skylighting is available, along with a simple Microsoft Excel based analysis tool

² <http://www.h-m-g.com/default.htm>

regarding their sizing. Such information does not however relate to more detailed roof configurations.

Basic formulas are reasonably well known to designers, and allow the effect of changes to building variables to be observed in a quantifiable manner. An example of such an equation describes the average daylight factor under a skylight (Littlefair 1998);

$$DF_{AV} = \frac{WT_g T_m T_f \theta}{A(1 - R^2)} \quad [2-6]$$

where,

W= area of atrium roof aperture

T_g = diffuse visible transmittance of glazing

T_m = maintenance factor for dirt (0.7 typical, 0.8 sloping glazing, 0.9 vertical glazing)

T_f = factor to allow for light blocked by the atrium roof structure

θ = angle of visible sky in degrees

A = total area of atrium surfaces

R = average reflectance of surfaces

It is not entirely clear from the text how to derive T_f, as it varies with viewing angle to the horizontal and with roof type (Figure 2-30). Further investigation/information is needed to clarify factors such as T_f. Whilst ultimately the equation is not especially accurate, and does not begin to approach the issue of light distribution, it is valid as a first step design aid. Physical tools such as nomographs, daylight protractors and Waldram diagrams are also traditional examples of simple design aids. Further examples of simple tools to be used at the beginnings of the design process are proposed by Hopkirk (1998) and Lassance (2002).

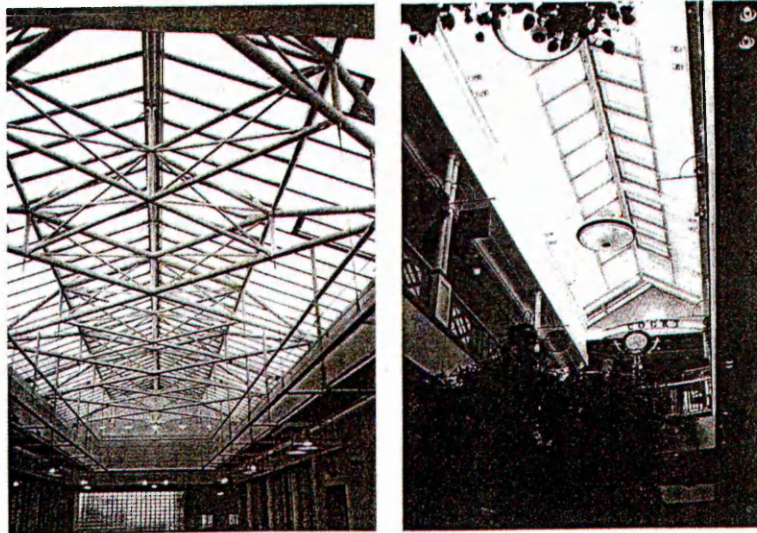
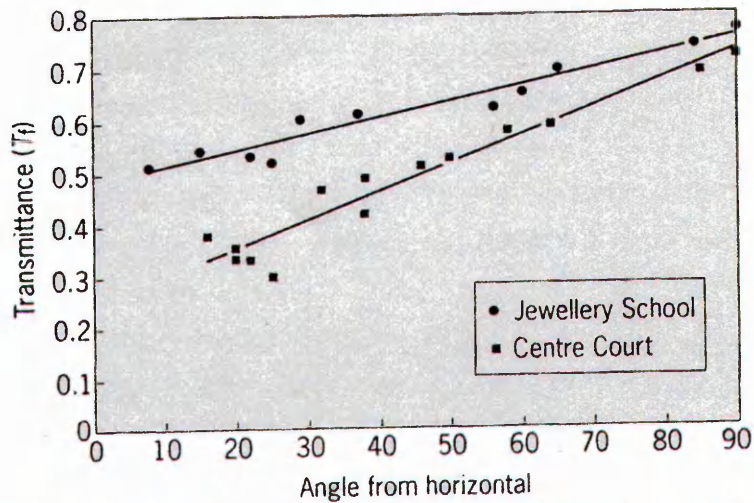


Figure 2-30: The varying nature of transmittance with angle from horizontal in the Jewellery School (left) and Centre Court (right) for application to a simple equation (Littlefair 1998).

2.8.2.2 Study of Precedents

A second approach involves identifying successful elements of existing buildings and adapting them to the current project. The precedent buildings could be specifically known to the design team (e.g. a previous project), or may be documented elsewhere (e.g. books, journals etc.). Marc Fontoynt's *Daylight performance of buildings* (1999) consists of three years of collaborative surveying of 60 European case studies, ranging from the ancient to the modern. The case studies are described in terms of geometry, daylight factors, material characterisation, visual comfort, homogeneity of distributions, luminous flux penetration through apertures (with diagrams), photographs, user comments and energy calculations e.g. Figure 2-31. An example of an individually

documented case study is Canada's first C2000 office, whose aim is to under halve the energy usage of a standard building (Carpenter et. al. 1998).

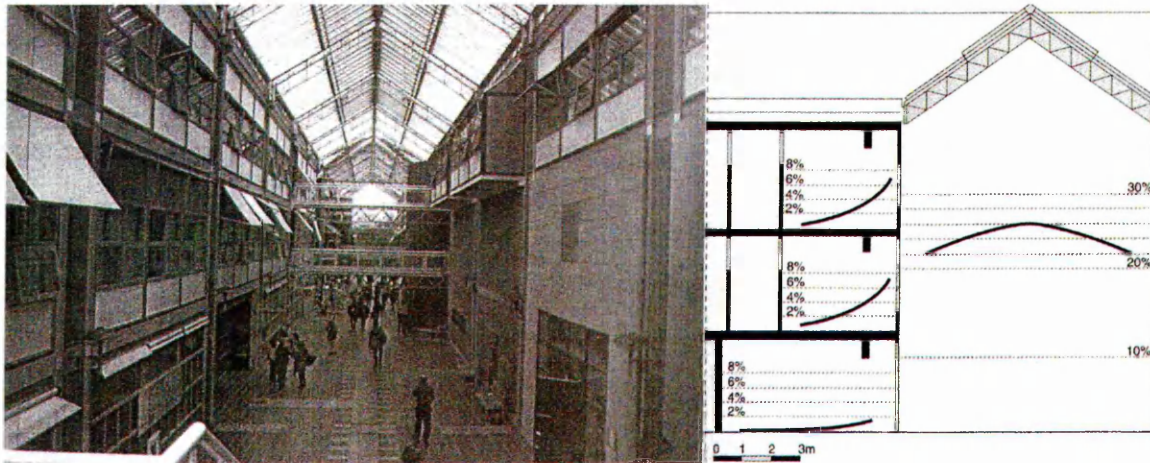


Figure 2-31: Photographs and analytical diagrams from case study buildings can assist designers in generating new designs e.g. Dragvoll University Centre, Trondheim, Norway (Fontoynt 1999).

Computer simulation of existing buildings can be run and changes to elements of the design (e.g. light shelves etc.) investigated to assess their impact on performance (e.g. daylighting). Such a methodology is proposed by Clarke et. al. (1998). Once the results for the specific building have been obtained, the simulations can be re-run with new climatic boundaries and archived for use in universal contexts. Should the project require it and resources permitting, surveying of existing buildings may be undertaken by the design team, though such scenarios are few and far between. Atif et. al. (1998) describe protocols for evaluating daylighting in buildings.

An important potential resource with regard to existing built solutions can be found in the occupants of the buildings. Hygge & Lofberg (1998) addresses this issue through the use of Post-Occupancy Evaluation (POE) questionnaires. They state that *'in reality, unless the occupants are totally satisfied with the facility they will never reach their full potential or totally accept the technology, especially if it is not perceived to be of immediate benefit to them'*. Findings from such POE questionnaires can assist in avoiding past mistakes and improving on existing designs.

2.8.2.3 Modelling

Modelling a design allows the architect to focus on single (or multiple) elements of the design. In ‘reducing’ the model, certain features can be focussed on thus this reduction and abstraction enables users to explore, understand, predict and document certain properties and behaviour of the modelled entity (Mahdavi 2004). Different models are required for the comprehension of different building parameters; an analysis of space would involve volumes, thermal performance concerns mass, whilst lighting combines volume with surface. Modelling here is broken down into two parts; physical modelling and simulation.

2.8.2.3.1 Scale Models

‘The use of scale models during the design process is the oldest method in design. They show the concept more effectively than sketches or perspective drawings. They allow the designer to study problems in all three dimensions.’ (Navvab 1996). Architects may use models for any project and at any stage of its design e.g. Morley (2000) found the use of a scale model as ‘invaluable’ in testing design options for an indoor cricket school, London.

Whilst physical models are an effective and accessible (given access to an artificial sky, else the model will need testing under the more erratic real sky condition) means of communicating design ideas, it is the finally realised space and not the model that is occupied, and thus how much faith can an architect place in them? The most comprehensive study compares illuminance measurements between an art gallery and corresponding model under the same real skies (Cannon-Brookes 1997). Once all the experimental error had been accounted for, the model was found to overstate actual values by 10-25% (Figure 2-32). The reasons for this were thought to be the difficulty in accurately measuring and modelling photometric properties (e.g. specular surfaces), and that as the model gets smaller, so the potential for error increases. Whilst caution was advised in placing quantitative confidence in models, they are still valid as qualitative tools.

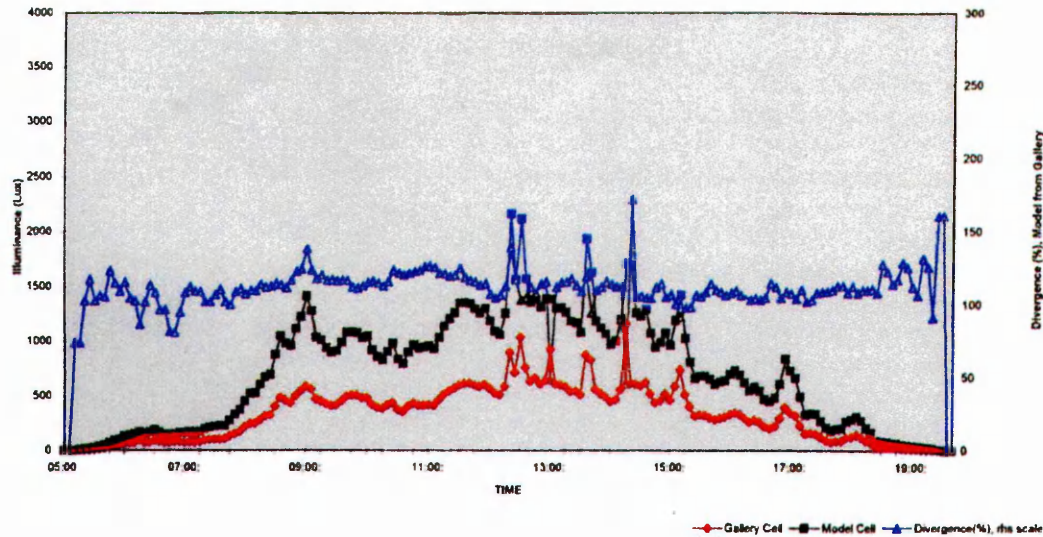


Figure 2-32: Illuminance measurements taken under overcast sky conditions were consistently higher in a scale model than from the full scale building (Cannon-Brookes 1997).

2.8.2.3.2 Computer Models

Computer modelling represents the greatest potential leap in the evolution of the design process. Advances in this field are rapid, and for example where less than 20 years ago it was stated that this approach to daylighting was limited due to the modelling of complex spaces and specular reflection (Spitzglas et. al. 1985), these shortcomings have since been overcome. Geebelen & Neuckermans (1998) state a gap in user need and current program delivery at the early stages of design. There exists no electronic counterpart for freehand sketching, and thus the use of CAD packages practically forces the designer to work at a level of detail that is unnecessarily high. Numerical values should be hidden from the user early on, and replaced with verbal descriptions. Once again, development is being made in this area. Tools such as Leso-DIAL allow a feel for quantitative levels to be experienced by the user through the use of intuitive inputs and fuzzy logic (Paule et. al. 1998). Ecotect³ incorporates a user friendly drafting interface with simple design tools that can be run very early on in the design process. As the project builds up in complexity, so the accuracy of output will improve, and the model can be exported to more specialised and accurate analysis programs. Where these programs holistically examine the building, other computer tools may focus on certain elements. Luminance mapping techniques could be used for

³ <http://www.squ1.com/site.html>

the positioning and sizing of daylighting systems (Compagnon 2004). SkyVision is a new specialist user-friendly tool that concentrates on skylight design in atria, and their sizing to meet target illuminance levels (Laouadi 2004). Its specific workings are detailed in Chapter 7. Glaser and Ubbelohde (2002) describe techniques for ordering data by tessellation, a relevant issue considering the potential for quantity of output to go unchecked through usage of such computer tools.

2.8.3 Which Tool is Appropriate?

With so many options it is obvious that there is no prevalent means for approaching the design process. Achieving the most successful daylit schemes will arise through a combination of many of the design tools and methods mentioned. Erwine (1998) conducted a study comparing the relative merits of physical modelling (reduced and full scale) and computer simulation through consulting the design team and client of a school in Oregon, USA. The computer model was seen as a verifying rather than a design tool due to high input and processing times. The program used was Lightscape; had programs such as Ecotect been considered the result may have been different. The scale model was used for both schematic design and design development, and to study qualitative impacts of the fenestration. Highest quantitative trust was placed in the full scale mock up, and the computer model, whilst qualitatively the full scale and scale models were best received. The scale model was chosen as the most indispensable tool in that it was *'easy to change, quick, least cost and believable to novices'*. The models were best for communicating the scheme to the client. Given the cost and detail required of the full scale mock-up, clearly it is a tool to be used later on in the design process. Disadvantages associated with scale modelling involved time and cost of construction, and access to sky simulators, problems which computer models can potentially overcome. The main criticism of computer models was the steep learning curve and the flatness on the screen of the information. All participants however expected the use of computer to become more prevalent within the next 7 years, as advances are made.

Better consistency and effectiveness of daylight design can be achieved through presentation of a constructive syllabus to architecture students. Students often use rules of thumb (which break down too easily), precedents, simple formula and tools, simple

scale models (ineffective for quantitative output) and computer models (often too complicated) (Mansy 2003, 2004). There is a need for a tool that;

1. is not limited to predetermined designs and/or conditions.
2. is not limited to a certain climate, location or orientation.
3. involves the impact of all relevant design variables into the analysis.
4. has an educational value i.e. suited for beginners and allows for experimental research and exploration of new ideas.
5. helps to make quick decisions when comparing alternative solutions.
6. provide both quantitative and qualitative evaluation.
7. helps the students to visualise the performance of daylighting systems.

The simplified Excel workbook suggested by Mansy may be a useful aid for design students though it is unlikely to catch on beyond classroom level. The seven criteria outlined are in effect covered by Ecotect. Further study would be welcomed to examine the use of such programs in architecture schools, and its trickle down into practice.

2.9 Conclusions

It can be seen that the re-establishment of daylighting as an architectural standard can be beneficial financially and psychologically, and that the atrium has a key role to play in medium to large buildings. The problem lies in the fact that insufficient reliable and accessible data exists for designers, as can be seen in poorly designed atria that result in increased energy loads and problems such as glare and overheating. Whilst a few successful individual schemes have been built, an effective vernacular has yet to emerge for any daylight climate to date.

It is appreciated that appropriate solutions will depend very much on local conditions, though general understandings of the various elements can be combined to generate successful designs. In breaking down the passage of flux from source to target deficiencies in knowledge begin to emerge. Whilst the behaviour of sky luminance and well properties are relatively well understood, the effects of the fenestration are not.

Most research has treated the atrium as an open-top light well, with the few studies that incorporate roof structure unable to provide conclusive suggestions for designers. There is virtually no work on the transmittance of daylight through the fenestration systems of real buildings. Uncertainty lies in how to strike the balance between maximum diffuse skylight admission whilst controlling incoming sunbeam. Furthermore, the behaviour of the complicated inter-reflections that occur between structural elements is poorly understood. Future work needs to focus specifically on roof transmittance in real atria. The effects of the atrium fenestration on spaces adjoining the well would also be welcomed e.g. to generate strategies regarding whether to place solar shading on the exterior of the roof, or on the openings to the adjoining spaces.

In order for any findings to be practically useful, they should be easily understood by designers, and any proposed methodology be user friendly and implementable early on in the design process, where decisions generally have most impact.

Finally, any definite daylight strategies will eventually need assimilation with other atrium aims and objectives. These include servicing needs such as thermal, ventilation and fire control, as well as architectural factors such as circulation, recreation, integration and communication.

3

Project Outline and Methodology

- 3.1 Outline: Aims and Objectives
- 3.2 Methodology: An Overview
- 3.3 Physical Illuminance Measurements
- 3.4 Photoanalysis with HemiView
- 3.5 Computer Simulation of Daylight in Buildings: Selecting the right tool
- 3.6 Summary

'While none of the work we do is very important, it is important that we do a great deal of it.' CATCH 22, JOSEPH HELLER

3.1 Outline: Aims and Objectives

3.1.1 Chapter Outline

This chapter reviews some of the findings of Chapter 2, and presents a case for the research undertaken. The aims and objectives of the thesis are stated, together with a general masterplan for the proposed work in Sections 3.1 and 3.2. The two principal buildings under investigation are introduced, and the three distinct methodologies (physical illuminance measurements, photoanalysis and computer simulation) are described in greater depths in Sections 3.3-3.5.

3.1.2 Current Gaps in Knowledge: A Very Brief Recap

It has been shown that in reverting to a more historical position by replacing artificial lighting with daylight, benefits in terms of energy savings, economics and psychology can be derived, yet there still exists a large gap between the potential and current actuality. Atria represent one means of achieving daylight objectives in medium to large scale non-residential buildings. The transmittance of a roof system is a useful performance descriptor as it is representative of the quantity of light flux entering the building, which could be used to illuminate the well itself, or spaces adjacent to the well. Unfortunately, the daylight performance of the roof remains the least understood area of atrium design. Past research into the effects of the roof are scarce, with the majority concentrating on scale model studies. The existence of information derived from measurements in real building is very limited.

Simple techniques such as applying the plan area of obstruction as an attenuating factor have been shown to underestimate losses due to blockage of light in the roof section. However, simple and easily implementable information early on is likely to be most useful as it is here where key decisions will have their greatest impact. The ability to accurately mimic a space using computers is less useful in terms of design, as it is seen by designers as a verifying tool, used further along in the process.

It is known that roof transmittance will vary with sky luminance distribution. Overcast sky conditions (with the accompanying daylight factor measurable quantity)

are well understood and widely used by designers as they are typical in temperate climates such as the UK, and represent ‘worst case’ design conditions. Given the limited scale of this project, it would appear to be sensible in the first instance to focus on these conditions over other sky types.

3.1.3 Aims and Objectives

The ultimate aim of this thesis is to greatly further the currently available information on the transmittance of daylight through atria fenestration systems, such that real daylighting benefits can be achieved in newly built (and through retrofitting, existing) atrium spaces. In order to achieve this grand aim, it is segmented into four objectives:

1. to assess the transmittance of daylight through skylights by conducting measurements in real working buildings under dynamic sky conditions
2. to propose and test a new photoanalysis technique whose aim is to rapidly assess the transmittance of daylight through skylights
3. to investigate further the multiple parameters of roof configuration, and their effect on transmittance, by comparing physically measured with computer simulated results
4. to propose useable advice for building designers, or at least suggest avenues for continuation of this research

3.2 Methodology: An Overview

The departure point from which all further experimentation and analysis stems, are the physically measured illuminance data from real buildings. This task involves identifying potential case study buildings, and the gathering of the required data over a sustained period of time. The methodology is described in Section 3.3, with results and analysis in Chapter 4.

Field gathered measurements represent the most realistic means of analysing the daylight performance of a building. There are however several limiting factors to such

methods. Firstly, a sufficiently long measuring period is required so as to obtain enough data for the specific sky condition examined. Secondly, to measure transmittance, the measuring equipment generally needs to be located immediately under the roof, towards the centre of the well. In practical terms, this may prove to be too challenging a barrier to overcome. Coupled with this, both these limiting factors are likely to influence the building owner towards denying permission for use as a case study. Thirdly, within the scope of most projects internal measuring points may only be available in one (or at the most, a few) position(s). Whilst this may result in the transmittance of the roof at the point of that measuring sensor, it is not necessarily representative of the overall average roof plane transmittance.

A photoanalysis process is proposed to overcome these factors. A hemispherical image of the roof looking upwards from inside the well is captured. The resultant view considers the roof element surfaces in three rather than the two the dimensions described by plan views, which have been shown by previous research to under-predict the transmittance of roofs. The image is processed in the hemispherical analysis program HemiView, to obtain the ‘gap fraction’. This is the proportion of visible sky/opening seen at that viewpoint. It is proposed that there will be a relationship between this value and the transmittance of the roof as perceived at that point. This relationship will depend on the glazing used at the openings (i.e. chiefly its transmittance) and the material properties of the blockage elements (i.e. how they behave regarding reflection). The methodology is described in Section 3.4.1-3.4.2, with results and analysis in Chapter 5.2-5.3.

This method of photograph capture coupled with simple analysis is quick and easy relative to sustained illuminance measurements. Practically, the process would therefore be far simpler to implement, and building owners would be more likely to grant permission. This would enable the rapid examination of many existing roof types.

In proposing such a methodology care must be taken to correctly define the limits of its use. The analysis treats all glazing as ‘gap’ and structure as ‘blockage’ whereas, in reality, glazing to some extent blocks light, in the same way that structure may reflect it. It is proposed that for the roofs studied in this thesis, these effects will be examined using computer simulations. Whilst the framework for the methodology may

therefore hold for the roofs specifically studied, the extent of these effects for any supplementary roof type can not be accurately known, and so empirically derived findings from this study may not necessarily apply to a whole range of roofs. Secondly, the proposed methodology may be strongly dependant on the position from which the photograph is taken, and as such, clear directions with regard to viewpoint need to be defined. Lastly, the transmittance of a roof will change with the sky luminance distribution, and so any application of findings might only apply under the sky conditions under which the experiment was conducted (i.e. overcast).

The photographs captured in the field represent the process that would be taken for application to further roofs. Such a process is however physically constricted by the locations from which the photograph may be taken, the upper resolution of the camera, and any obstructions which occupy a significant proportion of the field of view. The influences of these factors are investigated by repeating the process with images generated on a computer, where these three barriers are easily overcome. The findings will assist in defining limits of the proposed methodology. This process is described in Section 3.4.3 with the results and analysis detailed in Chapter 5.4-5.5.

It has already been stated that the best means of obtaining the lighting performance of an existing building is to take physical measurements within that building. As well as the length of measuring period discussed, there exist further limitations. The results can only be as accurate as the error margins within the experimental equipment and procedure. Secondly, the results found are representative of the point in time at which they were measured. Application to similar sky conditions etc. can only be considered to be an approximation (whose accuracy improves with increased sample size). Thirdly and already mentioned, there are practical constrictions as to the quantity of measuring points, and where they may be physically positioned. Finally, in measuring transmittance, photocells will not discriminate between light solely transmitted from the fenestration, and that which has been reflected back from the atrium well, and so as such, physically measured processes are only capable of measuring daylight factors, and not transmittance. It is for this reason that computer simulations are necessary. Section 3.5 describes the process of selecting the appropriate simulation program, whilst Chapter 6 is devoted to the specific methodology and findings from the simulations.

Compared to physically based measurements, analysis points can be positioned at any point in space, and in any quantity. Secondly, through manipulation of surface properties, the effects of certain attributes such as well contribution can be assessed (and in the case of obtaining transmittance, ignored). Finally, non-existent spaces can potentially be modelled. These may include proposed new buildings, or standardised roof forms.

In conducting computer simulations it is essential to be aware of their limitations. The results can only be as accurate as the effectiveness of the source code in describing real world events. Given the infinite interactions occurring in real world conditions, this poses a daunting task for the simulation program. In daylighting analysis, of particular importance are the sky models. With regard to this study, a reliance on the traditional overcast sky distribution can not hope to be entirely accurately representative of real world conditions for a significant proportion of the time. Further limitations involve the accurate entry of the scene into the program, specifically with regard to geometry and photometric properties. Whilst there are means of minimising error (through use of technical drawings, manufacturers data etc.) one must be mindful that the model is, and can only be, a representation of the real space.

The two means for illuminance derivation form a symbiotic relationship, the limitations of each method compensated for by the findings of the other. A schematic diagram illustrating the methodology strategy for the thesis can be seen in Figure 3-1.

Finally, the methodology and findings from the two case study buildings are applied to computer modelled roofs to examine the effect of roof type and to configure the photographic process (Chapter 7). This technique is then applied to several real buildings as a demonstration of its workings.

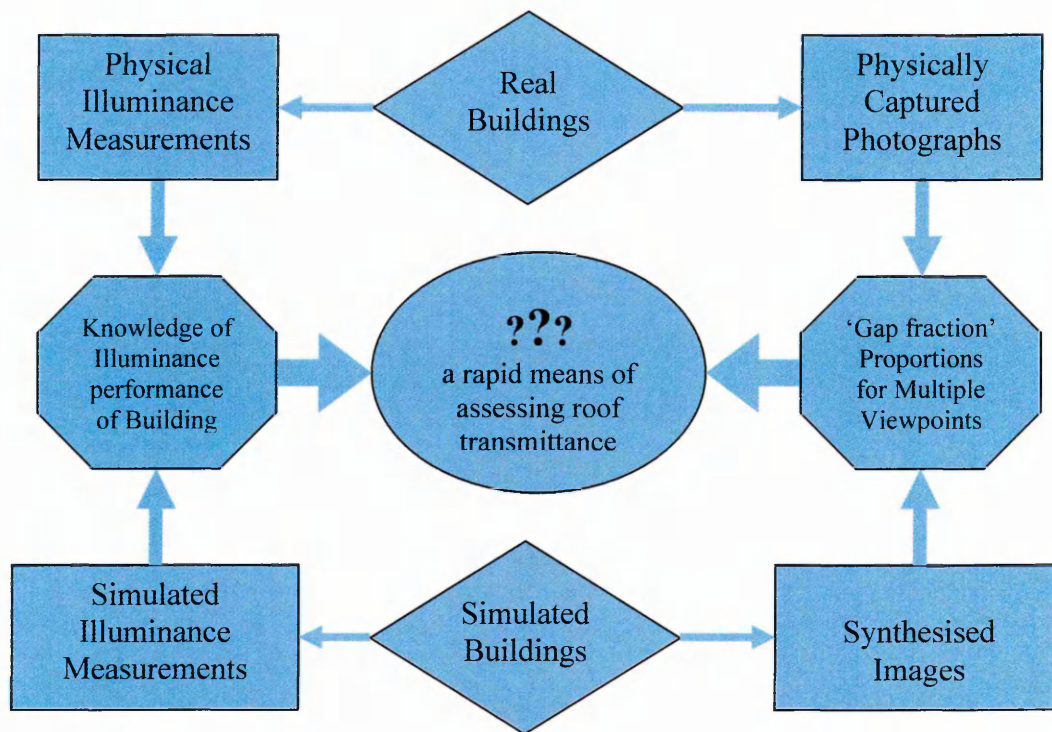


Figure 3-1: Schematic of methodology for this thesis.

3.3 Physical Measurements

3.3.1 Measuring Roof Transmittance

The transmittance of a transparent roof system at a point below the roof is the amount of light flux which passes through the system at that point relative to a 'no roof' scenario. It is expressed as a fraction or percentage. Under changing sky conditions, and hence differing luminous distributions, the value for the transmittance may vary. As has been discussed in Chapter 2, this study will consider overcast conditions. It can be seen that the equations for daylight factor and transmittance are very similar;

$$DF = \frac{E_{IN}}{E_{OUT}} \times 100\% \quad [3-1]$$

$$T_{ROOF} = \frac{E_{ROOF}}{E_{OPEN}} \times 100\% \quad [3-2]$$

where,

DF = daylight factor

T_{ROOF} = transmittance

E_{IN} = internal illuminance

E_{OUT} = unobstructed external illuminance (diffuse illuminance)

E_{ROOF} = illuminance immediately under roof

E_{OPEN} = illuminance immediately beneath where the roof system would potentially sit.

To physically measure a daylight factor at a point a photocell is normally positioned at that point, and a further one close to that point, with an unobstructed view of the sky. Usually this is achieved by placing it high above the ground plane e.g. on the roof of the building.

The process for measuring roof transmittance in a real building is similar. In practice it is not possible to measure the illuminance minus the roof without removing the roof (or measuring during the construction phase before the roof has been added), which is clearly impractical. The external photocell is therefore positioned as close as possible to the internal measuring position(s) on the outside of the roof system (Atif et. al. 1998).

The points(s) of internal measurement pose a greater conundrum. The plane in which the measurements should take place is immediately where the walls end, and the roofs begins i.e. at the top of the well, directly underneath the roof. The transmittance value will not be the same at every point on this roof plane. In an ideal scenario, values will be available at every point on the plane, and transmittance characteristics of the roof can be expressed as averages or with regard to distribution. Clearly this is impossible in terms of resources and the practicality of fixing large numbers of photocells over a high drop within a large bound area. As an aside, they would create a new physical plane near to the roof which would influence the results due to inter-reflection between photocells and roof. Redefining 'every point on the plane' as a very fine grid, the next best thing would be to have a coarser grid whereby results again could be expressed as an average, or distribution could be investigated through interpolation between grid points i.e. contours. The number of points in the grid would

represent measuring positions, with a finer grid giving a more complete picture. Again, this is impractical to perform in real buildings or even in scale models, which have a tendency to produce inaccurate results when dealing with fine components near openings, such as atria roofs (Cannon-Brookes 1997). This kind of analysis is much simpler with the aid of computer models, where real world practicalities can be bypassed. Such an analysis is described in Chapter 6.

For these physical measurements, it was not practical to suspend a grid of photocells over a large drop. The experiment is limited to taking internal illuminance measurements at one point. The exact location is of importance, and will vary from roof to roof, though its aim should be to capture the typical roof transmittance. Ideally this could be at the centre, though any area where the photocell 'sees' a typical configuration of that roof is deemed acceptable. The corresponding computer model point can be configured against the measured internal value, and subsequent adaptations to further model point values can be made.

A fundamental difference between measuring daylight factor and roof transmittance is that daylight factor considers light flux from any source of internally available luminance, be it a wall, a window, the floor etc. In measuring the transmittance of the roof we are concerned only with the impact of the roof. Unfortunately, the photocell can not discriminate between the origin of the flux, and so measured values are likely to be higher than the actual real transmittance value of the roof. Once again, the use of a computer model can help to overcome this shortcoming. In specifying the reflectance of any non-roof related surface as a pure light sink (reflectance=0%), the relative contribution from the well can be derived, and hence subtracted from the physically measured data. A further source of unwanted light flux is any artificial lighting system. Taking measurements at night (i.e. no daylight contribution) leaves only the contribution due to artificial lighting and again this can be subtracted from the daylight hour values (Atif et. al. 1998).

3.3.2 The Hardware

The illuminance data was measured using Skye Lux sensors (SKL 310) attached to DataHog 2 loggers (Figure 3-2). The exact pre-configuring of the photocells and loggers are detailed in Appendix A.



Figure 3-2: Skye DataHog and internal photocell used to measure and log illuminance.

Errors with photocells occur due to a number of factors (Hayman 2003). The use of a filter to fit the sensor to the V-lambda function, as is necessary to simulate the human visual response (i.e. photometry), has associated errors (recommended at 2.5% in the IDMP measurement guide) and may deteriorate over time due to bleaching. The photocells used in this experiment were brand new. The filter fitted to these sensors matched the CIE Standard Observer Curve to a high degree of accuracy (Figure 3-3).

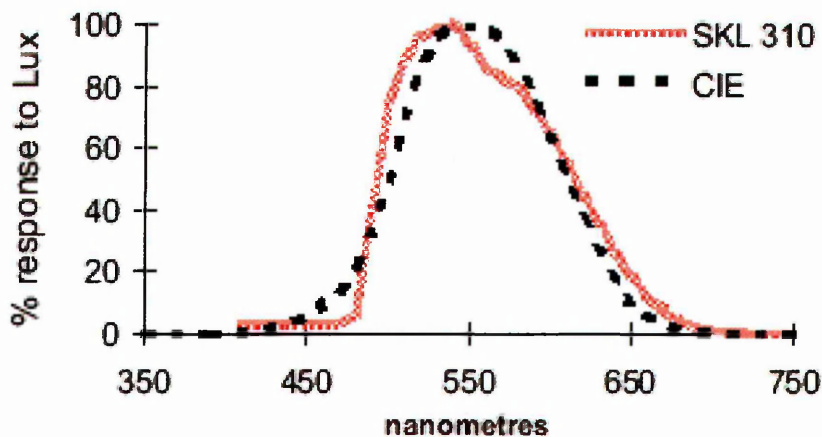


Figure 3-3: Response curve of SKL 310 photocell used relative to the CIE standard curve. The agreement is good (<http://www.skyeinstruments.com/>).

Photocells are also sensitive to temperature changes. More sophisticated hardware comes fitted with heating and cooling components to keep the temperature surrounding the cell constant (to $\pm 1^{\circ}\text{C}$), though the cells used in this experiment did not have such control. Error without temperature control could be up to -4.0% and $+2.4\%$ in Sydney (Standards Australia. AS1680.3). The accompanying literature stipulated a temperature coefficient of $\pm 0.1\%/^{\circ}\text{C}$. Photocells must also be cosine-corrected, to account for flux that is reflected off the cell at high incident angles to the surface normal. An uncorrected photocell characteristically under predicts illuminance.

Care must be taken in set-up to ensure the photocells are aligned to the horizontal (the direction of the measuring plane). This is more critical for high incident angles. For a photocell only 2° out from the horizontal, errors of up to 13% may occur for light at an incident angle of 75° (Hayman 2003). The literature for these specific sensors specified a 5% maximum cosine error to 80° . In this study, the intensity of light is stronger from zenith angles (three times greater than that of the horizontal, as is the attribute of a theoretically completely overcast sky), and so this error is not as significant as it could be, say if we were measuring vertical illuminance at the various cardinal points, or low altitude direct illuminance. In each case every effort was made to ensure the photocells were as level with the horizontal as possible.

Illuminance was measured every 30 seconds, and these values averaged and logged at 10 minute intervals. The 20 value per log averages (600s/30s) minimised the effects of erroneous single readings, and gives a clearer picture of changing sky conditions. For the constant overcast skies used in this study, it was expected that fluctuation would not be great over 10 minute periods. This logging period permitted 10.9 weeks of data storage before the memory bank of the loggers became full. Results were downloaded remotely in the first case study to ensure the equipment was functioning accordingly. This was not possible in the second case study, and thus the 10.9 week memory capacity was needed to obtain a sufficient number of acceptable skies.

Data from the loggers was downloaded using an RS232 cable and the associated specialist software SkyeLynx special edition. It was then exported to Excel where analysis could be made.

3.3.3 The Case Study Atria

3.3.3.1 *Selecting the Case Study Atria*

In ideal circumstances there would be sufficient time, resources and permission to conduct comprehensive experiments to isolate the effects of the following parameters on roof transmittance;

- geographical location (line of latitude)
- climate
- sky conditions
- external obstructions
- roof form
- materiality of roof (structure, glazing, shading)
- well properties

The scale of the project meant limiting the number of case studies from which illuminance measurements could be made. A major limitation in the availability of atrium roofs for this experimental work was the co-operation of the building owners. The use of real working buildings raised issues of health and safety in terms of the experiment protagonists during set-up, and to the general public from overhead logging equipment for its duration. An additional issue was the security of the equipment from the public with regard to deliberate or accidental sabotage. It was decided to study two atrium scenarios, one a simple linear A-frame roof, the other introducing more complexity, a monopitch roof which experienced over shading from large surrounding buildings. The roofs chosen were both part of this institution (Sheffield Hallam University), which greatly facilitated the proceedings with regard to access. A further advantage was the ready availability of architectural drawings, from which computer models could be generated.

3.3.3.2 *The Sheaf Building: A Simple Scenario*

3.3.3.2.1 *A Description*

The 'simple' case study used in this study was the Sheaf building, home of the School of Engineering at Sheffield Hallam University, which was completed in 1993. For a city centre site, the roof is relatively unobstructed, with the Owen building to the west obscuring a very small proportion of the sky dome. It is a 4-storey linear atrium, oriented east-west along its major axis. The approximate dimensions are 27m x 6m x 19m. The well is stepped in section, and has walkways crossing the width of the well about half way along its length. The roof is a simple A-frame structure, with large I-beams supporting a network of transoms and purlins. All structure is white steel, and the openings are double glazed. The surfaces of the well are predominantly white. The well and roof are shown in Figure 3-4, a-f.

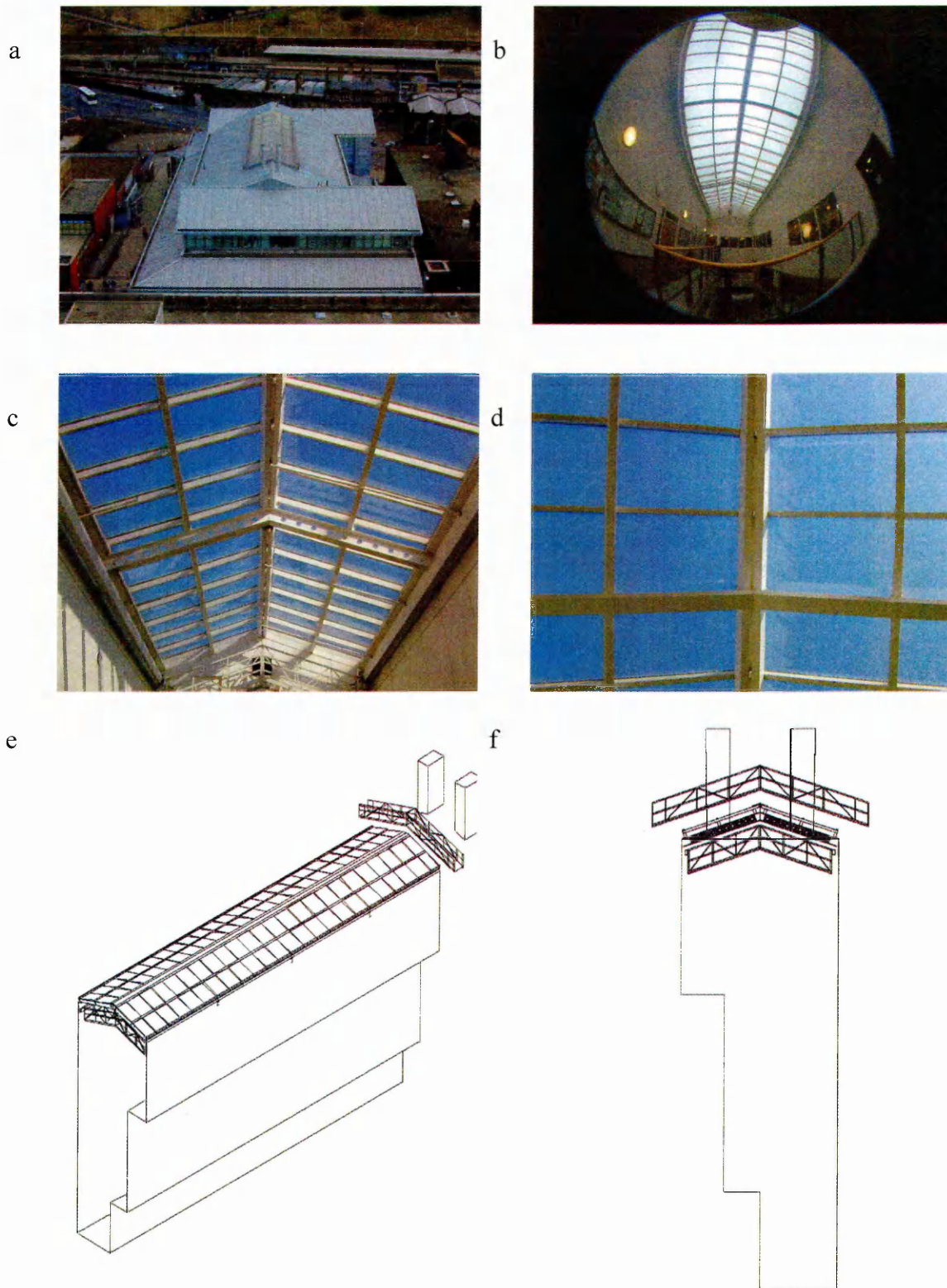


Figure 3-4: The Sheaf building: a. overhead view; b. internal fisheye view; c. the A-frame roof; d. roof panes close up; e. axonometric; f. section.

3.3.3.2.2 *Set-up and Rationale*

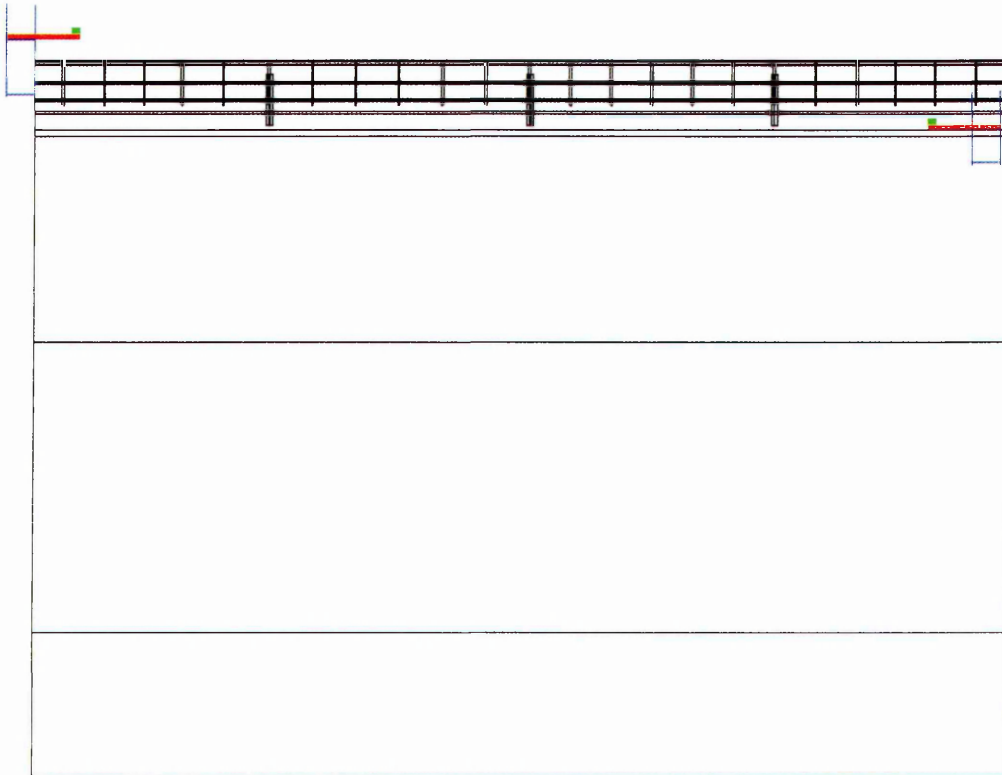
There were not many possibilities for the placement of the internal photocell. No point in the roof plane corresponded to solid surface underfoot. The nearest 'easy' possible location for the photocell was on the 3rd floor walkway, over 6m beneath the roof plane. At this depth, the influence of the well surfaces would begin to overshadow any conclusions drawn with regard to the roof transmittance. The only possible position at roof plane level would involve the use of the internal window cleaning gantry. This gantry was housed at the east end of the well. Theoretically, the gantry moves along the entire primary axis of the well, meaning that logging could take place at the centre if the gantry was 'parked' there. Permission for this was denied, both in terms of leaving the gantry parked at the centre of the well, and in terms of getting down and back up from the gantry at set-up/equipment removal time.

The photocell was safely fixed to a 2m long support that cantilevered 1.2m out from the gantry (see Figures 3-5, a-c). The photocell was just off the main central axis as viewed in plan, and level with the top of the well as seen in section. The repeating nature of the roof structure meant that it was likely results would have been similar from any point along the primary axis of the roof. Expected results may have been lower at the ends due to the influence of the end wall surfaces, as in this case. This observation was noted and any conclusions drawn must state this point. It is important to reiterate that the overcast illuminance measured, and derived daylight factor, is representative of daylight factor (transmittance + influence of well surfaces) at that point, and not of the entire roof.

The external photocell again took advantage of a window cleaning gantry as a point from which the photocell could be fixed. The same configuration (1.2m cantilever) as for the internal photosensor was used for the external photocell (see Figures 3-5 a, d & e). The photocell did not therefore see a totally unobstructed view of the sky vault, having three sources of obstruction; the window cleaning gantry, two slender flues from the Sheaf building and the Owen building as discussed previously. This would return slightly lower illuminance results than for a totally unobstructed photocell, and therefore lead to a falsely high daylight factor output. The extent of this magnitude was examined by obtaining the percentage of the sky vault as seen from the

external photosensor. A view from the photocell was generated with the rendering program Radiance of a CAD model of the Sheaf building and its surroundings, which was then processed in HemiView (these programs are discussed in Sections 3.4 and 3.5). This image can be seen in Figure 3-5, e. The value of visible sky was found to be 96%, that is to say, the obstructions block out 4% of the sky vault. If the sky had an even luminance distribution, we would expect subsequent external illuminance values to be 4% lower than for a completely unobstructed sky. These obstructions are situated towards the horizon of the image. The overcast skies under investigation are typified by luminances of thrice the intensity at the zenith angle than at the horizon. Coupled with small gains from the obstructions due to light reflection, the magnitude of illuminance loss is much lower, 2% would seem pessimistic. This is a relatively minor error.

a.



b.



c.



d.



e.

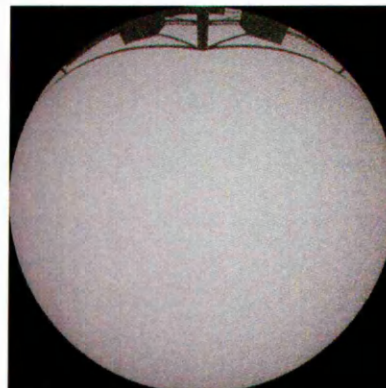


Figure 3-5: Location of Sheaf photocells: a. section - the photocells are located on service gantries at the left (external) and right (internal) ends of the well as seen on the page; b. view of internal logger; c. fisheye view from the internal logger; d. view of external logger; e. computer generated fisheye view from external logger.

3.3.3.3 *The Owen Atrium: A more Complex Scenario*

3.3.3.3.1 *A description*

The more 'complex' case study used in this thesis was the central atrium at Sheffield Hallam university. Constructed in 1993 (at the same phase of construction as the Sheaf building), the atrium's aims were to unite current blocks of accommodation from the late 1950's with new accommodation to form a recognisable 'heart' for the university and a 'reservoir of circulation' (Caldwell et. al. 1994). The existing accommodation consisted of three blocks of 5, 8 and 12 stories, the tallest of which, the Owen building, is the name for which we will refer to this case study.

The atrium is five stories deep and has approximate well dimensions of 50m x 18m x 16m whose major axis is oriented north-south. The atrium roof experiences over shading from the 12-storey high Owen building to the west, which climbs between five and seven stories above the well. The roof is a space deck structure whose load is transferred to steel columns so as to be structurally independent of the surrounding existing and new accommodation (Figures 3-6, b-d, g-h). The roof is monopitched and slopes towards the Owen building solving problems of solar access and smoke evacuation, though proved complex with regard to the potential for heavy snow loads to develop in the valley formed at the edge of the Owen building, and in terms of movement joints (Figures 3-6 a & g). The primary sides of the well consist of circulation walkways with adjacent accommodation to one side, and windowed classrooms to the other (Figures 3-6 e-f). The minor ends of the well contain large freestanding vertical circulation (south side), and circular seated areas (north side) respectively. The uppermost floor located above the classroom block forms a platform (used as an eatery) that is open to the roof (Figure 3-6 c).

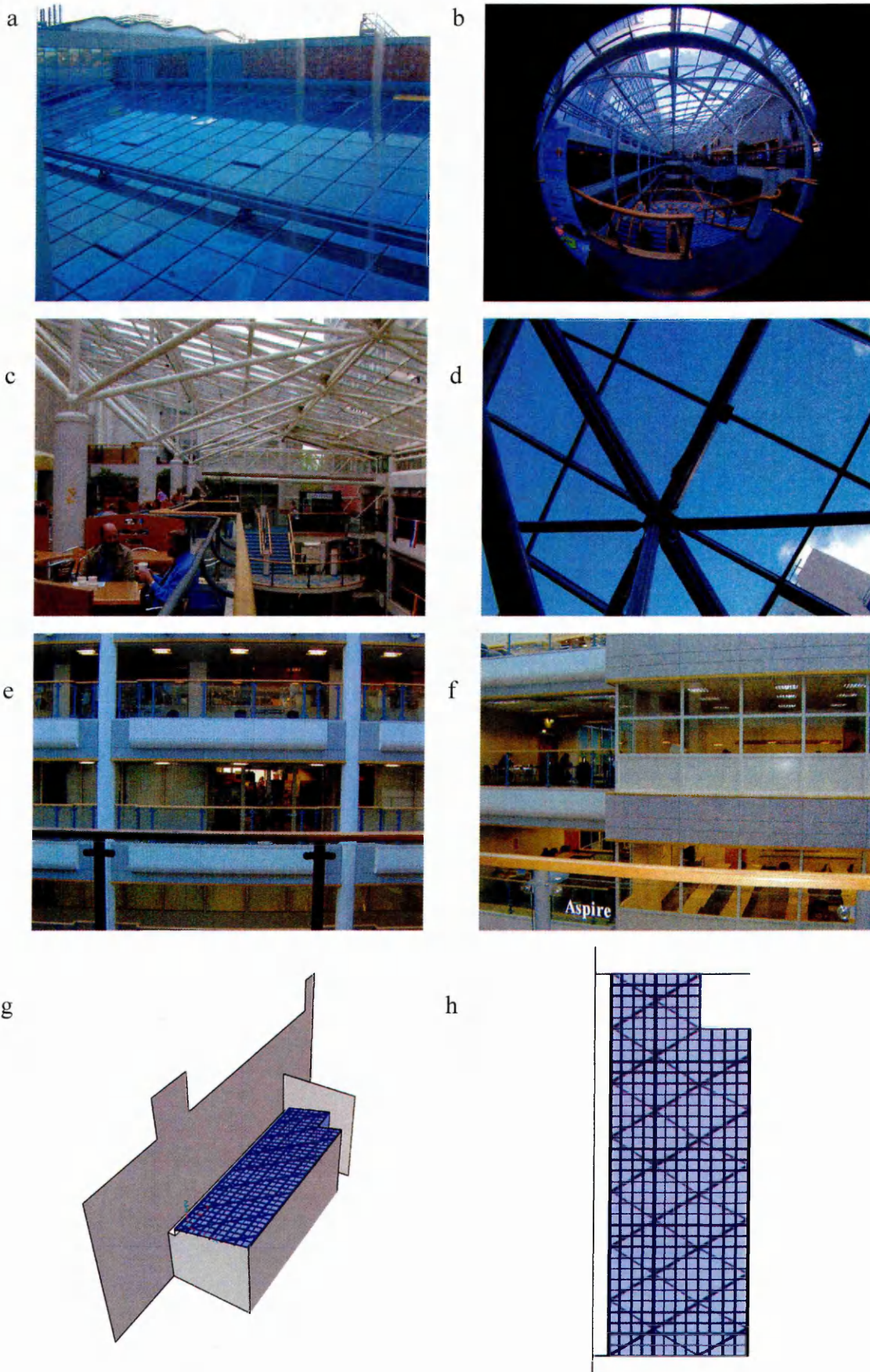


Figure 3-6; The Owen Building: a. external overhead view; b. internal fisheye view; c. internal view of space frame roof; d. close up of roof detail; e. adjacent corridors (west side); f. adjacent classrooms (east side); g. axonometric; h. roof plan.

3.3.3.3.2 Set-up and Rationale

The monopitched nature of the roof raises the issue of whereabouts within the vertical space of the roof volume to take internal measurements from. With other roof types, for example flat, A-framed (like the Sheaf) or pyramid, it is elementary that the measurement plane should if possible occur where the walls meet the roof. In this case, the roof meets the wall at different vertical displacements, and so the positioning measurement point in the Z-plane is not implied (Figures 3-7 a-c). Taking measurements from a low height (3-7 a) there is most potential for the influence of reflected flux from the higher facing wall. Taking measurements from a high position (3-7 c) misses out on seeing most of the roof with the photocell positioned horizontal. Somewhere in between (3-7 b) suffers from both of these drawbacks, but to a lesser extent for each.

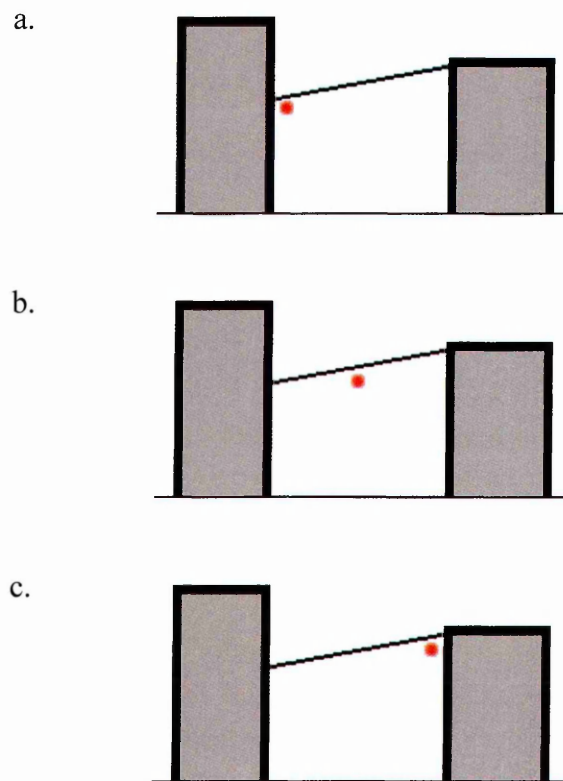


Figure 3-7: Potential depths within the roof from which 'transmittance' could be measured.

There were two potential locations for the internal measurement, without introducing undue practical difficulties (the space framed nature of the roof meant internal window cleaning gantries could not traverse the length of the roof, and hence

were not included in the final building designs). The first of these was around a walkway and balcony at the southern end of the well that crossed it at its uppermost point. Whilst this location was at the desired potential height within the roof volume, there were two shortcomings. Firstly, it was heavily under the influence of immediately adjacent side glazing, and a stepped 3-sided glazed atrium to the east. Whilst this was not necessarily a problem with regard to later comparison to the photoanalysis technique (indeed side apertures could form a direction for further investigation), this study focuses on top lit spaces, and this point of measurement represented too strong a divergence from this path. The second shortcoming was the access to the public of the walkway increased the likelihood of experimental sabotage.

The other possible measurement point was at the other end of the atrium (north side) located on top of a block of accommodation adjacent to the upper floor platform (Figure 3-8 a). Whilst there was also the presence of side glazing at this point of the atrium (the formation of the atrium through glazing a courtyard between several building masses meant that there were regions of vertical glazing at several points within the atrium), it was not in direct view of the measuring point. Access to the measuring point was via a service ladder, and thus the potential problem of public interference was avoided. The logger was fixed horizontally to a customised tripod 1.2m above the floor of the block, such that it cleared the height of the immediately surrounding handrails. It was positioned directly underneath a main axial beam, 1m in from the edge of the block. This was deemed to be the most appropriate position within the possible bounds of the block, with other locations being too close to side walls to see the roof sufficiently, or in direct line of the side glazing. A photo of the set-up and photocell view can be seen in Figures 3-8 b & c.

With the unobstructed case, one external photocell position sufficed. In this case, the influence of the Owen building was so great as to necessitate two measuring points. One of these would measure the unobstructed illuminance; the other just outside the glazing would measure an external obstructed illuminance value. By dividing the internal illuminance with the unobstructed external illuminance, the daylight factor in its traditional guise is derived. The obstructing Owen building is treated as part of the 'roof system' when the argument from a roof transmittance stance is made. In dividing the internal illuminance by the obstructed external illuminance, the effects of the roof

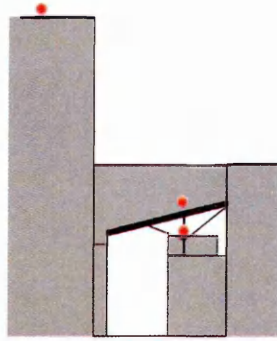
canopy (glazing and structure) are highlighted, and hence gives a closer value to 'transmittance' of roof if that roof were unobstructed.

The positioning of the obstructed external photocell should be as close as possible to the internal photocell. As in the Sheaf building, this photocell was fixed to an external window cleaning gantry that was accessed from a roof-side walkway. Unlike in the Sheaf building, the logger was fixed horizontally to a support running between the handrails of the balcony, thus avoiding obstruction from the gantry itself. The gantry was almost directly above the internal measuring point as viewed in plan (can be seen from internal photocell view (Figure 3-8 c)). The set-up configuration and photocell view can be seen in Figures 3-8 d & e.

The external unobstructed photocell should see 180° of the sky dome. This logger was fixed to a high part of the roof of the Owen building. The set-up configuration and photocell view can be seen in Figures 3-8 f & g. The minor obstruction in the field of view is due to the protrusion of the lift shaft through the roof surface. Access to the top of the lift shaft for measurement was not possible.

The Owen atrium deploys artificial lighting that operates throughout the day. As has been mentioned earlier, this potential source of error was resolved by subtracting the 'night' illuminance values from those measured during daylight hours.

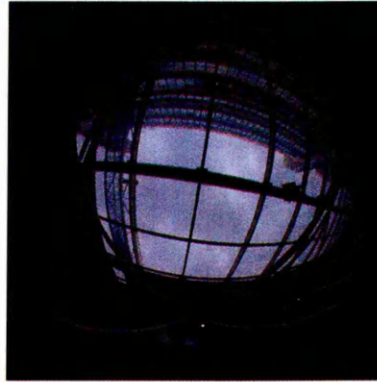
a



b



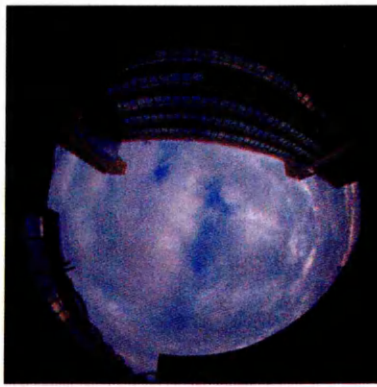
c



d



e



f



g

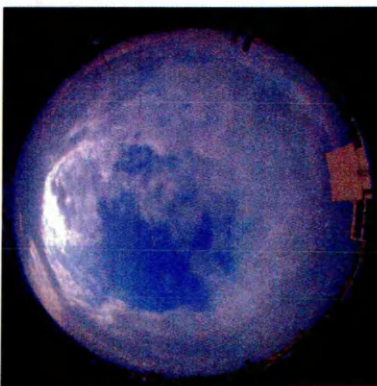


Figure 3-8: Location of Owen photocells: a. section - the internal photocell is located on top of a small block of accommodation, immediately beneath the roof. The obstructed photocell is fixed to a servicing gantry immediately above the internal photocell, on the outside of the roof. The unobstructed photocell is positioned at the top of the Owen building; b. view of internal logger; c. fisheye view from the internal logger; d. view of obstructed external logger; e. view from obstructed external logger; f. view of unobstructed external logger; g. view from unobstructed external logger.

3.3.4 Running the Experiment

3.3.4.1 Logging the Weather Conditions

Throughout the course of the logging period, a weather log was kept so as to ease the classification of sky types. Though it was found a graph of the external illuminance (in form and scale) was perhaps the most reliable guide to determining the sky conditions, the log provided a useful secondary source. Sky conditions were noted at three hour intervals from 9 a.m. to 6 p.m. The sources used were the Met Office¹, Metcheck² (for sky cover percentages), Yahoo weather³ and spot checks from the author. Results of the log are detailed in Appendix B.

3.3.4.2 Length of Logging Period

As mentioned in section 4.3, the logging capacity of the instrumentation at 10 minute logs was 10.9 weeks. A longer logging period was obtained in the Sheaf building as the results were downloaded at regular intervals. Measurements were conducted over the summer months in the Sheaf building (due to issues of access) and so a longer period was needed to obtain a sufficient number of overcast skies. Logging took place between the months of June and October 2002. 91 meaningful days were obtained over this period. Measurement in the Owen building was conducted within the 10.9 weeks (no downloading, due to practicality of roof access) with measurements occurring between February and April 2004. 68 meaningful days were obtained over this period.

¹ <http://www.met-office.gov.uk/education/archive/uk/>

² <http://www.metcheck.com/>

³ <http://weather.yahoo.com/forecast/>

3.4 Photoanalysis with HemiView

3.4.1 The HemiView Software

3.4.1.1 Hemispherical Imaging: A Background

The first hemispherical or *fisheye* lens was designed by Hill (1924) to assess cloud formation over the entire sky vault. The technology was soon adopted by architects for site investigation, and ecologists for studying the lighting environment under forest canopies (Evans & Coombe 1959). These early methods involved overlapping diagrams of sun paths onto the photographs. The first computerised program to analyse hemispherical imagery was called PISCES (Jupp et. al. 1980). Subsequent advances in information technology have led to increasingly advanced and user-friendly hemispherical imagery analysis packages. One of the most current of these is HemiView developed by the Helios Institute in Kansas, USA. The most recent release, version 2.1 is fully Windows compatible, supports a full spectrum of standard image formats and has configurable output to standard spreadsheets⁴. Whilst HemiView is used predominantly in the field of ecology, this study will apply the software to internal manmade environments.

3.4.1.2 HemiView: The Process

The first step was the acquisition of a hemispherical image. The photographs were taken using a Nikon Coolpix 950 digital camera, with fisheye lens adaptor (though this could be substituted for a traditional camera with film, which is then scanned in to a computer) (Figure 3-9).



Figure 3-9: Nikon 950 Coolpix camera with fisheye adaptor

⁴ Further information from HemiView manual pages and <http://www.delta-t.co.uk/>

The lens should sit completely level with the horizontal, with the operator beneath the lens, such that he is not captured in the image. The images should be referenced to magnetic north, though as the only output we will concern ourselves with is gap fraction (i.e. proportion of visible sky) which is calculated independently of orientation this step has been ignored. The ideal conditions under which the photograph should be taken are evenly overcast skies. This is so that contrasts within differing parts of the sky are minimal, thus facilitating the differentiation between sky and blockage. The presence of the sun in the image will result in high contrast within the sky, and potentially make blockage that is being directly illuminated by the sun appear as visible sky. The presence of clouds will result in contrast, making classification potentially problematic. If it is not possible to obtain an image under overcast skies, then just before sunrise or just after sunset are recommended, such that the sun is not in the field of view.

Once the photographs had been obtained, they were downloaded onto a computer and using Paint Shop Pro 6, any area of the image that was not under consideration (i.e. not part of the fenestration system) painted red. This was so that HemiView could 'ignore' these regions in its calculations. The image was saved as a bitmap, and opened in HemiView.

From the main screen the horizon circle was resized and dragged to cover the area of the photograph (Figure 3-10 a). Splitting the window enabled the circle to accurately and rapidly fit the image (Figure 3-10 b). As we were only concerned with the gap fraction output, various inputs, such as the date and geographical location could be ignored. HemiView has the capacity to calculate direct radiation arriving at the point of the lens, though a study of direct insolation was outside the scope of this study. This could be useful for future work, if sky conditions other than overcast are investigated.

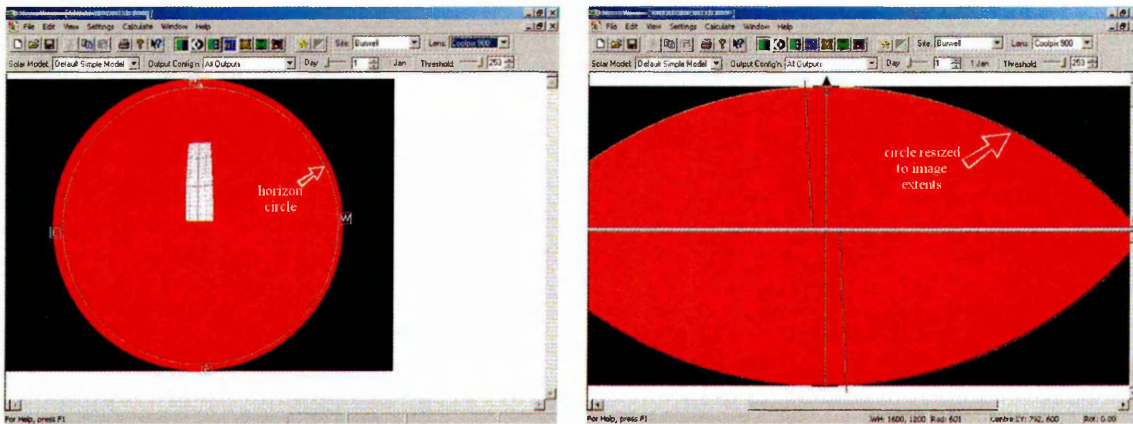


Figure 3-10: a. The horizon circle is resized to fit the arc of captured image; b. Splitting the window ensures accuracy of fit.

The appropriate lens is chosen - in this case the Nikon option (a linear 180° i.e. angular and Sigma 8mm are also available). This is necessary to correct for distortion in mapping from the zenith angle in three dimensions to the radius on resultant two dimensional images. This works via the application of a lens correction function, which comes in the form of a polynomial whereby the function passes through a radial distance of zero at a zenith angle (Θ) of 0° , and through radial distance 1 (i.e. the exact length of the radius of the two-dimensional image) at a zenith angle of 90° . A zenith angle of 0° corresponds to the horizon, whilst a zenith angle of 90° is in a directly upwards direction (Figure 3-11).

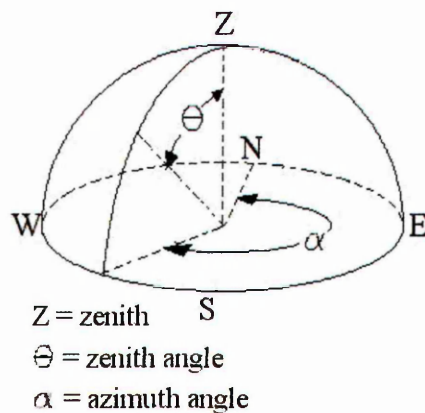


Figure 3-11: Terminology of sky dome (redrawn from HemiView manual p.7)

The correction function can be derived empirically or using information supplied by the lens manufacturers. An example of the correction function can be seen for the Sigma lens in Figure 3-12. The dotted line represents an angular lens, that is, a lens whereby the zenith angle is directly proportional to the zenith angle in the image.

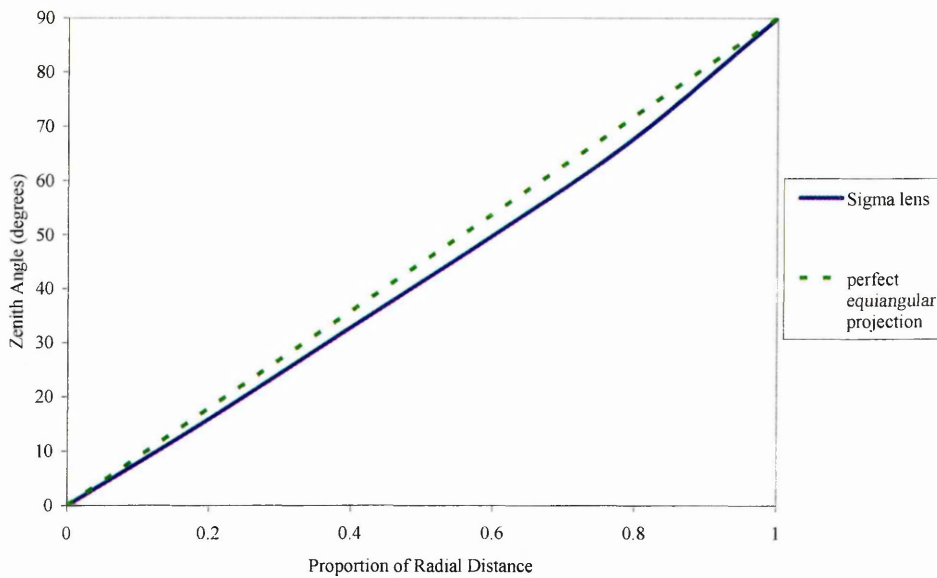


Figure 3-12: Correction factor applied by HemiView to actual camera lenses. The dashed line represents a theoretically perfectly equiangular projection (redrawn from HemiView manual p.9).

The image was then ready for classification. Firstly, the classifier menu was opened, and the option to 'ignore red' checked as previously discussed (Figure 3-13). HemiView uses a simple efficient threshold algorithm to classify an image. To quote from the manual, '*classification is achieved by determining a threshold intensity value, above which is classified as visible, and below which is classified as obscured. This technique is also known as segmenting an image, in that it divides a set of grey levels (intensity values) into a binary classification*⁵. The rationale behind having even skies that crisply contrast with the roof structure, as detailed above, now becomes evident.

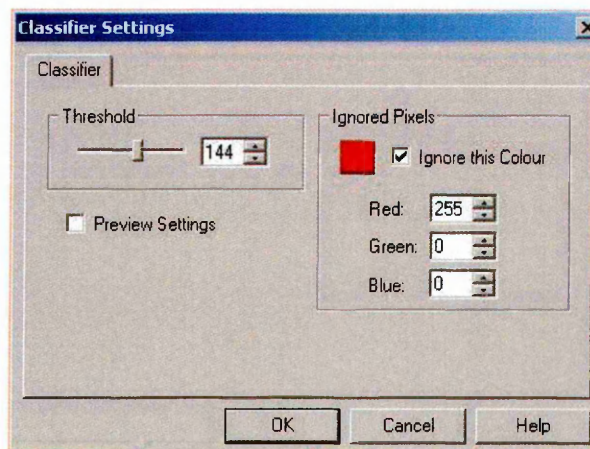


Figure 3-13: The classifier menu box. The threshold can be set, and the 'ignore red' option checked.

⁵ HemiView manual p.11

The simple method of classification makes the program fast and user friendly. However it lacks the intelligence to differentiate between, say, a dark patch of sky and light piece of structure that happen to have the same intensity. Much of the accuracy of the classification will rely upon the skills and consistency of the operator. A frequent ability needed is the fine judgement of visible sky gains in one part of the image to offset losses at other points. The classifying process is interactive. The screen can be toggled from the original image to the classified binary image and fine tunings made (Figure 3-14). A means of assessing the impact of the classification error is described later.

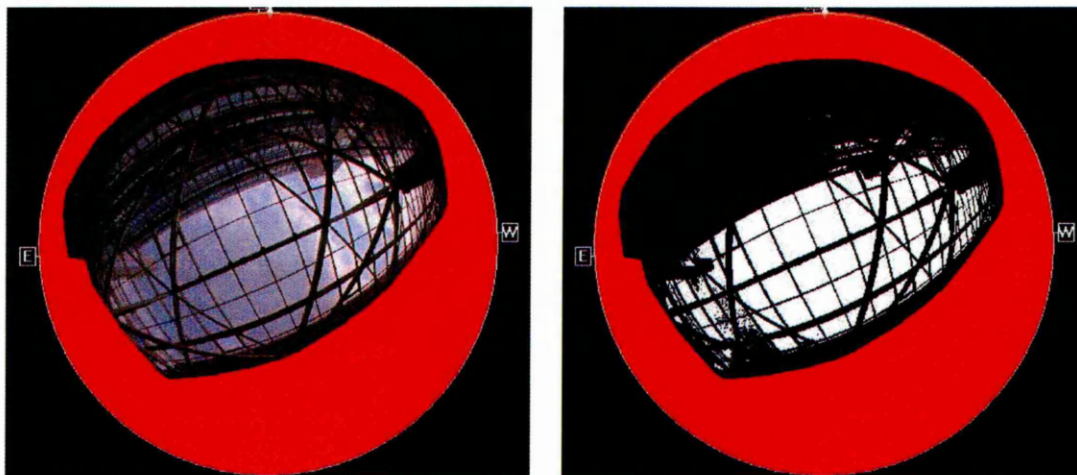


Figure 3-14: Toggling from the original image (left) to the classified image (right) facilitates the classification process.

Once classification is complete, HemiView is ready to calculate the output values. This is a speedy process, the calculations in this study taking no longer than about half a minute each. Output is sent to an Excel workbook. Toggling between the image and workbook is possible, such that amendments and re-calculation can occur, for example a change in threshold settings, or a change in date (perhaps for comparing solstice and equinox direct radiance). Opening subsequent images and calculating in the same manner sends the output to the same workbook, such that a whole series of images can easily be analysed collectively.

3.4.2 Methodology for Photo Derivation

3.4.2.1 The Base Position

An investigation into the premise that there exists a relationship between the transmittance of a roof and a fisheye image of that roof must begin with comparison between the transmittance measured at a point and an image captured from that exact point. In the first instance, a simple A-frame roof configuration in the rectilinear atrium well of the Sheaf Building at Sheffield Hallam University was examined. A value related to the transmittance of the roof was measured using photosensors positioned inside and outside the well. This measured value corresponds to the 'transmittance' as perceived from the point of the internal photocell i.e. suspended 1.2m over the well from an internal window cleaning gantry. Reasons for choosing this position have been detailed in Section 3.3. It is from here that a hemispherical image must be taken.

Taking a photograph from a position 1.2m over the edge of a high drop poses a practical challenge. At the time of writing there does not exist a reasonably priced manual shutter release for the digital camera. This is in contrast to manually operated cameras where a physical manual release mechanism is adopted rather than the more complicated electronic approach needed for digital camera apparatus. The only practical solution was to use the automatic timer on the camera. The Nikon 950 gives the option of a 3 second or 10 second timer. Regrettably, the facility for a user entered time is not supported. In practical terms, this meant that from the point at which the timer was set, there was a 10 second window in which to get the camera safely to the position of the photocell pointing directly upwards, and the operator to move beneath the field of view of the camera.

L-shaped profiled aluminium strips were fixed at either side of the support upon which the photosensor sat. A trolley was constructed from MDF which firmly supported the camera with the lens pointing directly upwards. The width of the trolley fitted securely within the aluminium strips, such that it smoothly and safely moved along the length of the support, as shown in Figure 3-15. The timer of the camera was set, and the trolley pushed out over the well to a position immediately adjacent to the photocell. It is appreciated that the centre of the lens is approximately 10cm displaced

from the ideal position (where the photocell sat), though this was unavoidable as the photocell and logger in its housing acts as the 'end of the line'. This left sufficient time for the operator to drop below the field of view of the lens. The trolley was retrieved using a cord fixed to its rear.

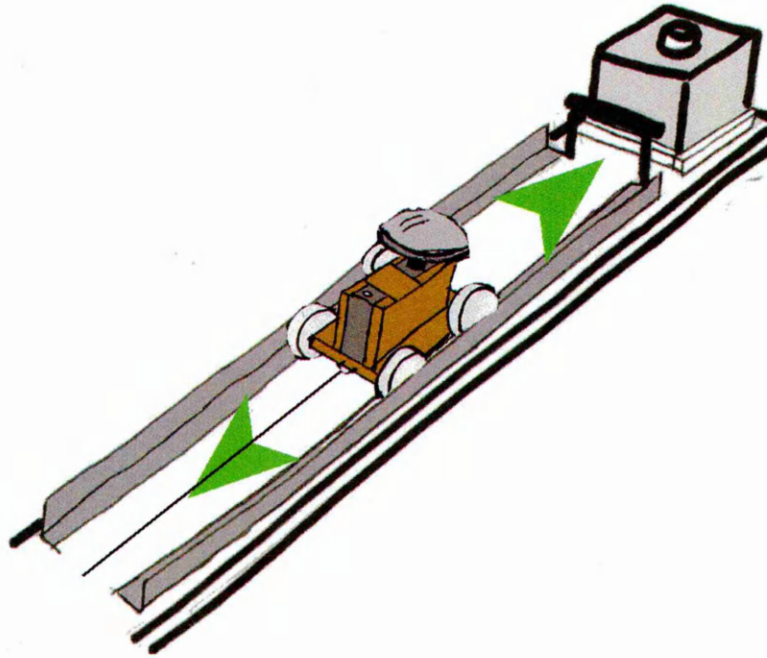


Figure 3-15: The trolley used to capture the image from the position of the photocell, suspended over the well.

The photo from the internal photocell position in the Owen building was by contrast far simpler to derive. A photo aimed directly upwards at the roof was taken manually from the exact photocell position under the supervision of a health and safety officer (due to access to high space).

3.4.2.2 Varying Location of Photograph

As can be seen the above methodology was challenging in many respects. It involved the time consuming construction of specialist hardware (in the case of the Sheaf building), as well as having to negotiate with the University's health and safety department with regard to accessing high spaces (in both cases). In many buildings the issue of access may prove to be an insurmountable obstacle, either as access may be refused, or that there simply are not the spaces in some buildings directly beneath the roof. If the method is to have any chance of success the whole process must be both

faster and with fewer complications. It is for this reason that photographs were taken from positions supplementary to that of the photocell position.

Within the Sheaf atrium photographs were taken from four further positions to the photocell position (S1). The first two were on the upper level walkway (level 3), in corner (S2) and central (S3) positions. In the case of this specific atrium, the walkway represented the least complicated and most rapid means of obtaining a photo close to the level of the roof structure. The corner position signified the closest match to the photocell position, whilst the central position was indicative of a field of view that perhaps encapsulates the fenestration system best (indeed if it were possible to suspend the photocell in midair, measurements would have been taken at the centre of the fenestration system). The second two were taken from the base of the well (level 0) at end (S4) and central (S5) positions. Some atria may not have circulation walkways within the well, and so the only place from which to take a photograph may be from the base of the well. Taking photos from these positions aimed to address this issue. The locations of these five viewpoints can be seen in Figure 3-16.

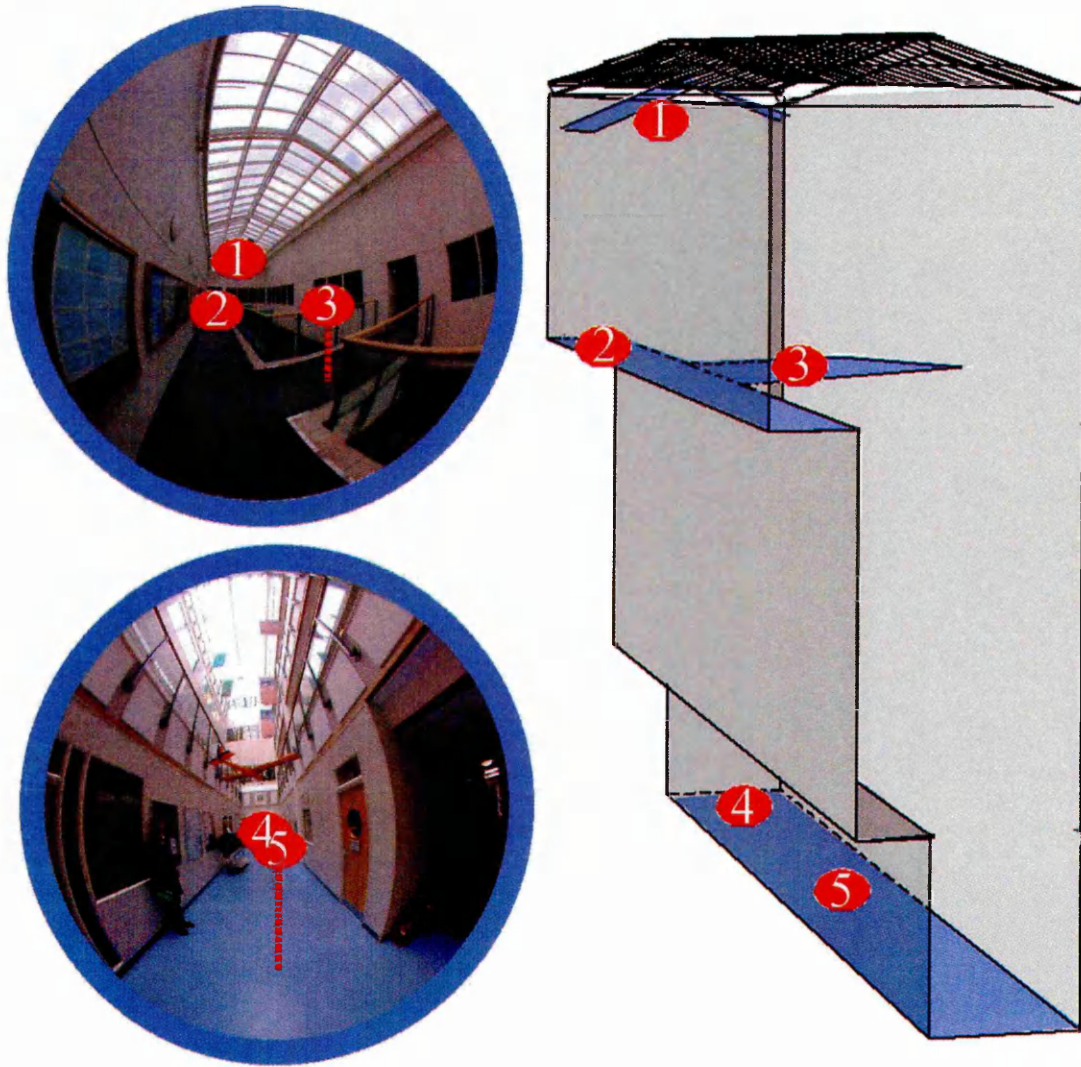


Figure 3-16: Photograph positions in the Sheaf building: S1 at photocell position, S2 & 3 top floor corner and centre, S4 & 5 ground floor end and centre.

Photos were taken at eleven supplementary positions to the photocell position image (O1) in the Owen building. From the same platform on which the photosensor sat, four further photos were taken (O2-O5). Each of these saw a slightly different arrangement of structure directly overhead. Two photos were taken from the high walkway at the other end of the well. The first was taken halfway across the bridge (O6) directly under a major junction of roof structural elements. The other was taken at the end of the bridge (O7). These photos represented the views from the opposite end of the well. O6 also represented the best approximation to accessing a position 'within' the roof section, being the most westerly of the positions measured along the minor axis, and sufficiently high up the well. Four photos were taken on the upper floor (O8-11). The first of these was towards the north end of the well on a seating platform. This

represented the best position to get to the centre of the well on the minor axis on the upper floor. The next three were taken from the cafe area that occupies the majority of the floor. The first of these (O9) was by the balcony at the edge of the well, the next (O10) in line (in the direction of the minor axis), in the centre of the floor space and the final one, again in line, by the end wall of the well (O11). These photos adequately sampled potential photo positions available on the floor. The upper floor is significant in that it represents the easiest way of getting close to the roof in most buildings (i.e. without the need to request access). The final photo (O12) was taken at the centre of the ground floor, as in the Sheaf building, to explore whether the technique could be extended to wells where the only access is at ground level. The positions can be seen in Figure 3-17.

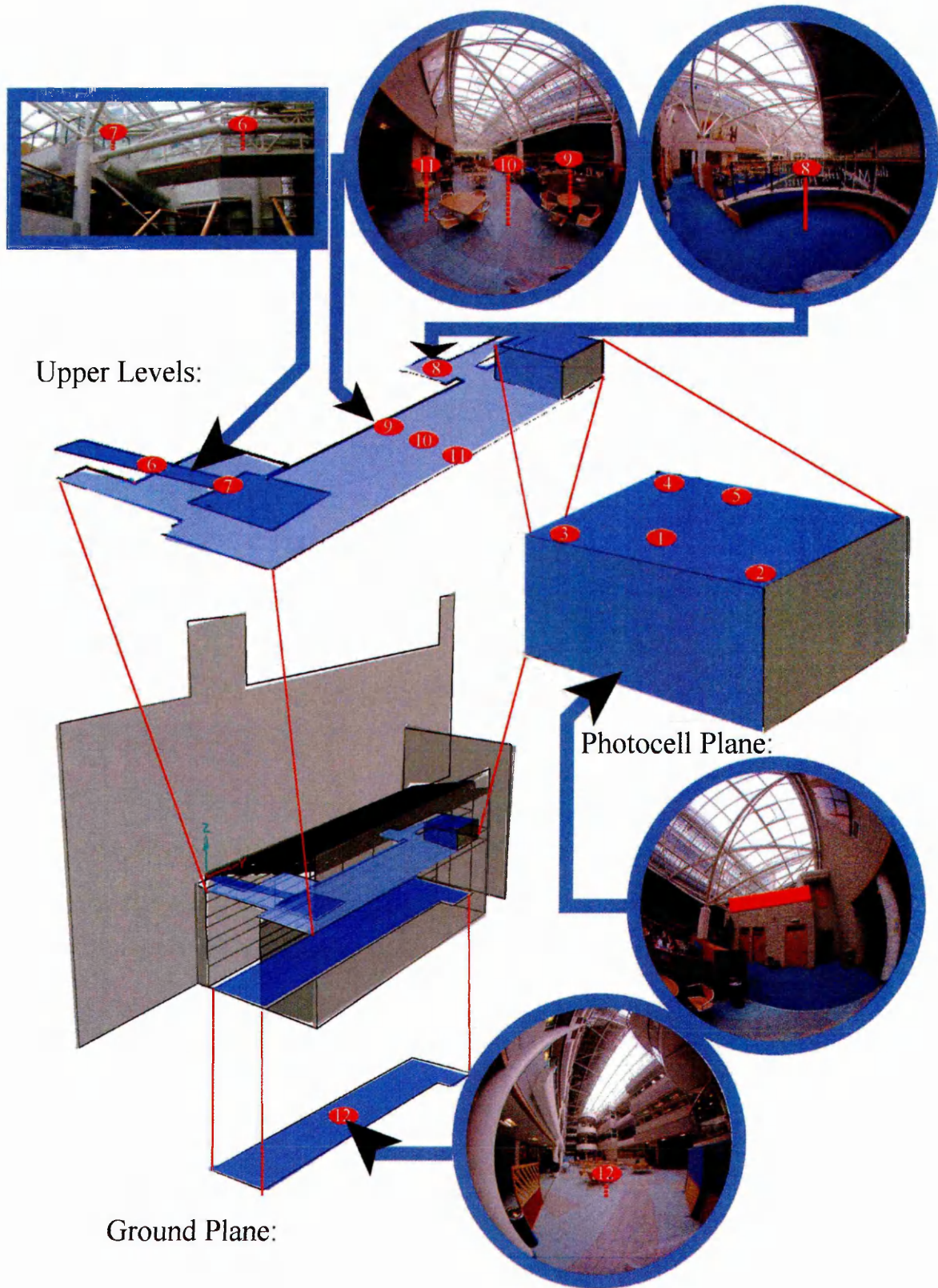


Figure 3-17: Photograph positions in the Owen building. O1 at photocell position, O2-5 photocell plane various positions, O6 & 7 on bridge centre and end, south end of well, O8-11 top floor moving west to east, O12 ground floor centre.

3.4.2.3 Varying Quality of Photograph

The resolution and quality of the image will have an effect on the ability of HemiView to analyse it. For these experiments, the highest setting (*hi*) of 1200x1200 pixels was used. In addition, some of the cameras quality settings were investigated, those being *normal* and *fine*. The *normal* and *fine* settings store the image as a JPEG file, that is to say it compresses the image. Clearly the *fine* setting will compress the image less than the *normal* image, though at the expense of taking up more space on the camera's memory card. The *hi* image is stored as an uncompressed TIFF file, and as such suffers from no loss in quality. Unfortunately for this scenario, there was only sufficient space on an 8MB memory card for one such photo, which could be problematic in the field if several photos are required. This problem can be avoided by having many memory cards, or downloading to a laptop on site (though this is a drain on battery power). It is appreciated rapid advances in technology have led to larger memory cards, as well as cameras with resolutions exceeding those of the camera used in these experiments, a camera that was considered 'top of the range' when purchased for this study. Photographs at each of the three qualities were taken from the four supplementary positions in the Sheaf building. Unfortunately, and due to the complexity of taking a photograph from the photocell position, only the *hi* quality setting was used. Varying the photo quality parameter was not investigated for the Owen building. All photos there were taken at the *fine* setting.

3.4.2.4 Processing the Image in HemiView

Once the photographs were downloaded they were opened in a paint program (Paint Shop Pro 6). The non-roof areas were painted red for reasons mentioned in section 3.4.1.2, and the images saved as bitmap files (compression leads to problems with HemiView recognising the red areas to ignore, and TIFF files are not supported). These will be referred to as *unadjusted* images. Still within the paint program, the images are then manually refined. For the Sheaf photos, areas of sky are flood filled with white, and where structure has been omitted in the images (perhaps due to a low quality, or region of sky brightness on the structure), it is intuitively drawn on in black. These images too are saved, and from now will be referred to as *adjusted* images. In their classified form at the *hi* camera accuracy setting, they may on occasion be referred

to as *reference* images, as they represent the 'correct' value for the roof. Similar *adjusted* images are created for the Owen building. These *adjusted* images were then manually adjusted such that the external buildings as visible from the camera position were painted white to produce an image as may be seen from an unobstructed site. These images will be referred to as *unobstructed* images (and the *adjusted* images may at times be referred to as *obstructed* in the case of the Owen building). This process can be seen in Figure 3-18.

The images were then opened in HemiView. For each Sheaf scenario (a certain image quality at a certain position) four HemiView calculations to obtain gap fraction were performed. Firstly, the *adjusted* image was analysed. Classification was unambiguous, as the pixel was either white i.e. sky, or non-white (/black) i.e. blockage. From the same scenario three calculations were performed from the *unadjusted* image; *classified*, *lower* and *upper*. The *classified* calculation was performed with the threshold set as close as possible to a description of the roof as the author saw it (i.e. the proportion of roof to sky in the total view appeared as close as possible to the proportion of blockage to gap in the classified view). The *lower* calculation represents the lower bounds at which the author believes a person may classify the image (all the structure appeared as black, possibly at the loss of some sky). The *upper* calculation represents the upper bounds at which the author believes a person may classify the image (all the sky appeared classified as white, possibly at the loss of some structure). The *lower* and *upper* values were used to assess possible sources of error in using the classifier on an *unadjusted* photo. There were thirteen scenarios comprised of the S1 (photocell) position taken at *hi* quality, and S2-S5 positions each taken at three qualities (*hi*, *medium* and *fine*). This gave 52 HemiView calculation outputs.

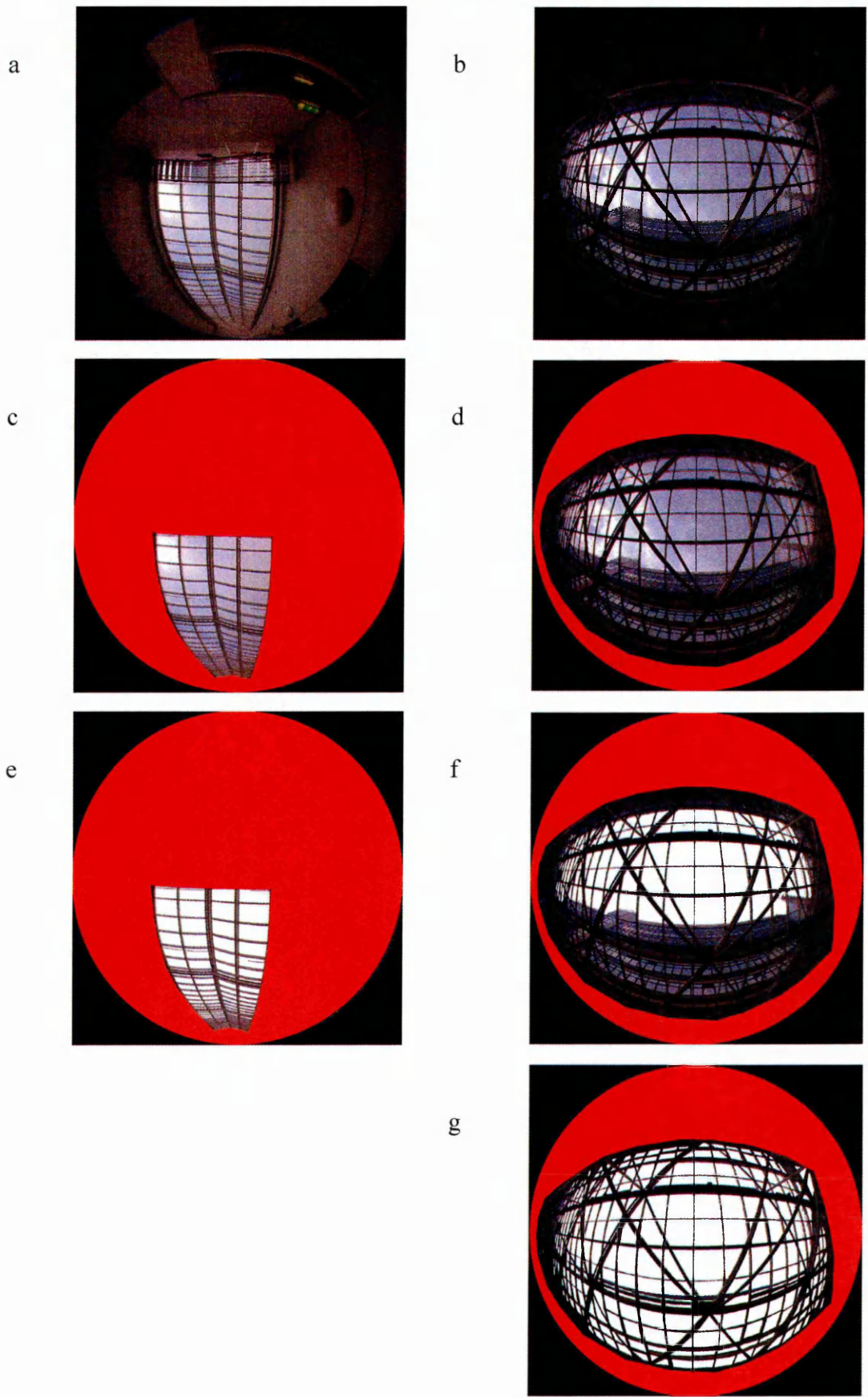


Figure 3-18: Processing the derived photographs: a. & b, original images (Sheaf, Owen); c & d unadjusted images (Sheaf, Owen); e & f adjusted images (Sheaf, Owen); g unobstructed image (Owen).

For each Owen photo position nine HemiView calculations were performed. The *unadjusted*, *adjusted* and *unobstructed* images were each classified to be as close a description of the roof as the author saw it, in a similar manner to the Sheaf building. It should be noted that for the *classified* results from the *obstructed* (*unadjusted* and *adjusted*) images the external obstructions were not classified entirely as blockage. An element of 'gap' was intuitively left to account for externally reflected flux contributions. This was possible due to luminance contrast about the obstructions as specularly reflecting window bands appeared lighter on the image. Without painting in the obstruction as black it would have been impossible to classify the obstruction entirely as blockage without the classification of most of the gap in the image as blockage too. Associated *lower* and *upper* bounds were derived through the same methodology. There were twelve photo positions (O1-O12), giving 108 HemiView calculation outputs.

The results are discussed in Sections 5.2 (simple case) and 5.3 (complex case).

3.4.2.5 *The Plan Area of Obstruction*

The plan area of obstruction (PAO) is the percentage of blockage of the roof when viewed from a plan perspective (focal point at infinity). Previous practice has been to take the PAO as a guide to the transmittance of a roof {BS 8206-2 p.21}. Later studies have shown this to be misleading {Sharples & Shea 1999}. The PAO's of the buildings in question were calculated by counting pixels using a standard utility from a plan image derived from CAD models of the roofs. The only significant source of error was the accuracy at which the models were drawn. The error is expected to be minimal. More traditional means of deriving the PAO include using standard measuring devices on architectural drawings, which is prone to greater error.

3.4.3 Deriving the Image using Radiance

3.4.3.1 *The Benefits of Image Generation from Radiance*

Physically taking a photograph of the roof is the most rapid means of deriving the gap fraction from HemiView. Three major drawbacks in this method become quickly apparent, being;

1. It is not practical to take the photo from any position, and specifically very challenging immediately under the roof. Viewpoint is restricted in the main to where access for the human operator is feasible.
2. At increasing distances from the roof, or where there are many distinct elements in the same part of the field of view, the resolution of the camera may not be accurate enough to define the elements. The result can be seen by dark regions where elements cluster together, or omitted elements where they are very far away.
3. Unevenness in sky luminance distribution (through clouds, the position of the sun etc.) increases ambiguity of the classification process.
4. Obstructions that are not relevant to the calculation may significantly reduce the available analysis region. In the case of the Sheaf building, the obstructions consisted of the overhead walkways, and the stepped nature of the well.

Generating the image synthetically bypasses all of these shortcomings. Images can be generated from any position in the model, looking in any direction and with any type of lens (e.g. wide, fisheye, orthographic projections). Setting the resolution to a high enough setting (limitless, though higher resolutions will be more computationally demanding) will allow all the necessary detail to be clearly defined. Specifying a uniform sky makes discrimination between structure and gap totally unambiguous. Finally, simplifying the model to include only the areas of interest resolves the issue of overhead obstructions.

3.4.3.2 *Generating the Images*

The models of the atria were created on AutoCAD, exported to Ecotect, and then rendered using the Radiance engine. The exact rationale and specific workings for this are detailed in Chapter 6. For both the Sheaf and the Owen scenarios, the roof was modelled as accurately as possible i.e. including all structural members (though omitting very small detail that would not influence the outcome such as connecting plates, bolts etc.). The well outlines were reduced to cuboids that essentially formed downwards extrusions of the roof footprints. This meant that the well was no longer stepped in the Sheaf building, and the overhead walkways were removed.

The appropriate resolution for the renderings was determined through incrementally increasing the parameter and an examination of the outputted image. The results can be seen in Figure 3-19, where an image of the Sheaf roof as seen at ground level has its resolution doubled from 512 through to 8192⁶. Low resolution images are characterised by jagged (antialiased) lines and omitted detail. At a resolution of 4096, all the relevant detail can clearly be seen, and is thus ready for classification in HemiView. A further doubling of the resolution to 8192 results in significantly increased render times, with little gain in image quality for our purposes. It can be seen also that a camera with a higher resolution may have been able to capture the detail far more effectively. The chosen resolution of 4096 was 3.4 times larger than the 1200 obtainable from the photographs, and as such the images contained 11.7 times more pixels.

Multiple hemispherical fisheye projections directed upwards were rendered by specifying several viewpoints within the Radiance information file (*.rif). Specific command line entry is described in box 3-1.

⁶ the derived circular fisheye images have the same resolution in the x and y directions, and strictly speaking are 512x512 etc., though are referred to as one number for brevity

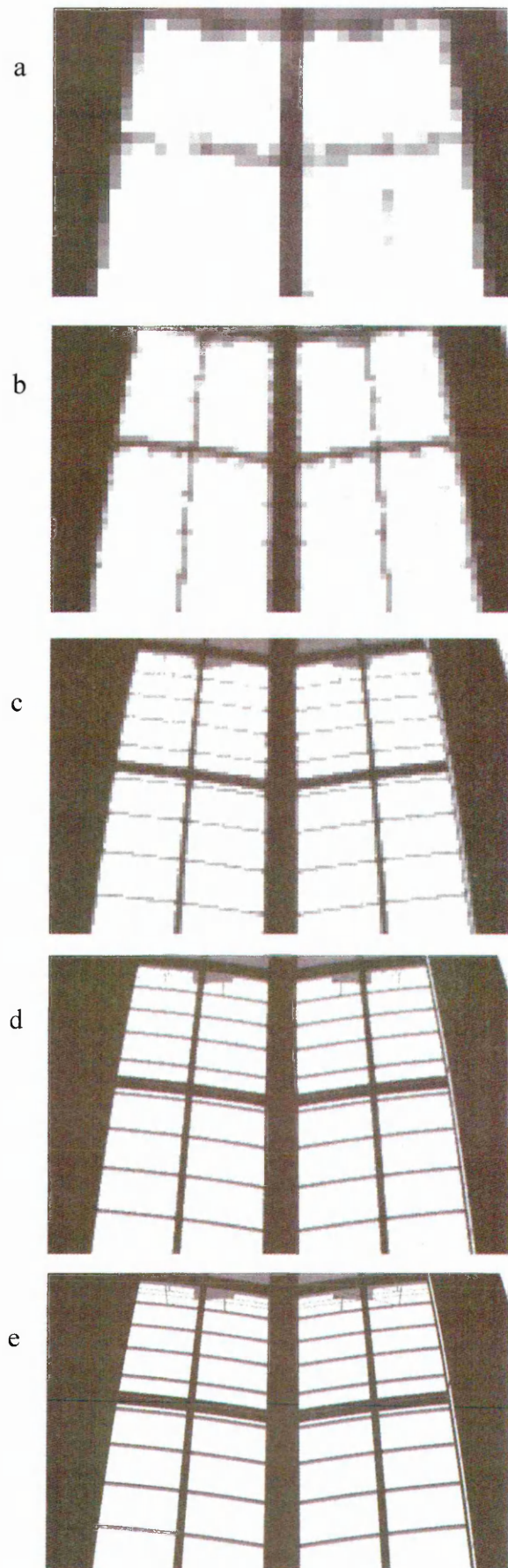


Figure 3-19; Detail of Sheaf roof as viewed from the ground at resolutions of a. 512, b. 1024, c. 2048, d. 4096 and e. 8192.

Box 3-1: Describing a viewpoint within Radiance

The following command line is entered into the *.rif file to describe a view;

```
view= name, view type, viewpoint, view direction vector,  
      view up vector, horizontal size, vertical size.
```

```
view= name -vtt -vp x y z -vd xd yd zd -vu xd yd zd -vh  
      val -vv val
```

For example, the following three views entered in the *.rif file would generate three hemispherical upwards pointing fisheye images, two at roof plane level (end and centre) and one at ground floor level (centre, working plane height) for a hypothetical well measuring 20m long x 5m wide x 10m deep.

```
view= roofcen -vth -vp 10 2.5 10 -vd 0 0 1 -vu 0 1 0 -vh 180  
      -vy 180  
view= roofend -vth -vp 0.1 2.5 10 -vd 0 0 1 -vu 0 1 0 -vh  
      180 -vy 180  
view= floorcen -vth -vp 10 2.5 0.8 -vd 0 0 1 -vu 0 1 0 -vh  
      180 -vy 180
```

The derived images are in Radiance picture format (*.pic). These are then converted to standard bitmap format (*.bmp) for further manipulation in a paint program.

An image was generated for the Sheaf case study at an end position along the primary axis. Further images were generated for the same plan position, but moving down the well at 2m increments up to the base of the well. Upon analysis, further images at closer intervals were generated where it was felt a large gradient of change in gap fraction occurred. A schematic can be seen in Figure 3-20. A similar downwards series was generated along a path in the centre of the well.

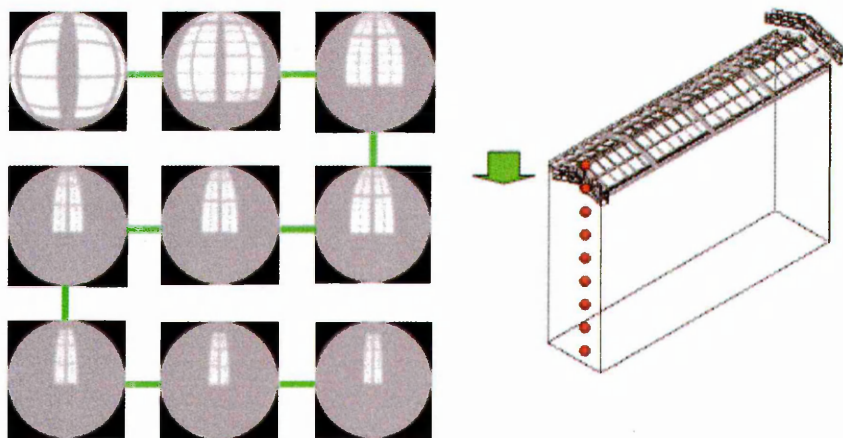


Figure 3-20: Schematic indicating incremental deepening of viewpoint within the well of the Sheaf building, at the end position.

Radiance fisheye views were generated for each of the photo positions in the Owen building. Images were also generated to parametrically investigate taking the photo at increasing depths within the well. Downwards paths were defined along the centre of the primary axis of the well in east, centre and west positions. The east and west positions were $1/8^{\text{th}}$ of the distance in from the well side (2.3m). Assuming a roof plane level at the west end of the well, images were generated at depths of 0m, 1m, 2m, 3m, 5m, 7m, 9m, 12m and 15m (base). At the centre and east positions, moving 'into' the roof was investigated, by generating images at -1m and -2m for both positions, and further at -3m and -4m at the east position, where the monopitch roof reaches its highest point. This arrangement can be seen in Figure 3-21.

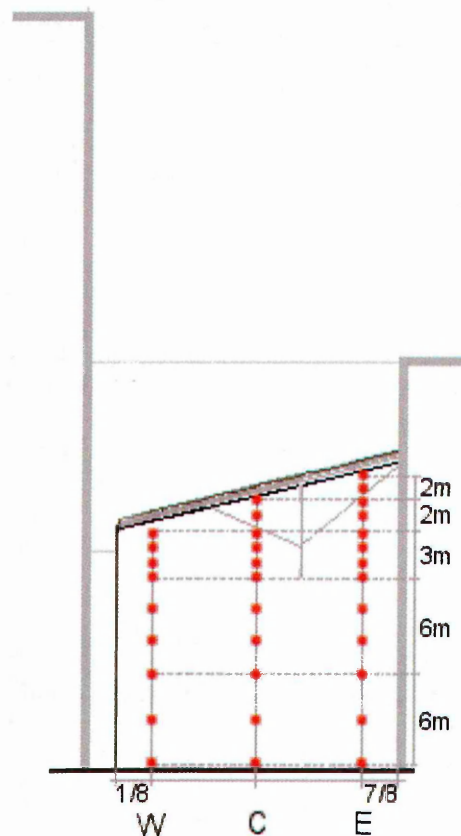


Figure 3-21: Location of Radiance derived fisheye images in the Owen building. 9 positions are chosen on the west sectional axis, 11 in the centre and 13 at the east axis.

The derived images are processed in a paint program in exactly the same manner as the photographs (i.e. non considered parts painted red). The HemiView procedure is different to the photograph method in one way - the lens type is changed from 'Coolpix 900' to 'Linear 180' to correspond to the hemispherical fisheye images generated.

3.5 Computer Simulation of Daylight in Buildings: Selecting the Right Tool

3.5.1 Computer simulation of daylighting: Outline

The past twenty years has seen rapid advances in the accuracy and application of computer programs in lighting simulation. The following section discusses the objectives of a computer program (known as global illumination models) to describe a lit environment. It then continues by describing various approaches to lighting simulation, including radiosity and ray-tracing, alongside discussion on validation work. Radiance emerges as the most accurate and hence appropriate computer based lighting simulator for the needs of this project.

3.5.2 The Objectives of a Global Illumination Model

The ability to determine in advance the (day)lighting performance of a building is advantageous in several ways. Synthetic visualisation will give the designer and client a good idea of how a building may look or 'feel' and appropriate amendments can be made early in the design process (changes to design are much more expensive once building work commences). In terms of quantitative analysis, design illuminance levels and glare analysis provide powerful tools that enable designers to more successfully plan opening sizes and positions, shading devices and artificial lighting and switching systems.

These dual advantages correspond to the two goals outlined by Roy (2000) with respect to computer simulation of lighting. The first of these is to provide a model that can produce convincing visualisations of a building, known as *photorealism*. The second is to produce a model that is accurate in its quantitative output, referred to as a *photometric* model (also known as *lighting visualisation* (Ward Larson & Shakespeare 1998). Figure 3-22 shows three images, the first being a photo of a real boardroom, the second a photorealistic rendering generated by Radiance, and the third containing quantitative illuminance values in the form of contours.



Figure 3-22: Three views of the same boardroom: a. a photograph; b. generated with Radiance; c. generated image including analysis information from Radiance (Ward Larson & Shakespeare 1998).

The ultimate objective of a global illumination model is ambitious; *'In an ideal world, an unskilled user would be able to take the model from any CAD system, quickly and easily set up the materials of the surface, hit a render button and a photometrically correct, photorealistic image would be displayed, giving easy access to all of the photometric data'* (Roy 2000). Annexed to that, the simulation should be rapid. At this moment in time, no such model exists. The complex interactions of light in the real world mean that global illumination models must be based on general assumptions, necessary to enable processors to handle the simulations with any kind of efficiency. Typically, the more simple a program, the easier and faster it will be to use, at the cost of perhaps a less meaningful output. Photometrically accurate results often come at the cost of high input and calculation time, and even then the model can not hope to 100% accurately simulate what occurs in a totally unpredictable world. The following sections outline the accuracy of several models, mainly in terms of quantitative accuracy as is relevant to this study. It should be noted that theoretically a model that produces photometrically accurate output is likely to be better equipped to generate photorealistic images.

3.5.3 Early Programs and Simple Models

Predating the use of computer modelling were empirical measurements (in models and real buildings) and theoretical models, as has been discussed in Chapter 2. One study compares Tregenza's model for the attenuation of light in an open top well with simulations in SuperLite and Radiance (wall and floor reflectance 0.8 and 0.2 respectively), not as a validation but as a comparison of method (Figure 3-23) (Tsangrassoulis & Bourdakis 2003). The divergence of the models for such a simple scenario is cause for concern.

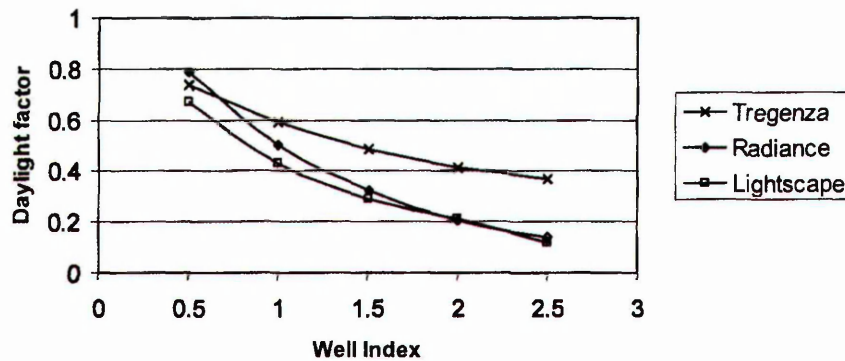


Figure 3-23: A comparison of a theoretical model and two computer programs (Tsangrassoulis & Bourdakis 2003).

SuperLite, developed by the Lawrence Berkley Laboratory, 1986, is part of the Adeline software which also includes Radiance (Erhorn et. al. 1998). A study exploring the accuracy of the SuperLite program along with LumenMicro against measurements taken in a real building, a physical model and the more powerful models of Lightscape and Radiance found it (and Lumen Micro) performs poorly (Ubbelohde & Humann 1998). It also states the necessity for all surfaces to be orthogonal and diffusely reflecting, a major shortcoming against other programs available. Ashmore & Richens (2001) state that the study is already slightly out of date, an indicator of the rapid development in computer simulation. Whilst not performing well when accurate results are required SuperLite has been found to be a useful early stage design tool. Roy's (2000) review on studies performed on various programs has shown SuperLite, Genelux, Adeline and Leso-DIAL to agree within 5% to measurements taken in a simple well. When more complexity is added (measurements in room adjacent to well, sawtooth roof) Adeline predicts within 10% with Genelux having generally a greater than 20% error.

Ecotect by Andrew Marsh uses the simple BRE Split-Flux method to calculate daylight factor at a point (Figure 3-24). Whilst the results seem acceptable for simple scenario's (such as at the early stages in the design process), it is not appropriate for the accuracy desired in this study.

As is often the case in computer simulation, an appropriate trade-off between simulation accuracy and time must be found.

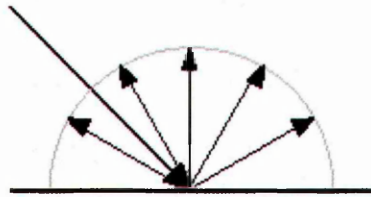


Figure 3-25: A Lambertian (perfectly diffuse) surface assumes no bias in any direction of reflection (Summerfield 2004).

The radiosity process is computationally expensive, though efficiency is improved by use of an iterative convergence technique, which Summerfield (2004) breaks down into three steps;

1. The direct component is calculated by finding the contribution to each patch by each light emitter (artificial or daylight) in the scene. This includes the formation of shadows
2. The indirect (diffuse) component is then calculated. Each patch is ranked according to the quantity of light flux reflected (the combined effect of quantity of direct illuminance received by a patch, and its reflectance). The light is then distributed amongst the other patches according to the form factors, and the process is repeated for each patch.
3. This process is repeated iteratively until there is no perceptible change in illuminances (a lighting equilibrium has been reached). As the number of times light is reflected increases, so the available amount of light for reflection decreases, as more is absorbed into the surfaces at each reflection. The user can set a cut-off point, say once 95% of light has been accounted for to terminate the calculation.

This results in a data structure containing red, green and blue values for each patch. From a defined viewpoint these values can be mapped onto a viewing plane resulting in a rendering of the scene. A distinct advantage of radiosity is that once the calculation has been performed, the values do not have to be recalculated for different viewpoints i.e. it is independent of view. This means that it lends itself well to QTVR

(quick time virtual reality) or VRML (virtual reality mark-up representation) (Ashmore & Richens 2001). This, along with the ease of use of leading programs such as Lightscape, may go a way to explain the popularity of radiosity programs with architects. It should be noted, however, that recalculation is necessary when changes to the scene are made, be it geometry (e.g. the movement of furniture) or lighting conditions (e.g. the diurnal passage of the sun).

A disadvantage to the radiosity approach is in its simplistic treatment of surface reflectance. Whilst in many cases reflectance will mostly be diffuse in nature, a failure to deal with specular reflection makes radiosity inappropriate for dealing with scenarios where there are a significant amount of highly specularly reflective surfaces. Such examples could include lightshelves, or atria wells with bands of specularly reflecting windows. Lack of quantifiable output in specular scenarios would also hinder any form of quantitative glare analysis. In a comparative study of simulation programs, all glazing had to be (unrealistically) removed from the calculations as Radiance (which uses backwards ray tracing) was the only program '*to support non-uniform BRDF's, specular to diffuse reflection and a proper treatment of transparent materials*' (Ashmore & Richens 2001).

Lightscape is capable of producing images that contain specular highlights. These are calculated by sending out rays through the view plane to the scene and then from where it strikes the scene a further ray at the same angle of reflection as incidence, to see if a specular surface is 'hit'. That being the case, a specular highlight can be added to the patch (as seen from the view plane). The resultant specular reflection does not in any way contribute to the quantitative results.

3.5.4.2 In Practice and Validation

Despite the widespread nature of radiosity programs, there appears to be limited published validation work. Khodulev & Kopylov (1996) conducted a vigorous comparison of three computer programs; Lightscape, Specter and Radiance. The criteria for judgement were based on comprehensiveness and physical correctness of scene description, completeness of global light propagation model, accuracy (numerical and visual) and user interface. In the first instance the programs were compared to a

simple model consisting of a white cube with a luminant source at its centre. The luminance distribution of the room was derived from Kajiyama's rendering equation (1986). Lightscape performed least well of the three with regard to physical accuracy. At the most accurate setting used an average error of 10.7% (under-prediction) was found. The simulation took 40 minutes. Radiance produced results with an average error of under 1% in 5 minutes. Similar results were found for visualisation. Radiance (and Specter) outperformed Lightscape in every department with the exception of interactivity of user interface. It was noted that much of the working of the program were hidden from the user (both within the program and the accompanying literature).

Ashmore & Richens (2001) compare Lightscape with RadioRay (no longer commercially available (Roy 2000)), Microstation and Adeline against measured daylight factors in a scale model. The results are displayed in Figure 3-26. All programs with the exception of RadioRay fall within the 20% error band as defined by the systematic error due to measuring the physical model. The computer programs were found to under-predict (0.1%-0.3% in terms of absolute daylight factor) though it was uncertain whether this error is significant due to the large experimental error. The general trends were found to be good. Whilst the model was not entirely straightforward (a small room off a larger volume), it did not contain real world complexities such as a structured glazed roof to the volume. In their study, Ubbelohde & Humann (1998) too found Lightscape to predict expected distribution patterns, though at an underestimation of one fifth. They also warn that *'the lack of scientific specificity about sky conditions used by Lightscape underlines our concern about the accuracy of the quantitative daylighting predictions'*. Miguet & Groleau (2002) proposes another radiosity based simulation tool by the name of SOLENE. It will be able to handle transparency and will attempt to incorporate specular surface interaction through future material libraries. It is unclear due to a lack of information whether this offers significant if any advantages over Lightscape.

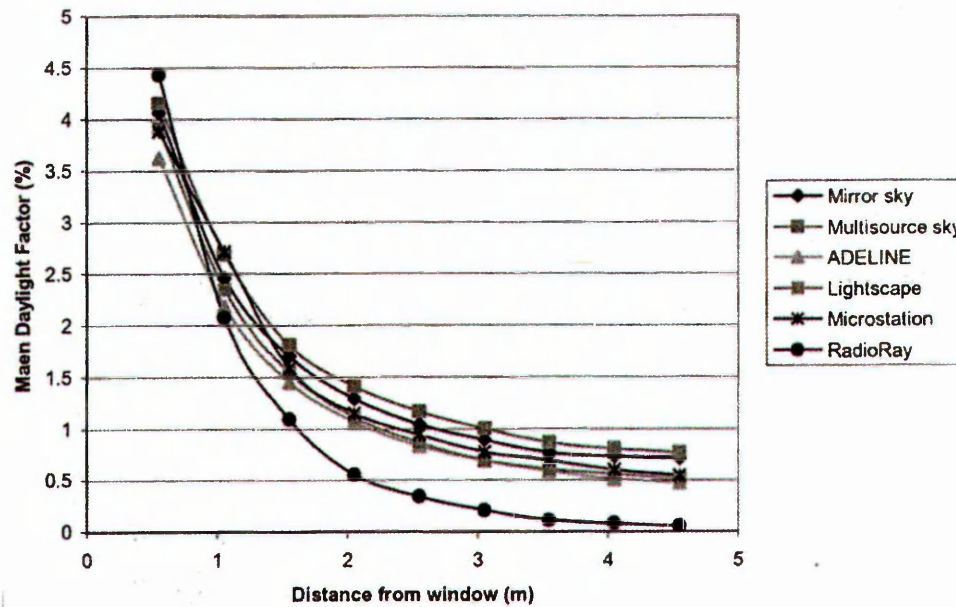


Figure 3-26: A comparison of 2 measured field datasets with 4 computer programs, including the most widely known radiosity program, Lightscape (Ashmore & Richens 2001 (figure from Roy 2000)).

3.5.5 Ray-tracing and Radiance

3.5.5.1 The Workings

This section deals with ray-tracing, though for our purposes it will focus only on Radiance developed by Greg Ward (Ward & Rubinstein 1988), which is a backwards ray tracer that adopts both a deterministic and stochastic approach. The most comprehensive resource for understanding the workings of Radiance is the text *Rendering with Radiance* by Ward Larson and Shakespeare (1998) and the in-program manual pages, and it is from these two sources that the majority of this section has referred to.

In conventional forward ray tracing, light is followed along linear geometric rays from the light source to the point of measurement. The principle shortcoming of this method is that most of the light leaving the source does not reach the scene, resulting in redundant computational effort. In tracing the ray from the point of calculation to the source (mathematically equivalent) only light relevant to the view is considered. To render a simple box room with a bare light bulb would take a month on the world's fastest computer using forward ray tracing, or 3 seconds using backwards ray tracing (Ward Larson & Shakespeare 1998).

There are two approaches within ray tracing; *deterministic* and *stochastic*. In the deterministic approach, light rays are sent directly to the light source, resulting in unnaturally sharp scenes with no inter-reflection between surfaces (Figure 3-27 a). Often a fixed ambient value is applied to the scene, resulting in 'flat' images. In the stochastic approach, rays are sent in a random direction. This relies to chance as to whether areas of known high luminance (i.e. sources such as luminaires or the sun) are hit (assuming thresholds have been set, and the simulation isn't allowed to go on indefinitely). A stochastic approach is a better approximation of what happens in the real world, and is therefore more accurate, though renders typically appear blotchy (Figure 3-27 b). A purely stochastic approach is far more computationally expensive. Radiance uses a hybrid deterministic and stochastic approach, to take advantage of both processes whilst maximising processor efficiency (Figure 3-27 c).

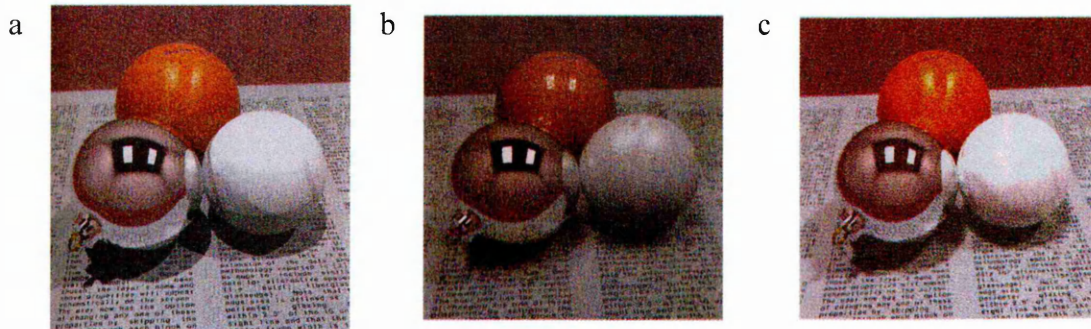


Figure 3-27: Image generation using a. purely deterministic approach, b. purely stochastic approach and c. the hybrid approach taken by Radiance (Ward Larson & Shakespeare 1998).

The central equation to Radiance is as follows (the equation is simplified to ignore the effects of participating media e.g. mist);

$$L_r(\theta_r, \phi_r) = L_e + \iint L_i(\theta_i, \phi_i) f_r(\theta_i, \phi_i; \theta_r, \phi_r) |\cos \theta_i| \sin \theta_i d\theta_i d\phi_i \quad [3-3]$$

where,

$L_r(\theta_r, \phi_r)$ = the value of a ray expressed in luminance

L_e = the luminance emitted due to the point being a source

$L_i(\theta_i, \phi_i)$ = the incoming luminance distribution

$f_r(\theta_i, \phi_i; \theta_r, \phi_r)$ = the bidirectional reflectance-transmittance distribution function (BRDF)

That is, the luminance from a point is equal to the sum of its self luminance and the incoming radiation adapted by the BRTDF of the surface. Within the integral, there will be peaks where either the luminance distribution function or the BRTDF are high, that is, around light sources or highly specular surfaces. Removing these from the integral will make the calculation more manageable. Radiance moves the direct light source component and purely specular components to a deterministic approach, and calculates the remaining indirect (diffuse) calculation stochastically. This splitting up of the calculation can be seen in Figures 3-28 and 3-29.

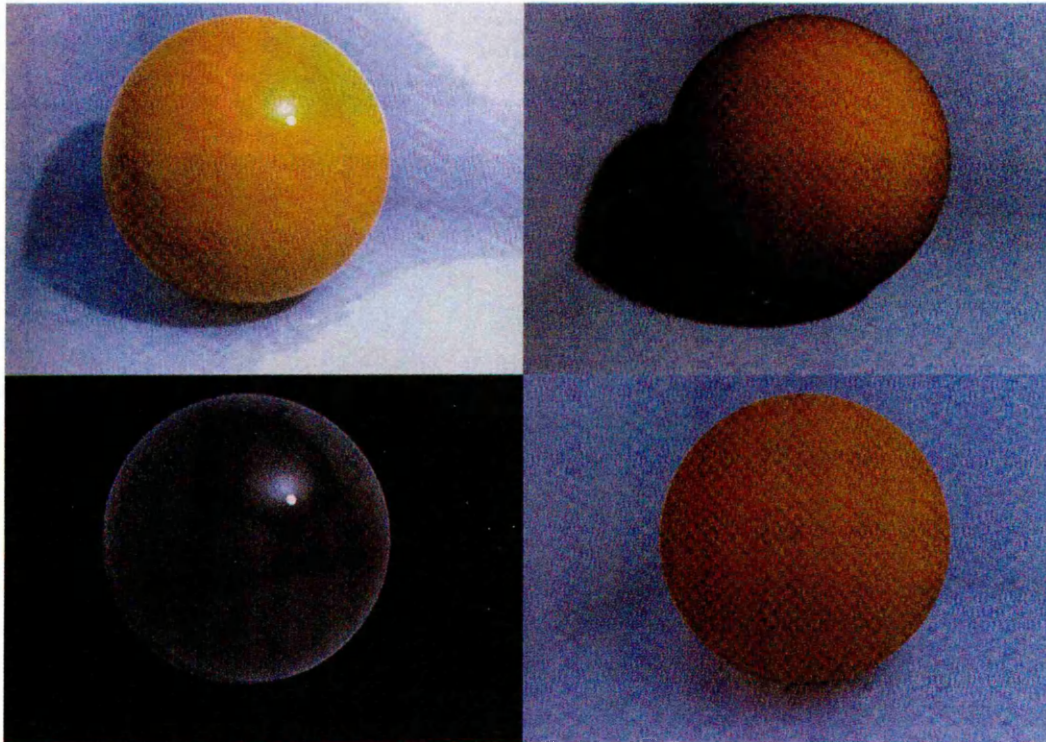


Figure 3-28: The completed view of the yellow sphere (top left) is the resultant combination of a direct light calculation (top right), indirect specular component calculation (bottom left) and diffuse calculation (bottom right) (Ward Larson & Shakespeare 1998).

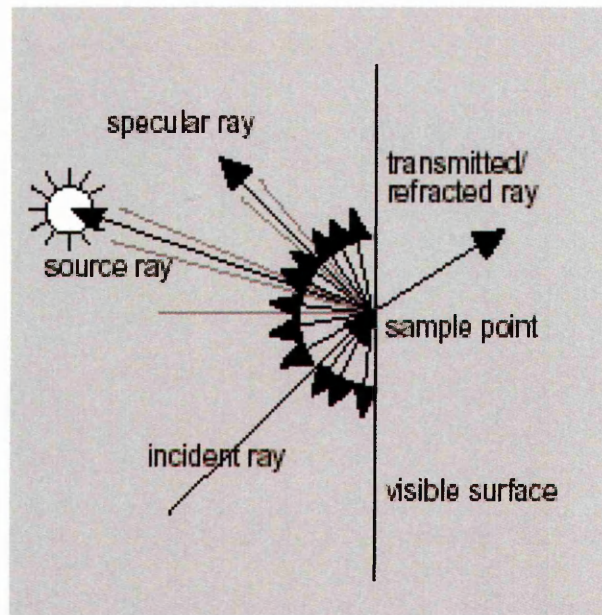


Figure 3-29: Incoming incident light to a surface is considered direct (deterministic tracing back to a source), indirect (hemispherical stochastic sampling) and specular terms (Summerfield 2004).

Deterministic ray-tracing occurs for all elements predefined as light sources. These could include luminaires and the sun, but not the sky which occupies a large area, and is better sampled stochastically. The sky should be defined as a `glow` material to imply it is an emitter of light, and that it is to be calculated stochastically. 'Shadow' rays are sent out towards these direct sources from the viewpoint through the viewing plane, thus determining the shadow distribution in the scene. An element of random sampling may occur to soften the sharp shadows that would otherwise form. Large light sources are subdivided into smaller rectangles to generate penumbras.

The direct contribution from highly specular surfaces such as a mirrored surface is included in the deterministic calculation by creating virtual light sources behind the specular surface. When a shadow ray is sent towards this virtual source, it is reflected back towards the actual source. This can also be applied to redirecting light systems such as prisms.

Radiance may also treat other surfaces as secondary light sources if they are described as an `illum` by the user, and calculation would occur deterministically. These include significant sources that do not emit light directly but may not be efficiently detected in a stochastic manner. A suitable example may be a small window in a deep room, where the window approaches the behaviour of a point source when

viewed from the rear of the room. As it occupies a relatively small area in the field of view, the chances of it being effectively sampled stochastically are low. `Illum`'s are not appropriate in this case, where large glazed openings are studied and as such should be sufficiently sampled by 'chance' hits.

Pure specular reflection is handled deterministically. The material `glass` is one such example. Other materials are likely to reflect both diffusively and specularly. These could be Gaussian materials such as `plastic` or `metal` or a user defined function such as a BRTDF material. Wherever possible, the Gaussian material should be used⁷. The specular component is again handled in a deterministic manner. Adding a surface roughness includes an element of Monte Carlo sampling to achieve a 'glossy' reflection (i.e. not perfectly crisp as you would find in a mirror). The diffuse reflection is handled in the ambient calculation. Setting the specular threshold determines the cut-off point at which Radiance will calculate the specular component separately, before considering it solely in the stochastic calculation. For example, with the threshold set at 0.2, any material with specularity below 20% will be calculated entirely in a stochastic manner.

The final part of the calculation is the indirect calculation, often called the ambient calculation. This accounts for the diffuse inter-reflection between surfaces, and such phenomena as colour bleeding and shadow grading. Monte Carlo sampling takes place in cosine weighted hemispheres at selected points with interpolation occurring between these points. The number of ambient divisions (`-ad`) determines the number of rays spawned from each hemisphere, whilst further subdivision of the hemisphere-ambient super-sampling (`-as`) - occurs where there is high variance within the hemisphere.

The number of ambient bounces (`-ab`) determines the amount of times a ray is reflected before it is ignored by the calculations. For example, with `-ab 3`, light may come from a source and bounce off three surfaces before it is killed. With `-ab 0`, the ambient calculation is turned off. Figure 3-30 shows possible indirect ray paths when increasing `-ab` from 0 to 1. Radiance keeps ambient information (i.e. position and results of hemisphere sampling) cached, and thus this information can be used during

⁷ email correspondence with Greg Ward, January 2004.

increasing ambient bounces. This reduces the potential amount of processing that may occur had new sampling had to take place for every possible bounce. The ambient accuracy ($-aa$) sets the maximum error permitted in the indirect calculation, and ambient resolution ($-ar$) determining the level at which further sampling between hemispheres is replaced by interpolation. The ambient parameters are critical to the accuracy and render times of a simulation, and are discussed in further depths with regard to experimental set-up in section 6.3.

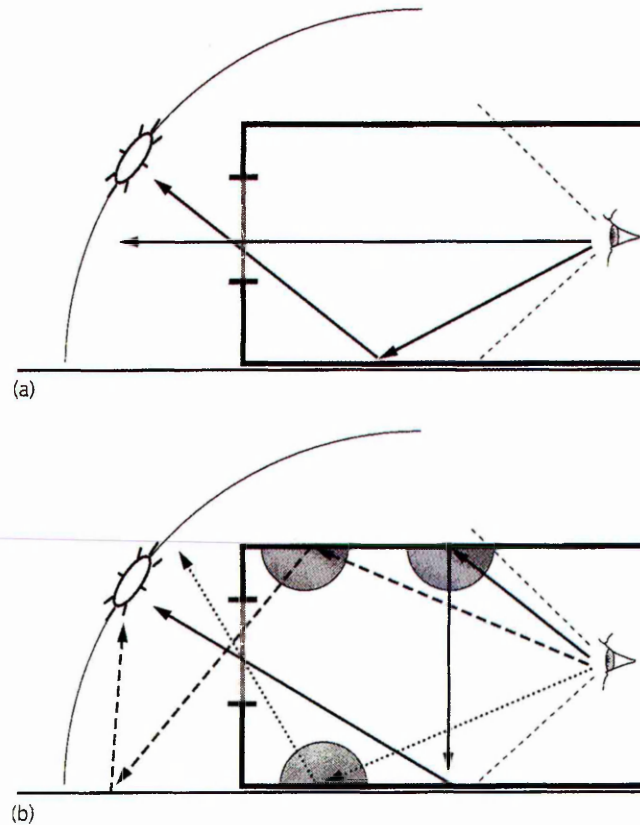


Figure 3-30: Possible combinations of reflection with ambient bounce parameter set at a. 0 and b. 1 (Ward Larson & Shakespeare 1998).

3.5.5.2 In Practice and Validation

Khodulev & Kopylov's (1996) comparison of three programs (discussed in Section 3.5.4.2) demonstrates the difference between forward and backwards ray-tracing. Whilst Radiance uses backwards ray-tracing, Specter employs a forward ray-tracing approach. The only numerical comparison of the output concerns a simulation simplified (and therefore unrealistic with regard to real world conditions) cube. Whilst Radiance arrived at accurate results (under 1% error) within 5 minutes, Specter could

only achieve such accuracy in the centre of the planes (purely symmetrical model, so could be floor, wall etc.). The most accurate results recorded at the edge of the well was a 1.5% error, though the calculation took 156 minutes. For the same simulation, errors at corner positions were still unacceptably high for such a simple model, at 8.8%.

The most thorough validation of Radiance was performed by Mardaljevic (1999). A 'gold standard' dataset of 754 unique sky luminances were mapped at Kew. These luminance patterns were inputted into Radiance using the `brightdata` modifier and illuminance in a simple room was simulated under these skies. The accuracy, particularly under overcast skies was found to be very good (Figure 3-31). Major divergences between measured and simulated results were attributed to error where the photocell could see the circumsolar region (i.e. not a fault of the simulation engine). Removal of these 'potentially unreliable' results further improved the correlation.

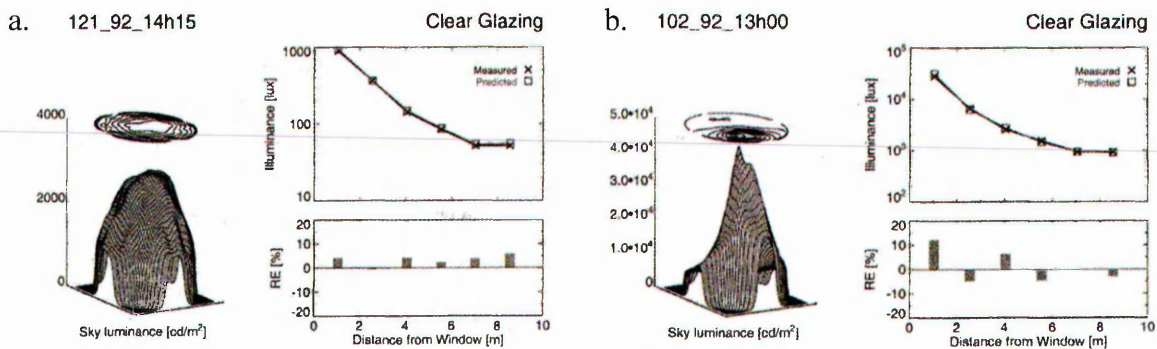


Figure 3-31: Results of sky luminance scan and illuminance values physically measured and predicted by Radiance for a. an overcast sky, and b. an intermediate sunny sky.

An experiment comparing measured illuminance data in a real atrium with Radiance found that for any particular sky condition, the model can potentially accurately simulate the daylight performance provided the relevant data such as geometry, materiality and sky conditions are inputted (Galasiu & Atif 2002). The range and distribution patterns of internal illuminance of the Radiance simulation were good, though differed in absolute terms by as much as 100% for direct sun conditions. This was attributed to the location of photocells and the simplified modelling of the glazing system. The agreement of within 20% under overcast skies was much better (Figure 3-32). Another comment to emerge was a reiteration of the importance of correctly

setting the rendering parameters in order to get meaningful results. Aizlewood et. al. (1998) too found a correct general form though an under-prediction. It was conceded that the program had possibly not converged to an answer, and that one or more of the ambient parameters were not set to a sufficiently accurate setting.

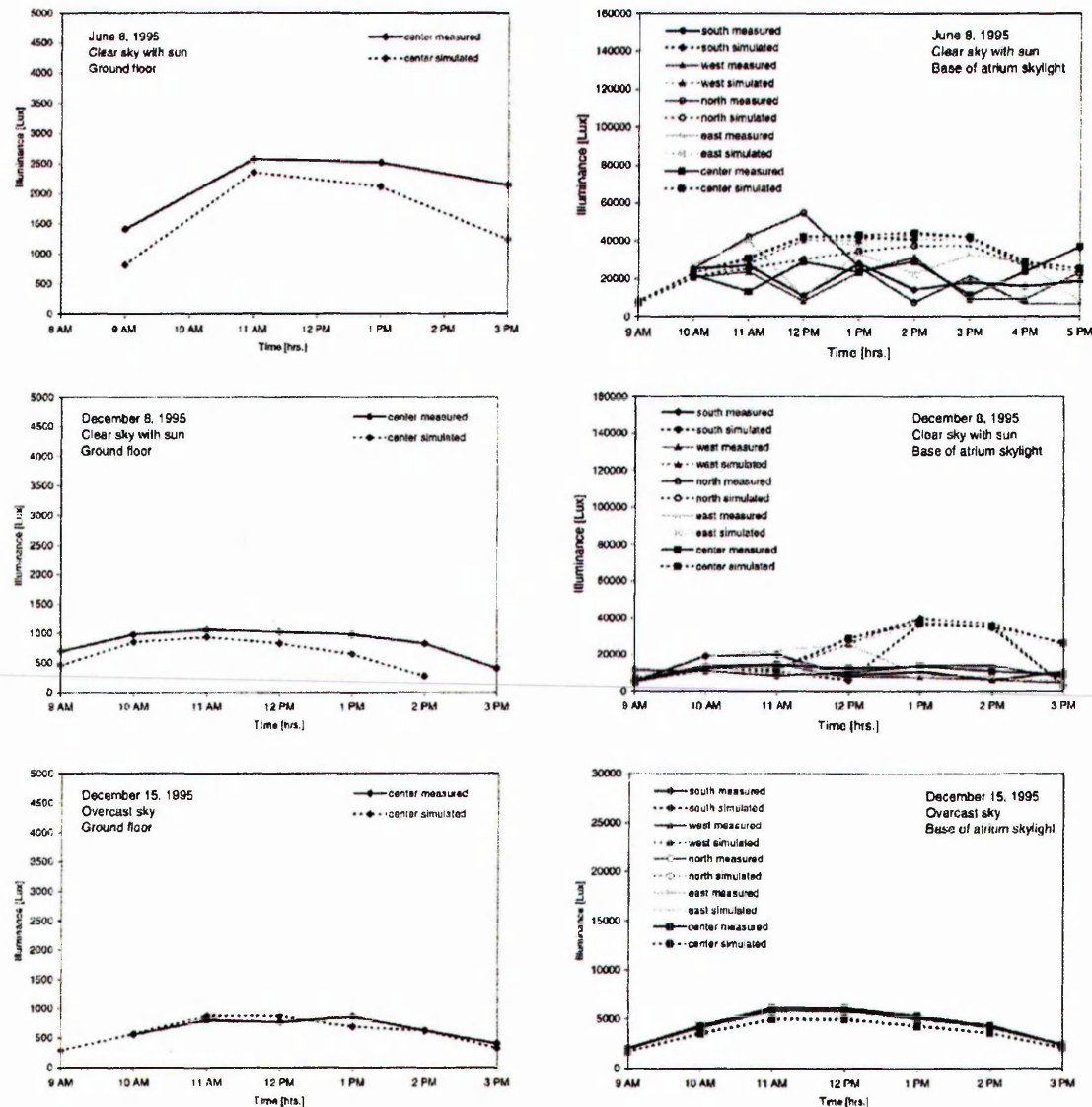


Figure 3-32: Illuminance values physically measured and predicted using Radiance in an atrium for 3 days (one overcast, two clear with sun) in positions at the base of the well, and immediately beneath the skylight (at central and the four cardinal directions) (Galasiu 2002). The agreement, particularly under the overcast sky was good.

Ng et. al. (1999) found an error of 8.1% between Radiance and measured daylight factors in a simple room (Figure 3-33). Radiance was then used to model an existing building to be converted to a museum. External obstructions (trees) were ignored due to their complexity. Instead, correction coefficients were applied such that

the simulation results would tie in to measurements taken from the field. A very reasonable match was found after an iterative process. The model was then used to test various louver and curtain scenarios. The point is made that daylighting is not an exact science, and a fluctuation of 20% can be expected from measured daylight data.

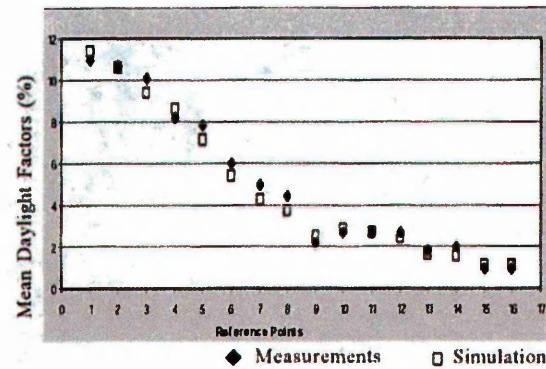


Figure 3-33: The close match between physically measured and simulated daylight factors in a museum space (Ng et. al. 1999).

A common criticism of Radiance is the lack of a user friendly interface (Ashmore & Richens 2001, Ubbelohde & Humann 1998). Whilst it is the total freedom of the program that allows the user a high level of control, it also makes the learning curve very steep. Importers from common CAD packages help with scene description, though DXF data often needs extensive and sometimes tiresome post-processing (Apian-Bennowitz 1998 et. al.). Executable programs within Radiance such as `rad` help to automate the simulation process. Moeck (1996) devised a program that uses Radiance to produce numerical and rendered results such that a non-experienced user can see the effects of making changes to a design on factors such as glare. Other features such as `pcond` attempt to display an image incorporating human visual perception, though there is little validation work on its effectiveness (Papamichael et. al. 1998). One striking advantage radiosity offered over Radiance was regarding animation. Radiance requires a re-rendering with every change in viewpoint. Summerfield (2004) suggests simulations at carefully positioned viewpoints mapped onto a contextual hemisphere and viewed using QTVR can be as effective as a walkthrough animation in describing an architectural scheme.

This study concerns quantitative accuracy. In Roy's (2000) review paper, he states '*...there is one package that appears on most of the comparative studies and seems to offer reliable results in a wide range of circumstances. This is the Radiance*

package...' and goes onto to say *'the Radiance package appears to be well positioned amongst all of the others, and seems to be able to produce a consistent level of accuracy when compared to theoretical, scale model and a selection of other simulation packages. The underlying theoretical models and their implementation appears to be the most well developed for photometric accuracy'*. A recent web based survey assessing the use of daylight simulation programs in design, consultancy and research returned 42 programs used by the 185 valid questionnaires highlighting the divide within the daylight simulation community (Reinhart & Fitz 2004). From the same survey however, Radiance and programs which make use of the Radiance engine comprised of over 50% of the selections. Radiance was chosen as the preferred global illumination model for this study.

3.6 Summary

This chapter has outlined the aims and objectives of the thesis. A methodology comprising three distinct elements was proposed, and their interaction explained. This involved the comparison of physically measured illuminance data with easily obtained photographic information, to enable the rapid analysis of transmittance through skylights. The supplementary use of computer simulations was deemed necessary to account for the practical shortcomings of real world techniques. The two case study buildings analysed in this study (Sheaf and Owen) were introduced and described in full detail. The procedure for physically measuring illuminance was described, together with the rationale for the positioning of the photocells. Chapter 4 describes the findings of the physically measured illuminance results. Next, the HemiView software was described, and the procedure for the photoanalysis technique explicated. This comprised image capture using a digital camera with a fisheye lens adaptor, and through image generation using computer rendering. The findings of this technique are presented in Chapter 5. Finally, the aims of a global illuminance model were discussed, and after a vigorous examination of the literature, Radiance was selected as the simulation program for use in this study. The results from the simulations are presented in Chapter 6.

4

Deriving Transmittance Values for Atria Roofs in Real Buildings

- 4.1 Introduction
- 4.2 The Sheaf Building: Results and Analysis
- 4.3 The Owen Building: Results and Analysis
- 4.4 Conclusions

'In Oceania at the present day, Science, in the old sense, has almost ceased to exist. In Newspeak there is no word for 'Science.' The empirical method of thought, on which all the scientific achievements of the past were founded, is opposed to the most fundamental principles of Ingsoc.' 1984, GEORGE ORWELL

4.1 Introduction

This chapter presents and discusses the results of the physically measured illuminance experiment described in Chapter 3. Separate analysis is made for both the simple (Sheaf) and complex (Owen) buildings in Sections 4.2 and 4.3 respectively. For each case study, the overall results are discussed, before they are classified into three sky types. Deeper analysis is made for overcast sky conditions, and the daylight factors at the measuring points are obtained. In the case of the Owen building, the effects of artificial lighting and the external obstruction are also discussed.

4.2 The Sheaf Building: Results and Analysis

4.2.1 Example Sky Types

The downloaded data was opened in a spreadsheet package. Data points outside the range of 6 am to 9 pm were removed. For the 91 day measuring period this left 8368 data points (each point comprising an internal and external illuminance). The internal illuminance was divided by the external illuminance at each of these points to derive a value related to transmittance, which would strictly be referred to as a daylight factor for the overcast conditions, or E_I/E_E for all others. Graphs for each day were created showing the temporal changes to internal and external illuminances, and to E_I/E_E (each of these skies can be seen in Appendix C). The dynamic nature of the sky meant most days experienced changing sky conditions, and hence luminance distributions (for example Figure 4-1).

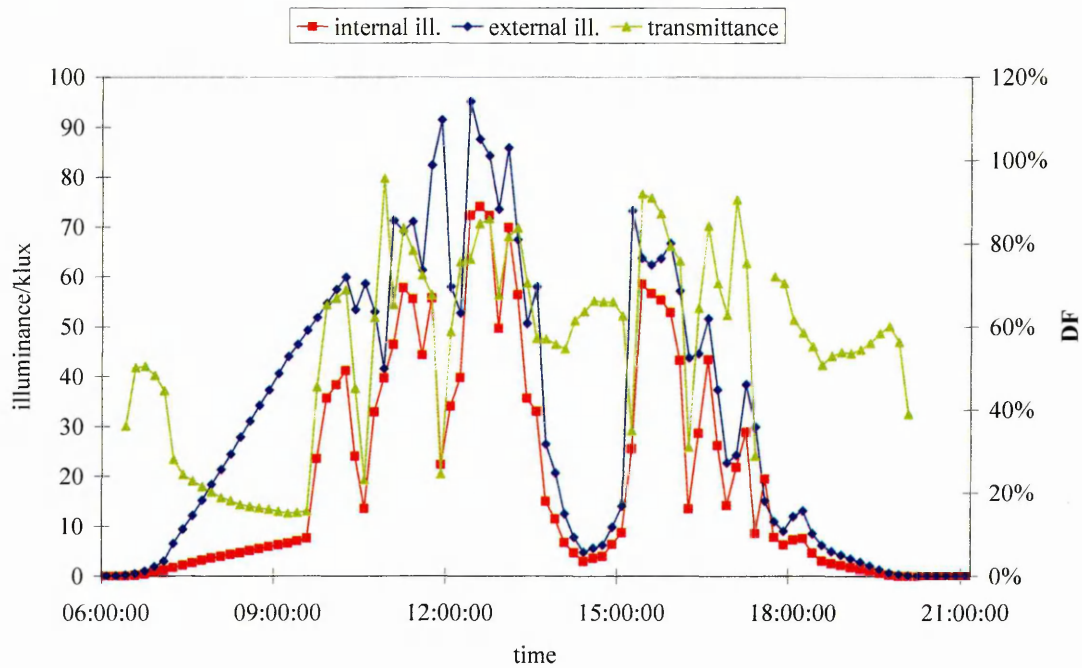


Figure 4-1: 7th September 2002. A demonstration of the dynamic nature of sky luminance distribution.

Figure 4-2 shows a completely overcast day. It is characterised by very low magnitudes of illuminance. The peak value of illuminance occurs at approximately midday, when even through the thick blanket of cloud, the influence of the sun of the zenith altitude is felt. The internal illuminance graph follows a similar form to that of the external graph, with a daylight factor of approximately 60%. The slightly jagged nature of the E_I/E_E line is due to a slight mismatch in clock synchronisation between the two loggers. Such an error would not be expected to affect the overall results where the peaks and troughs would average out to the correct 'flat line' average.

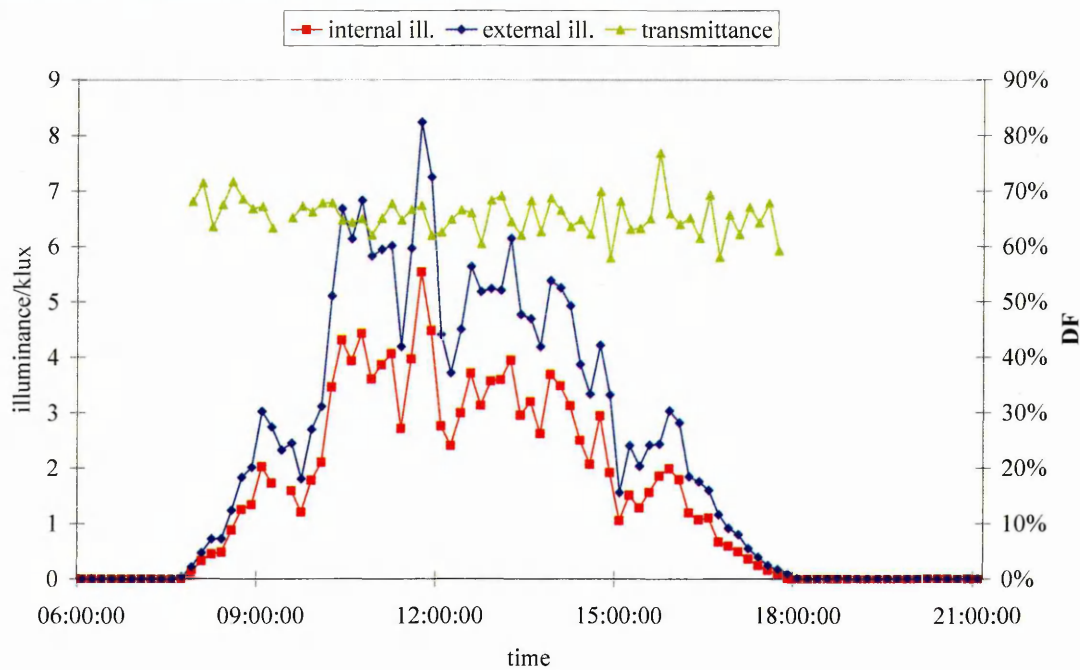


Figure 4-2: October 15th 2002. A completely overcast day.

Figure 4-3 shows a day with a completely clear sky. The graph of the external illuminance is approximately ten times the magnitude for that of the overcast day. The form is representative of the sun path (daily movement about the azimuth). The graph for the internal illuminance follows a similar form barring two phenomena; between 6 am and 10 am the gradient is far shallower, and throughout the day there are sharp troughs within the bell shaped curve. The shallower gradient early on in the day is due to the internal photocell not directly seeing the easterly sun due to overshadowing from the end of the Sheaf well. The troughs are due to blockage of direct light at the internal photocell by the primary structural roof elements as the sun passes overhead. These phenomena are more clearly seen when the values for all clear scenarios can be grouped together, as in Figure 4-4. Here, four phenomena are observed; the aforementioned low E_I/E_E values before 10 am and the troughs (whose depth and position will change dependant on time of year), as well as two further observations. After approximately 5pm, the E_I/E_E value drops to just below 60%. Figure 4-5 reveals that after these times, the magnitudes of illuminance are significantly lower, indicating that the low westerly sun is now obscured from both photocells by the overshadowing urban landscape, and thus the illuminances are a result of the sky glow only. Secondly, between 10 am and 5 pm, the E_I/E_E value rises gradually from about 70% to 85%. One possible explanation for this could be the westward moving sun creating more favourable relative scenarios for inter-reflection of direct light flux about the internal

photocell (positioned at the east end of the linear well). As this study focuses on overcast sky conditions, further investigation is not instigated.

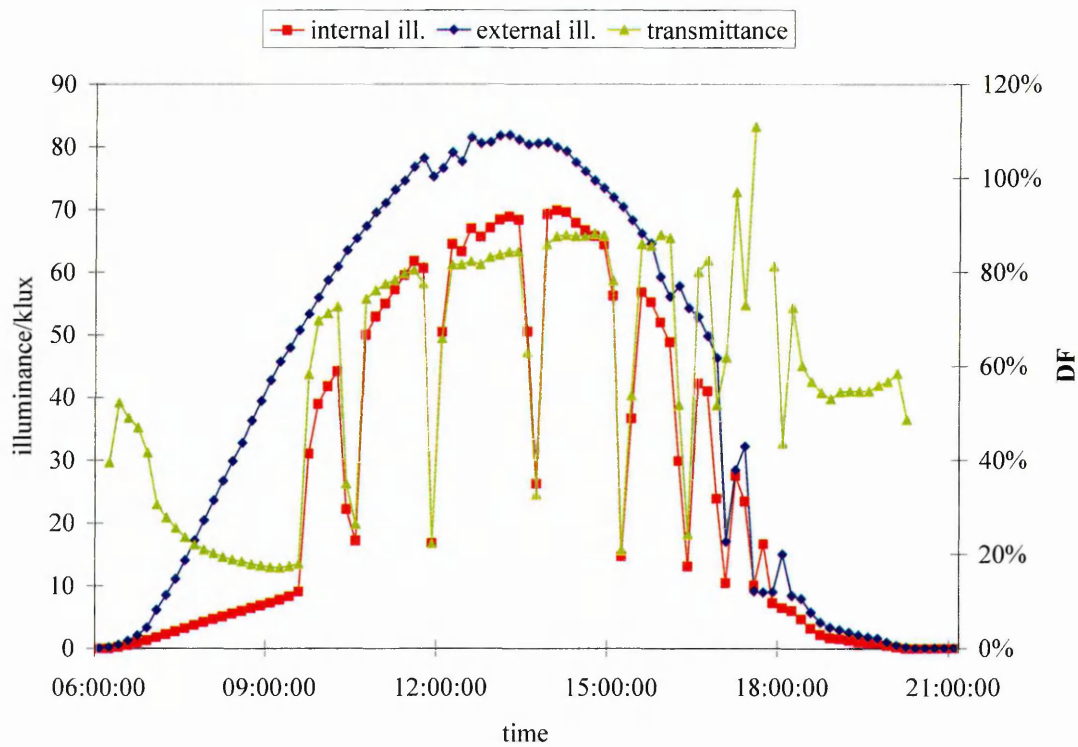


Figure 4-3: September 1st 2002. A day with clear skies

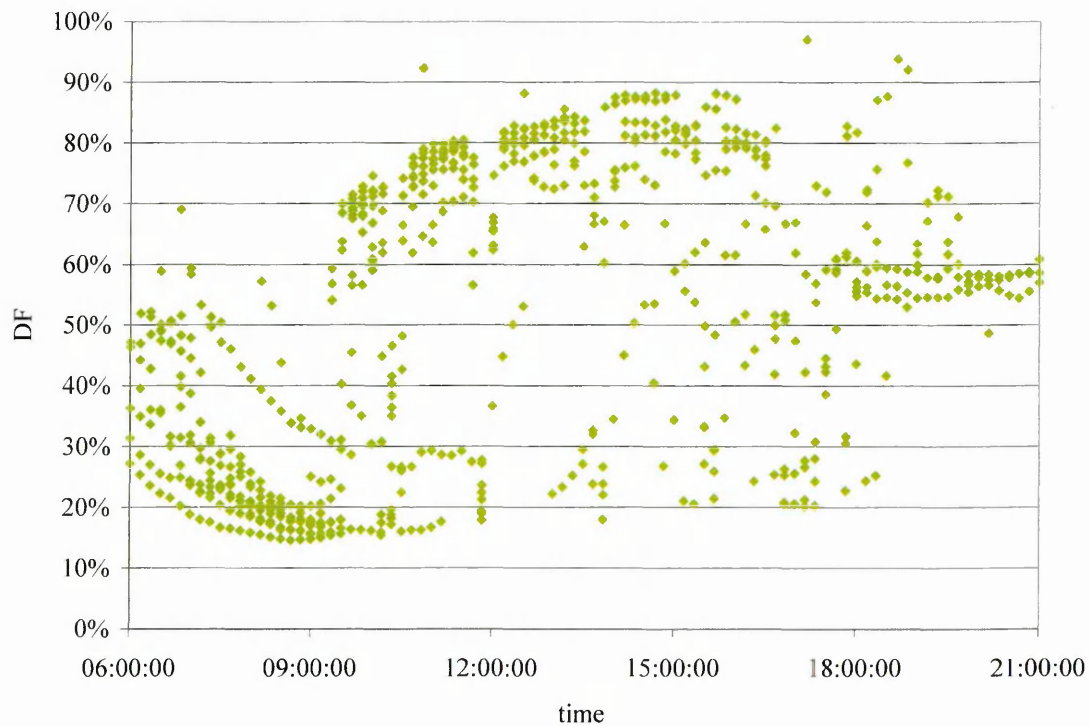


Figure 4-4: The variation of daylight factor over the course of a day under clear sky conditions.

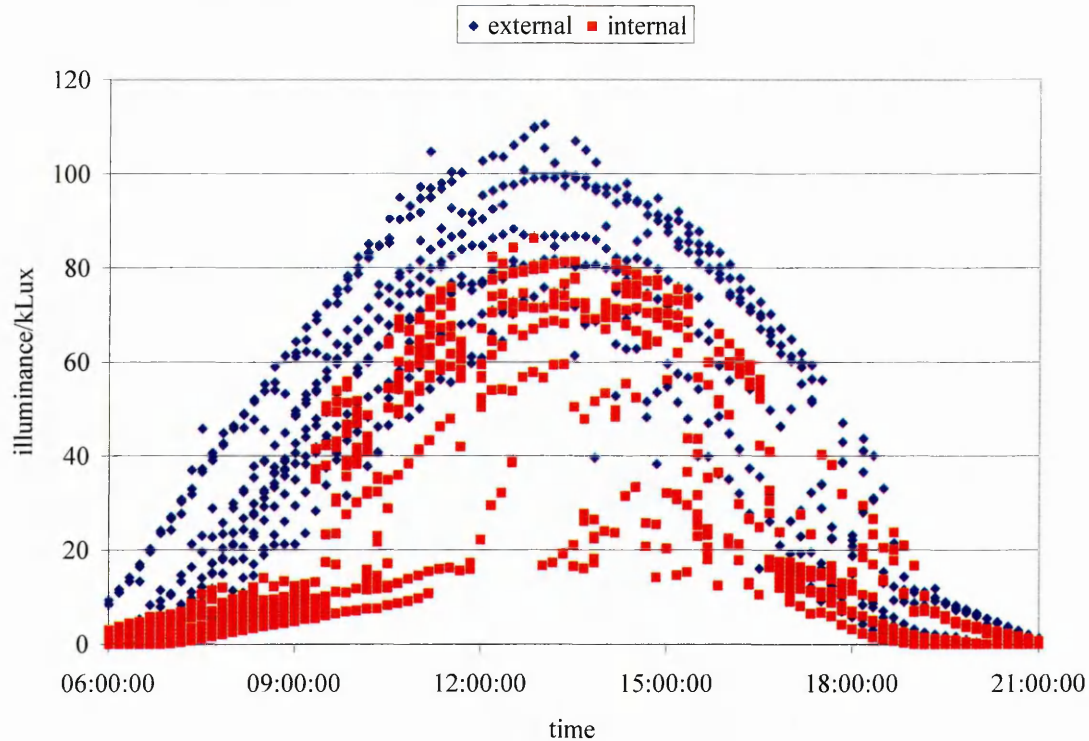


Figure 4-5: Illuminance values over the course of a day under clear skies.

4.2.2 Classifying Sky Conditions

The illuminance graph (Figure 4-6) for all 8368 points reveals several patterns. Its gradient would give an average E_I/E_E value (and hence daylight factor for overcast skies), though the several different skies represented ensures a ‘one line fits all’ strategy is unacceptable. It is for this reason the skies are broken down into 3 categories for classification; overcast, intermediate and clear. A fourth category of ‘null’ was included as for a very small sample of the points, where only one of the two loggers recorded a reading (due to mechanical failure).

The horizontal global illuminances as recorded by the external unobstructed photocell was the principal tool for classifying the skies. This was done by intuitively comparing the magnitude and temporal movements of illuminance with those expected for each sky type. There was good agreement between the classified skies and the logged weather conditions described in Section 3.3.4.1 (comprising independent descriptions, cloud cover percentage and spot checks by the author). The availability of site specific IDMP or sunshine duration data may have enabled the use of the classification techniques detailed in Section 2.4.1. The methodology used was adequate

for isolation of the overcast sky conditions as necessary for this study, though it is appreciated that should classification of sky conditions into finer boundaries have been required, a more robust method would have been necessary.

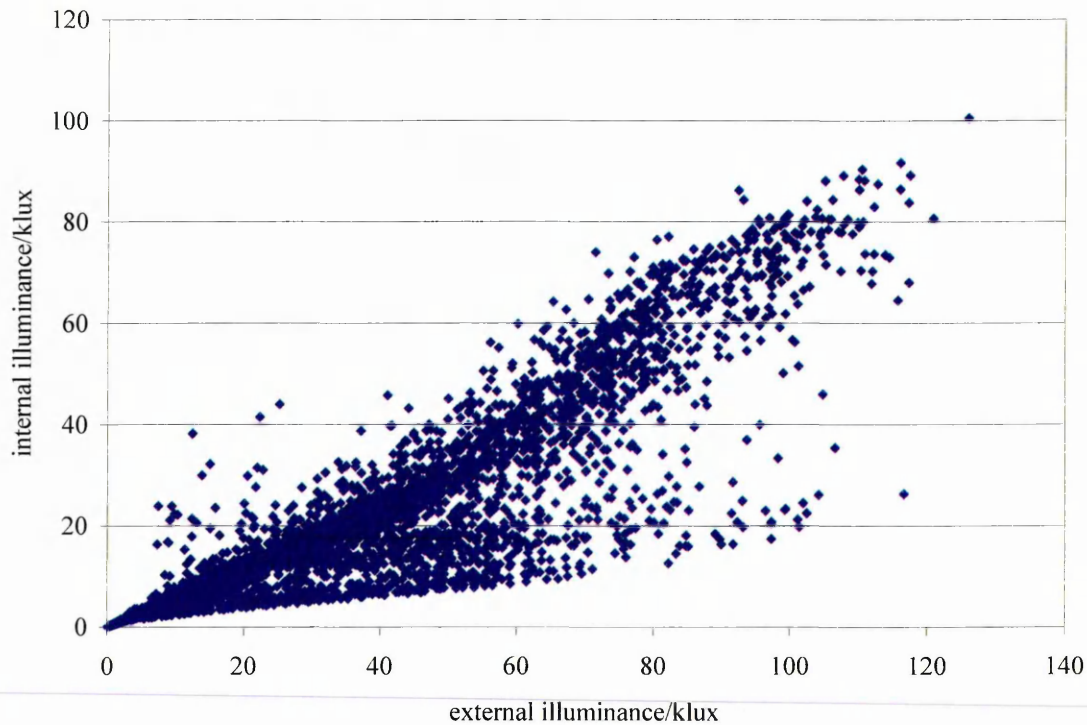


Figure 4-6: Internal illuminance against external illuminance for all sky conditions between 6 am and 9 pm.

Of the 8368 points, 972 (11.6%) were classified as overcast. 6590 (78.8%) were intermediate, 776 (9.3%) were clear and 30 (0.4%) null. The data was filtered to leave a measuring period of between 8 am and 6 pm. Whilst the original 6 am to 9 pm period was useful for visualising the entirety of a day's natural light cycle, it was felt the reduced period was more representative of the daylight occupancy period of the building. The dawn and dusk periods, characterised by very low magnitudes of illuminance, were more vulnerable to a distortion of the E_i/E_E values due to the greater impact of external influences such as user controlled artificial lighting that were more in effect at these times. This left a pool of 5614 values, 624 (11.12%) of which were overcast. The general distribution of sky types barely changed from the larger pool of sample points, and can be seen graphically in Figure 4-7. The 'intermediate' bracket is crude, and is often subdivided into further classes (hence its dominance here) namely intermediate overcast, intermediate mean and intermediate blue (Baker 1993 et. al.)

though for this study, isolating the overcast skies from the other sky types was sufficient.

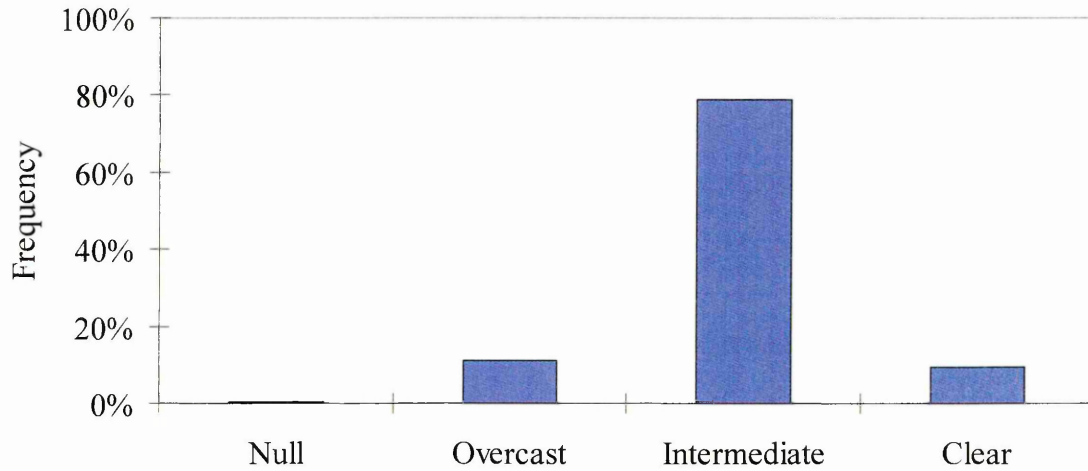


Figure 4-7: The distribution of sky into three bins, between 8 am and 6 pm, July to October 2002.

4.2.3 An Analysis of the Overcast Results

The illuminance results for the 624 overcast measurements are shown in Figure 4-8. The gradient of 0.603 indicates a daylight factor at the point of the internal photocell of 60.3% at a high significance level ($R^2=0.97$).

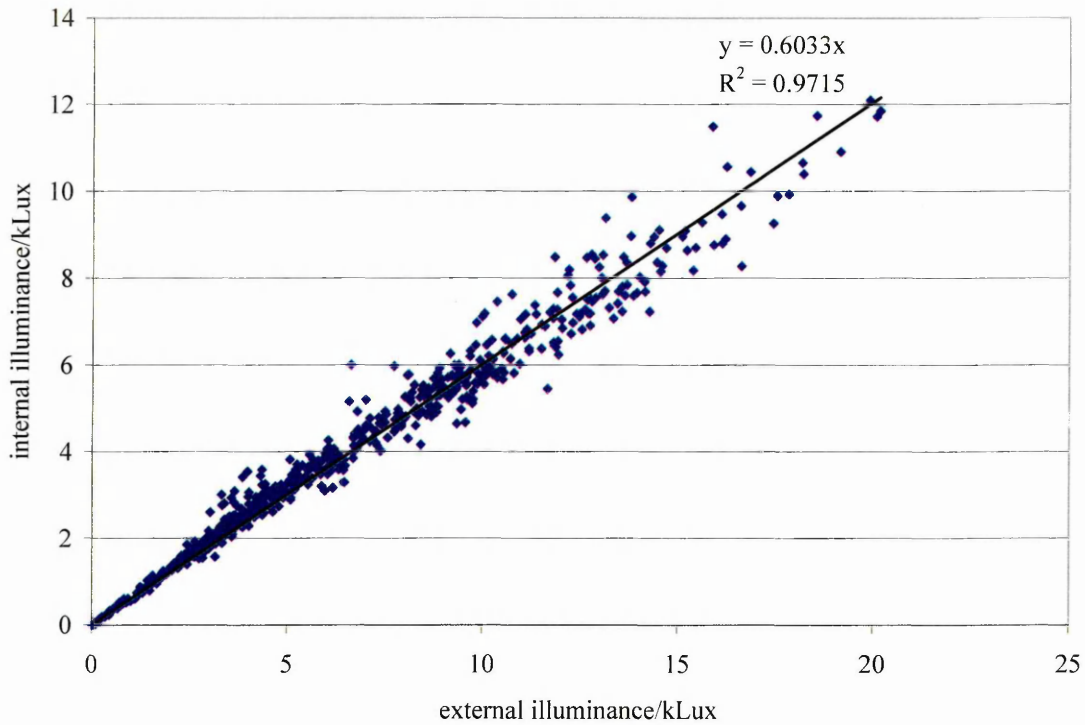


Figure 4-8: Internal illuminance against external illuminance under overcast skies between 8 am and 6 pm.

This daylight factor is several steps away from being indicative of the transmittance of the entire roof. Firstly, the result is influenced by illuminance gains at the internal photocell due to inter-reflections from the well. Simulation with the lighting program Radiance (Chapter 6) aims to isolate the effects of the well, and as such this measured daylight factor can be adjusted. Secondly, the measurement point may not correspond to the average transmittance of the roof over its entire plane. Again simulation with Radiance can reveal transmittance patterns for the roof, and the relationship to the physical measurement point. Those findings can be related back to this measured value.

4.3 The Owen Building: Results and Analysis

4.3.1 Sorting the Data

The data was opened in a spreadsheet package, and the data filtered to leave a measurement period of between 8 am and 6 pm for each day. For the 68 measurement days, this left 4079 data points (each point comprising an internal illuminance and two external illuminances). The internal illuminance value was divided by both the external obstructed photocell and the external unobstructed photocell value. The former represents a value related to the transmittance of only the roof system. The latter is representative of the transmittance of the roof system and the obstructions of the surrounding urban fabric (i.e. the obstructions are considered a part of the 'roof system'). Under overcast conditions, this value would be referred to as the daylight factor. Individual graphs were plotted for each of the measurement days.

The data points were classified as in the Sheaf building, into overcast, intermediate, clear and null categories, using the weather log and the individual day graphs for reference. The distribution can be seen in Figure 4-9. Of the 4079 measurement points, 481 (11.8%) were overcast, 3200 (78.5%) intermediate, 310 (6.6%) clear and 88 (2.2%) null. This distribution is remarkably similar to that observed in the Sheaf building, which occurred over the summer months. The lower percentage of clear skies is as expected, and the larger quantity of null points is due to the exclusion of some of the data points between 5 pm and 6 pm in February and early March, where sunset occurs before 6 pm. Breaking the intermediate category into finer distinctions would probably induce a divergence between the two datasets, with the Owen scenario having more intermediate overcast skies, and the Sheaf building having more intermediate blue skies.

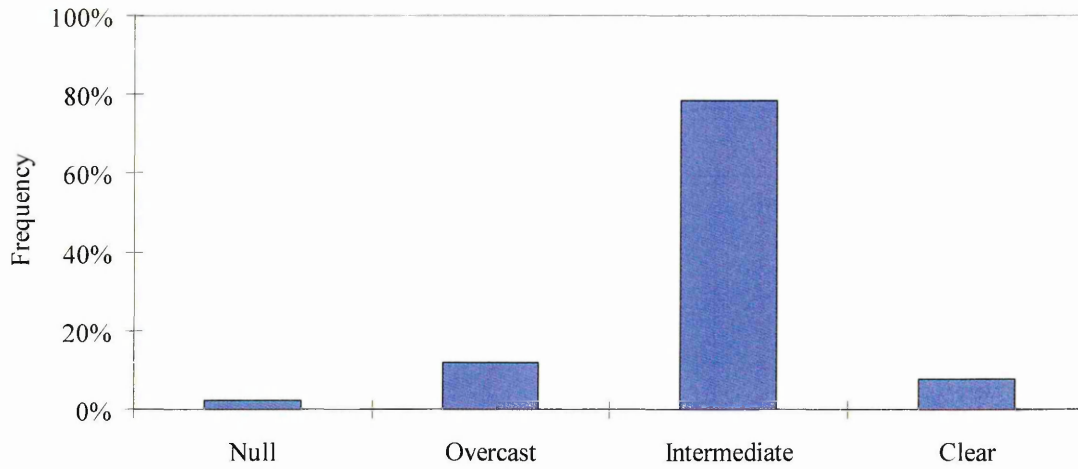


Figure 4-9: The distribution of sky into three bins, between 8 am and 6 pm, February to April 2004.

4.3.2 The External Obstructions

The effect of the obstructing urban fabric on light arriving at the atrium roof relative to the global illuminance can be seen in Figure 4-10.

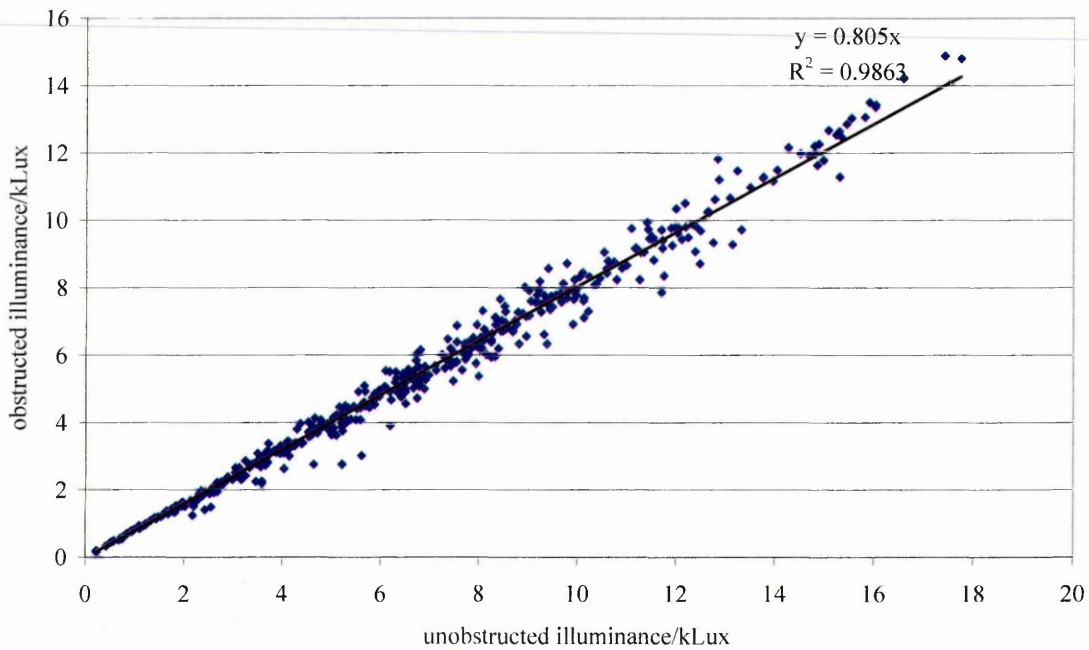


Figure 4-10: Obstructed external illuminance against unobstructed external illuminance under overcast skies.

The quantity of light flux falling on to the obstructed photocell is approximately 80% of the quantity of flux falling upon the unobstructed photocell ($R^2=0.99$). The

percentage of visible sky as seen from the obstructed external photocell was found to be 51% using HemiView (discussed in detail in Chapter 5). If the obstructing surfaces were pure light sinks, and the sky distribution uniform it might be expected that the two values would match. The 'extra' illuminance measured at the internal photocell is due to reflected flux from the surrounding buildings, and from a clear view of the most luminant part of the sky under overcast conditions (the zenith).

4.3.3 The Influence of Artificial Lighting

The Owen atrium contains several artificial lighting circuits controlled by a Building Energy Management System (BEMS). There is potential for artificial lighting within the atrium well between 5.45 am and 9.30 pm. The switching is controlled by a combination of daylight linked sensors handled by the BEMS, and user controlled overrides. It was expected that artificial lighting could influence the lighting levels recorded by the internal photocell. Figure 4-11 shows the illuminance levels logged at the internal photocell for sample days one week apart from February to April, with their corresponding sunrise and sunset times. The light levels drop to zero before sunrise and after sunset as expected, and the form of decay is characteristic of daylighting, not the flat lines observed for artificial lighting. Outside of daylight hours it is known that the artificial lighting was being deployed¹, and so it must be concluded that the quantity of artificial light flux arriving at the internal photocell position was negligible. All illuminances measured at the internal photocell were assumed to be as a result of natural daylighting.

¹ first hand observation by the author

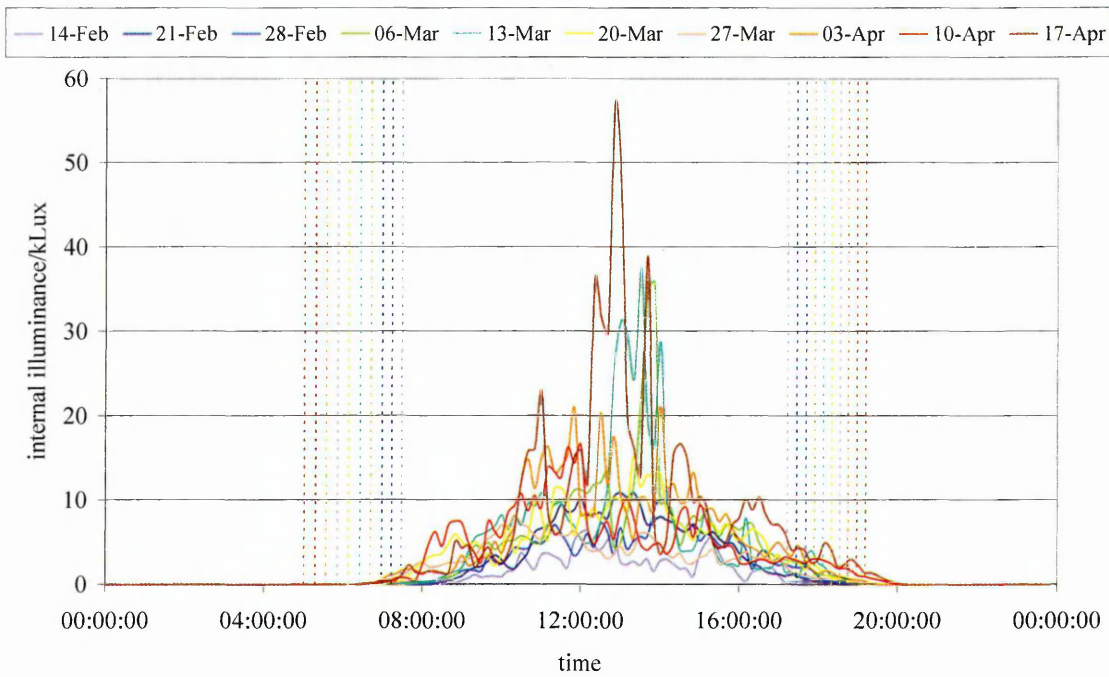


Figure 4-11: Illuminance levels for sample days one week apart from 14th February to 17th April 2004, with their corresponding sunrise and sunset times (the dashed vertical lines).

4.3.4 Example Sky Types

Figure 4-12 shows a day that is in the most heavily overcast. The illuminance values recorded at each of the three photocells follow similar trends throughout the course of the day, as is demonstrated by the flat E_I/E_E lines. The unobstructed external illuminance is consistently higher than the obstructed external illuminance, and therefore the E_I/E_E obstructed line is higher, at approximately 43%, than the E_I/E_E unobstructed (daylight factor) line at approximately 35%.

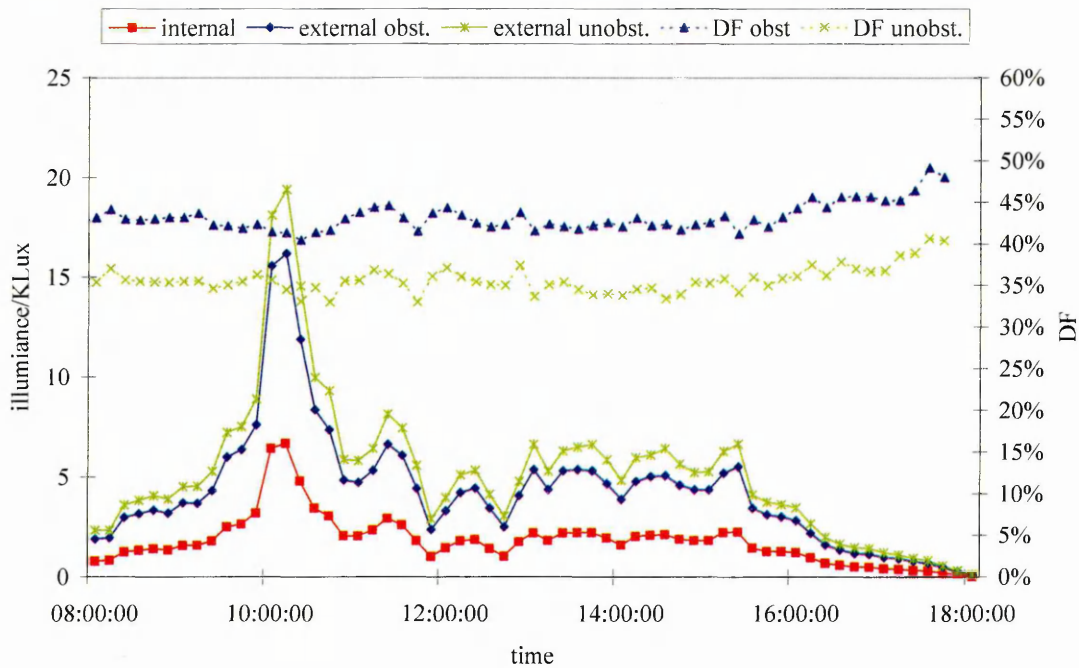


Figure 4-12: 12th March 2004. An almost entirely overcast day.

Figure 4-13 shows a day with clear skies. As with the Sheaf building, the magnitudes of illuminance are up to ten times that of an overcast day. The unobstructed external illuminance curve represents the path of the sun through the day, peaking at midday. The obstructed external illuminance line follows a similar yet more irregular curve until about 1 pm, at some points even exceeding the unobstructed external results. After 1 pm, the values drop sharply and gradually decay until sunset. The internal values rise slowly at the start of the day until just before 11 am. The graph then follows a turbulent form for approximately 2 ½ hours before falling to values even lower than at pre-11 am. It then tails off gradually towards sunset. The forms of the E_I/E_E lines are heavily influenced by the illuminance reading measured internally (with the internal photocell seeing only part of the sky dome due to the external obstructions). For both E_I/E_E lines (dashed lines in Figure 4-13) before 1pm, as the corresponding absolute external illuminance values are similar, the path is analogous. There is minor fluctuation about 15% pre-11am and major fluctuation between 15% and 50% until 1 pm. After 1 pm, the obstructed external E_I/E_E line hovers at about 36%, whilst the unobstructed external E_I/E_E line drops to 8% before rising to over 25% by sunset.

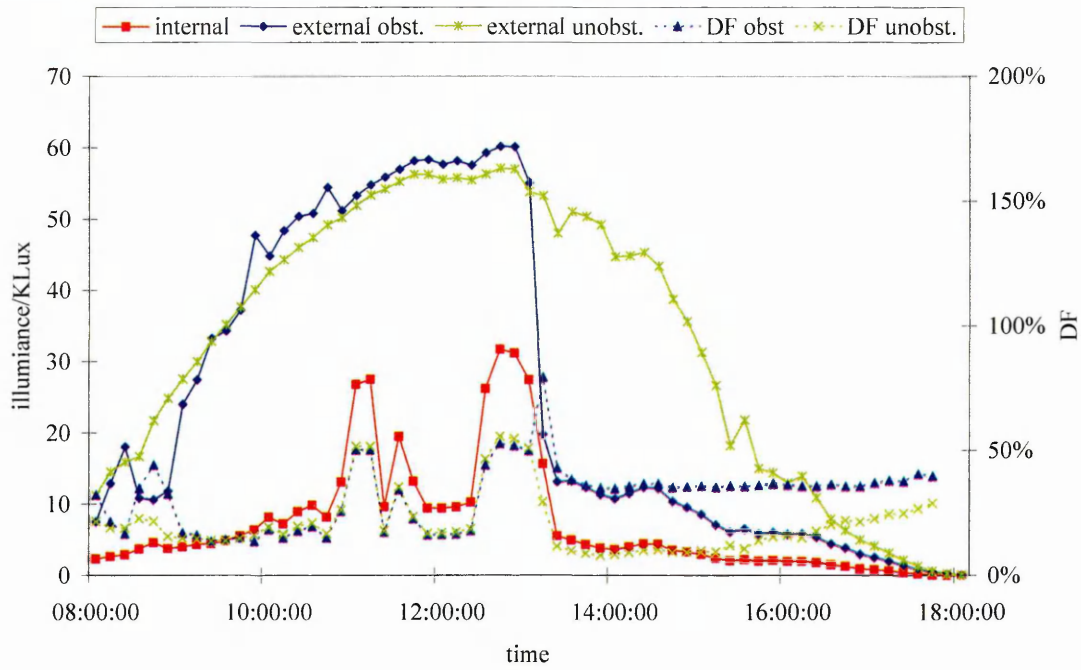


Figure 4-13: 2nd March 2004. A day with clear skies.

The illuminance values for all clear points can be seen in Figure 4-14. Again, the unobstructed external illuminances follow the daily passage of the sun, whilst the obstructed external values follow a similar path pre-1pm, in some cases exceeding the unobstructed values, and dropping off sharply going into the afternoon. The internal illuminances are generally low outside of the period between 10 am and 1 pm, where values are erratic.

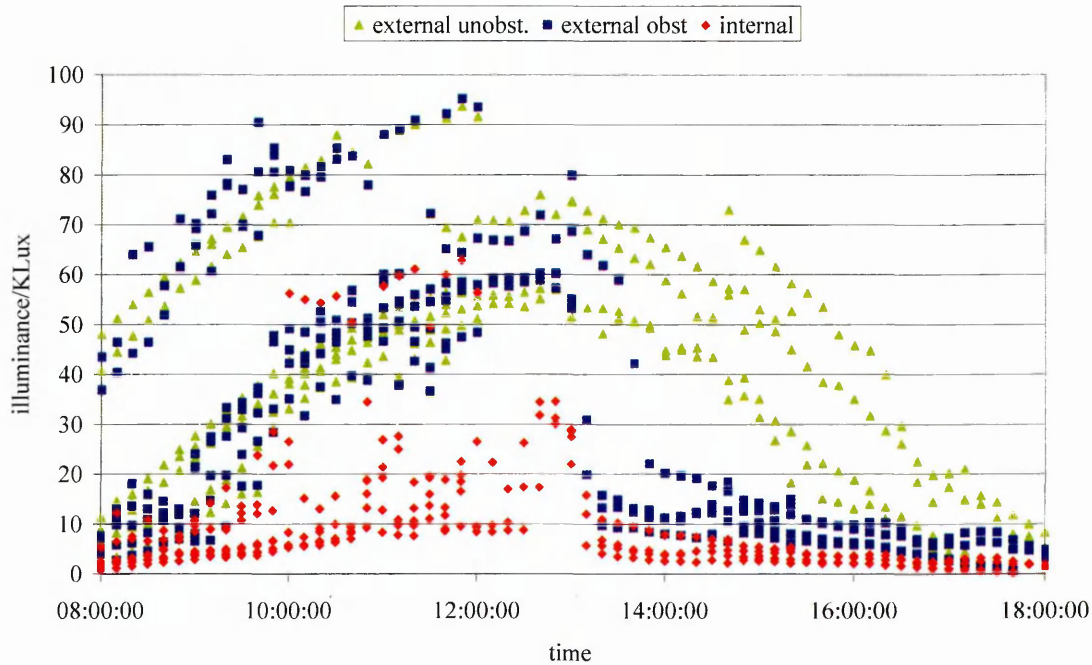


Figure 4-14: The variation of illuminance over the course of a day under clear skies.

The sharp drops in illuminance values as recorded at the obstructed external photocell are characteristic of the influence of direct solar insolation. The analysis program Ecotect (which is discussed in further detail in Chapter 6) was used as a virtual heliodon to establish at which times the obstructed position is in direct line of sight of the sun (Figure 4-15). On the 14th of February (measurement commences) the sun can be seen directly between 11.15 am and 1 pm from the obstructed position. This window widens to 10.30 am-1.15 pm on April 20th when measurement ceases.

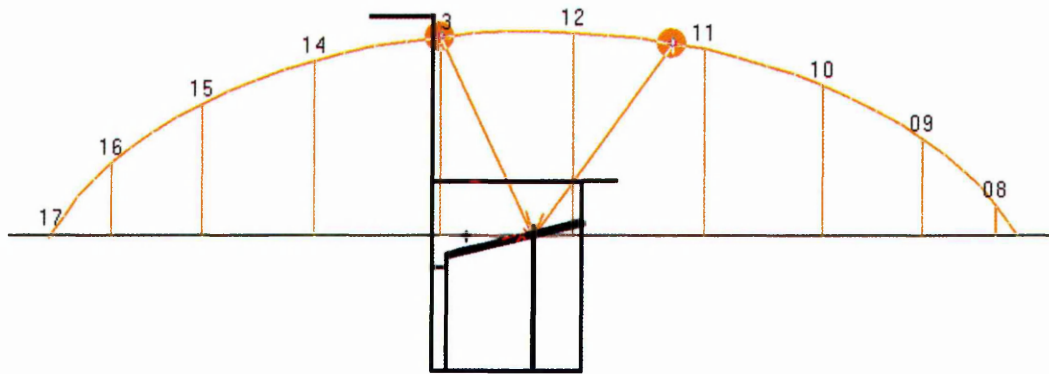


Figure 4-15: The obstructed measuring points are potentially under direct illumination between 11.15 am and 1 pm on February 14th.

The impact of the presence of direct illumination or lack of it on the results can be seen when observing the E_i/E_E values throughout the day (Figure 4-16). Before 11am, when the internal cell and obstructed cell do not have a direct line of sight of the sun internal illuminances and hence E_i/E_E values are low. The external obstructed values are much higher than expected. This is due to the facade of the Owen building, with its many specularly reflective surfaces redirecting light towards the photocell. These rays may not transmit through the roof to the internal photocell due to shallow angles of incidence under which reflectance prevails over transmittance with glass materials.

After 11 am and before 1 pm, the obstructed external values exceed the unobstructed values as the obstructed photocell is receiving light directly from the sun, and a reflection of the sun from the adjacent facade. The internal photocell during this period logs either high or low illuminance values, indicating that it is either in or out of

the line of the sun. The peaks and troughs are indicative of the influence of structural members obstructing the direct incoming rays at certain times of the day.

After 1pm, the obstructed and internal photocells again have no line of sight of the sun, though this time there is no adjacent reflective facade. The relatively constant E_I/E_E values of 35% are related to the transmittance of the diffuse sky illuminance under a clear sky luminance distribution. The unobstructed E_I/E_E values rise from about 5% to 25% over this period, as a result of the unobstructed external illuminance dropping at a much faster rate than the internal illuminance values which arise from the sky's glow only.

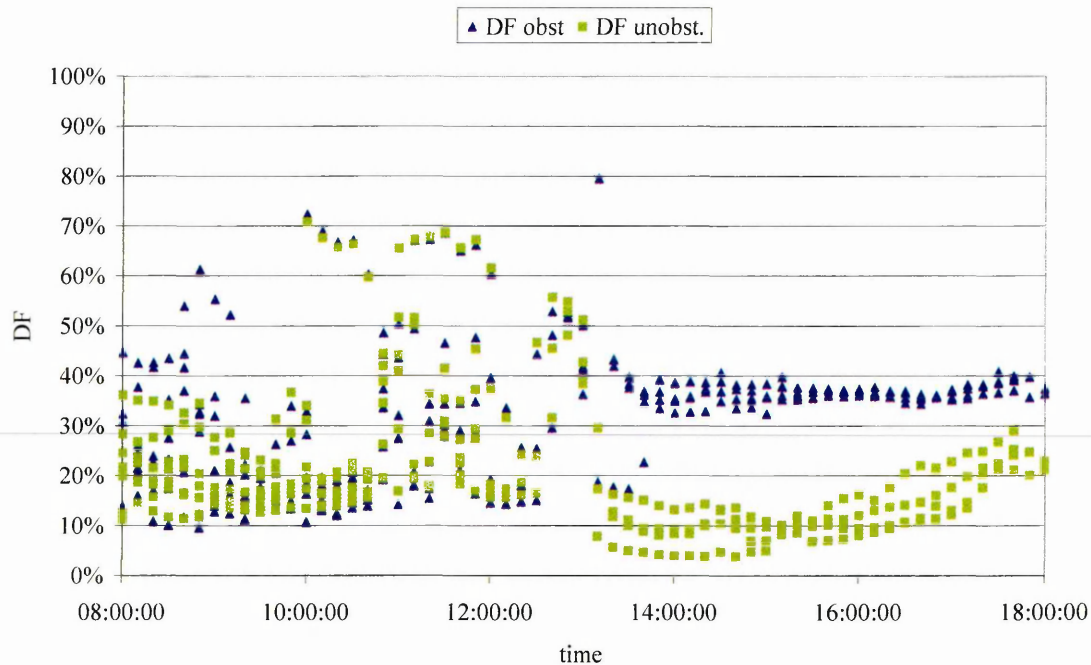


Figure 4-16: The variation of daylight factor over the course of a day under clear skies.

4.3.5 Overcast Skies Analysis

Figures 4-17 and 4-18 show the illuminance results for each of the 481 overcast measuring points for the obstructed and unobstructed photocell. The gradient of these lines gives a result that is related to the transmittance of the roof as measured from the point of the internal photocell. The gradient from the obstructed graph was 0.43 ($R^2=0.98$) and 0.35 ($R^2=0.96$) from the unobstructed graph.

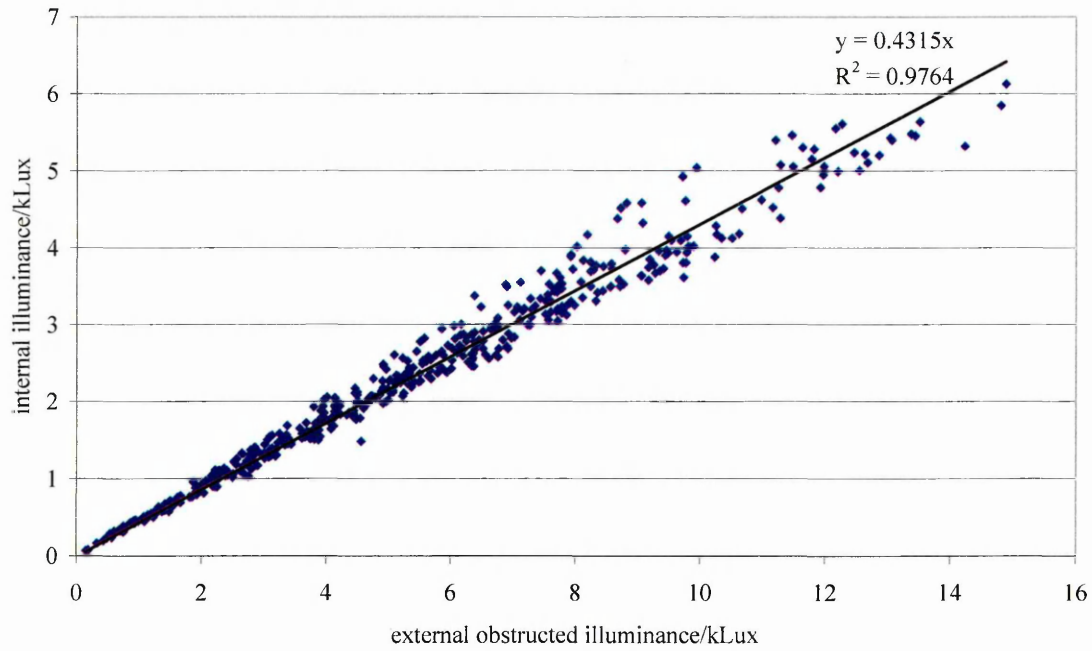


Figure 4-17: Internal illuminance against obstructed external illuminance under overcast skies.

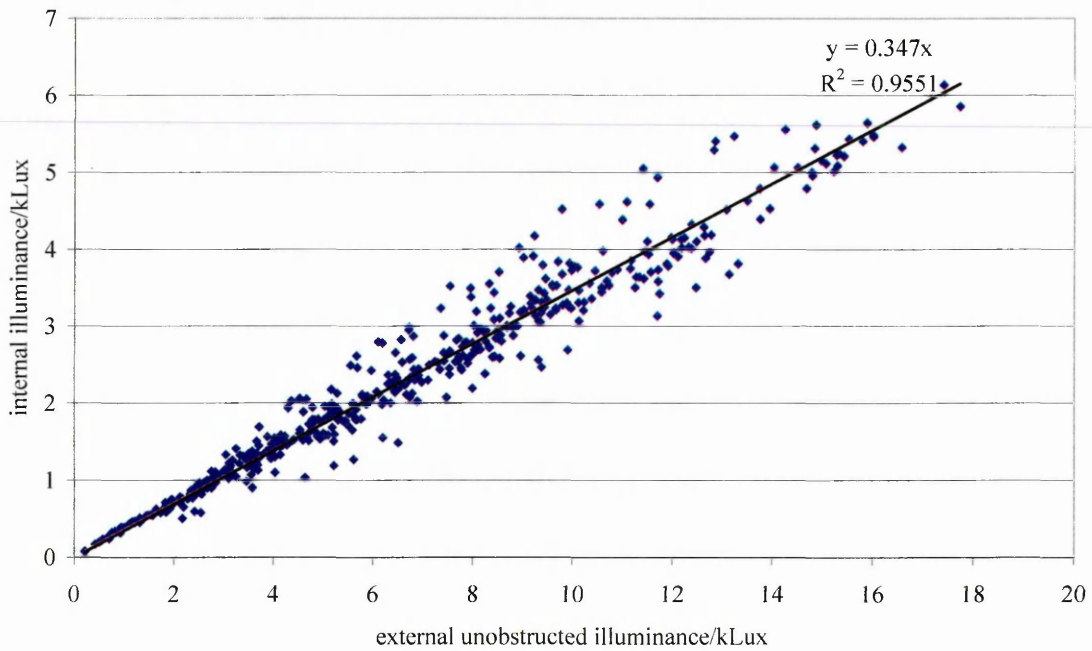


Figure 4-18: Internal illuminance against unobstructed external illuminance under overcast skies.

The two sets of results show good agreement, and it is as expected that the correlation is better in the obstructed case, as the two photocells (internal and obstructed external) are geographically closer, and the surrounding building obstructions are in effect a fixed variable for both. The distribution of derived E_I/E_E values can be seen in

Figure 4-19. Whilst there is a good concentration about the mean, the range of values seems high considering the sky luminance distribution is supposedly constant. The magnitude of the spread is as great as +/- 34% for the unobstructed E_I/E_E values (though only about 20% for the obstructed case).

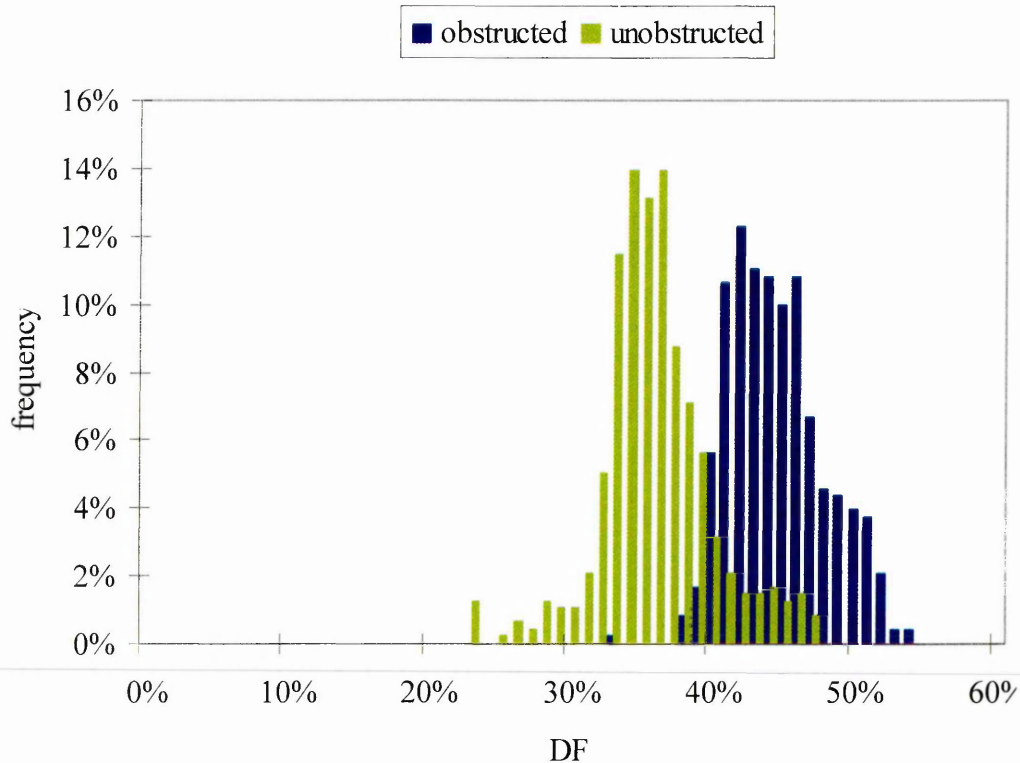


Figure 4-19: The distribution of DF (or more correctly, I_I/I_E in the case of the obstructed results) values derived from the obstructed and unobstructed external photocells.

A graph of daylight factor as a function of time reveals a potential explanation for the large range for the unobstructed skies (Figure 4-20). Small patterns can be seen within the time-bands described in Section 4.3.4 associated with a direct line of sight from the obstructed positions. This could mean that although some of the days classified as overcast may have had total cloud cover, this 'blanket' may not have been dense enough to totally prevent the intensely luminant disc of the sun from influencing proceedings. This would explain the isolated cases of low E_I/E_E values late in the afternoon from the unobstructed photocell, which may be gaining higher illuminance values than the internal photocell where the adjacent facade blocks the path to the setting sun. It would also explain the distinct isolated line of E_I/E_E values at 50% between 10 am and 1.30 pm. Here, the internal photocell has started seeing higher

luminance sky patches, which would offset any higher illuminance values recorded by the obstructed external photocell previously in the day due to reflections of higher luminance sky patches from the adjacent facade.

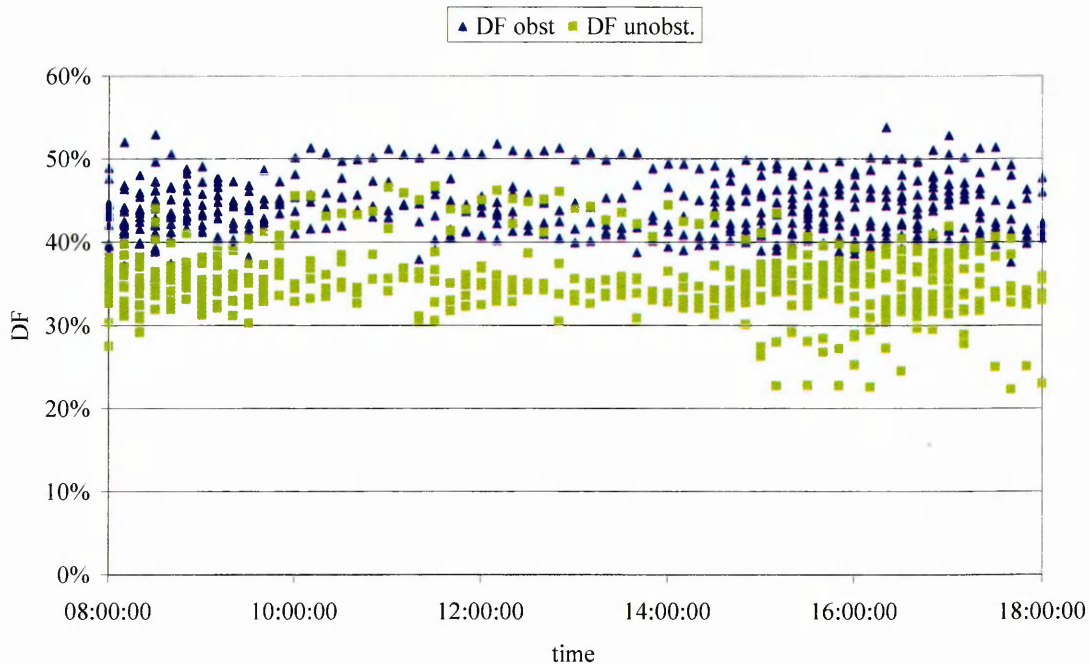


Figure 4-20: The variation of DF (or more correctly, I_I/I_E) over the course of a day under overcast skies.

As with the Sheaf study, these findings must now be translated to roof transmittances. This involves isolating the roof from external factors such as inter-reflection from the well and other non-roof members. The single internal measurement point must also be related to the distribution of results that would occur over the entire roof plane. These two factors are examined in Chapter 6 using computer simulation.

4.4 Conclusions

This chapter has detailed the results from illuminance measurements taken in two case study atria, a simple atrium and one with increased complexity. Internal measurements were taken at one point only due to resource limitations and practical considerations. The results from this one point will be used as a departure point when looking at an entire analysis plane generated through computer simulations in Chapter 6.

The calculated ratio of internal to external illuminances under overcast sky conditions correspond to daylight factor and not transmittance due to contributions from non-roof reflective surfaces. In the case of these experiments, the daylight factor was found to be 60% at the photocell position in the Sheaf building and 35% in the Owen building. The site was found to reduce illumination levels to 80% relative to an unobstructed view of the sky dome. The ratio of internal illuminance to an external illuminance measurement taken under similar site obstruction conditions was measured at 43%. Computer simulation can be used to specify the reflectance of non-roof elements to zero. This information can be used to derive transmittance values from the observed daylight factors from these experiments. Chapters 5 and 6 continue investigation into these case study atria, firstly through a photoanalysis technique, and following that the aforementioned computer simulations.

5

An Investigation of Skylight Gap Fraction through the Analysis of Hemispherical Imagery

- 5.1 Introduction
- 5.2 Results from a Simple Scenario: The Sheaf Building
- 5.3 Results from a Complex Scenario: The Owen Building
- 5.4 Results from Computer Generated Images: Sheaf
- 5.5 Results from Computer Generated Images: Owen
- 5.6 Synthesised Imagery: The Simple and Complex Results Discussed
- 5.7 Conclusions

'I believe in equality for everyone, except reporters and photographers' MAHATMA GANDHI

5.1 Introduction

This chapter presents the results from the photoanalysis technique described in Chapter 3. Sections 5.2 and 5.3 deal with the analysis of the photographs captured with a digital camera in the Sheaf and Owen buildings with respect to the base (photocell) position, the effect of taking photographs from elsewhere, and the legitimacy of using the classifier in HemiView to discriminate gap from blockage. The results for altering the quality of the image in the Sheaf building are also discussed. Sections 5.4 (Sheaf) and 5.5 (Owen) analyse the images generated through computer simulation, and attempt to relate these findings with the results from the physically acquired images. The Chapter concludes with some guidelines for future application of the photoanalysis technique.

5.2 Results from a Simple Scenario: The Sheaf Building

5.2.1 The Base Position

The calculated gap fraction at the photocell position (S1) as obtained from the *adjusted* image was found to be 61.2%. This figure is very close to the measured daylight factor of 61.6% as described in Chapter 4 (a difference of under 1%). This closeness must however be viewed with caution. Three factors need consideration. Firstly, the daylight factor was measured under an overcast sky, which has a heavy bias towards incoming light from the zenith of the sky. The photoanalysis assumption assumes a uniform sky, with no bias from any sky altitude. The second two factors concern the loss of illuminance arriving at points under the roof due to glazing and gains in illuminance due to the structure and the well walls acting as secondary sources of illuminance, as has been mentioned in Chapter 3. In this instance the luminance distribution conditions, the loss from the glazing and the gain from secondary surfaces offset each other almost exactly, making it appear at first glance that the transmittance is due entirely to light entering from those portions seen as visible sky from the photocell position. Chapter 6 will examine further the extent to which the glazing transmittance and structural reflectance play a role by simulation with the Radiance ray tracing program.

5.2.2 Varying Location of Photograph Position

The effects of taking the photographs from the supplementary positions are investigated by comparing the values for gap fraction from *adjusted* images at these positions with the value obtained at the S1. These values along with relative difference from the S1 are shown in Table 5-1.

Table 5-1: Gap fraction results from the five photo positions, and their deviation from the photocell value (S1).

Position	Gap Fraction	Relative Difference from S1
S1	61.2%	0%
S2	58.1%	-5.1%
S3	61.4%	0.3%
S4	68.1%	11.3%
S5	76.1%	24.4%

For photographs taken close to the photocell position i.e. from the 3rd floor, the match is good. The visible sky seen from the corner position is 5.1% lower than at the photocell, whilst from the central position the proportion of visible sky seen is only 0.3% greater.

It was thought that a possible reason as to why the corner position is 5% lower is the considerable view of the underside of the window cleaning gantry seen from that viewpoint. The underside of the gantry is clearly not seen from the photocell position (the photocell being clamped level with the gantry) (Figure 5-1). This region of the image had to be painted red and ignored in calculations. It is likely that this region has a higher proportion of gap than blockage compared to the rest of the roof area within the image. This is because the area of blockage gets higher with increasing distance from the viewpoint due to structural members receding in perspective and gathering close together. Omitting this region would return a falsely low value. The *adjusted* image from the photocell position was amended by painting out the area the gantry would occupy if projected up towards the roof in red. The region of analysis was now congruent to that of the 3rd floor corner position (S2). The image was analysed in HemiView. The gap fraction value of 61.6%, a difference of only 0.6% (and in the wrong direction) means that this is probably not the reason for the lower value.

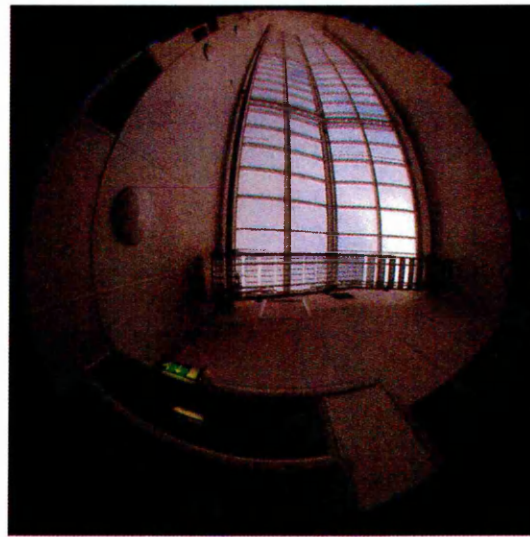
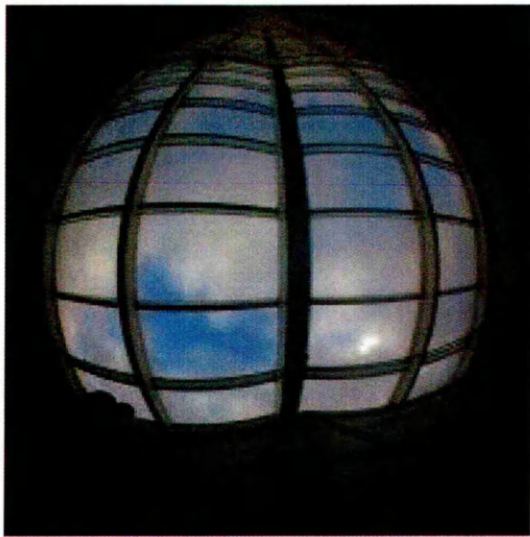


Figure 5-1: View from the S1 (left) and S2 (right). The gantry upon which S1 lies is clearly visible from S2.

Another possible reason for the lower value is the displacement in the horizontal plane further towards the corner. This has the effect of seeing the central purlin, a prominent member which runs the length of the image, from a more sideways view thus revealing more of its depth. This would give return a lower gap fraction value (due to higher blockage).

The central position may be slightly higher due to less of a perceived loss at the ends of the image. In the central position the members only converge for half the distance as from the end position. There is therefore less compressed region in the central image. Further discrepancies between the photocell position and 3rd floor positions can be attributed to slight error in defining the exact boundary between images when painting in the red 'ignore' areas. This error could potentially bias the results in either direction.

For photographs taken from the ground floor the agreement with the photo taken from the photocell position is less good. Both images return greatly higher values for gap fraction, 11.3% higher from the end position and 24.4% from the central position. There are two main reasons as to why these values are significantly higher. The first of these is the change of perspective. As the depth increases, so the perspective moves further towards the conditions for a plan view, that is to say, the focal point moves in the direction of infinity (Figure 5-2). This being the case, we would expect the gap fraction output to approach that of [100% - POA] (to get visible sky). The PAO for this

roof was measured to be 27%. This means the visible area in plan is 73%. As can be seen, the value at the end position of 68% does indeed approach it, whilst the 76% obtained from the central position exceeds it.

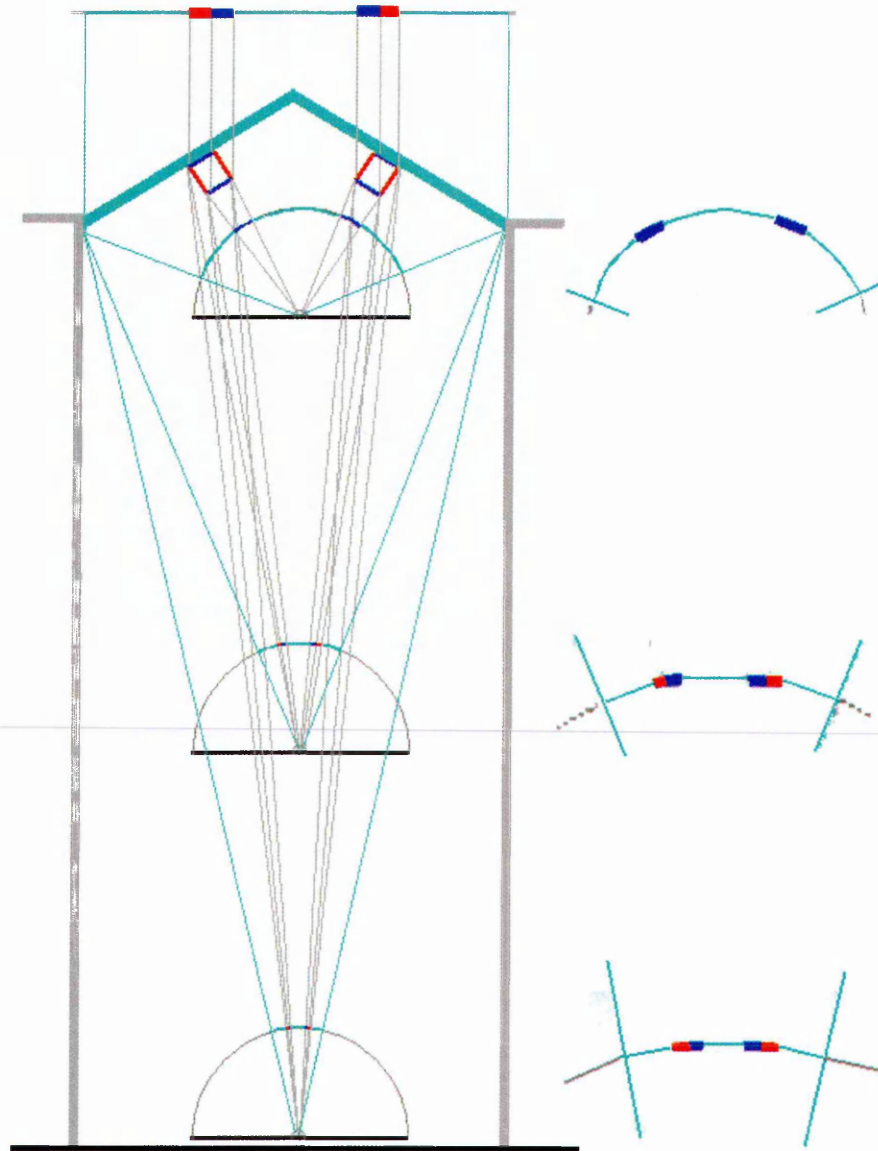


Figure 5-2: As the viewpoint moves deeper into the well (i.e. further from the roof), the area of interest diminishes, and the lines of perspective approach plan conditions (i.e. parallel).

The value of 76% at the centre position, even higher than the 'plan area of visible sky' leads us to the second reason as to the high values. As the depth changes from a position very close to the roof to one at the base of the atrium, the area of the hemispherical image the roof occupies (and the only part of the image we are concerned with) diminishes. This can clearly be seen by the narrowing of the field of view in

Figure 5-2. This tests the resolution of the camera to its limits, and where structural members appeared crisp in the upper positions they are jagged in the base images, and sometimes have part or even whole purlins missing. Painting on the structure to form the *adjusted* image can only be done to a certain extent, for example where members have been 'thinned out' if their width is greater than one pixel but less than two there is little option but to leave it thin. HemiView has no choice but to classify the thinned or omitted regions as gaps, even though they are patently not. Advances in camera resolution could go a long way to remedying the situation, and Section 5.2.4 will discuss the effects of image quality by comparing these results with photos taken at lower qualities.

Further possible sources of error concern the regions painted red. The overhead walkways, service gantry and stepped nature of the well meant that much of what may possibly have been visible at ground level had to be treated as section to ignore. This has the potential to shift the values higher or lower. As with the higher up positions, the exact boundary of well and roof too may be a slight source of error, which again could potentially shift results upwards or downwards. Neither of these factors would have the capacity to cause such an increase in gap fraction values measured from the base of the well.

The full effects of moving the point of image capture away from the roof are investigated further in Section 5.4 using the Radiance program.

5.2.3 Assessing the Legitimacy of the Classified Results

Table 5-2 shows the values of gap fraction returned by HemiView for the *classified* results. The photos were taken at the *hi* setting. The percentage differences between the *classified* reading and the base case result (S1 *adjusted*) as well as the difference between the *classified* reading and the *adjusted* reading from that position are shown.

Table 5-2: Reference and Classified gap fraction results from the five viewpoints, together with the relative differences between the classified results and S1 and the relative difference between the classified and reference results from that viewpoint.

Position	Reference Visible sky	Classified Gap Fraction	Relative Difference from S1 reference	Relative Difference from reference at that point
S1	61.2%	59.6%	-2.6%	-2.6%
S2	58.1%	58.4%	-4.6%	0.5%
S3	61.4%	63.8%	4.2%	3.9%
S4	68.1%	69.3%	13.2%	1.8%
S5	76.1%	78.7%	28.6%	3.4%

The discrepancies between the *classified* results and the base case results are similar to those between the *adjusted* results and the base case; the high up positions returning a low error, the low down positions returning higher errors. The direction and magnitude of these errors have been sufficiently discussed in the above section.

Amending the image in a paint program adds time to the process. Sufficient closeness between the classified and amended reference case should enable the method to be implemented on non-amended photos using the classifier in HemiView. The only editing to the photo would be the simple task of painting the non roof parts in red. The closeness of the *classified* results with the *adjusted* results taken from the same position is encouraging. In all cases, the difference is under 4%, and in all but one case (the photocell position), the classified case is an over-estimation.

The under-estimation at S1 is probably due to the sky conditions under which the image was taken. The need to plan in advance when the photo could be taken due to the presence of health and safety parties, coupled with the unpredictable nature of real dynamic sky conditions, meant that the photo taken from this position was captured under a partly cloudy sky. As has been discussed previously, this complicates the classification process, with the author having to visually match losses in white structure with gains from dark blue parts of the sky (Figure 5-3).

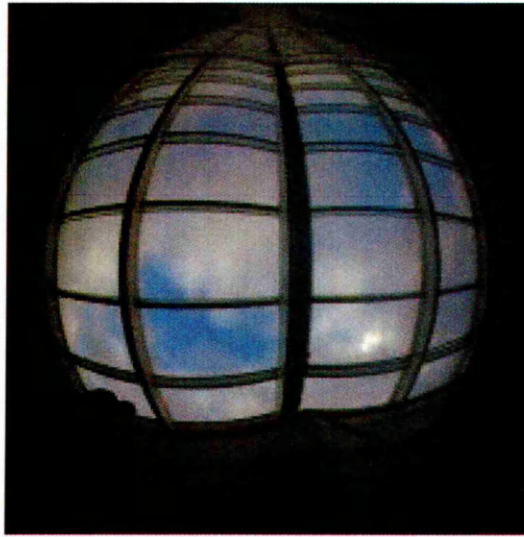


Figure 5-3: For practical reasons, the photograph at S1 could not be taken under even skies. The resultant partially cloudy sky made classification more problematic.

The slight overestimation occurring at the other points is due to there being slightly more blockage in the *adjusted* image. This is due to the elements intuitively painted on in black by the author. The slightly higher levels of gap fraction output is the price sacrificed for a faster process.

Table 5-3 shows the *lower* and *upper* bounds for gap fraction values within classification (as determined by the author) for photos taken under the *hi* camera setting.

Table 5-3: The lower and upper values of gap fraction reasonably possible for these scenarios and the relative differences to the adjusted value.

Position	Lower	Adjusted	Upper	Relative difference lower to adjusted	Relative difference upper to adjusted
S1	48.5%	61.2%	66.9%	-20.8%	9.3%
S2	56.9%	58.1%	66.2%	-2.1%	13.9%
S3	60.5%	61.4%	67.0%	-1.5%	9.1%
S4	66.9%	68.1%	72.4%	-1.8%	6.3%
S5	75.7%	76.1%	79.7%	-0.5%	4.7%

In every case, the *adjusted* case falls between the upper and lower bound. In every case bar the photocell position, the *lower* bound is only marginally less than the *adjusted* case. The anomalously low value at the photocell position is due to the cloudy sky under which the photo was taken. In order to include all the structure for classification, a large part of the sky was also considered as blockage. The closeness of the *lower* bound and *adjusted* case highlights the sharp contrast between gap and blockage when moving the classifier downwards from its maximum incrementally

(Figure 5-4, last five images moving from 180 to 140). It is relatively straight forward classifying an image in this way.

The *upper* boundary values fall further away from the *adjusted* case. The value recorded at S2 in particular seems high. This is attributed to a slightly uneven (though cloudless) sky luminance. More generally however, by moving the classifier upwards from its minimum incrementally, we can see the relative effects of moving one denomination seem visibly minimal compared to moving downwards from the maximum (Figure 5-4 first five images moving from 100 to 140). In fact, there are small changes in classification of blockage occurring due to variation in brightness over the structural members. It is not unimaginable that an inexperienced user could underestimate the amount of blockage. Moving the classifier downwards from the maximum however should minimise the error. As has already been seen, the match between the *classified* results and the *adjusted* results was good.

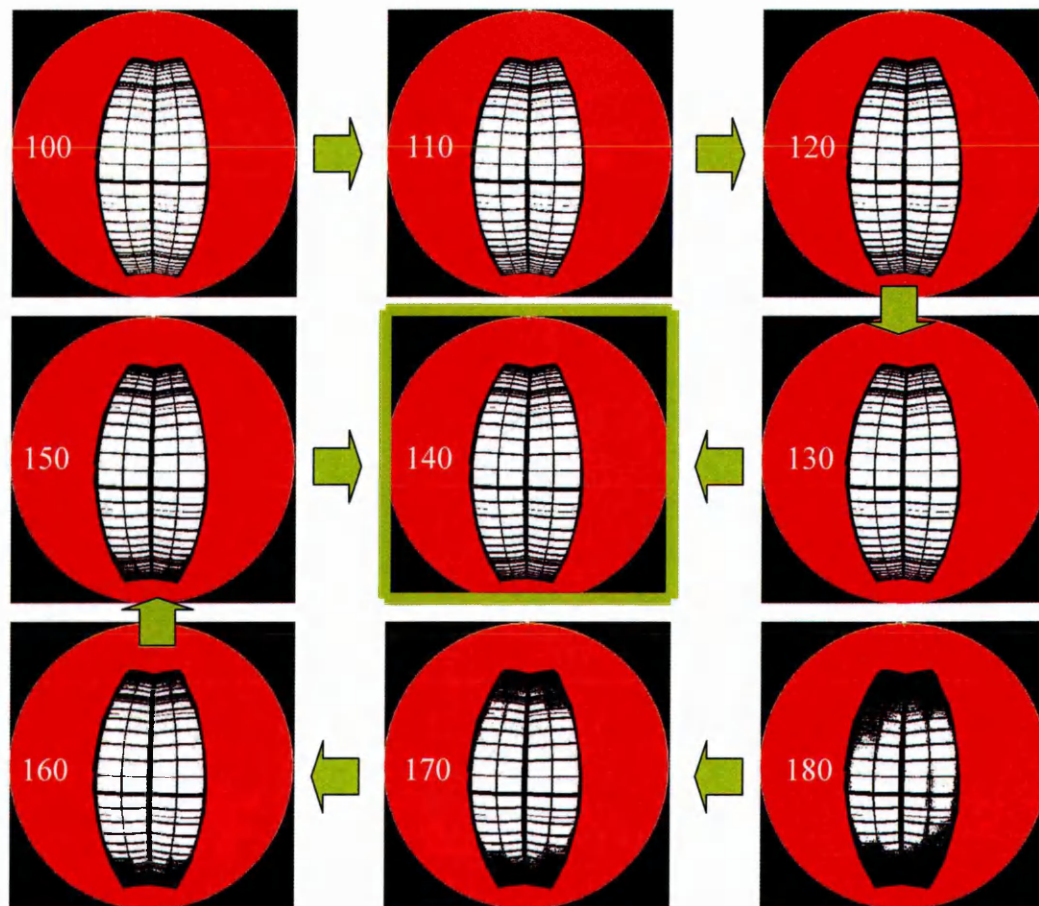


Figure 5-4; Assuming the image is classified with the threshold set at 140. Moving upwards in increments of 10, it is clear that by 180 too much of the image has been classified as blockage. Moving downwards in increments of 10, by 100 there is still ambiguity (example looks at position S3).

5.2.4 Varying the Quality of the Image

Table 5-4 shows the *classified* readings for the images taken at the three quality levels along with the errors associated relative to the *adjusted* image taken at the highest quality setting. As expected, there is a direct link between image quality and accuracy of results. The *hi* quality images produce the lowest average error (2.4%) followed by the *fine* setting (6.7%) and lastly the *normal* setting (7.8%).

Table 5-4: Classified gap fraction results from taking the photographs at the three quality settings of the camera for positions S2-5, along with the relative difference to the reference value.

Position	Adjusted <i>hi</i>	<i>Hi</i>		<i>Fine</i>		<i>Normal</i>	
		Classified	Relative difference	Classified	Relative difference	Classified	Relative difference
S2	58.1%	58.4%	0.5%	58.8%	1.2%	61.4%	5.7%
S3	61.4%	63.4%	3.9%	64.7%	5.4%	66.3%	8.0%
S4	68.1%	69.3%	1.8%	77.0%	13.1%	75.1%	10.3%
S5	76.1%	78.7%	3.4%	81.6%	7.2%	81.6%	7.2%
Mean			2.4%		6.7%		7.8%
STDEV.			1.55%		4.93%		1.92%

The encouraging closeness of the *adjusted* results and the *hi classified* results have been discussed above. The low standard deviation indicates that this slight over-estimation of gap fraction is of consistent magnitudes.

The compressed image (jpeg) formats perform less successfully. Even positions near the roof return reasonably high values for gap fraction. The large standard deviation at the *fine* images coupled with the high over-estimation of gap fraction demonstrates an increased ineffectiveness in methodology that accompanies a loss of image quality. The even larger over-estimation at a lower image quality is expected, though the low standard deviation shows the magnitude of this error is at least consistent. The higher the quality of the image, the more information it will contain. With more information, there exists a greater potential for subtle differences over small distances to be picked up. Consequently, the image will become more sensitive to classification. This is however balanced by the potential to pick up more useful information (roof structure in this case), and thus build up a more life-like/informed picture. It should not come as a surprise that the standard deviation is higher at the *fine* level than at the *normal* level. Whilst the results are likelier to be closer to the *adjusted*

hi cases (due to picking up more of the roof structure), there exists a greater potential to be inconsistent in the classifying (as can be seen by the error ranging from 1.2% to 13.1%). The fact that this is not extended to the *hi* setting must mean that the *hi* image contains sufficient information for accurate classification to surpass minor discrepancies between, say two points in the sky. The means and standard deviations are only based on four measurements, and as such can only be seen to give a snap shot of the situation. Slight variations in sky luminance between when the photos at different quality were taken may also have slightly influenced the results, as well as inconsistencies in defining the boundary of the area of interest and the ignored red region.

Table 5-5 shows the *adjusted* value with *upper* and *lower* bounds and error relative to the reference image taken at the *hi* quality. Table 5-6 surmises the average values of error from Table 5-5.

Table 5-5: Gap fraction results for the lower and upper boundaries at the three camera quality settings for positions S2-5.

Position	Quality	Lower	Adjusted	Upper	Relative difference lower to <i>Hi</i> adjusted	Relative difference adjusted to <i>Hi</i> adjusted	Relative difference upper to <i>Hi</i> adjusted
S2	<i>Hi</i>	56.9%	58.1%	66.2%	-2.1%	0%	13.9%
	<i>Fine</i>	55.6%	56.0%	64.2%	-4.3%	-3.6%	10.5%
	<i>Medium</i>	55.8%	60.4%	71.9%	-4.0%	4.0%	23.8%
S3	<i>Hi</i>	60.5%	61.4%	67.0%	-1.5%	0%	9.1%
	<i>Fine</i>	63.0%	63.0%	67.4%	2.6%	2.6%	9.8%
	<i>Medium</i>	64.0%	64.1%	71.9%	4.2%	4.4%	17.1%
S4	<i>Hi</i>	66.9%	68.1%	72.4%	-1.8%	0%	6.3%
	<i>Fine</i>	71.1%	72.1%	75.9%	4.4%	5.9%	16.7%
	<i>Medium</i>	73.9%	73.2%	78.9%	8.5%	7.5%	15.9%
S5	<i>Hi</i>	75.7%	76.1%	79.7%	-0.5%	0%	4.7%
	<i>Fine</i>	79.6%	78.2%	82.5%	4.6%	2.8%	8.4%
	<i>Medium</i>	74.3%	79.6%	85.6%	-2.4%	4.6%	12.5%

Table 5-6: Mean errors for the three camera quality settings

Quality	Mean of Relative difference lower to <i>hi</i> adjusted (standard deviation)	Mean of Relative difference adjusted to <i>hi</i> adjusted (standard deviation)	Mean of Relative difference upper to <i>hi</i> adjusted (standard deviation)
<i>Hi</i>	-1.5% (0.7%)	0% (0%)	8.5% (4.0%)
<i>Fine</i>	1.8% (4.2%)	1.9% (4.0%)	11.4% (6.7%)
<i>Medium</i>	2.0% (5.8%)	4.4% (1.6%)	14.0% (4.7%)

With the *adjusted* images the effects of loss in quality are even more clearly defined than for the *classified* results. As the image quality decreases, the gap fraction result increases due to a loss in structure captured by the camera (Figure 5-5).

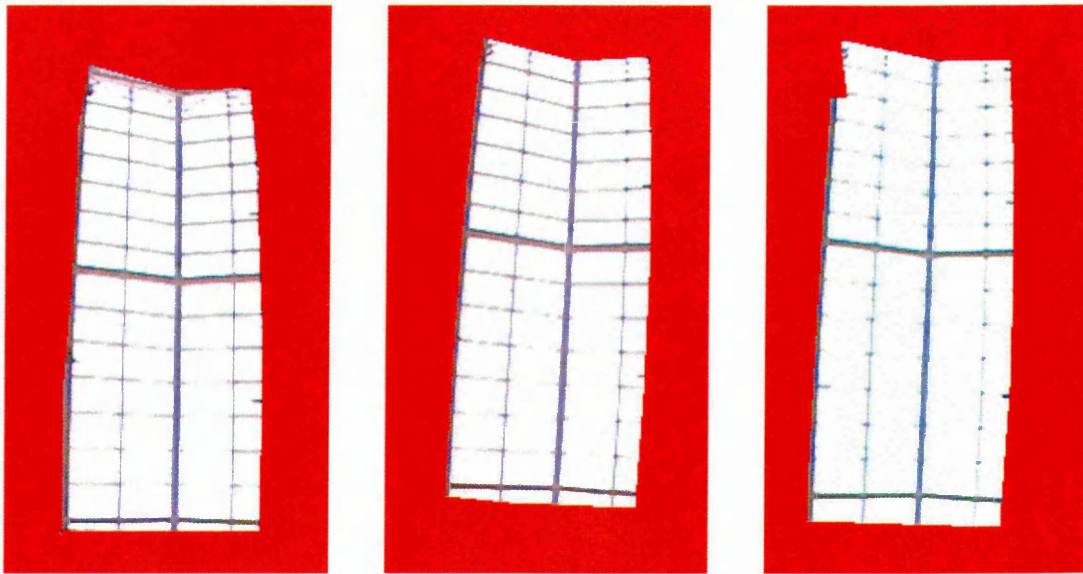


Figure 5-5: Detail from position S5 at *hi*, *fine* and *normal* quality (l-r). The *normal* image clearly omits detail present in the other images.

As was the case for the *hi* images, the *adjusted* image results are closer to the *lower* bound than to the *upper* bound. Again, this is due to being able to distinguish more clearly the point at which blockage turns to gap when moving the classifier downwards than trying to ensure the sky is completely clear at the loss of too much structure (as discussed Section 5.2.3). In most cases the lower error bound at *fine* and *medium* quality are positive. This indicates that even exhibiting a bias towards obtaining low gap fraction values the figure is still too high. Interestingly, in some cases (S4 *medium* and S5 *fine*) the *lower* bound of classification actually exceeds the *adjusted* case of its own quality (rather than just of the *hi adjusted*). This clearly demonstrates the effect of painting in some of the missing structure, and underlines the dangers of using images of low quality for classification without previous amendment. Even with the amendments, the gap fraction values are too high, indicating an insufficient level of structure drawn on. It is not possible to completely accurately amend the image to a point representing no loss of quality. It is too reliant on guesswork, and obstruction real width may lie between two discrete pixel numbers. For small obstructions, this error is magnified for example a strut that is 0.4 pixels wide can be drawn as one pixel wide or not represented at all. Over the course of a whole roof,

significant errors can and do arise. In any case, it is not time effective to redraw an entire roof in practice.

The results are displayed in their entirety in Figure 5-6.

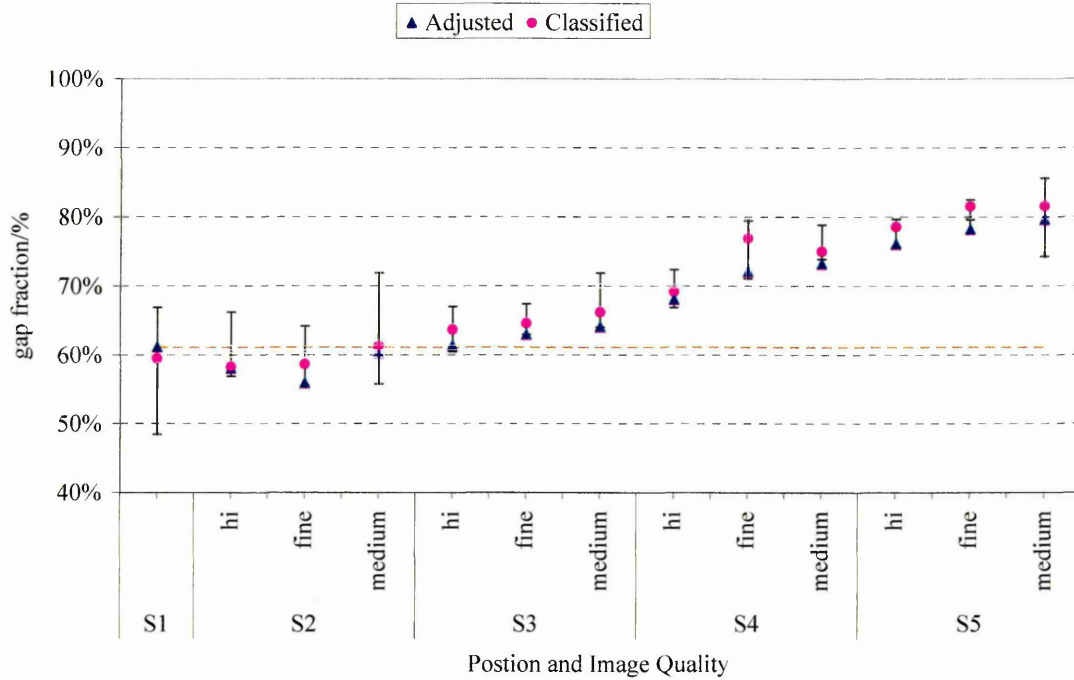


Figure 5-6: Overall results from the Sheaf building.

It is clear that taking the photo at the highest quality from a position as near as possible to the point of measurement is desirable. Images at low qualities should not be used as they return falsely high results due to missing out small structural detail that becomes significant over a whole roof. Interpolating from the highest quality setting available to the lowest one can see the loss in accuracy. The results achieved at the highest setting were sufficient. It is not unreasonable to expect even more accurate results extrapolating towards higher quality images that are becoming more the standard with advances in technology. Section 5.4 will look more closely at the effects of systematically moving the point of image capture away from the base case using Radiance.

5.3 Results from a Complex Scenario: The Owen Building

5.3.1 The Base Position

The calculated gap fraction at the photocell position as obtained from the *adjusted* image was found to be 32.6%. The gap fraction for the *unobstructed* image was found to be 52.2%. From these, the percentage of blockage due to roof structure and external obstructions can be derived, given that;

$$GF_O + SB + EB = 100\% \quad [5-1]$$

and

$$EB = GF_U - GF_O \quad [5-2]$$

so

$$SB = 100\% - GF_O - EB = 100\% - GF_U \quad [5-3]$$

where,

GF_O = obstructed gap fraction (i.e. *adjusted*)

SB = structural blockage

EB = external blockage

GF_U = unobstructed gap fraction

The percentage blockage due to external obstructions was 19.6%, with the blockage due to the roof structure 47.8%. This value is markedly higher than the measured PAO of 28.9% (a relative difference of 65%).

The gap fraction value of 32.6% is marginally lower than the measured daylight factor (unobstructed E_I/E_E) of 35% (Chapter 4). If all the 'gap' were gap, and all opaque surfaces pure light sinks, under uniform skies we might expect the gap fraction value of 32.6% to equate to the daylight factor of 35%. The fact that the daylight factor is a

measure taken under overcast which are not uniform in distribution, means a difference between the two values should be expected. Likewise, with the same 'gap as gap' and 'obstructions as light sinks' conditions, we might expect the *unobstructed* gap fraction of 52.2% to equate to the obstructed E_I/E_E value of 43%. In the case of the *adjusted* (obstructed) HemiView image, the gains from reflective elements in the scene (i.e. external obstructions, roof structure and internal well reflections) marginally outweigh losses due to the presence of glazing in the 'gaps'. In the case of the *unobstructed* HemiView image, the losses due to glazing outweigh the contribution due to reflective elements. This is discussed further in Chapter 6 with the benefit of comparison with Radiance simulation results.

5.3.2 Varying Location of Photograph Position

The HemiView output from all viewpoint positions can be seen in Table 5-7. The gap fractions as derived from the adjusted and unobstructed images are displayed together with each position's deviation from the result obtained from the photocell position (O1). From the two results from each position, the structure blockage and external blockage are calculated. The proportions of gap fraction, structure blockage and obstruction blockage can be seen in Figure 5-7.

The agreement between the photocell position (O1) and from photos taken from the same plane and locality is good, with the exception of O4. Percentage difference from O1 for gap fraction is under 5% for O2, O3 and O5 though O4 is 28% lower. Similar low differences are seen with the *unobstructed* and hence derived structure and external blockage results. The small differences between O1 and O2, O3 and O5 are due to slightly different viewpoints and hence arrangement of structure in the field of view.

Table 5-7: Adjusted and unobstructed gap fractions for the 12 Owen viewpoints, together with the differences from the O1 position, and derived structure blockage and external blockage values.

Position	Adjusted gap fraction	Relative difference from O1	Unobstructed gap fraction	Relative difference from O1	Structure Blockage	External blockage
O1	32.6%	-	52.2%	-	47.8%	19.6%
O2	32.6%	0%	48.6%	-6.9%	51.4%	16.0%
O3	34.0%	4.3%	52.7%	1.0%	47.3%	18.7%
O4	23.4%	-28.2%	47.0%	-10.0%	53.0%	23.6%
O5	32.6%	0%	53.0%	1.5%	47.0%	20.4%
O6	22.6%	-30.7%	40.5%	-22.4%	59.5%	17.9%
O7	36.6%	12.3%	55.9%	7.1%	44.1%	19.3%
O8	26.5%	-18.7%	55.1%	5.6%	44.9%	28.6%
O9	28.9%	-11.3%	50.0%	-4.2%	50.0%	21.1%
O10	30.3%	-7.1%	55.5%	6.3%	44.5%	25.2%
O11	33.7%	3.4%	55.1%	5.6%	44.9%	21.4%
O12	48.6%	49.1%	66.4%	27.2%	33.6%	17.8%
<i>Statistics for all positions;</i>						
Mean;	31.9%		52.7%		47.3%	20.8%
STDEV;	6.5%		5.9%		5.9%	3.4%
Coefficient of Variation;	20.4%		11.3%		12.5%	16.3%
<i>Statistics excluding O4,6,7,12;</i>						
Mean;	31.4%		52.8%		47.2%	21.4%
STDEV;	2.6%		2.5%		2.5%	3.9%
Coefficient of Variation;	8.3%		4.7%		5.3%	18.3%

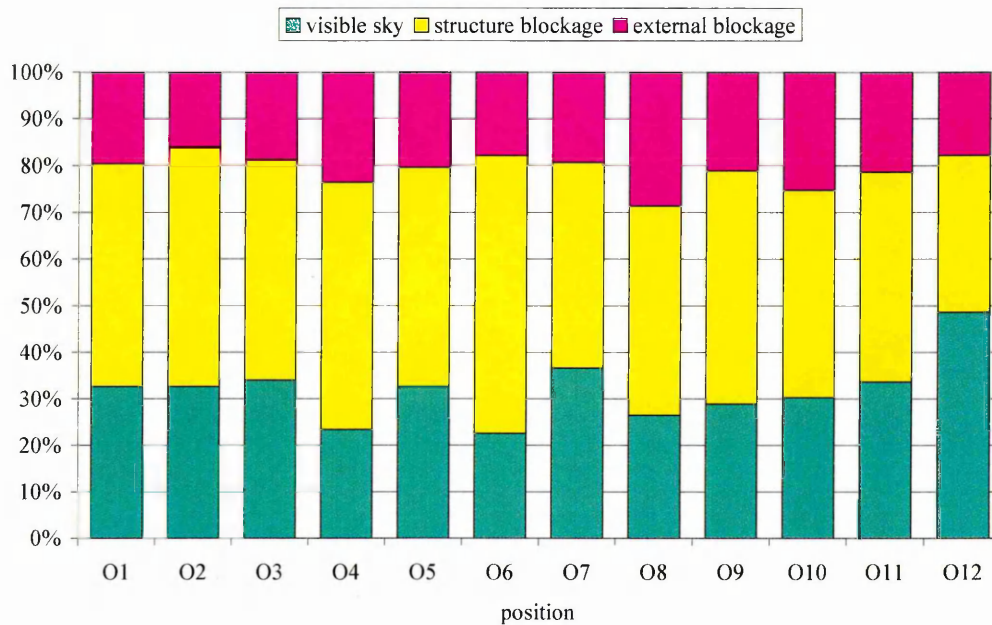


Figure 5-7: Visible sky, structure blockage and external blockage proportions as seen from the 12 viewpoints

The much larger difference between O1 and O4 is due to more than simply this. The field of view seen at O4 includes an area of side glazing in the well which is included in the analysis (Figure 5-8). The view through this is mainly of blockage from a combination of structure and the surrounding external built environment. The area was dark and therefore classified as blockage (either structure or external) hence the low *adjusted* gap fraction result. The low contrast within this dark patch made manual differentiation between roof structure or external blockage challenging, and thus it is likely the proportion of structure blockage may have been over-estimated (at 53%) relative to the external obstruction blockage (23.6%). The presence of this side glazing does contribute in actual terms to illuminance levels within the well. However, in the case of analysis of solely the roof, calculations ignoring the side glazing would have been more desirable, and as such this result is not representative of HemiView analysis made from the other positions.



Figure 5-8: The view at O4 sees an element of side glazing which was included in the analysis, though it is not representative of roof transmittance properties.

The two positions on the bridge at the other end of the well (O6 and O7) show poor agreement with the values calculated at the photocell position. The gap fraction seen at O6 is 30.7% lower and 12.3% higher at O7 than at O1. The low recorded value at O6 was due to the high density of roof structure immediately about where the photo was taken from, underneath a juncture of several structural elements (Figure 5-9). This is confirmed by the derived value of 59.5% for structure obstruction which is easily the highest value recorded of all the photos. The high value recorded at O7 is due to the presence of a secondary source of top glazing from an adjacent space which was

included in the calculation (Figure 5-10). As with the side glazing at O4 (though this time the glazing was relatively unobstructed), this glazing was not representative of the overall form and arrangement of the main roof.

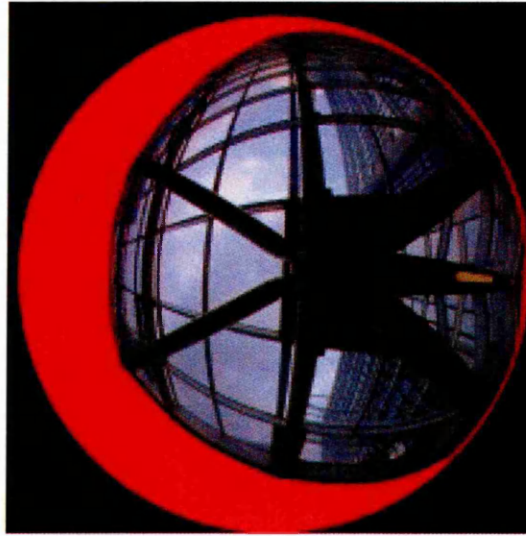


Figure 5-9: Position O6 lies immediately beneath a busy juncture of structural members.

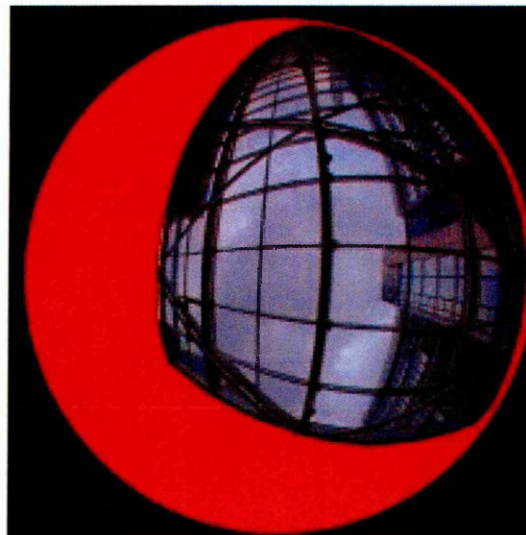


Figure 5-10: Position O7 sees an adjacent top-lit space, which was included in the analysis though is not representative of the overall roof transmittance.

The results from the upper floor (O8-11) exhibit a trend concerning movement across the minor axis (east to west). Moving eastwards across the well, *adjusted* gap fraction values rise from 26.5% to 33.7%. The *unobstructed* gap fraction values are 55% for all cases with the exception of O9 which is at 50%. Adjusting the images from 'obstructed' (referred to as *adjusted* in this study) to *unobstructed* is a process with scope for error dependant on where within each image the author decided the structure

had receded, the elements converged into too dense a patch and painting in the sky became too coarse a process. Whilst undertaking the analysis by a constant experimenter in one sitting reduces this error, it is possible that slightly erroneous results could occur. It is imaginable that the *unobstructed* value at O9 could be slightly low. Either taking this to be the case, or ignoring that point from consideration for the time being, it would appear that the proportion of structure obstruction at any point on the top floor plane remains constant (at approximately 45%) regardless of lateral displacement. The proportion of external obstruction diminishes moving from west to east i.e. away from the obstructing influence of the Owen building. As a comparison to the photocell position, those on the top floor have lower obstruction due to structural blockage and a higher blockage due to external obstructions (at any point). The lower external obstruction blockage value at the photocell position could be due to being higher up and hence being marginally less overshadowed. A more likely reason, and linked to the higher value of structure obstruction at O1 may mean that there is more structure obstructing the external 'obstruction'. The higher value of structure blockage at O1 is down to a closer proximity to the roof structure, and hence seeing more of the elements in section as well as in plan.

The *adjusted* gap fraction value calculated at the ground floor (O12) is 49.1% higher than that calculated at O1. The derived value for structural blockage at the ground floor was 33.6% as opposed to 47.8% at O1. As with the Sheaf building taking the photo deeper down the well leads to the blockage due to structure approaching the PAO (which is in this case 28.9%) due to the perspective of the roof approaching plan form. A further cause of the high value of gap fraction observed at the ground floor may be due to the loss in image quality discussed in section 5.2.4.

It can be seen that the calculated values at the photocell position for gap fraction, structure blockage and external blockage are close to the mean of all the photo results. This is encouraging and shows that there is potential to take photos from several possible points within the well. Removing the results which have been discussed as anomalous changes the mean averages little, though significantly reduces the spread of the results. The coefficient of variation for obstructed gap fraction falls from 20.4% to 8.3% and from 11.3% to 4.7% for *unobstructed* gap fraction. The coefficients of variation for the structural blockage is 5.3% (down from 12.5%) and 18.3% (up from

16.3%) for the external blockage. The relatively high value of coefficient of variation for the external blockage highlights an element of experimental error. The method adopted relied heavily on the intuition and consistency of the author when painting in the sky over the external obstruction, and could lead to minor inconsistency between processing images. Whilst this produced a standard deviation of just under 4%, this translates to a coefficient of variation of just under 20% when dealing with an element that only occupies about 20% of the view.

The excluded four results are excluded for two primary reasons. The first of these is 'localised factors', and the second concerns depth. In applying this method, it must therefore be stated that the photo should aim to capture a representative view of the roof, and thus not be taken where localised features could influence the results e.g. under large structural junctions or adjacent to other glazed areas. If the photo is to be taken next to a large area of additional glazing, that region should be painted red and ignored in the calculations. Secondly, the photo should be taken as close to the level of the roof plane as possible. Taking a photo too deep in the well will lead to the structure occupying lower proportions of the field of view. It should also be noted, as observed by the potentially erroneous result at O9, that if possible (time, access) photos from more than one position should be taken such that potential experimental error is highlighted.

5.3.3 Assessing the Legitimacy of the Classified Results

A comparison of gap fraction results between the *adjusted* obstructed (sky gap flood filled white) and *classified* obstructed (raw image) can be seen in Table 5-8. The *classified* results show a good agreement with the *adjusted* results. In all but two cases, the difference was under 5% in relative terms, as is demonstrated by the RMS of 3.1%. In the case of the Sheaf building, the *adjusted* cases (bar from the photocell position which was taken under a partly cloudy sky) returned lower gap fraction results than the *classified* cases due to structure in the reference cases being painted black. In this case, whether the *classified* exceeds the reference or vice versa is specific to the individual case. A primary reason for this is the classification concerning the external obstruction. The specular highlights on the windows of the main external obstructing element (the Owen building) would have been interpreted slightly differently for each case when

classifying the *adjusted* and *classified* image. A further reason is the slightly non-uniform sky luminance distributions. This may affect the classification process for the classified images where an element of intuitive offsetting of blockage and gap was required by the author. It should be re-iterated that these differences are small.

Table 5-8: A comparison between adjusted and classified gap fraction results.

Position	Adjusted gap fraction	Classified gap fraction	Relative difference classified to O1 adjusted	Relative difference classified to adjusted at that point
O1	32.6%	30.9%	-5.2%	-5.2%
O2	32.6%	32.9%	0.9%	0.9%
O3	34.0%	33.9%	4.0%	-0.3%
O4	23.4%	23.7%	-27.3%	1.3%
O5	32.6%	32.1%	-1.5%	-1.5%
O6	22.6%	23.5%	-27.9%	4.0%
O7	36.6%	37.2%	14.1%	1.6%
O8	26.5%	24.9%	-23.6%	-6.0%
O9	28.9%	28.9%	-11.3%	0.0%
O10	30.3%	30.9%	-5.2%	2.0%
O11	33.7%	32.3%	-0.9%	-4.2%
O12	48.6%	49.7%	52.5%	2.3%
			RMS:	3.1%

Tables 5-9 and 5-10 show the results of classifying the results to the *upper* and *lower* bounds of rational classification. As expected the *adjusted* value always falls within the *upper* and *lower* bounds. For both the *obstructed* and *unobstructed* images, the magnitudes of the *upper* bound exceed that of the *lower*. When classifying for the *upper* values, a significant proportion of the structure was omitted (classified as gap) to account for the darkest patches of sky luminance. In classifying for the *lower* bound, the main indicator was ensuring most of the specular flecks from the external obstruction were classed as blockage. This occurred closer to the *adjusted* value than the former in classifying for the *upper*. The mean of the differences are lower for the *unobstructed* images. This is expected, as the *unobstructed* images had been modified and as such classification was less ambiguous.

Table 5-9: Classification upper and lower bounds of the obstructed images.

Position	Lower	Adjusted	Upper	Relative difference lower to adjusted	Relative difference upper to adjusted
O1	31.2%	32.6%	34.6%	-4.3%	6.1%
O2	30.9%	32.6%	37.3%	-5.2%	14.4%
O3	33.1%	34.0%	36.2%	-2.6%	6.5%
O4	22.2%	23.4%	25.0%	-5.1%	6.8%
O5	30.1%	32.6%	40.9%	-7.7%	25.5%
O6	22.2%	22.6%	25.3%	-1.8%	11.9%
O7	35.5%	36.6%	41.0%	-3.0%	12.0%
O8	25.8%	26.5%	27.7%	-2.6%	4.5%
O9	27.0%	28.9%	31.1%	-6.6%	7.6%
O10	29.1%	30.3%	32.4%	-4.0%	6.9%
O11	30.7%	33.7%	36.2%	-8.9%	7.4%
O12	47.7%	48.6%	52.0%	-1.9%	7.0%
			Mean;	-4.5%	9.7%
			STDEV;	2.6%	5.6%

Table 5-10: Classification upper and lower bounds of the unobstructed images.

Position	Lower	Unobstructed	Upper	Relative difference lower to adjusted	Relative difference upper to adjusted
O1	52.1%	52.2%	60.5%	-0.2%	15.9%
O2	48.6%	48.6%	52.5%	0.0%	8.0%
O3	52.6%	52.7%	53.3%	-0.2%	1.1%
O4	46.8%	47.0%	53.6%	-0.4%	14.0%
O5	52.8%	53.0%	61.0%	-0.4%	15.1%
O6	40.5%	40.5%	44.0%	0.0%	8.6%
O7	55.8%	55.9%	60.7%	-0.2%	8.6%
O8	55.1%	55.1%	57.8%	0.0%	4.9%
O9	49.9%	50.0%	54.8%	-0.2%	9.6%
O10	55.5%	55.5%	56.3%	0.0%	1.4%
O11	54.8%	55.1%	58.0%	-0.5%	5.3%
O12	66.4%	66.4%	67.4%	0.0%	8.8%
			Mean;	-0.2%	7.8%
			STDEV;	1.8%	4.8%

A summary of the results with associated *upper* and *lower* bounds can be seen in Figure 5-11. The results for the *classified* images show sufficient agreement with the manually manipulated *adjusted* images to consider them suitably accurate for use. Using the classifier rather than manually altering the images is a far faster process. The only alteration needed to field captured images is the painting of non-considered regions in red.

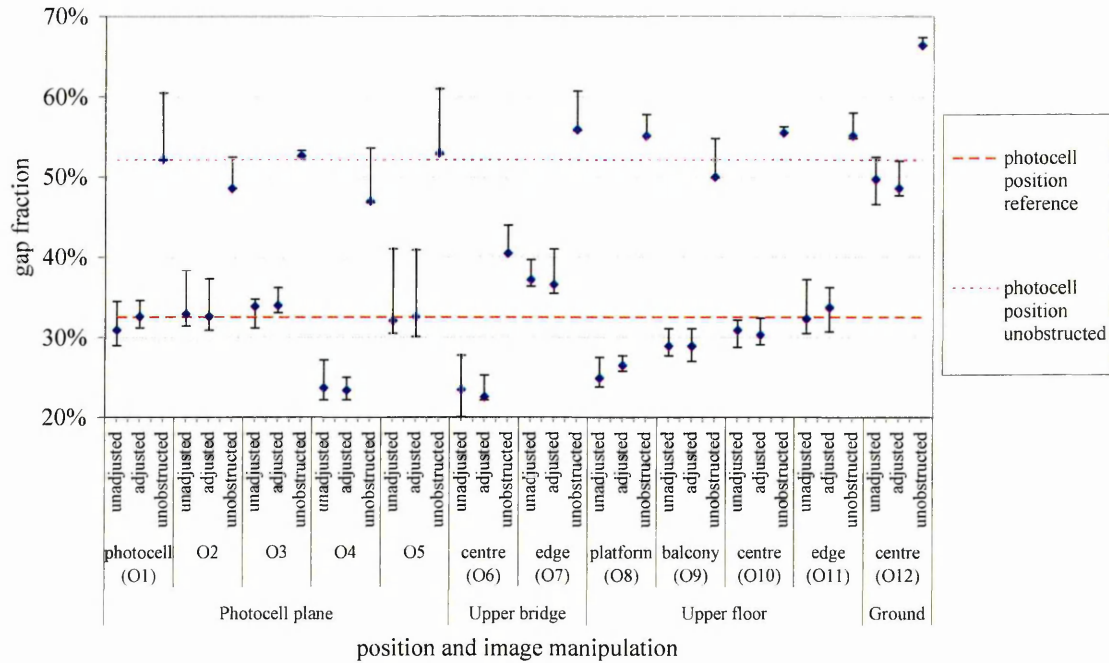


Figure 5-11: Overall results from the photographs analysed at the Owen building

5.4 Results from Computer Generated Images: Sheaf

The proportion of gap fraction seen from the increasing depths into the well at central and end positions can be seen in Table 5-11 and Figure 5-12. For both lateral positions the proportion of gap fraction drops sharply from the roof plane to a depth of about 4m (the most rapid change occurring between 0m and 2m) and from there the value remains relatively constant. In the case of the end position, this entails a rise from approximately 62% to 77%, a 19% relative increase, and from 53% to the same value at the centre position, a rise of 31%.

Table 5-11: Gap fraction values at end and central axis positions with increasing depth of the Sheaf building.

Well depth/m	Gap Fraction End	Gap Fraction Centre
0 (roof plane)	0.622	0.531
0.5	0.659	0.599
1	0.684	0.608
1.5	0.7	0.668
2	0.715	0.686
3	0.751	0.742
4	0.747	0.736
6	0.748	0.744
8	0.762	0.762
10	0.754	0.763
12	0.766	0.768
14	0.764	0.774
16	0.766	0.778
18 (base)	0.767	0.775

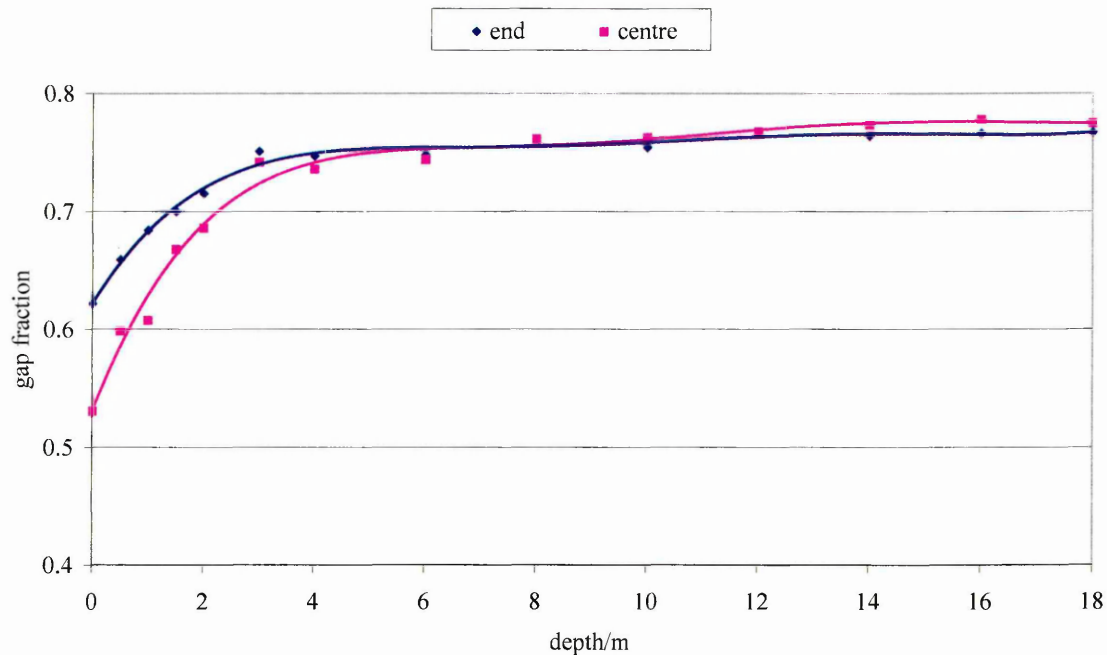


Figure 5-12: The effect on gap fraction of increasing depth from the roof plane at end and central positions.

This rise in the amount of gap seen is a result of seeing the roof geometry at a differing perspective. At the roof plane, very close to the roof structure, the structural elements 'surround' the view, with the side and base surfaces of the members occupying area within the field of view. As the depth increases, the quantity of structure seen in profile decreases, and the base of structure as seen from below predominates the field of view.

In the region between 0m and 4m, the proportion of gap seen at the end position exceeds that at the centre. The reason for this is that the central position is directly beneath a main roof I-beam. This roof beam only becomes visible in the field of view at the end position at increased depths within the well (Figure 5-13).

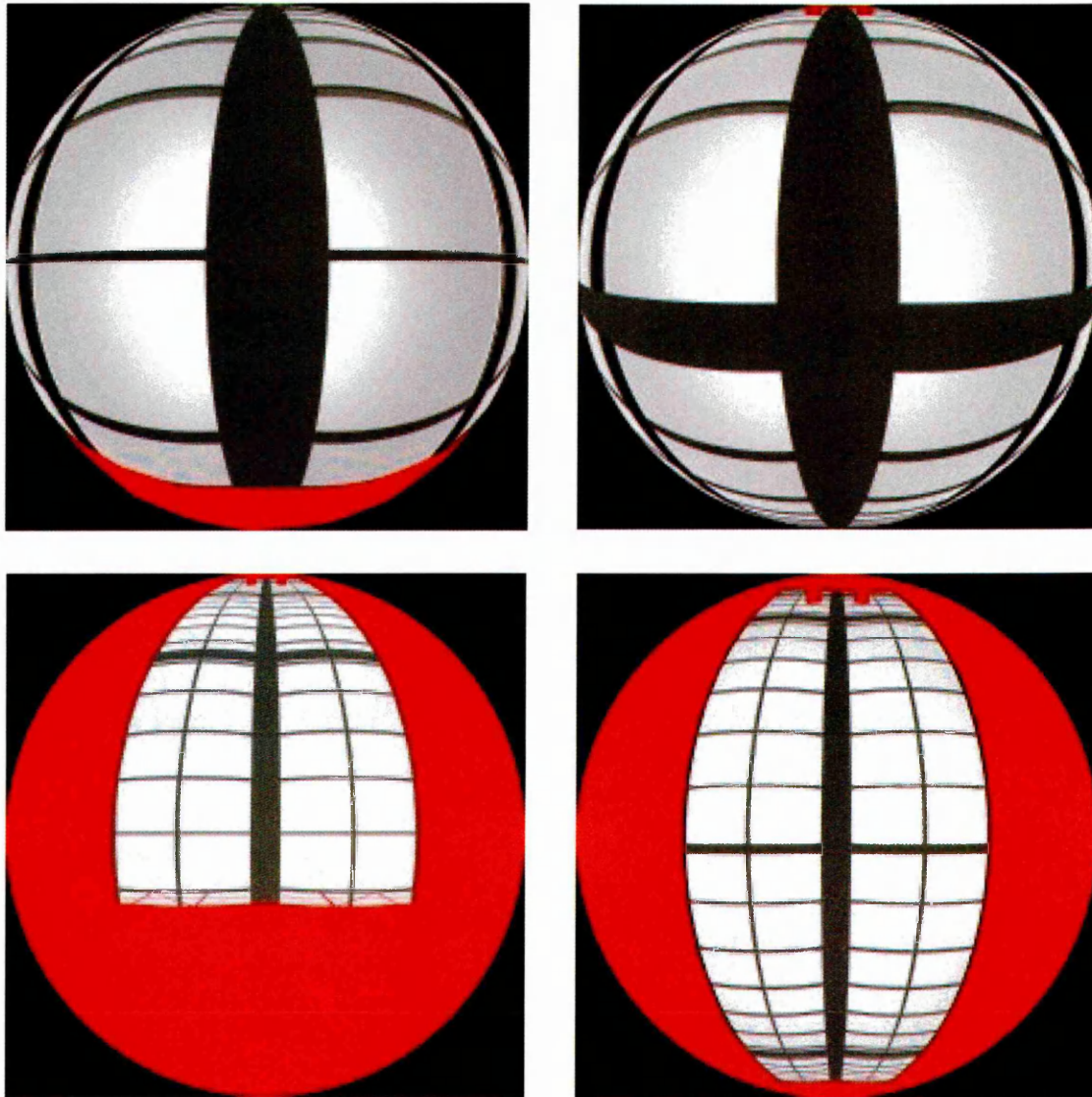


Figure 5-13: Views at end (left) and central (right) positions at depths of 0m and 4m. At roof plane level, the large cross beam occupies a significant proportion of the field of view at the central position. At the increased depth, the impact of this member has diminished.

In the case of this well, at depths of greater than 4m, changing the lateral or vertical displacement has little effect on the amount of visible sky seen. At the roof plane, the area of interest (i.e. the roof area, which is not painted red) is effectively 100%. At a depth of 4m into the well the area of interest occupies 62% of the hemisphere at a central position, and 43% at an end position (Figure 5-13). At these

levels most of the sectional views of the structure appear to have diminished due to perspective. The image has converged on a value for gap fraction, similar to the [PAO-1] of the roof.

Curiously, this value of 77% exceeds the [PAO-1] value of 73%. The sharpness of detail of the structural members even at the deepest viewpoint let alone at a depth of only 4m suggests that this is not due to the images missing detail, as was the case with the photographs physically taken at depth within the well. The CAD model used to generate the viewpoints was the same one as was used to determine the PAO and so any error in modelling should produce the same effect on both values. A possible source for the slightly higher than expected results of gap fraction concerns the Radiance rendering. The images required for HemiView analysis needed only the silhouette of the obstruction. In fact, more detailed renderings with subtle contrast variance over the surfaces are more prone to error in HemiView classification. Two means of generating the images in Radiance were adopted, both of which turned off the computationally expensive 'indirect' calculation. For the Sheaf building, a sunny sky at midday was used to illuminate the scene. In the case of the Owen building, an overcast sky was used and an arbitrary ambient value applied as the illuminating medium. The very high intensity of the sun may have saturated some obstruction to the point where it became 'whited-out' and as such was classified as gap rather than blockage. An example of this can be seen in Figure 5-14 where a small white gap runs the length of the structural member. Over the entirety of an image this could have caused the over-estimation of gap fraction. It is recommended that for the generation of images in Radiance for HemiView, an overcast or uniform sky should be used.

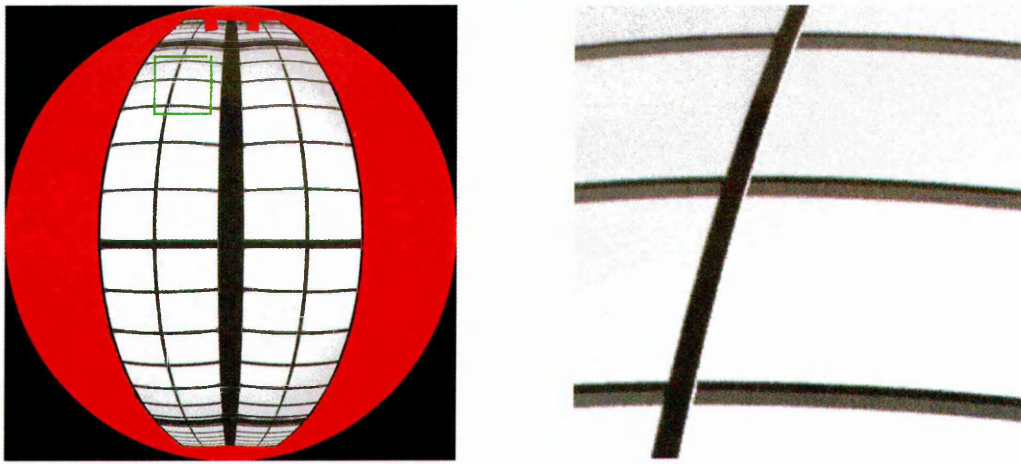


Figure 5-14: Narrow omissions of structure running along the length due to saturation of the side of the structural member by the intense light source (the 'sun').

The gap fraction results from the physically taken photographs can be approximated in viewpoint position to the Radiance derived images. The results of these are plotted as individual points in Figure 5-15. The photocell position is near to the end roof plane position. S2 and S4 are equated to the 'end' results at depths of 6m and 18m. Likewise, S3 and S5 are compared to the 'centre' results at 6m and 18m. Figure 5-16 reveals the crudeness of these comparisons. None of the views match exactly, though the closest is probably S3.

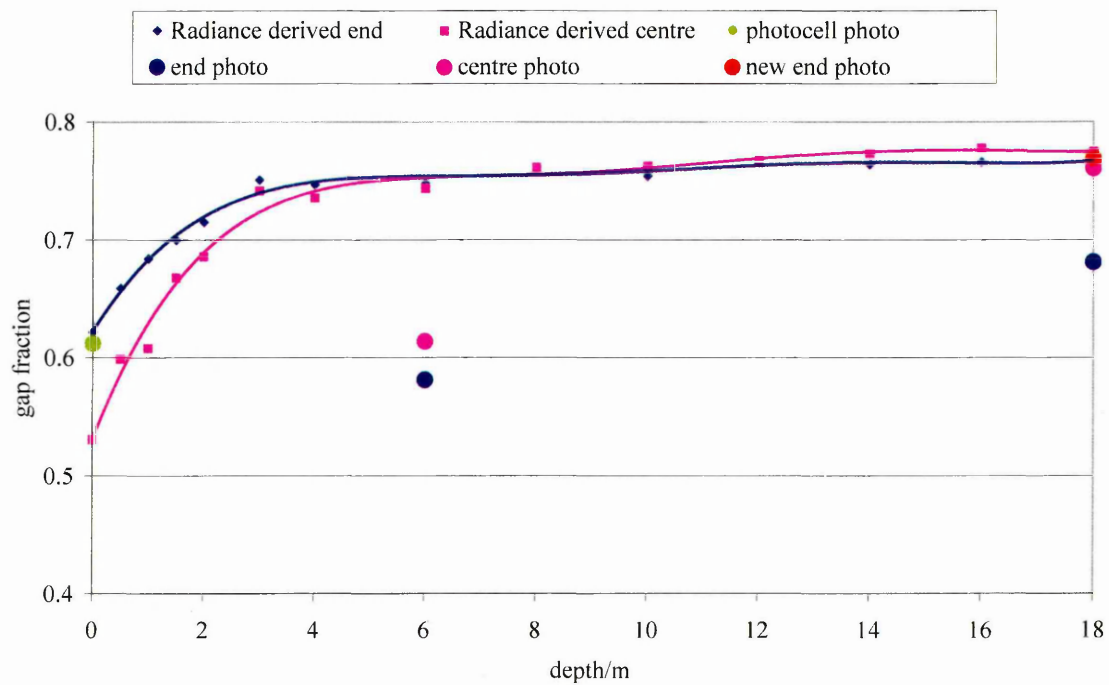
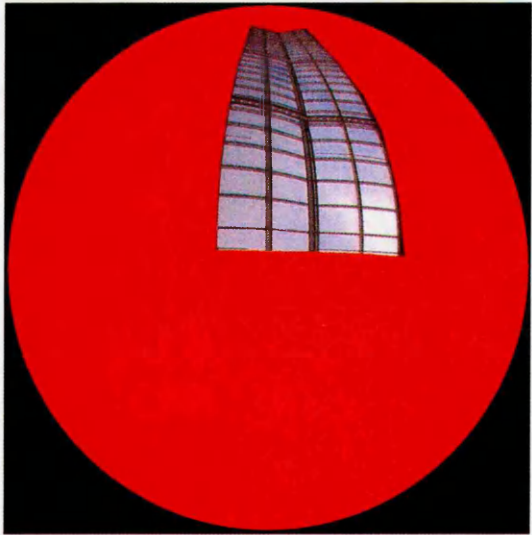
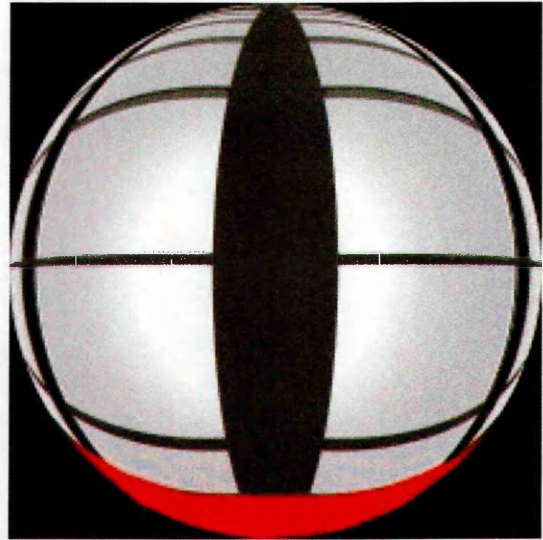


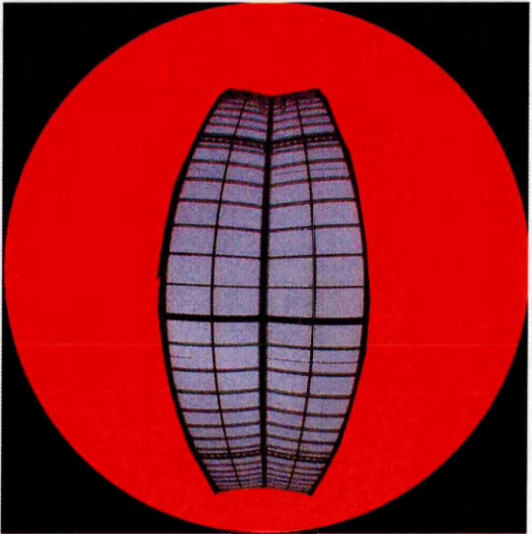
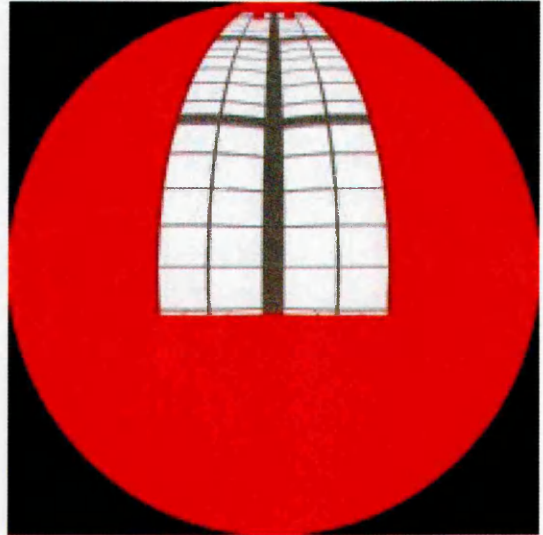
Figure 5-15: The gap fraction results from the physically captured photographs overlaid onto the curves from the generated images. The values fit with varying levels of success.



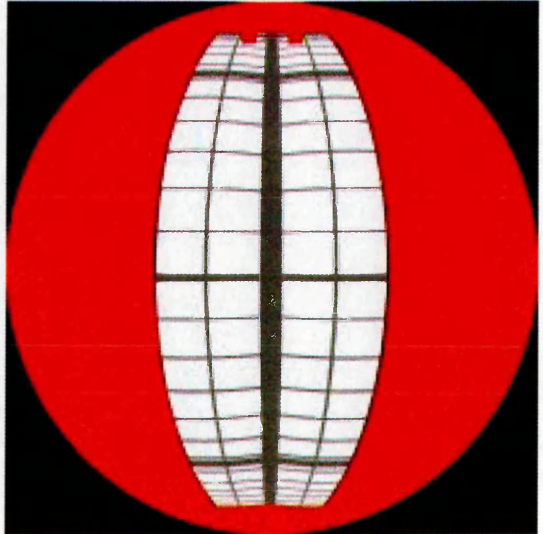
S1



S2



S3



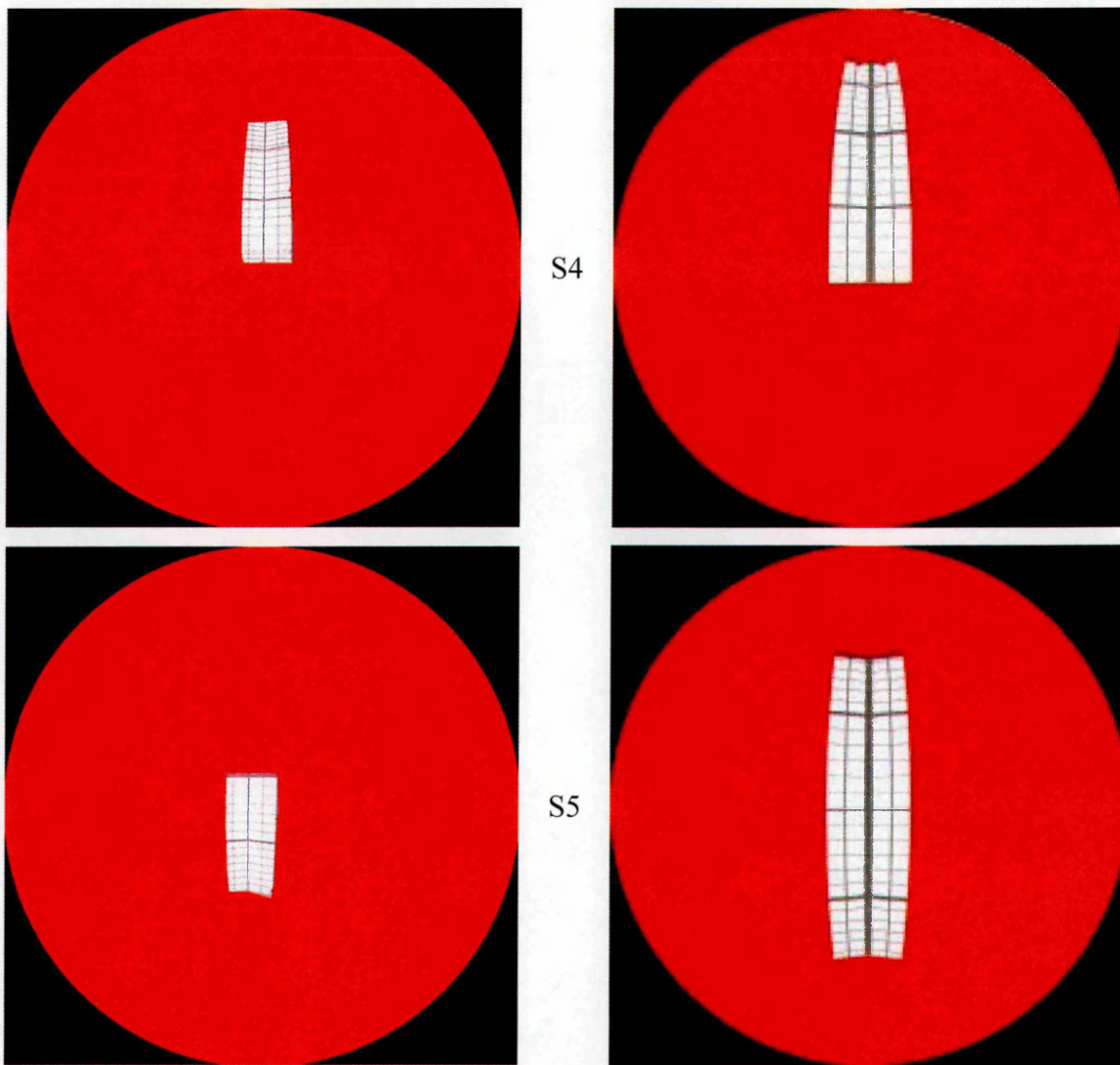


Figure 5-16: Side-by-side comparisons of the physically acquired photos (left) to the computer images (right) generated at the closest position to the former, for positions S1 (top) through to S5 (bottom).

At first glance the photocell result shows good quantitative agreement with the view generated at the end of the well level with the roof plane. Comparison of the images reveals the photocell position was slightly below the level of the roof plane, displaced slightly off centre. This being the case, the main structural spine of the roof constitutes a far greater blockage in the generated viewpoint than in the actual photograph. In the physical photograph, the structural elements receding into the distance resulted in too dense a zone of noise and consequentially the entire area was classified as blockage. In the computer derived view, the higher resolution ensured the areas at the top edge of the image were defined as gap. These two negating factors resulted in the perception of genuinely good agreement.

The S2 position values show a poor agreement, with 58% calculated from the corner photograph and 75% from the end generated image. Essentially the two images were taken from significantly different positions hence agreement was not expected. At this depth there was however little difference between the centre and end results from the generated views indicating that this observed difference was due to more than a difference in lateral position. The difference here was mainly a result of the distant parts of the roof being classified entirely as blockage in the photograph, and a combination of gap and blockage in the generated image.

A similar mismatch occurred at the centre position (S3). Here, the photo viewpoints were a better approximation of each other than at the corner/end viewpoint, as a walkway crossing the width of the well allowed a photo to be taken almost directly underneath the roof centre. The difference between the photo (61.4%) and the generated image (74.4%) is great, though not as great as at S2. The source of this divergence again can be found at the extreme ends of the roof. In the photograph, the structure converges to an area that is classified entirely as blockage in HemiView, whereas in the generated image the higher resolution ensured differentiation between gap and structure at the roof ends was possible. This occurred to less of an extent than at the corner position, as the ends of the roof are closer and (hence larger) to the central position. It is interesting to note the different shapes of the areas of interest, the top edges of the walls distorted to sharper curves in the photograph. This is due to the difference between the fisheye lens and the Radiance purely hemispherical algorithm. This is not an expected source of error, as the lens type had been set accordingly within HemiView.

A comparison of the photographs and generated images taken at the ground floor shows good agreement between the central position but poor agreement with the end position. A visual comparison shows the extent to which the overhead balconies occupy the field of view from the ground floor looking up, and as such the reduced area of interest available for analysis. The generated images did not suffer this fate, with the well detail (walkways etc.) omitted from the model. The central photograph value is very near to that of the generated image. Despite the differing sizes of analysis, the repeating nature of the roof ensures both fields contain a similar proportion of gap and blockage. As discussed, both values exceed the [PAO-1] value, in the case of the

photograph through omitted detail, in the case of the generated view due to the small quantity of washed out structure.

The end position photograph value of 68.1% is significantly lower than the generated value of 76.7%. It would, if anything, be expected that the gap fraction value for the photograph would exceed that of the generated image due to loss of structural detail. The reason for this conflict is the defined area of interest in the captured photograph. The edge of the atrium well had not been entirely painted in red, and thus contributed to the calculation as blockage. The calculation was repeated with the area of wall painted red, as can be seen in Figure 5-17. This new value for the photograph was 76.9%, a very near match with the generated image (Figure 5-15).

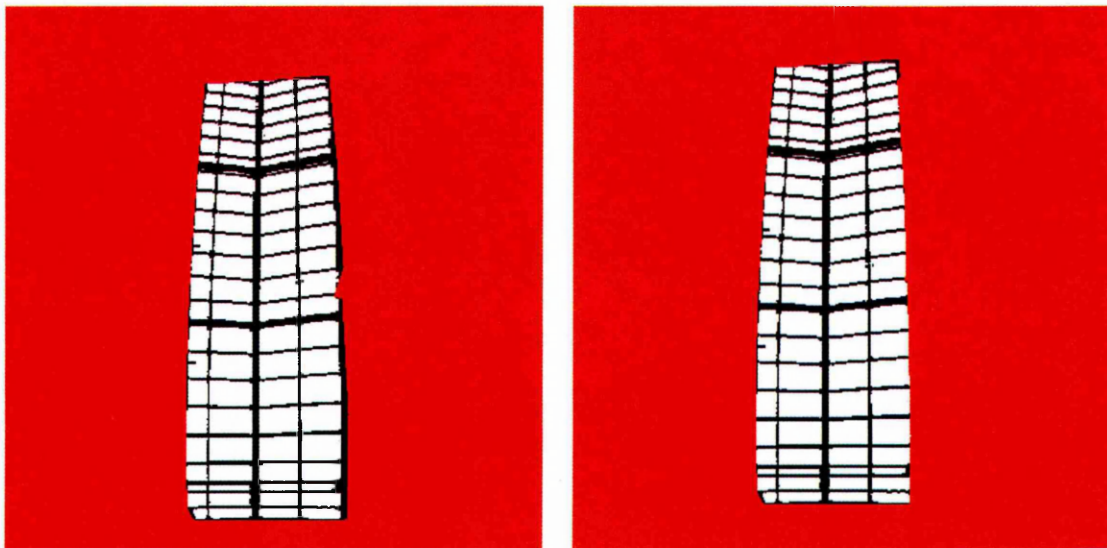


Figure 5-17: Comparison of photo S4 before (left) and after (right) modifying the right hand edge from black to red.

The comparison between the photographs and generated images has been useful in stressing the importance of accurately defining the field of analysis. In this instance, only a small area of well included in the calculation resulted in a reasonably large error. Defining the area with a sufficiently 'zoomed in' view and using tools such as 'smart edge selection' facilitates the process.

Discovery of error in the gap fraction result from the S4 photograph clearly has ramifications on previously stated analysis and trends of Section 5.2.2. The difference of 11.3% from the photocell value increases to 25.7%, a much better match to the 24.4% difference between the photocell position and the S5 viewpoint. This result implies that at such a vertical displacement from the roof, movement in the lateral

direction has little bearing on the calculated gap fraction seen at that point. Whilst quantitatively there may be minor alterations to the relationships describing the legitimacy of classified results, the basic conclusions previously discussed still hold. The *classified* image returns a marginally higher gap fraction than the *adjusted* image (whilst previously this difference was 1.8%, the agreement is now closer at 0.4% difference). The *adjusted* value still falls between the *upper* and *lower* bounds of classification, and closer to the *lower* than the *upper*, for the reasons stipulated in section 5.2.3.

5.5 Results from Computer Generated Images: Owen

5.5.1 Replicating the Physically Acquired Photograph Positions

The gap fraction results from the synthesised images for *obstructed* and *unobstructed* views can be seen in Table 5-12, along with the relative differences between the photograph derived values. On average the synthesised images returned gap fractions 30% higher in the *obstructed* cases and 20% in the *unobstructed* cases.

Table 5-12: Comparison of physically captured photograph with computer generated images for obstructed and unobstructed images.

Position	Obstructed gap fraction		Relative Difference	Unobstructed gap fraction		Relative Difference
	Photo	Synthesised		Photo	Synthesised	
O1	32.6%	49.6%	34.3%	52.2%	70.9%	26.4%
O2	32.6%	47.4%	31.2%	48.6%	67.8%	28.3%
O3	34.0%	51.6%	34.1%	52.7%	68.6%	23.2%
O4	23.4%	44.7%	47.7%	47.0%	63.4%	25.9%
O5	32.6%	36.4%	10.4%	53.0%	57.6%	8.0%
O6	22.6%	35.6%	36.5%	40.5%	60.1%	32.6%
O7	36.6%	50.3%	27.2%	55.9%	70.8%	21.0%
O8	26.5%	38.0%	30.3%	55.1%	64.4%	14.4%
O9	28.9%	41.7%	30.7%	50.0%	63.9%	21.8%
O10	30.3%	44.1%	31.3%	55.5%	65.4%	15.1%
O11	33.7%	46.6%	27.7%	55.1%	65.4%	15.7%
O12	48.6%	60.9%	20.2%	66.4%	73.8%	10.0%
Mean;			30.1%			20.2%

The *obstructed* and *unobstructed* values were used to obtain structure blockage and external obstruction blockage values as described in Section 5.3.1. A comparison with the photograph results can be seen in Figure 5-18. A relatively good agreement can be seen in the proportion of external obstruction values derived from the two methods. The difference concerns the ratio of visible sky to structural blockage. The same reasons as were found with the Sheaf building apply in this case too. The lower resolution of the camera as compared to the synthesised images resulted in a lot of distant parts of the roof being classified entirely as blockage, when in reality as is confirmed by the synthesised images, gaps exist. This phenomenon diminishes with increasing depth in the well. At the ground floor, the difference in gap fraction is 20% as opposed to the average value of 30%. The good agreement with the external obstructions is due to the fact that the obstructing facades consist of a few large unbroken surfaces rather than a large number of small surfaces. There is therefore less potential for error due to too low a resolution, even at increased distances from the obstruction.

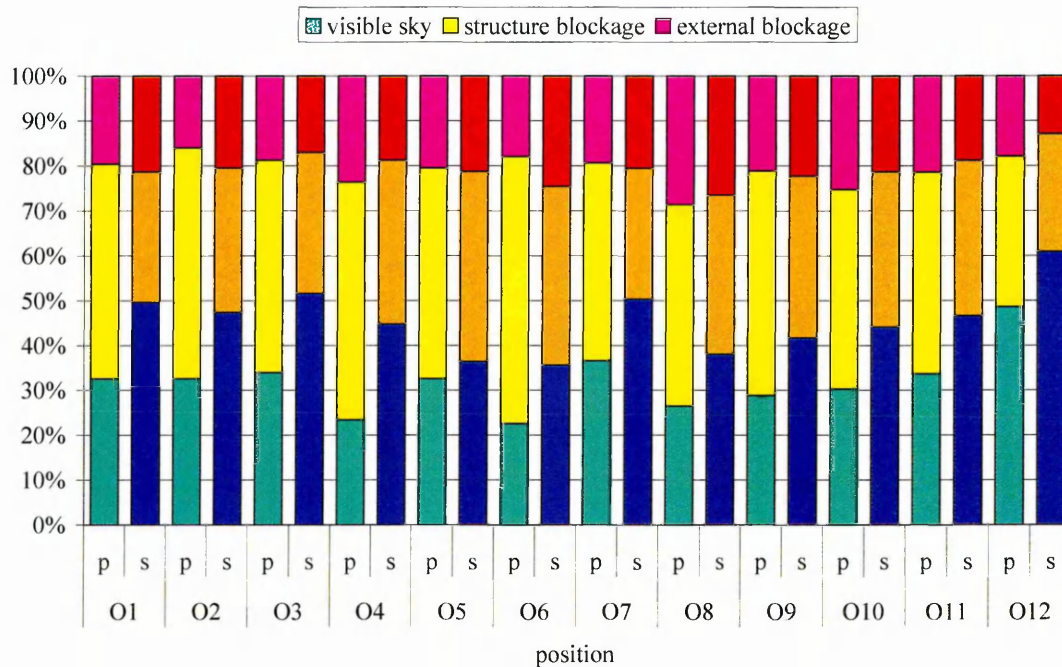
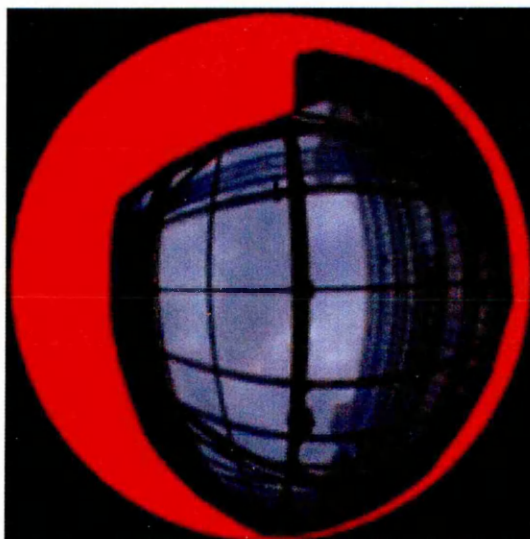


Figure 5-18: A comparison between physically captured photographs and generated images for visible sky, structure blockage and external blockage values.

The visual differences between the images can be seen in the series of images in Figure 5-19. The most striking immediate observation concerns the size of the area of interest where again the synthesised images have far less ignored red zones. Once more

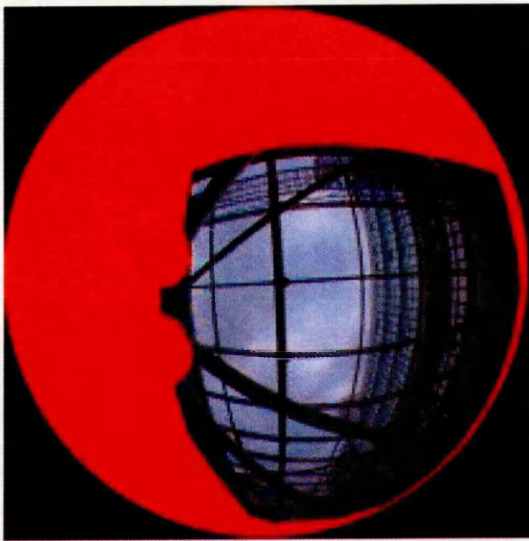
this is down to the difference between the fisheye lens and the Radiance hemisphere algorithm. The general arrangement and gap-blockage ratio appears congruent when comparing the zenith region of the images. At the edges where the roof recedes into the distance the much discussed differences between the photographs and corresponding synthesised images can be seen.

Further sources of difference include localised detailing which was not modelled in the computer representation. Examples of this include the window cleaning gantry, which can be clearly seen in the photographs from O1 to O5. In the adjusted images used for classification, the gantry was painted white so as not to influence the calculation. A further demonstration of detail in the real atrium can be seen in O6. The juncture of structure contains a roof plate. This was not entered into the computer model, as such detail would not influence results either in terms of HemiView analysis or illuminance calculations, unless the measuring point was at a close proximity. This was the case at O6, where the viewpoint was directly beneath the juncture at a distance of approximately 1m. Such localised detail is the cause of any significant difference between the photographs and the synthesised images with regard to the closeness of the external obstruction results as seen in Figure 5-18. In this case, the roof plate has obstructed a significant portion of the overshadowing facade, and thus the derived external obstruction value is lower than that derived for the synthesised image.

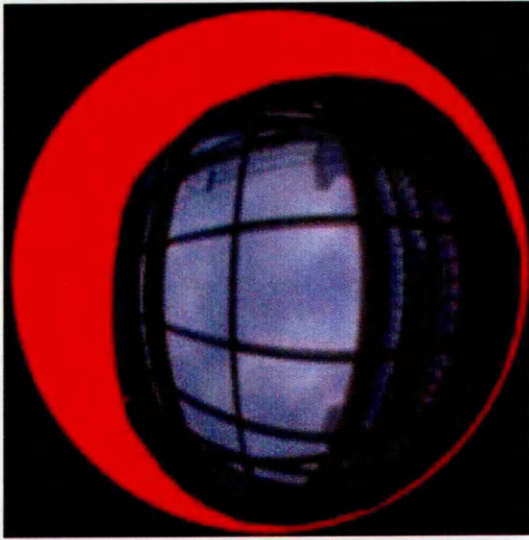
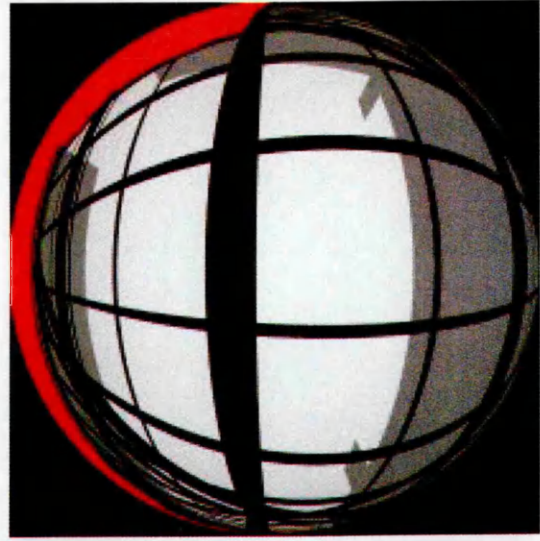


O1

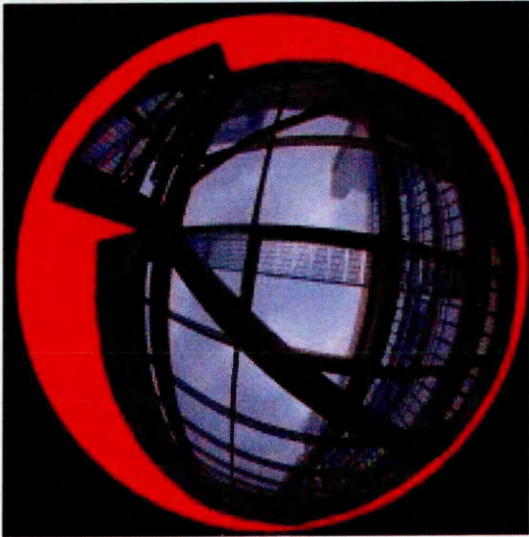
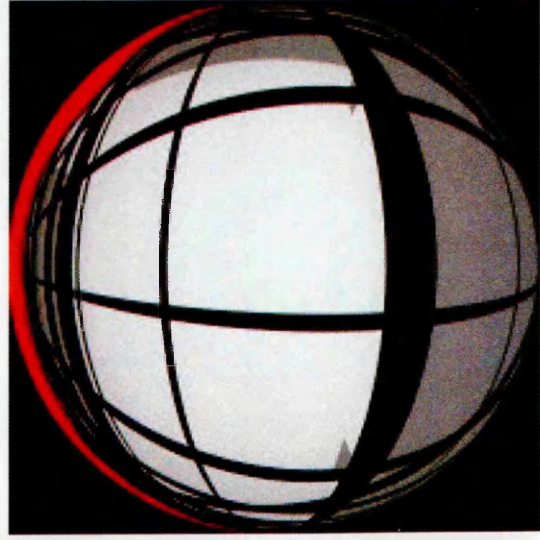




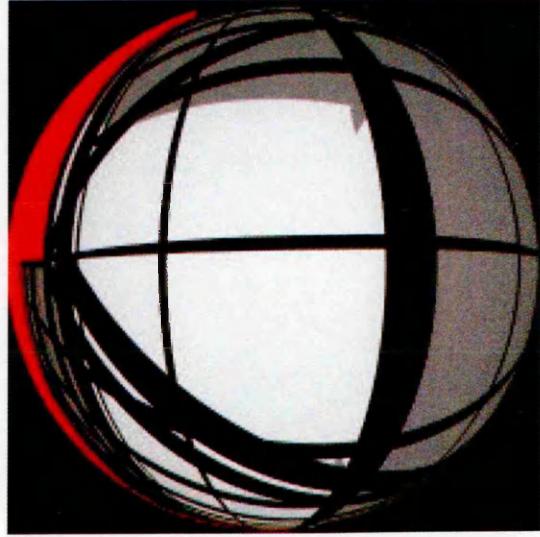
02

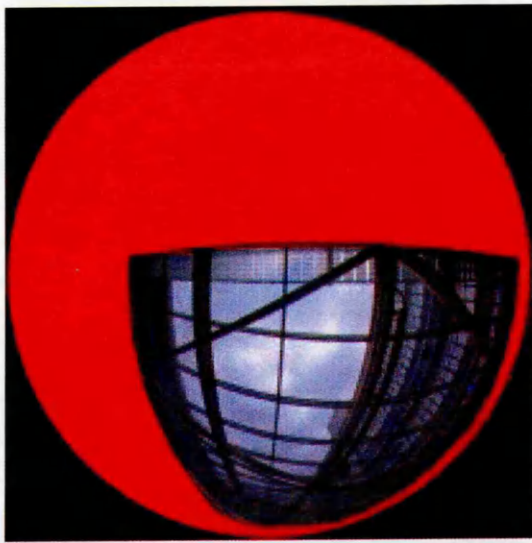


03

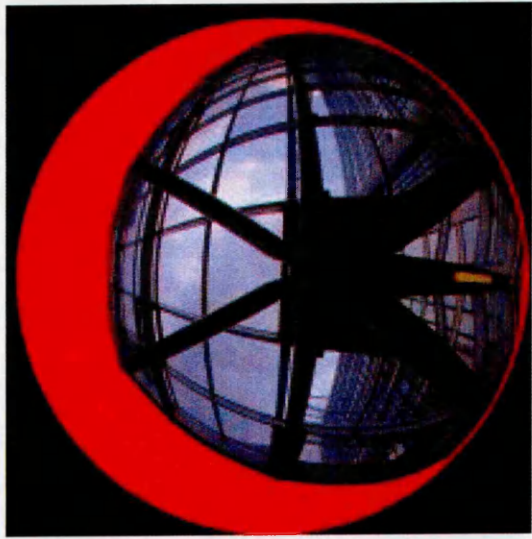
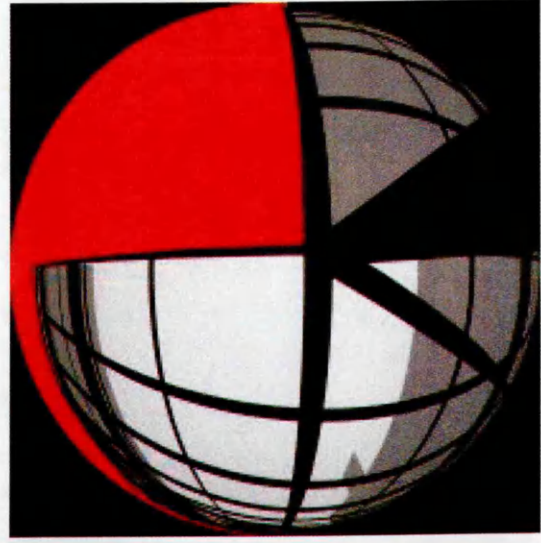


04

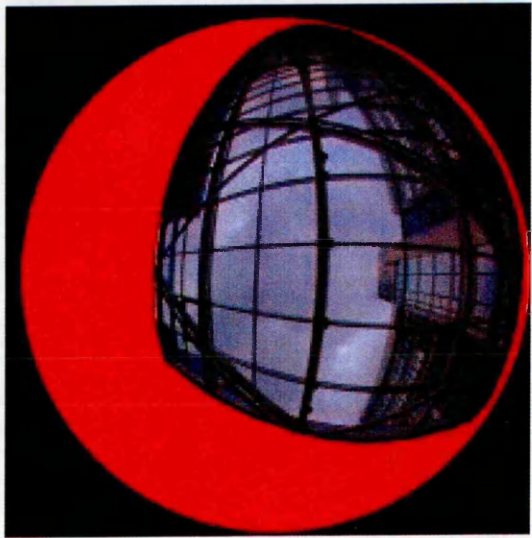
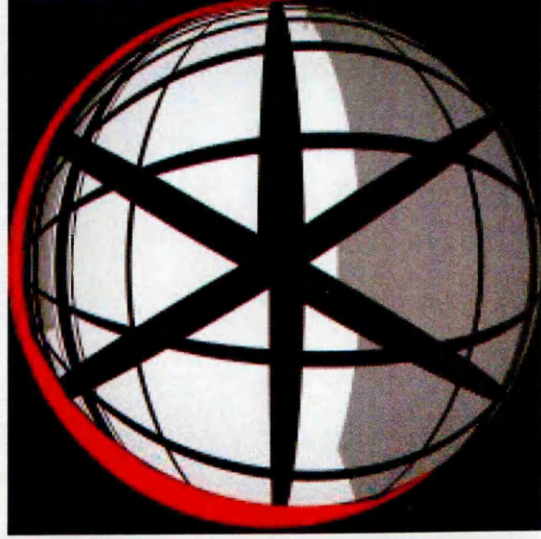




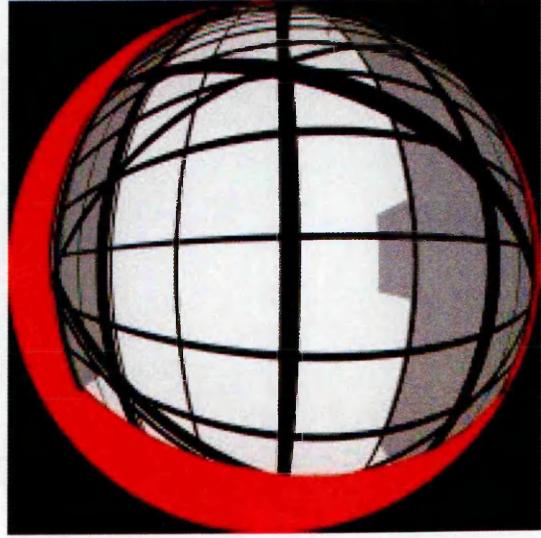
05

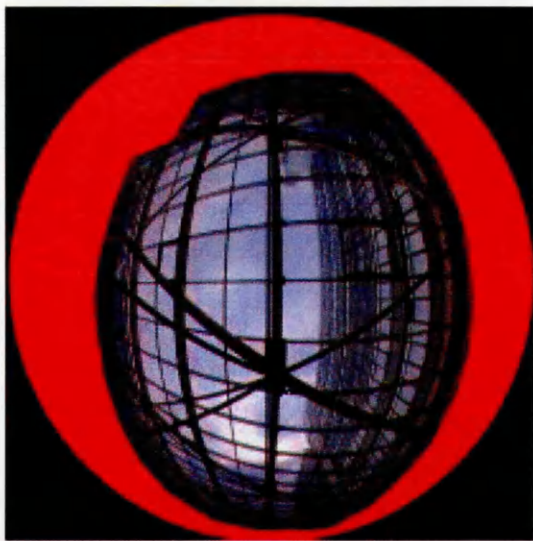


06

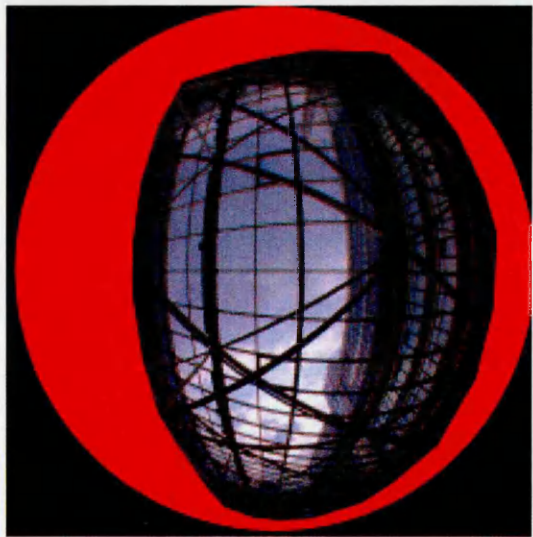


07

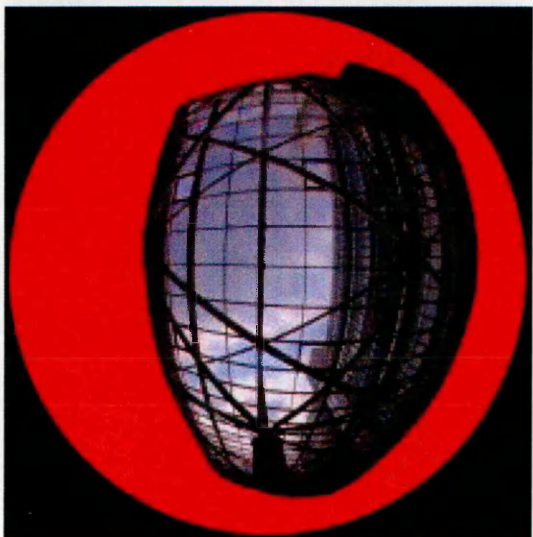
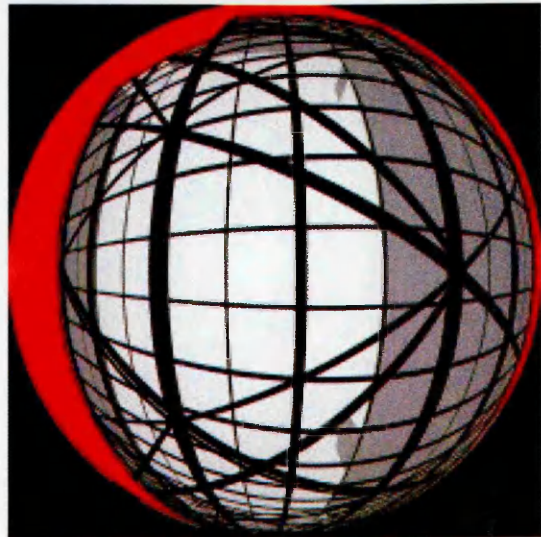




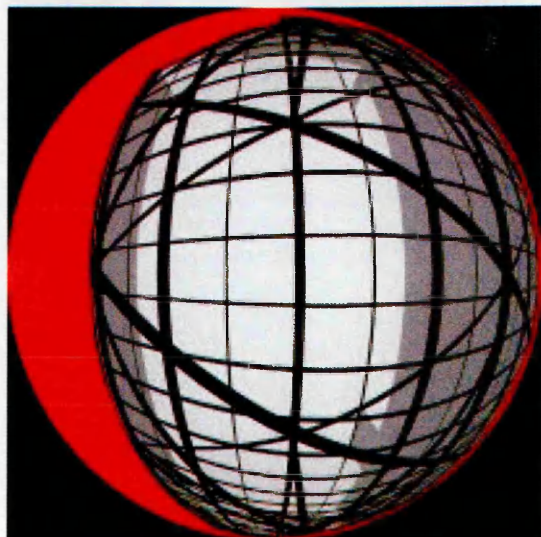
08



09



010



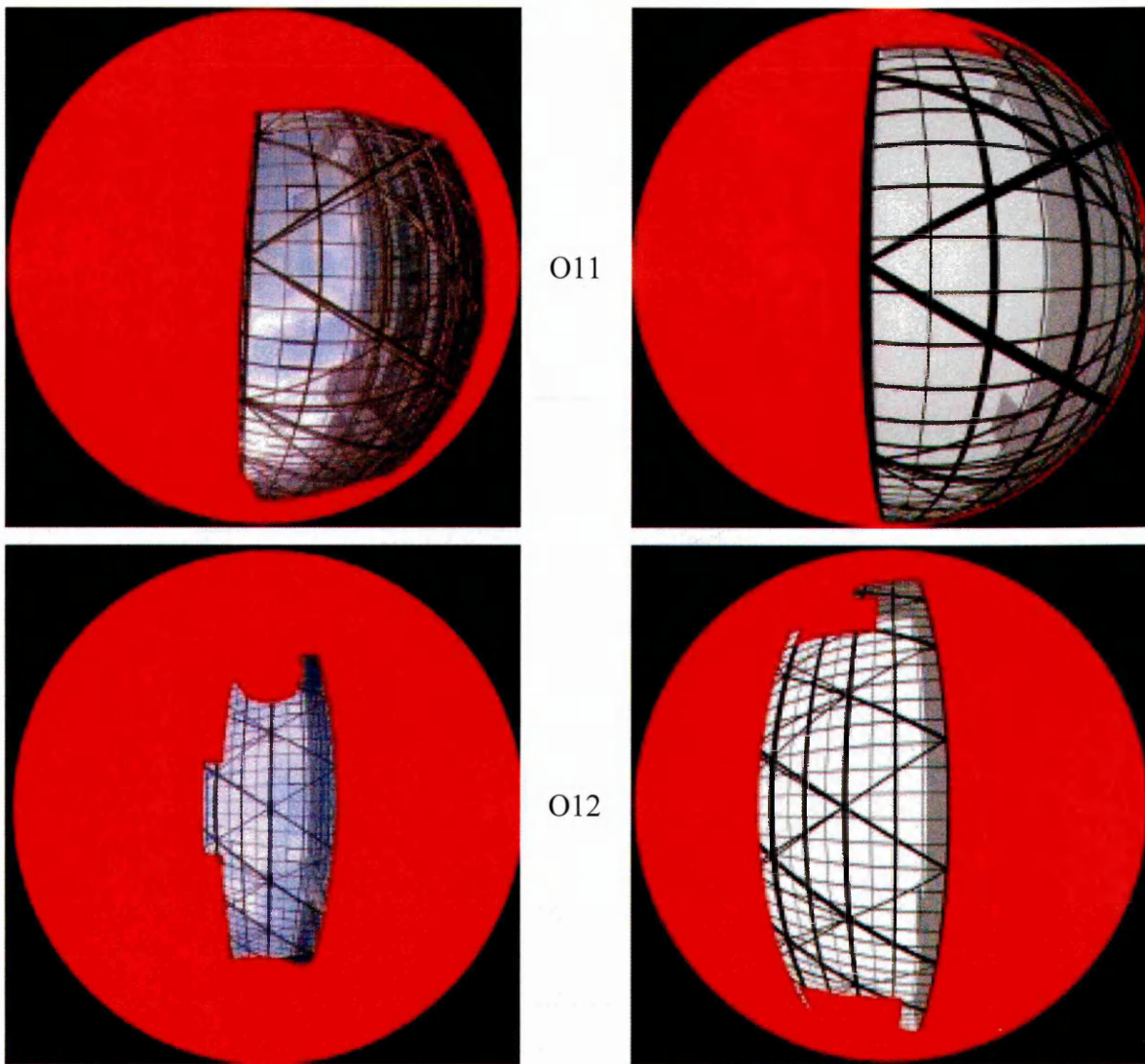


Figure 5-19: A side-by-side comparison of physically captured photographs (left) with computer images (right) generated from the corresponding position for position O1 (top) through to O12 (bottom).

5.5.2 Changing Depth of Photo Viewpoint: Owen

The *obstructed* gap fraction and the *unobstructed* gap fraction were calculated for the east, central and west positions for the synthesised images at the depths discussed in section 3.4.3.2. The results can be seen in Figure 5-20. For the *unobstructed* scenarios in the west position, gap fraction remains relatively constant at between 66% and 68%. For the central and end positions from the roof plane (0m) to the ground floor (15m) there is a gradual rise from just over 60% to 70%. At depths within the roof volume (between 0m and -4m) there are dramatic increases in gap fraction. In the east position at a depth of -4m, the value rises to 80.7%.

For the *obstructed* scenarios in the west position the value of gap fraction rises steadily from 33% at roof plane level to 56% at ground floor level. For the central and east positions the gap fraction remains relatively constant between 40% and 43%. The variance within these boundaries is greater in the central position (standard deviation 1.9%) than at the side position (standard deviation 0.7%). Once more, within the roof volume gap fraction values rise sharply. In the central position at -2m the value rises to 58%.

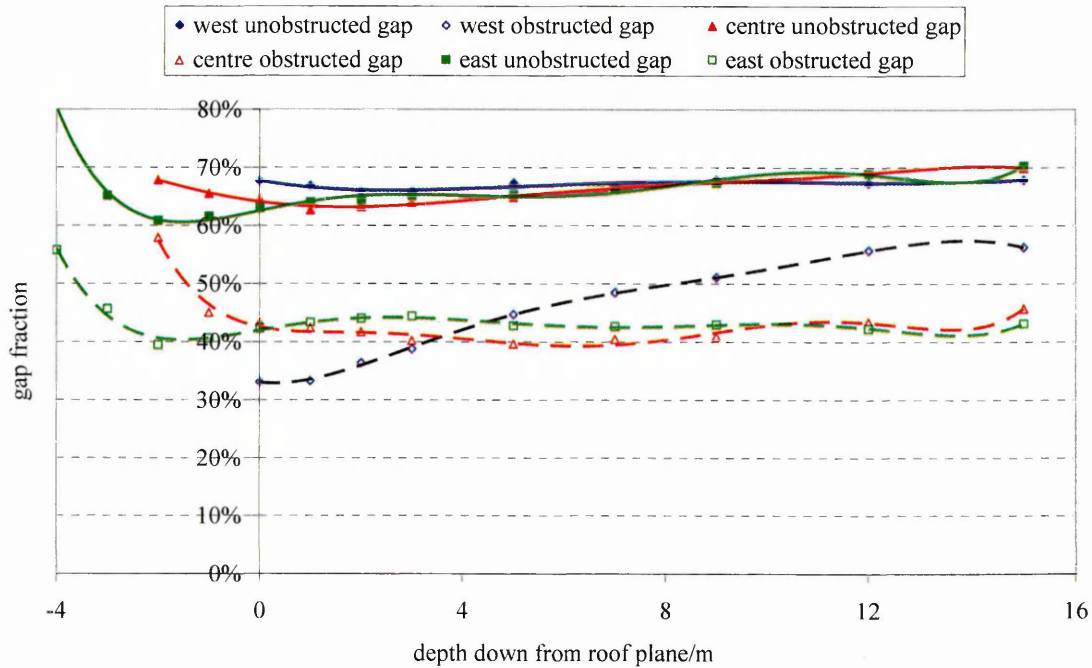


Figure 5-20: Gap fraction results from obstructed and unobstructed computer generated images with increasing depths within the well along west, central and east axis.

Separating these values into gap, structure blockage and obstruction blockage reveals the reasons for these trends (Table 5-13 and Figure 5-21).

Table 5-13: Visible sky and derived external and structure blockage values with increasing depths within the well along west, central and east axis.

Position	Depth/m	Obstructed visible sky	External blockage	Structure blockage
West	0	33.1%	34.6%	32.3%
	1	33.3%	33.6%	33.1%
	2	36.4%	29.5%	34.1%
	3	38.8%	27.1%	34.1%
	5	44.7%	22.6%	32.7%
	7	48.5%	18.2%	33.3%
	9	51.1%	16.8%	32.1%
	12	55.7%	11.6%	32.7%
	15	56.3%	11.6%	32.1%
	Centre	-2	58.0%	9.9%
-1		45.1%	20.5%	34.4%
0		43.5%	21.2%	35.3%
1		42.5%	20.3%	37.2%
2		41.8%	21.5%	36.7%
3		40.3%	23.8%	35.9%
5		39.7%	25.2%	35.1%
7		40.6%	26.0%	33.4%
9		41.0%	26.5%	32.5%
12		43.5%	25.6%	30.9%
East	15	45.8%	24.2%	30.0%
	-4	55.7%	25.0%	19.3%
	-3	45.6%	19.5%	34.9%
	-2	39.4%	21.4%	39.2%
	-1	40.6%	20.9%	38.5%
	0	42.3%	20.7%	37.0%
	1	43.3%	20.7%	36.0%
	2	44.0%	20.5%	35.5%
	3	44.4%	20.7%	34.9%
	5	42.7%	22.5%	34.8%
7	42.6%	23.6%	33.8%	
9	42.9%	24.4%	32.7%	
12	42.2%	26.7%	31.1%	
15	43.1%	27.2%	29.7%	

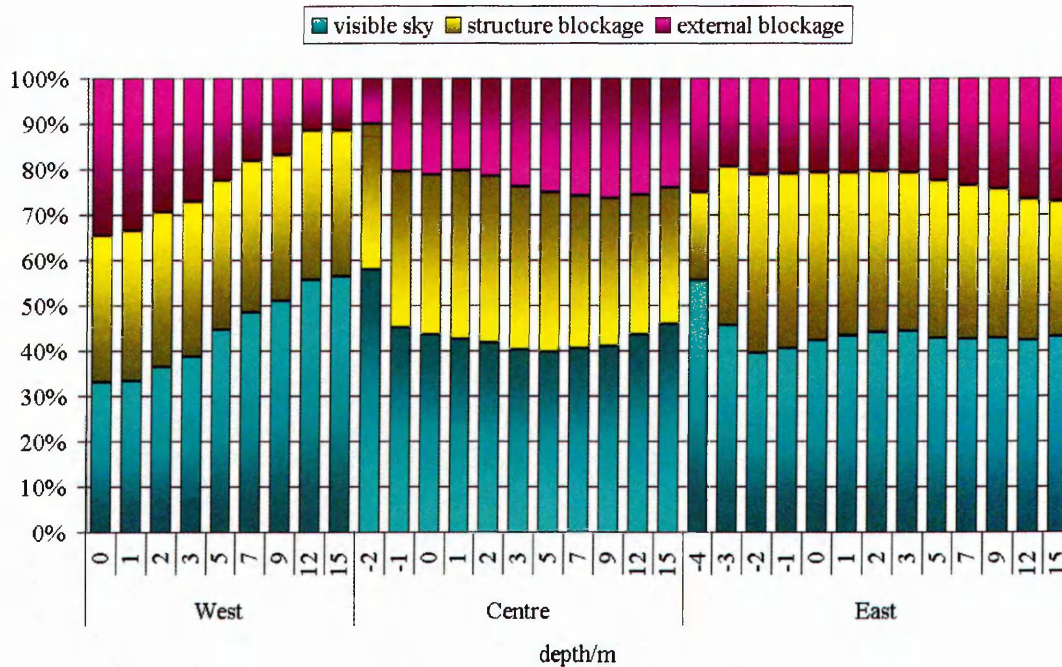


Figure 5-21: Visible sky and derived structure and external blockage values with increasing depths within the well along west, central and east axis.

At the west position as depth increases the obstruction due to external elements decreases (a drop from 35% to 12%). This can be seen visually looking at the series of images moving down the well in Figure 5-25. The west position is immediately adjacent to the principal obstructing facade of the atrium. With increasing distance into the well, the facade occupies less area within the images, hence less of a recorded external obstruction value.

There is a relative drop of 5.9% in structural blockage at 1m from the roof plane to the ground floor. This value appears low relative to other drops experienced in structural blockage from roof to base. The monopitched nature of the roof introduces complexity when considering the building in section that was not as evident in the symmetrical A-framed Sheaf roof. The lines of sight from the west position towards the roof run more parallel to the slope of the roof compared to more easterly positions. Changes to the perceived view of the structure are therefore not as great with regard to depth as for more easterly positions (Figure 5-22).

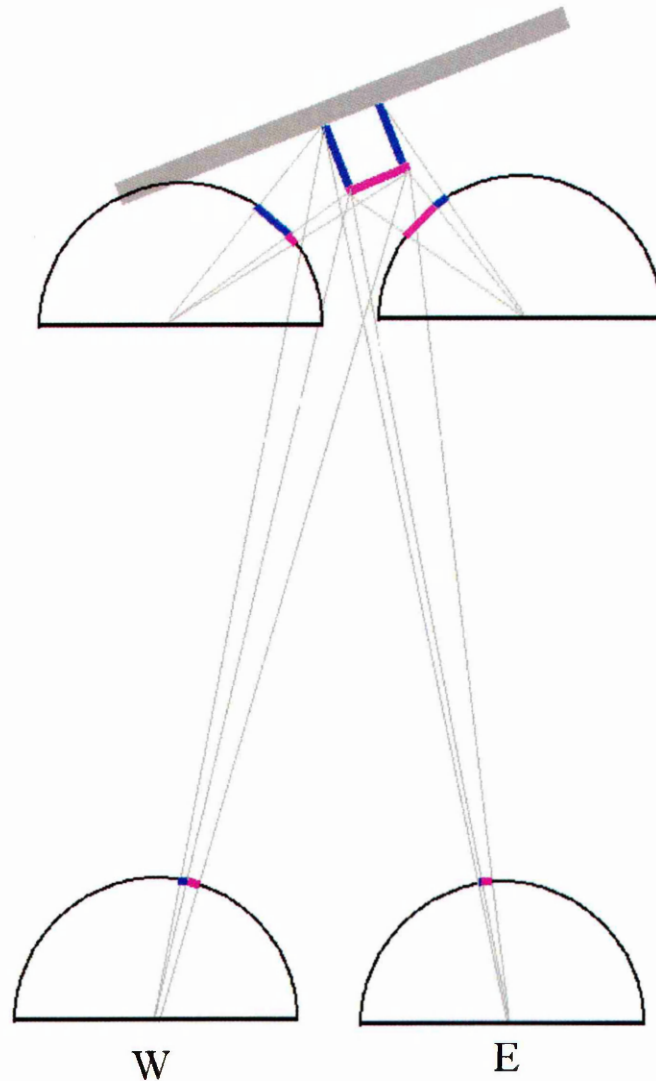


Figure 5-22: The relative drop at the east position, where the lines of sight are more perpendicular to the roof slope exhibit a greater change when moving from positions at the top to the bottom of the well. At the top the right side of the structure can be seen in section, whilst at the bottom the left side can be seen. At the west position, the general arrangement is the same at top and bottom, though the structure is smaller in the field of view.

The value of structure blockage is actually higher at 1m than at 0m. This is due to the emergence into the image of part of the space frame structure which extends into the well. This can be seen in Figure 5-25.

In the central position at depths beneath the roof plane, the structural blockage drops from a peak at 1m into the well to the base by 19.3% in relative terms. Again the value is higher at 1m than at 0m due to the space frame appearing in the field of view beneath the roof plane. Applying the metaphor of a painting to the image, the structure

can be considered the foreground, the external obstructions the mid-ground and the sky (gap) the background. The structure is the first matter to appear at the viewing plane, followed by the external obstructions and finally the sky. Trends observed with the roof structure due to increasing depth are therefore solely a result of these changes.

The effect of depth on external obstruction and visible gap are slightly clouded by the relative appearance of the roof structure at that point. The resultant portion of the hemispherical view that is not structure blockage i.e. [1-structural blockage] increases in depth, as the proportion of structure blockage decreases. If the structure were not there it would be expected that the proportion of external obstruction to decrease. With reference to Figure 5-23, the following can be stated;

$$\alpha = \tan^{-1}\left(\frac{w}{x}\right) - \beta \quad [5-4]$$

$$\beta = \tan^{-1}\left(\frac{w}{(x+h)}\right) \quad [5-5]$$

where,

α = obstruction blockage

β = gap fraction

w = width of opening

h = height of obstruction

x = depth in well of viewpoint

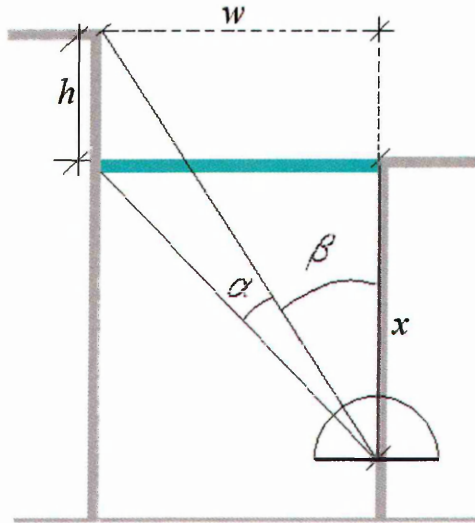


Figure 5-23: Illustration of geometric parameters defined in Equations 5-4 and 5-5.

Assuming w and h remain constant, increasing depth into the well would result in the ratio of gap to obstruction increasing, as can be seen in Figure 5-24.

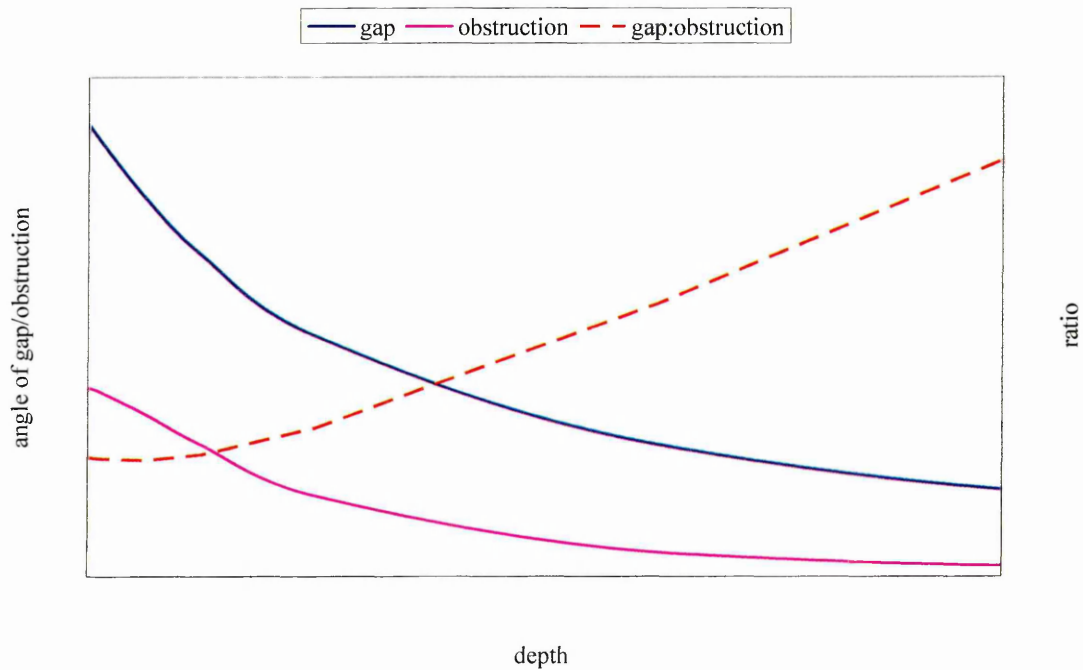


Figure 5-24: Assuming the width of the well and the height of any external obstructions remain constant, the proportion of gap to external blockage in the field of view will increase at increased depths within the well.

Whilst in the central position the size of the external obstruction does diminish relative to the whole hemisphere, the ratio to gap fraction (i.e. only in the concerned 'non-red' part of the hemisphere) increases up to a depth of 9m. At depths greater than 9m the ratio falls. At the central position for this specific arrangement of roof structure and with the non roof area ignored 9m represents the depth where the most efficient relative view of the obstruction can be seen. This phenomenon was not observed in the west position as it was so close laterally to the obstruction and thus the drop in depth led to a sharp drop of the obstruction blockage in the hemispherical views.

In the central position moving above the roof plane (i.e. into the roof) there is a large increase in gap fraction (25% relative difference between the 0m and -2m values). This is at the expense mainly of the external obstruction, whose value falls from 21.2% to 9.2% (a relative decrease of 57%). The reasons can be seen in Figure 5-25. At -2m the view is extremely localised to the immediate overhead glazing hence the high gap fraction value. The main structural beam has bent around concealing most of the obstructing Owen building behind it, hence the low external obstruction value. The value of structural obstruction also drops relatively by 9% over this distance, due to omitted structure of the space frame which is outside and beneath the field of view.

At the east position the trends are similar to those found in the centre of the well. The structural blockage drops from 37% to 30% (19% in relative terms) from 0m to 15m. This time the value at 0m is greater than at 1m due to the space frame already occupying a prominent position within the field of view at 0m. This reduction in structure obstruction is offset by a gain in external obstruction. This is due to the arrangement of roof structure either obstructing 'gap' or 'blockage'. If the well were deeper, the proportion of external obstruction would diminish with corresponding gains in gap fraction

At depths above the roof plane the image once more becomes subject to localised factors. Moving from 0m to -2m, the general trends as found moving down from the roof plane continue, as more of the profile of structural members of the space frame are seen. At a depth of -4m, the space frame no longer appears in the field of view (Figure 5-25) and so the structure blockage falls whilst the gap fraction rises.

From every position moving down the well has resulted in a reduction in the observed structure blockage. This is primarily for two reasons. The first of these is the same as was found in the Sheaf example that is, at increased depths less of the structure is seen in profile but only in 'plan' or underside plan thus resulting in values approaching the PAO of 28.9%. Secondly, and a factor specific to more complex roof structures, the roof members obstruct each other to a greater degree at increasing depths. Struts that are located directly above one another in plan can be seen simultaneously looking parallel to that view with an angular (i.e. perspective) lens, at close enough distances. Only at increased depth do they appear to overlap. In these examples where the maximum structural obstruction did not occur at the roof plane level, it was due to the space frame extending into the depth of the atrium. In every case from first instance where the entirety of the roof structure could be seen, there was a drop in structure obstruction with increased depth.

The reduction is greater at the central and east positions (19%, as opposed to 6% at the west position) as they are located under busier areas of roof structure (the average obstruction blockage from 0m to 15m is 32.9% at the west, 34.1% at the centre and 33.9% at the east), and therefore have higher obstruction values to begin with, where the viewpoint is from 'within' the structure. The structure also begins to 'obstruct itself' at shallower depths than the west position which is offset laterally from the busiest sections of the space frame and hence sees it in profile at greater depths.

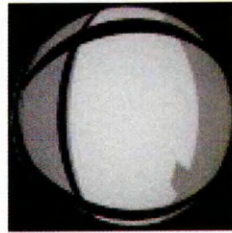
Depth

East

Centre

West

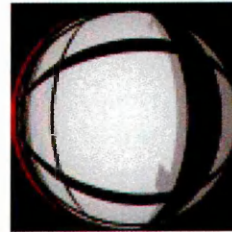
-4m



-3m



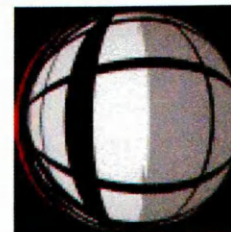
-2m



-1m



0m



1m



2m



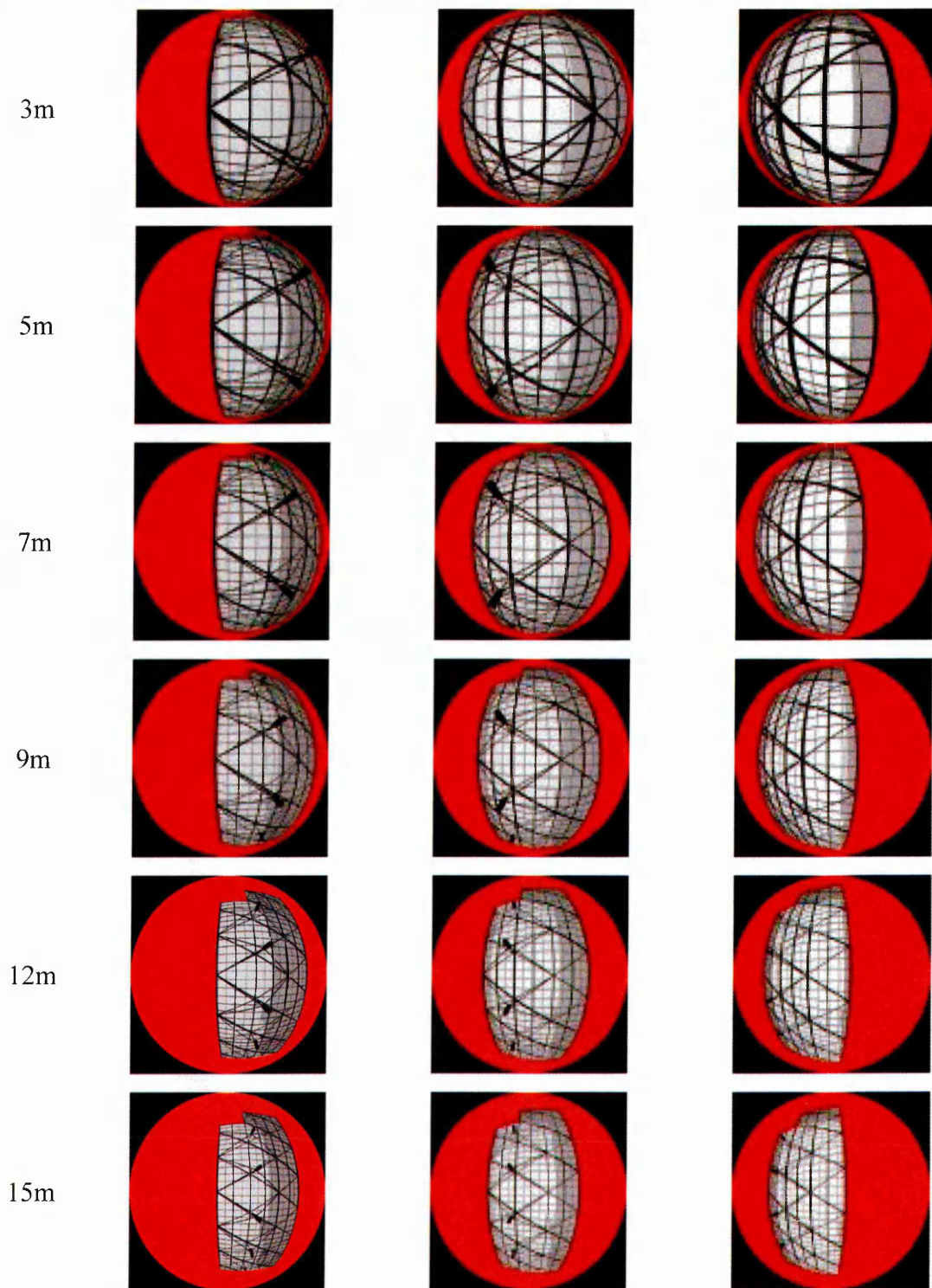


Figure 5-25: Computer generated views along east (left) centre (centre) and west (right) axis at depths within the roof plane (i.e. <math>< 0m</math>) through the roof plane (0m) up to a depth of 15m.

5.6 Synthesised Imagery: The Simple and Complex Findings discussed

In general the agreement between the physically captured photographs and the synthesised images was poor. Where agreement was good (e.g. at the photocell position in the Sheaf example) it was as a result of several negating factors rather than genuine congruence. The photographs tended to return lower values for gap fraction due to structure at increasing angles from the zenith forming regions of perceived total blockage. The magnitude of difference was approximately 30% in the Sheaf building and 30% (for *obstructed* images) in the Owen. This effect decreased at increased depths within the well, where both photograph and synthesised image converged towards plan gap/blockage proportions. The relatively good external obstruction correlation was due to the large solid surface of the obstruction, and thus factors such as image resolution did not play a significant factor.

In both the simple and complex roof roofs taking the photograph deeper within the well resulted in a loss in the quantity of structural blockage in the field of view. The drop was greatest in the zone closest to the roof plane. The plan area of obstruction will underestimate the amount of structural blockage at the top of atria wells. It would therefore seem dangerous to apply it as a correction factor for potential light entering an atrium well. Photographs should be taken as high up the well as is practical. The observed drops in structural blockage from maxima towards the top of the wells to minima at the bases ranged from 35% (Sheaf centre, though this high value is due to the influence of a large dominant overhead I-beam) to 19% (Sheaf end, Owen centre and east) to as low as 6% (Owen west, though this lower value was connected to viewing the monopitch roof at a skewed angle). Whilst the sample is too low to form definite conclusions, a correction factor of 20% applied to photos taken deep within atria wells where PAO conditions appear to have been reached does not seem unreasonable. Chapter 7 discusses this issue further.

The quantity of sky visible due to the presence of external obstructions is specific to viewpoint. In this study, on the side of the well closest to the obstruction, its influence was great at the top of the well and markedly reduced at the base. On the opposite side the influence of the obstruction increased towards the base of the well. Taking the photograph at the centre of the well helps balance out edge phenomena.

Moving into the depths of the roof makes images highly biased towards localised factors, as the whole roof form and structure is not contained within the field of view. Photographs should be taken at or beneath the roof plane, ensuring that the view seen is representative of the entire roof form and not likely to be influenced by localised factors e.g. structural joints, servicing gantries etc.

The observed difference between field captured and synthesised image was due to the higher resolutions capable in the generated images. The camera used captured images at a resolution of 1200x1200 (1.4 Megapixels). At the time of writing, the most powerful commercially available digital cameras specify a resolution of 8.3 Megapixels¹ (i.e. roughly 2900x2900) (Figure 5-26). This still falls short of the 4096x4096 (16.8 Megapixels) used to generate the images in this study. It is not unreasonable to expect a continued improvement in digital hardware. The areas vulnerable to the effects of insufficiently accurate resolution were the roof regions at relatively low altitude angles from viewpoints high up the well (where discrimination between structure and sky was hardest due to receding structural elements and the darker horizon part of the sky). If the roof examined were one of a generally repeating structure, it would be acceptable to paint these regions as red and ignored in the HemiView calculations. The field of interest would now contain only an arrangement of roof structure at sufficiently accurate resolutions for sky gap to be classified correctly.



Figure 5-26: The Canon EOS-1D Mark II, an example of the ever increasing advances in digital image acquisition hardware.

¹ Canon has unveiled its new EOS-1D Mark II camera, which it claims is the most powerful digital-SLR model in the world.
<http://www.itp.net/news/details.php?id=11782&category=>, 27 April 2004)

5.7 Conclusions

This chapter has described results from a method which assessed the gap fraction of a skylight in an attempt to correlate it to skylight performance. Systematic investigation into location of photograph and image quality have revealed that the photographs should be taken as close to the centre of the roof plane as possible, or at roof plane level where a view of the typical arrangement of the structure can be seen. At large depths within the well, images approach the conditions of a plan rendering, and have gap fraction values generally 20% lower than at the roof plane. Generating the images synthetically confirms the general trends found with manually capturing the images, though gap fraction values were markedly higher due to the increased resolutions possible. It is not at this stage possible to relate the findings of this chapter to the illuminance measurements described in Chapter 4 with any confidence. An investigation into the effects of the fundamental optical properties of the key skylight components is needed to explain the relationships found. Chapter 6 presents such an investigation using computer simulations to parametrically assess the impact of the various elements of the skylight.

6

Expanding Scenario Possibilities: Computer Simulation

- 6.1 Introduction
- 6.2 A Methodology for Lighting Simulation
- 6.3 Setting Radiance Ambient Parameters
- 6.4 Base Case Simulations: Results
- 6.5 Examining the Impact of Structural Reflectance and
Glazing Transmittance
- 6.6 Physical Illuminance Measurements and Computer
Simulations Compared
- 6.7 Conclusions

*'Well, that would not be necessary Mr. President. It could easily be accomplished with
a computer'* DR. STRANGELOVE, STANLEY KUBRICK

6.1 Introduction

Chapter 3 concluded that Radiance was the most appropriate simulation program for the needs of this study. The first part of this chapter describes its workings in this context. In Section 6.2 Ecotect is introduced as a suitable means to access the Radiance engine and display the results in a user friendly manner. Section 6.3 concerns the configuration of the Radiance ambient parameters.

The chapter continues with the output and analysis from the simulations. Section 6.4 details the illuminance at the photocell position and analysis plane for both case study buildings. The effect of the reflectance of the wall surfaces and the external obstructions (in the case of the Owen building) are also discussed. Section 6.5 discusses the need and implementation of further simulations with parametric changes made to the reflectance of the roof structural members, and the transmittance of the glazing. In Section 6.6, the simulated results are compared to the physically measured results from Chapter 4.

6.2 A Methodology for Lighting Simulation

6.2.1 A Step Back from Radiance

As has been discussed Radiance has been shown to accurately simulate the lighting environment of buildings (arguably more so than any other software available at this moment in time), and has been extensively validated in numerous studies. In order to perform a simulation, various input parameters are required, those being the building geometry, the photometric behaviour of its materials and the sky conditions (when modelling a daylight scenario). Radiance converts this data using the `onvoc` command into a description of the scene referred to as an *octree* file (denoted by the suffix *.oct*). The programs `rpict` (or `rview` for interactive rendering) and `rtrace` invoke a simulation either resulting in a picture (*.pic*) or as numerical value(s) at a point or defined grid (the output is piped to a file with the *.dat* suffix) respectively. A schematic of the process can be seen in Figure 6-1.

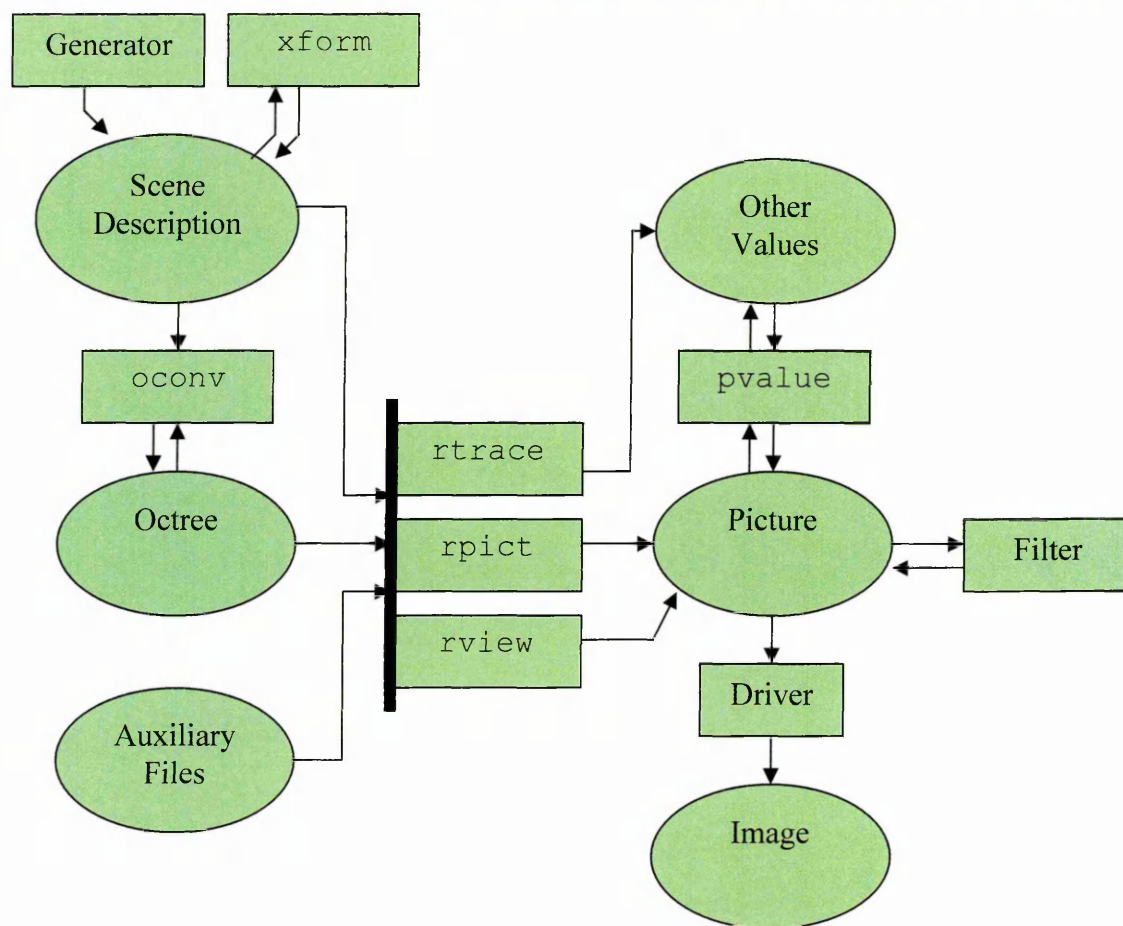


Figure 6-1: The workings of Radiance (adapted from Radiance manual pages)

Theoretically it is possible to enter all these data directly into Radiance. Geometry can be entered manually, using the three basic surface classes; polygon, sphere and cone¹. The x,y,z co-ordinates of each node within each shape (typically polygon in the case of the rectilinear elements occurring in these atria studies) are required. Thus, for each rectangular surface, twelve numbers to a high decimal degree of accuracy must be entered (the polygons must all meet exactly in order for the model to be 'light tight'). For a simple scene this may not be overly problematic. In the case of our atrium roofs, the large amounts of polygons (and at slightly irregular spacing to each other thus making the extensive use of image manipulators such as *xform* slightly redundant) means that geometry input through a standard CAD package is preferable. Indeed only the greatest Radiance enthusiast would wish to construct the entire scene geometry of a complicated scheme within a text editor in Radiance, such as has been done in Figure 6-2. This highly impressive rendering was extremely sophisticated in its time, though by the author's admission, the geometry entry took "a very long time"²

¹ *Rendering with Radiance* p.10

² discussion with John Mardaljevic September 2003



Figure 6-2: A rendering of an atrium space (Ward Larson & Shakespeare 1998).

A CAD package has two distinct advantages over entry within Radiance. Firstly, the entire process is more visually interactive. As a surface is drafted into the CAD package, it appears upon the screen. In Radiance it is text driven. The `objview` command can be invoked periodically as a check to ensure the model appears correct, though this can not be as effective as having a constant visual link. Secondly, software specifically designed for drafting will incorporate many tools which can significantly reduce the time and effort required to produce the same result, such as snaps which makes node entry more efficient, and increases the chances of a resultant 'light tight' model. Radiance has several programs which convert geometry from the most widespread CAD packages into Radiance format.

Radiance is a program (or rather series of over fifty interacting programs) that runs off a UNIX platform, and has a notoriously difficult learning curve. It is the flexibility that the program offers which gives the user ultimate freedom, yet at the same time for the first time user, provides a daunting hurdle. As well as familiarisation with the numerous programs comprising Radiance, the user will often have to acquaint himself with the UNIX operating system. Given that it is possible to create the geometry of the model outside of Radiance, to what extent could it be possible to bypass the heavy technical weight of the program without compromising the integrity of the output?

One possible solution is Desktop Radiance. This is a Windows release of the UNIX based Radiance program. Once downloaded (for free, like its bigger brother) it is

configured and a new menu appears within the AutoCAD toolbar. From here, materials, light sources and furniture can be added to the AutoCAD created geometry. Simulation is then achieved using the `rad` executable program. Rad is a program that "set (sic) up a rendering procedure and optimize (sic) the rendering process based on a few general parameters that you provide"³. Initial experimentation with this program has revealed that whilst it appears worthwhile in terms of image generation, consistently accurate numerical output was difficult to achieve whilst working within the bounds of the AutoCAD interface. It is appreciated that a large part of this may have been down to user inexperience. It should be noted that further development of Desktop Radiance has ceased⁴.

A method that was finally settled on was using the building analysis software Ecotect as a platform from which to access Desktop Radiance. The specific workings and advantages of using Ecotect are detailed later in this chapter. Figure 6-3 gives an overview of the simulation process.

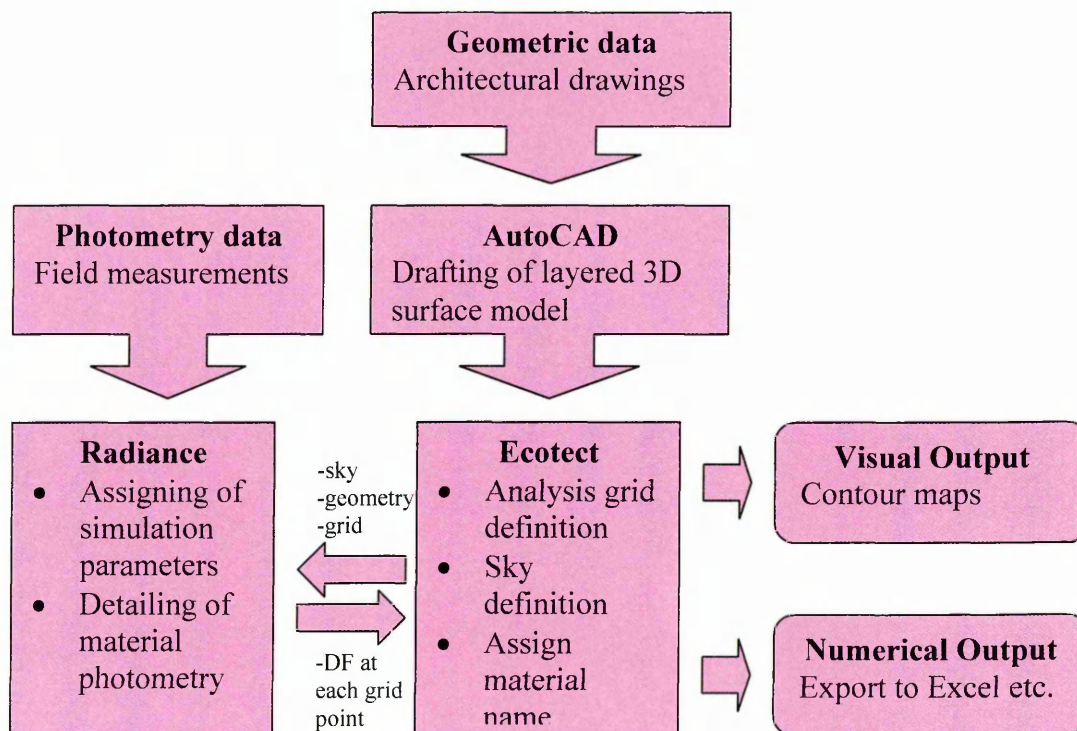


Figure 6-3: An overview of the simulation process used in this study

³ *Rendering with Radiance* p.107

⁴ discussion with John Mardalijeveic September 2003

6.2.2 Creating the Geometry

The case study atria chosen for this study have the advantage of being a part of this university. Architectural drawings were readily available, and it was from these that the building geometry could be accurately modelled. Error in translation was small, and dictated by the size of the intervals on the scale used to measure the lengths.

A model was created using AutoDesk's popular AutoCAD 2002 drafting program. The model was constructed using surfaces (the *3dface* command) rather than solids. Whilst this may have been more time consuming, Radiance does not support solid geometry. Members of like material were grouped in unique layers (e.g. glazing, transom, purlin etc.) such that specific materials could easily be attached to the correct members. When creating the glazing it was important to ensure the surface normal was pointing in the correct direction, that is, into the atrium. The right hand rule was used as an aid as in Figure 6-4. Whilst most of the geometry was created using surfaces, some elements of the roofs (such as the space frame in the Owen building) were tubular in form and hence not suitable for modelling using flat surfaces. Such elements were manually entered into the Radiance scene file using the `cylinder` primitive.

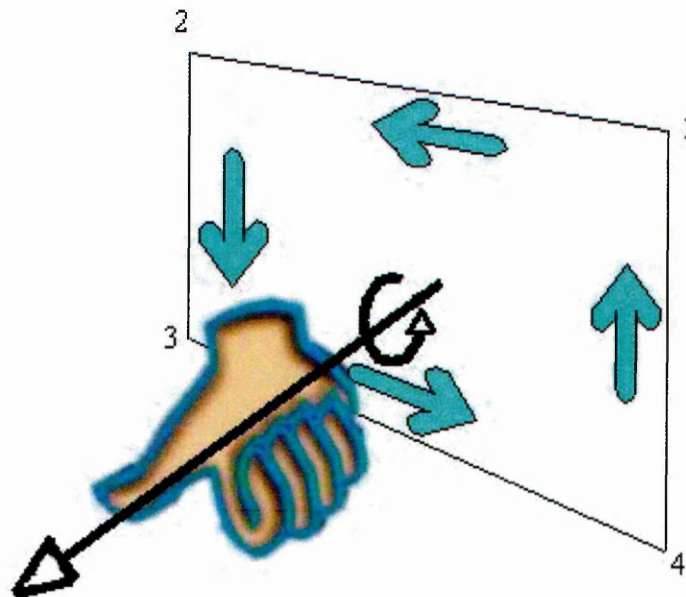


Figure 6-4: The right hand rule; With your right hand in the 'thumbs-up' position, and the thumb pointing in the direction of the surface normal (i.e. towards the inside of the atrium), the direction of the fingers indicate the direction in which the polygon nodes are to be drawn i.e. anti-clockwise.

The level of detail at which the model was drawn was a critical factor. Clearly modelling the atrium to a high a level of accuracy as possible (for example down to door knobs) and setting the rendering parameters to as high a level as possible will lead to the most accurate results. In practice however the more separate surfaces there are in the model, the more computationally expensive a simulation will become. Figure 6-5 shows the Sheaf building atrium modelled at two levels of accuracy. The 'accurate' model on the left contains almost 2000 separate surfaces. It includes a detailed profile of the well including windows overlooking the well, walkways, and balconies with handrails. The 'simple' model on the right contains the same roof yet the well is approximated to a simple box. The surfaces are given an average area weighted reflectance value that approximately describes what their contribution in terms of reflected light flux may be to a point at the roof plane level. It contains just over 600 surfaces.

As we are concerned with the effects occurring at roof level, the roof system is modelled to a high level of accuracy. Initial simulations showed there to be little difference in terms of numerical output between the simple and complex models. The time taken however for the complex simulation was markedly longer. Radiance does not distinguish between a surface on the main roof beam, and a face on a balcony at first floor level, whose effect on lighting conditions at roof level is next to nothing.

Whilst it can be seen that for visualisation the complex model is more useful (perhaps for an architect to show to a client) a stripped down approach is necessary in terms of lighting analysis to make the process efficient. Thus models which geometrically accurately describe the roof structure and glazing, whilst approximating the bulk of the surrounding well, were created. They were then exported to Ecotect.

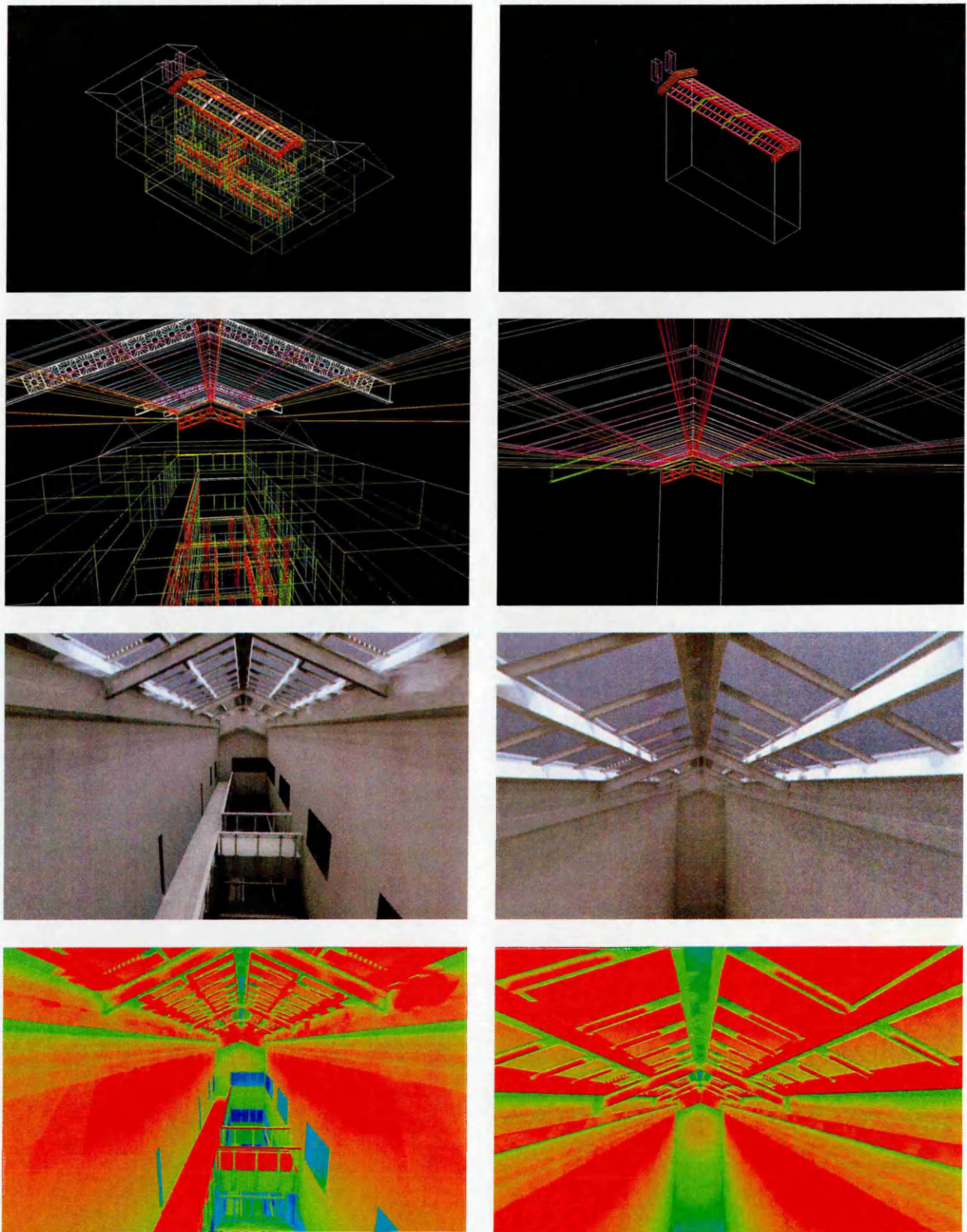


Figure 6-5: The Sheaf building modelled to a high (left) and low (right) level of detail, in isometric, internal perspective, Radiance rendered (with human sensitivity) and falsecolour views.

6.2.3 The Ecotect Platform

"ECOTECH v5.20 is the most comprehensive and innovative building analysis software on the market today" is the bold statement made by the authors of the program⁵. The software is aimed primarily at architects at the early stage of design, and integrates an intuitive modelling interface with simple environmental analysis (e.g. overshadowing, solar access, thermal comfort, acoustics etc.) (Roberts & Marsh 2001, Hagan 2003). Analysis output can be obtained from the very start, and as the complexity of the model increases, the accuracy of the analysis will respond accordingly. There is at the moment a scarcity of published validation work on the accuracy of these analyses. One study by Sethi examines the effect of various light shelf configurations on daylight factors on the floor of a simple room (Sethi 2003).

One of the greatest advantages of Ecotect is the potential for export to more powerful specialised analysis software. These include Energyplus (energy simulation program), WinAir4 (computational fluid dynamics) and Radiance. It is this export to Radiance that is relevant to this study.

Once the CAD models were imported (Ecotect supports *.dxf import) a material was added to each grouped layer. This was necessary for the creation of a scene file that Ecotect performs in the export to Radiance. The materials dialogue box is shown in Figure 6-6. Whilst it is possible to assign material characteristics within Ecotect, it was found to be faster and easier to make simple amendments to the scene files created by Ecotect using a simple text editor. This is described in greater detail in Section 6.2.4.

⁵ from the Ecotect help pages, by Dr. Andrew Marsh

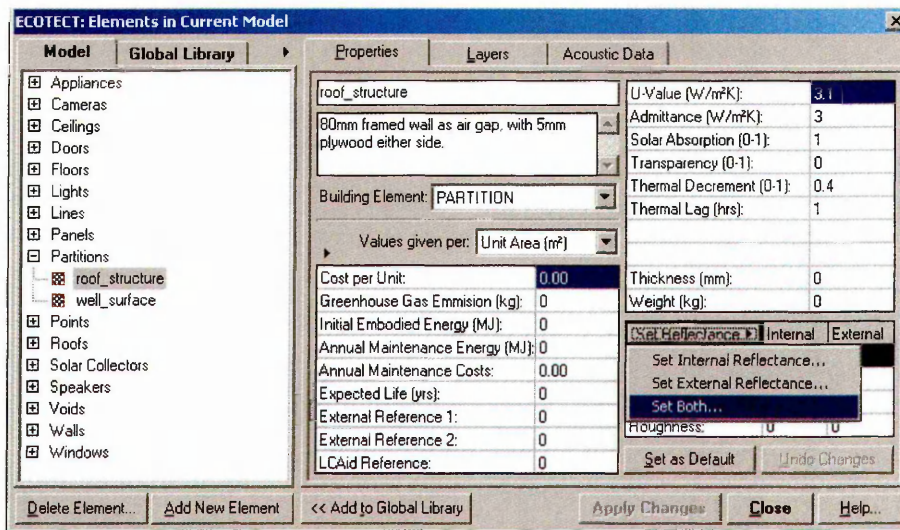


Figure 6-6: The materials dialogue box. Material names are assigned to geometry here, though in this work the actual properties are applied elsewhere.

An analysis grid was then defined. Ecotect takes the positions of the grid nodes and creates a file (*.pts). Radiance takes this information as a departure point, and returns the specified output at each of the points. In the case of the Sheaf building, a regular grid of 20x12 points was defined at the uppermost height of the well (Figure 6-7).

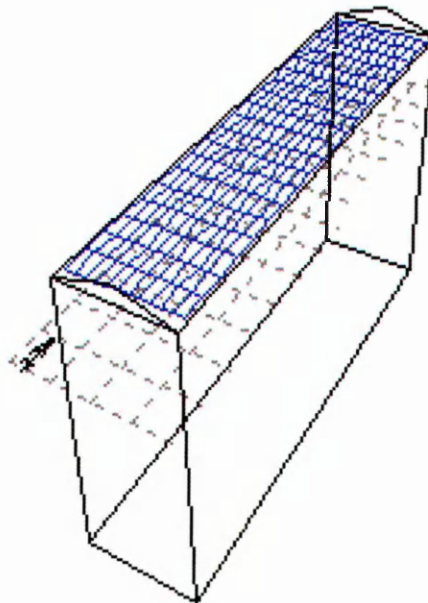


Figure 6-7; Position of analysis grid in the Sheaf building (the roof has been removed for clarity of display)

In the Owen building a grid of 20x12 points was also specified, with the 20 grid points located along the shorter axis (E-W), to more closely examine expected patterns when looking across the section of the monopitch (Figure 6-8).

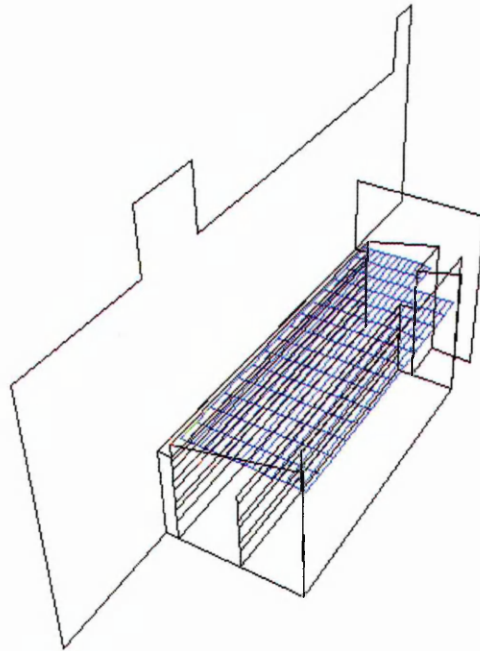


Figure 6-8; Position of analysis grid in the Owen building (the roof has been removed for clarity of display)

The model was then ready for export to Radiance. At the Radiance file conversion window (Figure 6-9), 'GridPt. Illuminance' (i.e. numerical output at the grid points) was selected as the action required (the other options being to produce rendered images). The sky type was then defined from a list of options. Available types include sunny and intermediate with or without sun, overcast and uniform. This study was concerned with the overcast scenario. Another option of 'daylight factor' is included. This option runs a simulation under overcast sky conditions, though sets the unobstructed sky illuminance value at 100 Lux. Any obstructed values will therefore have a ratio of 1:1 with the daylight factor e.g. a returned value of 5 Lux near to a ground floor window will also have a daylight factor of $5/100=5\%$. Whilst in reality, the unobstructed illuminance on an overcast day may be 100 times greater than 100 Lux, the actual daylight performance of a system under perfect overcast conditions will not change no matter what the absolute value for the illuminance may be. This is therefore a valid means to obtain daylight factor which, when directly underneath the roof and provided there is no contribution from the well in the form of light flux

reflected back up to the roof plane, is representative of the transmittance value of the roof system.

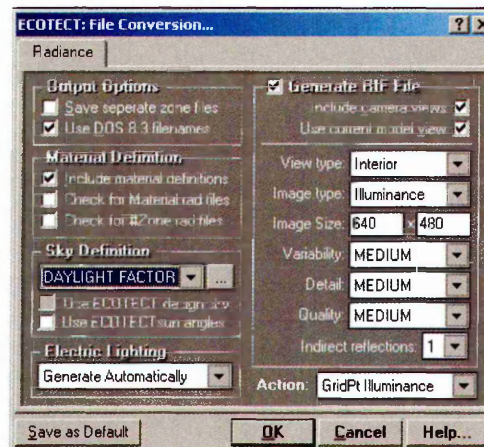


Figure 6-9: The Radiance file conversion window. The type of simulation is defined here (i.e. whether *rpict* or *rtrace* are invoked and other finer details).

Once prompted for a name for the simulation, Ecotect creates several files, a description of which can be seen in Table 6-1.

Table 6-1: The files created by Ecotect in the export to Radiance

File Name	Suffix	Description
Ambient file	*.amb	Stored data of ambient values around the scene. Useful for multiple renders of scenes that keep the same geometric and photometric properties.
Batch file	*.bat	Starts the simulation. Subsequent simulations with changes to photometric properties or ambient parameter changes are invoked using this. Changes to ambient parameters using <i>rtrace</i> were made here.
Data file	*.dat	The output (grid data) is stored here.
Octree file	*.oct	A description of the scene comprising information from the conversion of the *.rad files using the <i>oncov</i> program in Radiance.
Points file	*.pts	The positions of the analysis grid points exported from Ecotect
Radiance files	*.rad	<ul style="list-style-type: none"> sky.rad - a description of the sky conditions *.rad - a description of the photometry and geometry. Changes to the photometry are made here.
Information file	*.rif	Contains the rendering settings for a rendering using the <i>rad</i> executable. <i>rad</i> in this case was used to generate the <i>octrees</i> from which <i>rtrace</i> took its information.

When the simulation had finished, the results were imported back into Ecotect (Figure 6-10). The grid now contained values calculated by Radiance.

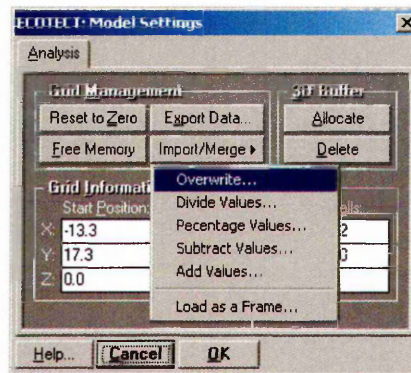


Figure 6-10: The Radiance grid point results are imported to the Ecotect grid.

Ecotect provides a simple and rapid means to display graphically the output onto the analysis grid. Figure 6-11 shows the analysis grid options and the same set of data presented using different means. The preferred choice of display to be used in this study is the shaded contour line. Varying the range of the maximum and minimum allows comparison between two datasets at the ends of the scale, whilst adjusting the spacing of the contours (Figure 6-11, f & g) moves from a jagged to a smooth contour map. The data can then be exported as a formatted ASCII data file (*.txt) and imported in a spreadsheet such as Excel for further analysis.

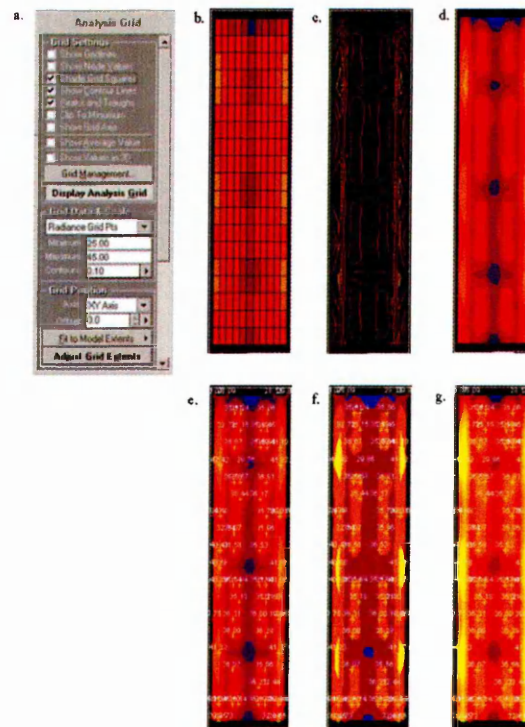


Figure 6-11: a. analysis grid options, b. shaded grid squares, c. contour lines (range 25-45% at 2% intervals), d. shaded contour lines, e. shaded contour lines with peak and trough values, f. as before, though range set at 25-40%, contours at 5% intervals, g. as in f, but at 0.1% intervals.

6.2.4 Procuring and Application of Material Photometric Information

6.2.4.1 Obtaining the Correct Data from the Field

Vital in obtaining meaningful results from a Radiance simulation is an accurate description of the material photometry. The output can only be as good as the input. There are several ways in increasing order of accuracy, ease and cost to derive photometric data from the field. The simplest involves holding up a greyscale chart divided into squares of incrementally increasing reflectance and matching the appropriate square with that of the surface. If the scale is divided into 10% increments, it should be possible to estimate a surfaces reflectance to an accuracy of 5% (absolute terms). This is a crude measure that is perhaps appropriate when aiming for an approximate rendering of a scene, though inappropriate where accuracy is required. A similar methodology involves comparison with known or typical surfaces. Such a methodology has been adopted by Galasiu in determining the reflectance values of atrium well surfaces in a similar study to this one (Galasiu 2002 et. al.). The *IESNA Lighting Handbook-Reference and Application Volume*⁶ was used as the source of reference.

A more quantifiable method involves the use of a luminance or illuminance meter. If an illuminance meter is to be used, a black cylinder placed over the sensor turns it into a focused probe (i.e. all incoming illuminance from the surroundings is blocked out). This method assumes the material is Lambertian (all light is reflected diffusely). A sample of known reflectance is placed next to the material to be measured in an area of evenly distributed illuminance. The reflectance of the unknown material is derived from the simple ratio of either the luminances or illuminances from the two materials;

⁶ Latest edition: Rae M, 2000, *IESNA Lighting Handbook*, Illuminating Engineering, 9th edition, ISBN 0879951508

$$\rho_{UNKNOWN} = \rho_{KNOWN} \times \frac{\alpha_{UNKNOWN}}{\alpha_{KNOWN}} \quad [6-1]$$

where,

ρ =reflectance

α =measured luminance or illuminance

This method was adopted in a study by Aizlewood et. al. (1997) that attempted to validate Radiance against a physical model of an atrium well under artificial sky conditions. The need for highly accurate results in that case made them then turn to the use of a commercial reflectometer. The samples of card representing the well surfaces in his model were of a simple and uniform nature. Despite that, for the white card measurements ranging from 81.5% to 89.8% were recorded, whilst values of 2.7% to 5.2% were measured for the black card, a factor difference of almost two. The side by side luminance method was used in another experiment, with the error being stated in the order of 3% (Ashmore & Richens 2001). This magnitude of error could lead to an error of 15% +/- 8% in mean daylight factor in a simple room as demonstrated through computer simulation using Lightscape.

The most accurate means of determining a surface's photometric qualities involves the use of a spectrophotometer. These machines measure a materials reflectance, chromaticity and specular reflectance though the high costs of these machines put them beyond the reach of this study.

As well as reflectance, Radiance can assign a material a value for specularity and roughness. Other than using expensive spectrometers, there exist few hard and fast means of determining specularity. *Rendering with Radiance* suggests a trial and error method that involves seeing whether the material looks correct in a render. Other than that, there exist some rules of thumb. In general, most non-metallic surfaces rarely have specularities exceeding 6%. Roughness can only be measured using extremely expensive atomic-force microscopes and ellipsometers, though other than that, trial and error is suggested within the range of 0 to 20%.

An alternative means of deriving the material characteristics is to consult the manufacturer's specifications. This has been done by Galasiu et. al. (2002) to determine various glazing transmittances in the modelling of an atrium. Where available, this method represents a good means to obtaining reasonably accurate photometric information.

For the case studies examined, the architectural drawings available did not stretch to the level of detail whereby material reflectance values were implicitly stated. The most accurate means of obtaining reflectance values from the field within the budget constraints of the project involved comparison of luminance ratios against a sample of known reflectance using a luminance meter. The luminance meter used was the Minolta LS-100 (Figure 6-12).



Figure 6-12: The Minolta LS-100 Luminance meter used to derive material surface reflectance.

The comparison material consisted of a white tile from Ceram Research, with a known reflectance of 0.87 (Figure 6-13). For each material type assessed, measurements were taken at several (at least 3) sample points across the material, and averages taken. The found reflectance values for the surfaces within the two case study atria can be seen in Table 6-2.

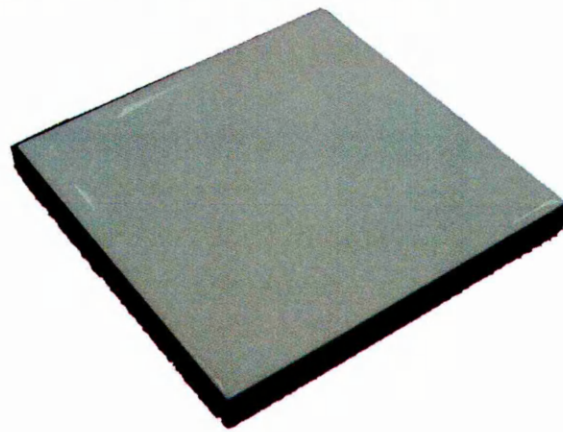


Figure 6-13: The reference material of known reflectance 0.87.

Table 6-2: Reflectance values for principle surfaces in the Sheaf and Owen buildings.

	Reflectance
<i>Sheaf Building</i>	
Roof structure	57.1%
Well walls	70.3%
Floor	11.4%
<i>Owen Building</i>	
Red brick external building	12.5%
Well wall dark	46.8%
Well wall light	67.6%
Tiled floor ground level	32.9%
Tiled floor top level	31.6%
Carpeted floor	8.5%
Roof structure	57.1%

The white paint used in both studies for the roof structure had an element of specularity. Without the manufacturer's specifications or expensive equipment, the exact value of this was unknown. A value of 3% was assigned as the specularity, which was found by comparison to materials in the extensive materials library annexed to Desktop Radiance. All other surfaces were assumed to be perfectly diffuse. The obstructing Owen building which could not be measured using the methodology described was estimated at 20% (including reflective windows) from *Rendering with Radiance*.

Roughness for all materials was ignored (i.e. set at 0%). Whilst useful for adding realism to synthesised imagery, in quantitative terms the slight random function of reflectance applied to a material due to its roughness would not significantly change the magnitude or distribution of the output.

A simple means of measuring the transmittance of a glazing involves taking a sample of the glass, and under controlled conditions finding the ratio of illuminance falling onto an illuminance meter with and without the glass acting as an obstructer. More complicated and expensive equipment such as spectrophotometers can more accurately describe the reflectance and transmittance characteristics over a range of wavelengths and incident angles (Van Nijnatten 2002). It was not possible to adopt either of these methods in the case study buildings. The architectural drawings stipulated 'double-glazed' as the glass type.

The computer program Optics version 5.1, freely available from Lawrence Berkley National Laboratories, was used to simulate the glazing configuration (Figure 6-14). The program allows the building of layered glazing configurations through selection from a highly extensive database (though users can create their own types from scratch). Two layers of 6mm 'generic clear glass' were arranged as in the schematic in the upper right part of the display in Figure 6-14. The reflectance and transmittance behaviour at varying wavelength is shown in the graph at the bottom of the display. The glazing can then be exported directly as a BRTDF material in a *.rad file for use in Radiance simulations. The double glazing simulated for the case study buildings had a transmittance of 78.5%.

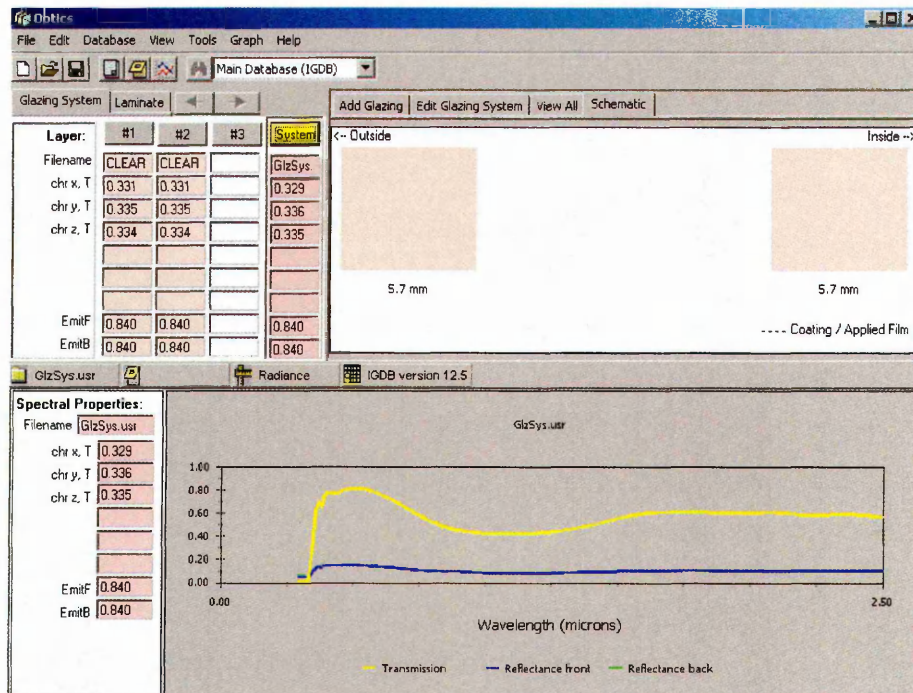


Figure 6-14: Optics5 allows the building of layered glazing systems from an extensive database of glass types and coated films.

6.2.4.2 Editing the *.rad File to Change Photometric Settings

The *.rad file firstly describes the materials present in the scene. A material in Radiance is described by combining arguments of a modifier, type and identifier. The following text describes a hypothetical material that could be used to describe the photometry of the well surfaces:

```
# an off white material with no specularity or roughness to
be used on the well surfaces
# modifier type identifier
void plastic well_surface
0
0
5 0.65 0.65 0.65 0 0
```

The first two lines of the text, pre-fixed with '#' are comment lines, useful as a label to the user or outsider but not a function actually performed by Radiance.

In the case of material definition, there is no modifier, so the text `void` is inserted as a placeholder.

The material type is `plastic`. Plastic is the most common type of material used in Radiance, and differs from the word 'plastic' as we conventionally know it. In general terms, it is an opaque material that is not a metal. In Radiance terms, a metal (metal) differs from a plastic in that its reflections are filtered by the metal's own colour characteristics. Other Radiance material types include `light`, `glass`, `dielectric` and `trans`.

The identifier is a unique name given to the material to differentiate it from other materials. In this case, we have called the material `well_surface`.

The next two lines refer to arguments for the modifier and type, and in the case of creating a material, there are no arguments, hence the two zero's.

The final line contains five arguments, denoted by the 5 at the start of the line. The next three arguments refer to the red, green and blue (RGB) reflectance values for the material. This study will focus on monochromatic colours, as we are only concerned with quantitative illuminance measurements (not colour appearance), and so the red, green and blue components will always be equal. The next argument concerns the specularity of the surface. The more specular a material, the more bias it will show in the direction of reflection. A theoretically perfect mirror will have a specularity function of 1. The final argument denotes the roughness of a material. This enables Radiance to simulate more accurately how materials in the real world actually behave. In the case of our off white well material, it is a perfectly diffuse (Lambertian) material, with a reflectance of 65%.

In describing the transmittance of the glazed elements in the atrium, Radiance uses a theoretical measure called transmissivity. This is *"the amounts of light that penetrates a surface excluding all interreflections among opposite interface surfaces of the transmitting medium. Whereas the measurable quantity is called transmittance and includes interreflections, it is necessary to convert the measured transmittance to the theoretical transmission for the Radiance glass primitive."*⁷. This is done by using the Equation 6-2, where T is the transmittance, and T_s is the transmissivity. Transmissivity values for transmittances between 0 and 1 are shown in Table 6-3.

$$T_s = \frac{(\sqrt{(0.8402528435 + 0.0072522239 \times T^2)} - 0.9166530661) \times T^{-1}}{0.0036261119} \quad [6-2]$$

Table 6-3: Transmissivity values for increments of transmittance

Transmittance (T)	Transmissivity (T _s)
0.1	0.10909
0.2	0.218166
0.3	0.327214
0.4	0.43622
0.5	0.545169
0.6	0.654047
0.7	0.762842
0.8	0.871538
0.9	0.980123
1	1.088581

⁷ Rendering with Radiance p.308

The following text describes glazing that could hypothetically be used for the glazing in the atrium:

```
# glazing with a transmittance of 70%
# modifier type identifier
void glass atrium_window
0
0
3    0.762842 0.762842 0.762842
```

Again, the glazing we shall use will transmit monochromatic light i.e. the same quantity of red, green and blue light is allowed through.

The BRTDF (bidirectional reflectance-transmittance distribution function) can be used to more accurately describe the reflectance properties of the front and back of the glazing system, and can specify a diffuse reflection and transmission. The function is applied to the created glazing primitive e.g. our `atrium_window` material.

```
modifier BRTDfunc atrium_window
10+  rrefl  grefl  brefl
      rtrns  gtrns  btrns
      rbrtd  gbrtd  bbrtd
      funcfile  transform
0
9+   rfdif  gfdif  bfdif
      rbdif  gbdif  bbdif
      rtdif  gtdif  btdif
A10 ..
```

where; r, g, b correspond to the red, green and blue channels

`rrefl`= ideal specular reflection of the surface

`trns`= ideal specular transmission

`brtd`= directional diffuse part of reflection and transmission

`fdif`= diffuse reflection component for front of surface

`bdif=` diffuse reflection component for back of surface

`tdif=` diffuse transmittance

The `BRTDF` directional diffuse reflections are not computed with Monte Carlo sampling as they are for the built-in types⁸. As the front and back surfaces of the glazing simulated in this instance were photometrically equal, it was felt that the `glass` primitive was sufficiently accurate for the needs of the study. Should the examination of the effect of glazing films or novel glazing types (e.g. prismatic glazing) become necessary, then the `BRTDF` material would be used. Andersen et. al. (2003) describe a way of measuring the `BRTDF` of a material through simulation of the arrangement using Radiance. This saves using expensive and time consuming use of photogoniometers.

Once the materials present in the model have been defined, they are applied to the geometry. Assigning the layers dummy materials in Ecotect means that this application has been automatically done. The following text describes the geometry of a wall plane in the well, with our `well_surface` material added to it;

```
well_surface polygon zone02.rad00000
0
0
12
-13.61  43.67  3.80
-13.61  16.62  3.80
-13.61  16.62 -14.45
-13.61  43.67 -14.45
```

The geometry type is `polygon`, which has been modified by the addition of the material `well_surface`. The identifier `zone02.rad00000` has been created by Ecotect. The next 12 numbers represent the four co-ordinates of the polygon nodes, expressed in terms of their x,y,z displacement from an origin (this polygon does not move in the x plane, and the width and heights of 27.05 and 18.25 derived from

⁸ *Rendering with Radiance* p.14

subtraction of one node value from another (i.e. $43.67-16.62$ and $3.8-(-14.45)$) represent the length and height of the well in metres).

The effect of changes to photometry (a simple change to the text at the top of the *.rad file) become apparent at each re-running of the simulation. Every time the batch file is invoked, the previous octree is deleted and a new one generated. This new octree will reflect the changes to the photometry. Results for many combinations of material possibilities can be rapidly achieved with only simple changes to the *.rad file and a re-running of the simulation. It is appreciated that the process of changing material properties can be automated using scripting techniques. This has the advantage of being able to manage simulations outside of standard office hours. This is however beyond the field of knowledge of this author, and whilst less elegant, the manual manipulation of the *.rad file produces the same results. The effects of varying the reflectance properties of the roof structure and the transmittance properties of the well are described later in Section 6.5.

6.3 Setting Radiance Ambient Parameters

6.3.1 The Simulation Parameters

Meaningful quantitative output from Radiance will depend heavily on correctly configuring the input parameters. The large number of parameters at the disposal of the operator results in an infinite combination of possibilities. These parameters must be set so as to maintain photometric accuracy, yet not at a prohibitive processing cost. Broadly speaking, the Radiance parameters can be split into six groups (Summerfield 2004).

1. View - regarding the viewing position, direction etc.
2. Pixel - pixel sampling and frequency
3. Direct - source sampling and subdivision, specular thresholds
4. Ambient - frequency and level of sampling in ambient calculation
5. Participating media - consideration of mist and turbidity etc.
6. Miscellaneous - network controls, file naming, reports etc.

The view and pixel commands are primarily concerned with viewpoints and quality of images, where this study is concerned with the numerical output at predetermined grid points. The direct parameters may be more relevant when considering artificial lighting, particularly large sources which require subdivision. This study concerns overcast skies, and hence there is no direct component (and even if the sun were included, its nature as a point defined at a 0.5° angle at infinite distance requires no subdivision). Participating media were not considered in this study. The following sections outline the relative effects of varying the ambient parameters, and an experiment to determine the correct ambient settings for simulation of the test atria.

6.3.2 The Ambient Parameters

There are essentially seven key ambient parameters within Radiance, being;

1. ambient value (-av)
2. ambient weight (-aw)
3. ambient divisions (-ad)
4. ambient supersample (-as)
5. ambient bounces (-ab)
6. ambient accuracy (-aa)
7. ambient resolution (-ar)

The following sections will describe the effect on accuracy and processing cost of each of these parameters. Initial simulations were run on the Sheaf (simple atrium) model to ascertain the best parameter combination for the multiple simulations later required for the varying configurations of structure reflectance and glazing transmittance.

6.3.2.1 Ambient Value and Weight

The ambient value is the average radiance in all directions of the visible scene, and is inputted by the user as a RGB value. The ambient weight determines the extent to which the assigned ambient value will dominate over calculated indirect values. Setting an ambient value may be useful for visualisation, where adding a constant

radiance to a scene may save on computational effort through perhaps achieving a similar appearance using less ambient bounces (see Section 6.3.2.3). Where quantitative accuracy is required, this 'estimation' of radiance is not relevant, and hence `-av` is set at zero (all indirect radiance is the result of stochastic calculation).

6.3.2.2 Ambient Divisions and Supersample

The number of ambient divisions sets the number of samples sent out from the sample hemisphere. The error in the Monte Carlo calculation of indirect illuminance will be inversely proportional to the square root of this number. In other words, the higher the value for `-ad` the more accurate the results will be. Conventionally its value is expressed as a factor of two (2^n). Supersampling means a spawning of further rays at areas within a hemisphere where variance is found to be large (e.g. at apertures). In this case, `-as` is set at a quarter of `-ad`, although the relative effects in terms of accuracy or computational cost of changes to the supersample value was found to be minimal.

The effects of varying `-ad` (with `-as` always set to a quarter of the `-ad` value) were investigated on the model of the Sheaf (simple) model. The reflectance and transmittance values were set at relatively high levels (structure 100%, glazing 90%, well surface 65%) as it is under these circumstances where there will be more light flux and hence potentially put most strain on the program. A reference case was simulated at very high settings for comparison (`-ab` 7, `-ad` 2048, `-as` 512, `-aa` 0.05, `-ar` 128). For the remaining simulations, ambient bounces were set to 7 and the accuracy at 10%. Table 6-4 shows the results.

Table 6-4: Effect of changing the `-ad` (with `-as`) parameter.

<code>-ad</code>	<code>-as</code>	Time	<i>h</i>	<i>m</i>	RER	RMSE
64	16	0	2		-1.49%	3.29%
128	32	0	4		-0.74%	2.31%
256	64	0	10		-0.95%	1.69%
512	128	0	23		-0.72%	1.21%
1024	256	0	58		-0.52%	0.85%
2048	512	2	47		-0.41%	0.73%

RER=relative error

RMSE=root mean square error

Figure 6-15 shows results at selected settings of $-ad$ for a measurement line across the width of the well (note the peaks and troughs related to the structural members). The results with 64 and 128 divisions are fairly erratic. This would be reflected in a rendering by a 'splotchy' appearance. By 512 divisions there is little deviation from the measurements found at the more accurate 2048 setting.

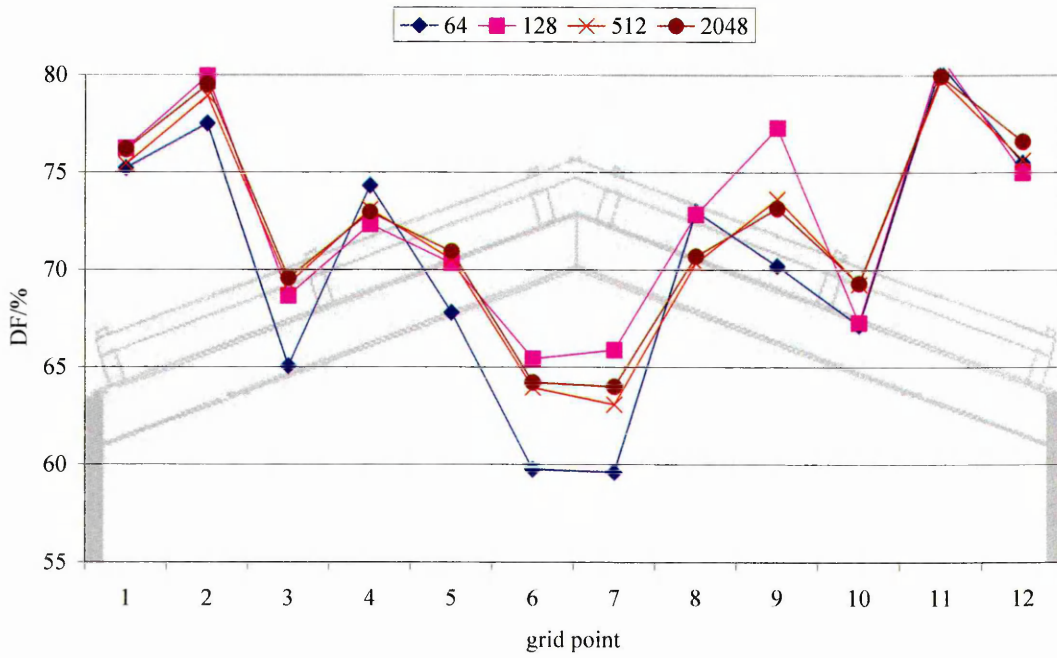


Figure 6-15: Effect of changing ambient divisions across one row of a grid in the Sheaf building.

Figure 6-16 illustrates in plan view the effect of varying the number of ambient divisions. At the low setting, the distribution is less smooth, due to interpolation based on chance hits which have designated a surface being either higher or lower in luminance than it actually is in reality. By the time the setting has been increased to 512, there is little visible difference with the higher accuracy setting of 2048.

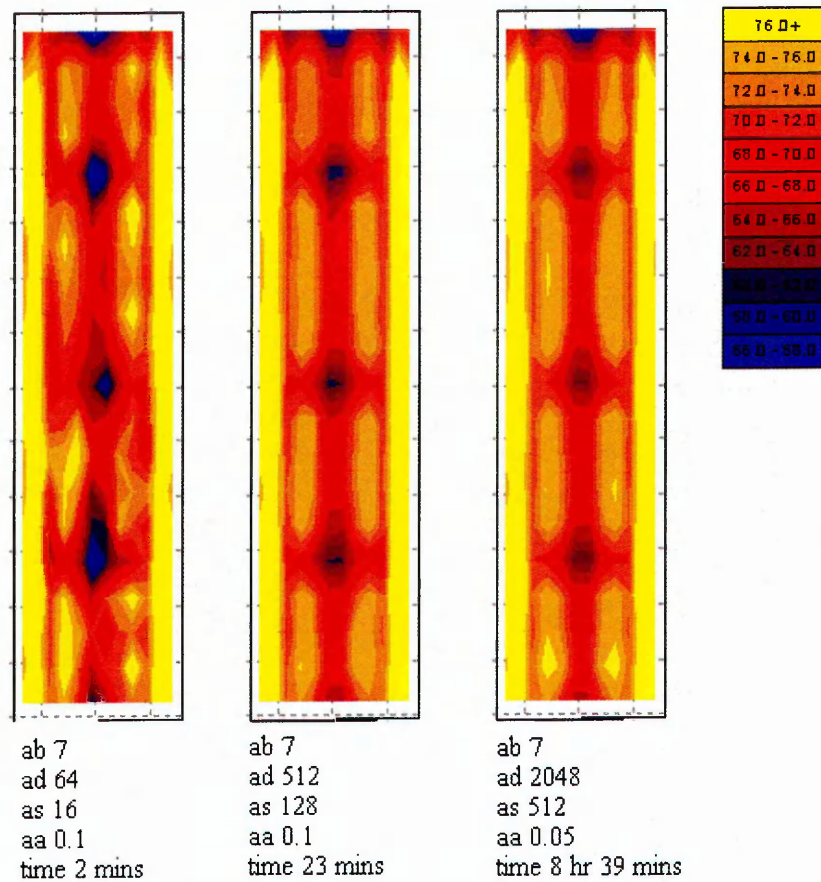


Figure 6-16: Three settings of ambient division. The results obtained at $-ad$ 64 are very coarse compared to those at $-ad$ 512. There is little noticeable improvement increasing $-ad$ to 2048, though the calculation is over 25 times longer.

Figure 6-17 shows the cost of computational time against accuracy due to increases in number of ambient divisions. The decay of the curve indicates a poor marginal return in accuracy at the expense of great computational power with increasing number of divisions. Similar findings were observed in corresponding pre-simulation parameter set-up experimentation for the Owen building. A setting of $-ad$ 512 and $-as$ 128 was ascertained to yield sufficiently accurate results for the purposes of this study.

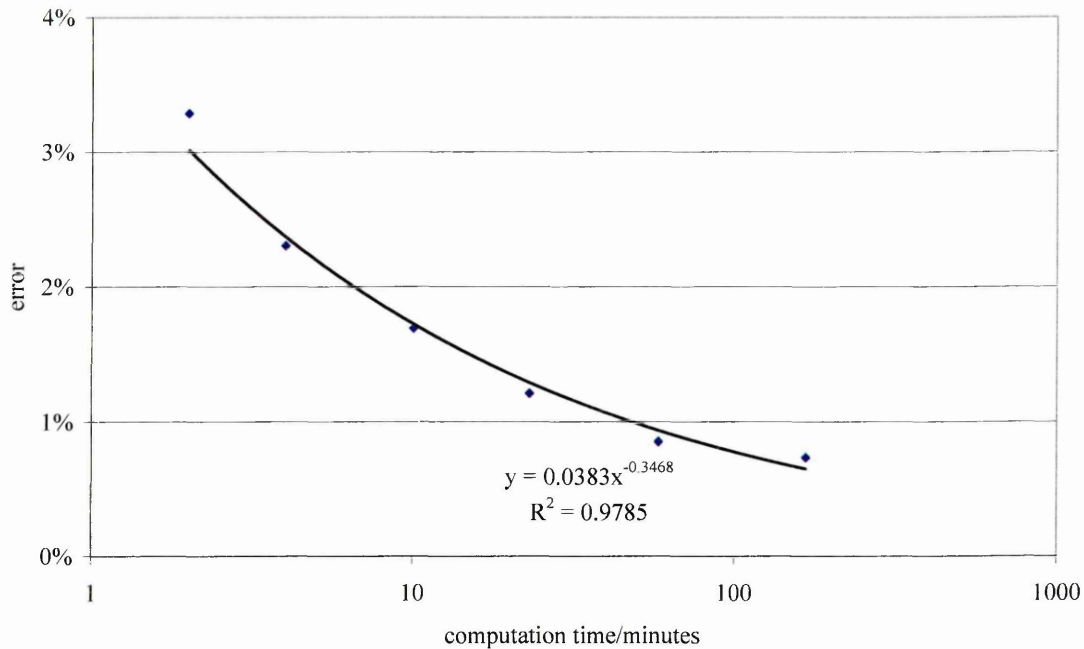


Figure 6-17: The cost in time of running a more accurate simulation by increasing the *-ad* parameter from 2^6 - 2^{11} (64-2048).

6.3.2.3 Ambient Bounces

The number of ambient bounces sets the maximum number of inter-reflections between surfaces the program calculates before reverting to the ambient value (though in this study, the ambient value is set to zero). That is to say, if *-ab* is set to four, sampling of a ray could occur at four separate surfaces after leaving the source (i.e. the sun or an artificial light, or three surfaces from the sky glow which is considered to be an indirect source). At a low number of ambient bounces, and assuming ambient value is set to zero, the program will tend to underestimate illuminance levels as the calculation is cut off well before all the light flux has been accounted for. Coupled with that, the distribution is likely to be inaccurate. As the number of bounces increases, the calculation will begin to converge at its true value till further increases in *-ab* make negligible difference. In terms of visualisation, acceptable results may be achieved with *-ab* set at 2 or 3, with perhaps the addition of an ambient value to brighten the scene. For accurate quantitative data, higher settings must be used. Parametric changes were made to the ambient bounce setting in the Sheaf model (*-ad* 512, *-as* 128, *-aa* 0.1, *-ar* 128). The results displayed in Table 6-5 and Figure 6-18 clearly show a convergence with increasing bounces, from about 5 onwards.

Table 6-5: Effect of increasing the $-ab$ parameter

$-ab$	time/m	RER	RMSE
1	2	-22.32%	22.84%
2	5	-12.85%	13.21%
3	17	-6.21%	6.50%
4	21	-2.54%	2.80%
5	22	-0.92%	1.33%
6	23	-0.69%	1.15%
7	23	-0.72%	1.21%

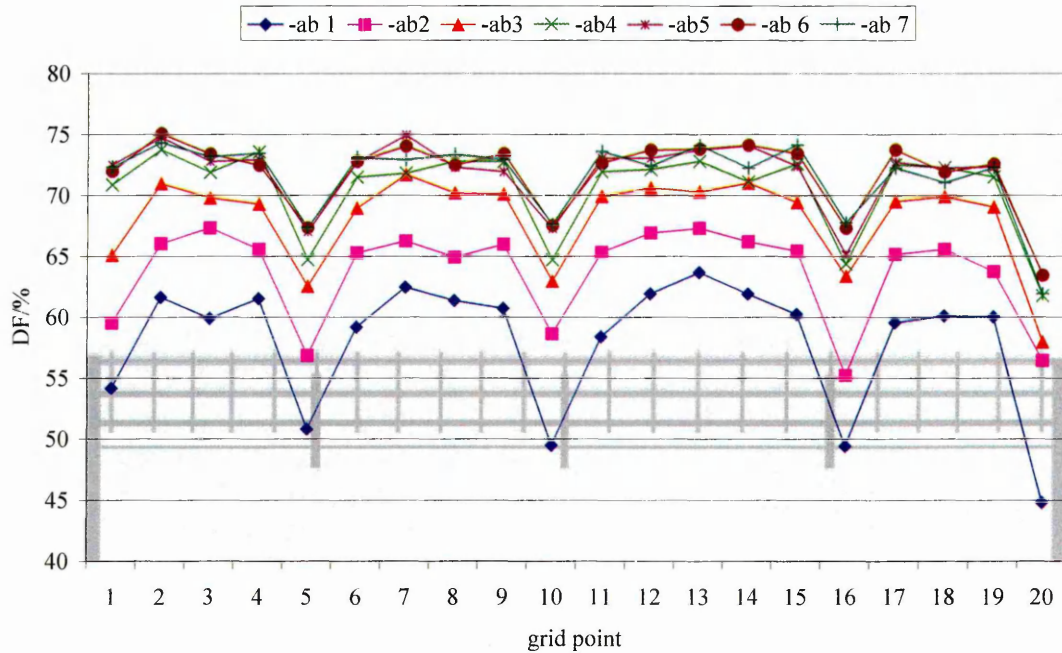


Figure 6-18: The effect of changing the $-ab$ parameter across an analysis row in the Sheaf building.

The effects on calculation time can be seen in Figure 6-19. The Radiance help guidelines stipulate a direct relationship between increasing the number of ambient bounces and calculation time⁹. Interestingly, in this case there appears to be sufficient cached ambient data at the resolution specified for Radiance to be able to efficiently interpolate the indirect calculation with considerable savings in time. It only took six more minutes to calculate at $-ab$ 7 rather than $-ab$ 3. From the results, it appears that the calculation has fully converged at about 5 ambient bounces. Seeing as there was no difference in calculation time between the two settings, a value of 7 was used in the experiments.

⁹ from Radiance online help http://floyd.lbl.gov/deskrad/param_table.htm

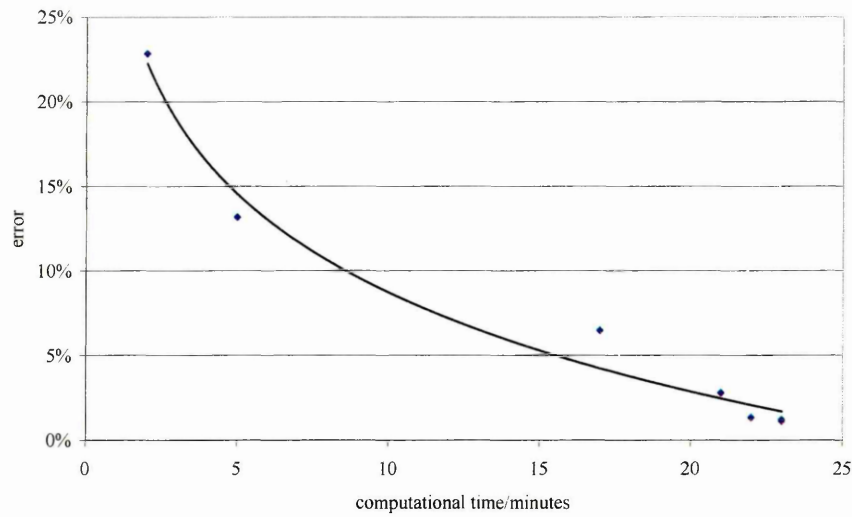


Figure 6-19: Error associated with varying $-ab$ parameter against computational cost Sheaf (for $-ab$ 1-7 note; $-ab$ 6 and 7 coincide)

In the case of the Owen building the simulations took much longer to run. The values at roof plane level seem to have converged after approximately 3 ambient bounces (Figure 6-20). Increasing the $-ab$ parameter from 3 to 4 resulted in an improved accuracy of under 0.25%, at a cost of over an hour and a half. If measurements were being made deeper in the well, it is appreciated a higher number of ambient bounces would need to be set. The base simulation of the atrium was performed with 7 ambient bounces. A value of $-ab$ 3 proved sufficiently accurate for the multiple simulations required to examine the effect of the glazing transmittance and structural reflectance.

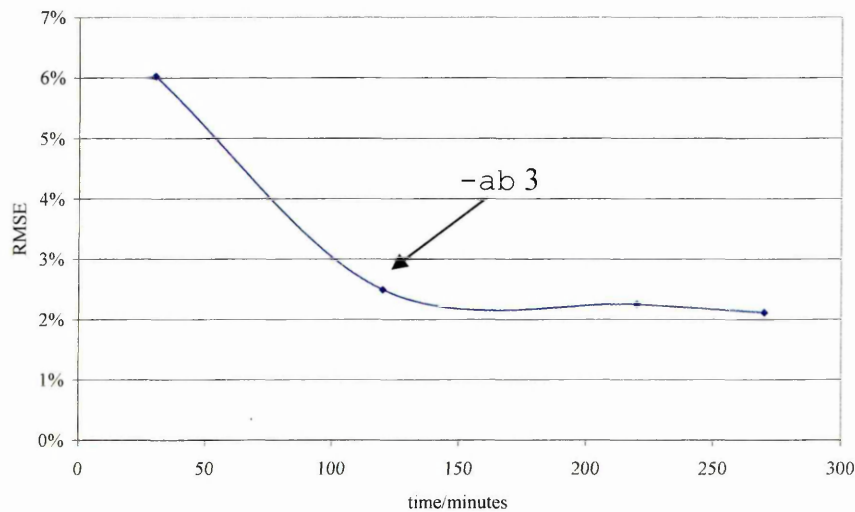


Figure 6-20: Error associated with varying $-ab$ parameter against computational cost for the Owen scenario ($-ab$ 2, 3, 4 & 7)

6.3.2.4 Ambient Accuracy and Resolution

Ambient accuracy ($-aa$) is the maximum error (expressed as a fraction) permitted in the indirect irradiance interpolation. The majority of the parameter set-up experiments were performed at $-aa = 0.1$, i.e. a maximum permitted error of 10%. This is at a more sensitive setting than the 0.15% recommended on the Radiance website for an 'accurate' rendering, and the 'high' setting in the `rad` executable program. Increasing the accuracy to 5% yielded marginally more accurate results (under 1% RMSE). This came at a huge time cost - a doubling in accuracy tripled the time taken for the calculation. This can rise to a quadrupling of time. A value of 0.1 was considered appropriate for the needs of this study.

Ambient resolution ($-ar$) relates to the ambient accuracy, the scene size and the cut off point at which further hemispherical sampling ceases and interpolation begins.

$$S_{min} = \frac{aa \cdot D_{max}}{ar} \quad [6-3]$$

S_{min} = minimum distance between sample points

D_{max} = maximum scene dimension

The maximum scene size can be found using the `getinfo` command. In the case of the Sheaf model it was found to be 59.99m (note; whilst the length of the well is only approximately 30m, the extra 30m in length is due to the external roof, which includes an element of necessary obstruction modelling). This length was 86m in the Owen scenario. Applying this information to the equation, $-ar$ set at 2^n intervals returned the following S_{min} values (Table 6-6);

Table 6-6: Minimum distances from after which stochastic hemispherical sampling takes place for various values of $-ar$.

$-ar$	S_{min}/cm Sheaf	S_{min}/cm Owen
32	18.7	28.9
64	9.3	13.4
128	4.7	6.7
256	2.3	3.4
512	1.1	1.7

That is, with resolution set at 32, further hemispheres are spawned in the Sheaf simulation where the distance between them is greater than 18.7 cm. Interpolation occurs where the distance is under 18.7cm. The assumption of interpolation can be made as the gradient of diffuse light over a scene is far shallower than the sharp contrasts typical of direct light sources. A setting of 128 (interpolation occurs for distances under 4.7cm) was found to give good results at acceptable calculation times (note; this also ties in with the accurate setting recommended on the Radiance website, though it is appreciated these are only guidelines, and results will vary depending on the model). Likewise, a more accurate setting of `-ar 256` (further hemispherical spawning at distances of greater than 3.4cm) was used in the Owen model due to its increased size.

6.4 Base Case simulations: Results

6.4.1 The Simple Scenario (Sheaf Building)

6.4.1.1 Roof Plane Results

The simulated daylight factor at the point of the internal photocell (S1) was 53.5%. This is 11.3% lower in relative terms than the value obtained using the photocells. The most obvious source of error concerns the value of glazing transmittance used in the Radiance scene file. The lack of reliable information any more detailed than "double-glazed" for the glazing type used in the roof system meant an estimate from Optics 5 had to be used. Further simulations revealed that a glazing of 88% entered into the Radiance scene file would result in a good agreement between physically measured and simulated daylight levels. A value this high however better describes a single clear pane of glass. The lower simulated values must therefore be a result of something else.

It was not expected either the geometry entry or the ambient parameter settings could be the cause of such an error. Both were undertaken at high accuracy settings. A likely source of error is in the Radiance treatment of the sky luminance distribution. The most rigorous validation of the Radiance rendering system found a good agreement between simulated and physically measured results (Mardalijevic 1999). These

simulations were performed with a sky distribution modified to match that under which the physical measurements were taken. Comparison between physically measured results and simulated results using the CIE standard overcast formula resulted in underestimations on the south and west surfaces (mean bias errors of -15% to -19%, root mean square errors of 22% to 28%) when measuring vertical illuminances. These errors are greater than those observed in this study, which introduces far more complexity than unobstructed vertical illuminance levels. It would not be an unreasonable presumption to believe that the simulation has successfully described the transmittance of the roof system, albeit with results of scaled down magnitudes.

The photocell was positioned towards the end of the well for pragmatic reasons discussed in Chapter 4. The array of 240 grid points in the simulation reveal how representative this point is to the performance of the entire roof. The mean daylight factor at the roof plane was 54.6% with a standard deviation of 5.2%. Dividing the standard deviation by the mean returns the coefficient of variation. This measure is a useful descriptor for this study of the extent of distribution across the analysis plane. A very low coefficient of variation means a plane with very even lighting distribution. A high value means high contrast across the pane. The coefficient of variation for the Sheaf analysis plane was 9.5%, and was as a direct result of the roof structure arrangement over the measurement grid points (Figure 6-21)

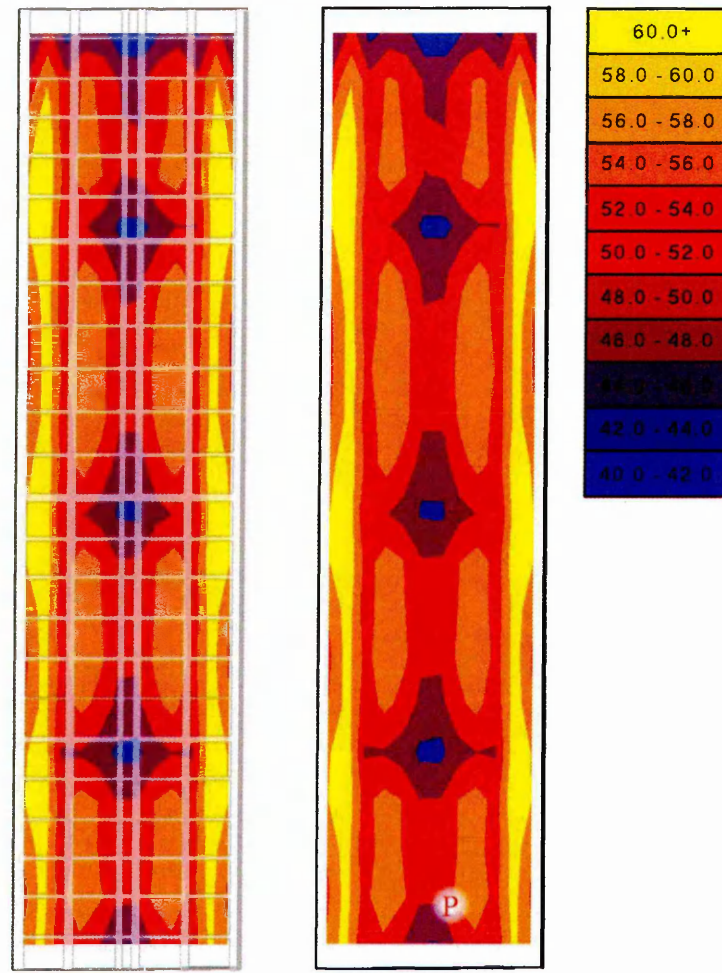


Figure 6-21: Analysis plane daylight factor results for the Sheaf building, with roof plan overlaid (left) and without (right). The photocell position is denoted by P.

The areas of roof plane with lower daylight factor than the photocell position were found underneath the central roof purlin and under the primary I-beams. Where the two crossed the daylight factors were lower still, with the only values lower to be found at the small regions very close to the east and west edges, which were obstructed by the opaque gable ends of the roof. The areas of roof plane with higher daylight factor than the photocell position occurred along the length of the well close to the sides where the photocell position was very close to the roof openings, and thus 'saw' less of the overall roof structure. The average daylight level values were 2.0% higher (relatively) than at the photocell position. The root mean square error of each individual grid point from the photocell point was 10.8%. That is to say, on average, values over the plane fluctuate above and below the photocell value by a magnitude of about 10%. The photocell position would seem to be a reasonably good descriptor of the roof (in as much as one measuring point ever can be). However, only through simulation (as in

this case) or by using many more sensors was performance across the whole plane possible.

6.4.1.2 The Well Contribution

In order to assess the impact of the well on daylight factor results, the simulation was run with the reflectances of the well surfaces set at 0% (light sinks). The average value for the roof plane fell from 54.6% to 52.5%. This can be seen visually in Figure 6-22.

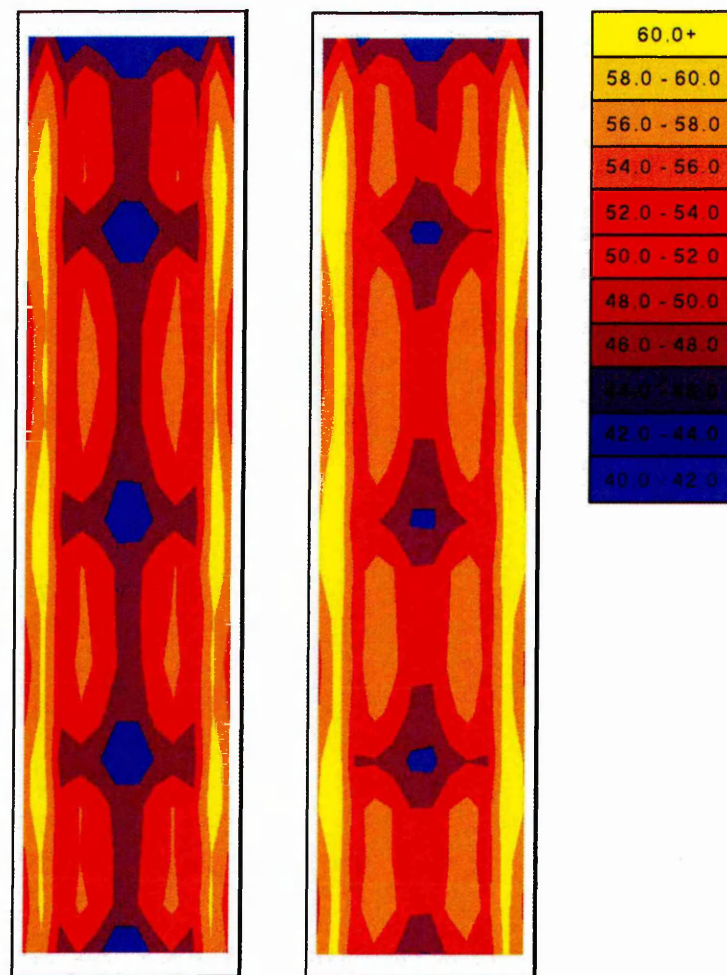


Figure 6-22: Analysis plane daylight factor results with the well reflectance set at 0% (left, i.e. transmittance at roof plane) and with a well of 70.3% reflectance (right)

The coefficient of variation at 10.7% is slightly higher than with a reflective well. This is because after 7 reflective bounces the light flux gained back at the roof

plane from the well acts as an ambient value marginally evening the distribution brought about by the roof structure. The root mean square difference between the photocell position and every other grid point remains almost exactly the same.

In relative terms, daylight factor are 3.9% higher with a reflective well than with a light sink values (by comparing like points from both scenarios). The coefficient of variation for this result was found to be 41%, seemingly high. A closer examination as to where the differences are greatest reveals that at both ends of the well the values obtained are notably higher (differences of up to 12% found). The reason for this is the influence of the gable ends which, when assigned a reflectance of 0%, significantly lower the daylight levels in the immediate vicinity. Removing the closest row of grid points from each end reduces the coefficient of variation to a more acceptable 24%. The relative contribution of the well to the analysis plane also drops to 3.5%.

6.4.2 The Complex Scenario (Owen Building)

6.4.2.1 Roof Plane Results

The simulated daylight factor at the position corresponding to the placement of the internal photocell (O1) was found to be 38.0%. The physically measured daylight factor was measured at 35.0%. The simulated result exceeds this result by 7.9% in relative terms (3.0% in absolute terms). Given the assumptions made in the model input the closeness of the results is extremely encouraging. The fact that the two results are so close adds confidence to the assumption that the simulation has accurately described daylight levels over the entirety of the analysis plane.

The most likely sources of error include inconsistency between the sky model and the actual sky luminance distribution, the estimation of the glazing transmittance properties from Optics 5 and the estimation of the reflective properties of the main obstructing external element in the scene. Small changes to any of these e.g. a lower glazing transmittance (perhaps caused by dirt accumulation) or a less reflective Owen building would lead to a near perfect match. The difference is already within the often quoted 20% error bounds in connection to daylight measurement.

The mean daylight factor over the whole analysis plane was 35.5% (standard deviation 5.5%). The daylight factor recorded at the photocell position was thus 7.2% higher than the average for the roof. The coefficient of variation of the grid points was 15.6%. The explanation for the variance can be seen by examining the roof plan over a contour map of daylight factors at the analysis plane (Figure 6-23). The highest values are to be found at small peaks to the west of the well (near the external obstruction) and towards east of the centre away from any major junction of roof structure. The peaks near the edge are due to the extreme proximity of the grid points to the roof thus seeing large (and unrepresentative relative to the overall roof form) areas of glazing in the fields of view. Row 1 is so far 'into' the roof structure it is possible it is above the level of some of the structural members. There are also some localised gains due to reflection from the adjacent obstruction. Troughs are to be found at the junctions of structure towards the west of the roof, where the actual roof is very close to the analysis plane. There are also lower daylight levels at the extreme east of the well adjacent to the well wall. Here the analysis plane is displaced furthest from the roof (going deep into the well) and is heavily influenced by the overshadowing well surface. The relatively coarse contours suggest that the 20x12 analysis grid was not sufficiently dense. Whilst this should not affect the average roof plane illuminance values too much it may skew patterns regarding distribution. If the experiment were to be repeated, this should be done using a finer analysis grid.

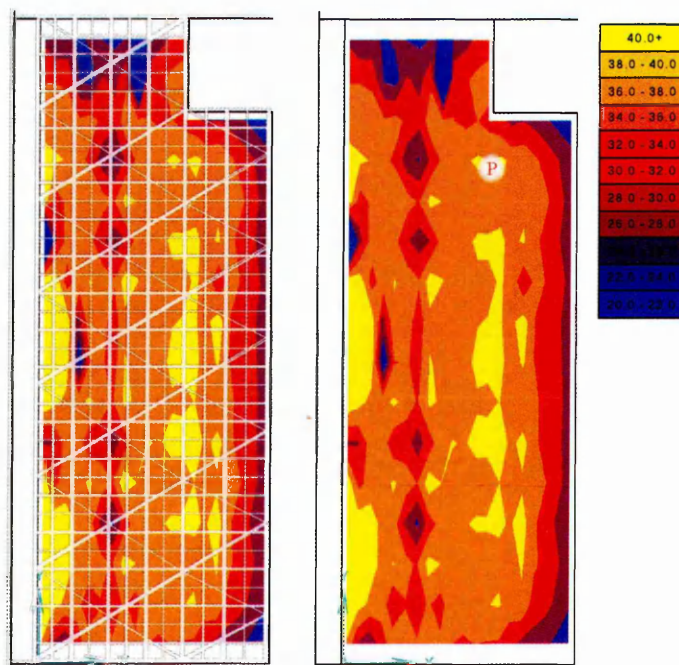


Figure 6-23: Daylight factor at analysis plane in the Owen building with the roof overlaid (left) and without (right) The photocell position is denoted by P

These patterns can be clearly demonstrated in Figure 6-24. For the majority of the well the daylight factor at the analysis plane does not deviate far from the 36% mark. The slight peak at grid point 1 is due to the extremely close proximity to the roof, and thus most of the measuring points saw predominantly open space. The external obstruction reflects a degree of light back into the space. The trough at grid point 7 is due to the major overhead structural junction (concerned with the space frame). Such a trough is not evident at grid point 13 (underneath the next major structural junction) as the analysis plane is at sufficient distance from the roof for localised factors to lose their significance. The gradual drop from grid points 16 to 20 is due to an increasing proximity to the edge wall.

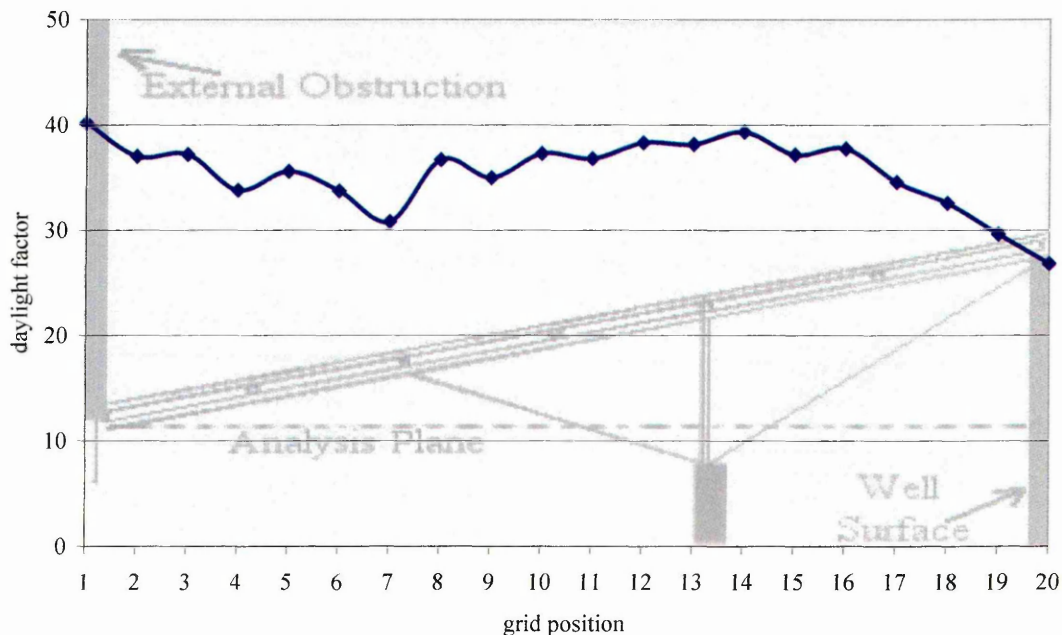


Figure 6-24: Average daylight factor per grid row in the N-S direction. The DF decreases with increasing proximity to the well surface that rises above the analysis plane.

6.4.2.2 External Obstruction Contribution

In order to assess the impact of the external obstructions, the simulation was re-run with the external context geometry removed (note; polygons removed that formed part of the well were replaced with unobstructed polygons to ensure the space remained 'light tight'). The relative difference from each measurement point was calculated. On average the unobstructed results were 32.4% higher than the obstructed results. Figure 6-25 shows the daylight factor results for a reflective and black box well, together with the relative difference between the two along measuring points on the primary axis of

the analysis plane. The effect of the obstruction is greatest (as expected) in the regions closest to it. The relative difference between the two simulations was just under 45% immediately adjacent to the obstruction, dropping to under 30% towards the east of the well where the obstruction has less influence. The two troughs correspond to the immediate overhead structure occupying the field of view as seen from the analysis points, the magnitude of the trough being greater at the structural joint closer (in the 'Z' direction) to the analysis plane.

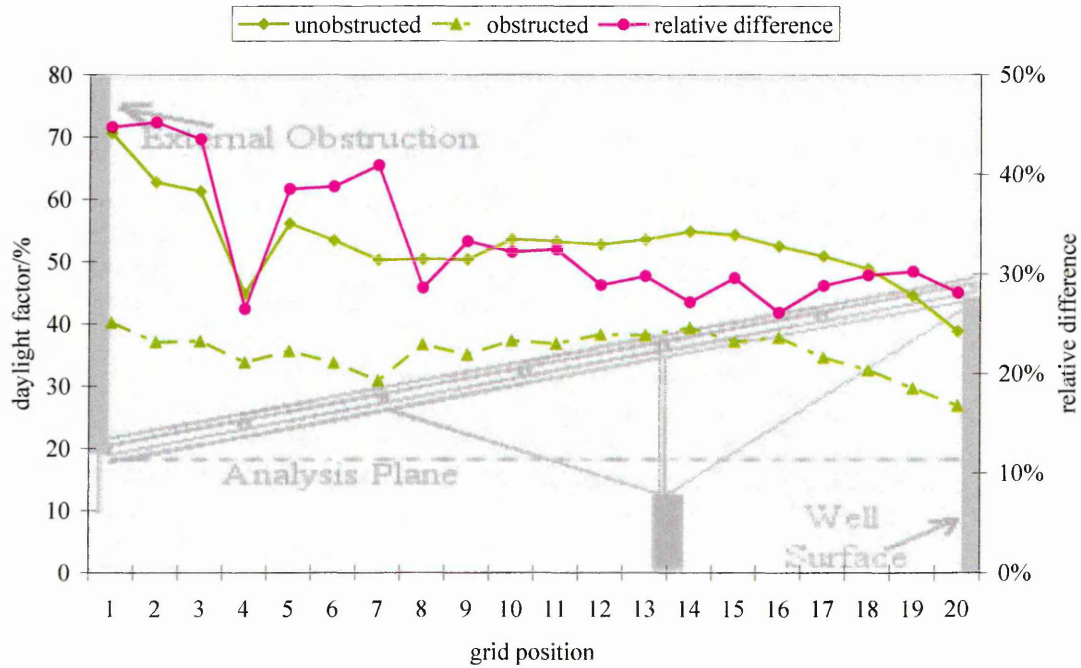


Figure 6-25: Average difference at analysis row between simulations with and without external obstructions.

It might be expected that there would be agreement between the unobstructed simulated results and the E_I/E_E results for the obstructed photocell. This is because the photocells used for the physical measurements have similar views to each other (roof structure aside), as does the analysis plane to the unobstructed external view (roof structure aside). Both aim to isolate the transmittance effects of the roof system alone. The simulated results are 26.4% higher than the physically measured result of 43.0%. Whilst a significant part of this difference may be due to the discussed possible divergence between real and simulated material properties, the magnitude of error is greater than found for the obstructed results.

There are two possible reasons for this. Firstly, the internal and external obstructed photocell were displaced several metres apart in the 'Z' direction. Whilst this was the closest in practice that the two could be positioned to each other, this gap still meant the external photocell saw more clear sky than the internal photocell (roof structure aside). This would lower the ratio of internal to external result as compared to if the two were located at the exact same point (impossible in reality to measure with and without the roof on at the exact same time). The second reason concerns the direction of the monopitch slope. Removing the primary obstruction reveals a large portion of the sky dome that is at close to a perpendicular angle to the roof plane. Transmittance through glazing is higher at such angles compared to at grazing angles. This could lead to higher internal measured daylight levels at the analysis plane. Scaling the unobstructed simulated result down by 8% (the difference found in the obstructed simulation), the simulated result is 13.9% higher than the physically measured value. It is quite reasonable for these possibilities discussed to have caused such an error.

6.4.2.3 The Well Contribution

The contribution from the well was assessed by re-running the simulation with well surfaces specified as light sinks. The simulation with a reflective well returned values 5.3% higher than for the black box scenario, with a difference of 3.5% observed at the photocell position (average of differences between corresponding grid points). There was a high coefficient of variation (82.3%) about that mean (Figure 6-26).

The high variation is due to the general trend occurring across the analysis plane. The difference between the two simulations, that is to say, the reflectiveness of the well carries a greater significance at the east than at the west i.e. towards the high end of the monopitch roof and hence the side wall. Differences between the simulations ranged from under 2% at the west end to over 15% in the east (Figure 6-27). For the majority of the analysis plane the illuminance contribution of the well is between 4% and 6%.

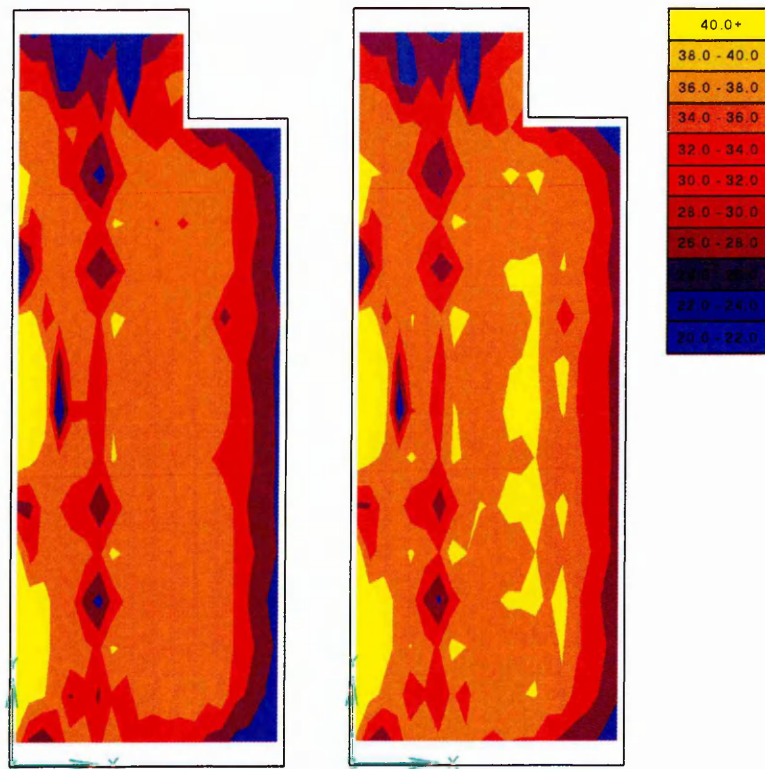


Figure 6-26: Analysis plane daylight factor results with the well reflectance set at 0% (left, i.e. transmittance at roof plane) and with a reflective well (right)

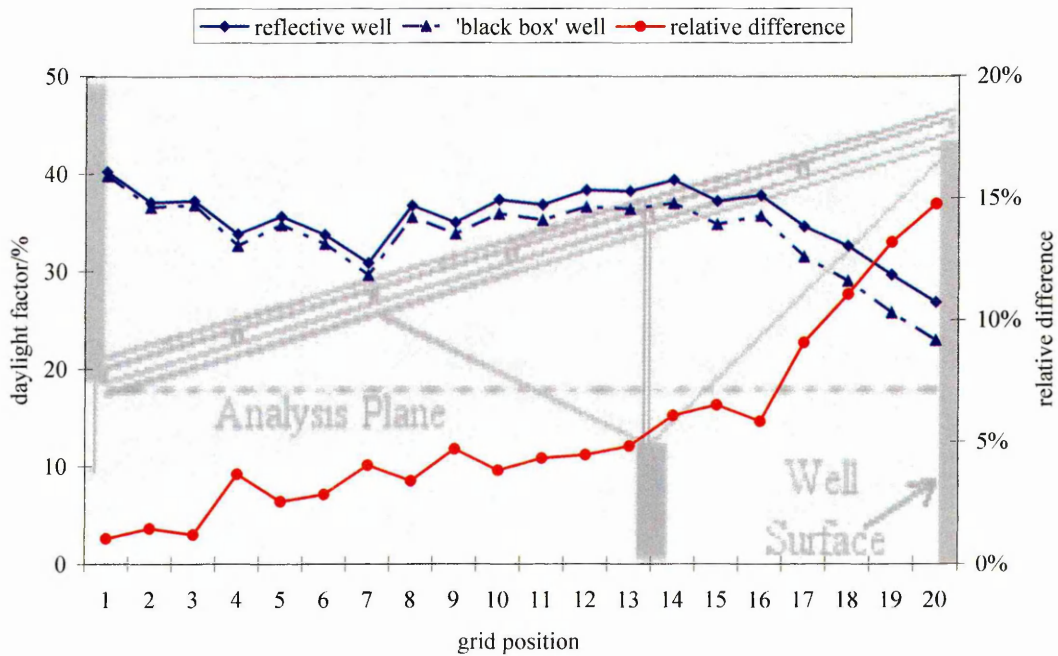


Figure 6-27: The contribution of the well to DF calculated at the analysis plane (from simulations with no external obstructions)

6.5 Examining the Impact of Structural Reflectance and Glazing Transmittance

6.5.1 The Need for Parametric Experimentation

Chapter 5 contrasted the findings of the physically measured illuminance data with the photographic image analysed data. Simply relating the gap fraction of visible sky to the transmittance does not consider illuminance gains from areas which would be classed as 'blockage', nor losses from regions which would be classed as 'gap'. In practical terms, glazing does not transmit 100% of incident light, and opaque surfaces reflect a certain percentage of light flux back into a scene. Through isolating the roof structural reflectance and glazing transmittance parameters, and making incremental changes, the relative effects and contributions of the two factors can be analysed.

6.5.2 Methodology

Simulations were performed for the same analysis grid as in the previous section. The ambient render parameters used in the Radiance simulation in the Sheaf building were `-ab 7, -ad 512, -as 128, -aa 0.1 and -ar 128` and `-ab 3, -ad 512, -as 128, -aa 0.1 and -ar 256` in the Owen building. For the both buildings simulations were run for roof structure reflectances of 0%, 20%, 40%, 60%, 70%, 80%, 90%, and 100%. The smaller increments (10% as opposed to 20%) at higher reflectance values are so as to examine more closely the region of reflectance values found in roof structural members, which typically are highly reflective. Specularity of the roof structure was set at 3% for the reasons discussed in Section 6.2.4.1. Roughness was set at 0% for all measurements. The values of glazing transmittance (note; the values were converted to transmissivity in the Radiance **.rad* file) simulated ranged from 40% to 100% at 10% increments, the 100% simulation consisting of a 'no glazing' scenario. These regular transmittance intervals could represent various glazing types available in architectural practice. The effect of dirt whilst not included specifically could be thought of as inclusive within these transmittance values, for example the 50% measurement could comprise a perfectly clean glazing system of transmittance 50% or a dirtier system of transmittance 55% with a layer of dirt reducing incoming flux by a further 5%. The reflectance of the well was set at 0%, so as to isolate solely the effects

of the interaction between glazing and structural reflectance. As all inter-reflection from internal well surfaces had been switched off, the daylight factor output equates to the roof transmittance. In the case of the Owen building, the external obstructions were removed from the model so as to observe only the impact of the two parameters under examination.

6.5.3 Findings: The Simple Atrium Scenario

6.5.3.1 Magnitudes

The twofold nature of varying structural reflectance and glazing transmittance can be seen in Figure 6-28. Increasing glazing transmittance increases the overall transmittance of the roof (as expected) as does increasing the structural reflectance. Increasing the glazing transmittance has a greater effect. This is due to the fact that any effect due to structural reflectance is dependant on light passing through the glazing in the first instance. In the case of this (and most atria) roof, the proportion of glazed area exceeds the area of structural blockage and so SC is more significant than IRC.

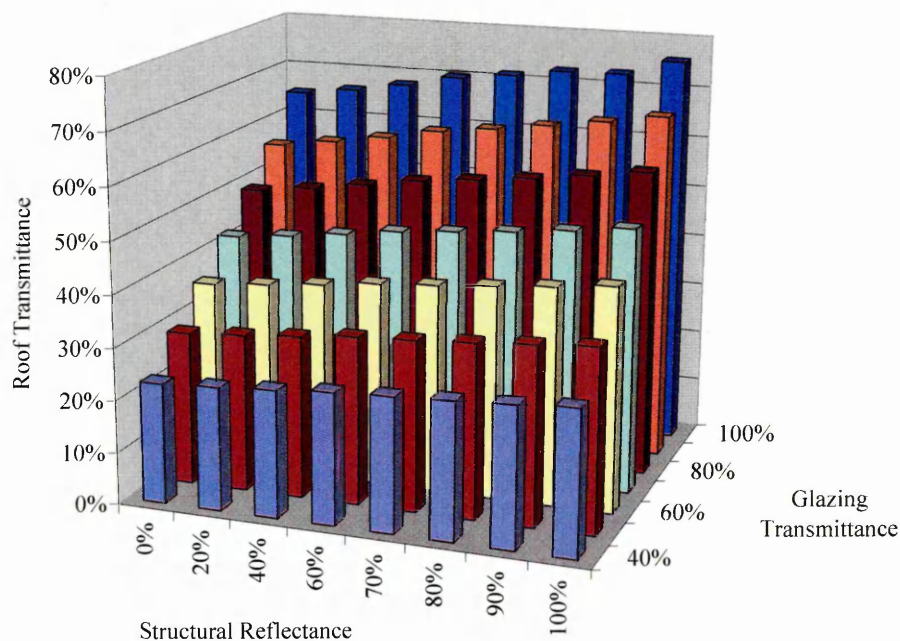


Figure 6-28: The effects of changing structural reflectance and glazing transmittance on overall roof transmittance

Increasing the reflectance of the structural members raises the transmittance of the roof. Over a range of reflectance values of 0% to 100%, this results in an increase in roof transmittance of approximately 20% (relatively), depending on the transmittance of the glazing. The relationship between structural reflectance and roof transmittance shows a good agreement when fitted to a second order polynomial (Figure 6-29 and Table 6-7). This relationship is specific to the configuration of the elements of this specific roof. It is not unreasonable to expect the form of these graphs to be the same for different roofs with similar arrangements of rectangular glazing separated by structure, even if the numerical values may differ.

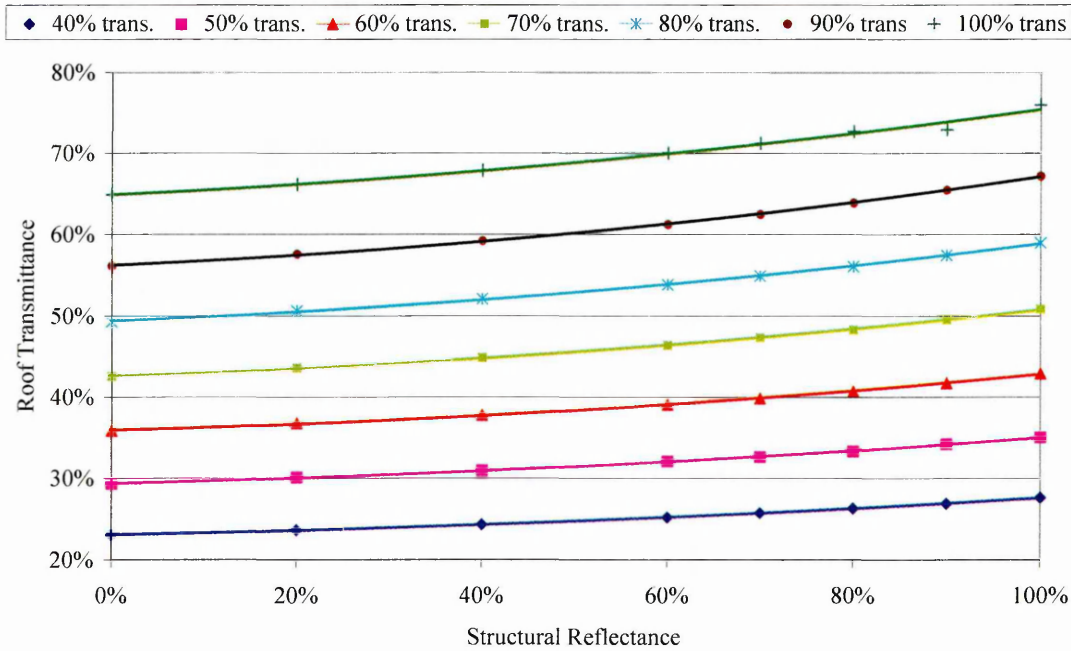


Figure 6-29: The effect of changing structural reflectance on overall roof transmittance for various levels of glazing transmittance

Table 6-7: Equations of lines derived from Figure 6-29

Glazing Transmittance	Equation of Line	R^2
40%	$y = 0.0238x^2 + 0.0212x + 0.2311$	0.9996
50%	$y = 0.0292x^2 + 0.0271x + 0.2947$	0.9993
60%	$y = 0.04x^2 + 0.0287x + 0.3603$	0.9992
70%	$y = 0.0449x^2 + 0.0365x + 0.4262$	0.9994
80%	$y = 0.0498x^2 + 0.0449x + 0.4935$	0.9993
90%	$y = 0.06x^2 + 0.0488x + 0.5626$	0.9994
100%	$y = 0.0516x^2 + 0.0531x + 0.6492$	0.9986

The relationship between roof transmittance and glazing transmittance was linear as expected (Figure 6-30). The transmittance of the glazing has a direct relationship with the quantity of light passing through to the internal space, and this is demonstrated by the straight lines on the graph. The R^2 values for these lines always exceeded 0.99. The gradient of the lines represent a value connected to the effect in roof transmittance due to the structural arrangement and reflectance of the structural members. This value will be referred to as the Transmittance Ratio (TR);

$$TR = \frac{T_{ROOF}}{T_g} \quad [6-4]$$

where,

TR= transmittance ratio

T_{ROOF} = overall roof transmittance

T_g = glazing transmittance

This can be rewritten as;

$$T_{ROOF} = T_g \times TR \quad [6-5]$$

With knowledge of the glazing transmittance and the TR for the reflectance of the structure, the overall roof transmittance can be easily derived.

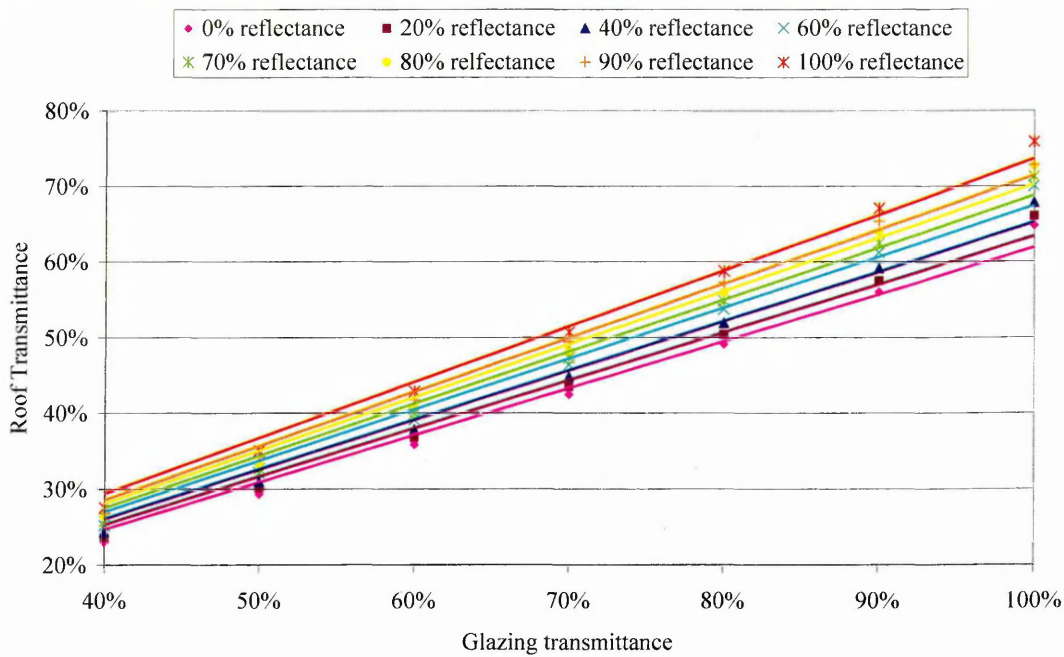


Figure 6-30: The effect of changing glazing transmittance on overall roof transmittance for various levels of structural reflectance

Plotting the derived TR values produced a relationship which was accurately described ($R^2=0.999$) by a second order polynomial with the equation (Figure 6-31);

$$TR = 0.0606\rho_s^2 + 0.0533\rho_s + 0.6212 \quad [6-6]$$

where ρ_s = structural reflectance

That is to say, the transmittance of the roof system will be at least the product of 0.6212 and the transmittance of the glazing used, rising to as high as 0.7351 times the glazing transmittance (when the structure reflects 100%). That is an almost 20% range confirming the trends discussed in Figure 6-29.

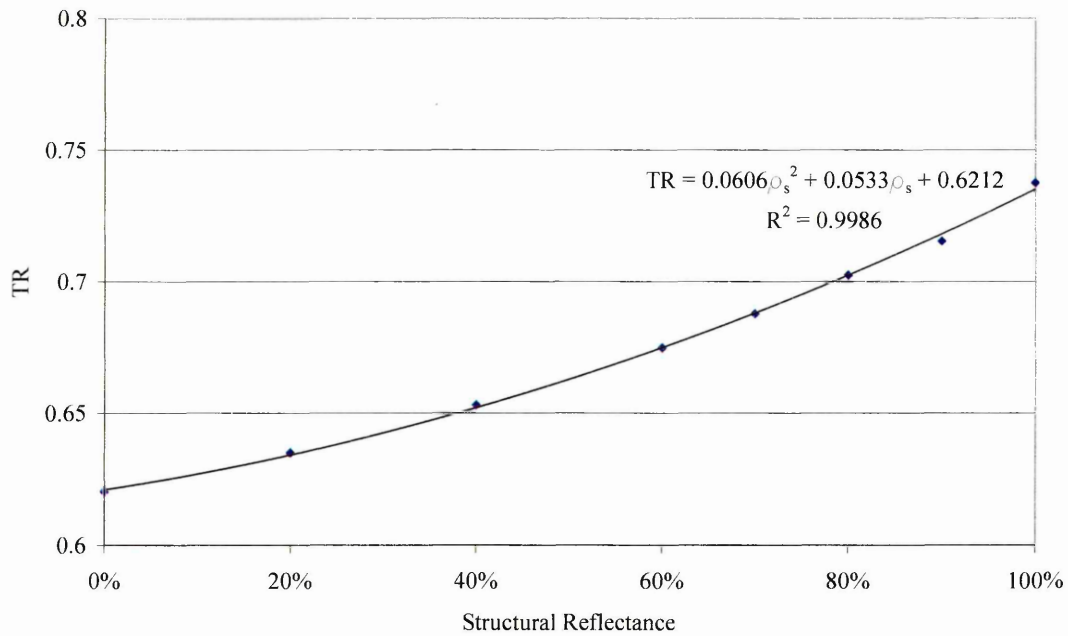


Figure 6-31: Structural reflectance against Transmittance Ratio

6.5.3.2 Distribution

Varying the structural reflectance and glazing transmittance parameters for this roofing configuration affects not only the magnitudes of daylight levels, but the distribution across the roof plane. Taking the coefficient of variation of the values obtained at the roof plane, the mean from the 56 simulations was approximately 10.5%. There is a 7% variation about this mean, as can be seen in Figure 6-32.

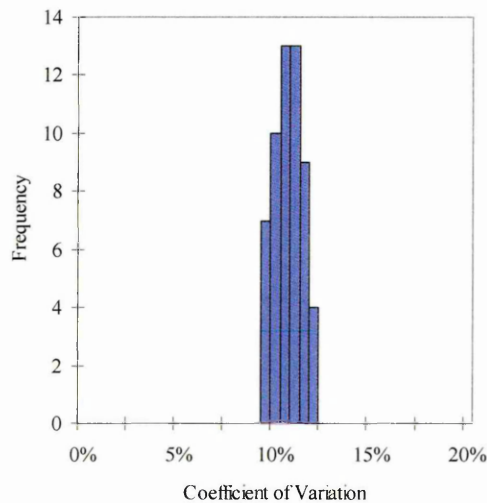


Figure 6-32: The distribution of values of Coefficient of Variation obtained for 56 simulations of the Sheaf building

Breaking this down further reveals the reasons for this variance. Figure 6-33 displays the coefficient of variation relative to the two investigated parameters. Two patterns emerge; the variation across the roof plane decreases with increasing structural reflectance (from 11% to 9%), and the variation increases with increasing glazing transmittance (between a 0.5% and 1% increase, dependant on the structural reflectance value). Both these phenomena are as a result of increased contrast within the scene. Increasing the glazing transmittance raises the luminance of the 'gaps' relative to the 'obstruction', whilst reducing the reflectance of the structure lowers the luminance of the 'obstruction' relative to the 'gaps'. The effect of increased contrast between gap and obstruction manifests itself by having a slightly larger spread of daylight values across the scene.

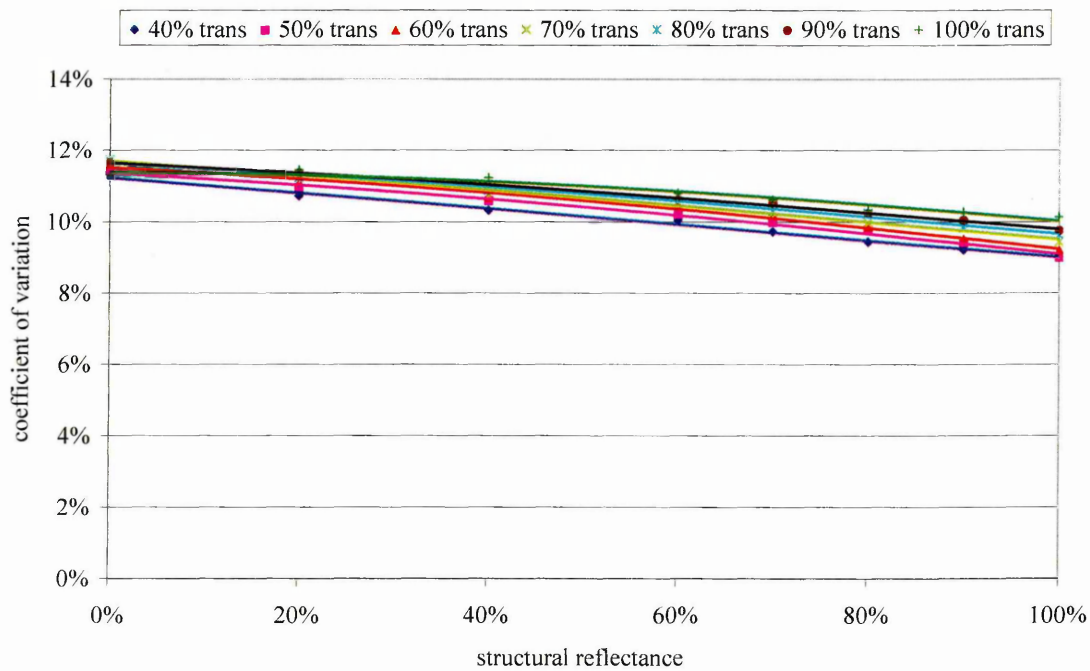


Figure 6-33: The effect of structural reflectance and glazing transmittance on coefficient of variation.

Whilst the ranges of the daylight levels may change, the general form of distributions stays the same. Figure 6-34 shows transmittance contours for the structural reflectance values investigated under a constant glazing transmittance of 80%. The 'peaks' and 'troughs' still correspond to the roof arrangement directly overhead. It is not possible with the human eye to observe the minor shift in distribution spread from the lowest structural reflectance value to the highest.

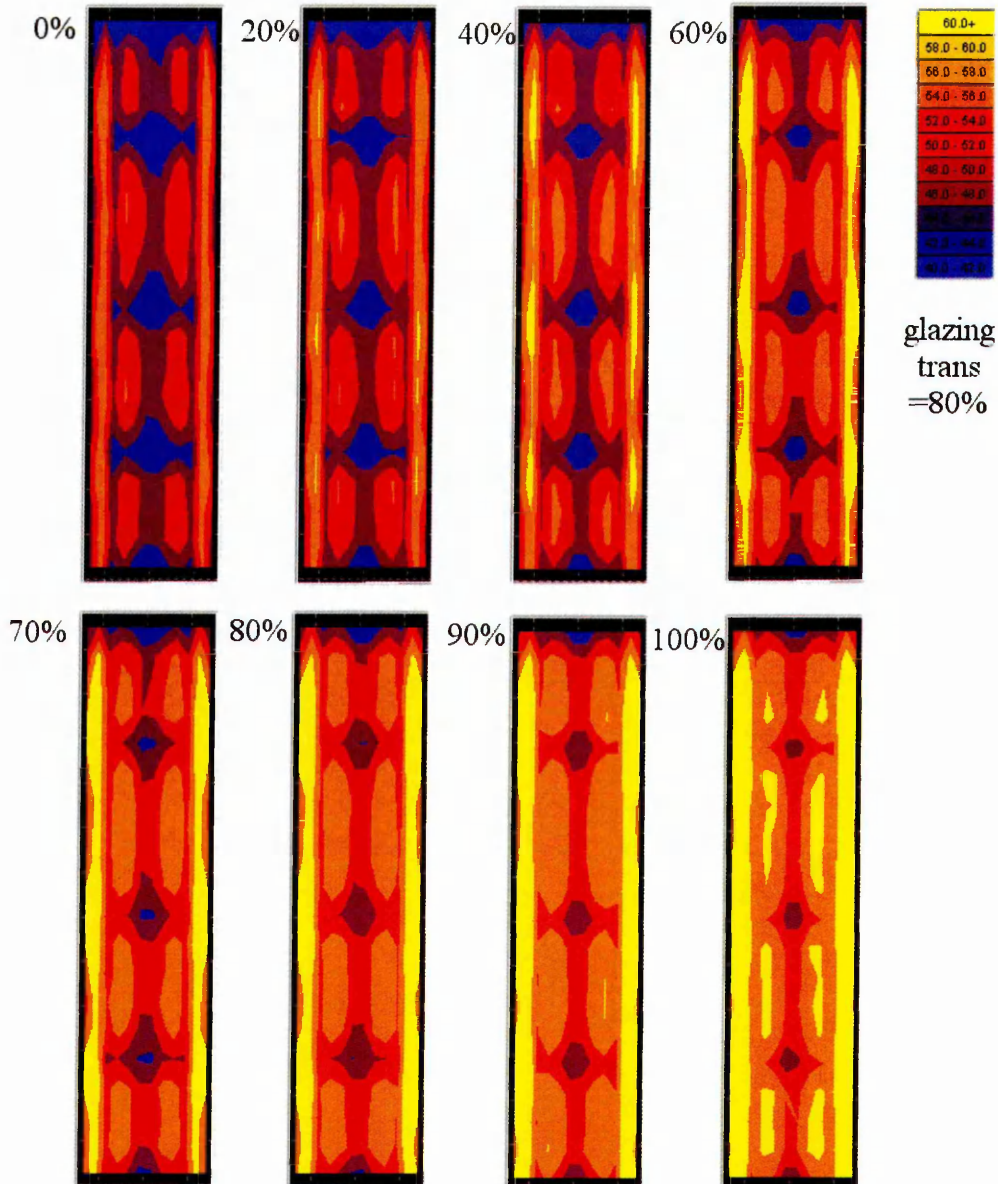


Figure 6-34: The effect of increasing the structural reflectance at 10% increments on transmittance of the roof for a fixed glazing transmittance of 80%.

This is confirmed when comparing two of the simulated scenarios, one with low levels of light (structural reflectance 40%, glazing transmittance 40%) to one with high light levels (structural reflectance 70%, glazing transmittance 80%). The distribution of transmittance values can be seen in Figure 6-35. Although at first glance the distribution appears tighter at lower settings, in relative terms the distribution for both planes is similar. The ratio of range to mean is 49.4% for the low light scenario, and 50.5% for the high light scenario. The general distribution appears to be the same for

both scenarios (Figure 6-36, a & b) whilst the magnitudes are significantly higher in the high light level scenario (Figure 6-36, c & d).

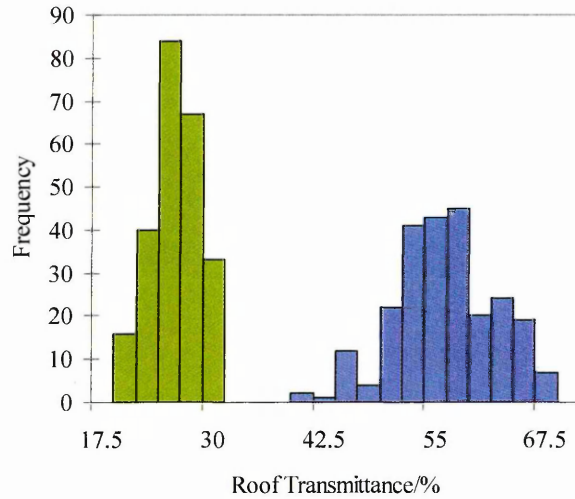


Figure 6-35: Histogram showing distribution of transmittance values measured at the analysis points at low (glazing transmittance 40%, structural reflectance 40%) and high value scenarios (glazing transmittance 80%, structural reflectance 70%)

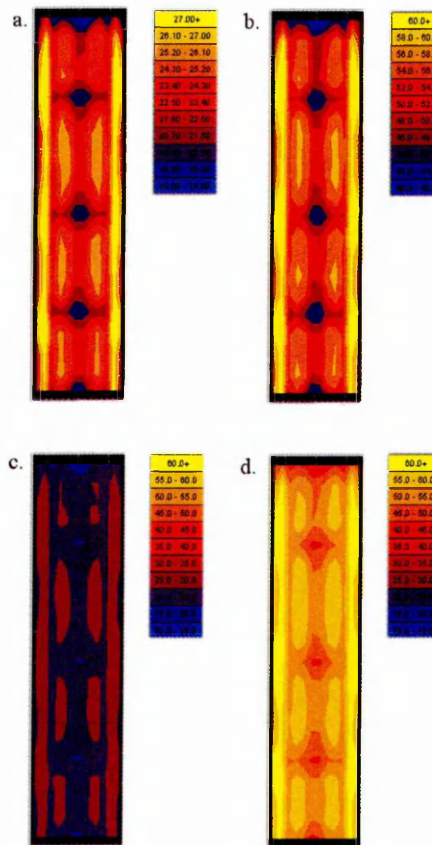


Figure 6-36: a. and c. show transmittance results for the 'low' light level scenario, b. and d. the 'high' light level scenario. The scale of data is set for a comparison of distribution between a. and b., and for magnitude between c. and d.

6.5.4 Findings: The Complex Atrium Scenario

6.5.4.1 Magnitudes

The trends observed in the simple scenario hold true for the more complex case study. Raising the reflectance of the structure and the glazing transmittance both lead to an increase in overall roof transmittance, with the glazing transmittance having the greater effect (Figure 6-37).

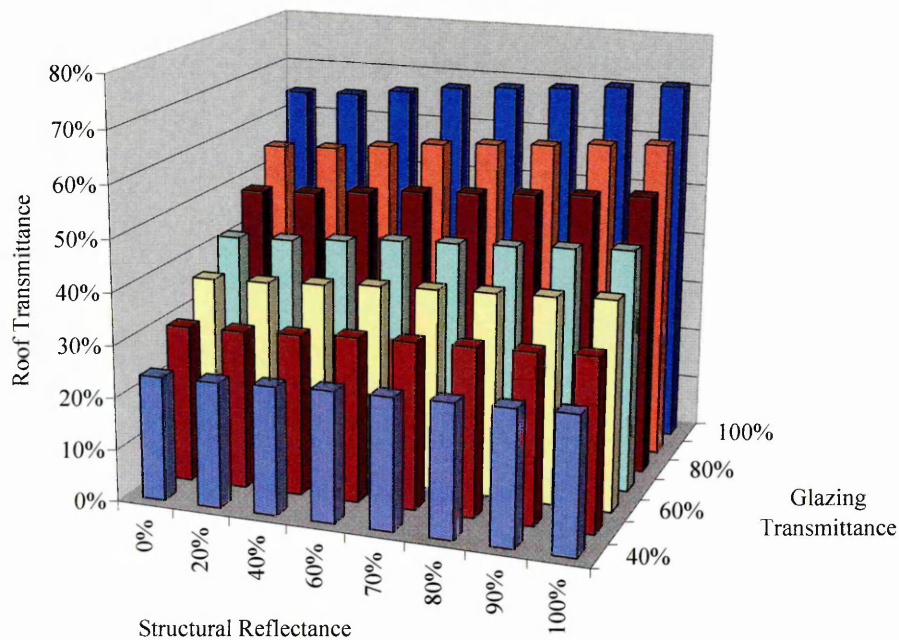


Figure 6-37: The effects of changing structural reflectance and glazing transmittance on overall roof transmittance

The relationship between structural reflectance and overall transmittance is similar to that observed in the simple scenario. The form of the curves again fit a second order polynomial (R^2 always over 0.99) (Figure 6-38 and Table 6-8). This time however the increase in overall transmittance is only approximately 10% over the range of structural reflectance values simulated. Interestingly, comparing the two roofs, the overall transmittance values are very similar at low structural reflectance values. It is only at the higher levels that the Sheaf scenario begins returning significantly higher overall transmittance values (up to 8% higher than Owen at reflectance 100%). This could be due to the monopitch nature of the Owen roof. At the east end of the analysis plane the distance from the actual roof elements are far greater than at any point in the

Sheaf scenario, and thus the localised effects of reflected flux from the structure take on less significance.

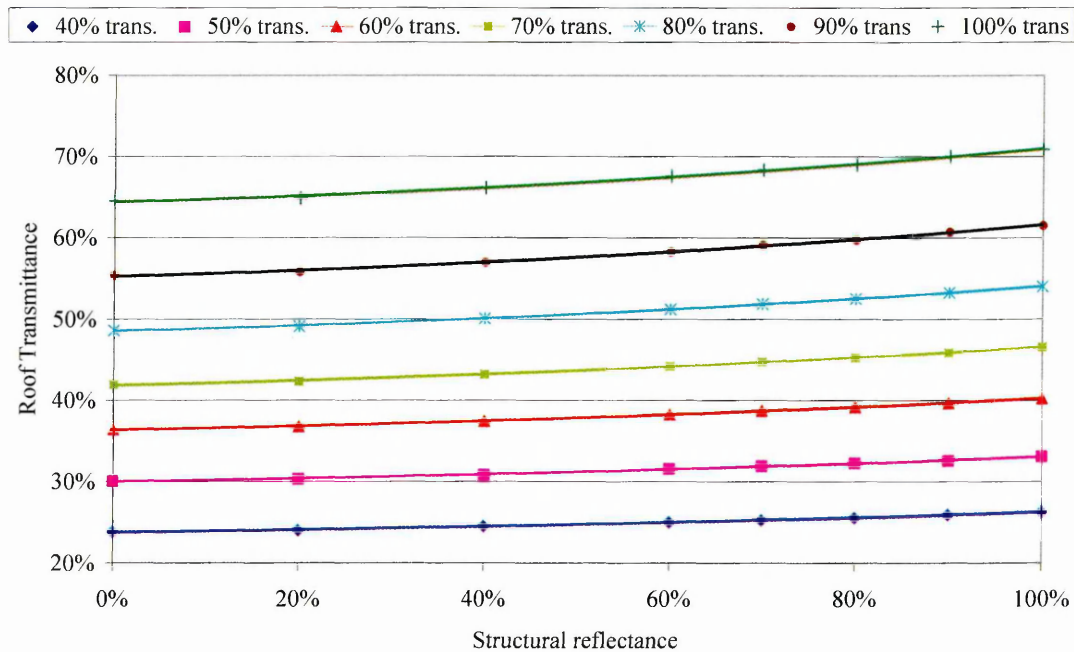


Figure 6-38: The effect of changing structural reflectance on overall roof transmittance for various levels of glazing transmittance

Table 6-8: Equations of lines derived from Figure 6-38

Glazing Transmittance	Equation of Line	R ²
40%	$y = 0.0116x^2 + 0.013x + 0.238$	0.9978
50%	$y = 0.0139x^2 + 0.0168x + 0.3008$	0.9966
60%	$y = 0.0188x^2 + 0.02x + 0.3644$	0.9991
70%	$y = 0.0216x^2 + 0.0255x + 0.4187$	0.9989
80%	$y = 0.0276x^2 + 0.0271x + 0.4857$	0.9992
90%	$y = 0.0329x^2 + 0.0306x + 0.5529$	0.9982
100%	$y = 0.0353x^2 + 0.03x + 0.6443$	0.9969

The relationship between glazing and overall transmittance once more is linear (Figure 6-39). Again the gradients represent TR values connected to the specific configuration of the roof. The lines for the Owen building are tighter together than in the Sheaf building (i.e. the range of TR values is greater in the Sheaf building than the Owen building). This is further demonstration of the greater influence of the structural reflectance parameter in the Sheaf building over that at the Owen building. It should be noted that the values returned from the 100% glazing transmittance simulation results do not fit the trend as closely as the other simulations (the same phenomenon can be observed in the Sheaf building). The 100% 'glazing transmittance' was actually run

without the glazing geometry i.e. open gaps in the model. The highest permissible transmissivity value for entry into the glass primitive in Radiance is 1 (which equates to a transmittance of a little over 90%). It is for this reason it is thought the 100% glazing transmittance values may vary slightly from the other simulations.

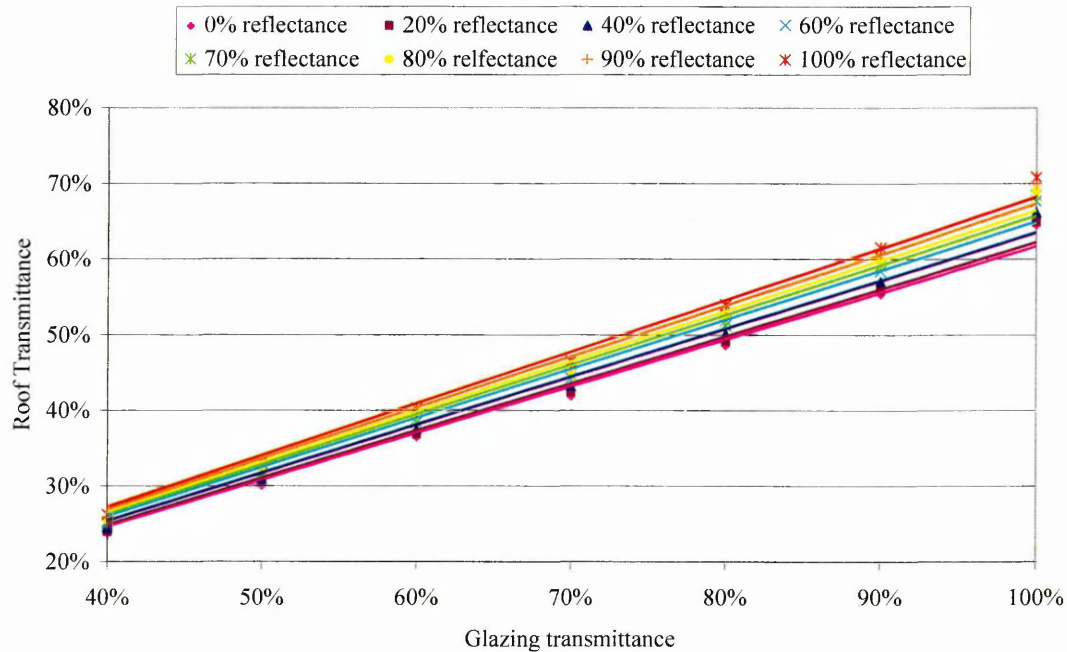


Figure 6-39: The effect of changing glazing transmittance on overall roof transmittance for various levels of structural reflectance

Plotting the curve for the TR (Figure 6-40) it can be seen that whilst the form is similar to that of the Sheaf building, the coefficients are lower. The equation for the curve again has an R^2 exceeding 0.99;

$$TR = 0.0338\rho_s^2 + 0.033\rho_s + 0.6167 \quad [6-7]$$

where,

ρ_s = structural reflectance

The transmittance of the roof system range between [0.6167-0.6835] the product of the transmittance value of glazing used. That is a range of approximately 10% confirming the trends discussed in Figure 6-38.

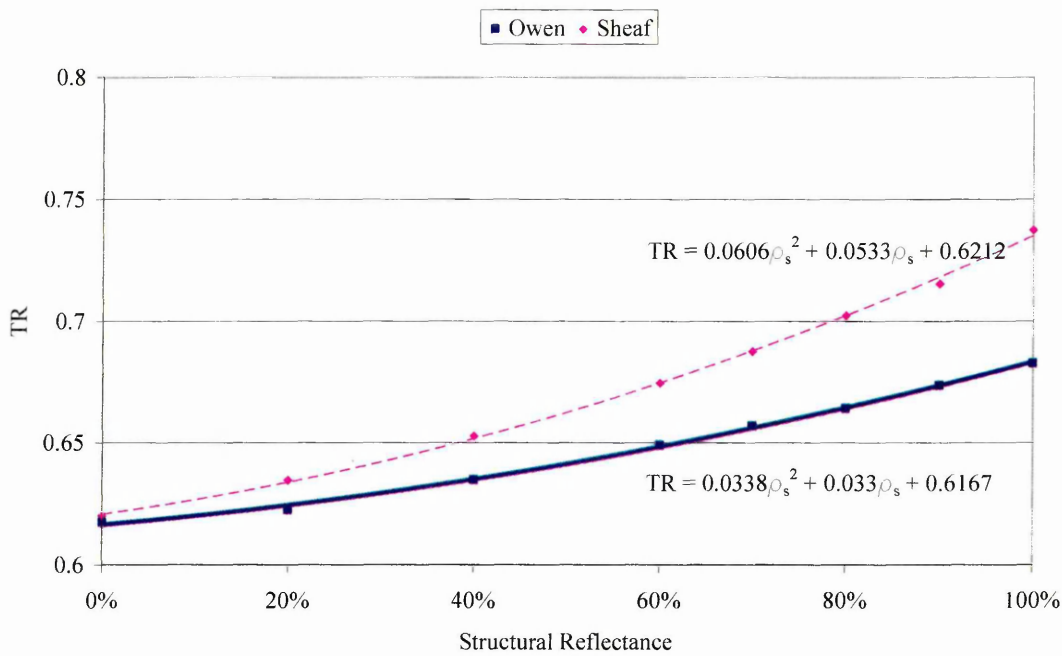


Figure 6-40: Structural reflectance against Transmittance Ratio for the Owen and Sheaf buildings. The coefficients are greater in the Sheaf building.

It is interesting to note that for structural reflectance set to 0%, the TR value for both the Sheaf and the Owen building are very similar (at approximately 0.62). The values for [PAO-1] for both roofs are also both very similar (73% Sheaf, 71.1% Owen). The contribution to daylight levels at the analysis plane due to reflection from the roof structure is however, potentially twice as great in the A-frame roof when compared to the monopitched roof. Figure 6-41 reveals the reason. The analysis plane is considered in two halves. For the A-frame roof, both these halves are equal (reflected along the apex of the roof) i.e. 'a' = 'b'. For the monopitch roof, the two halves are different, plane 'a' is much nearer the roof structure and as such will receive more of a lighting flux contribution from it. Plane 'b' is further away. A significant portion of potential flux reflected from the structure may never reach the plane due to the interaction with the light at the well surface.

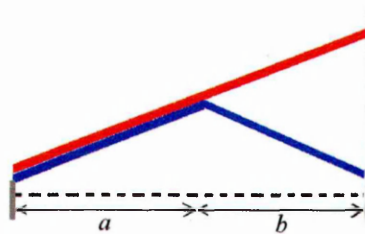


Figure 6-41: For the A-frame roof, there is symmetry about its apex and hence a and b is the same. In the monopitch, daylight levels at b will be lower due to the increased distance from the roof, and absorption of light flux at the atrium wall surface.

6.5.4.2 Distribution

The magnitude of the coefficient of variation values obtained in the Owen building (20%) were approximately twice that found at the Sheaf building (Figure 6-42). That is to say, there is a greater range of daylight levels recorded across the analysis plane in the Owen building. This is primarily for two reasons. The asymmetry of the Owen building meant highly contrasting daylight values were recorded say, between the areas at the west (very near the roof) and east (very near the wall) of the analysis plane. Secondly, the more complicated space frame structure resulted in a greater contrast of recorded daylight levels within the plane.

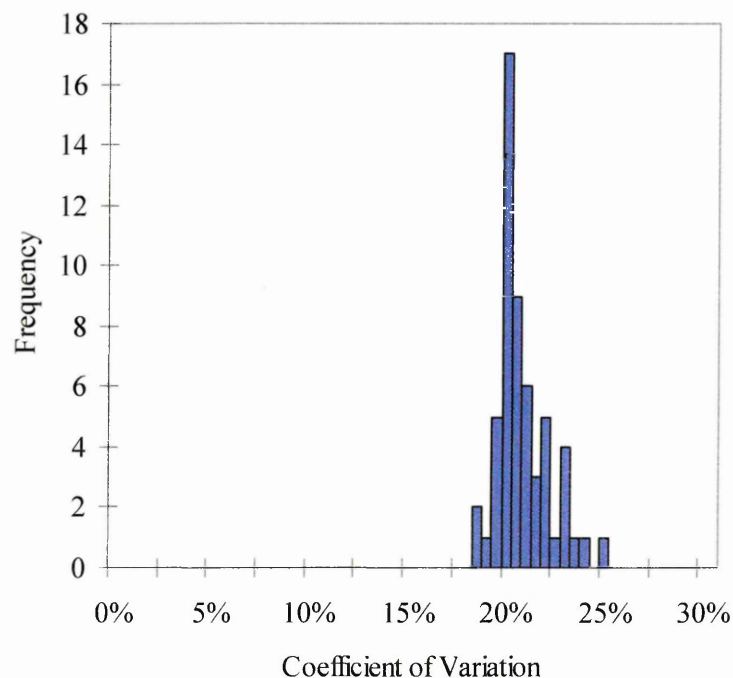


Figure 6-42: The distribution of values of Coefficient of Variation obtained for 56 simulations of the Owen building

A variation of 6.5% about this coefficient of variation of 20% was observed. This is similar to that found at the Sheaf. The coefficient of variation is higher at lower settings of structural reflectance (Figure 6-43) due to increased contrast between 'gap' and 'obstruction'. There is no clear pattern relating coefficient of variation to glazing transmittance as there was in the Sheaf building, though if anything, the trend has been reversed (i.e. lower coefficient of variation with increased glazing transmittance).

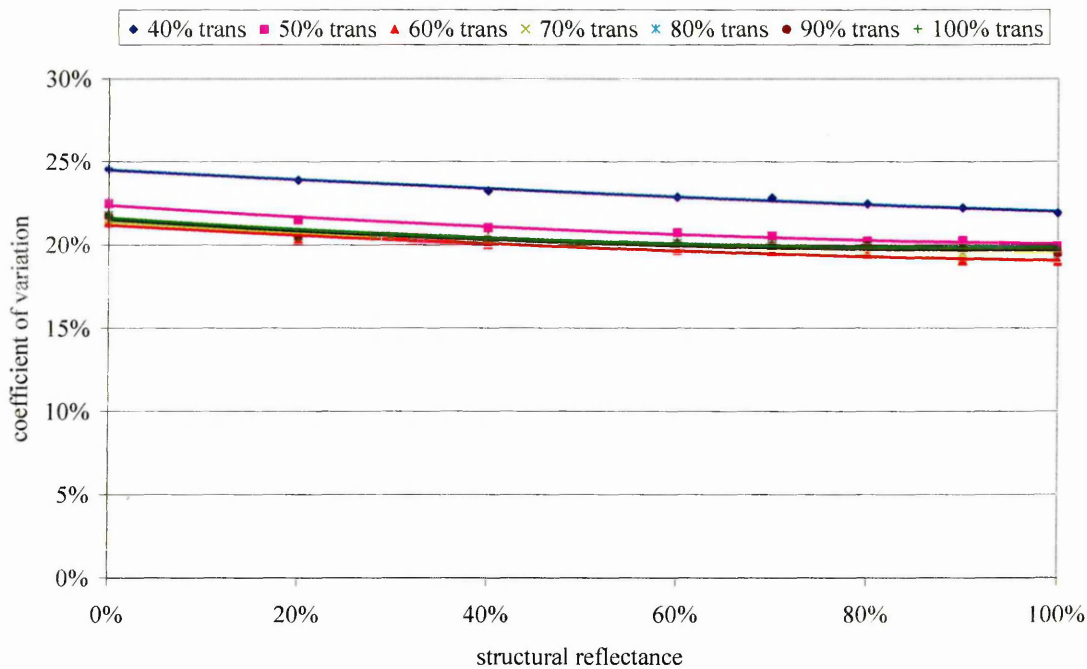


Figure 6-43: The effect of structural reflectance and glazing transmittance on coefficient of variation.

6.6 Physical Illuminance Measurements and Computer Simulations Compared

6.6.1 The Sheaf Building

The physically measured internal and external illuminance results obtained describe the daylight factor at one point beneath the roof. The TR polynomial used in conjunction with the glazing transmittance returns the average transmittance across the roof plane. In order for a comparison to be made between the two, the physically measured daylight factor must be converted to average transmittance across the whole plane. The information gleaned from the simulations was used to make this estimation. The daylight factor at the photocell point was 2.0% lower than the average roof plane. The contribution of the well to the roof plane illuminance values was 3.5%. Applying these factors to the measured daylight factor of 60.3%, an average roof plane transmittance of 59.4% is obtained. Entering the values for structural reflectance and glazing reflectance physically measured for the Sheaf building into Equation 6-6, the returned average roof plane transmittance is 53.9%. This is 9.2% lower than the physically measured result.

6.6.2 The Owen Building

The same process was deployed for comparison of physical and simulated results in the Owen building. The comparison was taken between the simulated result and both the physical results (obstructed and unobstructed external photocell).

6.6.2.1 Including External Obstructions

The measured daylight factor (i.e. totally unobstructed external photocell) at an internal point was found to be 35.0%. Through computer simulations, the photocell position illuminance levels were 7.2% higher than for the whole roof average. The reflective well contributed 5.3% illuminance and the blocking effect of the obstructions was 32.4%. Applying these factors to the measured daylight factor at a point, the estimate for average roof plane transmittance becomes 48.0%. The returned value for average roof plane transmittance when the structure reflectance and glazing transmittance values are inserted into Equation 6-7 was 51.4%. This is 6.7% higher than the measured result.

6.6.2.2 Excluding External Obstructions

The I_i/I_E value from the internal photocell and the obstructed external photocell was measured at 43.0%. This time the simulations were run without the external obstructions, as the two measurement points are relatively influenced to the same extent by the external environment. The illuminance value at the photocell point was 2.6% higher than the average roof plane value, and the well contributed 4.9%. Application of these factors returned an estimate for measured average roof transmittance of 39.8%. This is 22.5% lower than the 51.4% derived from Equation 6-7.

6.6.3 Discussion

The match between the derived polynomials and the measured results was good. In the case of the Sheaf building and the Owen building from the unobstructed external photocell (i.e. external obstructions considered) the difference was under 10% (or below approximately 6% Sheaf building, 2% Owen building in absolute terms), which is well

within acceptable error bounds for physical daylight measurement. Using the obstructed external photocell resulted in a less convincing match. The vertical displacement between the internal and external photocell has resulted in an increased difference between simulated and measured results. If the internal and external obstructed photocells were much closer, the difference in illuminance values between the two would have dropped, the E_I/E_E value would have risen, and the difference between measured and simulated would have been reduced.

The closeness of the simulated to the measured results is encouraging. This enables further roof types to be generated and analysed virtually, without the need for the more inconvenient and intensive physical measurement process. Chapter 7 pursues such a path. The differences between the measured and simulated results can be applied as multipliers to the roof transmittance equations (i.e. $\times 1.092$ for the Sheaf, and $\times 0.933$ for the Owen). In this way such multipliers can be added to other roof types simulated should real illuminance data become available.

6.7 Conclusions

This chapter has described the methodology for the simulation of daylighting in the two case study atria (Sheaf and Owen buildings). The agreement at the photocell position between measured and simulated results for both examples was good (Sheaf; simulated result 11.3% lower, Owen; simulated result 7.9% higher). The simulations enabled the relationship with regard to illuminance between the photocell position and average roof plane to be revealed. Likewise, the contribution of the well (thus converting daylight factor to transmittance) and in the case of the Owen building, the influence of the external landscape, were also isolated.

Simulations were run for both of the case study atria with parametric changes made to the structural reflectance and the glazing transmittance of the roof elements, with the well specified as a light sink. The relationship between overall transmittance and glazing transmittance was direct and linear. The influence of the structural reflectance was not as great as the glazing transmittance, and the relationship fitted a second order polynomial. The transmittance ratio (TR) was introduced, as the ratio of

roof transmittance to glazing transmittance at a specified value of structural reflectance. The plotting of the TR values for the structural reflectance intervals examined resulted in a second order polynomial. Thus a single expression for both roofs was found which describes the average transmittance across the roof plane with the glazing transmittance and structure reflectance as the dependant variables.

Using the isolated contributions of the well, external obstructions, and the relationship between photocell position and average roof plane results, the physically measured daylight factor results were converted to an estimate of average roof plane transmittance. These values were compared to the output from the aforementioned roof equations. The agreement was found to be very good (Sheaf; 9.2% lower than measured result, Owen; 6.7% higher than measured result). These differences can be applied to the roof equations to forge a link from the simulations to reality.

Chapter 7 adopts a similar methodology to investigate the influence of roof type through computer simulation. Should more physically measured results become available, a repetition of this methodology would further test the abilities of computers to accurately simulate real world conditions. The obtained transmittance information is then used in conjunction with the photographic technique, in an application to real buildings.



Expansion of Roof Typology and Application of Findings

- 7.1 Introduction
- 7.2 Computer Models: Approach
- 7.3 Results and Analysis
- 7.4 Application to the Field
- 7.5 Conclusions

'There are no such things as applied sciences, only applications of science.'

LOUIS PASTEUR

7.1 Introduction

The previous four chapters have looked in detail into the transmittance of two case study skylights. Whilst quantitative conclusions could be drawn, they were only applicable to the specific roofs studied, and thus the findings were of limited use in the examination of other roofs. This chapter extends the methodologies adopted in the detailed case studies to eight simulated generic roof types. The findings from these simulations enable the proposal of a method to estimate the transmittance and distribution at roof plane level of real skylights from a hemispherical image of that roof. The technique is demonstrated in several occupied existing buildings, and compared with output from the new program, SkyVision.

7.2 Computer Models: Approach

The first stage involved the modelling of eight roof types. They are applied to a hypothetical well with dimensions of 10m x 10m x 10m i.e. WI=PAR=SAR=1. The surfaces of the well were specified as light sinks so as to examine solely the effects of the roofs. The roofs modelled were as follows:

1. *Pyramid*: A square based pyramid roof, with a pitch angle of 45° . The structure is composed of rectilinear purlins at three cross sectional dimensions (150(wide) x200(deep) mm, 100x125mm and 50x75mm).
2. *Dome 1*: A lightly structured polygonal dome with 16 horizontal segments and 6 vertical segments. The structure is composed of short straight rectilinear elements arranged to form the curve of the dome. Two cross section types are used, 50x100mm and 25x75mm.
3. *Dome 2*: As *Dome 1*, though more heavily structured. A larger structural frame is inserted between the elements in *Dome 1* creating a dome with 32 horizontal segments and 11 vertical segments. The sizes of the inserted members are larger, with cross sections of 100x200mm and 75x150mm.

-
4. *Flat*: A flat grid comprising of two main beams (cross section 275x350mm) spanning both axis of the well, supporting a finer grid of smaller beams (cross section 100x150mm). The roof sits flush within a 'well lip' which extends 1m above the analysis plane (i.e. total well depth including roof = 11m). This is so that there is at least some distance (0.5m) between the base of the roof and the analysis plane for the pattern of the roof configuration to be detected by the measurement points. The reflectance of the lip is set at 100% so that it does not absorb any light and as such, the returned values are indicative of transmittance. It is appreciated that this will slightly influence the distribution of light towards the very edges of the analysis plane.
 5. *Waffle*: A waffle arrangement (representative of pre-cast concrete) with an element width of 160mm extending to a depth of 1m. The waffle separates the roof into a mesh of 10x10 window openings. As with the *flat* roof and for the same reasons, the waffle roof sits on a lip, of height 0.5m, reflectance 100%.
 6. *Sawtooth*: Four bays of sawtooth configuration (i.e. 2.5m wide) with glazing inclined at 64° to the horizontal. The angle between glazed section and opaque section was 90° . Each of the four glazed areas was separated by mullions (50x75mm) into 20 window openings. As with the *flat* and *waffle* roofs, there is a well lip of 1m to account for three support beams which extend beneath and support the sawtooth bays.
 7. *Monopitch Space Frame (The Owen Building)*: The monopitched space frame example of the Owen building is reproduced here as a comparison of roof type. The roof has been described in full detail in Chapter 3. Note: This roof applies to the well specified in Chapter 3, and not the 10m^3 hypothetical box introduced in this chapter.
 8. *A-Frame (The Sheaf Building)*: The A-frame example of the Sheaf building is reproduced here as a comparison of roof type. The roof has been described in full detail in Chapter 3. Note: This roof applies to the well specified in Chapter 3, and not the 10m^3 hypothetical box introduced in this chapter.

The exact PAO for each roof was calculated by generating a high resolution rendering of the plan view, and counting the pixels of gap and obstruction, or in the case of the more simple roofs, derived from the known dimensions of the roof elements.

An analysis plane was defined at the top of the well, comprising 20x20 points. This can be seen in Figure 7-1.

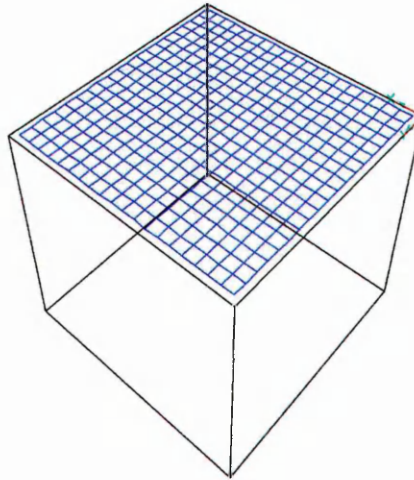


Figure 7-1: The 20x20 analysis grid assigned to the 10m3 black box, upon which various roofs were placed

Ten simulations to obtain daylight factors (i.e. transmittance) at the analysis plane were run for each roof type. These were at glazing transmittance 40% and 90%, and structural reflectance values of 0, 25, 50, 75 and 100%. Specularity of the structure was fixed at 3%, roughness 0%. Only two values of glazing were used due to the strong linear relationship found between glazing transmittance and overall roof transmittance in Chapter 6. When the graphs were plotted, and with the lines set to intercept the origin (i.e. 3 values of glazing transmittance for every value of structural reflectance), the value of R^2 always exceeded 0.99. The TR values were found for each value of structural reflectance. The results were graphed to obtain a second order polynomial that described the transmittance of that roof with regard to glazing transmittance and structural reflectance.

Pre-simulation ambient parameter analysis was performed as in Chapter 6. The following ambient parameter values were found to give reasonable accuracy at acceptable speeds for the purposes of a multiple simulation experiment such as this: -ab 3, -ad 1024, -as 256, -ar 128, -aa 0.1.

Aside from the plan rendering, five fisheye images were generated for each roof type. These were taken at the centre of the well, one roof plane level (0m), at depths of

1, 3 and 6m and one on the ground floor (i.e. 10m beneath the roof plane) (Figure 7-2). The resolution of these images was set at 4096x4096, as used in Chapter 5. The images were analysed in HemiView to obtain gap fraction values.

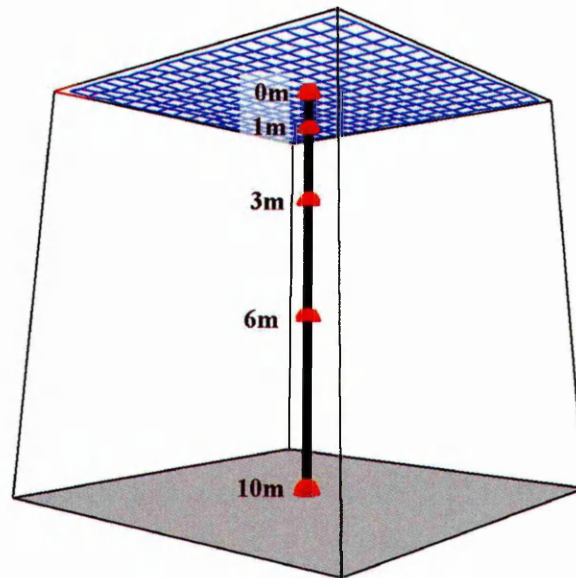


Figure 7-2: The depths at which hemispherical views of the roofs were generated for HemiView analysis

The following section describes the results of the simulations.

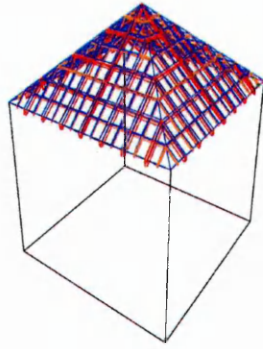
7.3 Results and Analysis

7.3.1 A Description of Result Presentation

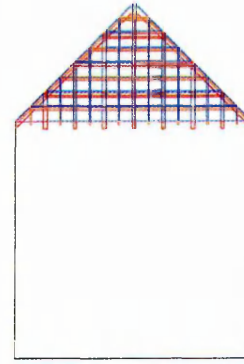
The results from the simulations of the computer modelled roof types are displayed in Figures 7.3-7-10 (parts a-n). Parts a and b show wireframe views of the roof types in perspective and in elevation. Parts c and d display DF (i.e. transmittance) contours over the analysis plane. The scale of c is set within an internal absolute scale highlighting minor variations across the plane. The scale of part d is set between 0-80% at 5% increments, to allow a rapid comparison between all the roof types. Part e shows graphically the average roof plane transmittance values (ordinate) plotted against the glazing transmittance values (abscissa). The five lines represent the five values of structure reflectance that were simulated. It should be noted that in the case of the

domes, the area of ceiling was excluded from the analysis. It is worth remembering therefore, that if a dome roof is to be used to cover a square well, the light admitting area of the well will be reduced (unless for some reason the dome overlaps the well). In the case of the pyramid, the outer row of simulation points were removed from the analysis as at points the structure of the roof cut through the plane, resulting in several zero readings. This left a resultant grid of 18x18. Part f plots the TR values (ordinate) derived from graph e (the gradients) against the value of structure reflectance (abscissa). The polynomial together with the R^2 value is also displayed. Part g is an indicator of the distribution of DF values across the analysis plane by plotting the coefficient of variation (ordinate) against the structure reflectance value simulated (abscissa). Lines at glazing transmittance of 40 and 90% are drawn. Part h displays a plan rendering of the roof. Parts i-m show the simulated fisheye views taken at the centre of the well looking upwards at depths of 0 (analysis plane), 1, 3, 6 and 10m (ground plane). In order to facilitate the application of these findings, the depths are later expressed as a fraction of the width of the well, and are referred to as relative depths. In this manner, the *monopitch* and *a-frame* roofs which have different widths can be compared. In the hypothetical well, the depths examined return relative depth intervals of 0, 0.1, 0.3, 0.6 and 1. In parts i-m for the *monopitch* roof (width 18m) photos are displayed at depths of 0, 2, 5, 9 and 15m (relative depths 0, 0.11, 0.28, 0.5 and 0.83) and at depths of 0, 0.5, 2, 4 and 6m (relative depths 0, 0.08, 0.33, 0.67 and 1) for the *a-frame* roof (width 6m). Part n plots the derived gap fraction output from HemiView (ordinate) against the relative depth of viewpoint. The dashed line is representative of [1-PAO] i.e. a depth of infinity.

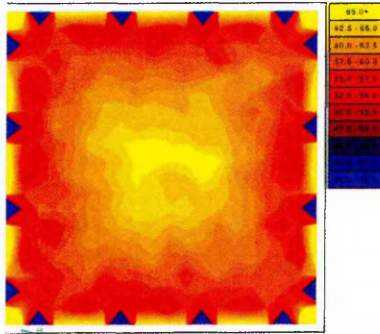
a.



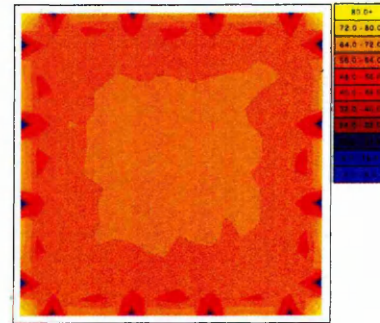
b.



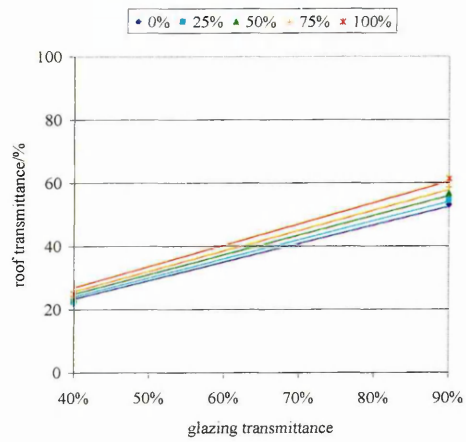
c.



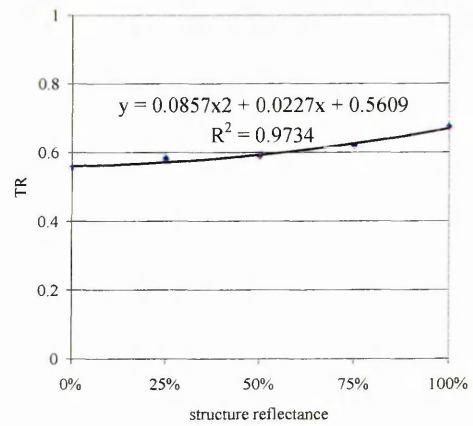
d.



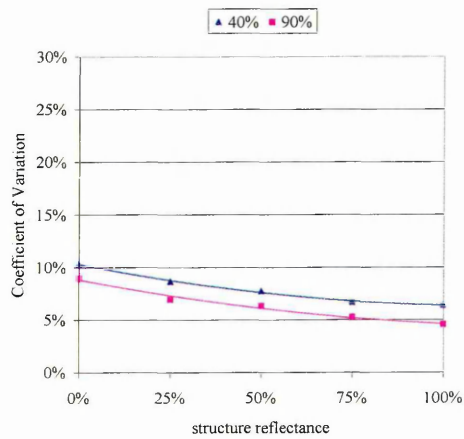
e.



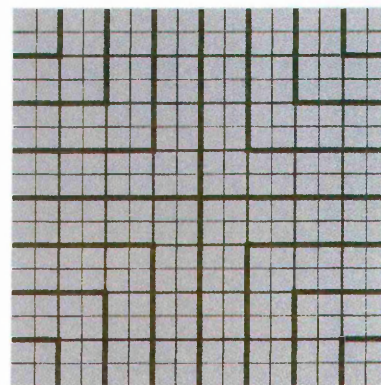
f.



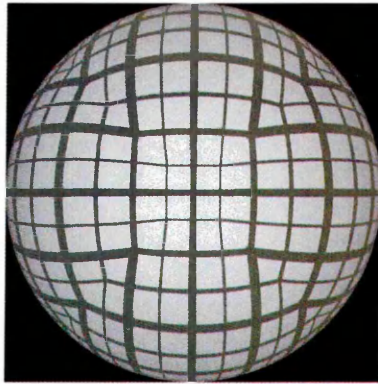
g.



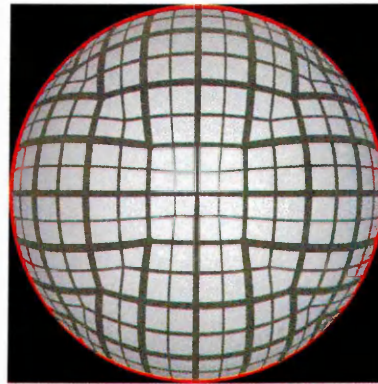
h.



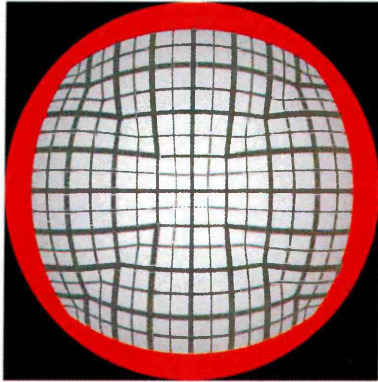
i.



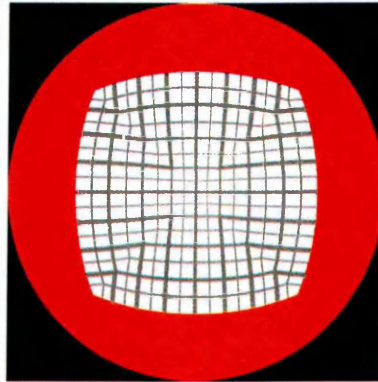
j.



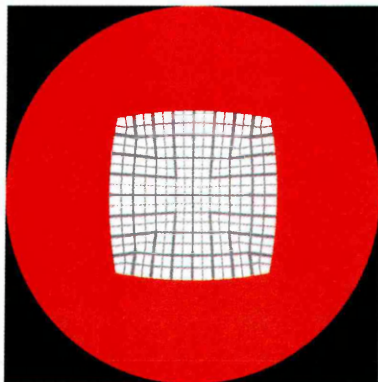
k.



l.



m.



n.

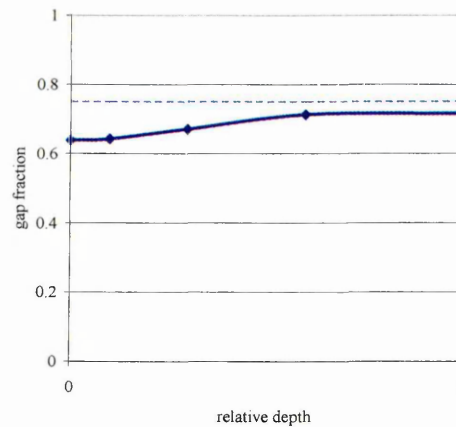
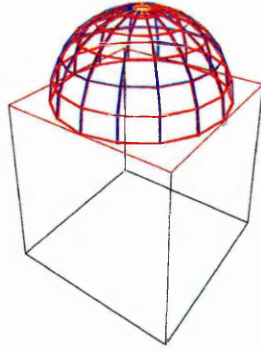
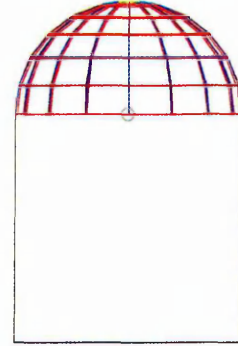


Figure 7-3: Pyramid: a. Wireframe perspective; b. Side Elevation; c. DF contours (glazing transmittance 90%, structural reflectance 75%) internal scale; d. DF contours (glazing transmittance 90%, structural reflectance 75%) comparative scale (contour range 0-80%, at 5% intervals); e. Overall transmittance against Glazing Transmittance; f. TR against structural Reflectance; g. Coefficient of Distribution against Structure Reflectance; h. Plan Rendering; i. Fisheye view roof plane; j. Fisheye view -1m; k. Fisheye view -3m; l. Fisheye view -6m; m. Fisheye view ground floor; n. HemiView returned gap fraction against Photograph depth.

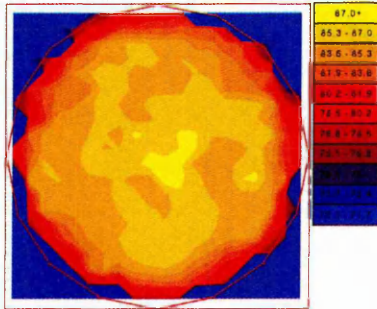
a.



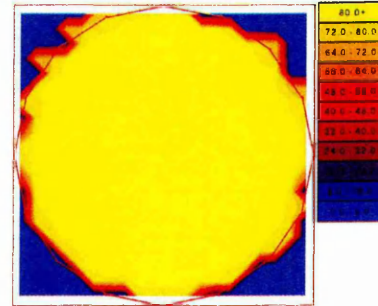
b.



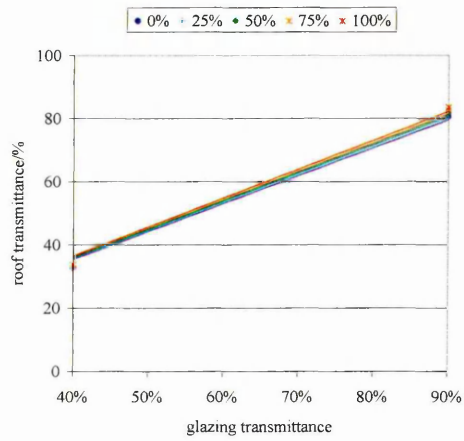
c.



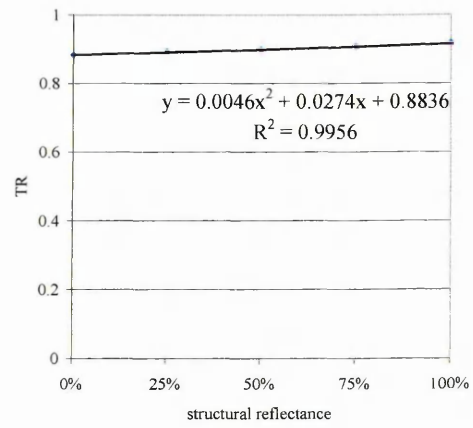
d.



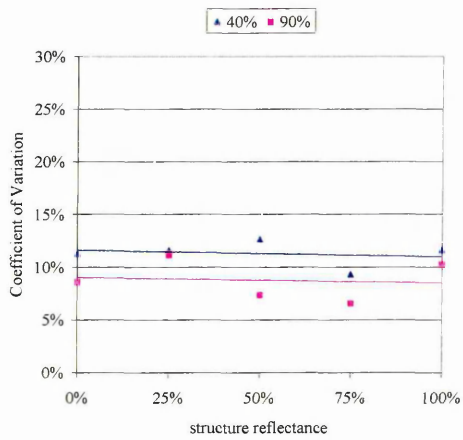
e.



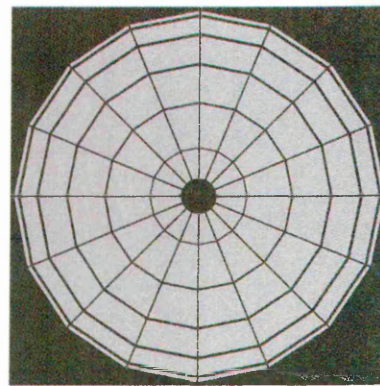
f.



g.



h.



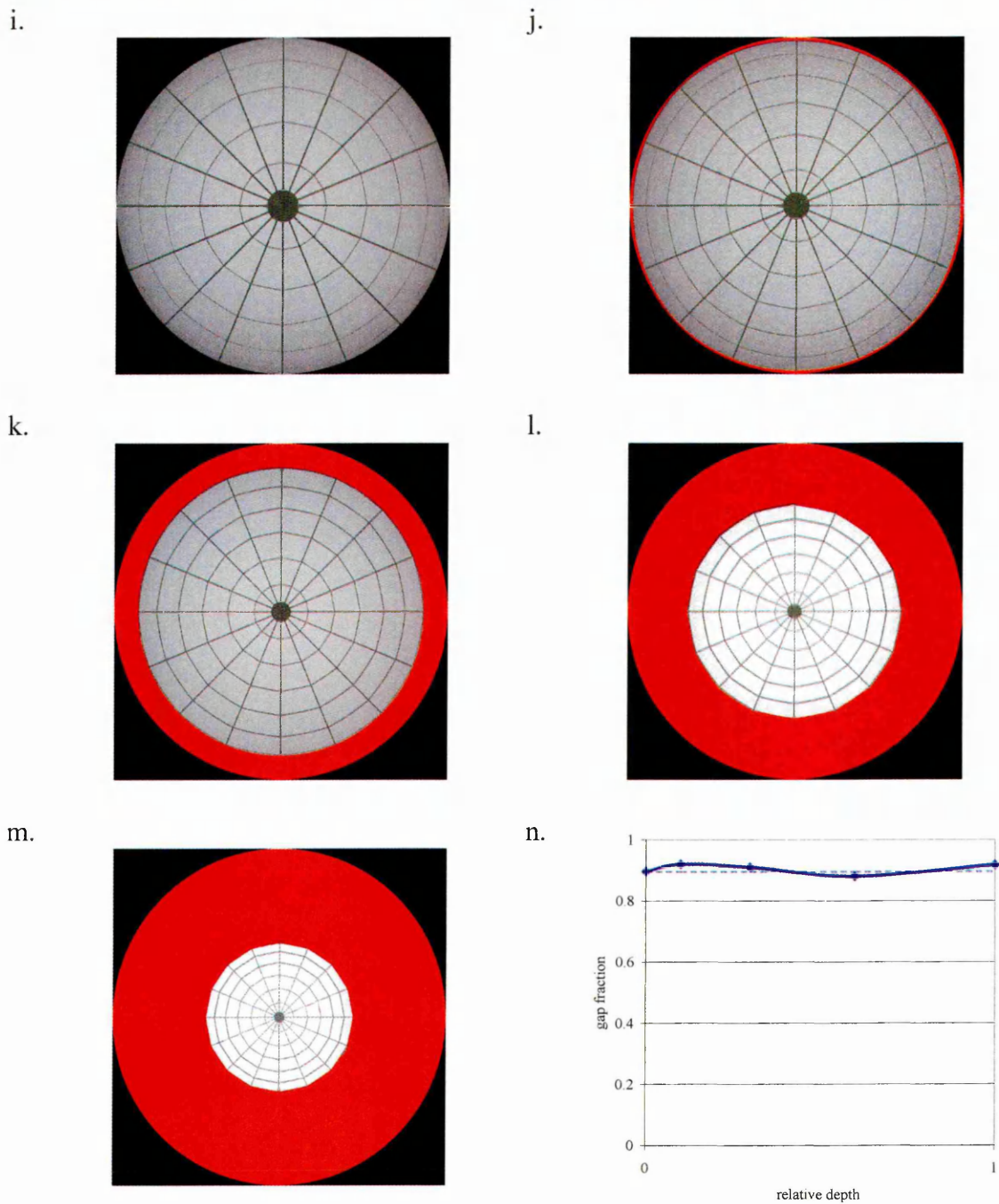
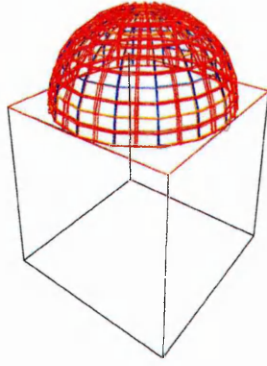
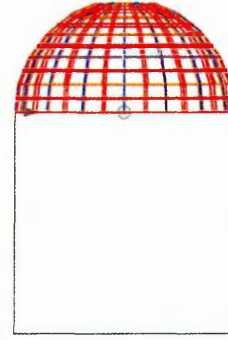


Figure 7-4: Dome 1: a. Wireframe perspective; b. Side Elevation; c. DF contours (glazing transmittance 90%, structural reflectance 75%) internal scale; d. DF contours (glazing transmittance 90%, structural reflectance 75%) comparative scale (contour range 0-80%, at 5% intervals); e. Overall transmittance against Glazing Transmittance; f. TR against structural Reflectance; g. Coefficient of Distribution against Structure Reflectance; h. Plan Rendering; i. Fisheye view roof plane; j. Fisheye view -1m; k. Fisheye view -3m; l. Fisheye view -6m; m. Fisheye view ground floor; n. HemiView returned gap fraction against Photograph depth.

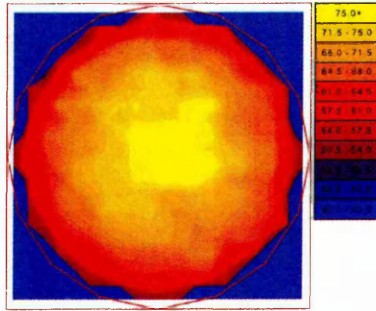
a.



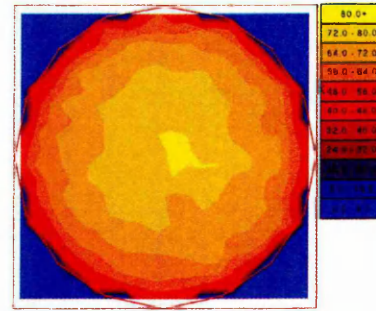
b.



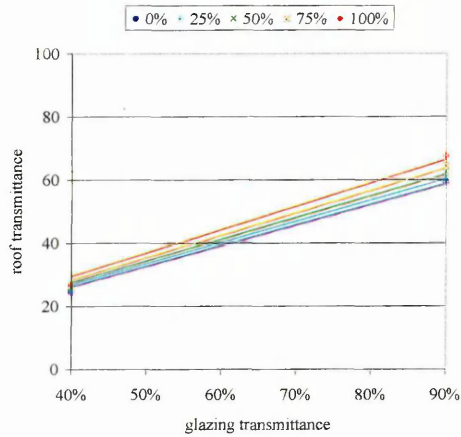
c.



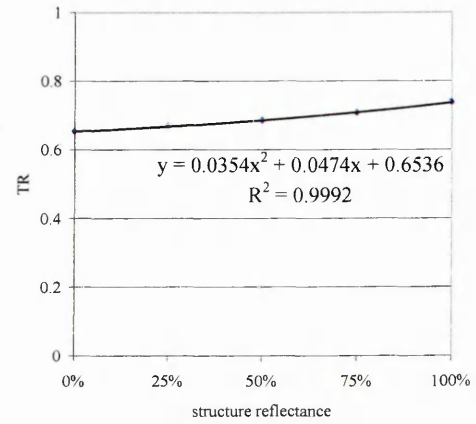
d.



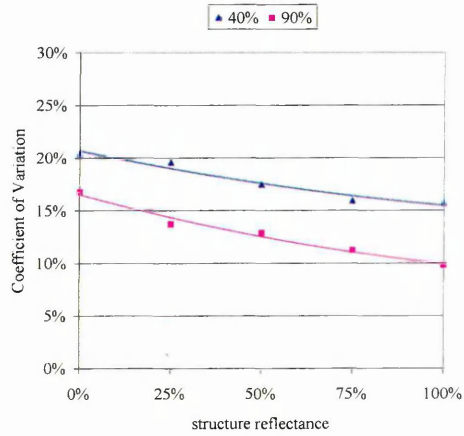
e.



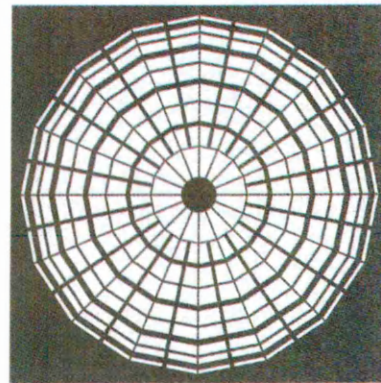
f.



g.



h.



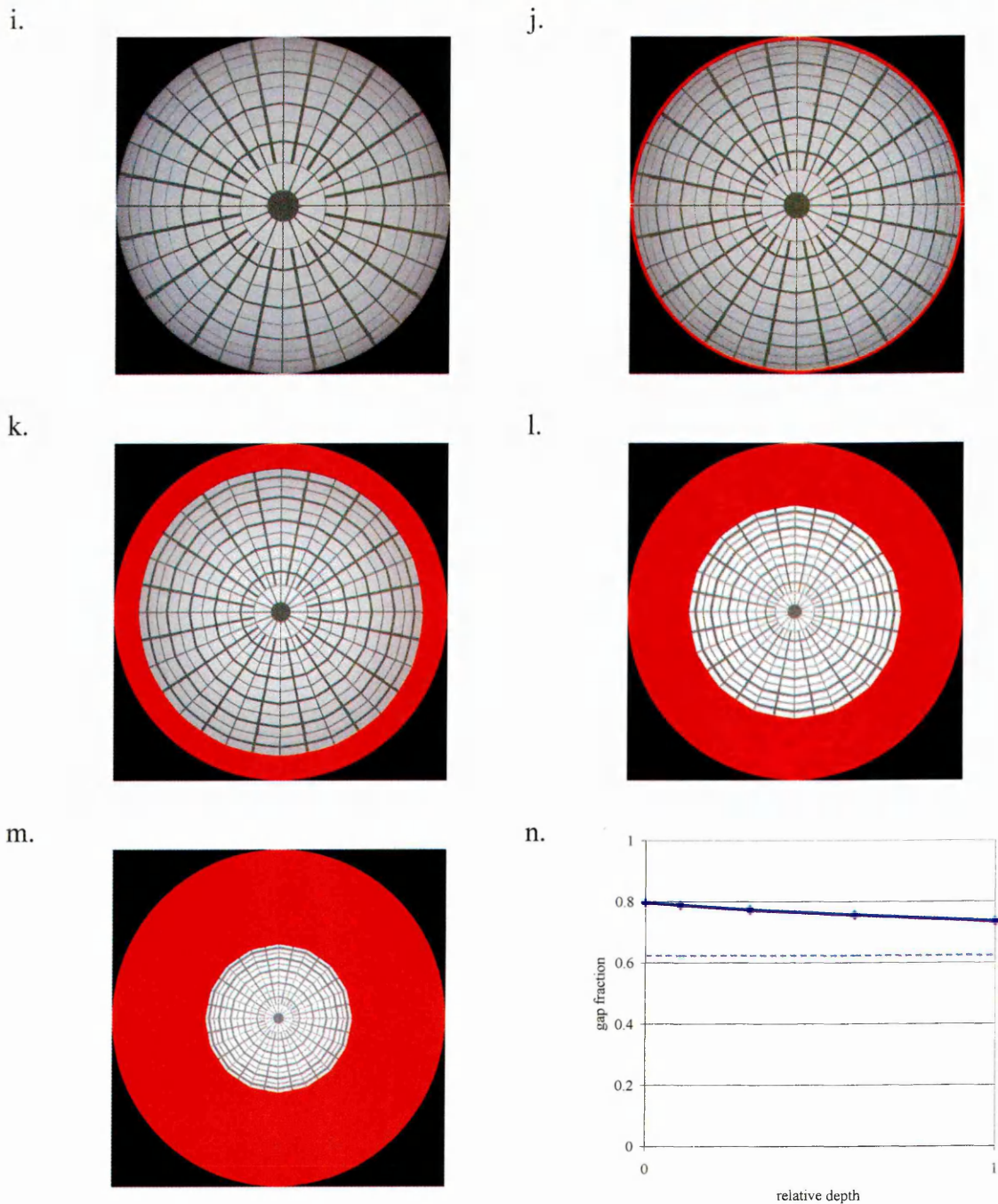
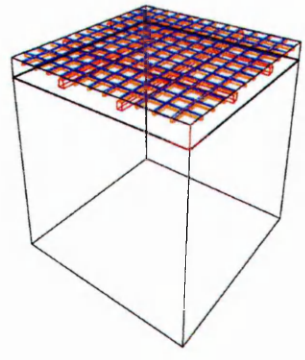
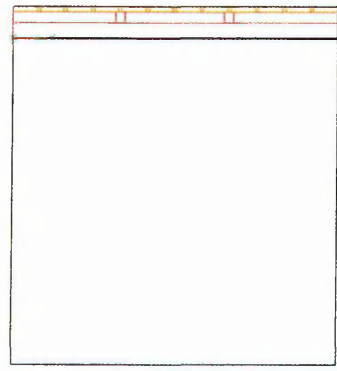


Figure 7-5: Dome 2: a. Wireframe perspective; b. Side Elevation; c. DF contours (glazing transmittance 90%, structural reflectance 75%) internal scale; d. DF contours (glazing transmittance 90%, structural reflectance 75%) comparative scale (contour range 0-80%, at 5% intervals); e. Overall transmittance against Glazing Transmittance; f. TR against structural Reflectance; g. Coefficient of Distribution against Structure Reflectance; h. Plan Rendering; i. Fisheye view roof plane; j. Fisheye view -1m; k. Fisheye view -3m; l. Fisheye view -6m; m. Fisheye view ground floor; n. HemiView returned gap fraction against Photograph depth.

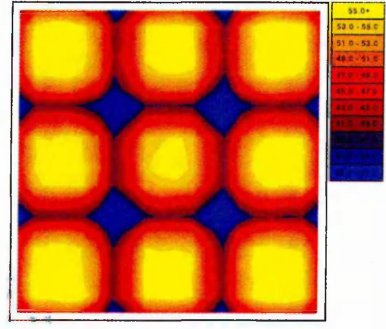
a.



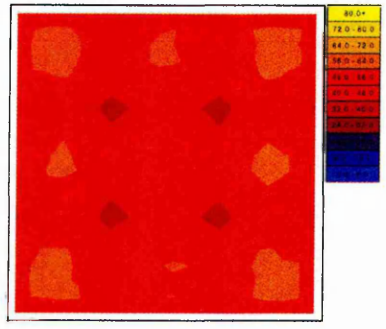
b.



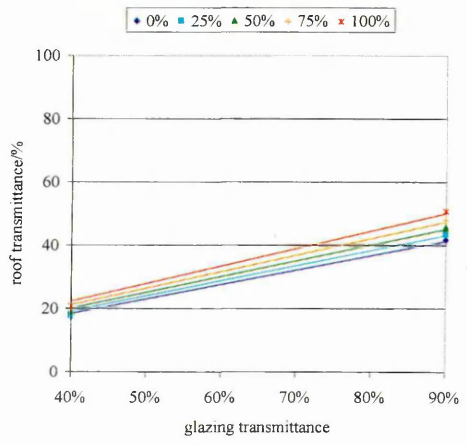
c.



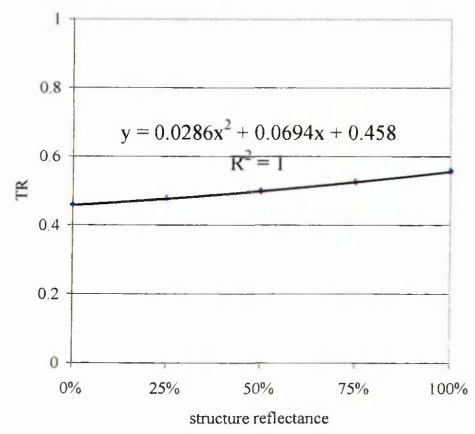
d.



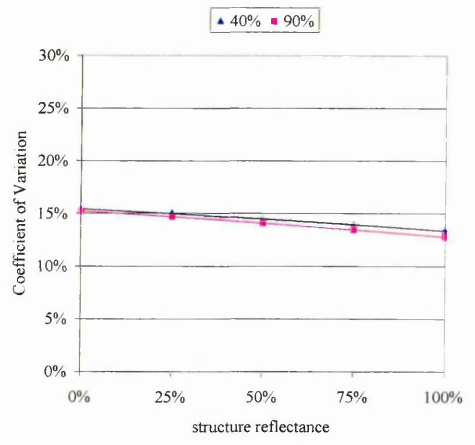
e.



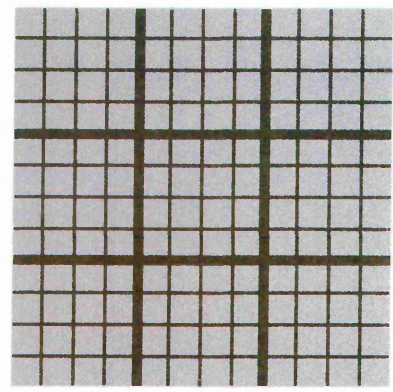
f.



g.



h.



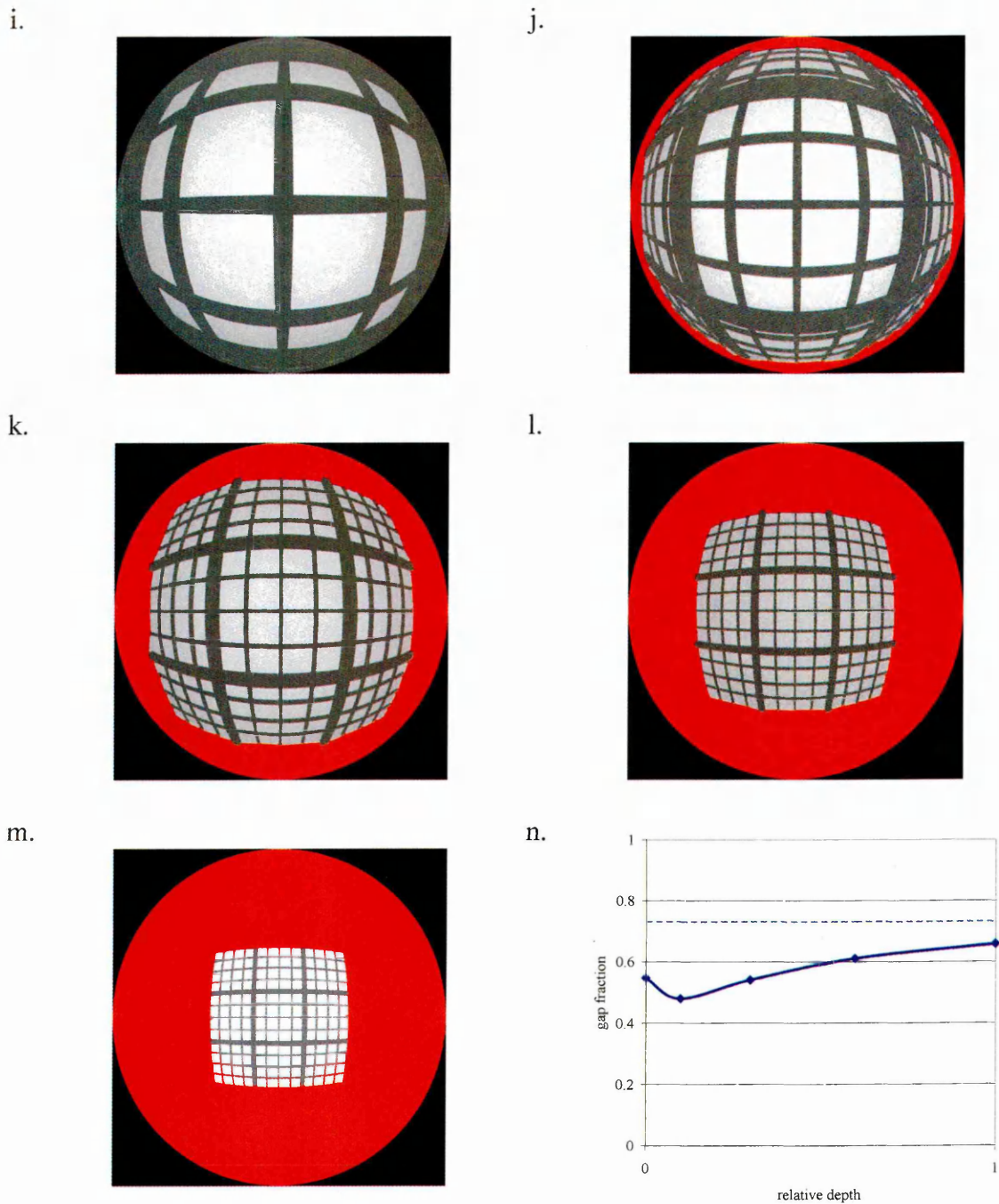
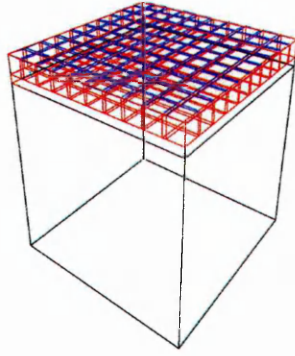
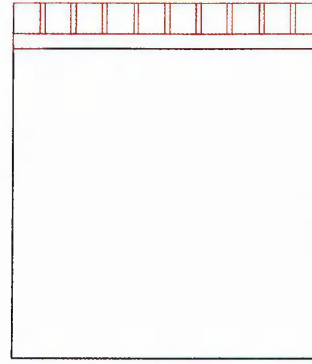


Figure 7-6: Flat: a. Wireframe perspective; b. Side Elevation; c. DF contours (glazing transmittance 90%, structural reflectance 75%) internal scale; d. DF contours (glazing transmittance 90%, structural reflectance 75%) comparative scale (contour range 0-80%, at 5% intervals); e. Overall transmittance against Glazing Transmittance; f. TR against structural Reflectance; g. Coefficient of Distribution against Structure Reflectance; h. Plan Rendering; i. Fisheye view roof plane; j. Fisheye view -1m; k. Fisheye view -3m; l. Fisheye view -6m; m. Fisheye view ground floor; n. HemiView returned gap fraction against Photograph depth.

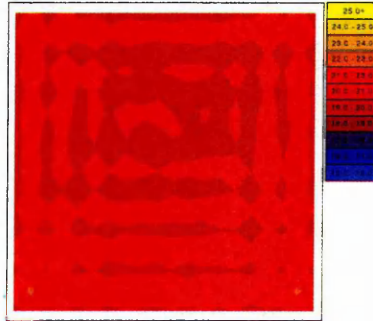
a.



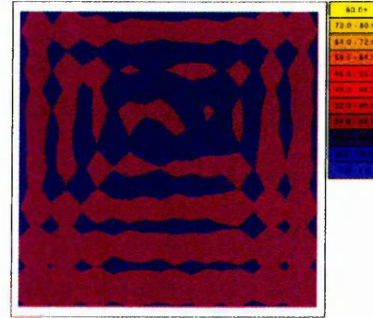
b.



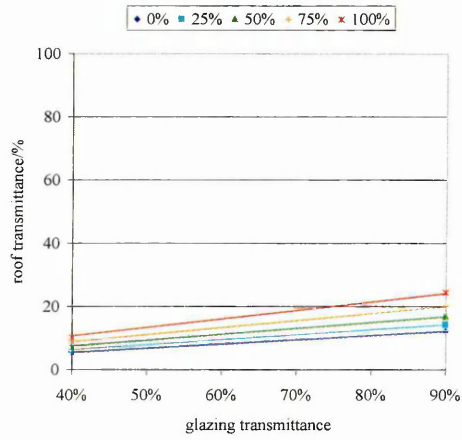
c.



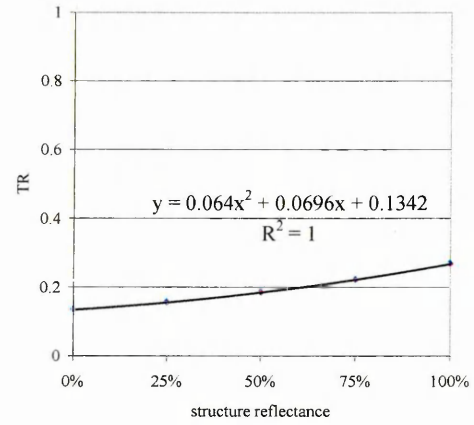
d.



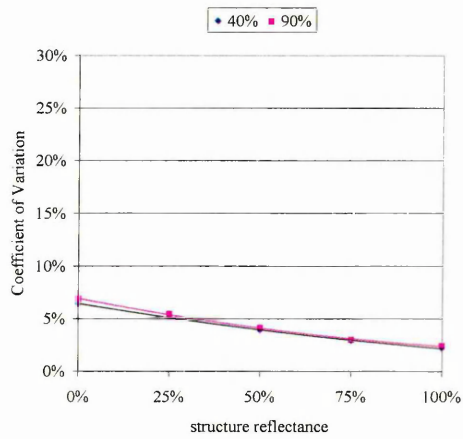
e.



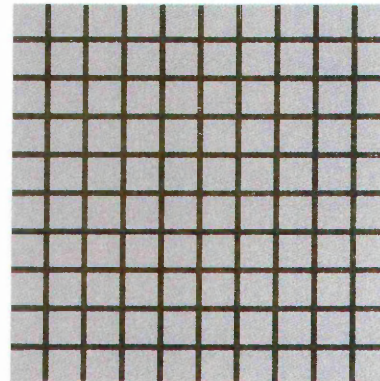
f.



g.



h.



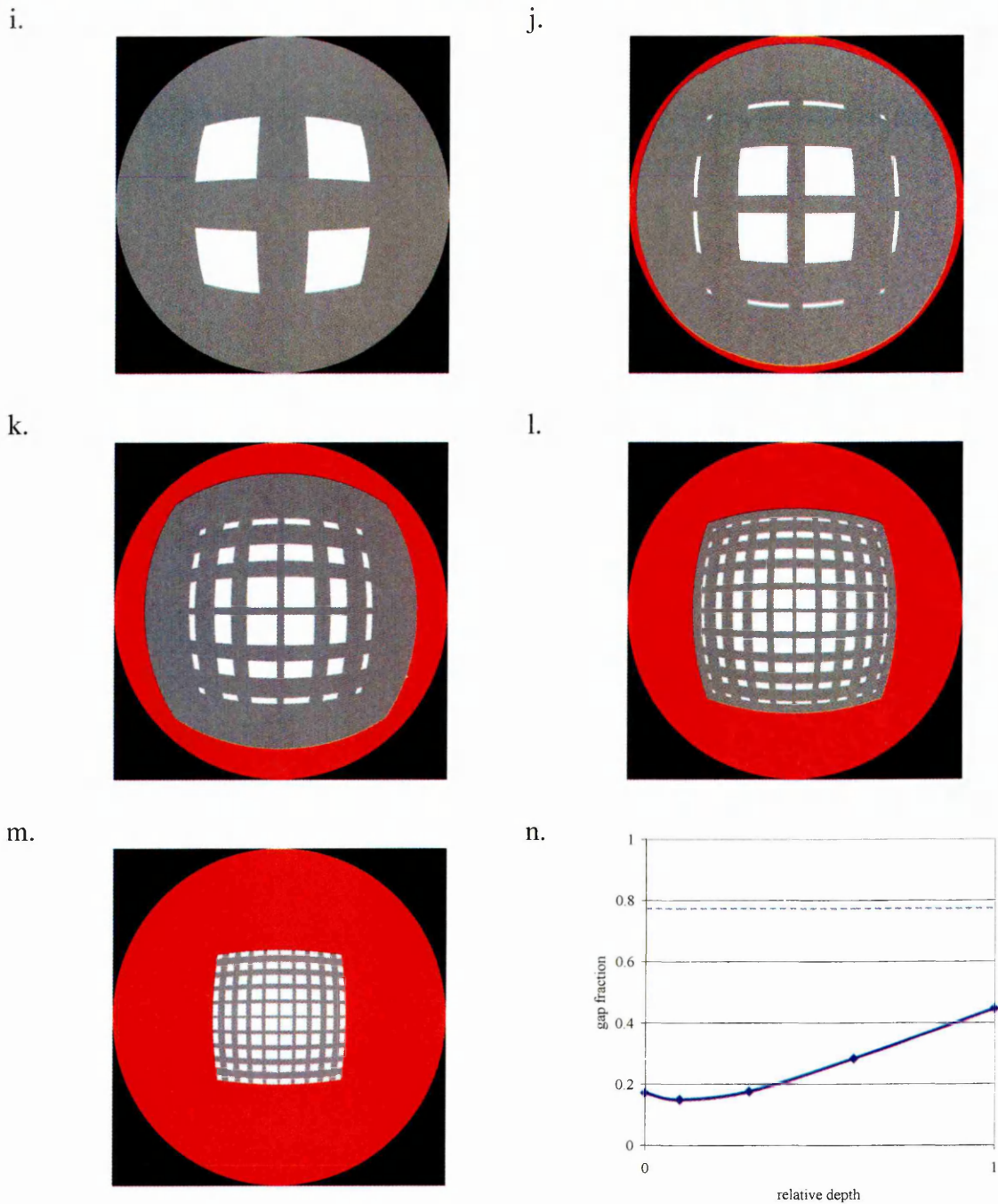
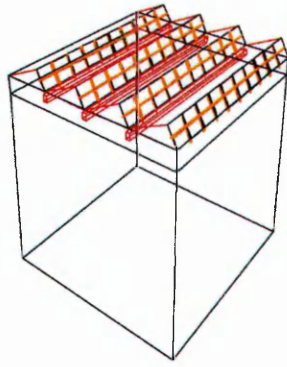
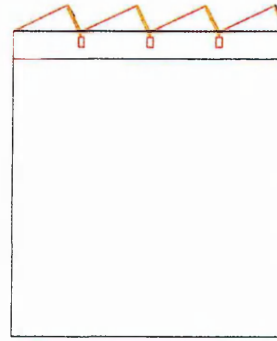


Figure 7-7: Waffle: a. Wireframe perspective; b. Side Elevation; c. DF contours (glazing transmittance 90%, structural reflectance 75%) internal scale; d. DF contours (glazing transmittance 90%, structural reflectance 75%) comparative scale (contour range 0-80%, at 5% intervals); e. Overall transmittance against Glazing Transmittance; f. TR against structural Reflectance; g. Coefficient of Distribution against Structure Reflectance; h. Plan Rendering; i. Fisheye view roof plane; j. Fisheye view -1m; k. Fisheye view -3m; l. Fisheye view -6m; m. Fisheye view ground floor; n. HemiView returned gap fraction against Photograph depth.

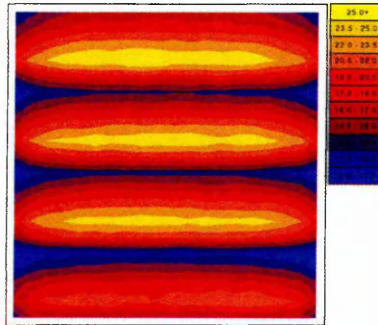
a.



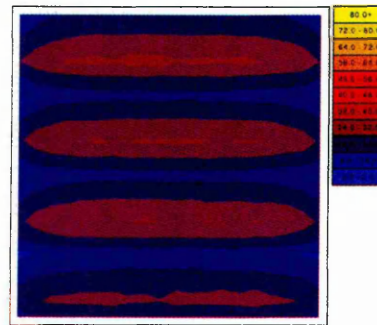
b.



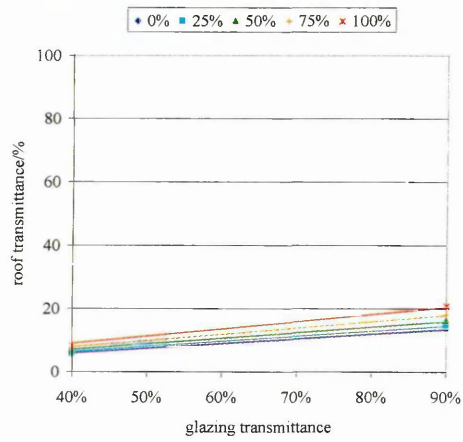
c.



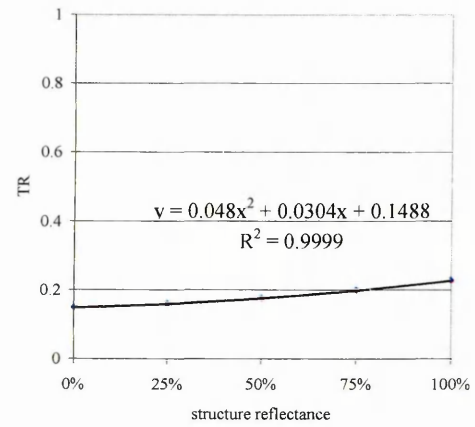
d.



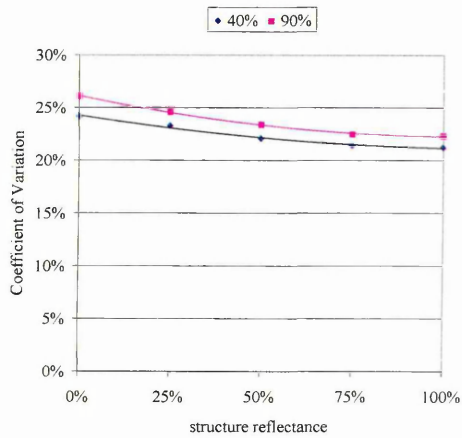
e.



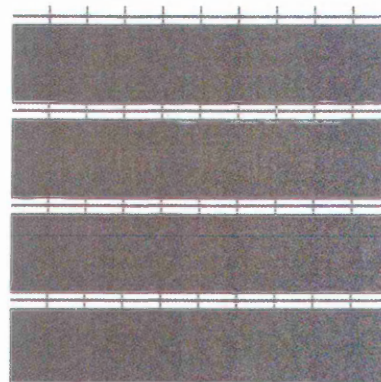
f.



g.



h.



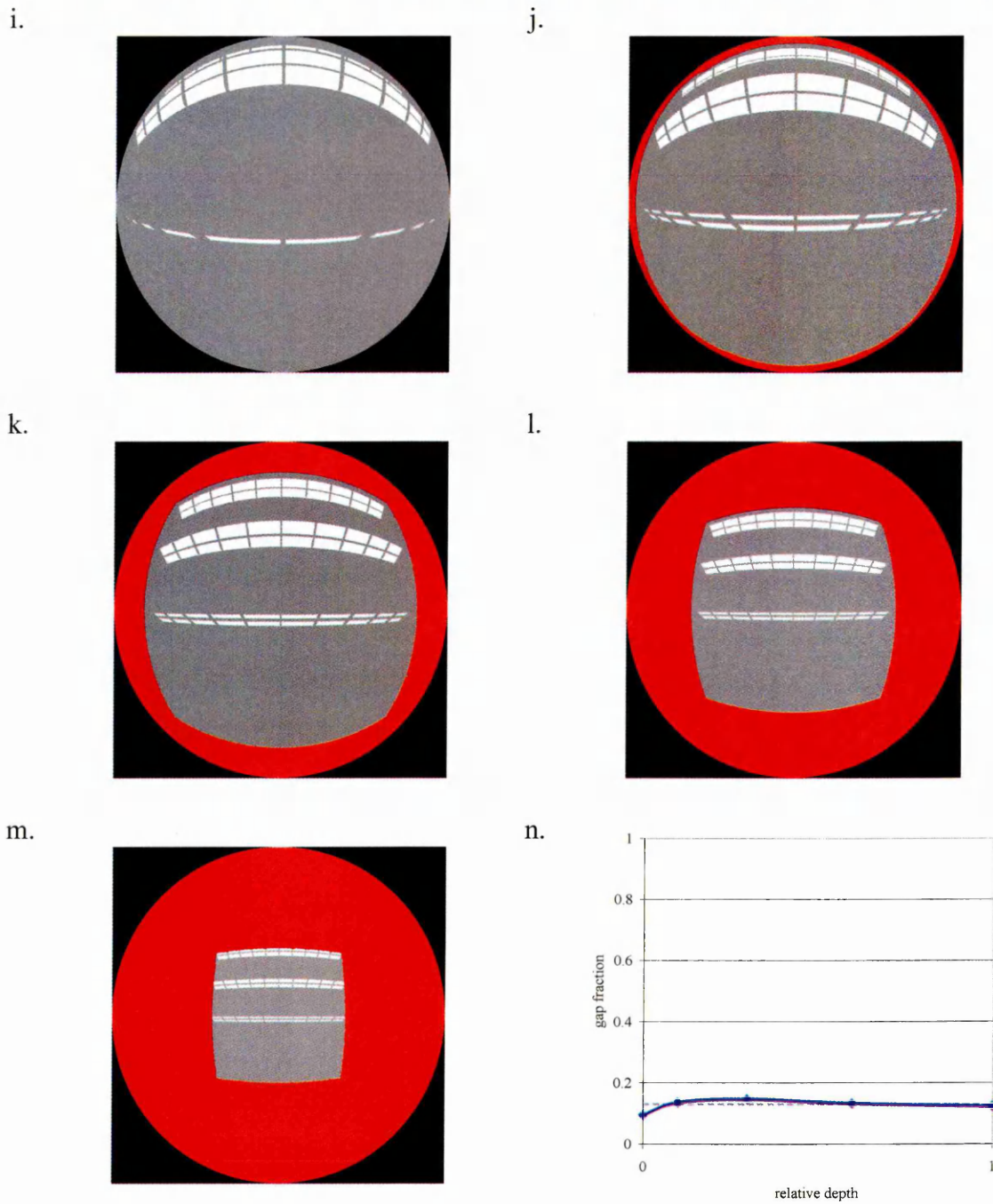
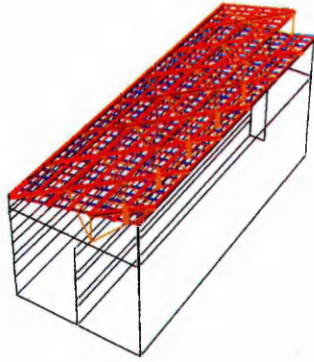
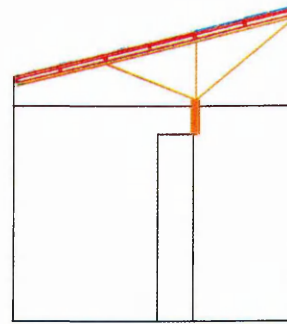


Figure 7-8: Sawtooth: a. Wireframe perspective; b. Side Elevation; c. DF contours (glazing transmittance 90%, structural reflectance 75%) internal scale; d. DF contours (glazing transmittance 90%, structural reflectance 75%) comparative scale (contour range 0-80%, at 5% intervals); e. Overall transmittance against Glazing Transmittance; f. TR against structural Reflectance; g. Coefficient of Distribution against Structure Reflectance; h. Plan Rendering; i. Fisheye view roof plane; j. Fisheye view -1m; k. Fisheye view -3m; l. Fisheye view -6m; m. Fisheye view ground floor; n. HemiView returned gap fraction against Photograph depth.

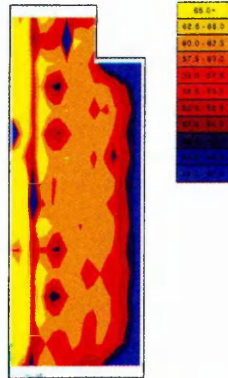
a.



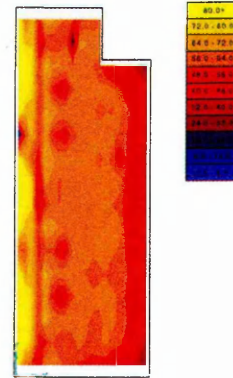
b.



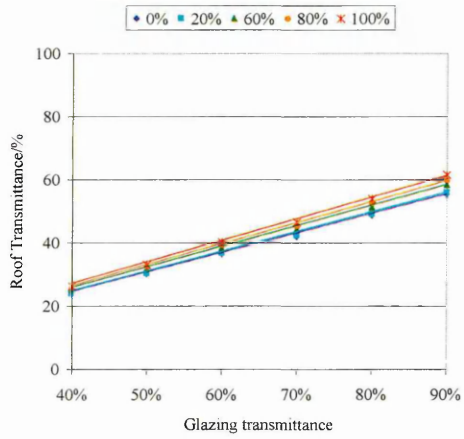
c.



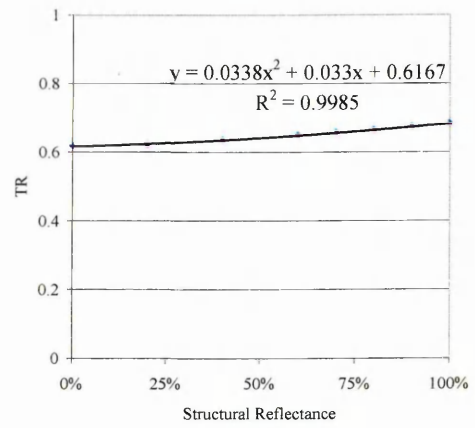
d.



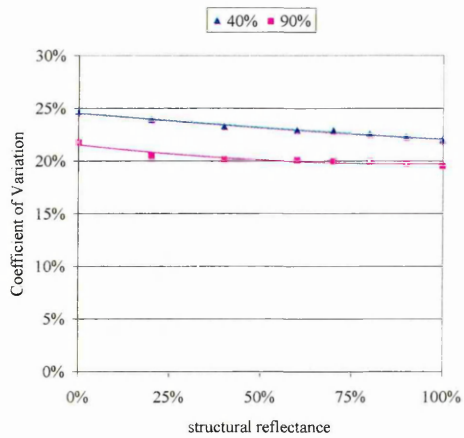
e.



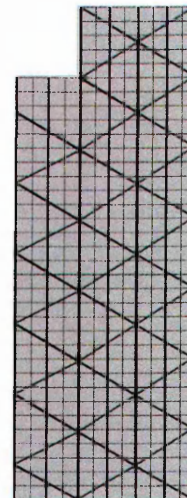
f.



g.



h.



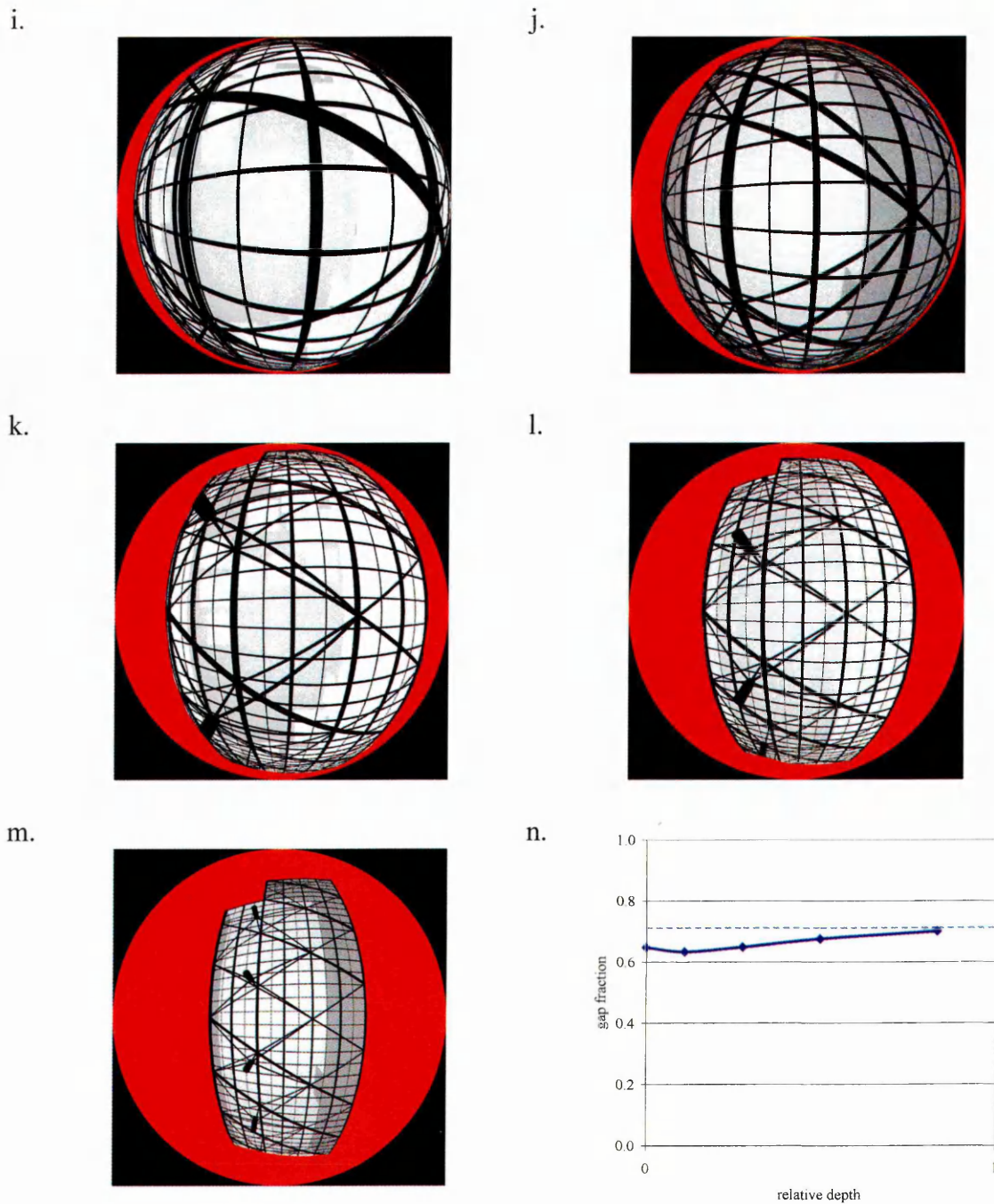
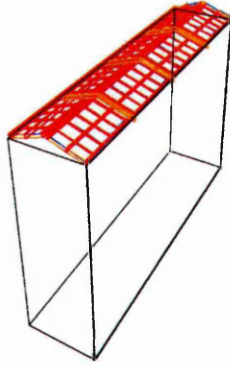


Figure 7-9: Monopitch Space Frame (Owen building): a. Wireframe perspective; b. Side Elevation; c. DF contours (glazing transmittance 90%, structural reflectance 75%) internal scale; d. DF contours (glazing transmittance 90%, structural reflectance 75%) comparative scale (contour range 0-80%, at 5% intervals); e. Overall transmittance against Glazing Transmittance; f. TR against structural Reflectance; g. Coefficient of Distribution against Structure Reflectance; h. Plan Rendering; i. Fisheye view roof plane; j. Fisheye view -2m; k. Fisheye view -5m; l. Fisheye view -9m; m. Fisheye view -15m; n. HemiView returned gap fraction against Photograph depth.

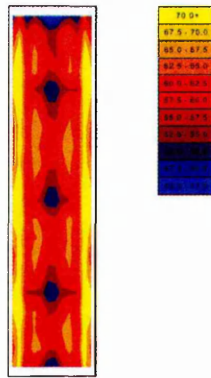
a.



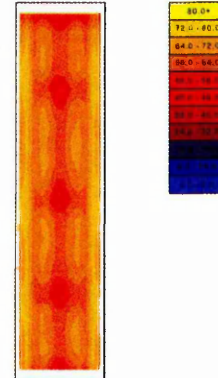
b.



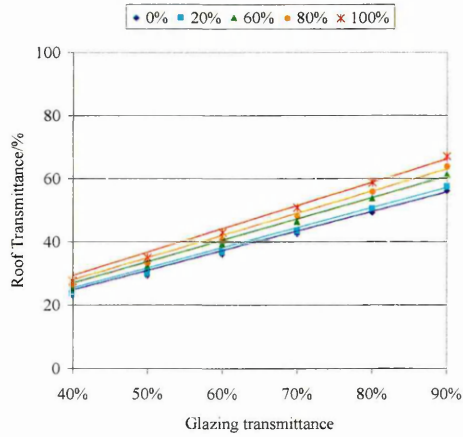
c.



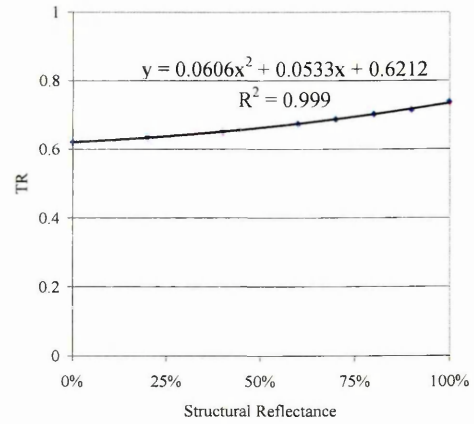
d.



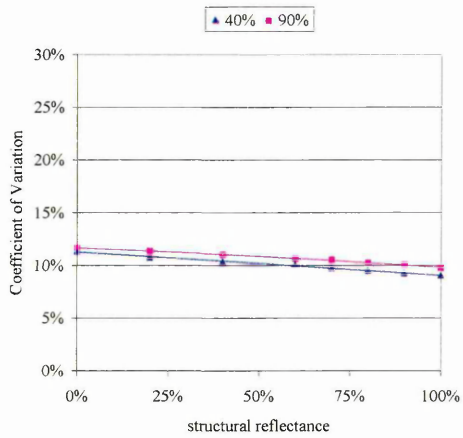
e.



f.



g.



h.



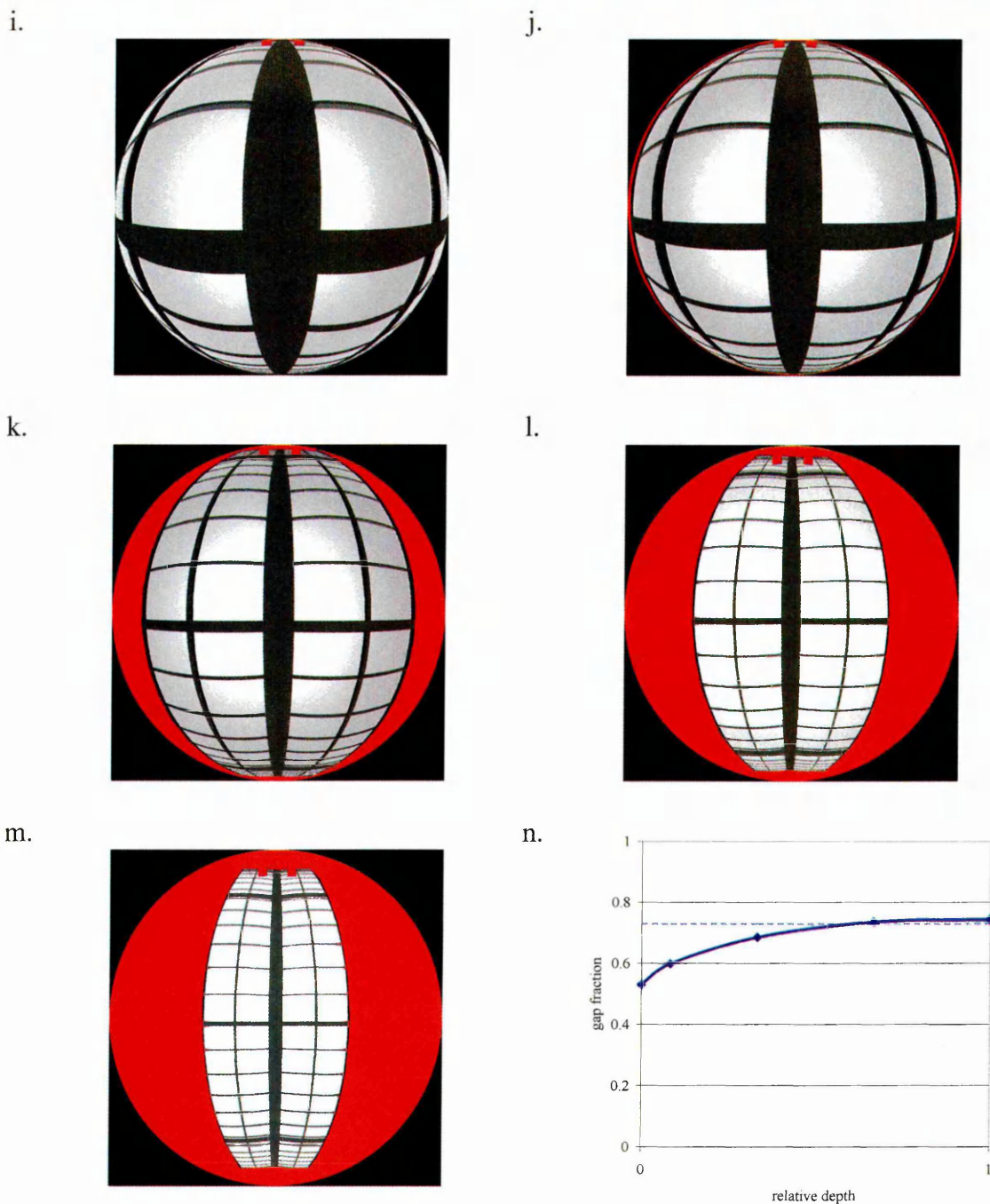


Figure 7-10: A-Frame (Sheaf building): a. Wireframe perspective; b. Side Elevation; c. DF contours (glazing transmittance 90%, structural reflectance 75%) internal scale; d. DF contours (glazing transmittance 90%, structural reflectance 75%) comparative scale (contour range 0-80%, at 5% intervals); e. Overall transmittance against Glazing Transmittance; f. TR against structural Reflectance; g. Coefficient of Distribution against Structure Reflectance; h. Plan Rendering; i. Fisheye view roof plane; j. Fisheye view -0.5m; k. Fisheye view -2m; l. Fisheye view -4m; m. Fisheye view -6m; n. HemiView returned gap fraction against Photograph depth.

7.3.2 Magnitudes of Transmittance

The graphs of TR against structure reflectance with the fitted polynomial equations describe the magnitude of transmittance of the various roofs. The R^2 values of these polynomials were in excess of 0.99 in all cases with the exception of the pyramid, there the fit was still a very good 0.97. The equation of the polynomial contains three coefficients (referred to here as a , b and c). Two of these (a and b) are dependant on the inter-reflected contribution of the roof structure, the third (c) is independent of this variable. These can be seen in Table 7-1, together with the Plan Area of Gap ([PAO-1]).

Table 7-1: The coefficients from the derived polynomials describing the TR relative to the structure reflectance of the 8 roof types simulated, as well as the PAG.

Roof:	a	b	c	PAG
pyramid	0.0857	0.0227	0.5609	0.749
dome1	0.0046	0.0274	0.8836	0.894
dome2	0.0354	0.0474	0.6536	0.623
flat	0.0286	0.0694	0.4580	0.731
waffle	0.0640	0.0696	0.1342	0.733
sawtooth	0.0480	0.0304	0.1488	0.129
monopitch	0.0338	0.0330	0.6167	0.711
a-frame	0.0606	0.0533	0.6212	0.730

In plan the *pyramid*, *flat*, *waffle*, *monopitch* and *a-frame* roofs had very similar blockages (70-75%). This can be seen visually in comparing the rendered plan views (part f). It was not possible to create a sawtooth roof with such an obstruction value (due to its nature), and the two *dome* types cover this mark in either direction. The shortcomings of traditional methods which use the plan as an indicator of transmittance are plain to see. Clearly, and despite the closeness of the PAG values, the transmittance values of all these roofs differ. In the case of the *waffle* roof, this difference is up to 400%. Whilst it is appreciated that there are probably very few (if any) *waffle* skylights in temperate climates such as the UK, it clearly demonstrates the interactions occurring in section that can not be predicted when looking in plan projection.

Likewise, the *dome 2* roof which had a lower PAG than every other roof (with the exception of the *sawtooth*) had the second highest (the highest being the lesser structured *dome 1*) TR values over the entire range of realistic structure reflectance values. This indicates that a dome skylight is the most efficient roof type for the

transmittance of daylight under overcast skies, at least on an analysis plane at roof level. It should be remembered however that this analysis plane excluded the regions of ceiling resultant of the fitting of a circular form to a rectilinear well, and as such a dome is perhaps not the most efficient means of covering such wells. Indeed, with the ceiling areas considered, the coefficients a , b and c drop to 0.0377, 0.0267 and 0.4907 respectively.

The TR polynomial curves can be seen plotted together in Figure 7-11. The roof that is most sensitive to structure reflectance is the *waffle* roof whose TR value doubles (from 0.13 to 0.27) over the range of structural reflectances. The *sawtooth* roof displays a similar trend though to a lesser extent (50% increase across the range of structure reflectance). The *pyramid*, *flat* and *a-frame* roof's TR values all rise approximately 20% over the range of structural reflectance values, with the *a-frame* being the best transmitter, followed by the *pyramid* and finally the *flat* roof. The transmittance of the *monopitch* and *dome 2* roofs are less sensitive to structure reflectance (relative TR range of just over 10%). This is probably as the analysis plane is further from the actual structural members compared to the *flat*, *a-frame* and *pyramid* which are close to the roof over their entirety, at the edges and around the circumference respectively. The minimally structured *dome 1* roof is barely affected by the reflectance of the structural members.

7.3.3 Distribution of Transmittance

The contour maps with internal scale (parts c) indicate the distribution of transmitted illuminance over the analysis plane of each of the roofs. For example, the separation of the plane into a 3x3 grid caused by the two main beams spanning the well in each direction for the *flat* roof (Figure 7-6 c). In the *dome* and *pyramid* roofs, the illuminance values are highest at the centres of the well, directly beneath the zenith/apex of the roofs. In the *a-frame* roof, illuminances are expectedly highest beneath the least structured parts of the roof, and lowest immediately the principal structural elements. In the *monopitch* roof the illuminances rise with increasing distance from the non-reflective high edge of the well. The *sawtooth* roof has intense bands of illuminance corresponding to the gains from the four lateral openings. The *waffle* roof has a relatively even distribution of illuminance across the analysis plane. Comparison

between the roofs is possible by examining parts d, whose scale is set from 0-80% transmittance at 5% intervals. This also rapidly reaffirms the trends of magnitude.

The coefficient of variation (the standard deviation divided by the mean) gives a relative description of the spread of an array of values. The coefficients of variation plotted against structure reflectance (parts g) were collated and displayed together (Figure 7-12). A low coefficient of variation indicates an even distribution across the roof plane. The roofs in order of evenness of distribution at the roof plane (from most to least even) is as follows; *waffle* (approximately 5%), *pyramid*, *dome 1*, *a-frame*, *flat*, *dome 2*, *monopitch*, *sawtooth* (approximately 25%).

For all cases, increasing the structural reflectance evened the distribution of illuminance across the analysis plane, due to a reduced contrast between 'gap' and 'blockage'. In comparing the effect of glazing transmittance on distribution an interesting discovery is made. For some roofs, increasing the glazing transmittance evens out the distribution (*monopitch*, *flat*, *pyramid*, *domes*) and in some instances the reverse holds true (*sawtooth*, *a-frame*, *waffle*). It was argued in Chapter 6 that decreasing the glazing transmittance was likely to even the distribution due to the aforementioned reduction of gap to blockage contrast. It is unclear as to why increasing the glazing transmittance should even out the distribution, though it is noted that the effect is most pronounced for the dome roofs and monopitch roof, where the analysis plane lies for the most part at relatively great distances from the actual roof elements. Further work in this area may reveal the reasons for this phenomenon.

Assuming the distribution of transmitted light through skylights within the assigned roof type group behaves similarly, then with the average roof plane transmittance, the glazing transmittance and structure reflectance values known, the standard deviation about that average can be estimated from the graph.

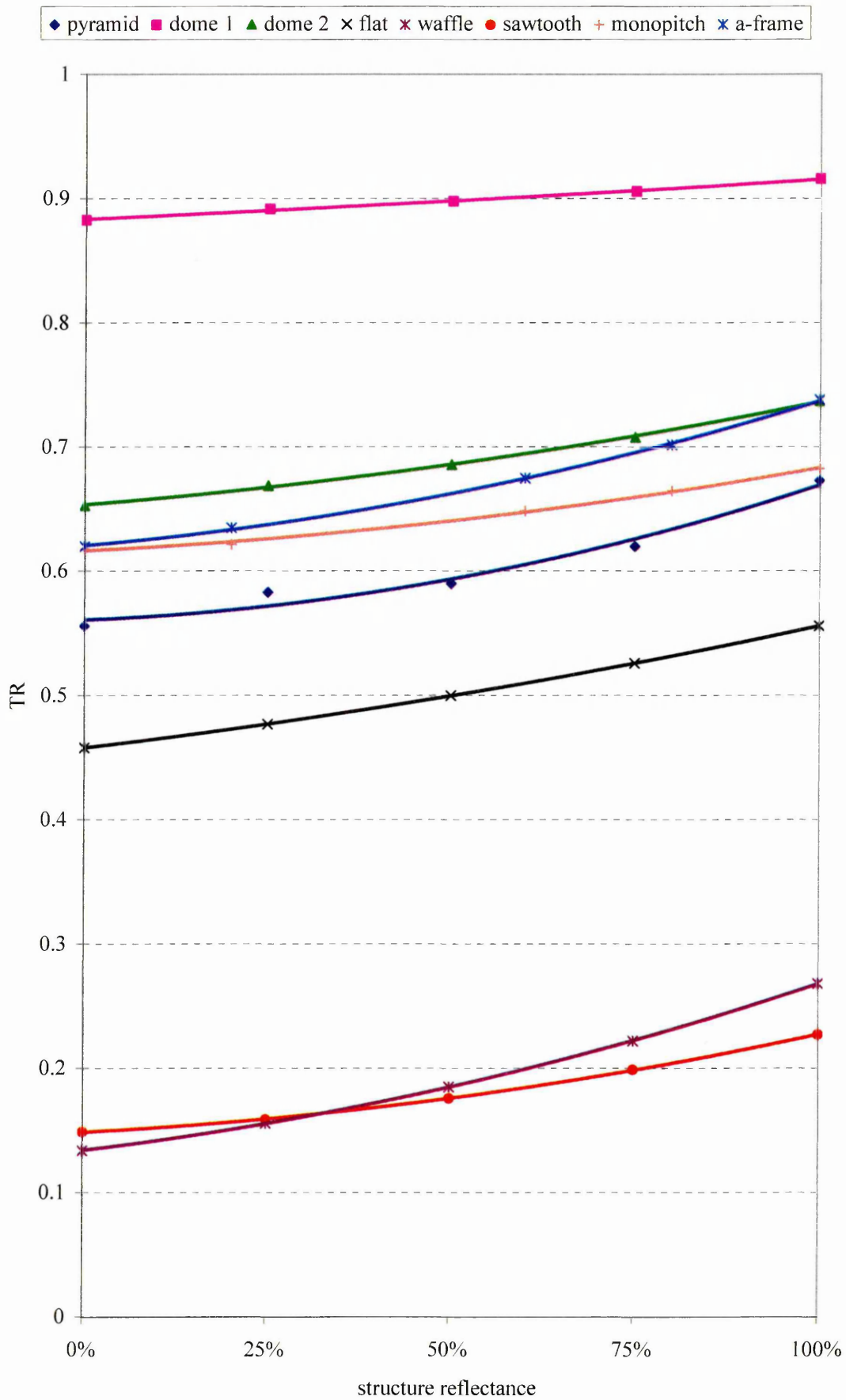


Figure 7-11: TR against structure reflectance for the eight roof types simulated

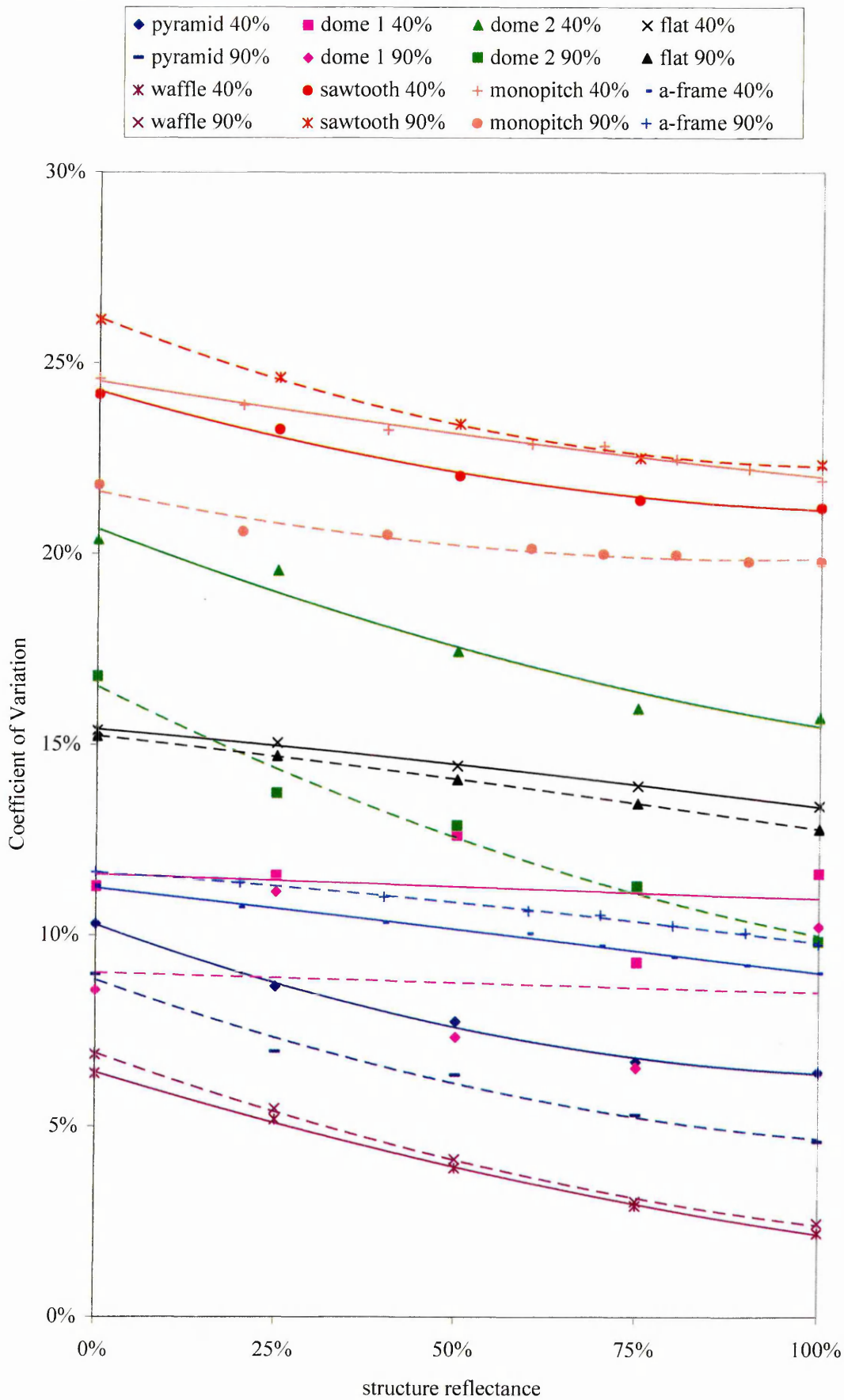


Figure 7-12: Coefficient of variation against structure reflectance for the eight roofs simulated

7.3.4 A Comparison of Results with SkyVision

SkyVision is a new design tool that calculates the daylighting and energy performance of skylights. It is freely available for download¹. The calculation is based on radiosity algorithms, and has been validated using model studies under real sky conditions (Laouadi & Arsenault 2004). It supports a wide range of sky models and roof types, and glazing input is linked to the Optics5 database. The modelled roofs were inputted in turn to the program. This on occasion involved a 'best match' strategy, for example, the *waffle* roof was described as flat, and the *sawtooth* roof stipulated as a monitor, with one transparent side opening and one opaque side opening. SkyVision does not include monopitch skylights. The depth of the well was set as low as was permissible (0.1m) such that the 'Daylight Factor - Floor' output represented transmittance at roof plane level. Clear double glazing was used in each instance, with a maintenance factor of 1 i.e. perfectly clean. Structural obstruction is considered by the program through the use of a 'frame factor', which is the proportion of the frame surface area with respect to the total skylight surface area. For the purposes of comparison to the Radiance derived roof plane transmittance results, the structure is assumed to have a reflectance of 0%. The results together with the difference from the Radiance output are shown in Table 7-2.

Table 7-2: SkyVision results for transmittance at roof plane level, together with the difference from the Radiance output

Roof	SkyVision	Radiance	% Difference
Pyramid	54%	44%	16.0%
Dome 1	63%	69%	-9.7%
Dome 2	44%	51%	-13.5%
Flat	50%	36%	39.4%
Waffle	50%	11%	376.1%
Sawtooth	7%	12%	-42.0%
A-frame	50%	49%	3.5%

Clearly, specifying the *waffle* roof as flat is incorrect, and the large difference can not be taken as representative of the accuracy of either program. Likewise, the approximation of the *sawtooth* roof appears to be too loose. The modelled roof had an inclined transparent opening, as opposed to the vertical opening of the monitor roof, hence the lower SkyVision result. The much lower Radiance result for the *flat* roof is

¹ <http://irc.nrc-cnrc.gc.ca/ie/light/skyvision/>

due to the proximity of the entirety of the roof to the analysis plane, and hence the influence of the arrangement and reflectance of the structural elements was at its greatest. Whereas Radiance considers this, the PAO entered as the frame factor in SkyVision was not representative of what occurs immediately beneath the roof. Using the gap fraction result from the hemispherical image at roof plane level (0.55) as the frame factor results in a transmittance value of 38%, a relative difference of 5% from the Radiance result. Where there was clearance between the analysis plane and the roof surfaces i.e. dome and pitched roofs, the agreement between the results was relatively good (MBE -1%, RMSE 12%), with differences in the main due to the discrete nature of input in SkyVision. Given the far more detailed model entry, it is likely the Radiance output was the more accurate, though as a fast design tool SkyVision performed well.

7.3.5 Effect of Viewpoint within the Various Roof Types

The individual roof type graphs of gap fraction against relative depth (part o) reaffirm the trend of gap fraction approaching the PAG that has been discussed in Chapter 5. In the case of the *waffle* roof, the divergence at shallow depths between PAG and gap fraction is particularly evident. For most roof types, this means increasing gap with depth, although in the case of the more heavily structured *dome 2* the gap fraction decreases with increasing depth. This observation helps explain the efficiency of the dome roof at transmitting daylight at the analysis plane level, as the amount of sky (luminous surface) seen is significantly greater than for the other roofs, despite the greater obstruction in plan. In the case of the minimally structured *dome 1*, the slenderness of the members means that the gap fraction value is already at the PAG, even at the analysis plane.

Another observation in some of the roofs is a small kink at shallow relative depths. This occurs for the monopitch, flat, sawtooth and waffle. Consultation with the generated images reveals the reason for this is that at the analysis plane for some of the roofs, the entirety of the roof is not visible. Taking the flat roof as an example (Figure 7-6 i-n) at the analysis plane, only the centre square of the formed 3x3 structural grid is visible. Moving the viewpoint downwards by 1m (relative movement of 0.1) brings the other eight major squares within the field of view. The glancing angle at which they are

visible increases the dominance of the blockage result, and hence the gap fraction value decreases. Moving further into the well (3m), the angle at which the external eight squares can be seen is closer to the normal (and hence plan perspective), and so the gap fraction increases, and continues to do so with increasing depths.

The gap fraction results for all the roof types are displayed together in Figure 7-13. At the analysis plane, for the roofs with similar PAO (i.e. all but the *domes* and the *sawtooth*) the range of gap fraction values is great. With increasing depths, they converge towards the PAG value of 70-75% (though the *waffle* roof still only reaches a PAG of about 45% at a relative depth of 1, despite having the greatest rate of increase). The kinks in some of the lines discussed above are also clearly visible.

The images generated and analysed were at the centre of the well. It was observed in Chapter 5 that discrepancies between gap fraction values from photos taken at different lateral positions are likely to be greater towards the top of the well, where the localised effect of 'structure obscuring structure' and viewing structural members over a wider possible range of three-dimensionality are more pertinent issues. In applying the photographic method to other atria where it is not possible to take the photograph at the centre of the well, taking a photo from an edge/corner etc. may prove to correlate better with these results when the photo is taken deeper within the well.

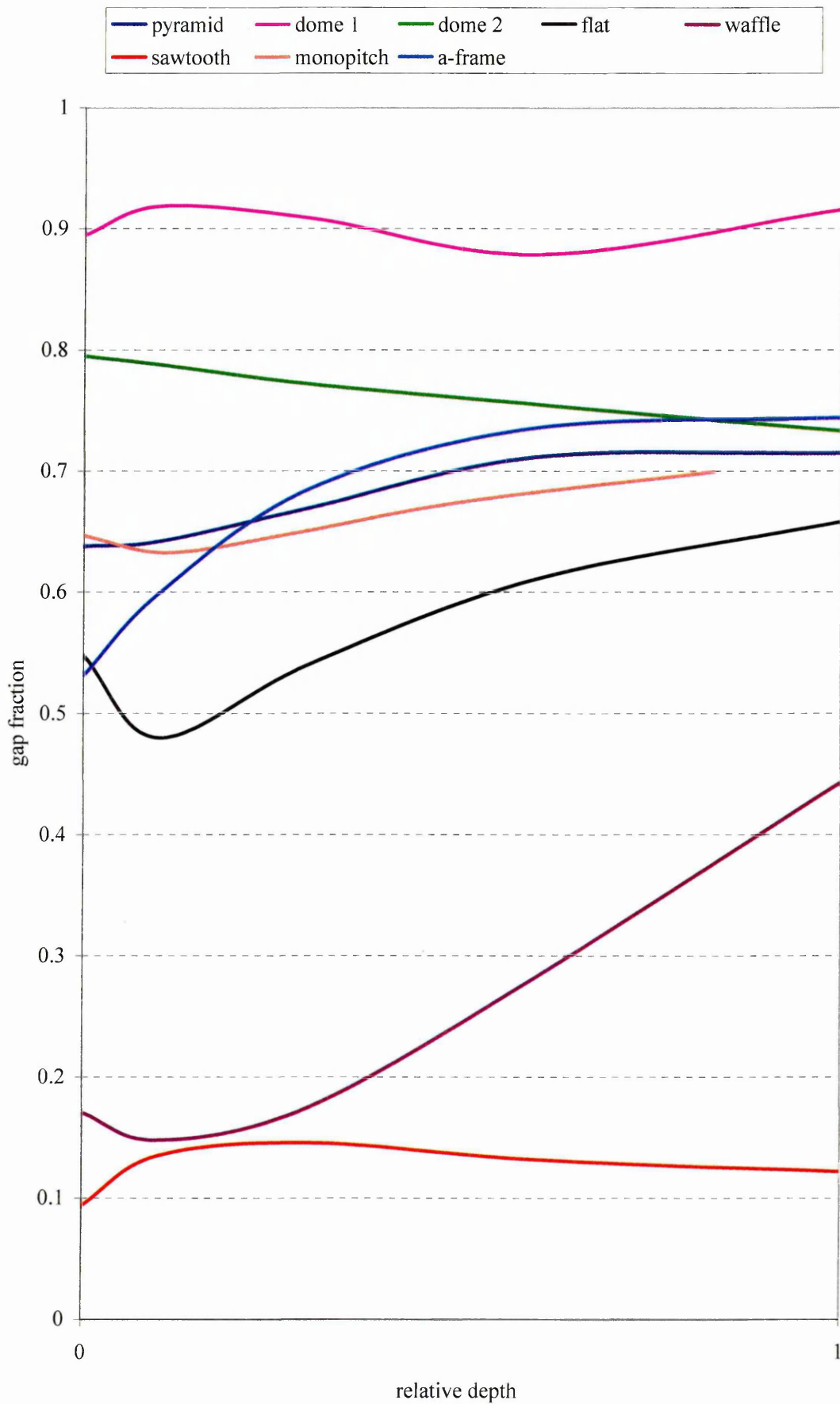


Figure 7-13: Gap fraction against relative depth for the eight roof types investigated.

7.3.6 Relating the Photograph to Transmittance of the Roofs

As has been discussed in Section 6.5 and stated in Equation 6-5, the transmittance of the roof can be defined by:

$$T_{ROOF} = T_g \times TR \quad [7-1]$$

where,

$$TR = a\rho^2 + b\rho + c$$

T_g = glazing transmittance

ρ = structure reflectance

The initial consideration of the HemiView output as corresponding to the transmittance of the roof must begin with the scene defined as it is considered in HemiView i.e. the glazed area is entirely gap ($T_g = 100\%$) and the structure acts as a pure light sink ($\rho = 0\%$). Inserting these into [7-1] results in the simplified equation;

$$T_{ROOF} = c \quad [7-2]$$

The polynomial equations derived to describe the TR functions of each roof type can be rearranged to express the coefficients a and b as simple ratios of c as follows (the ratios have been rounded to the nearest 0.05);

$$\textit{Pyramid} \quad TR = c(0.15\rho^2 + 0.05\rho + 1) \quad [7-3]$$

$$\textit{Dome 1} \quad TR = c(0.05\rho + 1) \quad [7-4]$$

$$\textit{Dome 2} \quad TR = c(0.05\rho^2 + 0.05\rho + 1) \quad [7-5]$$

$$\textit{Flat} \quad TR = c(0.05\rho^2 + 0.15\rho + 1) \quad [7-6]$$

$$\textit{Waffle} \quad TR = c(0.5\rho^2 + 0.5\rho + 1) \quad [7-7]$$

$$\textit{Sawtooth} \quad TR = c(0.3\rho^2 + 0.2\rho + 1) \quad [7-8]$$

$$\textit{Monopitch} \quad TR = c(0.05\rho^2 + 0.05\rho + 1) \quad [7-9]$$

The percentage difference of the coefficient c as derived from the transmittance simulations was calculated from the gap fraction results from the images at the various depths. These differences are displayed graphically in Figure 7-14 together with the percentage difference between the PAG (i.e. a photo taken at infinite, or approaching great depths). This graph is the critical link between the photographic technique and its application to the rapid assessment of roof transmittance of existing buildings. Once the photograph is taken, the percentage difference from the HemiView derived gap fraction and the coefficient c can be estimated with knowledge of the roof type, and the relative depth (i.e. well width and depth at which the photo was taken). This can then be inserted into the appropriate equation (7-3 to 7-10) and the average roof transmittance calculated with entry of the structure reflectance and glazing transmittance. Figure 7-12 can then be used to obtain the coefficient of variation, and together with the average roof transmittance, the standard deviation of transmittance values across the roof plane.

For example, say a hemispherical photograph was taken of a pyramid roof from the centre of the ground floor of a square atrium that is 15m wide and 9m deep. The transmittance of the glazing was 80%, and the reflectance of the structural members 65%, then the transmittance of the roof would be assessed as follows;

1. The gap fraction is calculated from HemiView. Let us suppose that the returned value was 0.7
2. The relative depth is calculated i.e. depth of photo viewpoint (9m) divided by the width of the well (15m), which in this case comes to 0.6.
3. From Figure 7-14, the percentage difference of c from the gap fraction at that depth and for that roof is found. In this case, the difference is -21.2%
4. The obtained gap fraction value is multiplied by this percentage difference i.e. $0.7 \times (1-0.212) = 0.5516$
5. This value is substituted for c in the relevant equation, in this case Equation 7-3. The equation for this roof becomes: $TR = 0.5516(0.15\rho^2 + 0.05\rho + 1)$
6. TR is calculated by substituting in the value of structural reflectance (0.65). This returns a TR of 0.604

-
7. The average roof plane transmittance is found by multiplying the TR by the glazing transmittance (80%). The average roof plane transmittance for this example is therefore 48%
 8. From Figure 7-12, the coefficient of variation for the specified roof type, structural reflectance and glazing transmittance is estimated. In this case approximately 6.5%
 9. The coefficient of variation is multiplied by the average roof plane transmittance to get the standard variation of transmittance. For this example, the standard deviation is 3.1%

The relationships found for the simulated roof types are specific to wells that are square in plan (PAR =1). The fitted finer accuracy of the polynomials is as a result of the specific arrangements of the elements, and the widths of the structural members and glazing, all relative to the defined analysis grid. Application to other atria roofs can therefore only be considered estimation. Future work could aim to investigate specific arrangements and combinations within each roof type further. The method suggested here is very much at the early stages of a potentially much longer research path. The nature of the method means that new findings and multipliers can be applied to the existing approach with minimal effort.

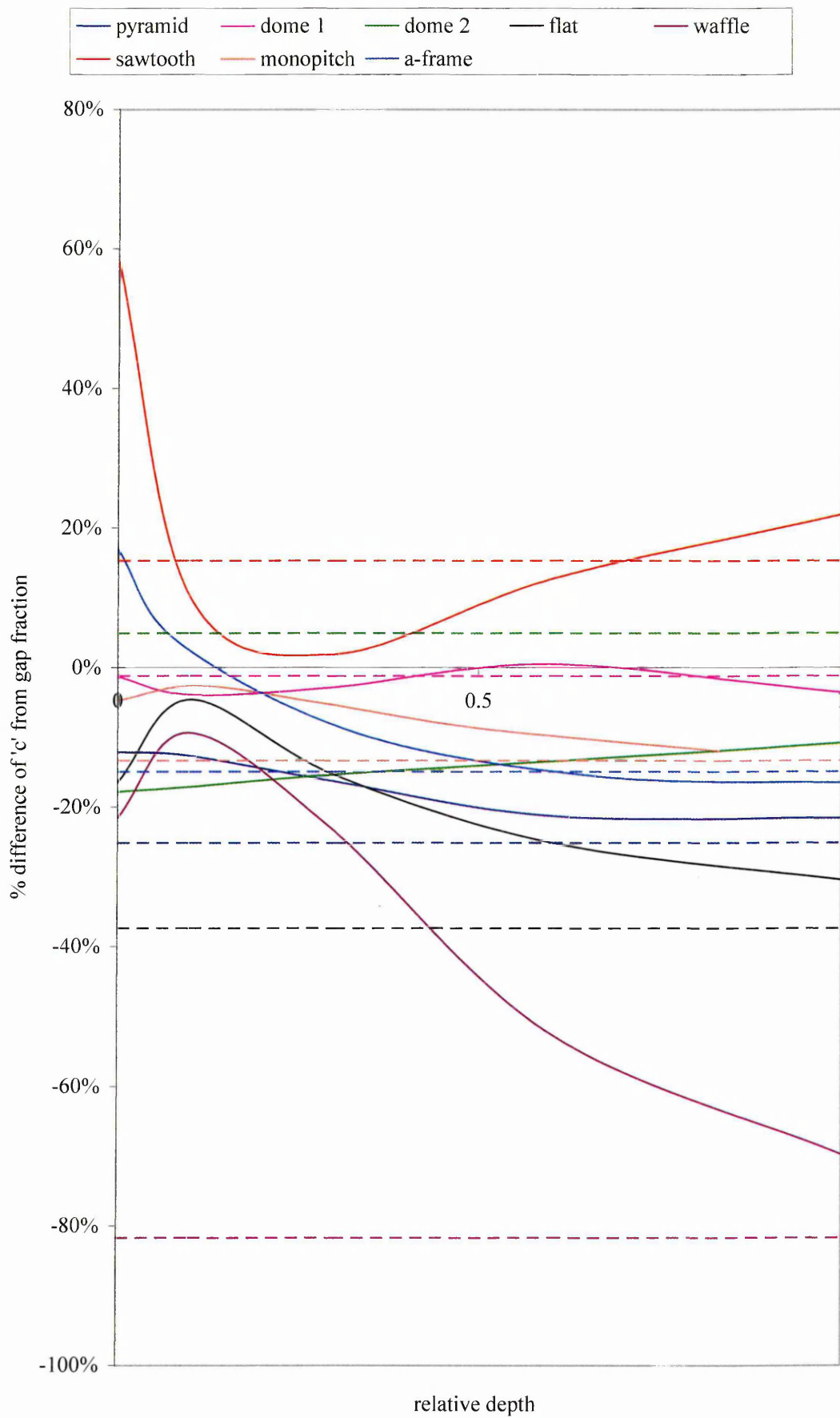


Figure 7-14: The % difference between coefficient c and calculated gap fraction. The dashed line represents the % difference of c from the PAG i.e. depth = infinity.

7.3.7 A Discussion on the Relevance of Application

The technique presented in this thesis is done so in conjunction with the hypothesis that in establishing daylight conditions immediately beneath the roof, predictions of daylight conditions in places deeper within the well and on other surfaces can be derived from traditional methods which treated the well as an 'open box'. The equation derived by Atif et. al (1994) represents an example of one such traditional simple method:

$$DF_{(Average)} = 46 \times T \times e^{(-WI+ER)} \% \quad [7-11]$$

where,

$DF_{(Average)}$ = average daylight factor on the floor of the well

T = transmittance of the top fenestration

WI = well index of the well

ER = effective reflectance of the atrium walls

There are several such equations derived from simple scale modelling, and although they agree in general form, they do not agree in terms of exact magnitudes. The availability of more powerful computer programs raise the possibility of repeating such studies in more a detailed manner, allowing applicability to a wide range of wells and reducing the ambiguities of having to chose between several existing formula. For demonstration purposes, reference will be made to Equation 7-11.

Let us further consider the example of the pyramid roofed atrium from Section 7.3.5. With dimensions of 15 x 15 x 9m, the atrium had a well index of 0.6 (from Equation 2-3). Say this well was finished with a white paint of reflectance 75%, and had bands of horizontal glazing 1m high running the length of each side over the three floors of the well. The surface are of the well was therefore 4 x 15 x 9m = 540m². Of this, the area of glazing constituted 3 x 4 x 15 x 1 = 180 m². Thus 360m² of the surface was of reflectance 75%, with the remaining portion glazed (assume total light sink in this instance i.e. 0%). The area weighted average for the entire well is 2/3 x 75% + 1/3 x 0% = 50%. The value of transmittance was calculated in Section 7.3.5 at 48%.

Substituting these values into Equation 7-11, the average daylight factor in the centre of the well was found to be 20%. The use of such simple methods allow designers to make quick informed decisions about their proposals, before they deploy more time and cost consuming measures. The single most important query that needs to be raised however, is how representative is the output from these processes of real world occurrences?

Without further illuminance measurements or modelling, it is not possible to state the accuracy of such an approach. Divergence from real world values will arise due to the discussed sources of error within this study, and through the limitations of existing well algorithms. In obtaining the daylight factor on the floor, the process outlined involved taking a photograph of the roof from the floor, from there calculating the transmittance immediately beneath the roof, and then working back down to obtain the floor measurements. This brings about the following question: Would it not make more sense to analyse a photograph in terms of lighting conditions with respect to lighting at that specific viewpoint? i.e. if the photograph is taken at ground level, the returned daylight results should be indicative of values at ground floor level, and not at the roof.

If we consider the example of the variation in gap fraction as seen through the waffle roof (Figure 7-13), one can see that there are massive changes over a relative depth distance of 1. In a position deep within a well, one would expect the gap fraction for a waffle roof and a flat roof (assuming equal PAO's) to be similar. In adopting the process described in this thesis, the transmittance at roof plane level (and hence subsequent output for DF at the floor) would be markedly lower for the waffle roof than for the flat roof. In reality, from the ground both would probably receive similar values of sky component, and the excess daylight transmitted at shallow angles from the flat roof would most likely be absorbed by surfaces at the top of the well (due to the glancing entry angles). In this instance, it would appear that the proposed technique may fail to describe with any accuracy real world conditions, though it is not possible to implicitly state this without further measurement or modelling. A method where the returned daylight results are representative of daylighting at the plane of the viewpoint may be more appropriate here.

The difference between the approach suggested in this work, and once where the image viewpoint immediately returns daylight results for that plane, is that the former is independent of contributions from well inter-reflection (for the first part of the calculation), whilst in the latter it is not. It was not within the scope of this study to investigate the effects of the well (geometry and surface) as well as the various roof variables. The consideration of introducing a further variable demonstrates the complicated inter-dependence of the various parameters in the daylighting of atrium buildings. Until such an expansion of this study is made, it is not possible to state which technique would work better. One point that does emerge is that the proposed methodology represents a good means of classifying various roof forms.

7.4 Application to the Field: Demonstration

7.4.1 Divergence between Real and Simulated Conditions: Application of the Photographic Method to Real Buildings

The relationships found between a hemispherical image of a roof and its transmittance have been based primarily on computer generated imagery and simulated illuminance results. In order to apply the technique to existing buildings, the divergence between virtual and real world conditions needs to be defined. This can be split into two parts:

1. The difference between a physically captured photograph, and a computer generated image. This has been discussed in Chapter 5.
2. The difference between computer simulated illuminance levels and real world illuminance levels. The difference between the real illuminance measurements reported in Chapter 4 and the computer simulations in Chapter 6 has been stated in the latter.

It was observed that the physically captured photographs resulted in lower values of gap fraction than the generated images. The magnitude of this difference was dependant on the roof type, the lateral location on the viewing plane and the depth within the well. The limited number of photos for comparison in this thesis did not provide the scope for a full parametric investigation. However, some trends could be

detected. The key areas within the field of view which caused the differences were at the ends of the skylights. This is where the structural members were furthest from the viewpoint, and thus they converged. This convergence caused the classified photograph image to register large end sections of the skylight as fully blockage. With the generated images, the finer resolution and more defined contrast between sky and structure enabled the geometrically correct gap fraction to be derived. This phenomenon is the result of a linear well, and is likely to be less marked for not excessively large atria which are squarer in plan. Likewise, the difference between the two methods of image derivation is reduced with increasing depth within the well, where the end structural members are viewed from less oblique angles.

The differences between the gap fraction output from the generated and physically captured images for the Owen and Sheaf buildings was calculated, and graphed against the relative depth within the well at which the images were concerned with (Figure 7-15). Chapter 5 discussed in more detail some of the larger differences between the two, with specific reasons stated. The four circled points (3 at the Owen, 1 at the Sheaf) were deemed to be non-representative of the generalised trends. For the purposes of application of the technique with this particular camera, it is proposed that an image conversion factor be applied to the physically captured image when dealing with linear atria. It was felt that although this factor can not be exactly quantified, with an element of intuition, its application would be preferable entering a gap fraction result potentially 25% lower than the actuality. The magnitude of the factor relative to the depth is defined by the line on the graph, with error zones of 33% and 50% shaded.

It is worth repeating that it is not suggested that this specific factor be carried over into future usage, unless a full investigation of the differences with justified quantifiable output is undertaken. The use of improved image acquisition hardware may make this problem redundant. An alternative means of avoiding the issue of the end regions in linear atria would be to paint these regions red and ignore them in the HemiView analysis. Provided the field of view contained sufficient information to describe the roof (i.e. a representative sample of a repeatable configuration) then the two methods of image derivation should correlate better. This is an area for future investigation.

Chapter 6 stated the differences between the computer simulated results, and the physically measured results. In the case of the Sheaf (*a-frame*) building, the simulated result was 9.2% lower than the measured result. In the case of the Owen (*monopitch*) building, the simulated result was 6.7% higher than the measured result. In the application of this method, the results for *a-frame* roofs were multiplied by 1.09, and the *monopitch* results were multiplied by 0.93. The magnitude of these factors could be subject to change with further detailed studies. Likewise, correction factors for the other roof types not physically measured in this thesis could be explored. In the meantime, no correction factor for the other roof types is applied. The derived numerical output is an estimation of the average roof plane transmittance.

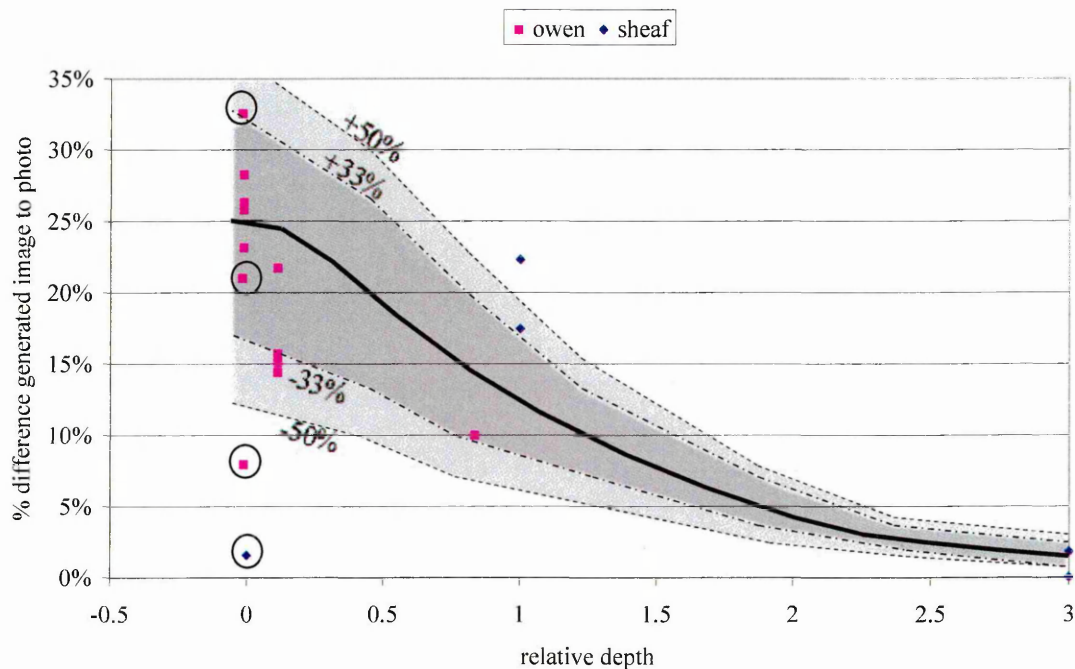


Figure 7-15: Correction factor to be applied to physically captured photographs using the specific set-up of this experiment, for linear atria.

7.4.2 The Buildings Selected and Methodology

The method was implemented on fifteen skylight types to obtain estimates for average roof plane transmittance. The criteria for selection were permission to take a photograph of the roof, and a general spread of roof types and scales. The Meadowhall Shopping Centre (Figure 7-16) provided six case studies. Further buildings examined include the Showroom Cinema, Natwest Offices, Orchard Square Shopping Centre, Blue Moon Cafe, Millennium Galleries, Winter Gardens, Sheffield Hallam University and TK Maxx department store.



Figure 7-16: The Meadowhall Shopping Centre, Sheffield, completed in 1990 incorporates a multitude of skylight types.

For each scenario, the following information was obtained:

- Name ID: The name of the building, with identifier if necessary.
- A hemispherical photograph of the roof looking upwards, as close to the centre as possible.
- Roof Type: The roof type of the measured building. If the roof is not one of the types modelled, then the closest match, or a hybrid is suggested. In the case of a hybrid, intuition is used in the application of the processes further on.
- Glazing Transmittance (T_g): An estimate is made on the glazing type and transmittance. Optics5 is used as a reference source. Should knowledge of the exact type of glazing used become available, then this could be substituted for the estimate. The method potentially allows several values of T_g to be entered, perhaps to obtain a range of overall transmittance.
- Structure Reflectance (ρ): An estimate based on the colour and material of the surface. The comprehensive Desktop Radiance material library is used as a reference. As with T_g as more information becomes available, this could be substituted for the estimate.
- Depth of Photograph (x): The depth beneath the roof plane at which the photograph was taken.
- Width of Skylight (w): The width of the skylight.

From this information, the following steps were taken to arrive at average roof transmittance:

-
- Relative Depth: The depth (x) divided by the skylight width (w).
 - Gap Fraction: The HemiView calculated gap fraction from red adjusted fisheye image of the roof. In the case of external obstructions, the image was intuitively classified to incorporate an element of extra gap to take into account reflected flux from the obstruction.
 - Image Conversion Factor: In the case of a linear skylight, the gap fraction obtained is multiplied by a conversion factor as described in Section 7.4.1 and Figure 7-15.
 - Deriving c from Gap Fraction: Achieved through use of Figure 7-14 as described in Section 7.3.5. Where the relative depth exceeded 1, an intuitive estimation was made, considering the relationship between the curve and the dashed PAG (depth at infinity) line.
 - Insertion of c to equation: From equations 7.3-10. In the case of hybrid roofs, the coefficients are averaged.
 - Simulation Conversion Factor: In the case of *monopitch* or *a-frame* roofs, a correction factor is applied based upon the findings of the detailed case studies of this thesis.
 - Average Roof Plane Transmittance: Through insertion of the above information into the relevant stated equation.
 - Coefficient of Variation: Achieved through use of Figure 7-12 as described in Section 7.3.3.
 - Standard Deviation across Roof Plane: The product of the coefficient of variation and mean roof transmittance.

The results from the application of the method are presented in Figures 7-17-7-

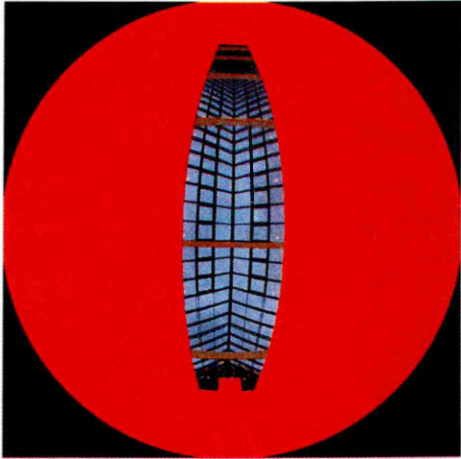
31.

Name ID:	Meadowhall A
Roof Type (see figure a):	A-Frame
Glazing Transmittance (T_g):	78% (clear double glazing)
Structure Reflectance (ρ):	20% (green paint)
Depth of Photograph (x):	8m
Width of Skylight (w):	6m
Relative Depth:	1.33
Gap Fraction (see figure b):	0.60
Image Conversion Factor:	$\times 1.08 = 0.65$
Deriving c from Gap Fraction (see figure c):	$\times 0.85 = 0.55$
Insertion of c to equation:	$T_{ROOF} = T_g 0.55(0.1\rho^2 + 0.1\rho + 1)$
Simulation Conversion Factor:	1.09
Average Roof Plane Transmittance:	48%
Coefficient of Variation (see figure d):	11.5%
Standard Deviation across Roof Plane:	5.1%

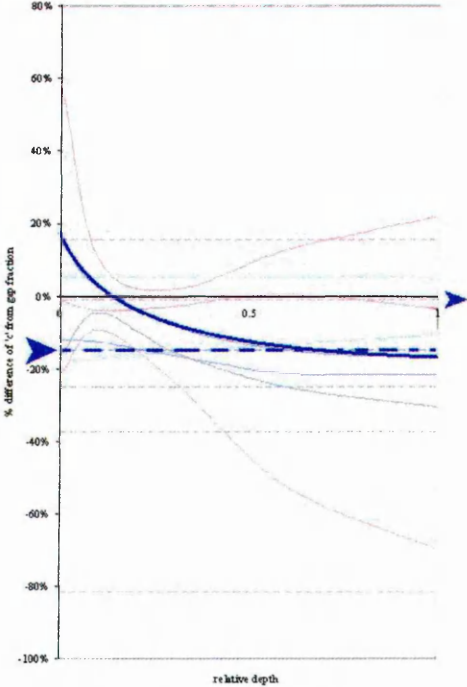
a.



b.



c.



d.

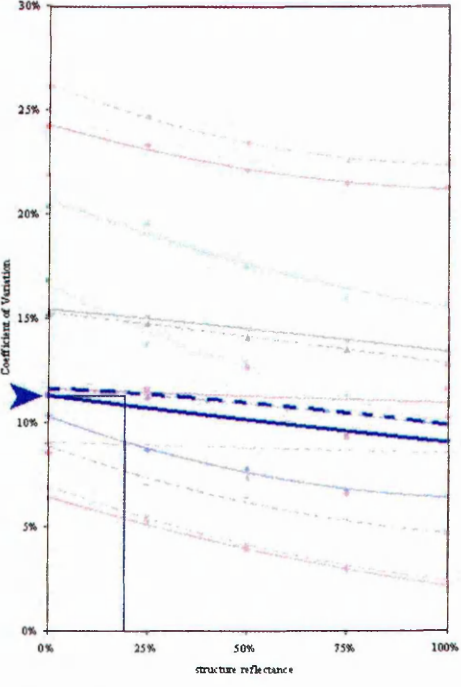


Figure 7-17: Meadowhall A: Box; Process to Obtain Average Roof Plane Transmittance; a. View of Roof; b. Hemispherical View of Roof; c. Difference between c and gap fraction at varying relative depth; d. Coefficient of Variation for each Roof.

Name ID:	Meadowhall B
Roof Type (see figure a):	Pyramid
Glazing Transmittance (T_g):	78% (clear double glazing)
Structure Reflectance (ρ):	20% (green paint)
Depth of Photograph (x):	14m
Width of Skylight (w):	10m
Relative Depth:	1.4
Gap Fraction (see figure b):	0.63
Image Conversion Factor:	N/A
Deriving c from Gap Fraction (see figure c):	$x \cdot 0.75 = 0.47$
Insertion of c to equation:	$T_{ROOF} = T_g \cdot 0.47(0.15\rho^2 + 0.05\rho + 1)$
Simulation Conversion Factor:	N/A
Average Roof Plane Transmittance:	37%
Coefficient of Variation (see figure d):	8%
Standard Deviation across Roof Plane:	3.0%

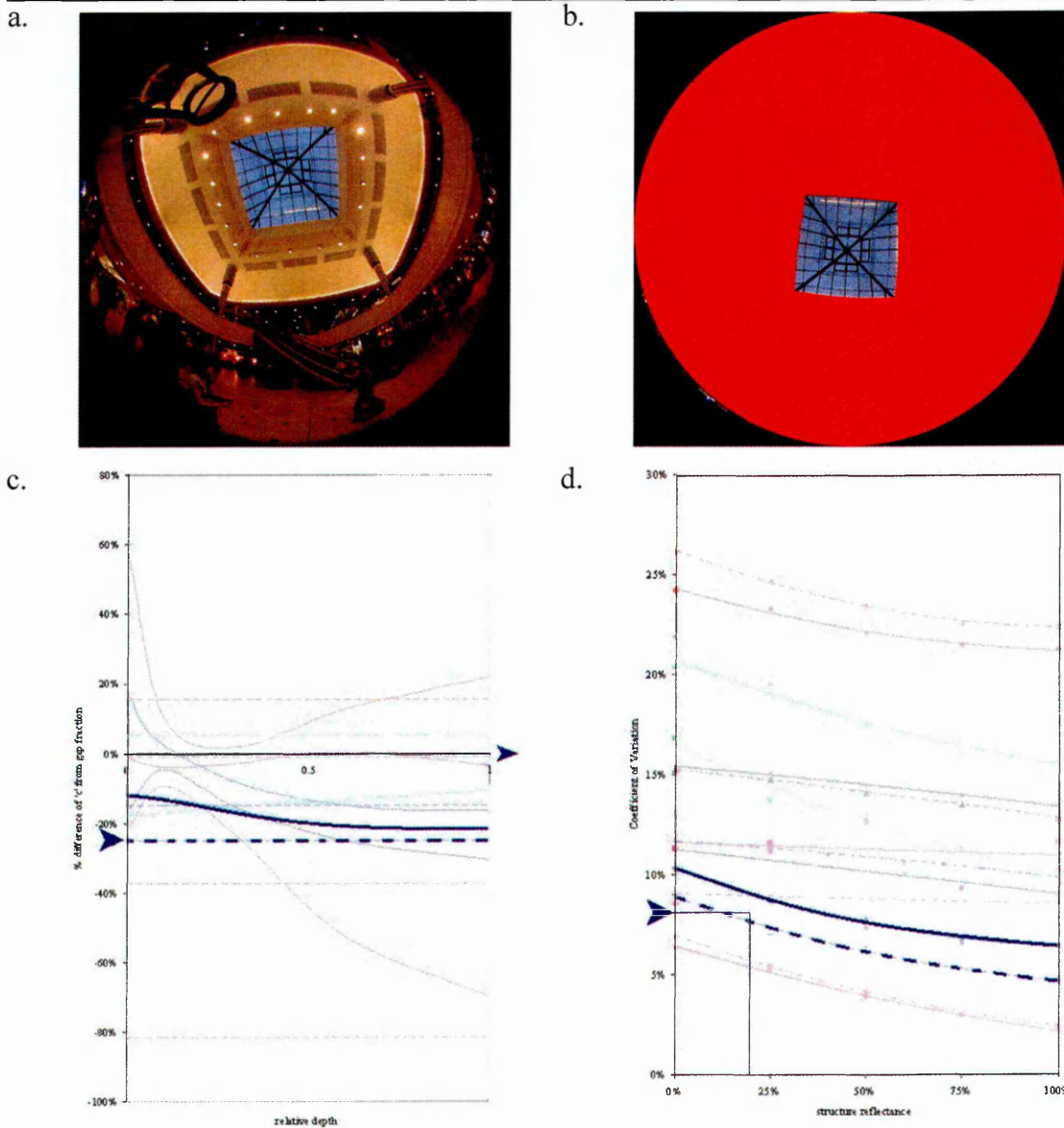


Figure 7-18: Meadowhall B: Box; Process to Obtain Average Roof Plane Transmittance; a. View of Roof; b. Hemispherical View of Roof; c. Difference between c and gap fraction at varying relative depth; d. Coefficient of Variation for each Roof.

Name ID:	Meadowhall C
Roof Type (see figure a):	Dome (2)
Glazing Transmittance (T_g):	78% (clear double glazing)
Structure Reflectance (ρ):	20% (green paint)
Depth of Photograph (x):	14m
Width of Skylight (w):	12m
Relative Depth:	1.17
Gap Fraction (see figure b):	0.64
Image Conversion Factor:	N/A
Deriving c from Gap Fraction (see figure c):	$\times 0.97 = 0.62$
Insertion of c to equation:	$T_{ROOF} = T_g 0.62 (0.05 \rho^2 + 0.05 \rho + 1)$
Simulation Conversion Factor:	N/A
Average Roof Plane Transmittance:	49%
Coefficient of Variation (see figure d):	17%
Standard Deviation across Roof Plane:	8.3%

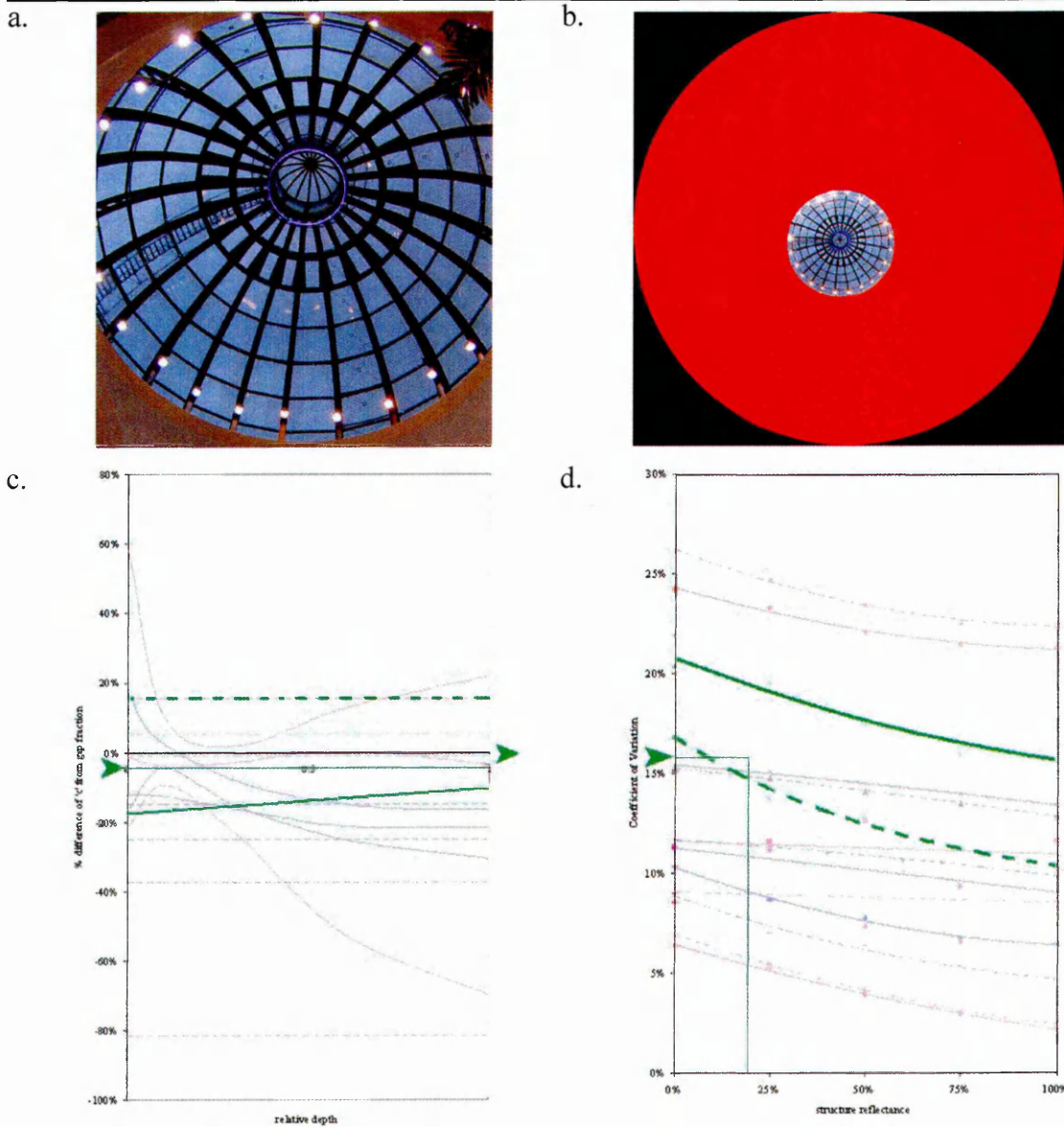


Figure 7-19: Meadowhall C: Box; Process to Obtain Average Roof Plane Transmittance; a. View of Roof; b. Hemispherical View of Roof; c. Difference between c and gap fraction at varying relative depth; d. Coefficient of Variation for each Roof.

Name ID:	Meadowhall D
Roof Type (see figure a):	Barrel (Hybrid A-Frame & Dome2)
Glazing Transmittance (T_g):	89% (clear single glazing)
Structure Reflectance (ρ):	20% (green paint)
Depth of Photograph (x):	1m
Width of Skylight (w):	6m
Relative Depth:	0.17
Gap Fraction (see figure b):	0.74
Image Conversion Factor:	N/A
Deriving c from Gap Fraction (see figure c):	$\times 0.92 = 0.68$
Insertion of c to equation:	$T_{ROOF} = T_g 0.68(0.075\rho^2 + 0.075\rho + 1)$
Simulation Conversion Factor:	N/A
Average Roof Plane Transmittance:	62%
Coefficient of Variation (see figure d):	13%
Standard Deviation across Roof Plane:	8.0%

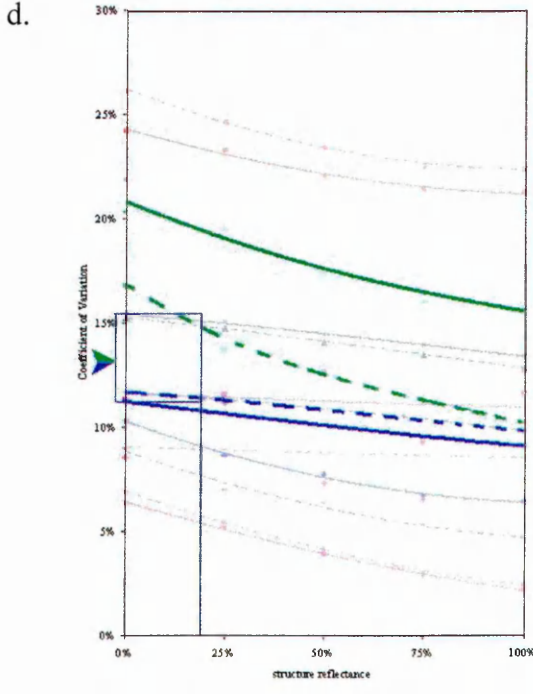
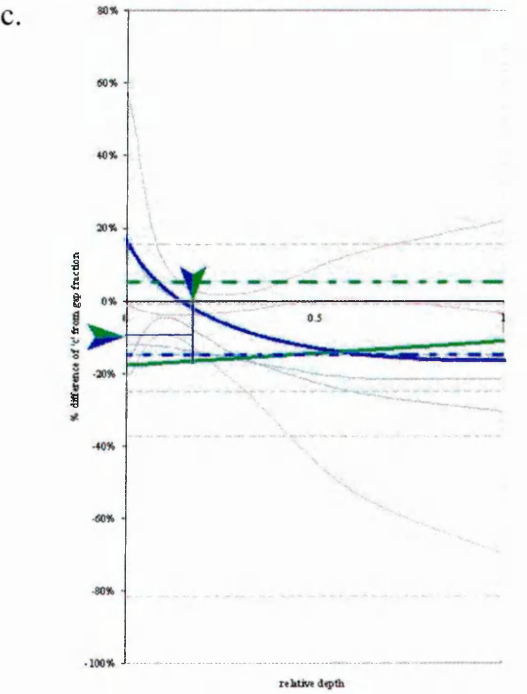
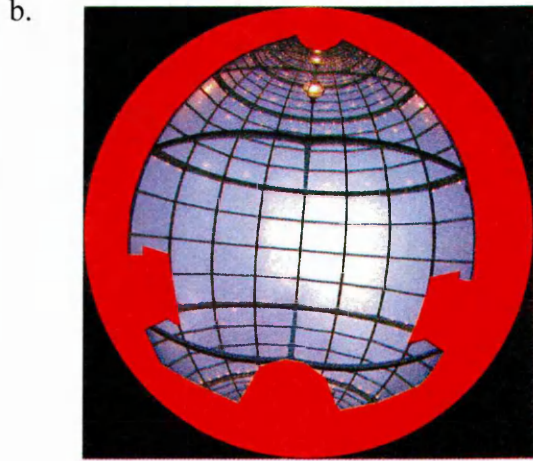


Figure 7-20: Meadowhall D: Box; Process to Obtain Average Roof Plane Transmittance; a. View of Roof; b. Hemispherical View of Roof; c. Difference between c and gap fraction at varying relative depth; d. Coefficient of Variation for each Roof.

Name ID:	Meadowhall E
Roof Type (see figure a):	Lantern (Hybrid Pyramid & Dome2)
Glazing Transmittance (T_g):	78% (clear double glazing)
Structure Reflectance (ρ):	20% (green paint)
Depth of Photograph (x):	11m
Width of Skylight (w):	8m
Relative Depth:	1.375
Gap Fraction (see figure b):	0.41
Image Conversion Factor:	N/A
Deriving c from Gap Fraction (see figure c):	$\times 0.89 = 0.36$
Insertion of c to equation:	$T_{ROOF} = T_g 0.36(0.1\rho^2 + 0.05\rho + 1)$
Simulation Conversion Factor:	N/A
Average Roof Plane Transmittance:	28%
Coefficient of Variation (see figure d):	12.5%
Standard Deviation across Roof Plane:	3.5%

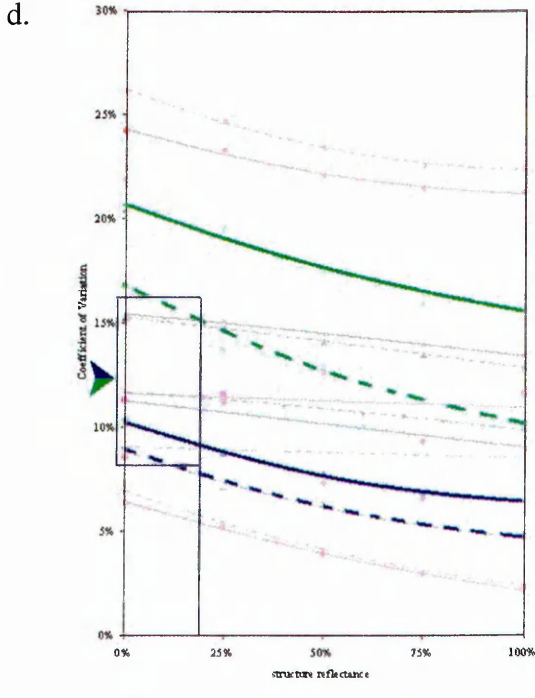
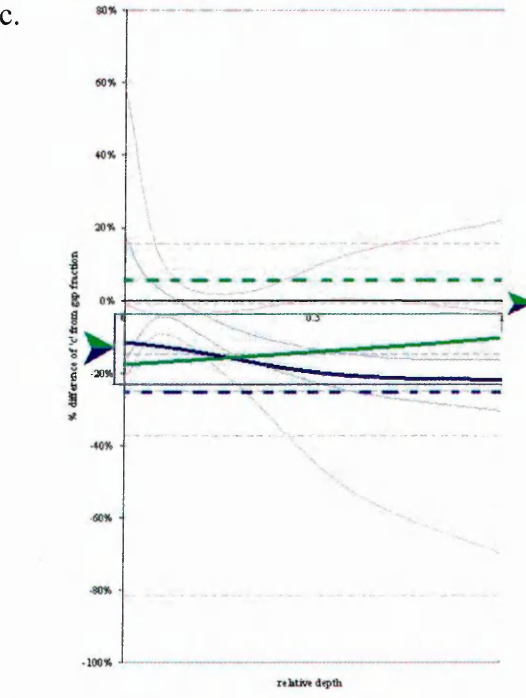
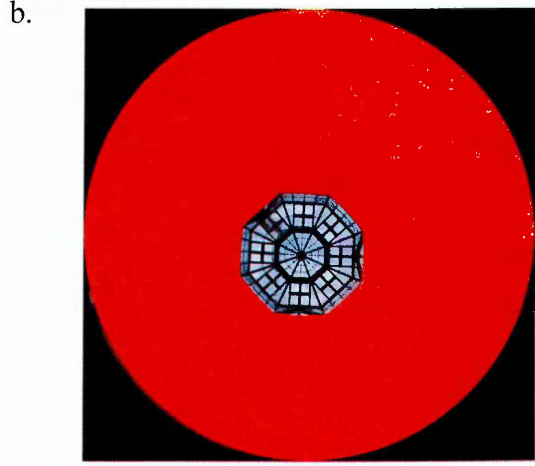
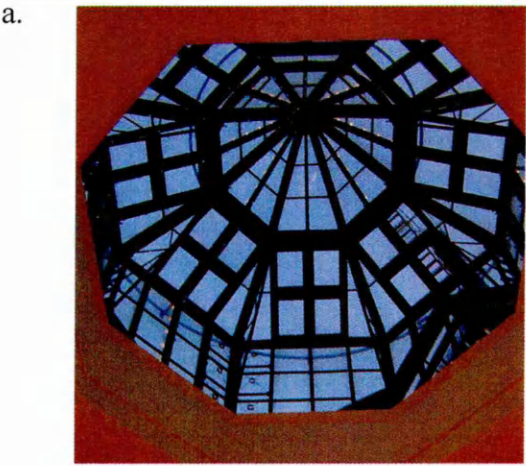


Figure 7-21: Meadowhall E: Box; Process to Obtain Average Roof Plane Transmittance; a. View of Roof; b. Hemispherical View of Roof; c. Difference between c and gap fraction at varying relative depth; d. Coefficient of Variation for each Roof.

Name ID:	Meadowhall F
Roof Type (see figure a):	Octagon (closest match Pyramid)
Glazing Transmittance (T_g):	78% (clear double glazing)
Structure Reflectance (ρ):	79% (brushed aluminium)
Depth of Photograph (x):	14m
Width of Skylight (w):	14m
Relative Depth:	1
Gap Fraction (see figure b):	0.62
Image Conversion Factor:	N/A
Deriving c from Gap Fraction (see figure c):	$x \cdot 0.78 = 0.48$
Insertion of c to equation:	$T_{ROOF} = T_g \cdot 0.48(0.15\rho^2 + 0.05\rho + 1)$
Simulation Conversion Factor:	N/A
Average Roof Plane Transmittance:	42%
Coefficient of Variation (see figure d):	6%
Standard Deviation across Roof Plane:	2.5%

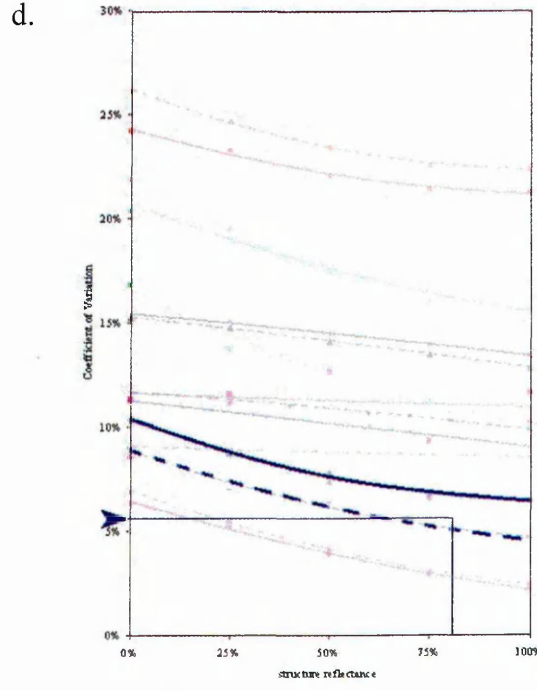
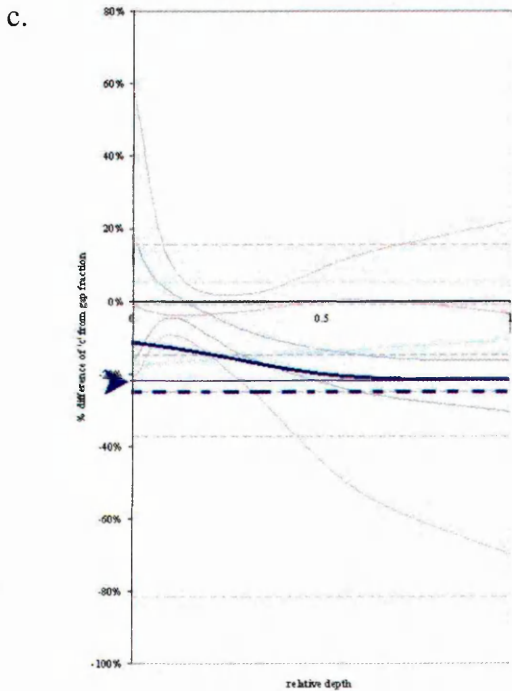
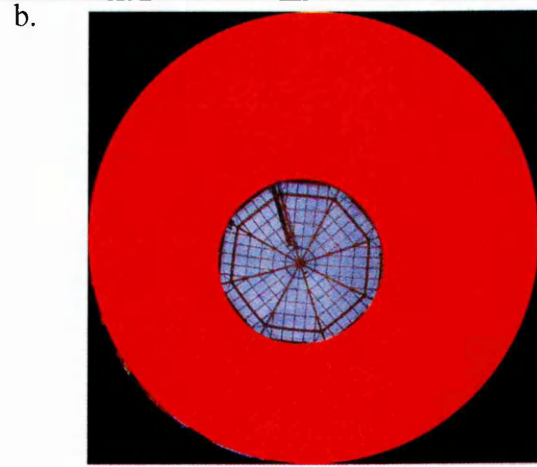
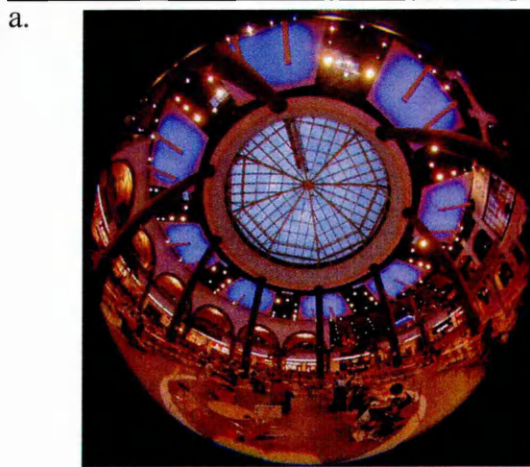


Figure 7-22: Meadowhall F: Box; Process to Obtain Average Roof Plane Transmittance; a. View of Roof; b. Hemispherical View of Roof; c. Difference between c and gap fraction at varying relative depth; d. Coefficient of Variation for each Roof.

Name ID:	Showroom Cinema
Roof Type (see figure a):	Pyramid
Glazing Transmittance (T_g):	78% (clear double glazing)
Structure Reflectance (ρ):	70% (white paint)
Depth of Photograph (x):	10m
Width of Skylight (w):	6m
Relative Depth:	1.67
Gap Fraction (see figure b):	0.73
Image Conversion Factor:	N/A
Deriving c from Gap Fraction (see figure c):	$x \ 0.77 = 0.56$
Insertion of c to equation:	$T_{ROOF} = T_g 0.56(0.15\rho^2 + 0.05\rho + 1)$
Simulation Conversion Factor:	N/A
Average Roof Plane Transmittance:	48%
Coefficient of Variation (see figure d):	6%
Standard Deviation across Roof Plane:	2.9%

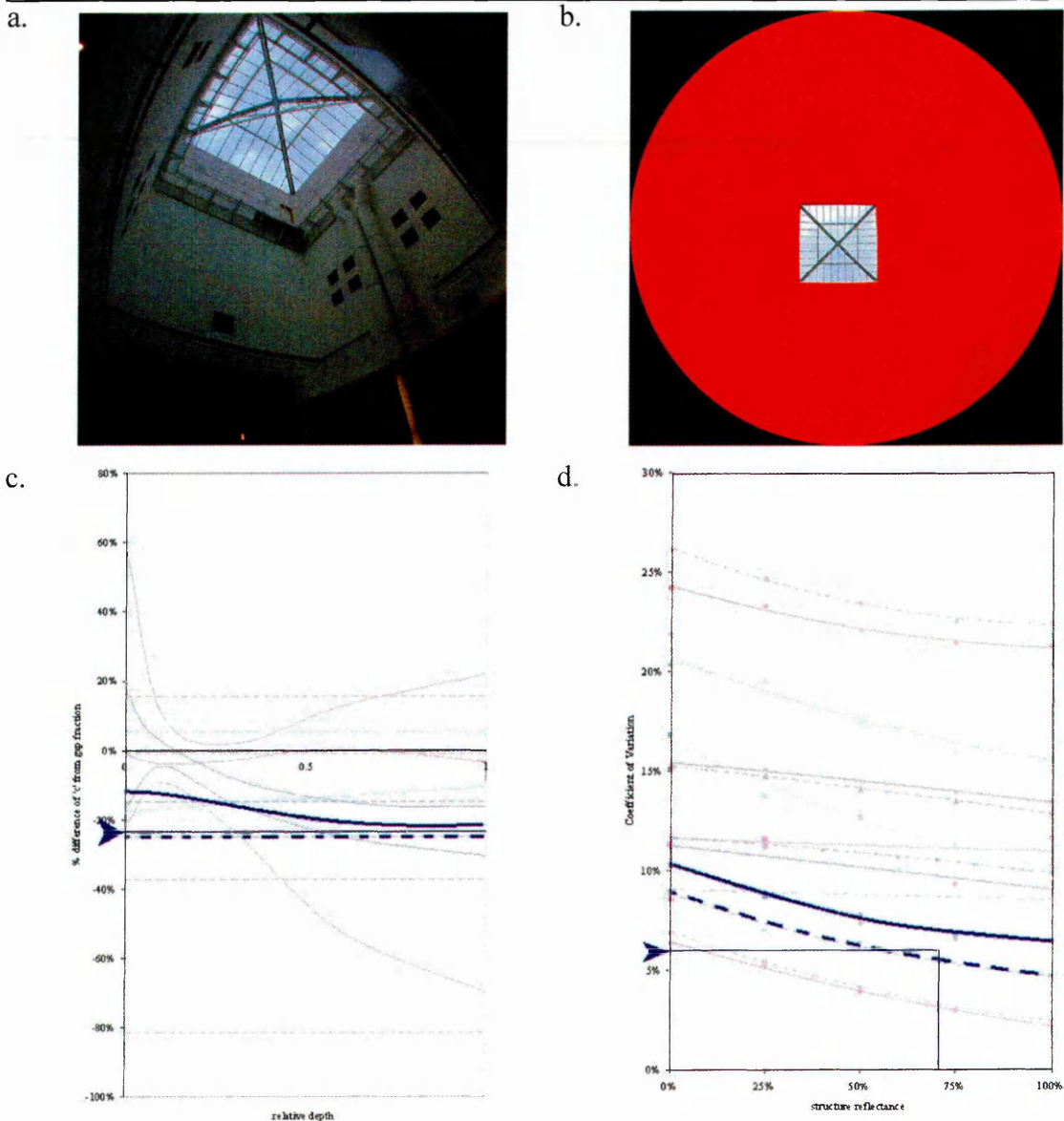


Figure 7-23: Showroom Cinema: Box; Process to Obtain Average Roof Plane Transmittance; a. View of Roof; b. Hemispherical View of Roof; c. Difference between c and gap fraction at varying relative depth; d. Coefficient of Variation for each Roof.

Name ID:	Natwest Offices
Roof Type (see figure a):	Monopitch
Glazing Transmittance (T_g):	78% (clear double glazing)
Structure Reflectance (ρ):	70% (white paint)
Depth of Photograph (x):	14m
Width of Skylight (w):	8m
Relative Depth:	1.75
Gap Fraction (see figure b):	0.68
Image Conversion Factor:	N/A
Deriving c from Gap Fraction (see figure c):	$\times 0.87 = 0.59$
Insertion of c to equation:	$T_{ROOF} = T_g 0.59(0.05\rho^2 + 0.05\rho + 1)$
Simulation Conversion Factor:	0.93
Average Roof Plane Transmittance:	45%
Coefficient of Variation (see figure d):	21%
Standard Deviation across Roof Plane:	9.5%

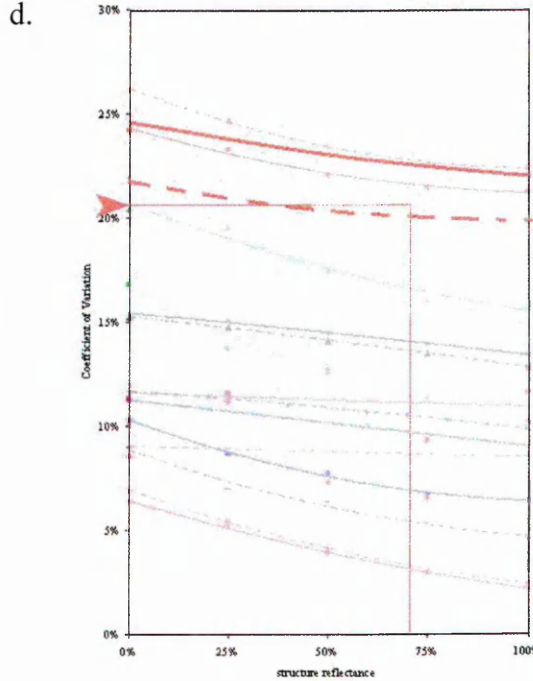
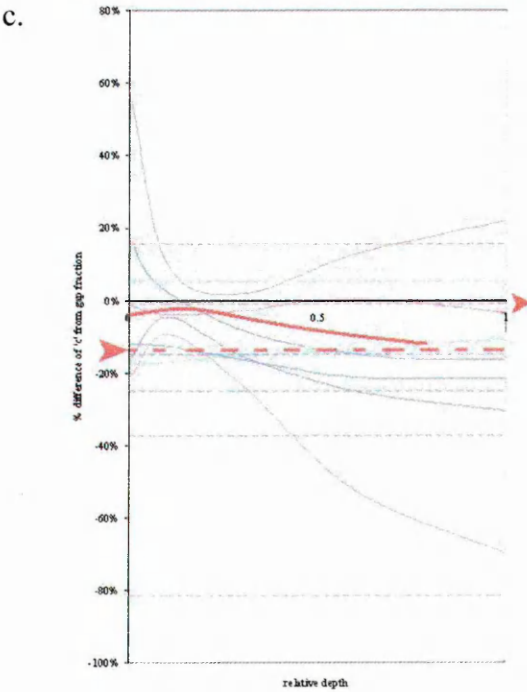


Figure 7-24: Natwest Offices: Box; Process to Obtain Average Roof Plane Transmittance; a. View of Roof; b. Hemispherical View of Roof; c. Difference between c and gap fraction at varying relative depth; d. Coefficient of Variation for each Roof.

Name ID:	Orchard Square shopping Centre
Roof Type (see figure a):	A-Frame
Glazing Transmittance (T_g):	85% (single glazed diffusing glass)
Structure Reflectance (ρ):	15% (dark green painted steel)
Depth of Photograph (x):	7m
Width of Skylight (w):	4m
Relative Depth:	1.75
Gap Fraction (see figure b):	0.62
Image Conversion Factor:	$\times 1.06 = 0.66$
Deriving c from Gap Fraction (see figure c):	$\times 0.87 = 0.57$
Insertion of c to equation:	$T_{ROOF} = T_g 0.57(0.1\rho^2 + 0.1\rho + 1)$
Simulation Conversion Factor:	1.09
Average Roof Plane Transmittance:	54%
Coefficient of Variation (see figure d):	11.5%
Standard Deviation across Roof Plane:	6.2%

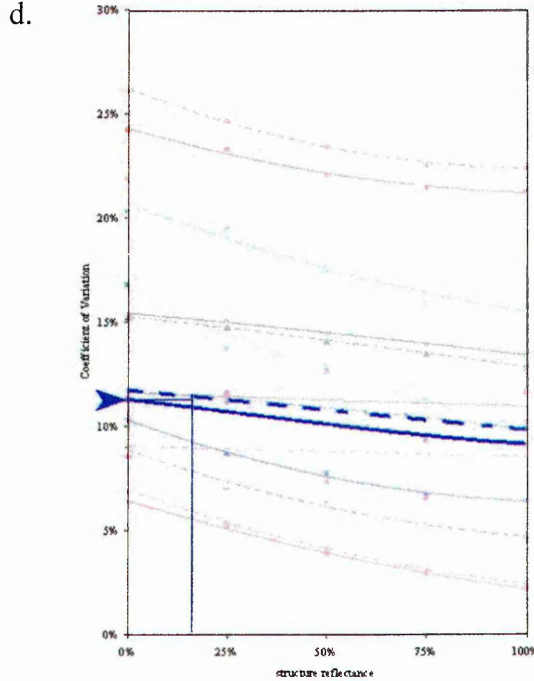
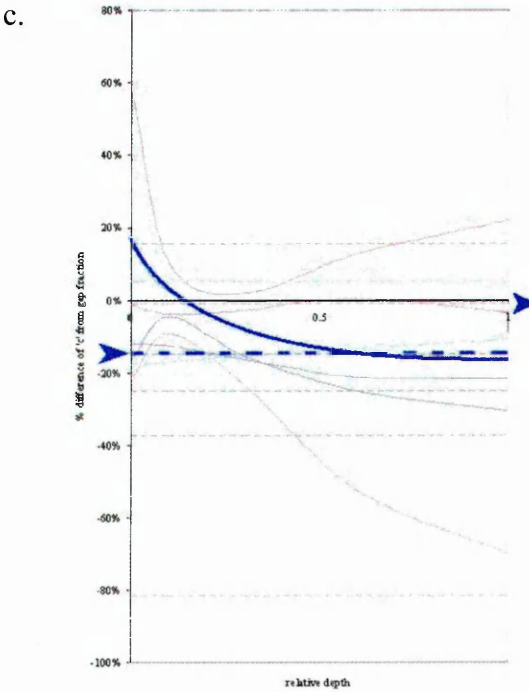
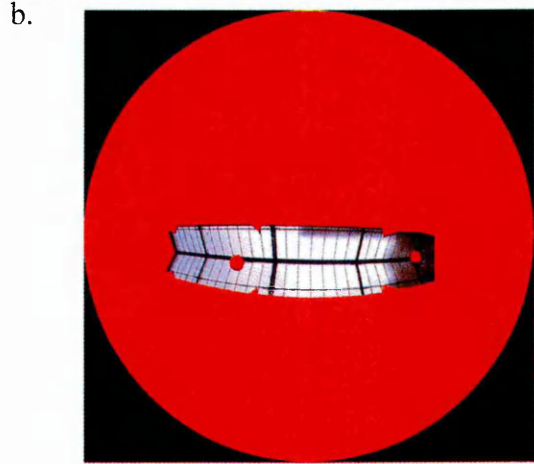


Figure 25: Orchard Square Centre: Box; Process to Obtain Average Roof Plane Transmittance; a. View of Roof; b. Hemispherical View of Roof; c. Difference between c and gap fraction at varying relative depth; d. Coefficient of Variation for each Roof.

Name ID:	Blue Moon Cafe
Roof Type (see figure a):	Hybrid A-frame and Pyramid
Glazing Transmittance (T_g):	86 % (triple glazed polycarbonate)
Structure Reflectance (ρ):	70% (white painted timber and iron)
Depth of Photograph (x):	8m
Width of Skylight (w):	3m
Relative Depth:	2.67
Gap Fraction (see figure b):	0.71
Image Conversion Factor:	N/A
Deriving c from Gap Fraction (see figure c):	$x \cdot 0.8 = 0.57$
Insertion of c to equation:	$T_{ROOF} = T_g \cdot 0.57 (0.125\rho^2 + 0.075\rho + 1)$
Simulation Conversion Factor:	N/A
Average Roof Plane Transmittance:	55%
Coefficient of Variation (see figure d):	8%
Standard Deviation across Roof Plane:	4.4%

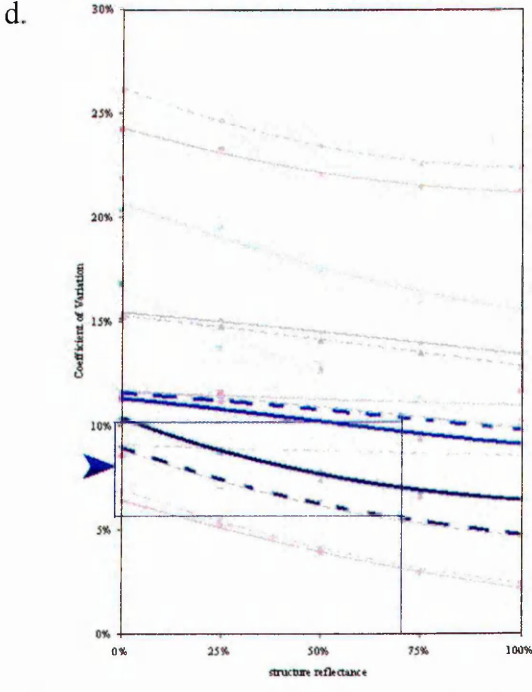
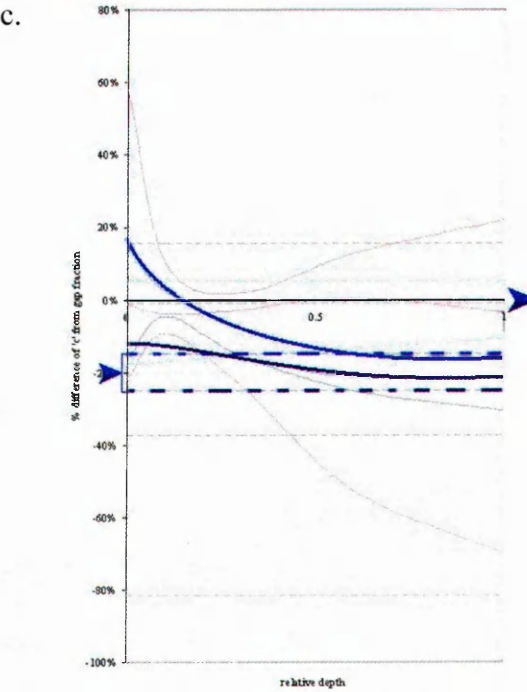
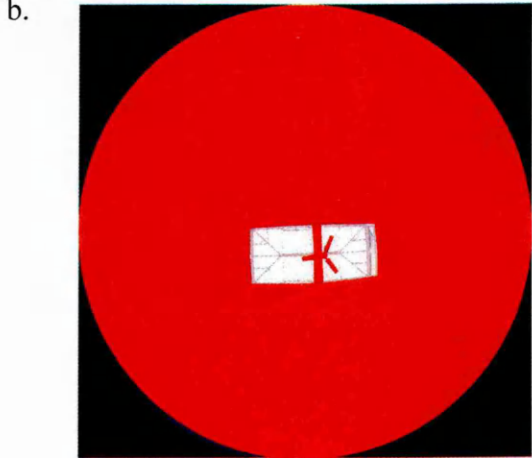


Figure 7-26: Blue Moon Cafe: Box; Process to Obtain Average Roof Plane Transmittance; a. View of Roof; b. Hemispherical View of Roof; c. Difference between c and gap fraction at varying relative depth; d. Coefficient of Variation for each Roof.

Name ID:	Millennium Galleries A
Roof Type (see figure a):	Barrel (hybrid Dome2 & A-frame)
Glazing Transmittance (T_g):	50% (glass block)
Structure Reflectance (ρ):	60% (exposed white concrete)
Depth of Photograph (x):	5m
Width of Skylight (w):	4.5m
Relative Depth:	1.11
Gap Fraction (see figure b):	0.42
Image Conversion Factor:	N/A
Deriving c from Gap Fraction (see figure c):	$\times 0.88 = 0.37$
Insertion of c to equation:	$T_{ROOF} = T_g 0.37(0.075\rho^2 + 0.075\rho + 1)$
Simulation Conversion Factor:	N/A
Average Roof Plane Transmittance:	20%
Coefficient of Variation (see figure d):	12%
Standard Deviation across Roof Plane:	2.4%

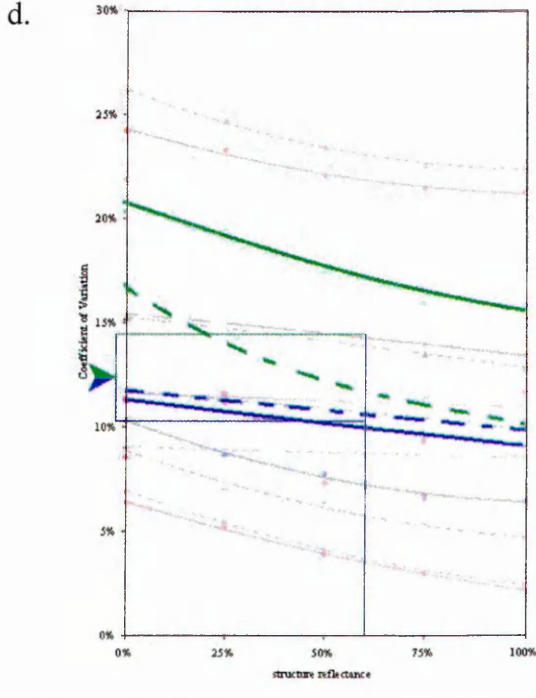
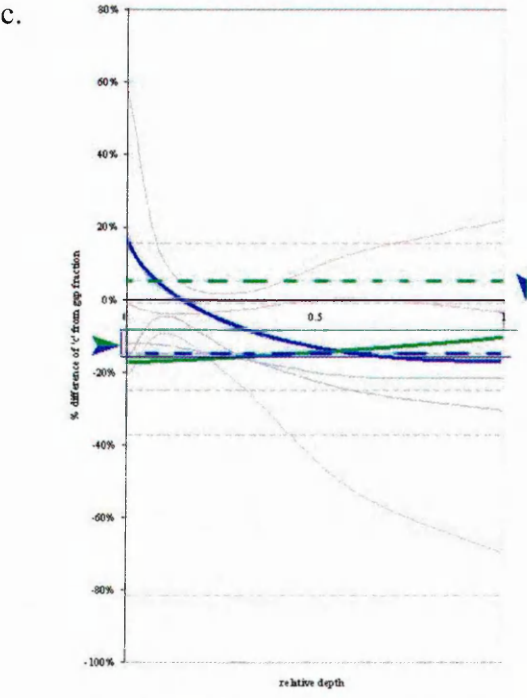
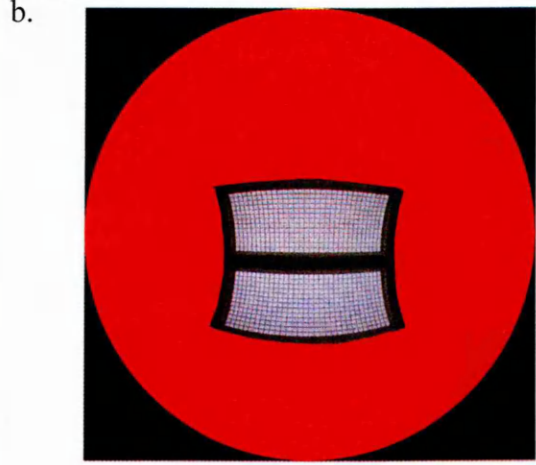
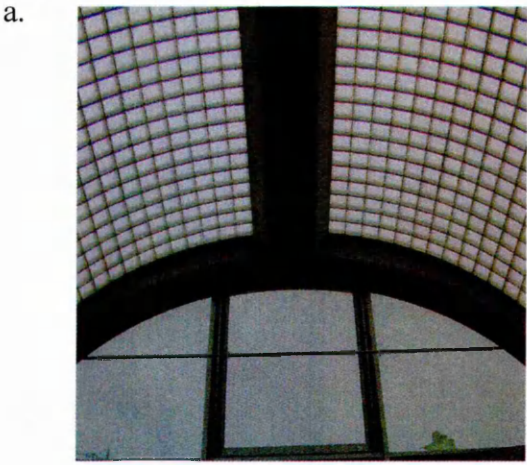


Figure 7-27: Millennium Galleries A: Box; Process to Obtain Average Roof Plane Transmittance; a. View of Roof; b. Hemispherical View of Roof; c. Difference between c and gap fraction at varying relative depth; d. Coefficient of Variation for each Roof.

Name ID:	Millennium Galleries B
Roof Type (see figure a):	Flat
Glazing Transmittance (T_g):	50% (glass blocks)
Structure Reflectance (ρ):	30% (exposed steel)
Depth of Photograph (x):	5m
Width of Skylight (w):	8m
Relative Depth:	0.63
Gap Fraction (see figure b):	0.59
Image Conversion Factor:	N/A
Deriving c from Gap Fraction (see figure c):	$x \cdot 0.76 = 0.45$
Insertion of c to equation:	$T_{\text{ROOF}} = T_g \cdot 0.45(0.05\rho^2 + 0.15\rho + 1)$
Simulation Conversion Factor:	N/A
Average Roof Plane Transmittance:	24%
Coefficient of Variation (see figure d):	14.5%
Standard Deviation across Roof Plane:	3.4%

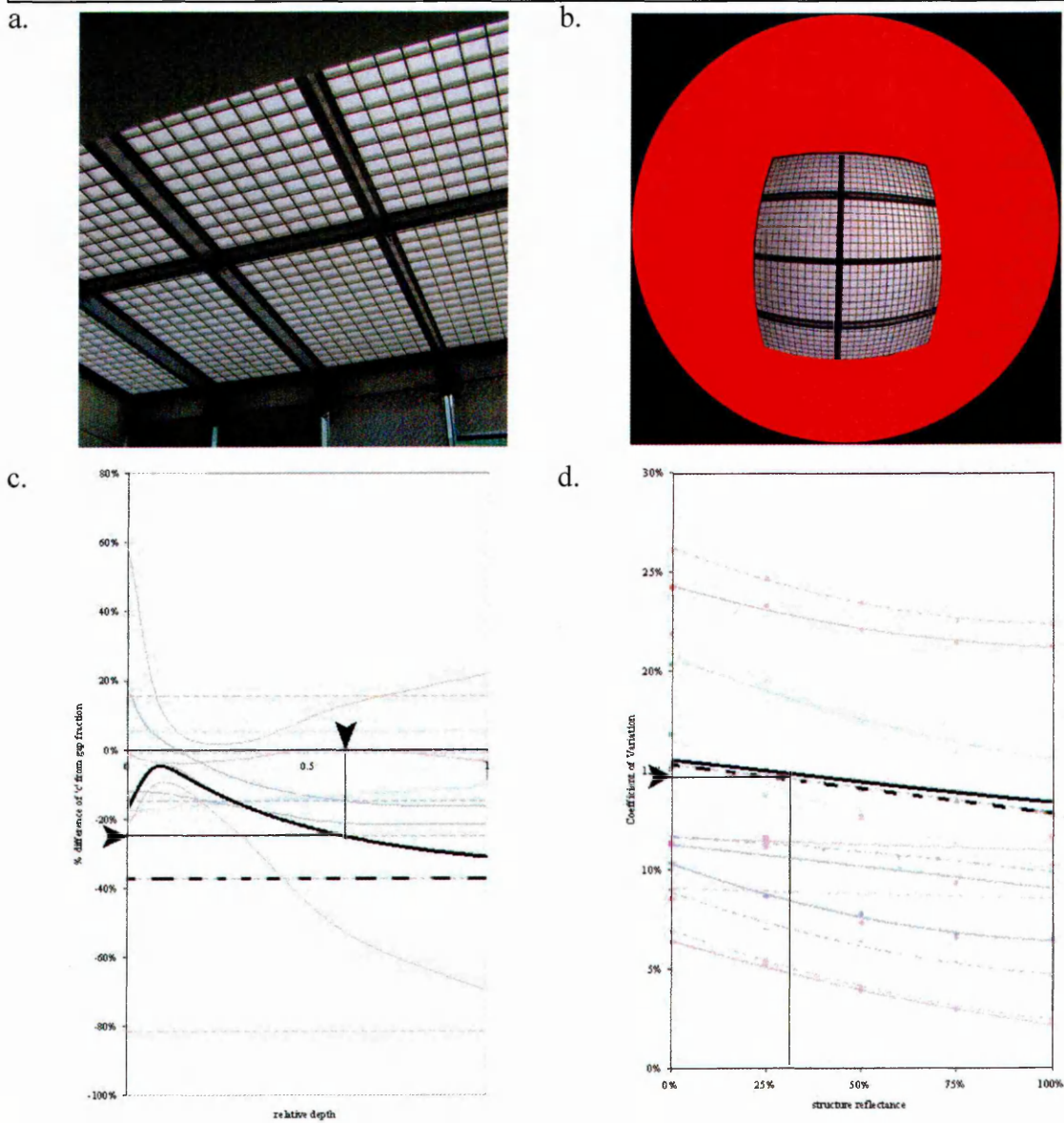


Figure 7-28: Millennium Galleries B: Box; Process to Obtain Average Roof Plane Transmittance; a. View of Roof; b. Hemispherical View of Roof; c. Difference between c and gap fraction at varying relative depth; d. Coefficient of Variation for each Roof.

Name ID:	Winter Gardens
Roof Type (see figure a):	Arch (closest match A-frame)
Glazing Transmittance (T_g):	78% (clear double glazing)
Structure Reflectance (ρ):	34% (glue laminated larch)
Depth of Photograph (x):	6m
Width of Skylight (w):	22m
Relative Depth:	0.27
Gap Fraction (see figure b):	0.55
Image Conversion Factor:	$\times 1.22 = 0.67$
Deriving c from Gap Fraction (see figure c):	$\times 0.94 = 0.63$
Insertion of c to equation:	$T_{ROOF} = T_g 0.63 (0.1\rho^2 + 0.1\rho + 1)$
Simulation Conversion Factor:	N/A
Average Roof Plane Transmittance:	51%
Coefficient of Variation (see figure d):	10.5%
Standard Deviation across Roof Plane:	5.4%

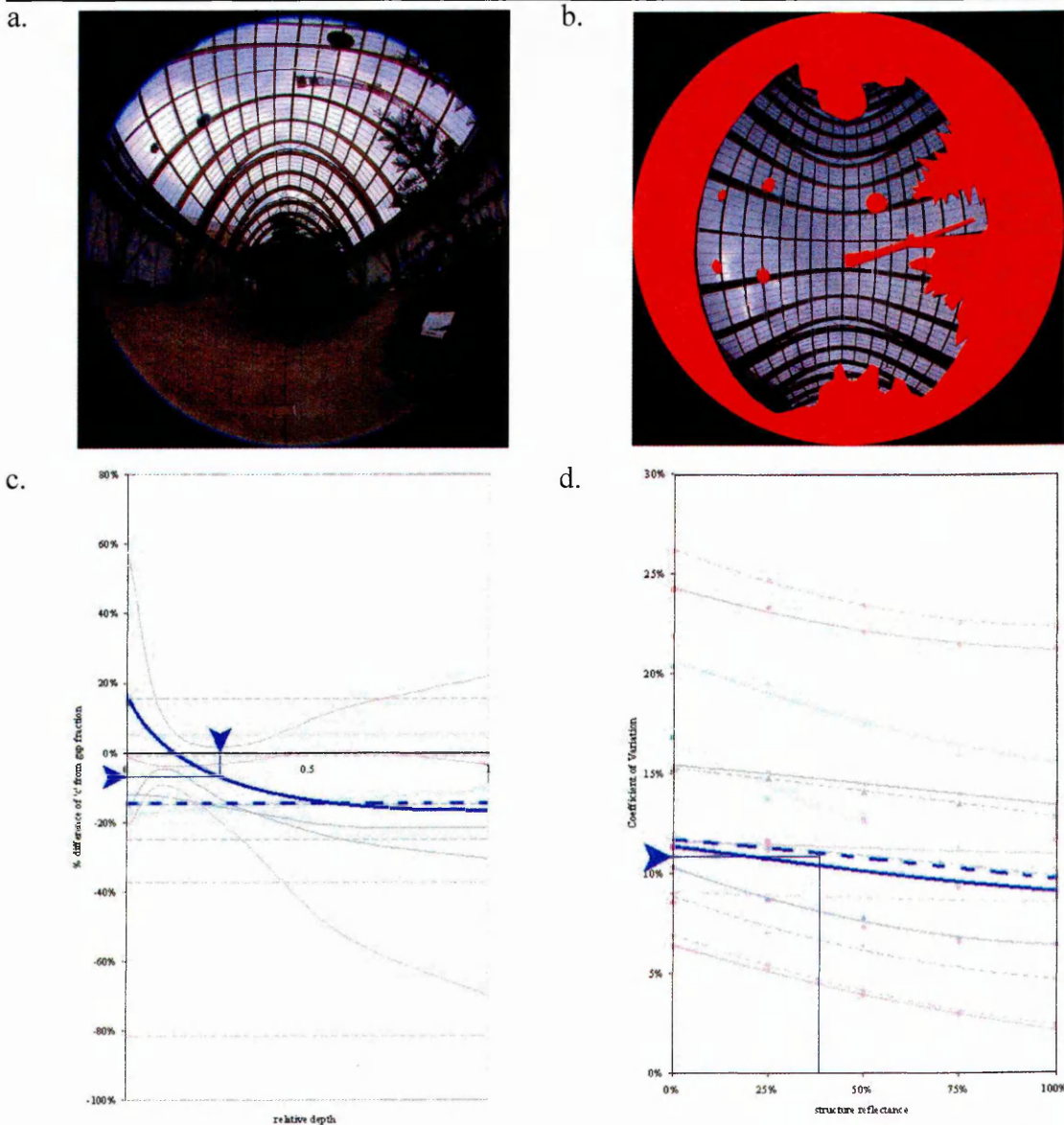


Figure 7-29: Winter Gardens: Box; Process to Obtain Average Roof Plane Transmittance; a. View of Roof; b. Hemispherical View of Roof; c. Difference between c and gap fraction at varying relative depth; d. Coefficient of Variation for each Roof.

Name ID:	Sheffield Hallam
Roof Type (see figure a):	Stepped Monopitch
Glazing Transmittance (T_g):	78% (clear double glazing)
Structure Reflectance (ρ):	58% (off white paint)
Depth of Photograph (x):	0m
Width of Skylight (w):	6m
Relative Depth:	0
Gap Fraction (see figure b):	0.45
Image Conversion Factor:	$\times 1.25 = 0.56$
Deriving c from Gap Fraction (see figure c):	$\times 0.96 = 0.54$
Insertion of c to equation:	$T_{ROOF} = T_g 0.54(0.05\rho^2 + 0.05\rho + 1)$
Simulation Conversion Factor:	0.93
Average Roof Plane Transmittance:	41%
Coefficient of Variation (see figure d):	21%
Standard Deviation across Roof Plane:	8.6%

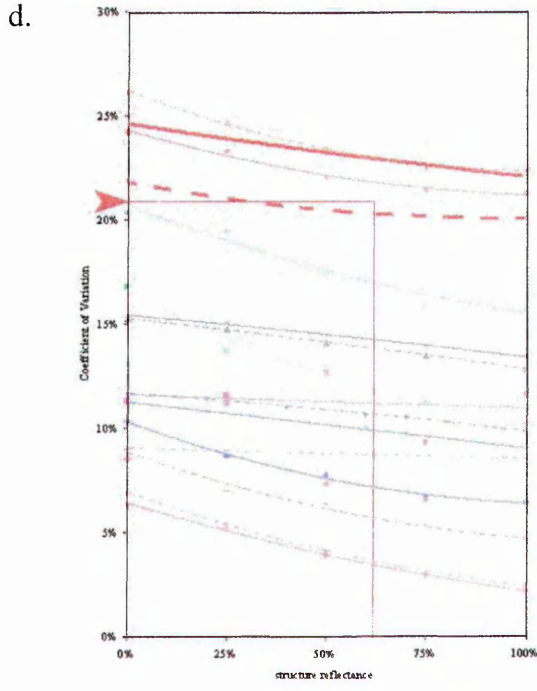
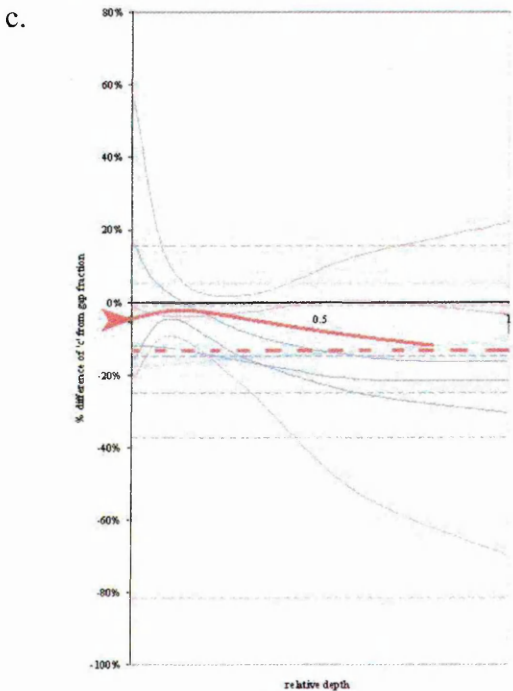
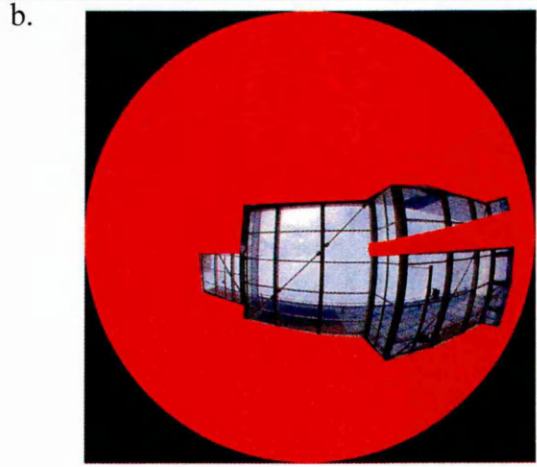


Figure 7-30: Sheffield Hallam: Box; Process to Obtain Average Roof Plane Transmittance; a. View of Roof; b. Hemispherical View of Roof; c. Difference between c and gap fraction at varying relative depth; d. Coefficient of Variation for each Roof.

Name ID:	TK Maxx
Roof Type (see figure a):	Partial Pyramid
Glazing Transmittance (T_g):	78% (clear double glazing)
Structure Reflectance (ρ):	70% (white painted steel)
Depth of Photograph (x):	8m
Width of Skylight (w):	8m
Relative Depth:	1
Gap Fraction (see figure b):	0.46
Image Conversion Factor:	N/A
Deriving c from Gap Fraction (see figure c):	$x \ 0.79 = 0.36$
Insertion of c to equation:	$T_{ROOF} = T_g 0.36(0.15\rho^2 + 0.05\rho + 1)$
Simulation Conversion Factor:	N/A
Average Roof Plane Transmittance:	31%
Coefficient of Variation (see figure d):	6%
Standard Deviation across Roof Plane:	1.9%

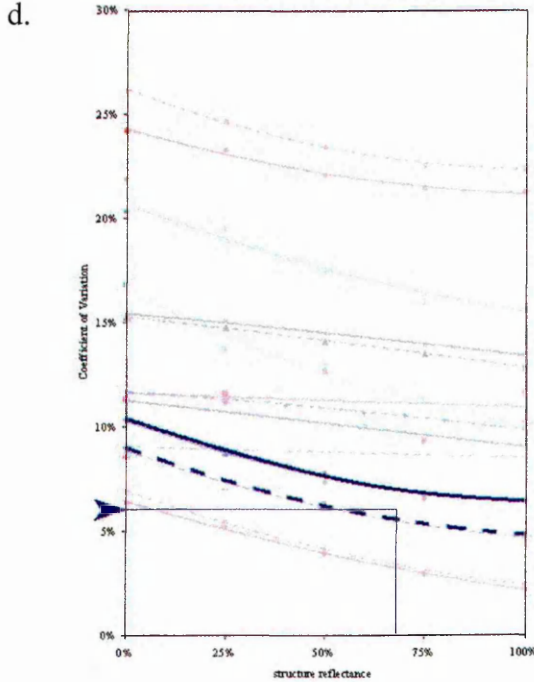
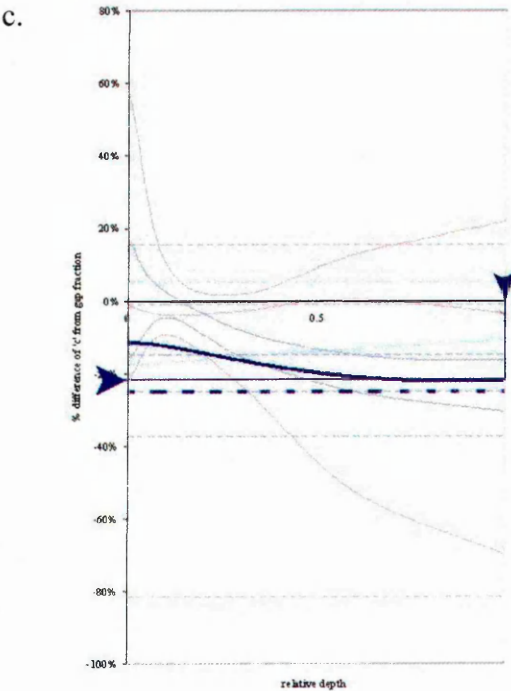
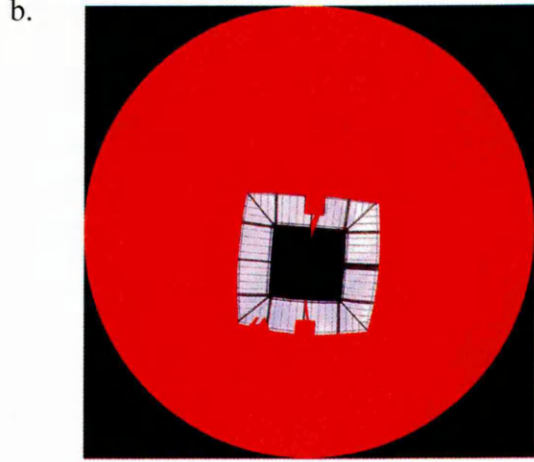
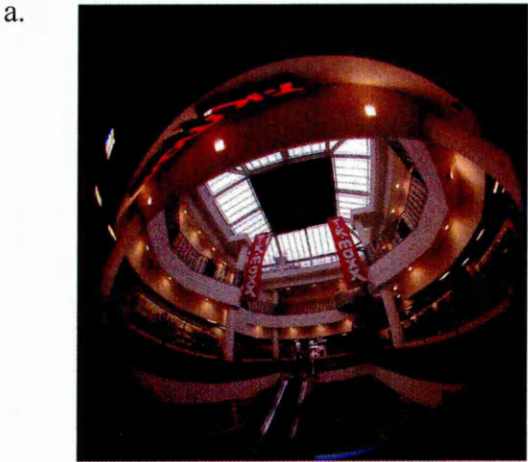


Figure 7-31: TK Maxx: Box; Process to Obtain Average Roof Plane Transmittance; a. View of Roof; b. Hemispherical View of Roof; c. Difference between c and gap fraction at varying relative depth; d. Coefficient of Variation for each Roof.

7.4.3 Discussion

The described method returned average roof plane transmittance values with standard deviations for the fifteen roofs examined. These can be seen in Table 7-3, which are ranked in order of overall roof transmittance.

Table 7-3: Transmittance results for the 15 roofs examined

Roof Name	Type	T_g	ρ	T_{ROOF}	St.Dev
Meadowhall D	barrel	89%	20%	62%	8.0%
Blue Moon Cafe	hipped a-frame	86%	70%	55%	4.4%
Orchard Square	a-frame	85%	15%	54%	6.2%
Winter Gardens	arched	78%	34%	51%	5.4%
Meadowhall C	dome	78%	20%	49%	8.3%
Meadowhall A	a-frame	78%	20%	48%	5.1%
Showroom Cinema	pyramid	78%	70%	48%	2.9%
Natwest	monopitch	78%	70%	45%	9.5%
Meadowhall F	octagon	78%	79%	42%	2.5%
Sheffield Hallam	stepped monopitch	78%	58%	41%	8.6%
Meadowhall B	pyramid	78%	20%	37%	3.0%
TK Maxx	partial pyramid	78%	70%	31%	1.9%
Meadowhall E	lantern	78%	20%	28%	3.5%
Millennium B	flat	50%	30%	24%	3.4%
Millennium A	barrel	50%	60%	20%	2.4%

The skylights studied had a range of average roof plane transmittance from 20-62%. It can be seen that overall transmittance was heavily influenced by the value of glazing transmittance inputted. The results were recalculated with fixed values for structure reflectance and glazing transmittance so as to make direct comparisons of the roof arrangements. A value of 70% was chosen for the reflectance (to represent a standard white finish), and 78% for the glazing (clear double glazing). The results can be seen in Table 7-4.

The range of average roof plane transmittance has reduced to 30-58%. Nevertheless, this is a clear demonstration of the potential impact of the roof arrangement on transmittance (a relative difference of approximately 100% between range extents).

Table 7-4: Transmittance results for the 15 roofs examined with $\rho = 70\%$ and $T_g = 78\%$

Roof Name	Type	T_{ROOF}	St.Dev
Meadowhall D	barrel	58%	7.0%
Winter Gardens	arched	55%	5.5%
Orchard Square	a-frame	54%	5.4%
Meadowhall A	a-frame	52%	5.7%
Meadowhall C	dome	51%	6.6%
Blue Moon Cafe	hipped a-frame	50%	4.0%
Showroom Cinema	pyramid	48%	2.9%
Natwest	monopitch	45%	9.5%
Meadowhall F	octagon	42%	2.5%
Sheffield Hallam	stepped monopitch	42%	8.8%
Meadowhall B	pyramid	41%	2.9%
Millennium B	flat	40%	5.2%
Millennium A	barrel	31%	3.4%
TK Maxx	partial pyramid	31%	1.9%
Meadowhall E	lantern	30%	2.7%

Results from the photoanalysis method were compared to output from SkyVision. Once more, an element of intuition was applied in roof type selection within SkyVision. Clear double glazing and structure with 0% reflectance were considered. The results are shown in Table 7-5.

Table 7-5: SkyVision output, together with difference from the photoanalysis method

Roof	SkyVision	Photoanalysis Method	% Difference
Meadowhall A	42%	47%	-10.0%
Meadowhall B	41%	37%	10.2%
Meadowhall C	44%	49%	-9.9%
Meadowhall D	49%	53%	-8.4%
Meadowhall E	25%	29%	-11.6%
Meadowhall F	43%	38%	13.4%
Showroom	48%	44%	10.1%
Natwest	n/a	46%	-
Orchard Square	45%	49%	-7.4%
Blue moon cafe	47%	45%	5.2%
Millennium Galleries A	30%	29%	1.8%
Millennium Galleries B	41%	35%	15.4%
Winter Gardens	47%	49%	-4.8%
Sheffield Hallam	n/a	42%	-
TK Maxx	31%	28%	9.0%
		MBE:	1.0%
		RMSE:	9.7%

Overall, the agreement between the two methods was good, with a RMSE of under 10%. This increases confidence in use of the photographic method to examine

existing roofs, although agreement with real measured data from these buildings would provide the best means of validation.

The entire process from image capture to final result was a rapid one. Total time spent per roof was typically under half an hour. Permission to take the photographs was granted in every instance by the building users. This is in sharp contrast to the lengthy logging periods, awkward experimental procedure and low chance of user permission in measuring illuminance within real buildings.

As with the application of any empirically derived data to subsequent situations, the condition that any result can only be a hypothetical approximation must be understood. Errors between calculated roof transmittance and actual roof transmittance can be classed into two categories; error intrinsic to the method, and error in its application. In the case of the former, it is appreciated that a simple method such as this one cannot hope to return values to the high degree of accuracy that complex and time intensive computer processes may be capable of. At present, there exist eight simple empirically derived roof equations linked to more comprehensive field studies in two real buildings. Whilst the agreement between the two buildings and the computer simulations was very encouraging, the assumption that this agreement will stretch to further roof types is just that. An advantage of the proposed method is that should further field data become available, it can be used to further calibrate and refine the findings already stated. Likewise, the simulation of further roof types e.g. barrel could remove some of the uncertainty of using crude hybrid roof methods. Such lateral thinking however does allow the user flexibility to examine potentially any roof form.

Error in application can be avoided by realising the limitations of the method. The standard deviation result obtained at TK Maxx of 1.9% is clearly erroneous (Figure 7-31 box). A brief glance at the roof form will reveal that the central blocked part of the roof will result in much greater contrast in distribution about the roof plane (Figure 7-31 a & b). As such, consideration of the roof as a pyramid is perhaps stretching the method too far. An alternative means could be to ignore the ceiling part in the HemiView calculation (painting it red) and consider the transmittance of the roof over a reduced area of opening.

As can be seen from Tables 7-2 and 7-3, a key strength of the method is the rapid comparison of many different roofs. Over time, and with the aforementioned creation of new roof types and further calibration, this could build into a large database of existing roofs. Combined with geographical location and archived typical illuminance levels (e.g. from IDMP stations), then yearly illuminance levels at roof plane level under overcast sky conditions for these roofs would be known. The entire process could be automated into one easy to use package as can be seen in the schematic diagram (Figure 7-32). With further experimentation as has been outlined in this thesis, the photographic technique could be extended to incorporate the effects of the well and thus illuminance levels on the various atrium surfaces (vertical and horizontal). The whole experiment could then be repeated to consider sky conditions other than overcast. This would leave a tool which could analyse a multitude of skylight types under different geometric settings and temporal conditions. This would provide a highly useful departure point for any designer considering incorporating an atrium into a scheme. More specialised and time intensive processes would then be pursued further along in the design process.

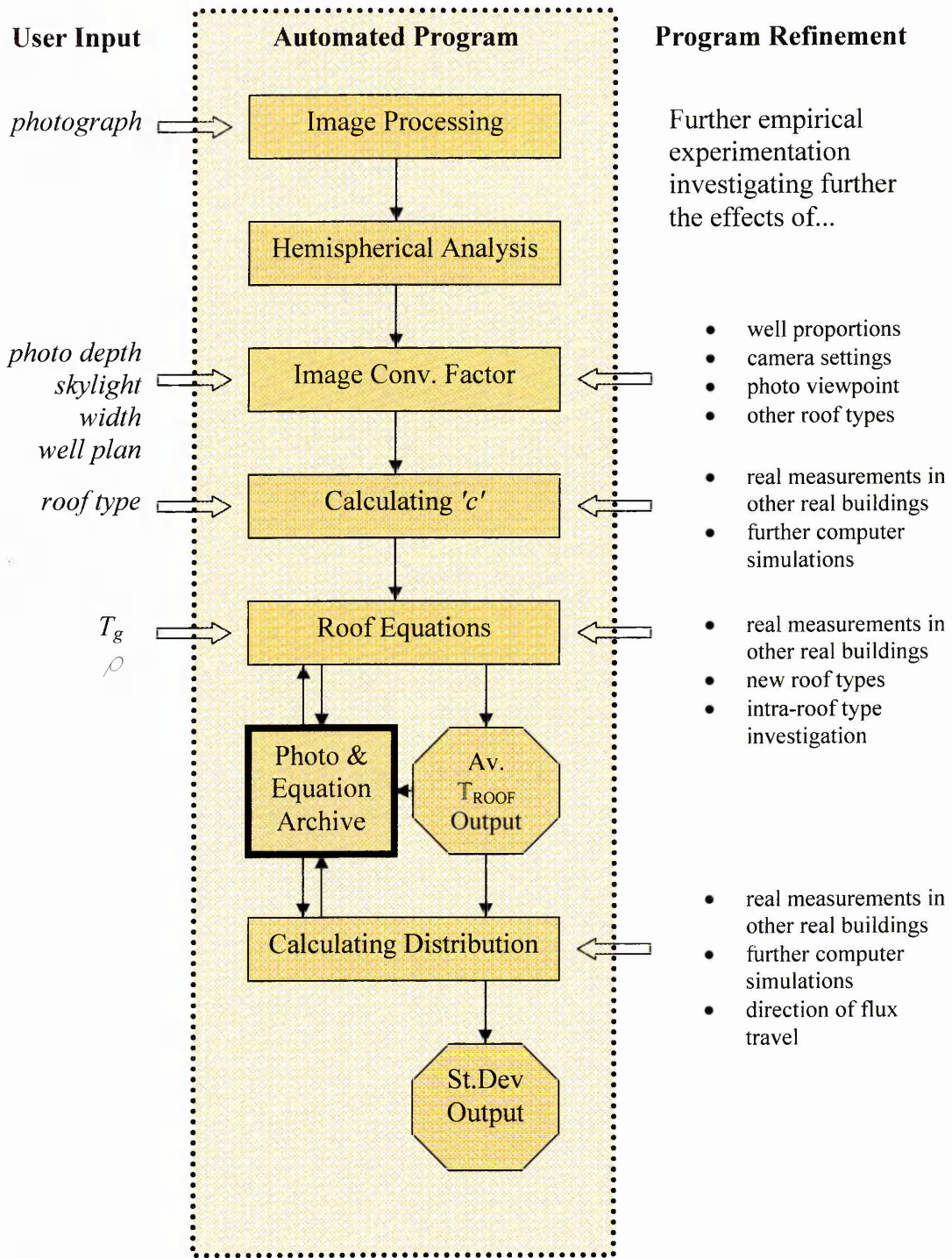


Figure 7-32: Schematic of possible automated program to assess roof transmittance using a photograph and simple input information

7.5 Conclusions

This chapter has taken the methodologies and findings from the two detailed case study buildings from Chapters 3-6, and extended the scope to include several more roof types, these being; pyramid, domes (two types), flat, waffle and sawtooth, as well as the existing monopitch and a-frame from the previous chapters. This was done through comparison of illuminance values obtained through computer simulation of standard roof types with generated images of the said roofs. Results were compared with output from SkyVision, and once large differences had been accounted for, the agreement was good. A method was described to relate the HemiView analysed photograph with empirically derived equations which described average roof plane transmittance. In the case of linear atria, a coarse image correction factor was suggested to account for compressed regions at the edges of the image. Without further experimentation it was not possible to tell whether such a factor needs application to more square skylights. Likewise, a simulation conversion factor was proposed for the a-frame and monopitch roofs where the difference between real and simulated illuminance values was known. Through further real measurements, it will be possible to refine these values for the a-frame and monopitch roofs, and to propose factors for the other roof types.

The method was applied to fifteen skylights across Sheffield. The results agreed well to output from SkyVision. The entire process proved to be fast and user friendly, significantly more so than real illuminance measurements. However, without access to further real measured data it is difficult to state how close in magnitude the calculated and actual values are. Assuming any error within Radiance to reality is consistent within the roof types simulated then the method has proved to be a rapid means of comparing many roof examples. A large database of existing real buildings could quickly be developed. Over time, other factors upon which daylighting in atrium buildings is dependant could be investigated and incorporated into the methodology. These may include the well geometry and surface properties and sky conditions. In conjunction with annual known illuminance data, artificial lighting system information, user behaviour and more, this could build into a self-sufficient tool for primary analysis of daylighting in atrium buildings. Alternatively, simply the roof transmittance information (either gathered personally, or from a universal database) could be used as a

departure point for designers to apply to other processes and methods with which they are comfortable.



Conclusions

- 8.1 Summary
- 8.2 Suggestions for Future Work

'I never make predictions, and I never will' PAUL GASCOIGNE

8.1 Summary

This study has aimed to further the current understanding of the transmittance properties of atria roofs. Chapter 2 has demonstrated that the daylighting of buildings is important from the standpoints of energy (economic, environmental) and human wellbeing. Atria represent one possible means of implementing daylighting strategies in medium to large scale buildings. Whilst there has been plentiful research undertaken in the field of daylighting and atria, for the most this work focuses on the well, and consist of model studies, generally physical modelling, under artificial skies. These studies are compromised by a reliance on the sky simulators and the possible level of detail and accuracy of the models.

The effects of the fenestration system have been stated to be the least understood area of atrium design (Aizlewood 1995). Very few studies have looked at the transmittance of atria roofs in real buildings (whose measurement pose significant practical challenges), and no one study that this author could find compares several real roof situations under the umbrella of one methodical process. Taking the plan area of obstruction as a multiplying factor has been shown to poorly describe the transmittance of roofs. At present a designer can rely on dated studies of physically modelled roofs, or through simulations of their proposed schemes, either physically or through computer simulation. Such processes are time consuming, and are generally not implemented at the early stages of the design, and besides which, neither are a guarantee of quantitative accuracy. There was the need for a process that could, with minimal levels of time and effort, assess the transmittance of real roofs, such that the information would be of use to roof and lighting engineers.

Solving the aim of the thesis was approached through a three pronged methodology (real illuminance measurements – a photoanalysis technique – computer simulations), the practicalities and rationales of which were described in Chapter 3. Illuminance measurements were conducted in two real buildings under dynamic skies. These buildings were chosen as they represented two different roof types, with the second case study – the Owen building – introducing further complexity in the form of significant external obstructions. Also of vital importance was the permission of the building owner, the ready availability of architectural drawings, and the guaranteed

safety of the measuring equipment. For reasons of practicality and financial consideration, it was only possible to measure internal illuminance from one measuring point. Due to the time constraints of the research, only overcast skies were considered. Chapter 2 demonstrated that these were the sky conditions most common in climates such as where this research was undertaken, and are familiar to designers through their use as worst case scenarios. The results of these real illuminance measurements were presented in Chapter 4. The daylight factor at the internal measurement point was found to be 60% in the Sheaf building and 35% in the Owen building. A further measure in the Owen building – the ratio of internal illuminance to external illuminance just outside the roof (i.e. under similar levels of site obstruction) - was found to be 43%.

Hemispherical images of these roofs were analysed in the program HemiView to obtain the gap fraction – the proportion of visible sky as seen from the image viewpoint – in an attempt to establish a technique that could rapidly assess the transmittance of real atria roofs. The images were obtained initially through physical capture using a digital camera with fisheye lens, and later generated using computer modelling, to bypass some of the practical issues that arose through the field technique (i.e. the limited viewpoint positions, insufficiently high resolutions, obstructing elements, uneven sky luminance distributions). The results from these experiments were presented in Chapter 5. The image taken should aim to capture a representative view of the roof. Localised factors e.g. immediate large structural junctures, will bias the result. Increasing the distance from the roof from which it is viewed will result in a gap fraction approaching [1-PAO] as the conditions of view approach that of a plan rendering. Gap fraction results from the computer generated images were significantly greater than from the physically captured images, due to an increased resolution and even skies, enabling the compressed extreme ends of the roofs to be classified correctly. Advances in possible resolutions of digital cameras should in the future reduce the gap between field captured and computer generated images.

The measured illuminance values represented daylight factors at one point in the roof plane, and it was evident from the offset that a relationship between gap fraction and roof transmittance must be dependant upon the structural reflectance and glazing transmittance of the roof components. It was necessary to run computer simulations, to obtain roof transmittance over the whole analysis plane and to investigate the effects of

the two aforementioned parameters. Chapter 3 presented the merits of radiosity and ray-tracing based global illuminance models, and finally Radiance was selected as the most appropriate program for the purposes of this study, based upon its superior quantitative accuracy. Chapter 6 described a methodology for its use which involved an interaction with the program Ecotect, and included the setting of the Radiance ambient parameters. Agreement between the measured results and the simulated results from that point were good (simulated result 11.3% lower in the Sheaf building, 7.9% higher in the Owen building), well within the often quoted 20% accuracy band regarding physical measurement of daylight. The relationship between the illuminance at the photocell point, and the rest of the analysis grid, as well as the contribution of the well and light attenuating factor of the external obstructions enabled an estimate of average roof plane transmittance, with the measured result as the departure point. Multiple simulations of the roofs with the structure reflectance and glazing transmittance parameters systematically modified resulted in the derivation of polynomial equations that described the average roof plane transmittance with regard to these two parameters. The agreement between these equations and the physically measured results was very good (calculated result 9.2% lower in the Sheaf building, 6.7% higher in the Owen building).

Chapter 7 broadened the findings of the two case study atria through a repetition of the methodology on six further computer modelled roof types. Polynomial equations relating structure reflectance and glazing transmittance were derived for each of these roofs, which were compared to output from the specialist skylight program SkyVision. Aside from large differences which could be explained, agreement was good. These equations were simplified by expressing the first two coefficients in terms of third (c). The differences between this coefficient and the gap fraction obtained at varying relative depth (from 0 to 1) as well as from the plan area of gap (depth=infinite) for each roof were expressed graphically. This enabled an estimate of average roof plane transmittance to be estimated from a hemispherical photograph of that roof, based upon the empirical findings of the research. The graphed relationship of coefficient of variation to structure reflectance and glazing transmittance for these roofs coupled with the average roof plane transmittance enabled an estimate of the standard deviation of transmittance values across this plane. A correction factor for converting the physically captured gap fraction results to the computer generated magnitudes upon which these

findings are based was tentatively proposed for linear atria, with the caveat that it applies only to the camera used for this study, and that it was not based on a significant number of results, and so further investigation was necessary. The differences found between the simulated and measured illuminance results discussed in Chapter 6 were applied as correction factors to the a-frame and monopitch examples. The technique was demonstrated in fifteen real buildings in Sheffield. The process was fast, user friendly and met with no objection from current building users, which is a significant advance on time consuming and awkward real illuminance measurement methods. Without further reference to such data, it is not possible to tell how accurately the new method has fared, however the good agreement with SkyVision output and results from these 15 roofs was encouraging. What could be seen was the speed at which multiple roofs could be compared against one another, and in that sense, and combined with the findings of the simulations of the sample roof types on the same well, this represents an advance on previous studies of atrium fenestration systems. As such, the aim of further understanding the transmittance of atrium roofs has been realised. With the knowledge of the findings of this research, a designer could use the information from the examined case studies, or apply the photoanalysis technique to any other existing building.

8.2 Suggestions for Future Work

Direction for future work falls into two distinct categories:

1. Validation and refinement of the proposed technique
2. Extension of the technique

The most glaring shortcoming of the work in this thesis is the limited quantity of real illuminance measurements, that is, there exist daylight factors at one point for two buildings. To be able to assess the overall transmittance of the roofs with more confidence, more measuring points across the roof plane are needed. With respect to the two case study buildings, provided the skies are classified in the same manner, such a task could still be accomplished, although as has been stated in Chapter 3, the potential positions for the photocells were very limited. Using additional photocells linked to the logger may make it easier to suspend the measurement device in an

awkward position (due to a smaller size and lighter weight than an integrated logger and photocell (though this may be offset by the gained weight of the cable to the logger)). More preferable would be the study of further real roof transmittances. This has the advantage of being able to study other roof types. This could either be through existing data or conducting field measurements. Using existing data would remove the need for measurement, and provided the exact position of measurement and the capability to accurately model the atrium were available, the method could be reapplied. With the case of field measurements, this would again involve negotiating with building owners, and overcoming practical hurdles. It could be a good time to potentially consider more than one internal measurement point. If this is possible, it would be preferable if all internal illuminance measurements were taken simultaneously (as well as with the unobstructed external illuminance). The findings from measurement and simulation of new case study buildings would add legitimacy to the findings of this thesis, as well as refining the correction factors applied to monopitch and a-frame roofs suggested, and possibly suggesting correction factors for other roof types.

Easier to achieve would be a continuation of the computer modelling and subsequent parameter investigation. At present, eight roof types have been modelled (although *dome 1* is probably unrepresentative of real roofs). The proposed method to derive roof transmittance can only be considered work in progress. Further simulations would include investigating more roof types e.g. barrel, to limit the need for the crude hybrid roof approach adopted for some of the examples in Chapter 7. The effect of the nature of roof structure could also be investigated within each roof type. It could be seen that the coefficients for the *dome 1* and *dome 2* roof polynomial equations were different, despite a similar form. Only through further simulation can these observed trends be quantified, and the method refined in accordance.

In Chapter 7 an image correction factor was proposed to be applied to linear atria, and dependant on depth of viewpoint. Further work here is necessary, both with regard to the plan proportions of the skylight (i.e. its squareness or linearity), and to see if there are still divergences between the synthesised images and possible field captured images from different, and more sophisticated digital cameras.

Finally in terms of refinement, the process lends itself well to automation. The chief barrier, or need for human entry (and therefore inconsistency), would lie in the processing and classification of the hemispherical images. This could remain a manually entered part of the process, although still integrated within an automated system. This would enable the build up of a global database of average roof plane transmittance (with standard deviation across the plane) of existing roofs.

The next suggestions concern the extension of the technique to cover daylighting and atrium roofs in a more holistic manner. The most obvious next step is a repetition of the study under other sky conditions than overcast. This will bring factors such as orientation and latitude into consideration. With the knowledge of how the roof will perform under a range of sky conditions, and local information about probable annual sky type percentages, an estimation of the annual transmittance patterns can be made. If more detailed IDMP illuminance data is available, then absolute internal illuminance can be estimated. This can help in the selection of the appropriate atrium roof, openings into the well and artificial lighting system selection.

This study has concentrated on transmittance of atria roofs, and as such illuminance levels were considered at a horizontal roof plane, looking upwards. The derived values are representative of the quantity of daylight entering the well, and act as a departure point for further analysis. Attempts could be made to develop the photoanalysis technique to consider illuminance levels at horizontal planes at different heights within the well (e.g. the ground floor). This would involve the parametric investigation of well geometric and surface configurations. Likewise, illuminance levels on vertical analysis planes could also be investigated. These are arguably more useful in terms of daylighting strategies in spaces adjacent to the well, where the potential for the greatest energy savings exist. This would involve the measurement or simulation of illuminance levels on the vertical faces of the well, and in spaces adjacent to the well. These results could be compared to hemispherical imagery from within the well, or from images captured from within these adjacent spaces.

The roofs simulated consisted of simple generic forms, to which values for the reflectance of the structure and transmittance of the glazing could be applied. More complex fenestration systems, incorporating shading elements (e.g. louvers) or

intelligent layered skins have not been investigated. The increased emergence of such systems (at present principally on vertical facades, though potentially on inclined and horizontal glazing) would make the incorporation of these elements a desirable addition.

The visual nature of the photoanalysis technique raises the possibility of combining the transmittance analysis with some form of glare analysis from the derived photographs. Processes such as High Dynamic Range (HDR) imagery could be implemented at the image capture stage of the method. This may even have the advantage of making the image easier to classify in HemiView, as the lower luminance regions of sky towards the horizon (under overcast skies) may not appear as relatively dark compared to the zenith point on an HDR image.

Possible ultimate goals of the findings from these processes and techniques could involve the publication of design guides which would be disseminated directly to the architectural profession. They could also be used in consultation for the generation of official daylighting standards in buildings.

9

Bibliography

'It is a very sad thing that nowadays there is so little useless information.' OSCAR WILDE

-
- Aizlewood M 1995, "The daylighting of atria: a critical review", *ASHRAE Transactions*, vol. 101, no. 2, pp. 841-857.
- Aizlewood M, Butt J, Isaac K & Littlefair P, 1997, "Daylight in atria: a comparison of measurement, theory and simulation", *Proceedings Lux Europa, Amsterdam*.
- Aizlewood M, Isaac K & Littlefair P. 1996, "A scale model study of daylighting in atrium buildings", *Proceedings of the IESANZ, Perth, Australia, November*.
- Aizlewood M, Laforgue P, Carroll W, Butt J, Mittanchey R & Hitchcock R, 1998, "Data sets for the validation of daylighting computer programs", *International Daylighting Conference, Ottawa, Canada, May 10-13* pp. 157-164.
- Al-Turki I & Schiler M 1997, "Predicting natural light in atria and adjacent spaces using physical models", *Solar Energy*, vol. 59, no. 4-6, pp. 241-245.
- Andersen M, Rubin M & Scartezzini J-L, 2003, "Comparison between ray-tracing simulations and bi-directional transmission measurements on prismatic glazing", *Solar Energy*, vol. 74, no. 2, pp. 157-173.
- Apian-Bennwitz P 1994, "Designing an apparatus for measuring bidirectional reflection/transmission", *SPIE 13 International Symposium on Optical Materials and Technology for Energy Efficiency and Solar Conversion, Freiburg, Germany* pp. 697-705.
- Aschehoug O 1992, "Daylight in glazed spaces", *Building Research & Information*, vol. 20, no. 4, pp. 242-245.
- Asdrubali F 2003, "Daylighting performance of sawtooth roofs of industrial buildings", *Lighting Research & Technology*, vol. 35, no. 4, pp. 343-359.
- Ashmore J & Richens P 2001, "Computer simulation in daylight design: A comparison", *Architectural Science Review*, vol. 44, no. 1, pp. 33-40.
- Atif M & Boyer L 1991, "Effective top-glazing and internal wall area for efficient daylighting in atria", *Proceedings of the Biennial Congress of the International Solar Energy Society, Denver, Colorado, August* pp. 2805-2810.
- Atif M & Galasiu A 2002, "Energy performance of daylight-linked automatic lighting control systems in large atrium spaces: report on two field-monitored case studies", *Energy and Buildings*, vol. 35, no. 5, pp. 441-461.
- Atif M, Boyer L & Degelman L, 1995, "Development of atrium daylighting prediction: from an algorithm to a design tool", *Journal of the Illuminating Engineering Society*, vol. Winter, pp. 3-11.
- Atif M, Love J & Littlefair P, 1998, "Monitoring protocols and procedures for daylighting evaluation of buildings", *International Daylighting Conference, Ottawa, Canada, May 10-13* pp. 55-62.
- Baker N 2000, "We are all outdoor animals", *Architecture, City, Environment, Proceedings of PLEA, Cambridge, UK* pp. 553-555.

-
- Baker N, Fanchiotti A & Steemers K, 1993, *Daylighting in architecture: a European reference book* James & James.
- Battle G 2001, "Kyoto or bust", *World Architecture*, October.
- Bednar M 1986, *The New Atrium* McGraw Hill.
- Bell J & Burt W 1995, *Designing buildings for daylight* Building Research Establishment. ISBN 1 86081 026 8
- Bodart M & De Herde A 2002, "Global energy savings in offices buildings by the use of daylighting", *Energy and Buildings*, vol. 34, pp. 421-429.
- Boubekri M 1995, "The effect of the cover and reflective properties of a four-sided atrium on the behaviour of light", *Architectural Science Review*, vol. 38, pp. 3-8.
- Boubekri M & Anninos W 1996, "Daylighting efficiency of an atrium: part III - the four-sided type", *Architectural Science Review*, vol. 39, pp. 179-186.
- Bouchet B & Fontoynt M 1996, "Day-lighting of underground spaces: design rules", *Energy and Buildings*, vol. 23, pp. 293-298.
- Boyce P 1998, "Why daylight?", *International Daylighting Conference, Ottawa, Canada, May 10-13* pp. 359-366.
- Boyce P, Hunter C & Howlett O, 2003, "The benefits of daylight through windows", Report, Lighting Research Centre, Rensselaer Polytechnic Institute, Troy, New York 12180-3352, *Sponsored by: Capturing the Daylight Dividend Program*.
- Boyer L 1990, "Preliminary design considerations for daylighting in atria", *Proc. 15th national passive solar conference, Austin, Texas* pp. 189-194.
- Boyer L 1998, "Daylight energy savings in large underground urban structures", *International Daylighting Conference, Ottawa, Canada, May 10-13* pp. 123-130.
- Boyer L & Kim K 1988, "Empirically based algorithms for preliminary prediction of daylight performance in toplighted atriums", *ASHRAE Transactions*, vol. 94, no. 1, pp. 765-781.
- Boyer L & Song K 2002, "Daylighting prediction and sunlighting strategies for atrium design in hot countries", *ASHRAE Transactions*, vol. 100, no. 1, pp. 676-682.
- BRE 1986, "Estimating daylight in buildings: part 1", *Building Research Establishment Digest* no. 309.
- Bryn I 1995, "Atrium buildings from the perspective of function, indoor air quality, and energy use", *ASHRAE Transactions*, vol. 101, no. 2.
- BS 8206-2 1992, *Lighting for buildings-part 2: Code of practice for daylighting*.
- Calcagni B & Paroncini M 2004, "Daylight factor prediction in atria building designs", *Solar Energy*, vol. 76, no. 6, pp. 669-682.

-
- Calcagni B, Filippetti F & Paroncini M, 2000, "Daylighting analysis of an atrium building", *World Renewable Energy Congress VI* pp. 645-648.
- Caldwell I, Bryan J, Croft C, Smith R, Sutcliffe M & Lawson B, 1994, "The heart of a new university", *Architects Journal*.
- Cannon-Brookes S 1997, "Simple scale models for daylighting design: analysis of sources of error in illuminance prediction", *Lighting Research & Technology*, vol. 29, no. 3, pp. 135-142.
- Capeluto I 2003, "The influence of the urban environment on the availability of daylighting in office buildings in Israel", *Building and Environment*, vol. 38, pp. 745-752.
- Carpenter S, Kokko J, Galasiu A & Atif M, 1998, "Daylighting performance of green on the grand: Canada's first C2000 office", *International Daylighting Conference, Ottawa, Canada, May 10-13* pp. 139-146.
- Clarke L, Hand J & Janak M, 1998, "Integrated performance appraisal of daylight buildings", *International Daylighting Conference, Ottawa, Canada, May 10-13* pp. 71-78.
- Cole R J 1986, "Justifying daylight: A question of cost", *Proceedings International Daylighting Conference, Long Beach, California, November* pp. 104-110.
- Cole R J 1990, "The effect of the surfaces adjoining atria on the daylight in adjacent spaces", *Building and Environment*, vol. 25, no. 1, pp. 37-42.
- Compagnon R 2004, "Solar and daylight availability in the urban fabric", *Energy and Buildings*, vol. 36, pp. 321-328.
- Cooksy C, Loveland J, Millet M & Vanags A, 1991, "'Limits of the sky'. Testing and evaluation of the current state-of-the-art in mirror-box sky simulation", *Proceedings of the biennial congress of the International Solar Energy Society, Denver, Colorado, August* pp. 2753-2760.
- Coyne S, Cowling I & Jardine P, 1998, "Daylighting for the human occupant", *CIE Symposium on Lighting Quality, Ottawa, Canada* pp. 197-205.
- Degelman L 1998, "Daylighting design tools - Do we have the right stuff?", *International Daylighting Conference, Ottawa, Canada, May 10-13* pp. 11-17.
- Degelman L 1998, "A daylighting design tool based on life-cycle cost simulation", *International Daylighting Conference, Ottawa, Canada, May 10-13* pp. 45-52.
- Degelman L, Molinelli J Jr. & Kim K, 1988, "Integrated daylighting, heating and cooling model for atriums", *ASHRAE Transactions*, vol. 94, no. 1, pp. 812-825.
- Dewey E & Littlefair P 1998, "Rooflight spacing and uniformity", *Lighting Research & Technology*, vol. 30, no. 3, pp. 119-125.

Douvoulou E & Pitts A 2000, "Glazed spaces in the Mediterranean climate: design of glazing and shading devices in atria", *Architecture, City, Environment, Proceedings of PLEA, Cambridge, UK* pp. 292-293.

DTI 2001, *Digest of United Kingdom energy statistics 2001* National Statistics Publication.

Dumortier D, Fontoynt M & Avuac-Bastie P, 1994, "Daylight availability in Lyon", <http://idmp.entpe.fr/library/papers/daylyon.pdf>.

Ecotect, <http://www.squ1.com/site.html> (checked 30/7/2004).

Ehrlich C, Papamichael K, Lai J & Revzan K, 2002, "A method for simulating the performance of photosensor-based lighting controls", *Energy and Buildings*, vol. 1444, pp. 1-7.

Erhorn H, de Boer J & Dirksmoller M, 1998, "Adeline - An integrated approach to lighting simulation", *International Daylighting Conference, Ottawa, Canada, May 10-13* pp. 21-28.

Erwine B 1998, "North Clackamas high school: case study evaluation of daylight design tools", *International Daylighting Conference, Ottawa, Canada, May 10-13* pp. 131-138.

Evans G & Coombe D 1959, "Hemispherical and woodland canopy photography and the light climate", *Journal of Ecology*, vol. 47, pp. 103-113.

Fontoynt M 1998, "Daylighting performance of buildings: 60 European case studies", *CIBSE National Lighting Conference* pp. 321-326.

Fontoynt M 1999, *Daylight performance of buildings* James & James.

Fontoynt M 2002, "Perceived performance of daylighting systems: lighting efficacy and agreeableness", *Solar Energy*, vol. 73, no. 2, pp. 83-94.

Franta G, Olgyay V, AIA & Hainline J, 2003, "Daylighting: Creating effective sunlight control", *Proceedings of the SOLAR Conference, Austin, Texas, June 21-26* pp. 839-844.

Galasiu A & Atif M 2002, "Applicability of daylighting computer modelling in real case studies: comparison between measured and simulated daylight availability and lighting consumption", *Building and Environment*, vol. 37, no. 4, pp. 363-377.

Geebelen B & Neuckermans H 1998, "Lighting tests in architectural design", *International Daylighting Conference, Ottawa, Canada, May 10-13* pp. 171-177.

Gillette G 1989, "Atrium roof glazing: Energy and daylighting implications", *Construction Specifier*, vol. 42, no. 3, pp. 44-51.

Gillette G & Treado S 1988, "The daylighting and thermal performance of roof glazing in atrium spaces", *ASHRAE Transactions*, vol. 94, no. 1, pp. 826-837.

Glaser D & Ubbelohde S, "Techniques for managing planar daylight data", *Building & Environment*, vol. 37, issues 8-9, pp. 825-831.

-
- Gordes J, Gouchoe S & Kalland S, 2003, "Rating the states for energy security", *Proceedings of the SOLAR Conference, Austin, Texas, June 21-26* pp. 455-462.
- Gordon H & Andersson B 1989, "U.S. participation in international atrium research", *Proceedings 14th National Passive Solar Conference, Denver, Colorado* pp. 105-108.
- Hagan S 2003, "Five reasons", *Harvard Design Magazine*, vol. Spring/Summer.
- Harrison R 1998, *The effect of the roof upon daylighting in the atrium environment*, M.Phil, University of Sheffield.
- Hayman S 2003, "Daylight measurement error", *Lighting Research & Technology*, vol. 35, no. 2, pp. 101-110.
- Heerwagen J 1986, "The role of nature in the view from the window", *Proceedings International Daylighting Conference, Long Beach, California, November* pp. 430-437.
- Heschong Mahone Group, <http://www.h-m-g.com/default.htm> (checked 30/7/2004).
- Heschong L & Wright R 2002, "Daylighting and human performance: Latest findings", *ACEEE Summer Study on Energy Efficiency in Buildings*, vol. 9, p. 8.91-8.104.
- Hestnes A & Aschehoug O 1995, "Daylighting in atria", *International Solar Energy Society UK section* no. 64, pp. 6-9.
- Hill R 1924, "A lens for whole sky photographs", *Quarterly Journal of the Royal Meteorological Society*, vol. 50, pp. 227-235.
- Hopkinson R 1963, *Architectural physics: Lighting Her Majesty's Stationary Office*.
- Hopkirk N 1998, "Simple design tool for lighting, lighting plus heating and cooling energy in an office adjacent to an atrium", *International Daylighting Conference, Ottawa, Canada, May 10-13* pp. 105-112.
- Hung W & Chow W 2001, "A review on architectural aspects of atrium buildings", *Architectural Science Review*, vol. 44, pp. 285-296.
- Hygge S & Lofberg H 1998, "Lessons from daylighting of real case studies", *International Daylighting Conference, Ottawa, Canada, May 10-13* pp. 79-86.
- Igawa N & Nakamura H 2001, "All sky model as a standard sky for the simulation of daylight environment", *Building and Environment*, vol. 36, pp. 763-770.
- Inoue T 2003, "Solar shading and daylighting by means of autonomous responsive dimming glass: practical application", *Energy and Buildings*, vol. 35, pp. 463-471.
- Iwata T & Tokura M 2003, "Survey on workers' response to automated blinds and lighting control systems in an office", *International Daylighting RD&A* no. 5 March, pp. 7-10.
- Iyer-Raniga U 1994, "Daylighting in atrium spaces", *Architectural Science Review*, vol. 37, pp. 195-208.

Jain A 2003, "Optimising the control strategies for switchable glazing for energy and daylight in an office building", *Proceedings of the SOLAR Conference, Austin, Texas, June 21-26* pp. 809-813.

Janak M 1998, "The run time coupling of global illumination and building energy simulations", *International Daylighting Conference, Ottawa, Canada, May 10-13* pp. 113-120.

Johnsen K 1998, "The direction of IEA Task 21 - Daylight in buildings", *International Daylighting Conference, Ottawa, Canada, May 10-13* pp. 3-10.

Julian W 1998, "Daylighting standards, codes and policies", *International Daylighting Conference, Ottawa, Canada, May 10-13* pp. 265-269.

Jupp D, Anderson M, Adomeit E & Witts S, 1980, "PISCES: a computer program for analysing hemispherical canopy photographs", *CSIRO Technical Memorandum 80/23*, vol. Canberra, p. 25.

Kainlauri E, Lehman G & Vilmain M, 1991, "Comparative studies of five atriums on the effects of orientation, exposure and design on daylighting, temperature, and stratification of air", *Proceedings of the biennial congress of the International Solar Energy Society, Denver, Colorado, August* pp. 2787-2792.

Kajiya J 1986, "The rendering equation", *Computer Graphics (SIGGRAPH '86 Proc.)*, v.20, August pp. 143-150.

Karayel M, Navvab M, Ne'eman E & Selkowitz S, 1986, "The rendering equation", *Computer Graphics (SIGGRAPH'86 Proceedings)*, v.20, August pp. 143-150.

Khodulev A & Kopylov E 1996, "Physically accurate lighting simulation in computer graphics software", *Graphicon '96: The 6th International Conference on Computer Graphics and Visualisation, St.Petersberg, Russia*.

Kim G, Boyer L & Degelman L, 1994, "Effect of perimeter balconies on daylighting in atria", *EDRA Proceedings*, vol. 25, pp. 117-123.

Kim K & Boyer L 1986, "Development of daylight prediction methods for atrium design", *Proceedings International Daylighting Conference, Long Beach, California, November*.

Kim K & Boyer L 1988, "Daylight prediction and measurement for three-sided multi-storey atriums under overcast and clear skies", *ASHRAE Transactions*, vol. 94, no. 1, pp. 783-797.

Kischkoweit-Lopin M 2002, "Overview over daylighting systems", *Solar Energy*, vol. 73, no. 2, pp. 77-82.

Kittler R 1986, "Luminance models of homogeneous skies for design and energy performance predictions", *Proceedings International Daylighting Conference, Long Beach, California, November* pp. 31-37.

Kittler R & Darula S 1999, "Specification of the local daylight climate and the importance of overcast sky conditions", *Light & Engineering*, vol. 7, no. 4, pp. 15-21.

-
- Kittler R & Darula S 2002, "Parametric definition of the daylight climate", *Renewable Energy*, vol. 26, pp. 177-187.
- Kittler R & Ruck N 1984, "Definition of typical and average exterior daylight conditions in different climatic zones", *Energy and Buildings*, vol. 6, no. 3, pp. 253-259.
- Kotani H, Narasaki M, Sato R & Yamanaka T, 2003, "Environmental assessment of light well in high-rise apartment building", *Building and Environment*, vol. 38, pp. 283-289.
- Lam W 1983, "Sunlighting as formgiver for architecture", *International Daylighting Conference, Phoenix, Arizona* pp. 77-84.
- Lam W 1986, *Sunlighting as formgiver for architecture* Van Nostrand Reinhold Company Ltd.
- Lane T 2001, "Colour me beautiful", *Building*, December.
- Laouadi A & Atif M 2000, "Daylight availability in top-lit atria: prediction of skylight transmittance and daylight factor", *Lighting Research & Technology*, vol. 32, no. 4, pp. 175-186.
- Laouadi A & Atif M 2001, "Prediction models of optical characteristics for domed skylights under standard and real sky conditions", *7th International IBPSA Conference, Rio de Janeiro, August* pp. 1101-1108.
- Laouadi A, Atif M. & Galasiu A. 2003, "Methodology towards developing skylight design tools for thermal and energy performance of atriums in cold climates", *Building and Environment*, vol. 38, pp. 117-127.
- Laouadi A 2004, "Design with SkyVision: A computer tool to predict daylighting performance of skylights", *CIB World Building Congress, Toronto, Canada, May 2-7*, pp. 1-11.
- Laouadi A & Arsenault C 2004, "Validation of SkyVision", *Research Report, Institute for Research in Construction, IRC-RR-167*.
- Lassance G 2002, "A pre-design aid support for architectural daylighting", *Proceedings of SKSB (Sharing Knowledge in Sustainable Building)*, www.iris.ba.cnr.it/sksb/papers/19-360.pdf.
- Lee F 1992, "Insights into the daylighting effect of the external obstructions", *CIBSE National Lighting Conference* pp. 294-308.
- Leslie R 2003, "Capturing the daylight dividend in buildings; why and how?", *Building and Environment*, vol. 38, pp. 381-385.
- Li D & Lam J 2001, "Evaluation of lighting performance in office buildings with daylighting controls", *Energy and Buildings*, vol. 33, pp. 793-803.
- Li D & Lam J 2002, "An investigation of daylighting performance and energy saving in a daylighted corridor", *Energy and Buildings*, vol. 35, issue 4 pp. 365-373.

-
- Li D, Lau C & Lam J, 2004, "Overcast sky conditions and luminance distributions in Hong Kong", *Building and Environment*, vol. 39, pp. 101-108.
- Littlefair P 1982, "Effective glass transmission factors under a CIE sky", *Lighting Research & Technology*, vol. 14, no. 4, pp. 232-235.
- Littlefair P 1989, *Innovative daylight systems* BRE IP 22/89.
- Littlefair P 1993, *Measuring daylight* BRE IP23/93.
- Littlefair P 2000, "Key issues of solar shading", *Building Services Journal*, vol. November.
- Littlefair P & Aizlewood M 1998, *Daylight in atrium buildings* BRE IP3/98.
- Littlefair P & Phillips G 1988, "Daylight under rooflights", *Building Services CIBSE Journal*, vol. 10, no. 4, pp. 61-62.
- Liu A, N. M. & J. J. 1991, "Geometric shape index for daylight distribution variations in atrium spaces", *Proceedings of the Biennial Congress of the International Solar Energy Society, Denver, Colorado, August*, vol. 3, no. 1, pp. 2781-2786.
- Loe D, Mansfield K and Rowlands E 1994, "Appearance of the lit environment and its relevance to lighting design: an experimental study", *Lighting Research & Technology*, vol.26, no.3, pp 119-129.
- Loe D 2003, "Quantifying lighting energy efficiency: a discussion document", *Lighting Research & Technology*, vol. 35, no. 4, pp. 319-329.
- Love J 1998 a, "Daylighting case studies: installations in the Calgary area", *International Daylighting Conference, Ottawa, Canada, May 10-13* pp. 147-154.
- Love J 1998 b, "Daylighting control systems: Directions for the future based on lessons from the past", *International Daylighting Conference, Ottawa, Canada, May 10-13* pp. 299-306.
- Mahdavi A 2004, "Reflections on computer building models", *Building and Environment*, vol. 39, pp. 913-925.
- Mansy K 2003, "A simplified method to quantify savings due to incorporation of daylight into architectural design", *Proceedings of the SOLAR Conference, Austin, Texas, June 21-26* pp. 797-802.
- Mansy K 2004, "A user-friendly procedure to visualize the hourly quantitative performance of daylighting systems", *Solar Energy*. vol. 77, pp. 373-380.
- Mardalijevic J 1999, *Daylight simulation: Validation, sky models and daylight coefficients*, PhD, De Montfort University, Leicester, United Kingdom
- Markou M, Kambezidis H, Bartzokas A, Katsoulis B & Muneer T 2004, "Sky type classification in Central England during winter", *Energy*. In press, corrected proof.

-
- Matusiak B & Aschehoug O 1998, "Daylighting systems for linear atria at high latitudes", *International Daylighting Conference, Ottawa, Canada, May 10-13* pp. 333-340.
- Matusiak B, A. O. & L. P. 1999, "Daylighting strategies for an infinitely long atrium: an experimental evaluation", *Lighting Research & Technology*, vol. 31, no. 1, pp. 23-34.
- McCluney R & Bornemann H 1986, "Time rate of changing daylight", *Proceedings International Daylighting Conference, Long Beach, California, November* pp. 24-30.
- Mead P 2003, "The medical significance of daylight in design", *Proceedings of the SOLAR Conference, Austin, Texas, June 21-26* pp. 835-838.
- Michel L & Scartezzini J-L 2002, "Implementing the partial daylight factor method under a scanning sky simulator", *Solar Energy*, vol. 72, no. 6, pp. 473-492.
- Miguet F & Groleau D 2002, "A daylight simulation tool for urban and architectural spaces- application to transmitted direct and diffuse light through glazing", *Building and Environment*.
- Millet M 1998, "Experiencing daylight in architecture", *International Daylighting Conference, Ottawa, Canada, May 10-13* pp. 351-358.
- Milne M & Zurich J 1998, "Daylight prediction techniques in energy design tools", *International Daylighting Conference, Ottawa, Canada, May 10-13* pp. 89-95.
- Moeck M & Selkowitz S 1996, "A computer-based daylight systems design tool", *Automation in Construction*, vol. 5, pp. 193-209.
-
- Moore T, Carter D & Slater A, 2000, "Lighting for turbulent spaces", *Building Services Journal*, vol. May.
- Muneer T 1998, "Evaluation of the CIE overcast sky model against Japanese data", *Energy and Buildings*, vol. 27, pp. 175-177.
- Nakamura H, Oki M, Hayashi Y & Itawa T, 1986, "The mean sky composed taking into account of the relative sunshine duration", *Proceedings International Daylighting Conference, Long Beach, California, November* pp. 38-50.
- Navvab M 1996, "Scale model photometry techniques under simulated sky conditions", *Journal of the Illuminating Engineering Society*, vol. Summer, pp. 160-172.
- Navvab M & Selkowitz S 1984, "Daylighting data for atrium design", *Ninth National Passive Solar Conference, Columbus, Ohio, September* pp. 495-500.
- Navvab M, Karayel M, Ne'eman E & Selkowitz S, 1984, "Analysis of atmospheric turbidity for daylight calculations", *Energy and Buildings*, vol. 6, no. 3, pp. 293-303.
- Neal T & Sharples S 1992, "The influence of well geometry on daylight levels in atria", *Proceedings CIBSE National Lighting Conference* pp. 342-345.
-

-
- Ng E, Lam K & Wu W, 1999, "The application of computer simulation techniques to the design and preservation of a national monument", *6th International Building Simulation Conference, Kyoto, Japan*.
- Onaygil S & Guler O 2003, "Determination of the energy saving by daylight responsive lighting control systems with an example from Istanbul", *Building and Environment*, vol. 38, pp. 973-977.
- Oretskin B 1982, "Studying the efficacy of light wells by means of models under an artificial sky", *Proceedings of the 7th ASES Passive Conference* pp. 459-463.
- Ozturk L 2003, "The effect of luminance distribution on interior perception", *Architectural Science Review*, vol. 46, pp. 233-238.
- Papamichael K, Hitchcock R, Ehrlich C & Carroll B, 1998, "New tools for the evaluation of daylighting strategies and technologies", *International Daylighting Conference, Ottawa, Canada, May 10-13* pp. 37-44.
- Parpairi K, Baker N, Steemers K & Compagnon R, 2002, "The luminance differences index; a new indicator of user preferences in daylit spaces", *Lighting Research & Technology*, vol. 34, no. 1, pp. 53-68.
- Paule B, Bodart M, Citherlet S & Scartezzini J, 1998, "'Leso-DIAL' daylighting design software", *International Daylighting Conference, Ottawa, Canada, May 10-13* pp. 29-36.
- Pearson A 2000, "Clear choices", *Building* no. 21.
- Pfrommer P, Lomas K, Seale C & Kupke C, 1995, "The radiation transfer through coated and tinted glazing", *Solar Energy*, vol. 54, no. 5, pp. 287-299.
- Place W, Coutier P, Fontoynt M, Kammerud R, Andersson B, Bauman F, Carroll W, Wahlig M, Webster T, 1986, *The impact of glazing orientation, tilt, and area on the energy performance of roof apertures*, Lawrence Berkley Laboratory, University of California, LBL-18838.
- Rahim R, Baharuddin & Mulyadi R, 2004, "Classification of daylight and radiation data into three sky conditions by cloud ratio and sunshine duration", *Energy and Buildings*, vol. 36, no. 7, pp. 660-666.
- Rea M, Rutledge B & Maniccia D, 1998, "Beyond daylight dogma", *International Daylighting Conference, Ottawa, Canada, May 10-13* pp. 215-222.
- Reinhart C 2004, "LIGHTSWITCH-2002: A model for manual and automated control of electric lights and blinds", *Solar Energy*.
- Reinhart F & Fitz A 2004, "Key findings from an online simulation survey on the use of daylight simulation programs", *Proceedings of the ESIM Conference, Vancouver, Canada, June 9-11*.
- Roberts A & Marsh A 2001, "ECOTECH: Environmental prediction in architectural education", *Architectural Information Management 19th eCAADe Conference Proceedings, Helsinki (Finland) 29-31 August* pp. 342-347.

-
- Robinson-Gayle S, Kolokotroni M, Cripps A & Tanno S, 2001, "ETFE foil cushions in roofs and atria", *Construction and Building Materials*, vol. 15, pp. 323-327.
- Rouanet S & Bobkowicz A 2003, "First solar daylighting aerogel panels: A green vision comes true!", *Proceedings of the SOLAR Conference, Austin, Texas, June 21-26* pp. 821-825.
- Roy G 2000, *A comparative study of lighting simulation packages suitable for use in architectural design*, Murdoch University, Australia.
- Roy G, Hayman S & Julian W, 1998, "Sky modelling from digital imagery", *The University of Sydney, Murdoch University, Australia*.
- Ruck N 1986, "An analysis of available skylight data for daylighting", *Proceedings International Daylighting Conference, Long Beach, California, November* pp. 51-65.
- Saridar S & Elkadi H 2002, "The impact of applying recent facade technology on daylighting performance in buildings in eastern Mediterranean", *Building & Environment*, vol.37, pp.1205-1212
- Saxon R 1983, *Atrium buildings: development and design* Architectural Press.
- Saxon R 1994, *The atrium comes of age* Longman.
- Selkowitz S 1998, "The elusive challenge of daylighted buildings: A brief review 25 years later on", *International Daylighting Conference, Ottawa, Canada, May 10-13* pp. 231-235.
- Selkowitz S & Lee E 1998, "Advanced fenestration systems for improved daylight performance", *International Daylighting Conference, Ottawa, Canada, May 10-13* pp. 341-348.
- Seshadri T 1960, "Equations of sky components with a CIE standard overcast sky", *Proceedings India Academy of Science, Paper 57A*, pp. 233-241.
- Sethi A 2003, "A study of daylighting techniques and their energy implications using a designer friendly simulation software", *Proceedings of the SOLAR Conference, Austin, Texas, June 21-26* pp. 689-694.
- Sharples S & Lash D 2004, "Reflectance distributions and vertical daylight illuminances in atria", *Lighting Research & Technology*, vol. 36, no. 1, pp. 45-57.
- Sharples S & Mahambrey S 1999, "Reflectance distributions and atrium daylight levels: a model study", *Lighting Research & Technology*, vol. 31, no. 4, pp. 165-170.
- Sharples S & Neal T 1993, "A model study of the influence of roof structure on daylight levels in atria type buildings", *3rd European Conference on Architecture, Florence, May* pp. 161-164.
- Sharples S & Shea A 1999, "Roof obstructions and daylight levels in atria: a model study under real skies", *Lighting Research & Technology*, vol. 31, no. 4, pp. 181-185.

-
- Sharples S & Shea A 2000, "Daylight transmission of atrium roofs under overcast and partly cloudy skies", *Lighting Research & Technology*, vol. 32, no. 3, pp. 153-156.
- Sharples S, Stewart L & Tregenza P 2001, " Glazing daylight transmittances: a field survey of windows in urban areas", *Building and Environment*, vol. 36, pp. 503-509.
- Shea A 2000, *Roof transmittance and daylight levels in top-lit atria: a model study*, M.Phil, University of Sheffield.
- Smith G 2004, "Materials and systems for efficient lighting and delivery of daylight", *Solar Energy Materials and Solar Cells*. In press, corrected proof.
- Song K & Boyer L 1994, "Instrumentation system for evaluating daylighting performance in sunlit atria with design-stage scale models", *ASHRAE Transactions*, vol. 100, no. 1.
- Spitzglas M, Navvab M & Selkowitz S, 1985, "Scale model measurements for a daylighting photometric database", *Journal of the Illuminating Engineering Society* no. Fall, pp. 41-60.
- Spring M 2001, "Art surgery", *Building* no. 48.
- Spring M 2004, "Playtime", *Building*, 2 July, pp. 38-42.
- Standards Australia.AS1680.3 1991, "Interior lighting part 3: Measurement, calculation and presentation of photometric data", *Standards Australia, North Sydney*.
- Stroud Foster J & Harington R 1990, *Structure and fabric part 2* The Mitchell Publishing Company Ltd.
- Summerfield A 2004, *Synthetic imagery for architecture: computer simulation of visual context under daylight*, PhD, University of Sydney, Australia.
- Szerman M 1992, "Daylighting in adjacent rooms connected to an atrium by artificial sky measurements", *Building Research & Information*, vol. 20, no. 6, pp. 357-359.
- Terman M, Fairhurst S, Perlman B, Levitt J & McCluney R, 1986, "Daylight deprivation and replenishment: A psychobiological problem with a naturalistic solution", *Proceedings International Daylighting Conference, Long Beach, California, November* pp. 438-445.
- Treado S & Gillette G 1986, "The daylighting and energy performance of building atria", *Proceedings International Daylighting Conference, Long Beach, California, November* pp. 360-373.
- Treado S, Gillette G & Kusuda T, 1984, "Daylighting with windows, skylights and clerestories", *Energy and Buildings*, vol. 6, no. 4, pp. 319-330.
- Tregenza P 1984, "Predicting daylight from cloudy skies", *Energy and Buildings*, vol. 6, no. 3, pp. 261-266.
- Tregenza P 1997, "Daylight attenuation in top-lit atria", *Lighting Research & Technology*, vol. 29, no. 3, pp. 151-157.

-
- Tregenza P, Stewart L & Sharples S 1999, "Reduction of glazing transmittance by atmospheric pollutants", *Lighting Research & Technology*, vol. 31, no. 4, pp. 135-138.
- Tsangrassoulis A & Bourdakis V 2003, "Comparison of radiosity and ray-tracing techniques with a practical design procedure for the prediction of daylight levels in atria", *Renewable Energy*, vol. 28, no. 13, pp. 2157-2162.
- Tsangrassoulis A & Santamouris M 2000, "A method to estimate the daylight efficiency of round skylights", *Energy and Buildings*, vol. 32, pp. 41-45.
- Tsangrassoulis A, Santamouris M & Asimakopoulos D, 1996, "Theoretical and experimental analysis of daylight performance for various shading systems", *Energy and Buildings*, vol. 24, pp. 223-230.
- Ubbelohde M & Humann C 1998, "A comparative evaluation of daylighting software: SuperLite, LumenMicro, Lightscape and Radiance", *International Daylighting Conference, Ottawa, Canada, May 10-13* pp. 97-104.
- Van Nijnatten P 2002, "A spectrophotometer accessory for directional reflectance and transmittance of coated glazing", *Solar Energy*, vol. 73, no. 3, pp. 137-149.
- Veitch J 2001 a, "Lighting quality contributions from biopsychological processes", *Journal of the Illuminating Engineering Society*, vol. 30, no. 1, pp. 3-16.
- Veitch J 2001 b, "Psychological processes influencing lighting quality", *Journal of the Illuminating Engineering Society*, vol. 30, no. 1, pp. 124-140.
- Vischer J 1986, "The effects of daylighting on occupant behaviour in buildings: New directions for research", *Proceedings International Daylighting Conference, Long Beach, California, November* pp. 419-429.
- Ward G & Rubinstein F 1988, "A new technique for computer simulation of illuminated spaces", *Journal of the Illuminating Engineering Society*, vol. 17, no. 1.
- Ward Larson G & Shakespeare R 1998, *Rendering with Radiance: The art and science of lighting visualization* Morgan Kaufmann Publishers, Inc.
- Webb N (ed.), Rich P, Wood J, Vieglais D & Burek K, 1996, "HemiView User Manual Version 2.1", *Helios Environmental Modelling Institute, LLC*.
- Weiner J & Milne M 2003, "Sizing skylights for daylighting landscaping in an atrium", *Proceedings of the SOLAR Conference, Austin, Texas, June 21-26* pp. 803-808.
- Weiss M 2004, "Atrium buildings: Subjective reactions to the daylighting performance of new glazing materials", *Lighting Journal-Rugby* pp. 16-23.
- Willbold-Lohr G 1989, "Daylighting in glazed atria", *2nd European Conference on Architecture, Paris, December* pp. 16-20.
- Windheim L & Daly L 1983, "Case study: Lockheed building 157. Deep daylighting/innovative lighting concepts for a large office building.", *International Daylighting Conference, Phoenix, Arizona* pp. 143-147.

Wotton E 1998, "Daylighting codes, standards and policies", *International Daylighting Conference, Ottawa, Canada, May 10-13* pp. 271-278.

Wotton E & Borkow B 1983, "An investigation into the effects of windows and lighting in offices", *International Daylighting Conference, Phoenix, Arizona* pp. 405-411.

Wright J 1996, "An illuminance prediction model for atria", *CIBSE National Lighting Conference* pp. 157-165.

Wright J & Letherman K 1998, "Illuminance in atria: review of prediction methods", *Lighting Research & Technology*, vol. 30, no. 1, pp. 1-10.

Zonneveldt L & Mallory-Hill S 1998, "Evaluation of daylight responsive lighting control systems", *International Daylighting Conference, Ottawa, Canada, May 10-13* pp. 223-230.

Appendix **A**

Configuring the Dataloggers

This experiment used three Data Hog 2 logging devices with attached photosensors. The loggers measured approximately 10cm^3 . The loggers connect to a PC through an RS232 cable. Each sensor is slightly unique, and comes with a manufacturer's calibration factor (expressed as $\mu\text{A}/\text{kLux}$). They are also fitted with seven internal resistors, one of which must be selected depending on the scale of illuminance values expected. Those used in this experiment were the (approx.) $100\text{k}\Omega$ resistors. For each of the three loggers, the following channel configurations were set;

Software Channel; 00 (sets the software channel)
 Hardware Channel; 33 (sets the hardware channel i.e. location of photocell)
 Gain; 3 (selects the $100\text{k}\Omega$ resistor)
 Scale Code; 1 (selects $Ax + B$ scaling)

One of the sensors had multiple software channels. In this case all other channels were turned off (scale code = 5) to save on memory.

The Calibration factors were then set. These were derived using the following formula;

$$\text{Full Scale Value} = 2.000 / (\text{Sensor Output } [\mu\text{A per unit}] \times \text{Feedback Resistor } [\text{M}\Omega])$$

The following full scale values (derived from the appropriate resistor value and sensor output) were used for each of the three sensors. Values were entered as 5 digits plus a decimal point;

Table A-1: Scale Values Used for the Configuration of the Photocells

Photocell	Sensor Output/ $\mu\text{A}/\text{kLux}$	Resistor Value/ $\text{M}\Omega$	Scale Value
1	0.145122	0.10029	137.42
2	0.141159	0.10029	141.27
3	0.113800	0.09986	175.99

The output was therefore in kLux. Comparison of each sensor output was double checked against a cosine corrected photocell placed adjacent to it. Agreement was found to be good.

The sensors were instructed to measure the illuminance every 30 seconds (setting 06) and log an average of these values every 10 minutes (setting 10). With one channel, logs at 10 minutes can be made for 10.9 weeks without overwriting of memory with new data.

The internal clocks were synchronised in turn by comparison to an independent wrist watch, accurate to +/- 1 second.

Battery life for the loggers running on six fresh type-C cells (total 9 Volts) is approximately 14 weeks.

Appendix

B

The Weather Log

Sources of Data

The following weather log in conjunction with the unobstructed global illuminances measured by the dataloggers (whose results in their entirety are displayed in Appendix C) was used to classify the sky conditions. Measurements were taken four times daily at three hourly intervals between 9am and 6pm. Five indicators were used, which were:

1. The Meteorological Office website; <http://www.met-office.gov.uk/education/archive/uk/>. Manchester weather station, 53°28'46" - 2°14'55", 26 miles from Sheffield.
2. The Meteorological Office website. Waddington weather station, 53°10'6" 0°32'20", 48 miles from Sheffield.
3. Spot checks by the author
4. Yahoo email weather alerts, Sheffield;
http://weather.yahoo.com/forecast/Sheffield_UK_c.html.
5. Cloud cover percentage from Metcheck, for South Yorkshire;
<http://www.metcheck.com/48hrforecast.asp?lat=53&lon=-1&locationID=67&Arr=163&Country=UK&Coastal=>.

It was not possible to obtain complete information from each source for every measurement day. Sources 1 and 2 were the most consistent and trustworthy means, and it is for this reason they were included, despite their distance from the sites. Manchester and Waddington represented the closest matches available, and whilst it data from these stations can not be applied to Sheffield, they may serve as an indicator. Where there is missing information in method 3, is due to the author not being present on in Sheffield. Where there is missing information in sources 4 and 5, it was due to inabilities to access the necessary internet sites or errors on the page. Despite the shortcomings, the 5 sources combined with the measured unobstructed global illuminance data served as a sufficient indicator of sky type for the needs of this study.

The log is displayed between 10th July and 16th October 2002, and 13th February to 20th April 2004.

Table B-1: The Weather Log

<i>Date</i>	<i>Time</i>	<i>1. Met Office: Manchester</i>	<i>2. Met Office: Waddington</i>	<i>3. Spot Checks by the Author</i>	<i>4. Yahoo Alert: Sheffield</i>	<i>5. Cloud Cover</i>
2002						
10-Jul	9am	partly cloudy	partly cloudy	partly cloudy		44%
	12pm	mostly cloudy	mostly cloudy	mostly cloudy		49%
	3pm	mostly cloudy	rain showers	mostly cloudy		51%
	6pm	mostly cloudy	showers	mostly cloudy		58%
11-Jul	9am	showers	partly cloudy	partly cloudy		81%
	12pm	thunderly showers	rain showers	partly cloudy		68%
	3pm	showers	rain showers	partly cloudy		45%
	6pm	rain showers	partly cloudy	partly cloudy		41%
12-Jul	9am	partly cloudy	mostly cloudy	partly cloudy		38%
	12pm	showers	mostly cloudy	partly cloudy		57%
	3pm	rain showers	mostly cloudy	partly cloudy		54%
	6pm	showers	mostly cloudy	partly cloudy		71%
13-Jul	9am	clear	clear			20%
	12pm	partly cloudy	partly cloudy			24%
	3pm	mostly cloudy	mostly cloudy			38%
	6pm	partly cloudy	clear			39%
14-Jul	9am	mostly cloudy	partly cloudy			
	12pm	mostly cloudy	mostly cloudy			
	3pm	mostly cloudy	mostly cloudy			
	6pm	mostly cloudy	mostly cloudy			
15-Jul	9am	mostly cloudy	clear			
	12pm	partly cloudy	partly cloudy			
	3pm	partly cloudy	mostly cloudy			
	6pm	mostly cloudy	mostly cloudy			
16-Jul	9am	partly cloudy	mostly cloudy	partly cloudy		
	12pm	partly cloudy	rain	partly cloudy		53%
	3pm	clear	mostly cloudy	partly cloudy		26%
	6pm	clear	mostly cloudy	clear		27%
17-Jul	9am	mostly cloudy	mostly cloudy	mostly cloudy		29%
	12pm	mostly cloudy	no significant weather.	mostly cloudy		29%
	3pm	mostly cloudy	no significant weather.	mostly cloudy		36%
	6pm	mostly cloudy	no significant weather.	mostly cloudy		37%
18-Jul	9am	mostly cloudy	mostly cloudy	bright cloudy		61%
	12pm	partly cloudy	mostly cloudy	mostly cloudy		59%
	3pm	mostly cloudy	mostly cloudy	partly cloudy		70%
	6pm	mostly cloudy	mostly cloudy	mostly cloudy		77%
19-Jul	9am	overcast	mostly cloudy	bright cloudy	mostly cloudy	67%
	12pm	overcast	mostly cloudy	bright cloudy	mostly cloudy	51%
	3pm	overcast	overcast	bright cloudy	mostly cloudy	52%
	6pm	rain	rain			65%
20-Jul	9am	mostly cloudy	mostly cloudy			86%
	12pm	rain showers	rain showers			74%
	3pm	mostly cloudy	stormy			46%
	6pm	rain showers	thunderly showers			52%
21-Jul	9am	mostly cloudy	rain			

	12pm	mostly cloudy	overcast			
	3pm	mostly cloudy	overcast			
	6pm	partly cloudy	mostly cloudy			
22-Jul	9am	overcast	drizzle	mostly cloudy	mostly cloudy	
	12pm	no data	overcast	bright cloudy	mostly cloudy	93%
	3pm	drizzle	mostly cloudy	overcast	mostly cloudy	96%
	6pm	drizzle	mostly cloudy	overcast	mostly cloudy	97%
23-Jul	9am	mostly cloudy	overcast	mostly cloudy	partly cloudy	93%
	12pm	showers	mostly cloudy	partly cloudy	showers	94%
	3pm	drizzle	mostly cloudy	partly cloudy	partly cloudy	96%
	6pm	drizzle	mostly cloudy	partly cloudy	mostly cloudy	95%
24-Jul	9am	mostly cloudy	rain showers	partly cloudy	partly cloudy	93%
	12pm	mostly cloudy	mostly cloudy	bright cloudy	partly cloudy	98%
	3pm	mostly cloudy	mostly cloudy			98%
	6pm	mostly cloudy	mostly cloudy			98%
25-Jul	9am	overcast	rain		partly cloudy	62%
	12pm	overcast	mostly cloudy		mostly cloudy	68%
	3pm	overcast	mostly cloudy		mostly cloudy	79%
	6pm	drizzle	rain		mostly cloudy	83%
26-Jul	9am	mostly cloudy	partly cloudy	mostly cloudy	mostly cloudy	
	12pm	partly cloudy	clear	almost clear	fair	60%
	3pm	clear	clear	almost clear	fair	12%
	6pm	clear	clear		partly cloudy	12%
27-Jul	9am	drizzle	mostly cloudy	mostly cloudy	mostly cloudy	94%
	12pm	partly cloudy	mostly cloudy		partly cloudy	87%
	3pm	partly cloudy	clear		partly cloudy	18%
	6pm	partly cloudy	partly cloudy		partly cloudy	19%
28-Jul	9am	mostly cloudy	clear		partly cloudy	
	12pm	partly cloudy	partly cloudy		partly cloudy	
	3pm	clear	partly cloudy		partly cloudy	
	6pm	partly cloudy	clear		partly cloudy	
29-Jul	9am	mostly cloudy	hazy	partly cloudy	partly cloudy	
	12pm	mostly cloudy	mostly cloudy	partly cloudy	partly cloudy	95%
	3pm	mostly cloudy	partly cloudy	partly cloudy	partly cloudy	93%
	6pm	mostly cloudy	mostly cloudy	partly cloudy	partly cloudy	91%
30-Jul	9am	hazy	partly cloudy	overcast	haze	76%
	12pm	thunderstorm	thunderstorm	overcast	haze	73%
	3pm	mostly cloudy	rain showers	overcast	haze	81%
	6pm	overcast	rain	overcast	thunderstorm	83%
31-Jul	9am	rain	rain	overcast	light rain	
	12pm	rain	drizzle	overcast	light rain	99%
	3pm	rain	hazy	overcast	fog	90%
	6pm	drizzle	hazy	overcast	fog	84%
01-Aug	9am	drizzle	rain	overcast	fog	86%
	12pm	rain	rain	overcast	heavy rain	96%
	3pm	rain	rain	overcast	rain	100%
	6pm	rain	rain	overcast	rain	100%
02-Aug	9am	rain	mostly cloudy	overcast	mostly cloudy	99%
	12pm	drizzle	mostly cloudy	overcast	mostly cloudy	99%
	3pm	mostly cloudy	partly cloudy	mostly cloudy	mostly cloudy	71%
	6pm	partly cloudy	mostly cloudy	partly cloudy	partly cloudy	70%
03-Aug	9am	fog	partly cloudy			71%
	12pm	partly cloudy	mostly cloudy			66%

	3pm	rain showers	partly cloudy			68%
	6pm	partly cloudy	mostly cloudy			65%
04-Aug	9am	rain	mostly cloudy			
	12pm	rain showers	mostly cloudy			
	3pm	rain showers	showers			
	6pm	rain showers	mostly cloudy			
05-Aug	9am	partly cloudy	rain showers	overcast	mostly cloudy	
	12pm	mostly cloudy	rain showers	mostly cloudy	mostly cloudy	80%
	3pm	mostly cloudy	mostly cloudy	mostly cloudy	mostly cloudy	51%
	6pm	mostly cloudy	mostly cloudy			56%
06-Aug	9am	mostly cloudy	mostly cloudy	mostly cloudy	mostly cloudy	89%
	12pm	mostly cloudy	mostly cloudy	mostly cloudy	mostly cloudy	73%
	3pm	mostly cloudy	mostly cloudy	partly cloudy	partly cloudy	45%
	6pm	mostly cloudy	mostly cloudy	partly cloudy	partly cloudy	45%
07-Aug	9am	hazy	hazy	mostly cloudy	haze	
	12pm	rain showers	mostly cloudy	mostly cloudy	partly cloudy	83%
	3pm	showers	thunderstorm	mostly cloudy	mostly cloudy	86%
	6pm	rain	thunderstorm	mostly cloudy	mostly cloudy	92%
08-Aug	9am	mostly cloudy	rain	partly cloudy	partly cloudy	96%
	12pm	mostly cloudy	rain	bright cloudy	partly cloudy	89%
	3pm	overcast	mostly cloudy	bright cloudy	partly cloudy	88%
	6pm	rain	mostly cloudy	bright cloudy	partly cloudy	92%
09-Aug	9am	rain	rain	rain	rain	88%
	12pm	rain	rain	rain	rain	88%
	3pm	rain	rain	rain	light rain	90%
	6pm	rain	rain	rain	rain	93%
10-Aug	9am	drizzle	drizzle		mostly cloudy	
	12pm	overcast	rain showers		mostly cloudy	
	3pm	overcast	mostly cloudy		mostly cloudy	
	6pm	mostly cloudy	mostly cloudy		partly cloudy	
11-Aug	9am	overcast	mostly cloudy		partly cloudy	
	12pm	mostly cloudy	rain showers		mostly cloudy	
	3pm	drizzle	mostly cloudy		mostly cloudy	
	6pm	drizzle	overcast		mostly cloudy	
12-Aug	9am	mostly cloudy	rain	mostly cloudy	mostly cloudy	
	12pm	partly cloudy	mostly cloudy	mostly cloudy	mostly cloudy	
	3pm	clear	partly cloudy	partly cloudy	partly cloudy	63%
	6pm	partly cloudy	clear	partly cloudy	partly cloudy	49%
13-Aug	9am	mostly cloudy	clear	mostly cloudy	partly cloudy	98%
	12pm	mostly cloudy	mostly cloudy	mostly cloudy	partly cloudy	98%
	3pm	mostly cloudy	mostly cloudy	mostly cloudy	partly cloudy	96%
	6pm	mostly cloudy	mostly cloudy	mostly cloudy	mostly cloudy	90%
14-Aug	9am	mostly cloudy	partly cloudy	partly cloudy	partly cloudy	73%
	12pm	mostly cloudy	partly cloudy	mostly cloudy	partly cloudy	74%
	3pm	mostly cloudy	clear	partly cloudy	mostly cloudy	54%
	6pm	mostly cloudy	clear			40%
15-Aug	9am	mostly cloudy	clear		partly cloudy	44%
	12pm	mostly cloudy	mostly cloudy		partly cloudy	39%
	3pm	mostly cloudy	mostly cloudy		partly cloudy	50%
	6pm	partly cloudy	mostly cloudy		partly cloudy	46%
16-Aug	9am	partly cloudy	clear	partly cloudy	fair	
	12pm	mostly cloudy	clear	clear	partly cloudy	81%
	3pm	mostly cloudy	partly cloudy	clear	partly cloudy	51%

	6pm	partly cloudy	clear		partly cloudy	37%
17-Aug	9am	mostly cloudy	hazy		fog	70%
	12pm	mostly cloudy	partly cloudy		partly cloudy	51%
	3pm	mostly cloudy	mostly cloudy		partly cloudy	9%
	6pm	partly cloudy	mostly cloudy		partly cloudy	20%
18-Aug	9am	rain	thunderstorm		partly cloudy	
	12pm	hazy	thunderstorm		partly cloudy	
	3pm	thunderstorm	rain		partly cloudy	
	6pm	mostly cloudy	mostly cloudy		partly cloudy	
19-Aug	9am	partly cloudy	mostly cloudy	mostly cloudy	mostly cloudy	85%
	12pm	mostly cloudy	mostly cloudy	mostly cloudy	partly cloudy	87%
	3pm	rain	mostly cloudy	overcast	partly cloudy	80%
	6pm	mostly cloudy	rain showers	overcast	rain	73%
20-Aug	9am	hazy	mist	overcast	mostly cloudy	84%
	12pm	partly cloudy	mostly cloudy	mostly cloudy	mostly cloudy	83%
	3pm	rain showers	mostly cloudy	mostly cloudy	mostly cloudy	78%
	6pm	showers	mostly cloudy	mostly cloudy	mostly cloudy	71%
21-Aug	9am	clear	partly cloudy	partly cloudy	fair	53%
	12pm	clear	clear	partly cloudy	partly cloudy	49%
	3pm			partly cloudy	partly cloudy	50%
	6pm			partly cloudy	partly cloudy	50%
22-Aug	9am			partly cloudy	partly cloudy	67%
	12pm			bright cloudy	partly cloudy	69%
	3pm			mostly cloudy	partly cloudy	71%
	6pm			mostly cloudy	partly cloudy	74%
23-Aug	9am			overcast	partly cloudy	89%
	12pm			overcast	partly cloudy	89%
	3pm			overcast	partly cloudy	83%
	6pm				partly cloudy	75%
24-Aug	9am					40%
	12pm				mostly cloudy	47%
	3pm				showers	47%
	6pm				mostly cloudy	43%
25-Aug	9am				mostly cloudy	
	12pm				mostly cloudy	
	3pm				mostly cloudy	
	6pm				mostly cloudy	
26-Aug	9am				mostly cloudy	
	12pm				mostly cloudy	
	3pm				mostly cloudy	
	6pm				mostly cloudy	
27-Aug	9am				sunny	
	12pm				fair	
	3pm				partly cloudy	
	6pm				partly cloudy	
28-Aug	9am				partly cloudy	
	12pm				partly cloudy	
	3pm				partly cloudy	
	6pm				partly cloudy	
29-Aug	9am				mostly cloudy	
	12pm				mostly cloudy	
	3pm				mostly cloudy	
	6pm				partly cloudy	

30-Aug	9am				mostly cloudy	
	12pm				mostly cloudy	
	3pm				partly cloudy	
	6pm				partly cloudy	
31-Aug	9am				partly cloudy	
	12pm				partly cloudy	
	3pm				mostly cloudy	
	6pm				partly cloudy	
01-Sep	9am				partly cloudy	
	12pm				partly cloudy	
	3pm				partly cloudy	
	6pm				fair	
02-Sep	9am	partly cloudy	partly cloudy			
	12pm	partly cloudy	mostly cloudy		partly cloudy	
	3pm	mostly cloudy	mostly cloudy		mostly cloudy	
	6pm	mostly cloudy	partly cloudy		mostly cloudy	
03-Sep	9am	hazy	mostly cloudy		fog	
	12pm	mostly cloudy	mostly cloudy		partly cloudy	
	3pm	mostly cloudy	mostly cloudy		mostly cloudy	
	6pm	mostly cloudy	mostly cloudy		partly cloudy	
04-Sep	9am	hazy	mist		haze	
	12pm	mostly cloudy	partly cloudy		haze	
	3pm	mostly cloudy	partly cloudy		haze	
	6pm	partly cloudy	mostly cloudy		haze	
05-Sep	9am	hazy	hazy		haze	
	12pm	mostly cloudy	partly cloudy		haze	
	3pm	rain showers	mostly cloudy		haze	
	6pm	rain	mostly cloudy		haze	
06-Sep	9am	mostly cloudy	mostly cloudy		partly cloudy	
	12pm	rain	drizzle		partly cloudy	
	3pm	rain	rain showers		light rain	
	6pm	mostly cloudy	rain		light rain	
07-Sep	9am	clear	clear			
	12pm	showers	mostly cloudy		mostly cloudy	
	3pm	partly cloudy	rain showers		heavy rain shower	
	6pm	partly cloudy	rain showers		mostly cloudy	
08-Sep	9am	partly cloudy	fog		partly cloudy	
	12pm	mostly cloudy	partly cloudy		partly cloudy	
	3pm	mostly cloudy	mostly cloudy		partly cloudy	
	6pm	partly cloudy	mostly cloudy		partly cloudy	
09-Sep	9am	overcast	mist			
	12pm	rain	rain	rain	fog	
	3pm	rain	rain	rain	heavy rain	96%
	6pm	rain	mostly cloudy	overcast	heavy rain	97%
10-Sep	9am	mostly cloudy	partly cloudy	partly cloudy	partly cloudy	38%
	12pm	mostly cloudy	partly cloudy	partly cloudy	partly cloudy	29%
	3pm	mostly cloudy	partly cloudy	partly cloudy	partly cloudy	22%
	6pm	mostly cloudy	partly cloudy	partly cloudy	partly cloudy	17%
11-Sep	9am	clear	clear			23%
	12pm	clear	partly cloudy	clear	sunny	20%
	3pm	clear	mostly cloudy	partly cloudy	sunny	15%
	6pm	clear	hazy	bright cloudy	sunny	14%
12-Sep	9am	hazy	mist	bright cloudy		86%

	12pm	hazy	partly cloudy	partly cloudy	haze	83%
	3pm	partly cloudy	partly cloudy	partly cloudy	haze	71%
	6pm	clear	partly cloudy	partly cloudy	haze	54%
13-Sep	9am	clear	mostly cloudy	mostly cloudy	haze	77%
	12pm	clear	partly cloudy	partly cloudy	partly cloudy	72%
	3pm	partly cloudy	mostly cloudy	mostly cloudy	partly cloudy	39%
	6pm	mostly cloudy	mostly cloudy		partly cloudy	6%
14-Sep	9am	hazy	hazy		haze	73%
	12pm	hazy	overcast		haze	68%
	3pm	hazy	overcast		haze	42%
	6pm	hazy	drizzle		haze	17%
15-Sep	9am	mostly cloudy	mostly cloudy			
	12pm	mostly cloudy	mostly cloudy			
	3pm	mostly cloudy	mostly cloudy			
	6pm	mostly cloudy	mostly cloudy			
16-Sep	9am	mostly cloudy	mostly cloudy	overcast		76%
	12pm	mostly cloudy	overcast	overcast		85%
	3pm	mostly cloudy	overcast	overcast		91%
	6pm	mostly cloudy	mostly cloudy	overcast		93%
17-Sep	9am	mostly cloudy	hazy	overcast		76%
	12pm	mostly cloudy	mostly cloudy			74%
	3pm	mostly cloudy	overcast			75%
	6pm	mostly cloudy	overcast			83%
18-Sep	9am	mostly cloudy	mostly cloudy	overcast		98%
	12pm	mostly cloudy	mostly cloudy	overcast		98%
	3pm	mostly cloudy	mostly cloudy	overcast		97%
	6pm	mostly cloudy	mostly cloudy	overcast		96%
19-Sep	9am	mostly cloudy	mostly cloudy	overcast		97%
	12pm	mostly cloudy	overcast	overcast		92%
	3pm	mostly cloudy	mostly cloudy	overcast		81%
	6pm	mostly cloudy	showers	overcast		66%
20-Sep	9am	mostly cloudy	mostly cloudy	overcast		78%
	12pm	mostly cloudy	mostly cloudy	overcast		72%
	3pm	mostly cloudy	mostly cloudy	mostly cloudy		69%
	6pm	mostly cloudy	mostly cloudy	mostly cloudy		69%
21-Sep	9am	hazy	mostly cloudy			65%
	12pm	hazy	mostly cloudy			65%
	3pm	mostly cloudy	mostly cloudy			67%
	6pm	partly cloudy	mostly cloudy			70%
22-Sep	9am	partly cloudy	rain showers			
	12pm	mostly cloudy	rain showers			
	3pm	mostly cloudy	rain showers			
	6pm	mostly cloudy	rain showers			
23-Sep	9am	clear	clear	partly cloudy		25%
	12pm	partly cloudy	partly cloudy	partly cloudy		20%
	3pm	partly cloudy	partly cloudy	partly cloudy		21%
	6pm	mostly cloudy	clear	partly cloudy		35%
24-Sep	9am	clear	mostly cloudy	clear		9%
	12pm	partly cloudy	mostly cloudy	partly cloudy		10%
	3pm	partly cloudy	mostly cloudy	overcast		10%
	6pm	mostly cloudy	mostly cloudy	mostly cloudy		10%
25-Sep	9am	hazy	mostly cloudy	partly cloudy		48%
	12pm	mostly cloudy	partly cloudy	mostly cloudy		63%

	3pm	mostly cloudy	mostly cloudy	partly cloudy	70%
	6pm	mostly cloudy	mostly cloudy	partly cloudy	74%
26-Sep	9am	partly cloudy	clear	clear	88%
	12pm	partly cloudy	partly cloudy	partly cloudy	87%
	3pm	mostly cloudy	mostly cloudy	partly cloudy	56%
	6pm	mostly cloudy	mostly cloudy	partly cloudy	44%
27-Sep	9am	mostly cloudy	mostly cloudy	overcast	92%
	12pm	rain	mostly cloudy	overcast	90%
	3pm	mostly cloudy	mostly cloudy	overcast	86%
	6pm	mostly cloudy	mostly cloudy	overcast	80%
28-Sep	9am	overcast	mostly cloudy		84%
	12pm	overcast	mostly cloudy		81%
	3pm	overcast	mostly cloudy		82%
	6pm	hazy	mostly cloudy		86%
29-Sep	9am	hazy	hazy		
	12pm	hazy	hazy		
	3pm	hazy	mostly cloudy		
	6pm	mostly cloudy	mostly cloudy		
30-Sep	9am	mostly cloudy	mist	partly cloudy	
	12pm	partly cloudy	mostly cloudy	partly cloudy	
	3pm	mostly cloudy	mostly cloudy	partly cloudy	
	6pm	mostly cloudy	mostly cloudy	haze	
01-Oct	9am	partly cloudy	mostly cloudy	partly cloudy	
	12pm	mostly cloudy	mostly cloudy	partly cloudy	
	3pm	mostly cloudy	mostly cloudy	partly cloudy	
	6pm	rain	no sig. weather	partly cloudy	
02-Oct	9am	hazy	hazy	mostly cloudy	
	12pm	hazy	hazy	bright cloudy	
	3pm	mostly cloudy	hazy	bright cloudy	
	6pm	mostly cloudy	hazy	mostly cloudy	
03-Oct	9am	rain showers	partly cloudy	partly cloudy	
	12pm	mostly cloudy	partly cloudy	partly cloudy	
	3pm	partly cloudy	partly cloudy	partly cloudy	
	6pm	clear	clear		
04-Oct	9am	mostly cloudy	mostly cloudy		
	12pm	mostly cloudy	mostly cloudy		
	3pm	partly cloudy	mostly cloudy		
	6pm	partly cloudy	mostly cloudy		
05-Oct	9am	rain	mostly cloudy		
	12pm	rain	mostly cloudy		
	3pm	drizzle	mostly cloudy		
	6pm	drizzle	mostly cloudy		
06-Oct	9am	partly cloudy	mostly cloudy		
	12pm	partly cloudy	mostly cloudy		
	3pm	mostly cloudy	mostly cloudy		
	6pm	mostly cloudy	partly cloudy		
07-Oct	9am	mostly cloudy	overcast		
	12pm	mostly cloudy	mostly cloudy	hazy	
	3pm	mostly cloudy	mostly cloudy	bright cloudy	
	6pm	mostly cloudy	mostly cloudy	hazy	
08-Oct	9am	mostly cloudy	mostly cloudy	bright cloudy	
	12pm	mostly cloudy	mostly cloudy	bright cloudy	
	3pm	mostly cloudy	mostly cloudy	bright cloudy	

	6pm	mostly cloudy	overcast	hazy	
09-Oct	9am	partly cloudy	partly cloudy	mostly cloudy	
	12pm	mostly cloudy	partly cloudy	mostly cloudy	
	3pm	mostly cloudy	mostly cloudy	hazy	
	6pm	mostly cloudy	mostly cloudy		
10-Oct	9am	mostly cloudy	overcast		
	12pm	mostly cloudy	mostly cloudy		
	3pm	mostly cloudy	overcast		
	6pm	mostly cloudy	overcast		
11-Oct	9am	mostly cloudy	overcast		
	12pm	overcast	overcast	overcast	
	3pm	overcast	mostly cloudy	overcast	
	6pm	rain	mostly cloudy		
12-Oct	9am	rain	drizzle		
	12pm	rain showers	rain		
	3pm	partly cloudy	hazy		
	6pm	clear	mostly cloudy		
13-Oct	9am	mostly cloudy	hazy		
	12pm	mostly cloudy	hazy		
	3pm	mostly cloudy	hazy		
	6pm	rain	rain		
14-Oct	9am	rain	rain	overcast	
	12pm	rain	rain	overcast	
	3pm	rain showers	showers	overcast	
	6pm	mostly cloudy	mostly cloudy	overcast	
15-Oct	9am	rain	rain	overcast	
	12pm	rain	rain	overcast	
	3pm	rain	drizzle	overcast	
	6pm	mostly cloudy	rain	overcast	
16-Oct	9am	mostly cloudy	rain	mostly cloudy	
	12pm	mostly cloudy	rain showers	mostly cloudy	
	3pm	rain showers	rain showers	partly cloudy	
	6pm	partly cloudy	mostly cloudy	partly cloudy	

2004

13-Feb	9am	hazy	hazy		
	12pm	hazy	drizzle		
	3pm	drizzle	mostly cloudy		
	6pm	drizzle	rain		
14-Feb	9am	fog	rain		
	12pm	rain	rain		
	3pm	rain	rain		
	6pm	mostly cloudy	rain		
15-Feb	9am	mostly cloudy	mostly cloudy		
	12pm	clear	mostly cloudy		
	3pm	mostly cloudy	mostly cloudy		
	6pm	mostly cloudy	mostly cloudy		
16-Feb	9am	clear	overcast	partly cloudy	partly cloudy
	12pm	hazy	mostly cloudy	partly cloudy	partly cloudy
	3pm	hazy	mostly cloudy	overcast	mostly cloudy
	6pm	mostly cloudy	hazy	overcast	mostly cloudy
17-Feb	9am	overcast	hazy	mostly cloudy	light rain
					100%

	12pm	rain	rain	overcast	mostly cloudy	100%
	3pm	mostly cloudy	mostly cloudy	overcast	mostly cloudy	100%
	6pm	partly cloudy	rain	overcast	mostly cloudy	100%
18-Feb	9am	partly cloudy	mostly cloudy	partly cloudy	fair	27%
	12pm	partly cloudy	drizzle	partly cloudy	mostly cloudy	26%
	3pm	partly cloudy	mostly cloudy	mostly cloudy	mostly cloudy	31%
	6pm	mostly cloudy	rain showers	mostly cloudy	mostly cloudy	31%
19-Feb	9am	partly cloudy	clear	partly cloudy	partly cloudy	91%
	12pm	partly cloudy	partly cloudy	partly cloudy	partly cloudy	97%
	3pm	partly cloudy	mostly cloudy	partly cloudy	partly cloudy	74%
	6pm	clear	partly cloudy		fair	54%
20-Feb	9am	partly cloudy	partly cloudy		partly cloudy	2%
	12pm	clear	partly cloudy		partly cloudy	2%
	3pm	clear	clear		partly cloudy	3%
	6pm	clear	clear		partly cloudy	6%
21-Feb	9am	clear	hazy		haze	33%
	12pm	partly cloudy	hazy		haze	19%
	3pm	mostly cloudy	hazy		partly cloudy	
	6pm	partly cloudy	hazy		mostly cloudy	
22-Feb	9am	clear	mostly cloudy		mostly cloudy	
	12pm	partly cloudy	showers		partly cloudy	
	3pm	partly cloudy	showers		light snow shower	
	6pm	mostly cloudy	snow showers		partly cloudy	
23-Feb	9am	partly cloudy	clear		fair	
	12pm	partly cloudy	showers		partly cloudy	
	3pm	mostly cloudy	partly cloudy		partly cloudy	
	6pm	partly cloudy	clear		fair	
24-Feb	9am	drizzle	rain		light drizzle	
	12pm	mostly cloudy	rain		mostly cloudy	
	3pm	overcast	rain		mostly cloudy	
	6pm	rain showers	sleet		mostly cloudy	
25-Feb	9am	clear	clear		fair	
	12pm	mostly cloudy	partly cloudy	partly cloudy	partly cloudy	
	3pm	mostly cloudy	mostly cloudy	partly cloudy	partly cloudy	100%
	6pm	partly cloudy	partly cloudy	partly cloudy	fair	99%
26-Feb	9am	partly cloudy	partly cloudy	partly cloudy	fair	43%
	12pm	mostly cloudy	mostly cloudy	partly cloudy	partly cloudy	60%
	3pm	showers	mostly cloudy	partly cloudy	showers	93%
	6pm	showers	mostly cloudy	partly cloudy	partly cloudy	61%
27-Feb	9am	clear	showers	partly cloudy	partly cloudy	38%
	12pm	showers	mostly cloudy	partly cloudy	partly cloudy	25%
	3pm	showers	mostly cloudy	partly cloudy	partly cloudy	55%
	6pm	snow showers	partly cloudy	partly cloudy	light snow shower	71%
28-Feb	9am	partly cloudy	snow showers		partly cloudy	98%
	12pm	mostly cloudy	snow showers		partly cloudy	98%
	3pm	mostly cloudy	snow showers		partly cloudy	98%
	6pm	mostly cloudy	snow showers		mostly cloudy	90%
29-Feb	9am	clear	snow showers		partly cloudy	14%
	12pm	partly cloudy	partly cloudy		partly cloudy	12%
	3pm	showers	mostly cloudy		partly cloudy	
	6pm	showers	clear		partly cloudy	
01-Mar	9am	hazy	hazy		fair	
	12pm	hazy	hazy		partly cloudy	

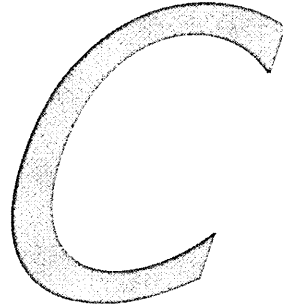
	3pm	hazy	clear		fair	
	6pm	clear	clear		fair	
02-Mar	9am	hazy	hazy		sunny	16%
	12pm	hazy	hazy		sunny	42%
	3pm	hazy	partly cloudy		partly cloudy	96%
	6pm	hazy	hazy		partly cloudy	98%
03-Mar	9am	hazy	hazy		partly cloudy	100%
	12pm	mostly cloudy	hazy		partly cloudy	100%
	3pm	rain	mostly cloudy		fair	100%
	6pm	rain	rain		haze	100%
04-Mar	9am	hazy	mist		haze	79%
	12pm	mostly cloudy	hazy		partly cloudy	50%
	3pm	mostly cloudy	hazy		partly cloudy	18%
	6pm	showers	hazy		partly cloudy	21%
05-Mar	9am	fog	fog		fog	100%
	12pm	hazy	hazy		fog	100%
	3pm	showers	hazy		fog	83%
	6pm	rain showers	hazy		light rain	77%
06-Mar	9am	mostly cloudy	hazy		mostly cloudy	63%
	12pm	mostly cloudy	mostly cloudy		partly cloudy	40%
	3pm	rain showers	mostly cloudy		partly cloudy	57%
	6pm	mostly cloudy	showers		partly cloudy	49%
07-Mar	9am	clear	rain		mostly cloudy	
	12pm	rain	mostly cloudy		partly cloudy	
	3pm	rain showers	showers		partly cloudy	
	6pm	mostly cloudy	partly cloudy		showers	
08-Mar	9am	mostly cloudy	mostly cloudy	mostly cloudy	mostly cloudy	38%
	12pm	mostly cloudy	mostly cloudy	mostly cloudy	mostly cloudy	44%
	3pm	partly cloudy	mostly cloudy	mostly cloudy	mostly cloudy	13%
	6pm	mostly cloudy	mostly cloudy	mostly cloudy	mostly cloudy	9%
09-Mar	9am	mostly cloudy	clear	mostly cloudy	mostly cloudy	28%
	12pm	mostly cloudy	mostly cloudy	partly cloudy	partly cloudy	25%
	3pm	mostly cloudy	mostly cloudy	partly cloudy	partly cloudy	95%
	6pm	mostly cloudy	mostly cloudy	mostly cloudy	partly cloudy	97%
10-Mar	9am	snow showers	snow showers	overcast	mostly cloudy	100%
	12pm	rain showers	snow showers	overcast	light snow shower	100%
	3pm	mostly cloudy	hail showers	mostly cloudy	mostly cloudy	100%
	6pm	snow showers	snow showers	mostly cloudy	mostly cloudy	100%
11-Mar	9am	overcast	hazy	overcast	haze	100%
	12pm	mostly cloudy	hazy	mostly cloudy	haze	100%
	3pm	mostly cloudy	showers	overcast	mostly cloudy	100%
	6pm	hazy	hazy	overcast	haze	100%
12-Mar	9am	snow showers	hazy	overcast	fog	100%
	12pm	overcast	snow showers	overcast	haze	100%
	3pm	hazy	rain	overcast	fog	100%
	6pm	hazy	mist	overcast	fog	100%
13-Mar	9am	rain	drizzle		fog	97%
	12pm	mostly cloudy	mostly cloudy		mostly cloudy	65%
	3pm	partly cloudy	rain showers		mostly cloudy	84%
	6pm	partly cloudy	rain showers		light rain	92%
14-Mar	9am	rain	rain	overcast	light rain	100%
	12pm	rain	rain	overcast	light rain	100%
	3pm	mostly cloudy	rain showers	partly cloudy	light rain	100%

	6pm	rain showers	rain showers	partly cloudy	light rain	100%
15-Mar	9am	mostly cloudy	mostly cloudy	partly cloudy	partly cloudy	100%
	12pm	no data	mostly cloudy	overcast	light rain	100%
	3pm	overcast	rain	mostly cloudy	showers	100%
	6pm	mostly cloudy	mostly cloudy	overcast	light rain	100%
16-Mar	9am	mostly cloudy	mostly cloudy	mostly cloudy	mostly cloudy	100%
	12pm	mostly cloudy	overcast	overcast	partly cloudy	100%
	3pm	mostly cloudy	mostly cloudy	overcast	mostly cloudy	100%
	6pm	mostly cloudy	mostly cloudy	mostly cloudy	mostly cloudy	100%
17-Mar	9am	mostly cloudy	mostly cloudy	mostly cloudy	partly cloudy	83%
	12pm	mostly cloudy	mostly cloudy	partly cloudy	partly cloudy	66%
	3pm	mostly cloudy	mostly cloudy	partly cloudy	partly cloudy	89%
	6pm	mostly cloudy	mostly cloudy	partly cloudy	partly cloudy	74%
18-Mar	9am	drizzle	rain	overcast	light drizzle	100%
	12pm	rain	rain	overcast	mostly cloudy	100%
	3pm	rain	mostly cloudy	overcast	partly cloudy	100%
	6pm	partly cloudy	mostly cloudy	mostly cloudy	partly cloudy	87%
19-Mar	9am	rain	rain	overcast	light rain	91%
	12pm	rain	rain	mostly cloudy	mostly cloudy	100%
	3pm	mostly cloudy	partly cloudy	partly cloudy	partly cloudy	99%
	6pm	mostly cloudy	showers	partly cloudy	partly cloudy	96%
20-Mar	9am	rain	mostly cloudy	overcast	light rain	100%
	12pm	rain	rain	mostly cloudy	rain	100%
	3pm	rain showers	duststorm	mostly cloudy	mostly cloudy	100%
	6pm	rain showers	rain showers	mostly cloudy	light rain	92%
21-Mar	9am	rain showers	mostly cloudy	mostly cloudy	light rain	79%
	12pm	showers	partly cloudy	overcast	partly cloudy	88%
	3pm	rain showers	rain showers	mostly cloudy	showers	100%
	6pm	rain showers	rain showers	mostly cloudy	partly cloudy	100%
22-Mar	9am	rain showers	rain showers	partly cloudy	partly cloudy	100%
	12pm	rain showers	rain showers	partly cloudy	partly cloudy	94%
	3pm	showers	showers	partly cloudy	showers	93%
	6pm	mostly cloudy	showers	partly cloudy	partly cloudy	98%
23-Mar	9am	partly cloudy	partly cloudy	partly cloudy	partly cloudy	73%
	12pm	mostly cloudy	mostly cloudy	mostly cloudy	mostly cloudy	85%
	3pm	mostly cloudy	rain showers	partly cloudy	partly cloudy	99%
	6pm	mostly cloudy	rain showers	overcast	partly cloudy	94%
24-Mar	9am	showers	mostly cloudy	overcast	partly cloudy	98%
	12pm	mostly cloudy	rain showers	overcast	partly cloudy	100%
	3pm	rain showers	hail showers	partly cloudy	partly cloudy	100%
	6pm	mostly cloudy	rain showers	partly cloudy	partly cloudy	100%
25-Mar	9am	rain	mostly cloudy	overcast	mostly cloudy	100%
	12pm	rain	mostly cloudy	mostly cloudy	mostly cloudy	100%
	3pm	rain	rain showers	overcast	partly cloudy	100%
	6pm	mostly cloudy	partly cloudy	overcast	partly cloudy	100%
26-Mar	9am	mostly cloudy	fog	mostly cloudy	mostly cloudy	81%
	12pm	rain	overcast	overcast	light rain	82%
	3pm	rain	overcast	mostly cloudy	mostly cloudy	100%
	6pm	overcast	rain	mostly cloudy	mostly cloudy	100%
27-Mar	9am	drizzle	overcast		mostly cloudy	70%
	12pm	rain	overcast		mostly cloudy	81%
	3pm	mostly cloudy	overcast		partly cloudy	100%
	6pm	mostly cloudy	overcast		mostly cloudy	99%

28-Mar	9am	mostly cloudy	mostly cloudy		mostly cloudy	97%
	12pm	mostly cloudy	mostly cloudy		mostly cloudy	99%
	3pm	partly cloudy	mostly cloudy		partly cloudy	99%
	6pm	partly cloudy	mostly cloudy		partly cloudy	100%
29-Mar	9am	mostly cloudy	overcast	mostly cloudy	mostly cloudy	100%
	12pm	mostly cloudy	mostly cloudy	overcast	mostly cloudy	99%
	3pm	mostly cloudy	mostly cloudy	overcast	mostly cloudy	100%
	6pm	mostly cloudy	mostly cloudy	mostly cloudy	mostly cloudy	100%
30-Mar	9am	partly cloudy	fog	hazy	mostly cloudy	99%
	12pm	mostly cloudy	hazy		mostly cloudy	99%
	3pm	mostly cloudy	partly cloudy		partly cloudy	99%
	6pm	hazy	clear		partly cloudy	78%
31-Mar	9am	hazy	hazy		cloudy	95%
	12pm	partly cloudy	hazy		haze	
	3pm	clear	hazy		partly cloudy	
	6pm	hazy	hazy		partly cloudy	
01-Apr	9am	hazy	rain		fog	
	12pm	hazy	hazy		fog	
	3pm	mostly cloudy	mostly cloudy		fog	
	6pm	mostly cloudy	mostly cloudy		fog	
02-Apr	9am	mostly cloudy	rain		light rain	
	12pm	mostly cloudy	overcast		mostly cloudy	
	3pm	mostly cloudy	mostly cloudy		partly cloudy	
	6pm	rain	partly cloudy		thunder	
03-Apr	9am	partly cloudy	rain		light rain	
	12pm	rain	mostly cloudy		partly cloudy	
	3pm	rain	mostly cloudy		light rain	
	6pm	rain	rain		light rain	
04-Apr	9am	mostly cloudy	mostly cloudy		light rain	
	12pm	mostly cloudy	mostly cloudy		partly cloudy	
	3pm	rain	rain		light rain	
	6pm	mostly cloudy	rain		partly cloudy	
05-Apr	9am	rain	mostly cloudy	overcast	light rain	
	12pm	mostly cloudy	rain showers	partly cloudy	partly cloudy	100%
	3pm	hail	partly cloudy	partly cloudy	partly cloudy	98%
	6pm	rain	partly cloudy	overcast	partly cloudy	99%
06-Apr	9am	rain	mostly cloudy	overcast	mostly cloudy	100%
	12pm	no data	rain	overcast	rain	100%
	3pm	no data	rain	partly cloudy	partly cloudy	98%
	6pm	thunderstorm	mostly cloudy	partly cloudy	partly cloudy	72%
07-Apr	9am	mostly cloudy	mostly cloudy	partly cloudy	mostly cloudy	100%
	12pm	mostly cloudy	rain	mostly cloudy	mostly cloudy	100%
	3pm	hail	thunderstorm	overcast	partly cloudy	98%
	6pm	thunderstorm	mostly cloudy	partly cloudy	partly cloudy	87%
08-Apr	9am	mostly cloudy	mostly cloudy	partly cloudy	fair	61%
	12pm	mostly cloudy	mostly cloudy	mostly cloudy	partly cloudy	80%
	3pm	mostly cloudy	rain	partly cloudy	partly cloudy	100%
	6pm	mostly cloudy	showers	partly cloudy	partly cloudy	99%
09-Apr	9am	mostly cloudy	hazy		partly cloudy	62%
	12pm	mostly cloudy	clear		mostly cloudy	68%
	3pm	drizzle	mostly cloudy		mostly cloudy	100%
	6pm	drizzle	rain		mostly cloudy	100%
10-Apr	9am	mostly cloudy	mostly cloudy		mostly cloudy	100%

	12pm	mostly cloudy	mostly cloudy		partly cloudy	100%
	3pm	mostly cloudy	mostly cloudy		mostly cloudy	100%
	6pm	mostly cloudy	mostly cloudy		mostly cloudy	
11-Apr	9am	hazy	overcast		mostly cloudy	
	12pm	hazy	overcast		mostly cloudy	
	3pm	mostly cloudy	mostly cloudy		partly cloudy	
	6pm	mostly cloudy	overcast		partly cloudy	
12-Apr	9am	drizzle	mostly cloudy		mostly cloudy	
	12pm	rain	mostly cloudy		partly cloudy	
	3pm	rain	rain		mostly cloudy	
	6pm	partly cloudy	mostly cloudy		mostly cloudy	
13-Apr	9am	partly cloudy	clear		fair	
	12pm	mostly cloudy	clear		partly cloudy	
	3pm	mostly cloudy	partly cloudy		partly cloudy	
	6pm	mostly cloudy	clear		partly cloudy	
14-Apr	9am	mostly cloudy	mostly cloudy	partly cloudy	mostly cloudy	
	12pm	overcast	mostly cloudy	mostly cloudy	mostly cloudy	100%
	3pm	mostly cloudy	mostly cloudy	mostly cloudy	mostly cloudy	98%
	6pm	mostly cloudy	mostly cloudy	mostly cloudy	mostly cloudy	98%
15-Apr	9am	hazy	hazy	hazy	haze	100%
	12pm	mostly cloudy	overcast	partly cloudy	mostly cloudy	100%
	3pm	overcast	mostly cloudy	mostly cloudy	fair	100%
	6pm	rain	mostly cloudy	mostly cloudy	mostly cloudy	100%
16-Apr	9am	rain	hazy	overcast	mostly cloudy	100%
	12pm	rain	hazy	overcast	light rain	100%
	3pm	rain	mostly cloudy	overcast	light rain	100%
	6pm	rain	hazy	overcast	light rain	100%
17-Apr	9am	hazy	hazy		haze	8%
	12pm	rain showers	partly cloudy		partly cloudy	11%
	3pm	mostly cloudy	partly cloudy		partly cloudy	80%
	6pm	rain	partly cloudy		partly cloudy	89%
18-Apr	9am	rain	rain		light rain	100%
	12pm	rain showers	drizzle		partly cloudy	100%
	3pm	rain showers	rain		partly cloudy	
	6pm	mostly cloudy	rain		light rain	
19-Apr	9am	mostly cloudy	partly cloudy	partly cloudy	partly cloudy	
	12pm	mostly cloudy	partly cloudy	partly cloudy	partly cloudy	53%
	3pm	partly cloudy	partly cloudy	partly cloudy	partly cloudy	32%
	6pm	rain showers	partly cloudy	partly cloudy	partly cloudy	36%
20-Apr	9am	partly cloudy	clear	clear	partly cloudy	33%
	12pm	mostly cloudy	partly cloudy	partly cloudy	partly cloudy	100%

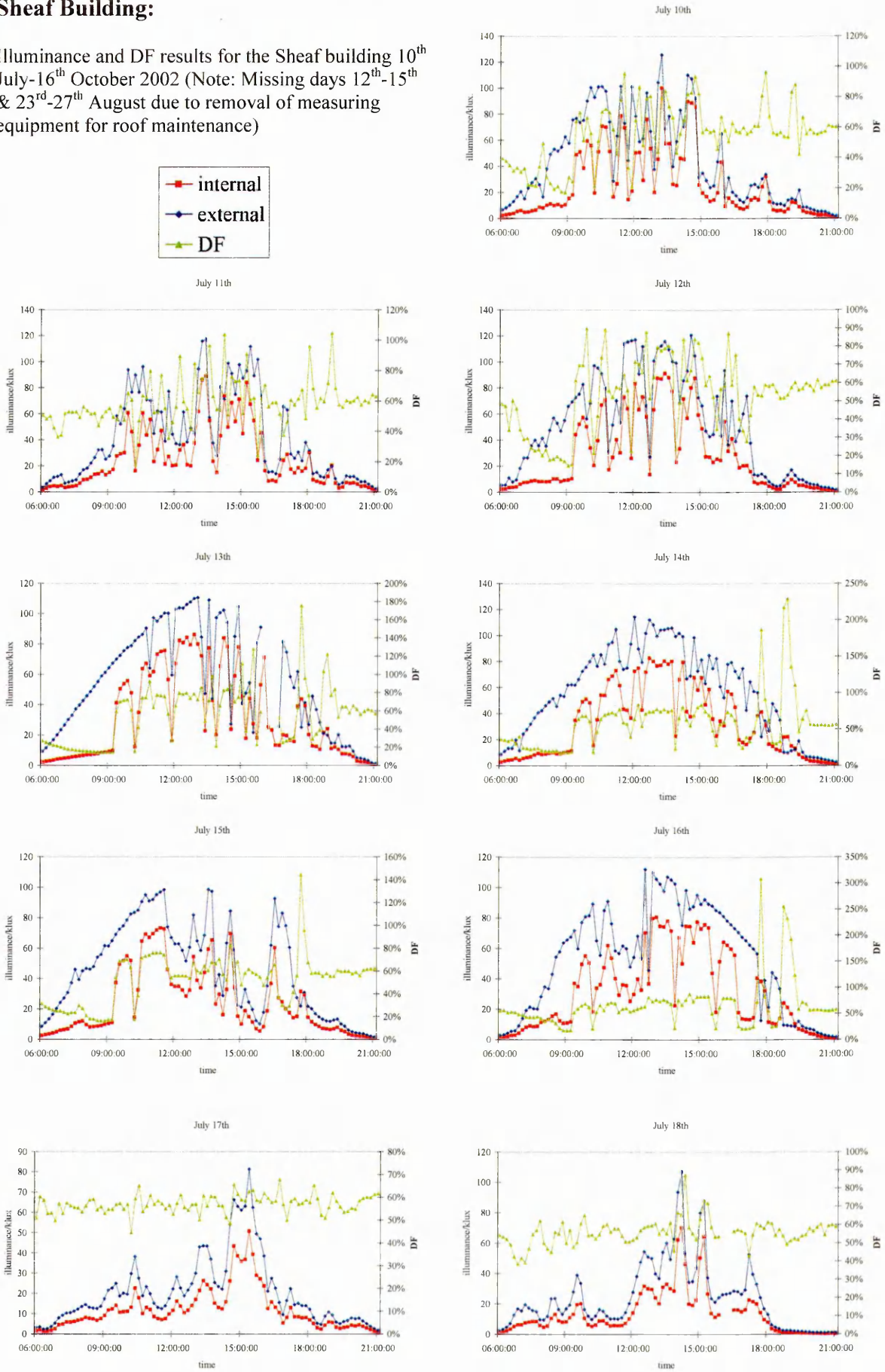
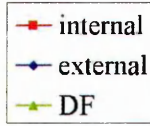
Appendix

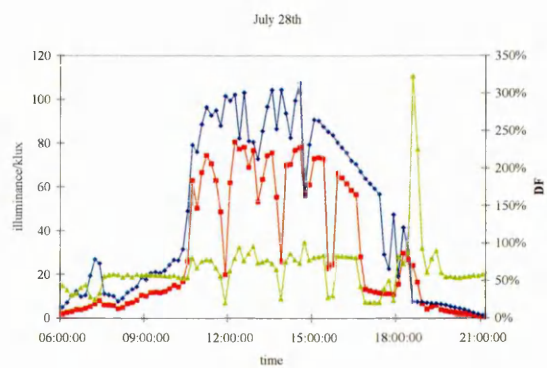
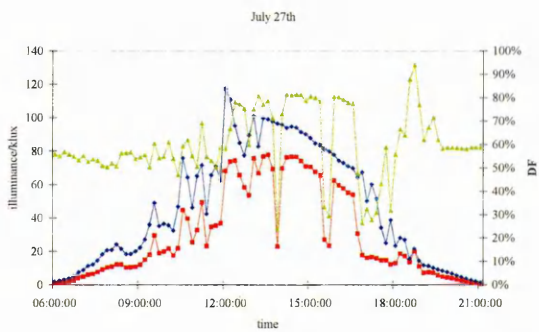
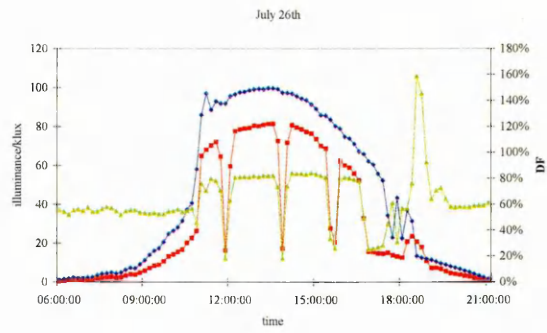
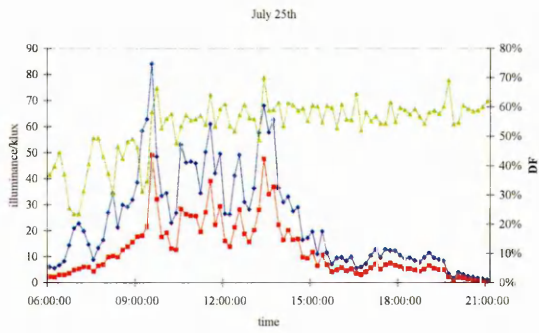
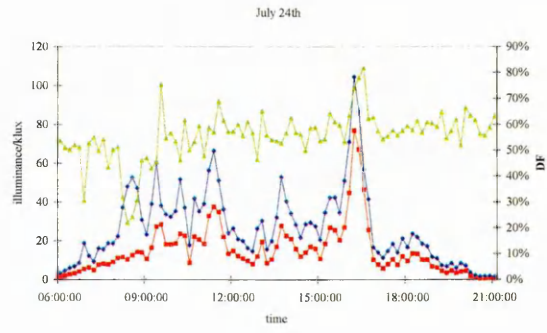
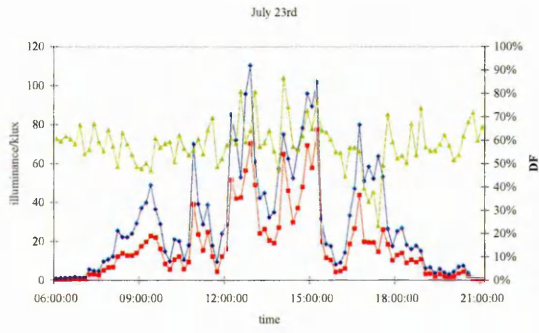
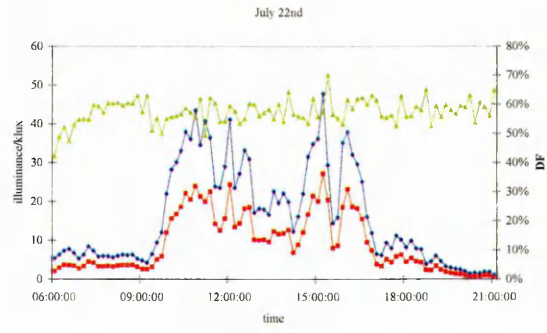
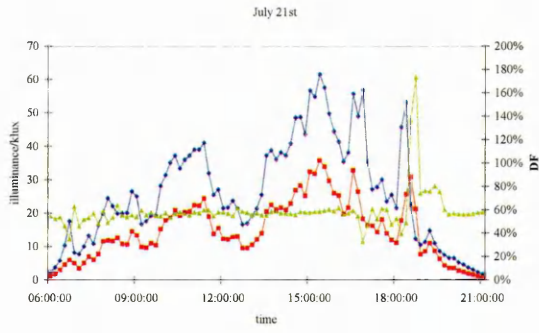
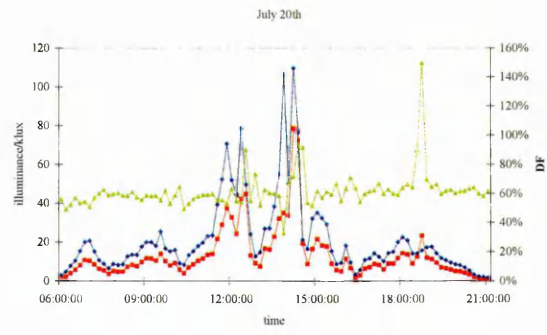
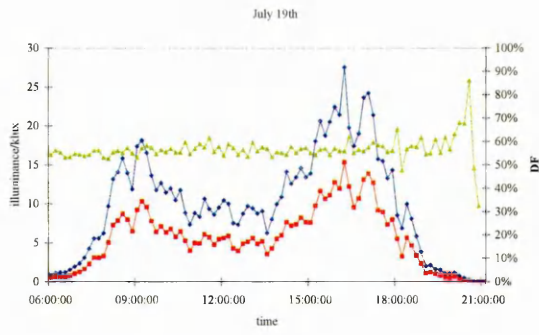


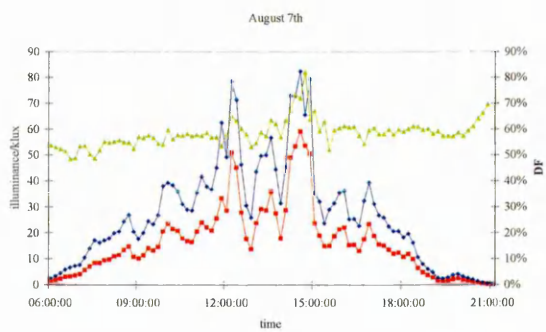
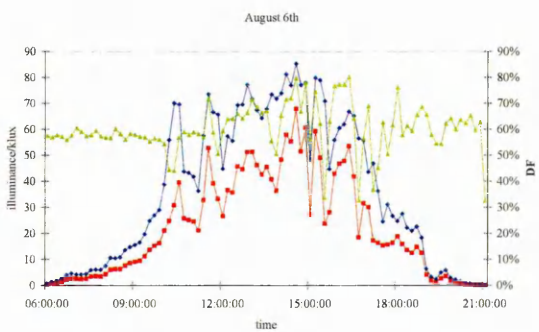
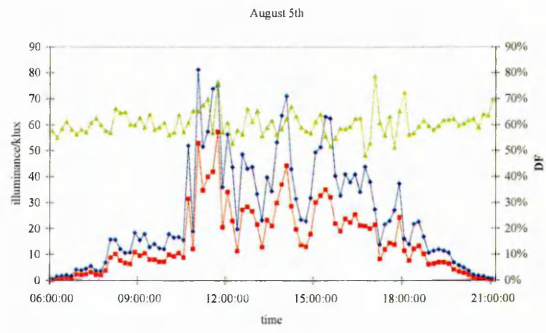
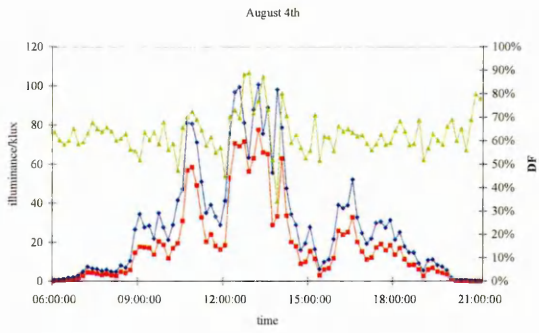
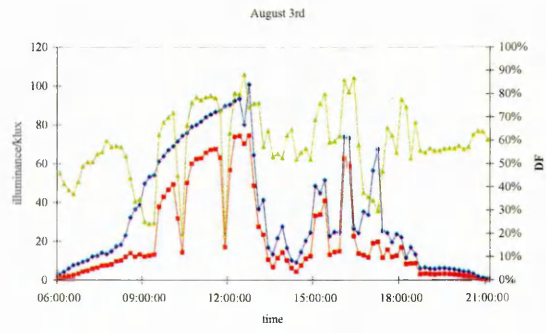
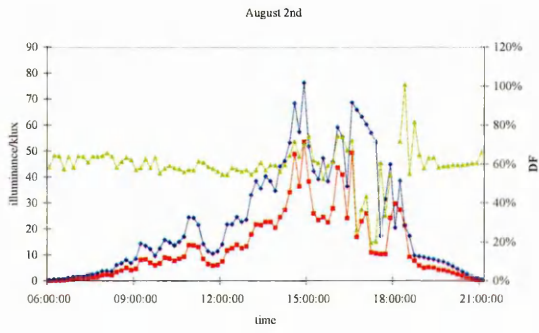
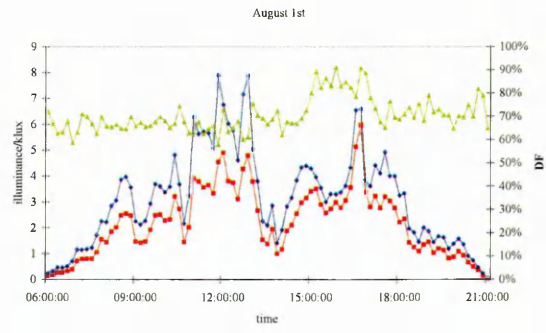
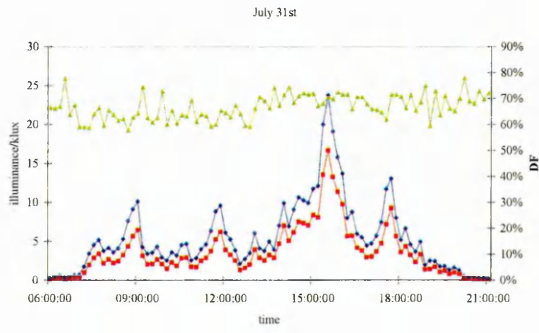
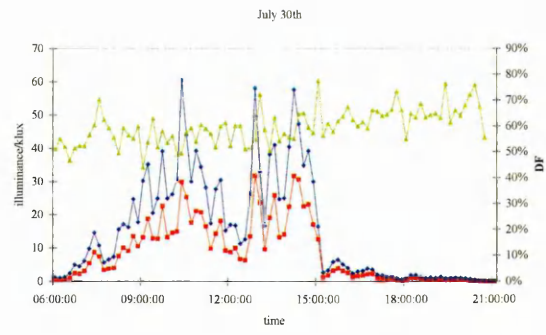
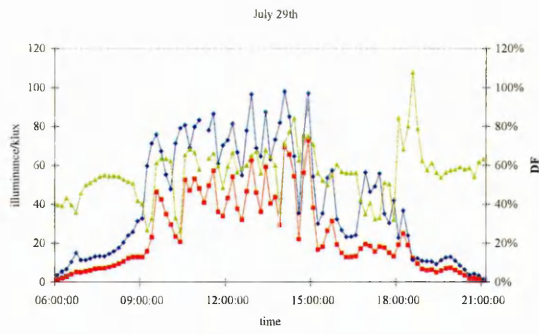
**Full Illuminance Results from
Sheaf and Owen Buildings**

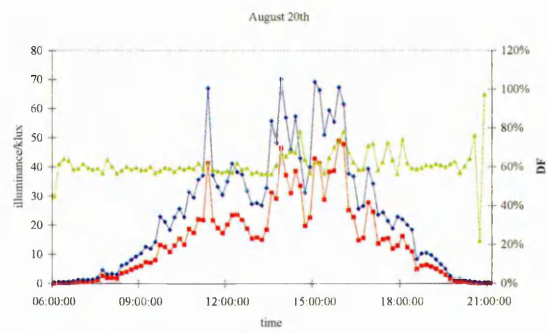
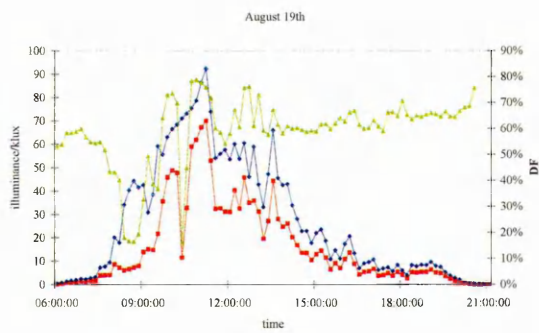
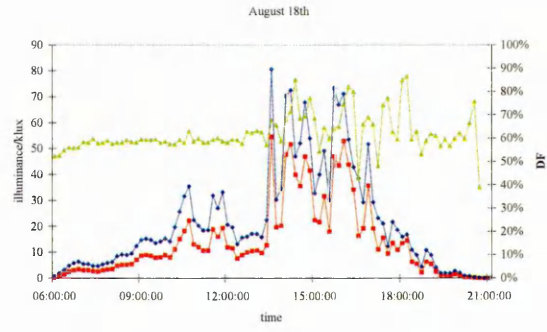
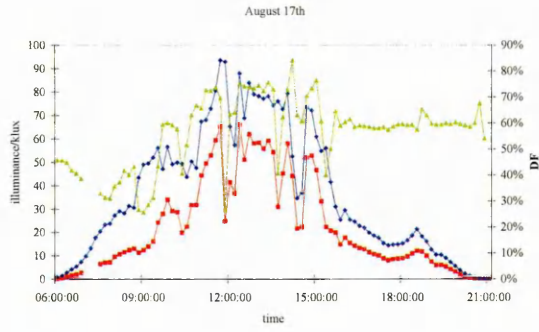
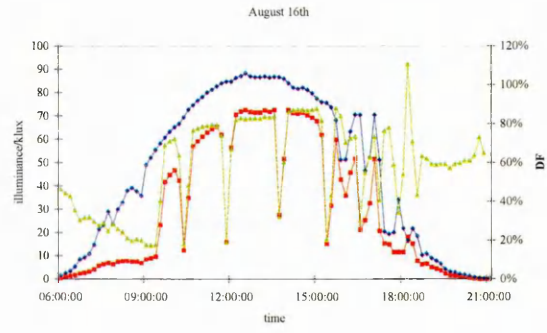
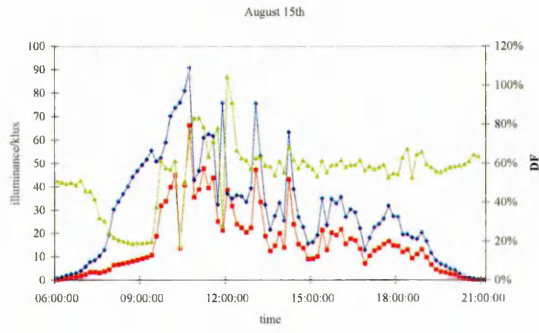
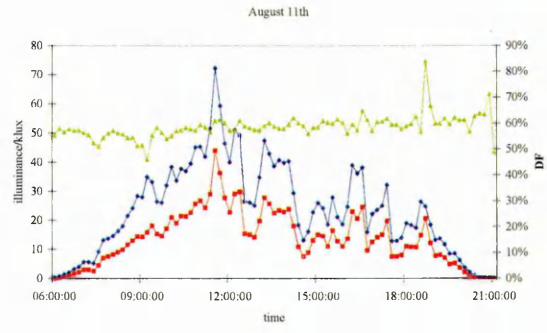
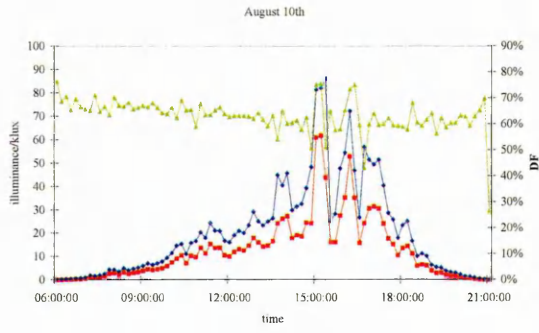
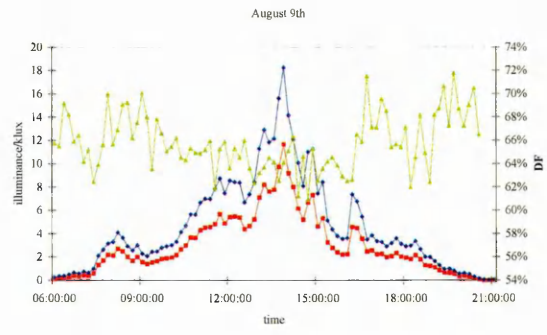
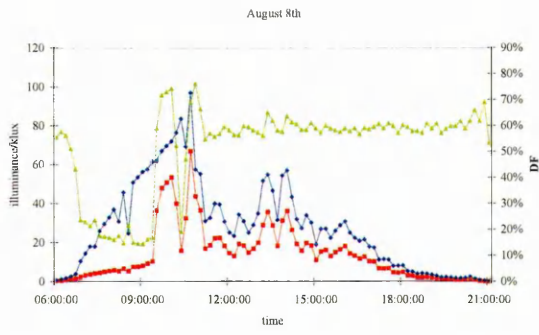
Sheaf Building:

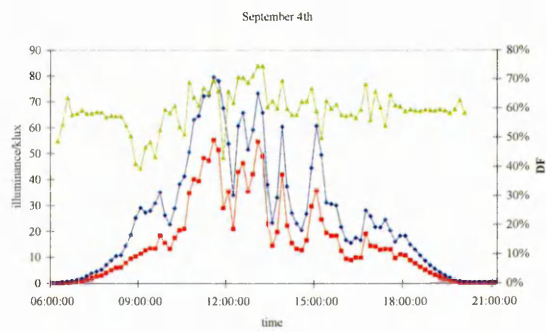
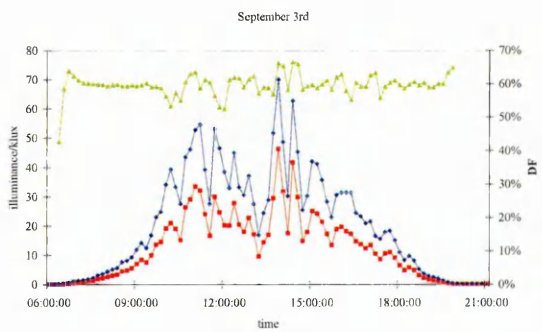
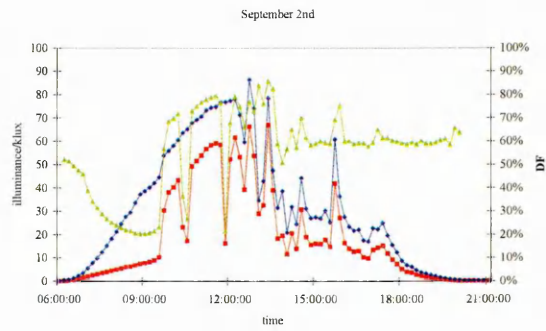
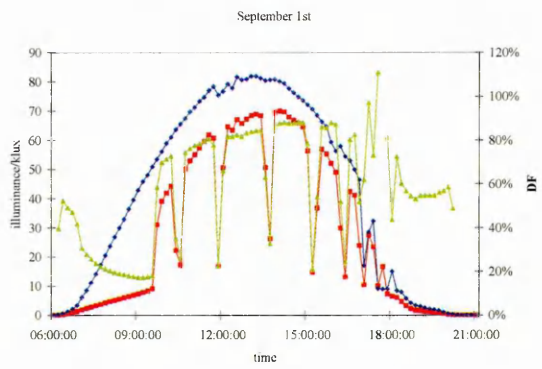
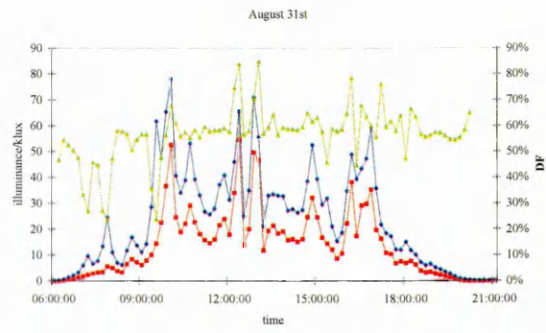
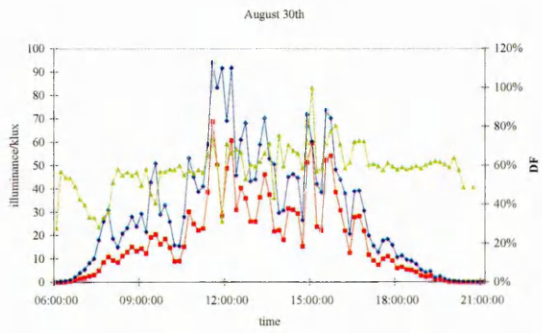
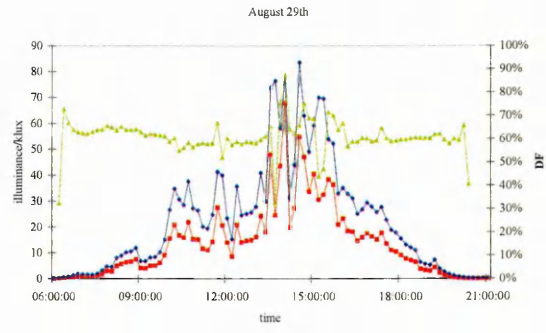
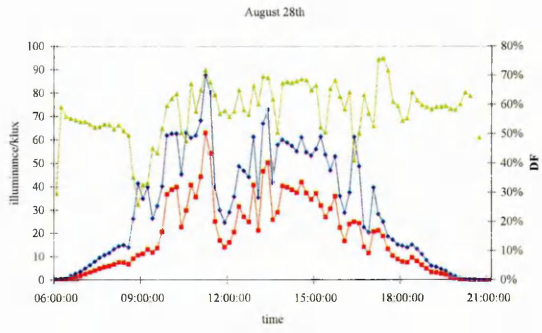
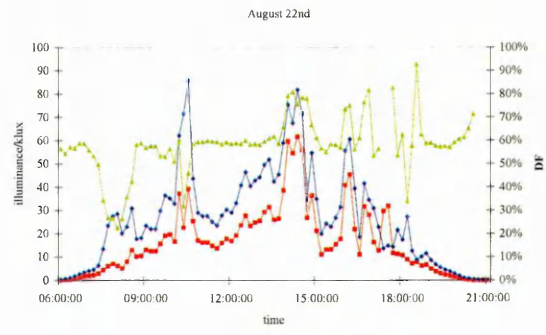
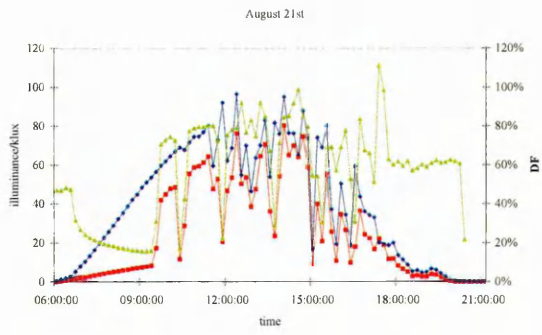
Illuminance and DF results for the Sheaf building 10th July-16th October 2002 (Note: Missing days 12th-15th & 23rd-27th August due to removal of measuring equipment for roof maintenance)

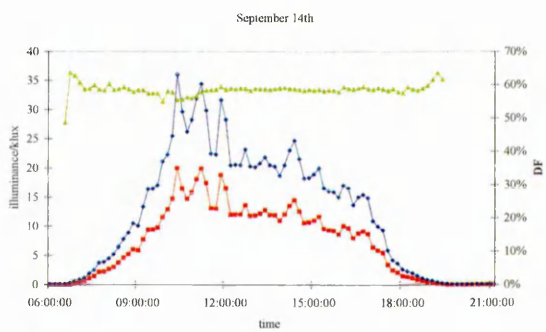
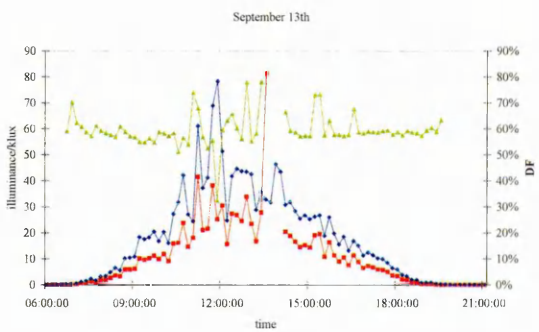
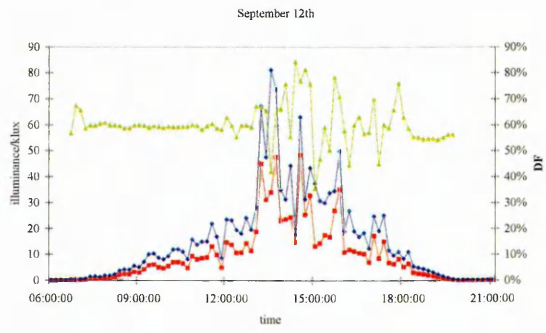
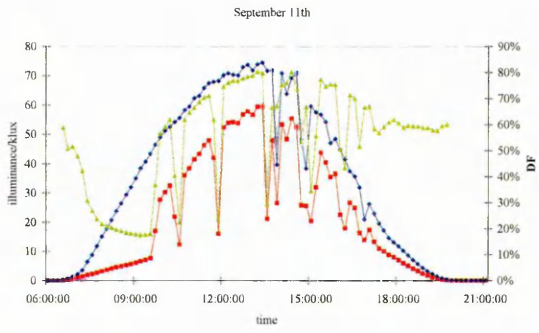
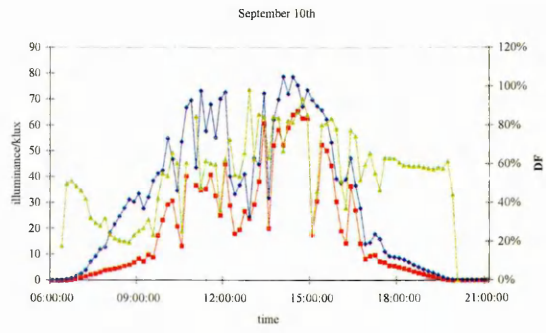
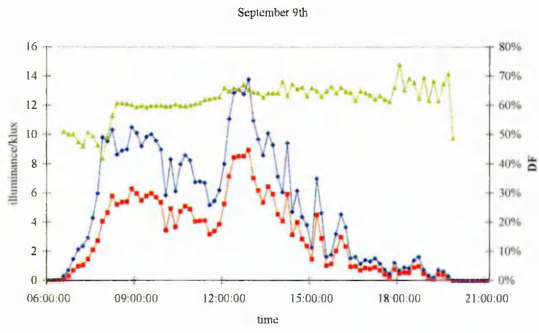
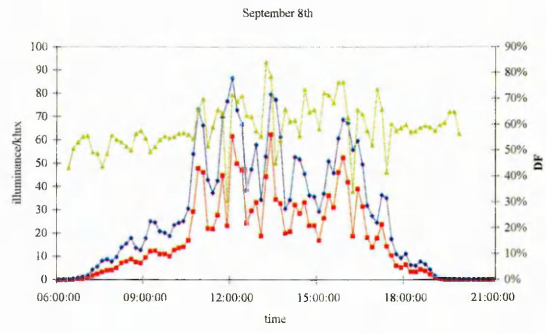
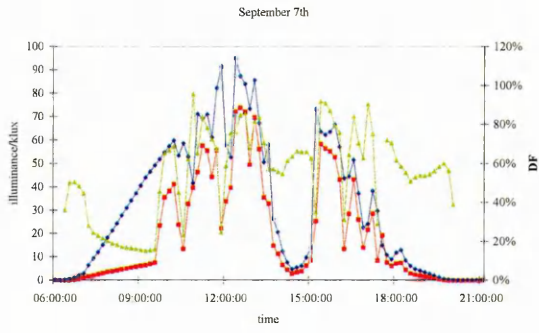
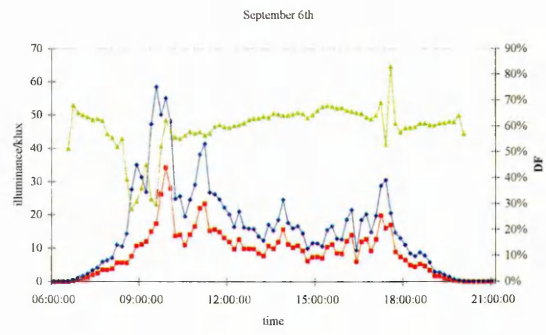
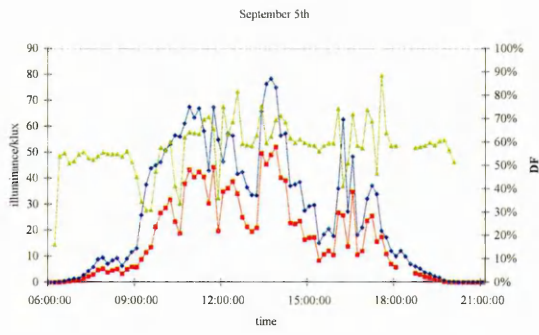


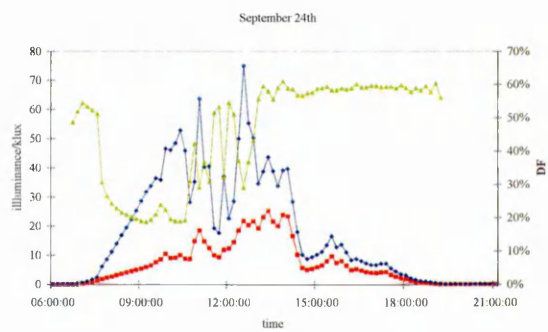
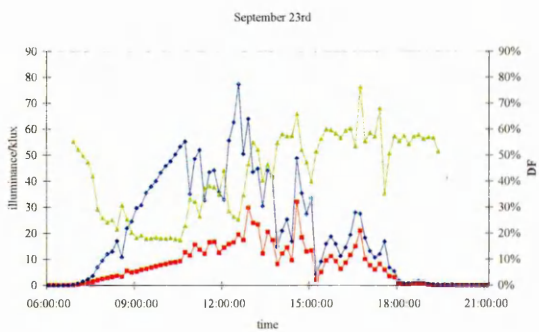
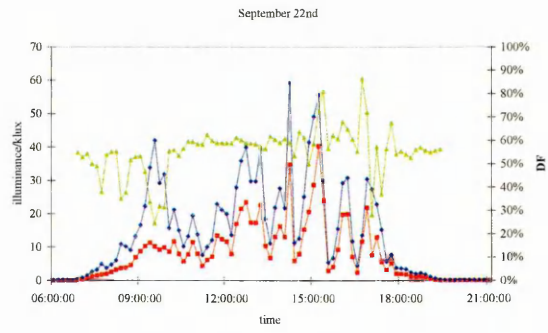
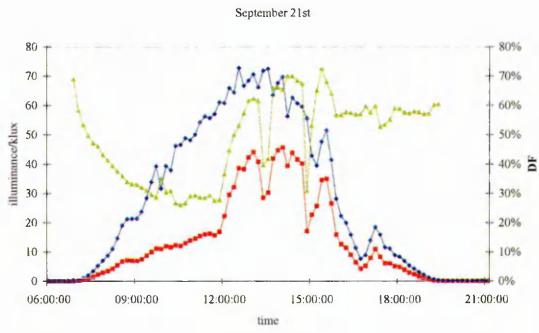
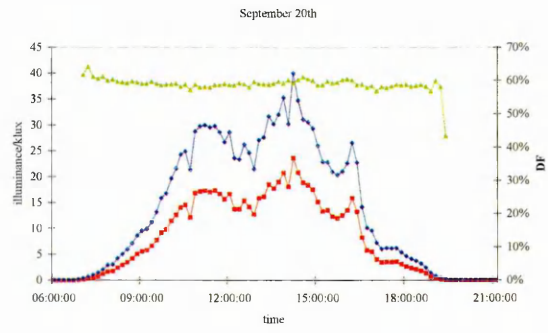
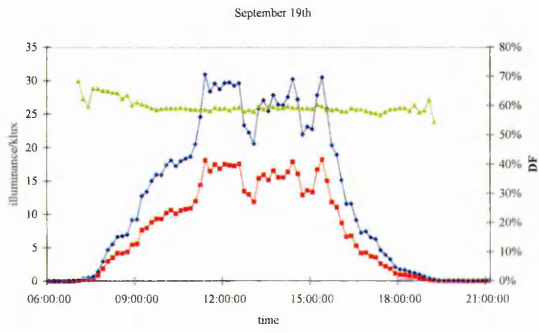
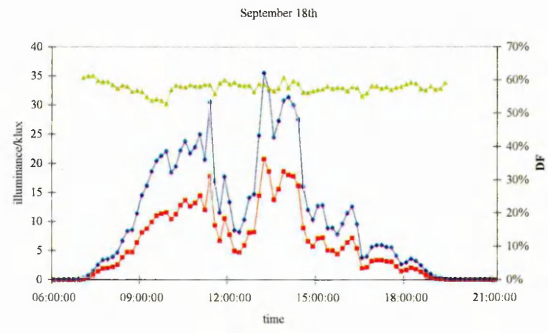
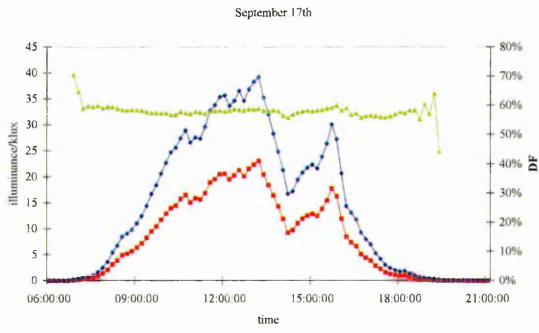
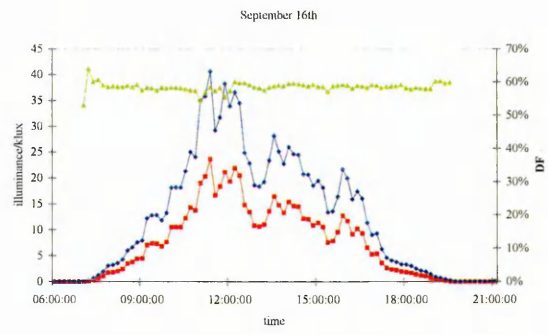
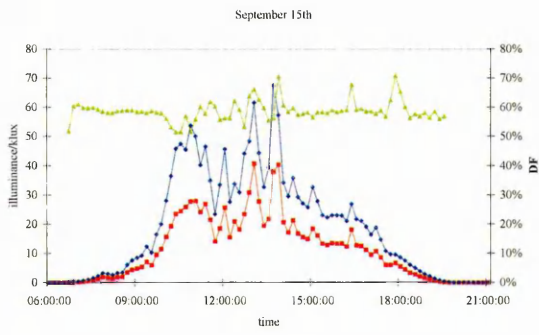


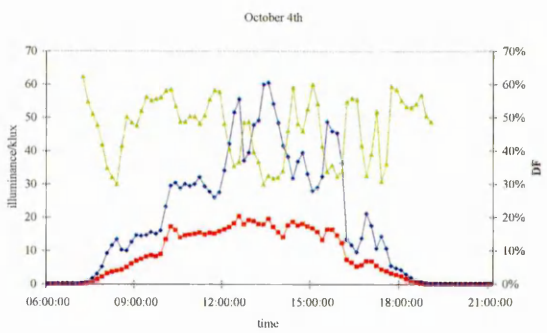
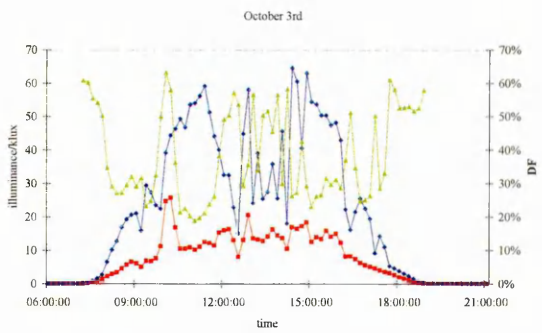
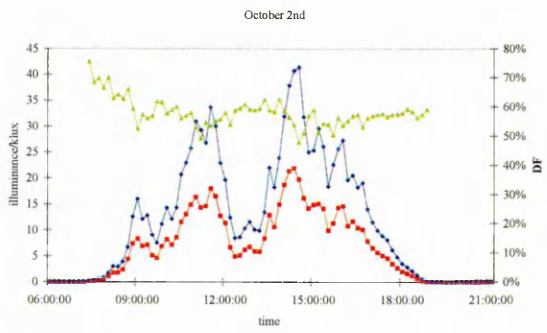
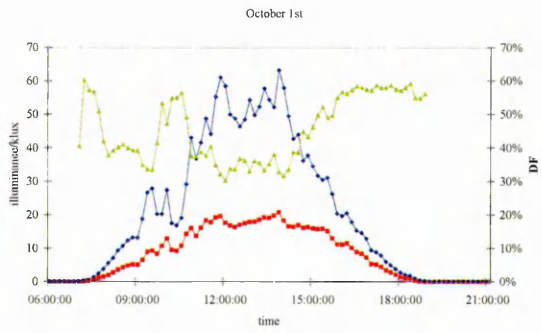
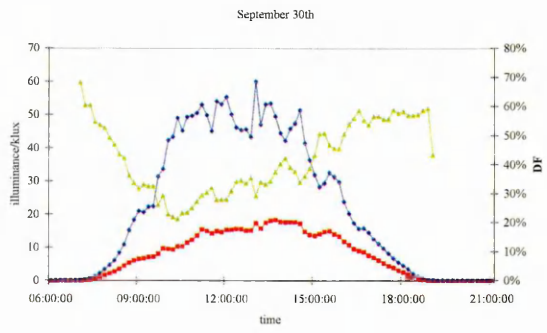
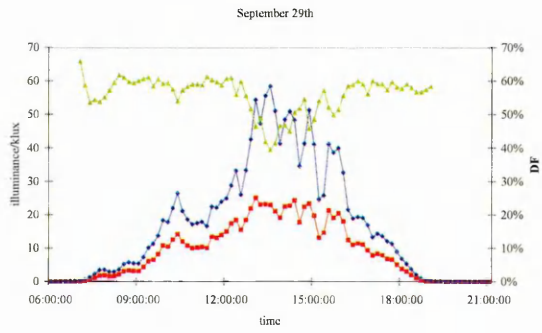
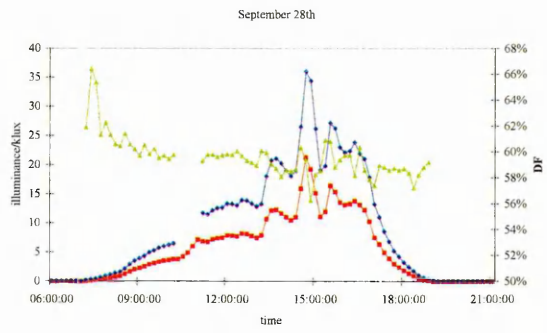
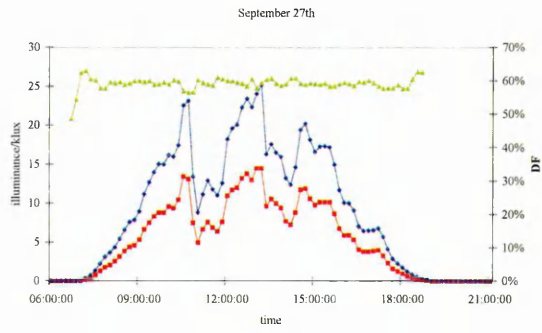
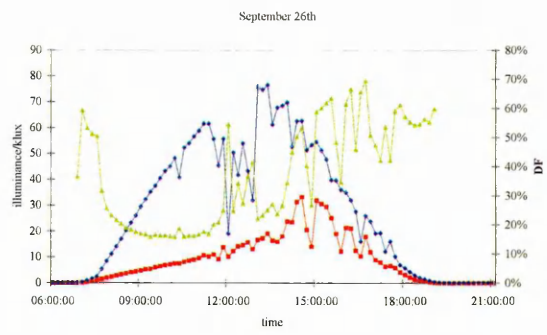
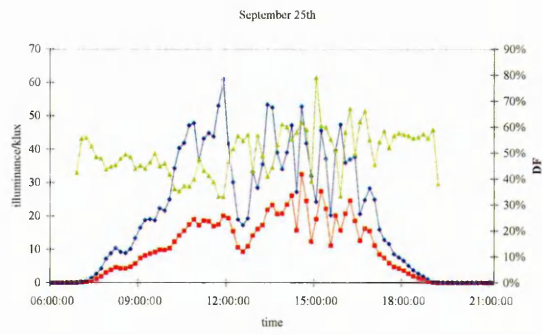


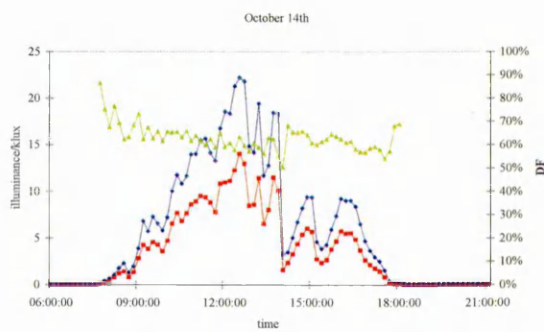
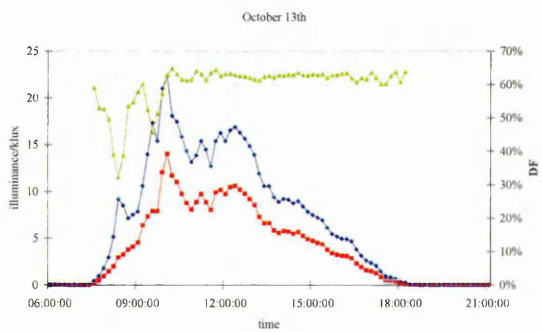
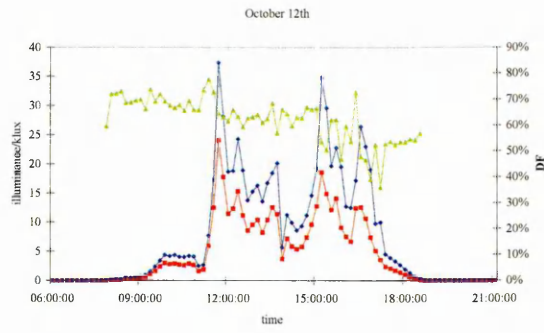
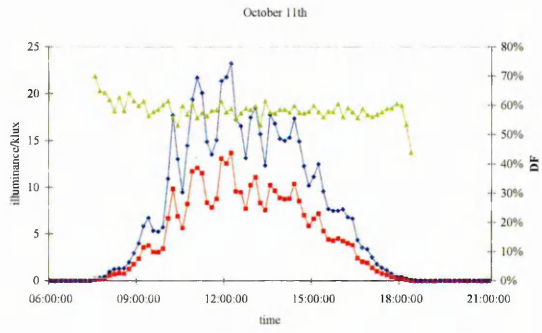
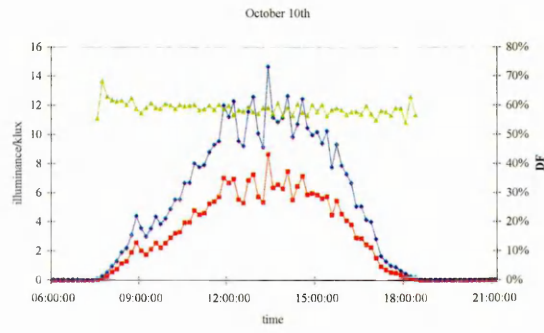
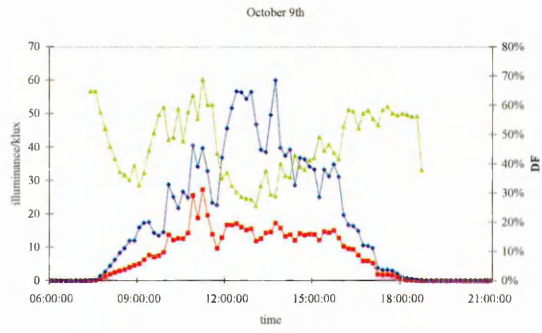
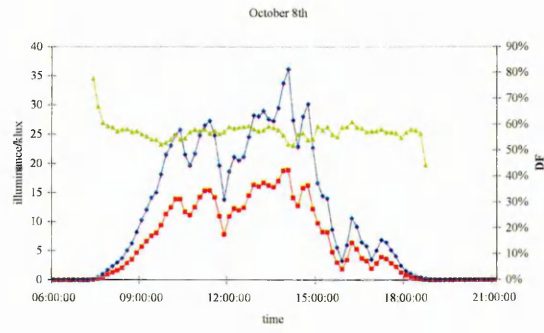
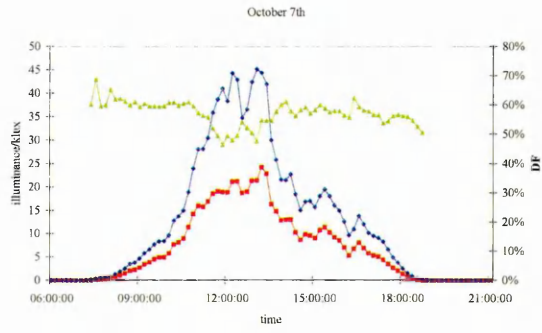
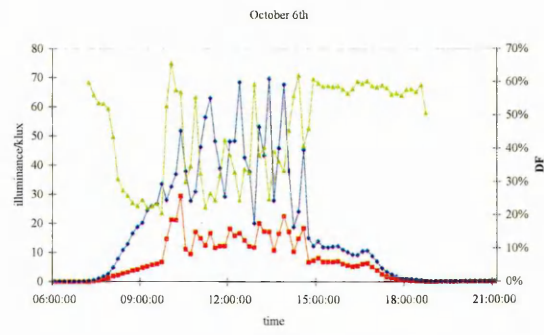
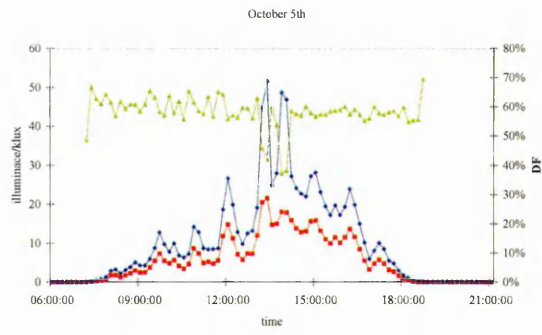


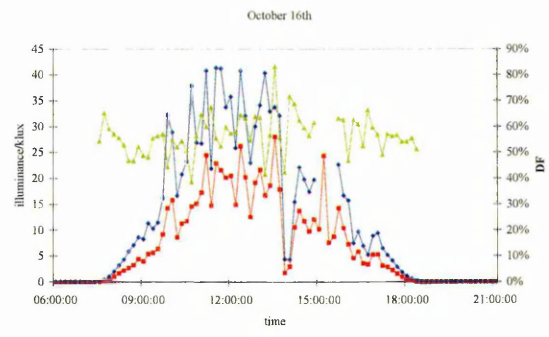
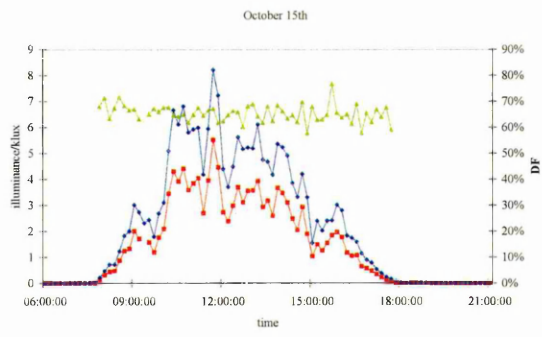






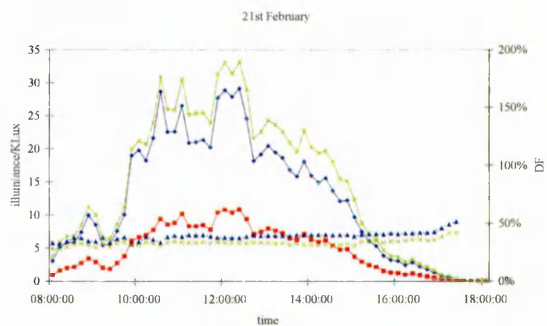
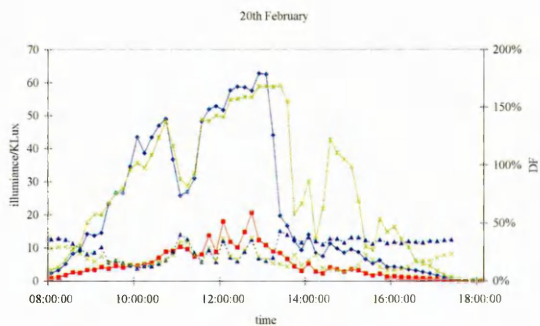
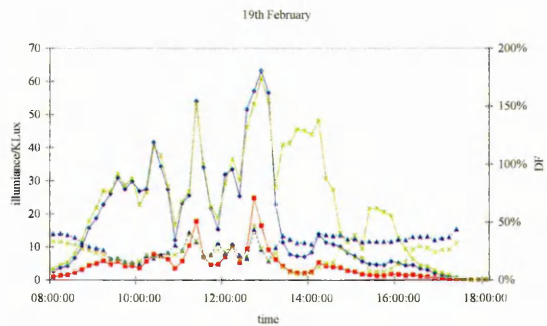
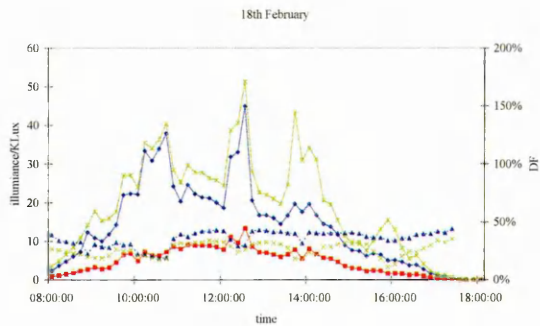
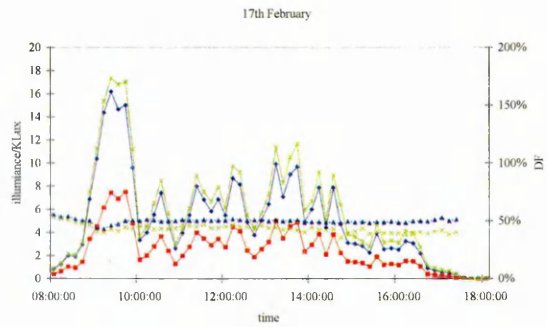
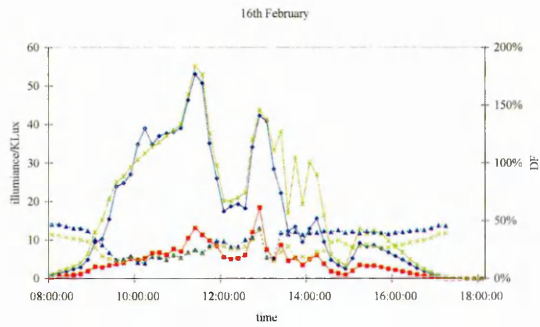
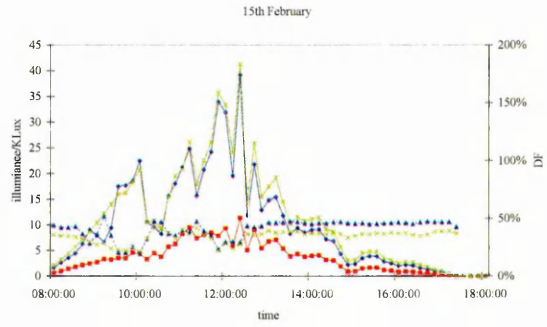
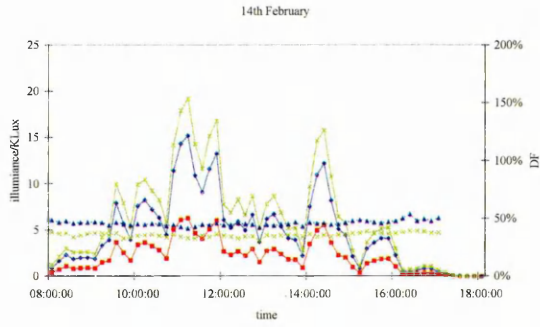
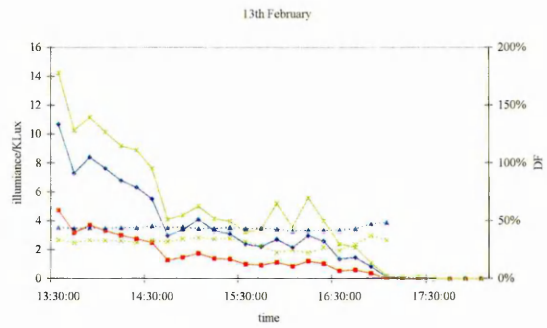
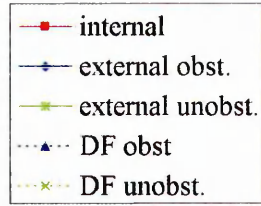


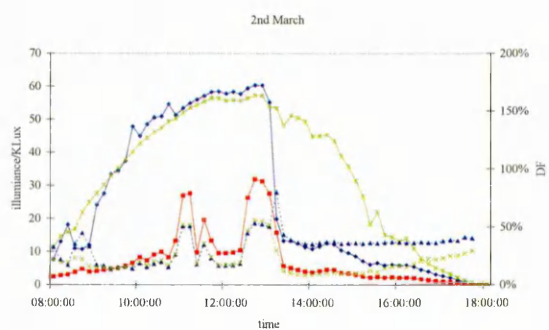
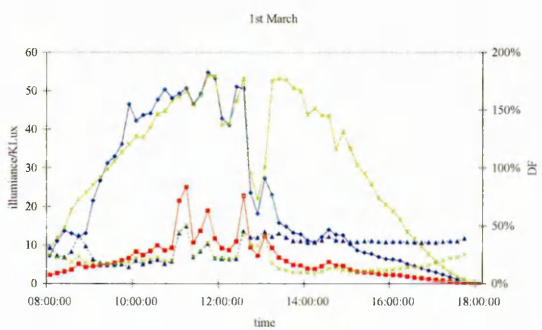
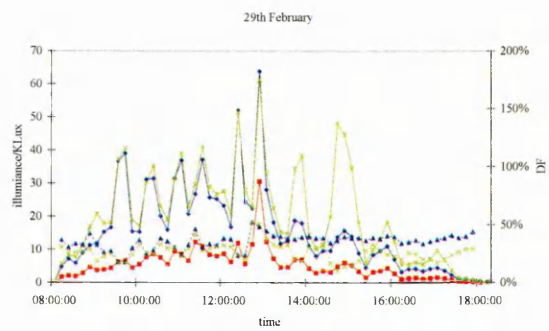
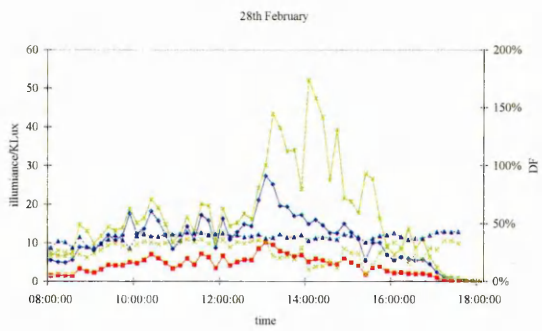
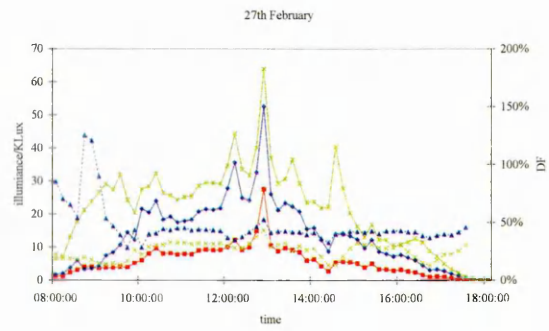
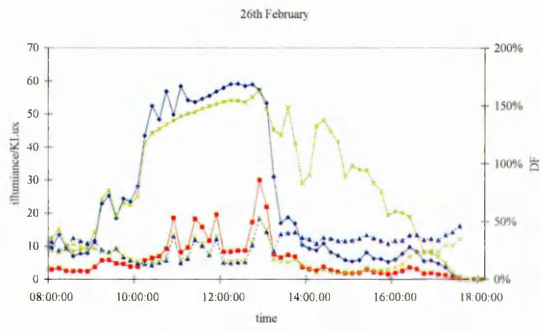
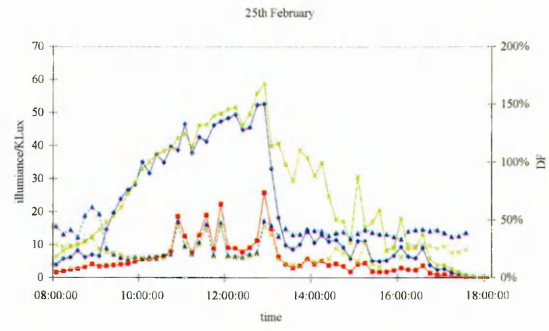
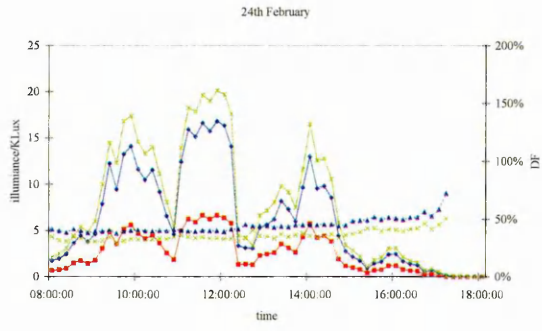
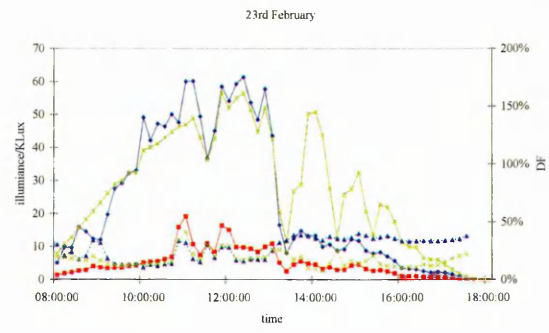
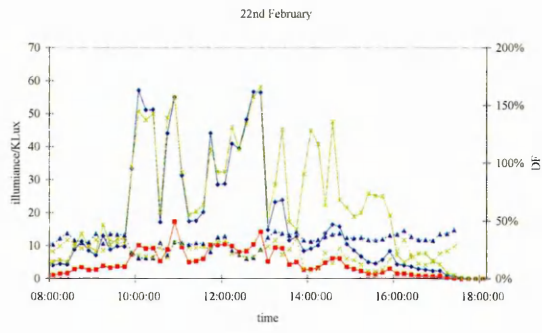


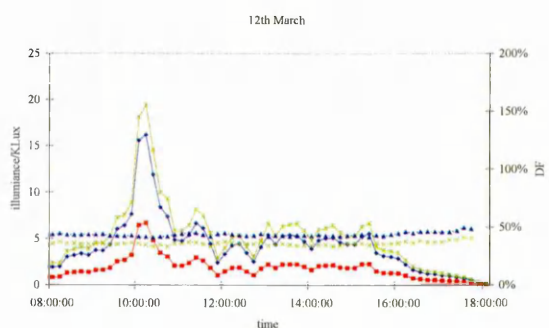
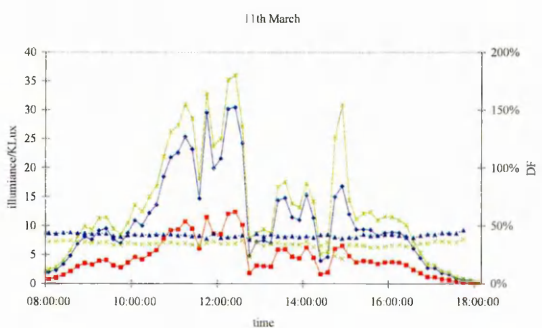
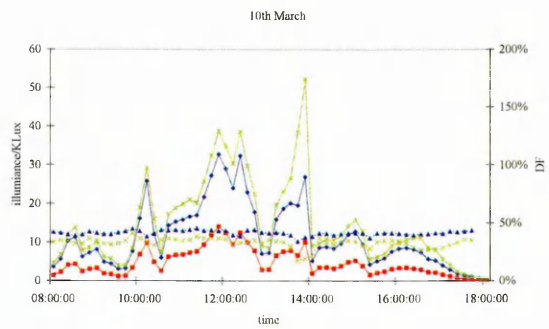
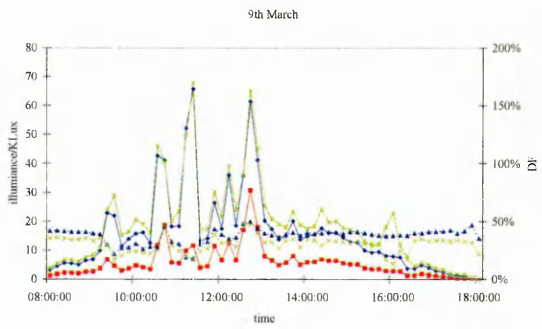
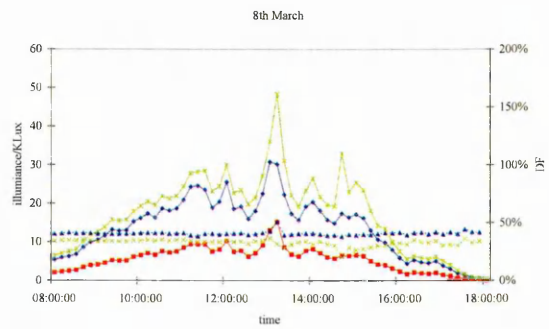
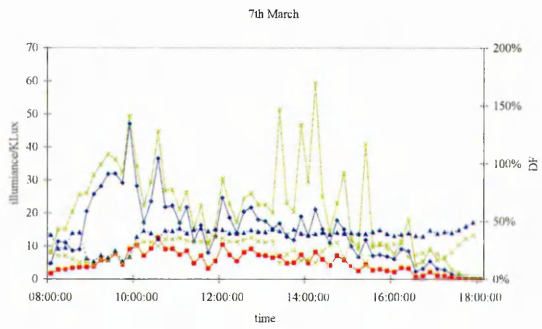
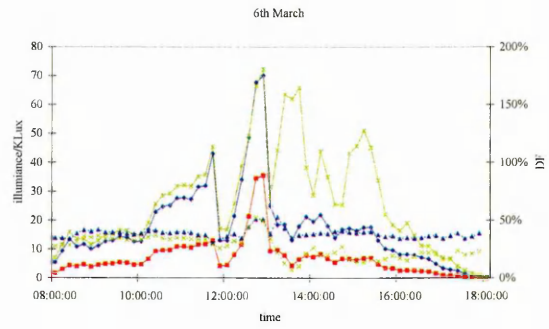
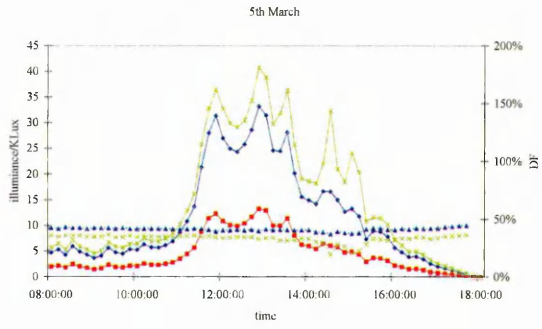
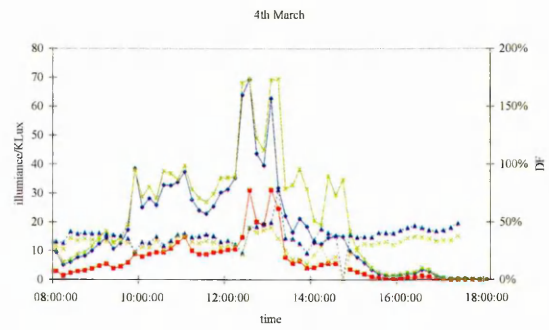
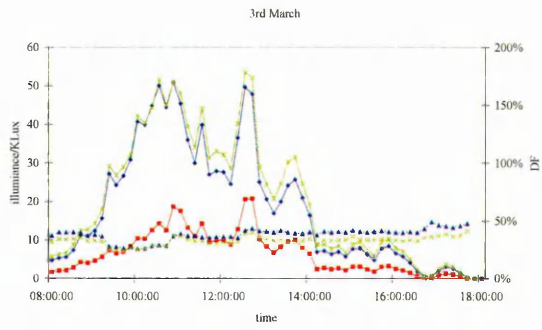


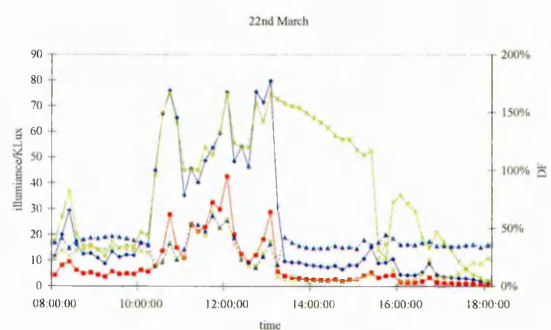
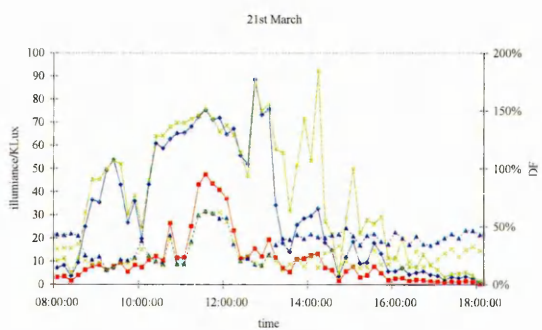
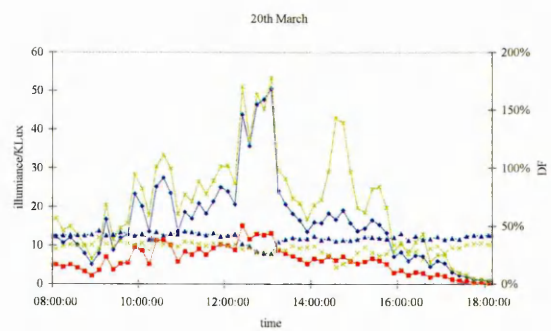
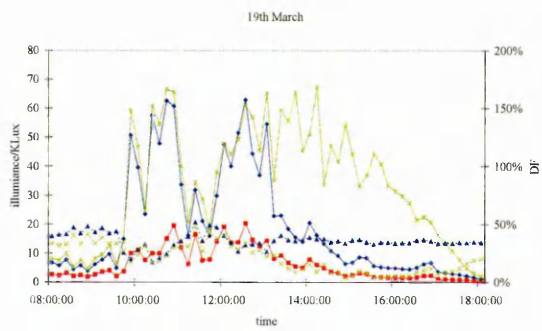
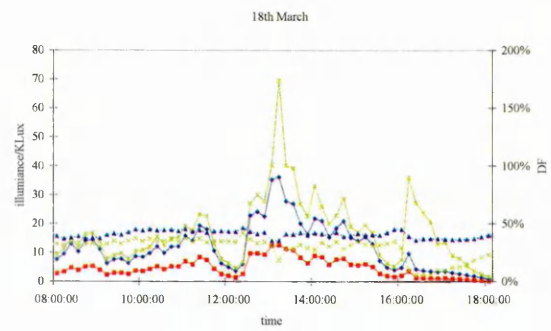
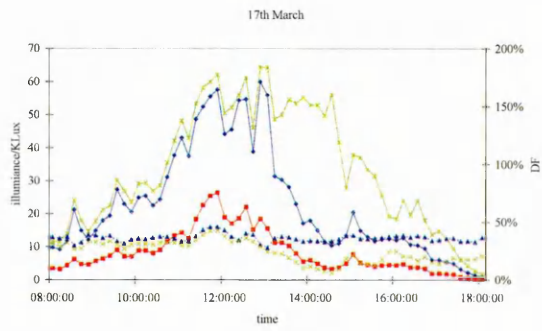
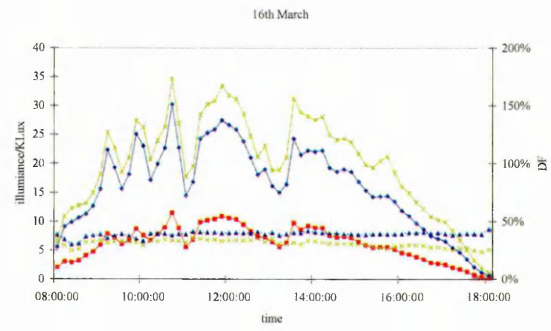
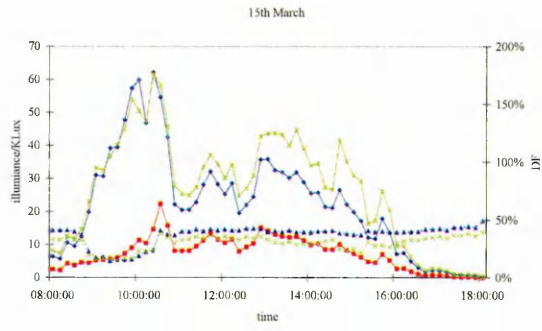
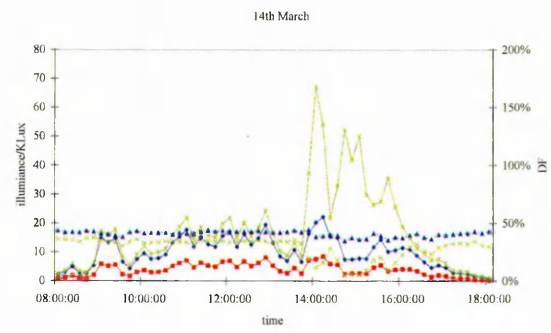
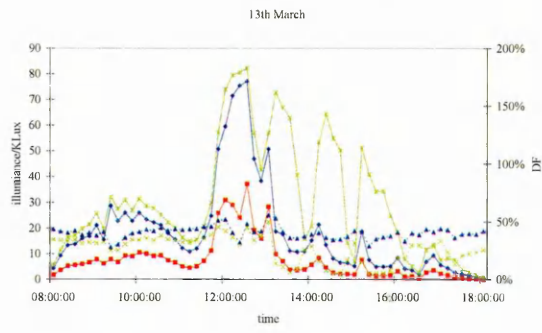
Owen Building:

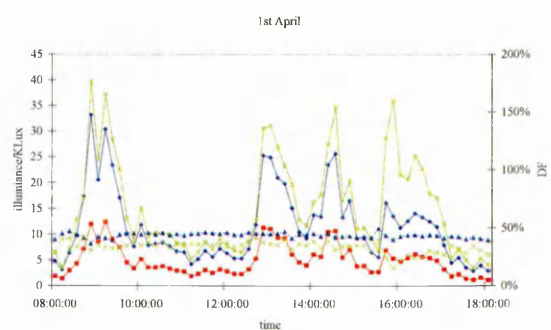
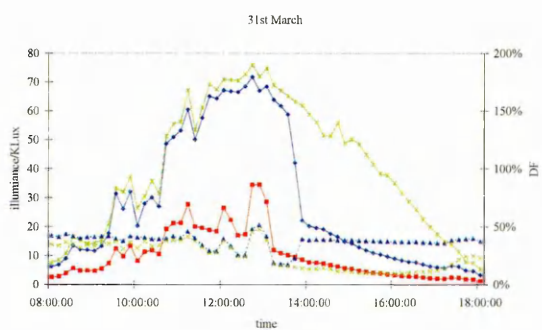
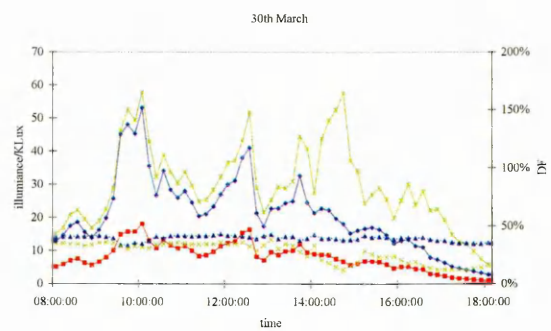
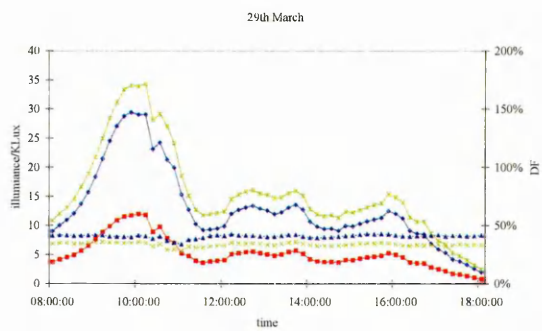
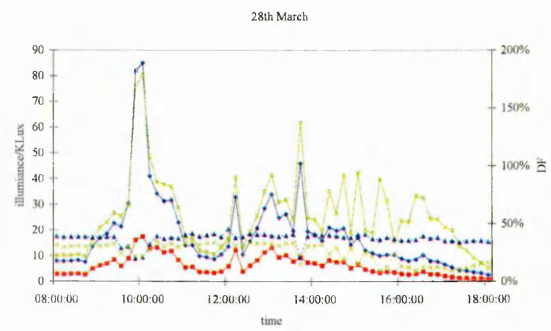
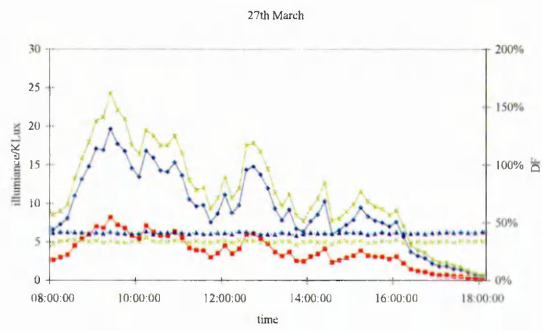
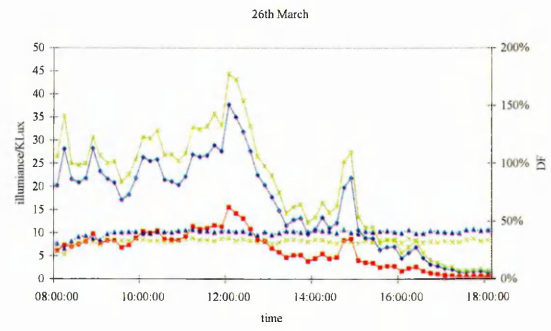
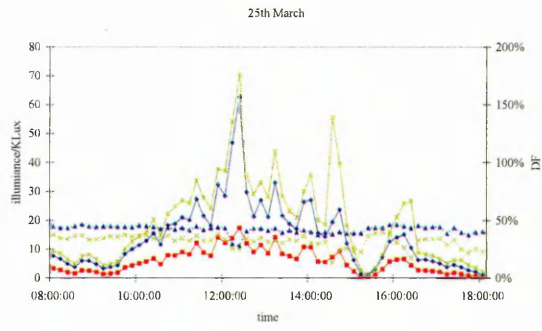
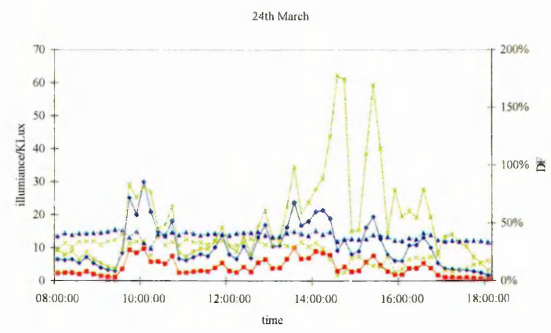
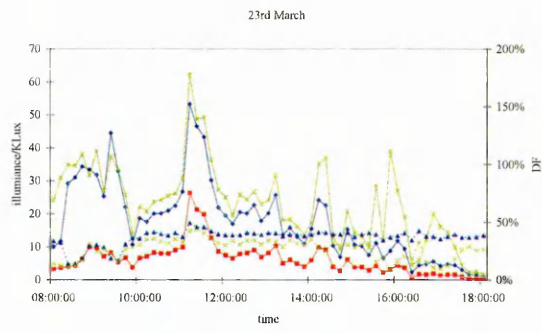
Illuminance and DF results for the Owen building
13th February-20th April 2004.

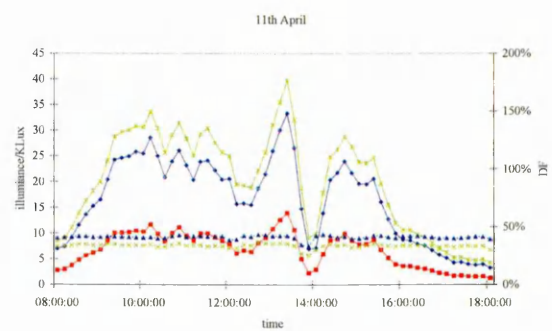
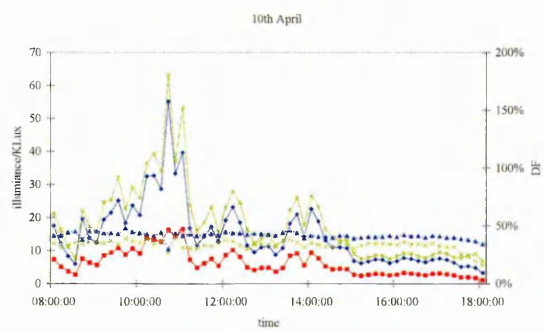
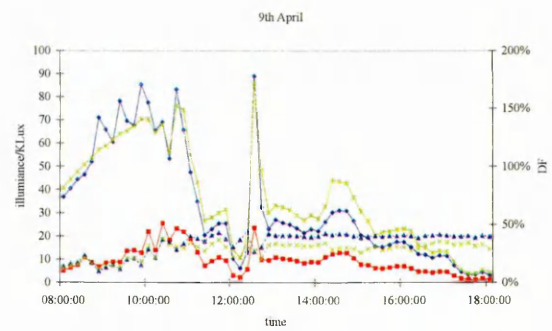
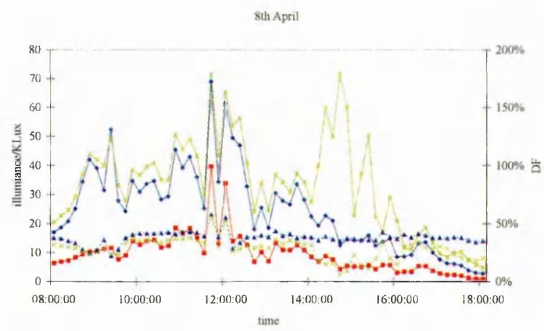
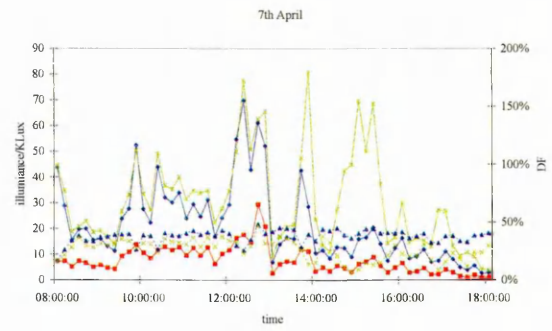
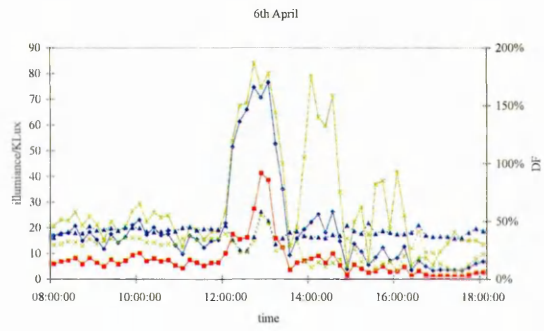
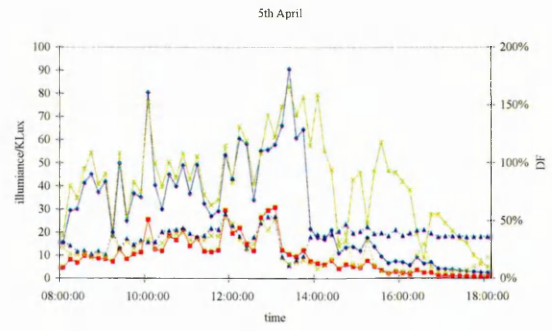
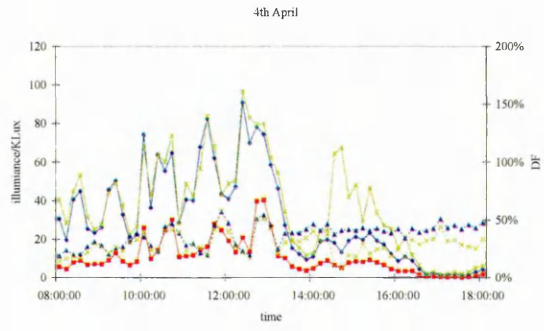
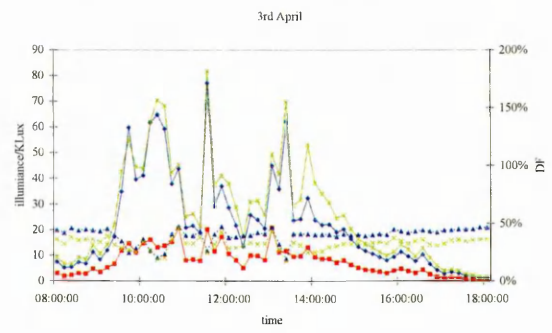
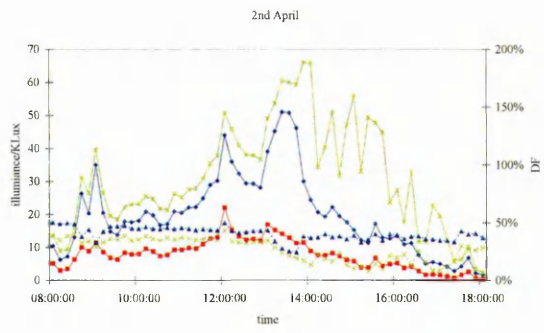


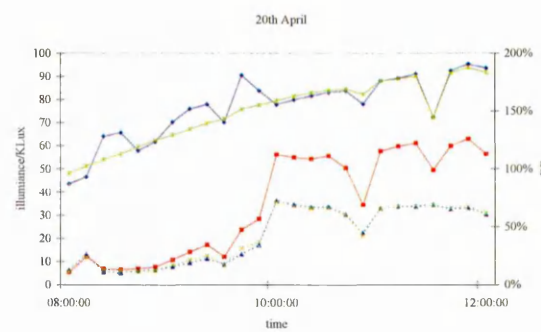
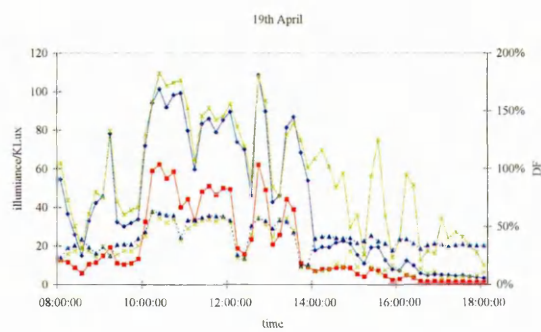
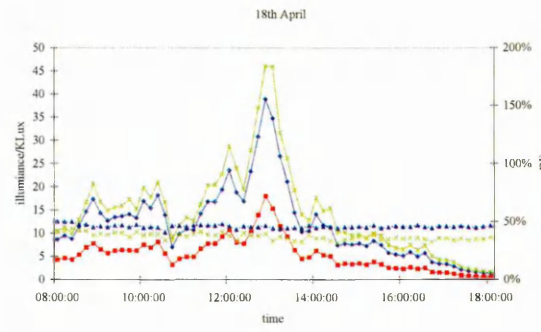
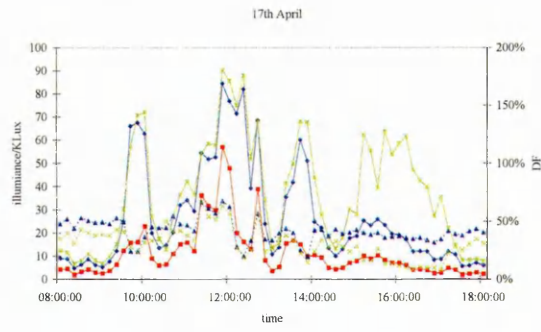
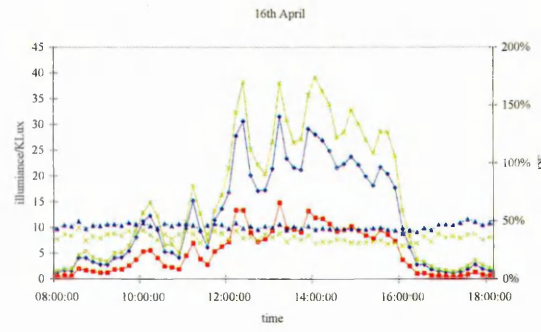
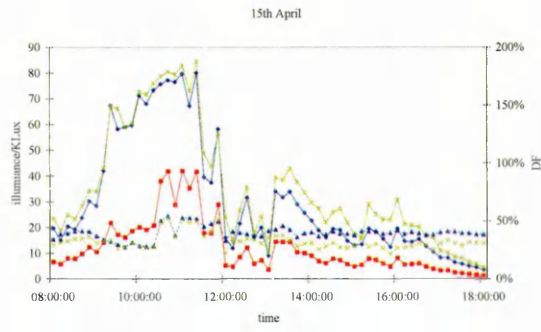
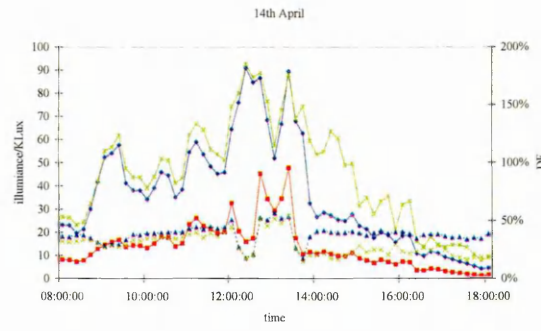
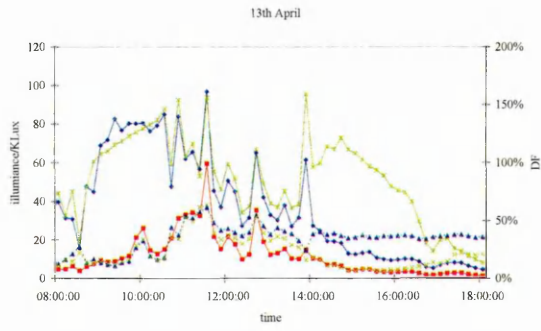
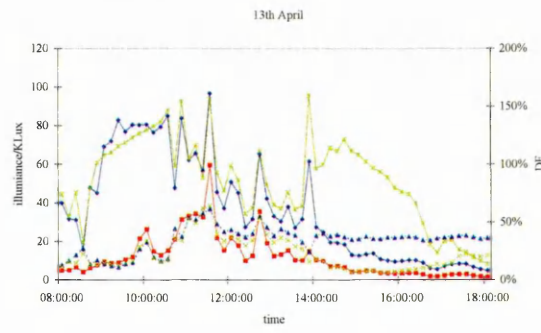
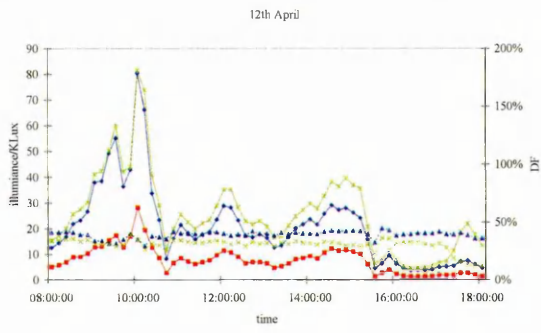












DX234068

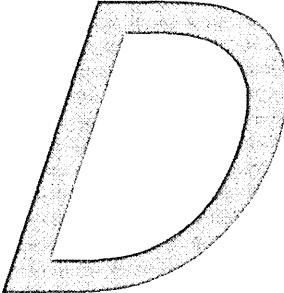
Awarding Body : SheffieldHallam

Thesis By : LASH Daniel

**Thesis Title : ASSESSING THE DAYLIGHT TRANSMITTANCE OF
ATRIA ROOFS IN REAL BUILDINGS**

We have assigned this thesis the number given at the top of this sheet.

**THE BRITISH LIBRARY
DOCUMENT SUPPLY CENTRE**

Appendix 

Statistical Equations

Here follows a list of statistical definitions with accompanying equations, used in this thesis.

The **mean** (\bar{x}) of a set of data is defined as the sum of all the items (where one item = x) in the range divided by the total number of items in the range (n). Its units relate to x .

$$\bar{x} = \frac{\sum x}{n} \quad [\text{D-1}]$$

The **standard deviation** (σ) is a statistical measure of spread or variability. It is expressed as the root of the average of the squares of deviations about the mean of a set of data. Its units relate to x .

$$\sigma = \sqrt{\frac{\sum (x - \bar{x})^2}{n}} \quad [\text{D-2}]$$

The **coefficient of variation** (V) expresses the standard deviation in relative terms to the mean of a set of data. It is expressed as a percentage.

$$V = \frac{\sigma}{\bar{x}} \times 100\% \quad [\text{D-3}]$$

The **relative error** (RER) is the ratio of absolute error to the true, specified, or theoretically correct value of the quantity that is in error. It is expressed as a percentage.

$$RER = \left(\frac{\text{predicted} - \text{measured}}{\text{measured}} \right) \times 100\% \quad [\text{D-4}]$$

The **mean biased error** (MBE) is the mean of a series of relative errors obtained for that series, expressed as a percentage.

$$MBE = \left(\frac{1}{n}\right) \sum_{i=1}^N \left(\frac{\text{predicted}_i - \text{measured}_i}{\text{measured}_i} \right) \times 100\% \quad [D-5]$$

The **root mean square error** (RMSE) is the root mean of a series of squared relative errors, expressed as a percentage.

$$RMSE = \sqrt{\left(\frac{1}{n}\right) \sum_{i=1}^N \left(\frac{\text{predicted}_i - \text{measured}_i}{\text{measured}_i} \right)^2} \times 100\% \quad [D-6]$$